Comparison of Recompression and SHANSEP Strength-Deformation Properties of Undisturbed Boston Blue Clay from Automated Triaxial Testing

by

Anne Heim Estabrook

B.S. Civil Engineering, University of California at Berkeley, 1989

Submitted to the Department of Civil Engineering
in partial fulfillment of the requirements for the degree of

Master of Science in Civil Engineering

at the

MASSACHUSETTS INSTITUTE OF TECHNOLOGY

May 1991

Author .....
Department of Civil Engineering
May 17, 1991

Certified by .....
Charles C. Ladd
Professor
Thesis Supervisor

Certified by .....
John T. Germaine
Geotechnical Laboratory Director
Thesis Supervisor

Accepted by .....
Ole S. Madsen
Chairman, Departmental Committee on Graduate Students

Comparison of Recompression and SHANSEP Strength-Deformation Properties of Undisturbed Boston Blue Clay from Automated Triaxial Testing

by

Anne Heim Estabrook

Submitted to the Department of Civil Engineering
on May 17, 1991, in partial fulfillment of the
requirements for the degree of
Master of Science in Civil Engineering

Abstract

This thesis presents the results of Recompression triaxial strength testing performed on undisturbed samples of Boston Blue Clay obtained at the Central Artery/Third Harbor Tunnel Special Testing Program site in South Boston. Background is given about the South and East Boston sites, the sampling program and the laboratory testing program. The automated stress path triaxial apparatus implemented for this research program and the laboratory procedures used are described in detail. Data are summarized from the various types of consolidation testing employed (CK_0–TX consolidation, standard oedometer tests, and constant rate of strain consolidation tests) and the stress history of each site is evaluated.

The Recompression technique was used for a comprehensive program of K_0 consolidated-undrained triaxial compression and extension tests run on both Sherbrooke block and fixed piston tube samples from the South Boston site. The influence of large changes in overconsolidation ratio on undrained shear behavior was studied by running tests on samples from different depths and by varying the preshear consolidation stress. A comparison of these data is made with results from the SHANSEP testing program reported by Mr. de La Beaumelle, and the UU and CIUC tests performed by Haley & Aldrich. Recommendations are made for use of Recompression tests in future testing programs.

Thesis Supervisor: Charles C. Ladd
Title: Professor

Thesis Supervisor: John T. Germaine
Title: Geotechnical Laboratory Director

Acknowledgments

I thank my thesis supervisor, Professor Charles Ladd, for his meticulous handling of the data, technical guidance, and attention to the details of this thesis. Thanks also to Doctor Jack Germaine, for his patient instruction and supervision of my laboratory work.

I thank the sponsors of this project, Haley & Aldrich, and Bechtel/Parsons Brinckerhoff, for funding my research. I especially thank Gretchen Young of H&A, an engineer who's not afraid to get her hands dirty (or waxy), for her help with preparing samples and checking and summarizing data.

I owe thanks for all of the great memories of Boston and MIT that I will be taking with me to a truly wonderful group of friends. In particular I thank my roommates, Mary Lynn and Matthew. Thanks to my lab partner, Axel, who is a lot more patient than I am, and to my other office mates for providing countless unproductive (but entertaining) hours of political debate, sports talk, snack-getting, MIT bashing, and general, unfocused procrastinating. Thanks to Chuck and Youssef for the letting me monopolize their Mac for the past month, and only complaining some of the time. Thanks to Roseanna for running with me three times a week, even though her mother wouldn't approve. Very special thanks to all current members and members emeritus of the GNO for all of the fabulous activities, aerobics networking, celebrity gossip, New Hampshire weekends, etc., and especially Claire, for nominating me for membership. Last but not least, thank you Michael, for niceness above and beyond the call of duty.

Finally, thank you Mom and Dad for your unconditional support of all of my endeavors.

Contents

List of Figures

List of Tables

Chapter 1

Introduction

1.1 Description of Central Artery/Third Harbor Tunnel Project and Special Testing Program

The Central Artery and Third Harbor Tunnel (CA/T) Project is a $5 billion, multi-year project currently underway in Boston, Massachusetts. The primary objective of the project is to decrease congestion in the Boston area by: 1) depressing a portion of Interstate 93 (called the Central Artery) through the downtown; and 2) extending Interstate 90 (the Massachusetts Turnpike) via a tunnel below the Boston harbor to provide a third tunnel connection with Logan airport. A joint venture of Bechtel and Parsons Brinckerhoff (B/PB) are managing the CA/T project for the Massachusetts Department of Public Works.

One early phase of the project consists of geotechnical investigations. The total alignment of the project was divided into five areas for purposes of geotechnical investigations, with contracts for each area being awarded to geotechnical consulting firms. Haley & Aldrich, Inc. (H&A) of Cambridge, MA has responsibility for two of the five areas (Areas 01 and 02).

1.1.1 Background

Most of the alignment within Areas 01 and 02 includes a marine clay deposit, known locally as Boston Blue Clay (BBC). A representative stratigraphy consists of: 15 to 40 feet of miscellaneous fill, organic soil and/or marine sand; from 25 feet to 100 feet of Boston Blue Clay; various types of glacial deposits, including glacial till; and argillite bedrock. The upper portion of the BBC deposit is generally quite firm due to desiccation, but becomes progressively softer with depth and may be near normally consolidated within the lower portion. The roadway elevations vary significantly, and include a sunken tube tunnel under Boston harbor, cut-and-cover tunnel sections, U-shaped "boat" sections, at grade sections, embankments and viaducts.

Construction involves a wide variety of geotechnical problems. Examples include the design of temporary and permanent lateral support systems and assessment of bottom stability for deep excavations, and predictions of both short and long term deformations for the boat sections. Moreover, the overall size and cost of the project, combined with unprecedented excavation depths within the BBC, warrant use of the most advanced design analysis rather than reliance on empirical techniques. This in turn requires highly reliable estimates of the engineering properties of Boston Blue Clay.

H&A identified a list of geotechnical design issues and the corresponding engineering properties of BBC that are summarized in Table 1.1. Accurate determination of these parameters, especially undrained stress-strain-strength properties, was recognized as being vital to the safe, timely and economical completion of these sections of the CA/T project.

1.1.2 Approach for Determining the Engineering Properties of Clay Deposits

The common approach for a project of this type always includes a combination of laboratory tests run on undisturbed samples and in situ testing. However, the exact nature, scope, and objectives of each component vary considerably depending upon

local conditions, the experience and expertise of the geotechnical firm, and the uniqueness of the project. For example, typical practice for characterizing Boston Blue Clay has generally focused most heavily on conventional laboratory testing (e.g., standard oedometer and triaxial tests), the Standard Penetration Test, and perhaps another in situ test such as the field vane.

As a general rule, laboratory testing is best suited for determination of most of the engineering properties listed in Table 1.1. However, this requires specialized testing in order to minimize the adverse effects of sample disturbance and to properly account for stress-strain-strength anisotropy. Also, such laboratory testing is both expensive and time consuming and hence is restricted to representative samples. On the other hand, in situ penetration testing can obtain essentially continuous data at relatively low cost and is therefore best suited to assess spatial variations in the general nature of clay, i.e., how its "strength" changes with depth and along the alignment. But in situ penetration tests cannot produce reliable strength-deformation properties due to the empirical nature of existing interpretation techniques. However, some specialized in situ tests may be better suited to measure certain properties such as the in situ coefficient of earth pressure at rest (K_0).

Because of the unusual scope and complexity of the CA/T Project, Haley & Aldrich developed the Special Testing Program (STP) described in Section 1.1.3. The following gives a brief summary of its objectives and rationale:

1. Develop a very comprehensive set of soil properties at two representative sites using state-of-the-art sampling techniques and a variety of advanced laboratory testing devices, including automated triaxial stress path cells. This new data set will be compared to existing information (mostly obtained at MIT on *Resedimented* BBC) and to results from conventional lab testing programs. And most importantly, correlations between Normalized Soil Properties (NSP) and overconsolidation ratio (OCR) can be used throughout the alignment with minimal additional testing.

2. Use special in situ testing devices to assess those properties that are difficult to

obtain from laboratory testing, such as initial modulus and K_0. This includes earth pressure cells (EPC) and self-boring pressuremeter (SBP) tests.

3. Evaluate the capability of new in situ penetration devices, such as the piezo-cone penetrometer (CPTU) and Marchetti dilatometer (DMT), to assess spatial variations in strength and/or stress history.

1.1.3 Objectives and Scope of H&A Special Test Program (STP)

1. Measure the engineering properties of the BBC using both Recompression and SHANSEP testing methods to develop Normalized Soil Properties (NSP) correlations using very high quality samples.

2. Attempt to develop correlations between engineering properties obtained from state-of-the-art laboratory testing on very high quality samples and properties obtained from more routine tests on conventional piston tube samples.

3. Attempt to develop reliable correlations between clay engineering properties determined from laboratory and in situ tests for BBC.

The scope of the STP as initially defined by H&A in February of 1990 involved nine subcontractors and hundreds of field and lab tests. Table 1.2 summarizes organizations involved with each testing activity. The sampling and field testing programs were to take place at two sites, called South Boston and East Boston, whose locations are shown in Figure 1-1.

Field Testing Program

At South Boston, the program called for two borings to obtain fixed piston tube samples at 8 – 10 foot intervals through the clay layer plus one 24 inch – 30 inch slurry stabilized caisson from which 9 inch diameter undisturbed block samples would be taken at the same elevations as the tube samples. Piezometers were to be installed

in the boreholes for measurement of in situ pore pressures and for possible use in hydraulic fracturing tests to estimate K_0. Multiple tests of each method were specified to evaluate repeatability and provide some redundancy in case of questionable data. Figure 1-2 shows a plan of the proposed field program at South Boston as well as a list of types of test and approximate numbers.

At East Boston, the testing program was similar except that no block samples were to be taken. Figure 1-3 shows a plan and list of the East Boston field program.

Laboratory Testing Program

All of the laboratory testing specified was to be performed either by H&A, J.T. Germaine & Associates, or MIT. Haley & Aldrich was responsible for the bulk of the "conventional" triaxial and oedometer tests as well as most of the index tests. J.T. Germaine & Associates radiographed all of the samples and performed a program of K_0 consolidated-undrained direct simple shear (CK_0UDSS) and constant rate of strain consolidation (CRSC) tests on the samples. MIT refers to a contract between H&A and MIT's Office of Sponsored Research Programs. Under this contract, MIT would construct several automated stress path triaxial cells and then conduct special K_0 consolidated–undrained (CK_0U) and drained (CK_0D) triaxial tests to develop strength-deformation properties of BBC as a function of OCR, the applied stress system, and the drainage conditions during shear. Tests to estimate the in situ K_0 and how it varies with OCR would also be run using the automated triaxial cells and/or lateral stress oedometers.

Tables 1.3 and 1.4 summarize the laboratory tests outlined for H&A and MIT on samples obtained from the South Boston and East Boston sites, respectively. Note that in these tables tests performed by J.T. Germaine & Associates are included under the MIT heading.

1.2 Objectives and Scope of the MIT Research Program

The first objective of the MIT Research Program was to design and construct four automated stress path triaxial cells. This task represented most of the initial work on the project and was absolutely essential for successful execution of the unprecedented number of planned triaxial tests. The second task was to perform an experimental program having the following objectives.

1. Conduct K_0 consolidated-undrained triaxial compression and extension (CK_0UC and CK_0UE) tests using the SHANSEP technique to obtain undrained stress-strain-strength parameters as a function of overconsolidation ratio (OCR). These tests would provide data showing how Normalized Soil Properties (NSP) varied as a function of: type of shearing (compression or extension); type of sample (tube versus block); depth within BBC; and site location (South Boston versus East Boston). The results would also be compared to prior data obtained at MIT on Resedimented BBC and with data from conventional UU and CIU triaxial compression tests.

2. Conduct CK_0UC/E tests using the Recompression technique in order to compare these NSP v. OCR relationships with those obtained from the SHANSEP test program and from conventional strength tests.

3. Conduct several K_0 consolidated-drained triaxial compression and extension tests (CK_0DC and CK_0DE) using both the SHANSEP and Recompression techniques in order to determine the effects of drainage on stress-strain-strength behavior. Some special stress path tests would also be run to simulate conditions during installation of diaphragm walls and subsequent excavation.

4. Perform tests using the automated stress path triaxial cells and/or MIT's Lateral Stress Oedometer (LSO) to estimate the in situ K_0 and how K_0 varies with overconsolidation ratio.

The scope of the MIT testing program as originally proposed by H&A is summarized in Tables 1.3 and 1.4, as previously mentioned. This summary gives a general idea of the numbers of tests performed, though significant changes in the original numbers and types of tests were made during the course of the testing program. These changes were made with H&A's approval due to: lack of sufficient soil samples (mainly at East Boston); addition of more tests of a certain type because of unexpected results or experimental problems; and elimination of some tests considered less important. An exact listing of the tests performed is provided later in Chapters 2 and 4, but suffice it to say that the number of triaxial tests performed was unprecedented.

The MIT Research Program started March 15, 1990, and is due to expire June 15, 1991. Dr. Charles C. Ladd, Professor of Civil Engineering, and Dr. John T. Germaine, Senior Research Associate and Director of the Geotechnical Laboratory, acted as Co-Principal Investigators. Dr. Germaine was responsible for design and construction of the four automated triaxial cells and daily supervision of the two Graduate Research Assistants who performed the triaxial test program, Mr. Axel de La Beaumelle and Ms. Anne H. Estabrook. Mr. Octavio J. Ortega assisted Dr. Germaine with development of the four triaxial cells and ran several tests as an Undergraduate Research Opportunities Program (UROP) student. Dr. Ladd was responsible for checking and presenting the experimental results. Ms. Gretchen Young of Haley & Aldrich then took over most of this responsibility in December, 1990 as a MIT Visiting Engineer. She also provided vital coordination between the H&A and MIT testing programs.

1.3 Organization of Thesis

This thesis is closely linked with a companion thesis written by Axel de La Beaumelle. Table 1.5 summarizes the contents of both theses for convenient reference.

All of Chapters 1 through 4 are common to both theses. These Chapters include the introduction (Chapter 1), detailed background information about the testing sites, sampling program, and objective and scope of the laboratory program (Chapter 2),

details about the automated triaxial equipment and testing procedures used (Chapter 3), and sample characteristics and distribution of MIT tests (Chapter 4).

Most of Chapter 5, which presents a summary of the stress history and consolidation properties at the two sites, is also in both theses. However, de La Beaumelle's thesis contains additional material in Section 5.5 concerning the measurement of the coefficient of earth pressure at rest (K_0).

Chapter 6 in each thesis is different. De La Beaumelle covers the results of the SHANSEP triaxial testing program, in which he was more heavily involved. He presents his results and then compares them with previous data obtained from testing programs performed on Resedimented BBC in Chapter 7. This thesis presents the results of the Recompression tests, for which the author was solely responsible, in Chapter 6 and compares them with results from MIT's SHANSEP triaxial tests and from H&A's UU and CIU triaxial tests in Chapter 7.

Chapter 8 consists of summary, conclusions, and recommendations, and is obviously unique to each thesis.

Appendix A in each thesis expands on the Chapter 3 (equipment and procedure). Appendices B and C in de La Beaumelle include plots from all of the SHANSEP tests run and Lateral Stress Oedometer test data, respectively. Appendix B in Estabrook includes the Recompression test plots. Tabulated data from all triaxial tests, SHANSEP and Recompression, are included in MIT research report R91-10.

Although de La Beaumelle and Estabrook performed CK_0DC/E and special stress path triaxial test using the SHANSEP and Recompression techniques the results are not presented in the theses due to time constraints. These data will be furnished by MIT in a separate report to H&A.

Table 1.1: Geotechnical Issues to be Evaluated (Modified from H&A, 1990)

Geotechnical Issue	Engineering Properties
Excavation Bottom Stability	Strength
Design Lateral Pressures	K_0, K_a, K_p
Excavation-related Soil Displacements	Strength, Stiffness, K_0
Soil/Wall Adhesion	Strength
Short-term Settlement, Heave	Stiffness, Coefficient of Subgrade Reaction
Long-term Settlement, Heave	Stress History, Compressibility, Permeability
Bearing Capacity	Strength
Slurry Wall Trench Stability	Strength, K_0

Table 1.2: List of Special Testing Program Subcontractors

	Planned Subcontractor	Testing Activities
Lab	J.T. Germaine and Associates	See Tables 1.3 and 1.4
	MIT	See Tables 1.3 and 1.4
	Haley & Aldrich, Inc.	See Tables 1.3 and 1.4
Field	Applied Research Associates	Cone Penetrometer, Dilatometer
	University of New Hampshire	Self-Boring Pressuremeter, Field Vane
	New England Foundation Co., Inc.	Drill Caisson for Block Sampling
	University of Massachusetts	Earth Pressure Cells
	Sherbrooke University	Block Sampler
	Haley & Aldrich, Inc.	Menard Pressuremeter
	Guild Drilling Co., Inc.	Control Borings for Piston Tube Sampling, Piezometers and assist SBP, MEN, FV, and EPC tests

Table 1.3: Summary of Tests to be Performed at MIT and by H&A at the South Boston Test Site

Test		MIT			H&A		
		Tube	Block	Total	Tube	Block	Total
Radiography		20	70	90	0	0	0
Index	Standard Handling	0	0	0	20	10	30
	Hydrometer	0	0	0	10	10	20
	Specific Gravity	0	0	0	6	5	11
	Salt Concentration	0	0	0	10	5	15
Triaxial	UUC	0	0	0	20	10	30
	CIUC	0	4	4	20	10	30
	CK_0UC						
	•Recomp. $\sigma'_{vc} = \sigma'_{vo}$	4	10	14	0	0	0
	•Recomp. $\sigma'_{vc} \neq \sigma'_{vo}$	4	10	14	0	0	0
	•Recomp. U/R	0	6	6	0	0	0
	• SHANSEP	4	6	10	4	8	12
	CK_0UE						
	•Recomp. $\sigma'_{vc} = \sigma'_{vo}$	0	6	6	0	0	0
	•Recomp. $\sigma'_{vc} = 0.1 \rightarrow 0.5\sigma'_{vo}$	0	8	8	0	0	0
	•SHANSEP	4	5	9	0	0	0
	CK_0UD (Recomp.)	0	6	6	0	0	0
	CK_0DC						
	•Recomp.	0	6	6	0	0	0
	•SHANSEP	0	3	3	0	0	0
	CK_0DE						
	•Recomp.	0	6	6	0	0	0
	•SHANSEP	0	3	3	0	0	0
Oedometer	Standard	0	0	0	30	25	55
	CRSC *	10	15	25	0	0	0
DSS *	CK_0UDSS						
	•Recomp.	0	10	10	0	0	0
	•SHANSEP	4	10	14	0	0	0
	CK_0UDSS @ 90°						
	•Recomp.	0	4	4	0	0	0
	•SHANSEP	0	4	4	0	0	0
	CK_0DDSS @ 90°						
	•Recomp.	0	4	4	0	0	0
	•SHANSEP	0	4	4	0	0	0
Test to Evaluate K_0		0	15	15	0	0	0

* By Germaine and Associates

Table 1.4: Summary of Tests to be Performed at MIT and by H&A at the East Boston Test Site

Test		MIT	H&A
Radiography		20	0
Index	Standard Handling	0	20
	Hydrometer	0	20
	Specific Gravity	0	10
	Salt Concentration	0	5
Triaxial	UUC	0	30
	CIUC	2	5
	CK_0UC		
	•Recomp. $\sigma'_{vc} = \sigma'_{vo}$	5	0
	•Recomp. $\sigma'_{vc} \neq \sigma'_{vo}$	5	0
	•Recomp. U/R	0	0
	• SHANSEP	15	0
	CK_0UE		
	•Recomp. $\sigma'_{vc} = \sigma'_{vo}$	0	0
	•Recomp. $\sigma'_{vc} = 0.1 \rightarrow 0.5\sigma'_{vo}$	6	0
	•SHANSEP	12	0
	CK_0UD (Recomp.)	0	0
	CK_0DC		
	•Recomp.	0	0
	•SHANSEP	3	0
	CK_0DE		
	•Recomp.	0	0
	•SHANSEP	3	0
Oedometer	Standard	0	25
	CRSC *	10	0
DSS *	CK_0UDSS		
	•Recomp.	0	0
	•SHANSEP	12	0
	CK_0UDSS @ 90°		
	•Recomp.	0	0
	•SHANSEP	4	0
Test to Evaluate K_0		5	0

* By Germaine and Associates

Table 1.5: Summary of Contents of SM Theses by de La Beaumelle and Estabrook on MIT Research Project with H&A

Chapter Number	Contents	Common to Both	de La Beaumelle	Estabrook
1	Introduction	×		
2	Background	×		
3	Automated Triaxial Equipment and Testing Procedures	×		
4	Sample Characteristics	×		
5	Stress History and Consolidation Properties (Added information on K_0)	×	×	
6	Results of SHANSEP Triaxial Strength Testing Program		×	
7	Comparison with Triaxial Data on Resedimented BBC		×	
6	Results of Recompression Triaxial Strength Testing Program			×
7	Comparison with SHANSEP Triaxial and UUC and CIUC Data			×
8	Summary, Conclusions and Recommendations		×	×
9	List of References		×	×
Appendix A	Automated Triaxial Equipment and Testing Procedures	×		
B	SHANSEP Consolidation and Strength Plots		×	
B	Recompression Consolidation and Strength Plots			×
C	Lateral Stress Oedometer Data		×	

Note: Tabulated data for all SHANSEP and Recompression tests are included in MIT research report R91-10.

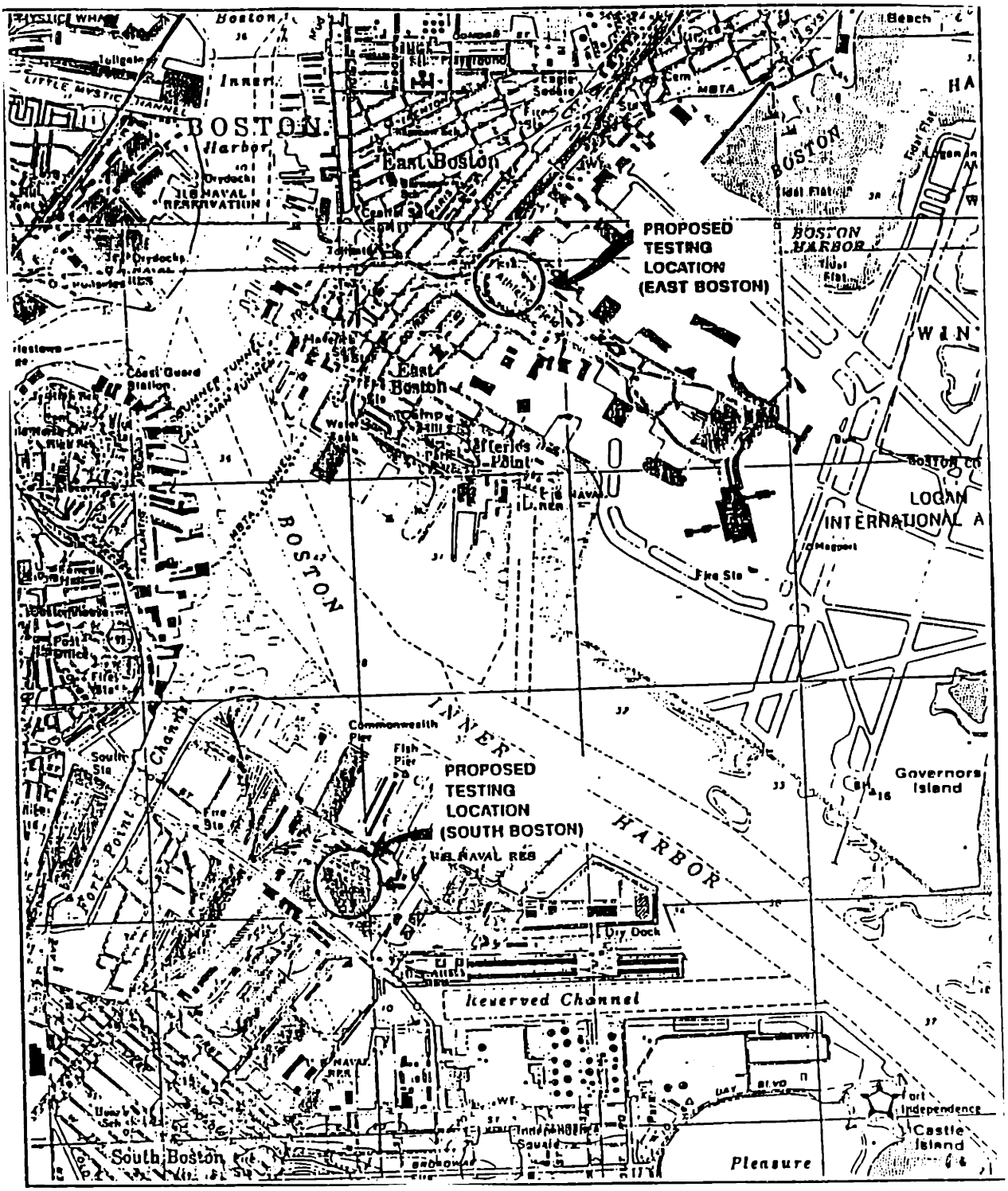

Figure 1-1: Location of Test Sites (after H&A, 1990)

SCHEMATIC OF SOUTH BOSTON SITE

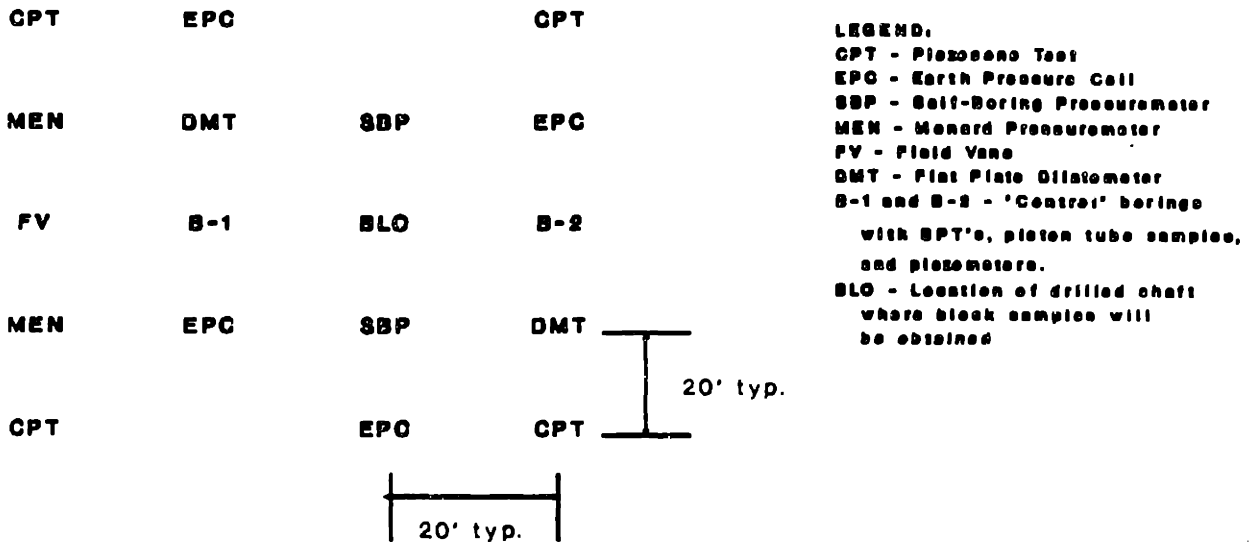

FIELD TEST	NUMBER LOCATIONS (TESTS PER LOCATION)
Pressuremeter	
Menard	2 (4)
Self-Boring	2 (10)
Piezocone	4
Dilatometer	2 (150)
Earth Pressure Cell	4 (1)
Field Vane (possible)	1 (20)

Figure 1-2: Proposed Layout of Field Program at South Boston Test Site

SCHEMATIC OF EAST BOSTON SITE

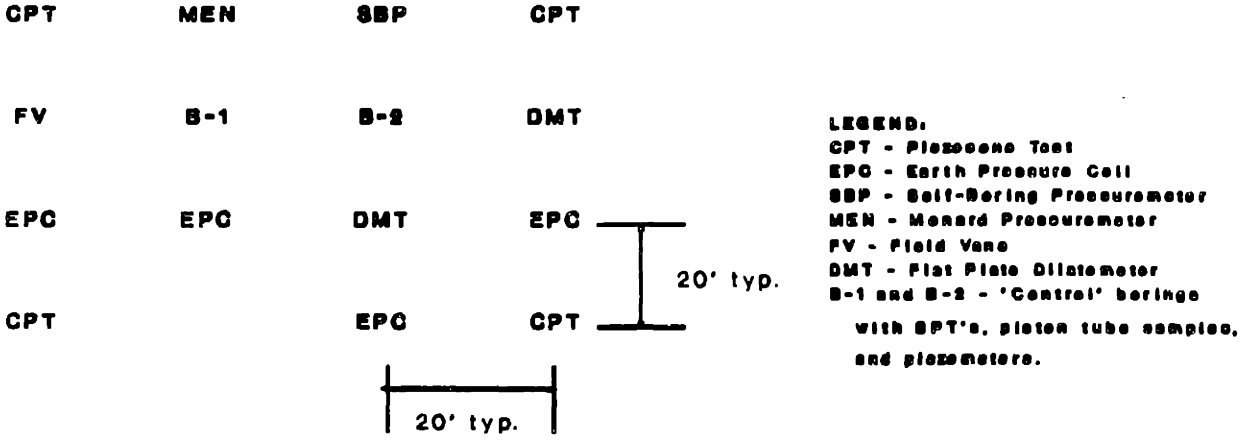

FIELD TEST	NUMBER LOCATIONS (TESTS PER LOCATION)
Pressuremeter	
Menard	1 (4)
Self-Boring	1 (10)
Piezocone	4
Dilatometer	2 (150)
Earth Pressure Cell	4 (1)
Field Vane (possible)	1 (15)

Figure 1-3: Proposed Layout of Field Program at East Boston Test Site

Chapter 2

Background

2.1 General Test Site Characteristics

The Central Artery/Tunnel project includes the construction of a large number of underground structures that will require extensive excavations to unprecedented depths and widths into Boston Blue Clay (BBC). Therefore, in order to satisfy the design requirements for such a large scale project, a thorough knowledge and understanding of the site's soil conditions, especially the BBC, are necessary. This section will therefore concentrate on factors especially important to clay behavior.

Haley & Aldrich (1990) states : "the subsurface soil conditions along the proposed roadway alignment vary, but are dominated by glacial and marine deposits having combined thicknesses which exceed 200 feet locally. Subsurface conditions along much of the alignment in Geotechnical work areas 01 and 02 consist of 15–40 feet of fill and organic deposits overlying up to 100 feet of marine 'Boston Blue Clay' (BBC). Glacial till and Argillite bedrock typically underlie the clay".

From previous experience in the greater Boston area, the top portion of BBC exhibits relatively high overconsolidation ratios due to desiccation, becoming less overconsolidated with depth and perhaps reaching an almost normally consolidated condition. Near the bottom of the clay, overconsolidation ratios of less than 1.5 have previously been measured by H&A and were also observed at the two test sites. Kenney (1964) stated that for the Boston area: "The soils making up the lower clay

deposit would be expected to have a common consolidation history and might be overconsolidated, depending on the amount of erosion and subsequent soil deposition which occurred". Therefore, overconsolidation could be due to a prior unloading from erosion greater than the subsequent deposition.

In order to investigate representative soil conditions, the program devised by Haley & Aldrich included extensive testing at two sites. The sites are located in South and East Boston (see Figure 1-1) and were chosen for several reasons : significant clay thickness, ready access (including after construction, if possible), lack of prior deep foundations which may have affected the clay, and lack of underground obstructions. The South Boston site comprises the bulk of the testing program, while the East Boston site is intended to provide information on the applicability of the Special Testing Program results to other locations.

To verify the suitability of these sites, pilot borings and piezocone testing were used to confirm stratigraphy. Fixed piston tube samples were obtained and radiographed to confirm appropriate test elevations, while piezometers were installed to measure in situ pore pressures. These data provide soil stratigraphy and profiles of unit weight, pore pressure and effective overburden stress. Note that the CA/T Project Elevation equals NGVD plus 100.00 feet.

Figure 2-1 represents the soil profile for the South Boston (SB) test site. About 20 feet of fill and 17.5 feet of sand overlie 103 feet of BBC. Within the BBC, SPT N values decrease with depth from about 10 to usually zero for the bottom 50 feet. Figure 2-2 shows the in situ state of stress for SB. The total vertical stress (σ_{v0}) was computed for the total unit weight (γ_t) values listed in Figure 2-1. The pore (water) pressure, u, was obtained from an observation well in the fill and four piezometers in the BBC. The u profile (and equation) in Figure 2-2 accounts for some salt in the pore water and reflects a piezometric water elevation that increases and then decreases with depth (i.e., PWE $\approx$ 102, 104 and 99 feet at elevation = 74, 25 and -30 feet, respectively). The effective stress profile σ'_{v0} (and equation) in Figure 2-2 were obtained by subtracting u from σ_{v0}. Figure 2-2 also shows the approximate variation in overconsolidation ratio (OCR) with depth based on data contained in Chapter

5. The substantial decrease in OCR with depth make the site ideal for specialized testing since the soil varies from a desiccated stiff clay at the top to "soft" clay with the lower 50 feet.

The typical soil profile for the East Boston (EB) site is represented in Figure 2-3. About 18 feet of fill and 5 feet of sand are underlain by 91 feet of BBC. The SPT N values again vary from around 10 at the top to essentially zero for the bottom 40 feet. As for the SB site, Figure 2-4 illustrates the state of stress in situ at EB. The various profiles were calculated in the same fashion as for the SB site, except for the pore pressure u which was derived using a linear PWE (PWE≈108 and 104.5 feet at elevation 87.7 and -3.3 feet, respectively). Some difficulties were encountered in defining an approximate OCR profile, because values of preconsolidation pressure σ'_p from some constant rate of strain tests (CRSC) were inconsistent with the K_0-triaxial consolidation and standard oedometer results.

2.2 Sampling Program

Figure 2-1 shows the tube locations from two borings at the South Boston (SB) site. A total of 37 two foot long samples were obtained with a 3 inch (76mm) diameter fixed piston sampler; 12 of them from boring SB2-21 at intervals varying from 8 to 10 feet, and 25 samples at intervals of 2 and 6 feet for SB2-23. For East Boston, a total of 8 tubes at intervals of 10 feet were extracted from the ground to a depth of 105 feet (See Figure 2-3).

In addition, nine-inch diameter block samples of the clay were obtained, using sophisticated sampling techniques developed at Sherbrooke University, Quebec. The sampling was performed within a 24-inch to 30-inch diameter caisson drilled under bentonite slurry. Using this method, two holes were drilled at the South Boston site, and a total of 11 samples were recovered at the locations shown in Figure 2-1.

The quality of the tube sampling was evaluated using radiography, an indispensable part of the overall testing program.

2.3 Laboratory Testing Program

The laboratory testing program can be divided into four major parts: radiography and sample quality, classification and index properties, consolidation testing, and undrained strength testing.

2.3.1 Radiography and Sample Quality

Radiography has been a standard procedure at MIT for the last 13 years. Based on this experience, radiography can show the following (Jamiolkowski et al. 1985):

1. Variations in soil types, especially granular versus cohesive materials.
2. Macrofabric features resulting from bedding planes, varves, fissures, shear planes, etc.
3. Presence of "intrusions" such as sand lenses, stones, shells, calcareous nodules, peaty materials, drilling mud, etc.
4. Voids and cracks due to gas pockets.
5. Variations in the degree of sample disturbance, ranging from barely detectable curvature adjacent to the sample edges to gross disturbance as evidenced by a completely contorted appearance and large voids and cracks (most often occurring at the ends of the tube).

> "Many of these features may not be readily identified from visual inspection of the extruded samples, at least without trimming or breaking it apart. Hence radiography provides a nondestructive means for selecting the most representative and/or less disturbed portions of each tube for engineering tests. It also helps in planning the overall testing program based on the amounts of suitable material."

The low cost of radiographs ($65 per tube), compared to the cost of running consolidation tests and sophisticated strength tests on disturbed and/or nonrepresentative soil

specimens warrant the use of radiography for every tube sample being considered for engineering tests. Radiographs for block samples could not be obtained, because the X-rays were unable to resolve features in the thick samples. An example radiograph can be seen in Figure 2-5.

The amount of recovery and quality of all tube and block samples is given in Tables 4.1 through 4.3 and discussed in Chapter 4. Once the amount and quality of soil available for testing was known, the testing started by performing (quick) "index" tests.

2.3.2 Classification and Index Properties

The next phase of the testing program is to determine the classification and index properties of the soil. To obtain an adequate knowledge of these properties, the following measurements were made:

- Water contents and torvane strengths taken at the end of each sample, and also from material adjacent to soil used for all engineering tests;
- Atterberg limits tests on each sample;
- Grain size distribution (using hydrometer analysis) and specific gravity tests performed on approximately 10 tube samples.

In addition, "special" tests such as carbonate content (done at the University of Massachusetts, Amherst), salt concentration and pH tests were run on a limited number of samples.

The approximate number of tests performed at MIT and H&A, plus specific procedures and results, are presented and discussed in Chapter 4.

2.3.3 Consolidation Testing

The first column in Table 2.1 lists the consolidation parameters to be obtained from the consolidation test program, namely:

- The preconsolidation pressure (σ'_p), which equals the "yield stress" measured during one-dimensional (1-D) drained loading.

- The compressibility parameters defined as $d\epsilon/d\log\sigma'_{vc}$ measured during virgin compression (CR), during recompression (RR) and during swelling (SR).

- The coefficient of consolidation (C_v) for both normally consolidated (NC) and overconsolidated (OC) clay during loading and unloading.

- The coefficient of permeability or conductivity (k) versus void ratio (e), wherein e vs. log k is usually linear with a slope defined by $C_k = de/d\log k$.

- The coefficient of earth pressure at rest (K_0) for NC clay and how it varies with overconsolidation ratio (OCR).

Table 2.1 also lists the four types of consolidation tests that were run for the Special Test Program, along with their planned and actual utilization in providing information regarding the different consolidation parameters. As discussed in Chapter 5, the clay below the upper portion of the drying crust often exhibited pronounced "S-shaped" compression curves. This unexpected behavior caused substantial changes in the test program because essentially continuous compression curves were required for reliable estimates of the preconsolidation pressure. Fortunately, MIT's automated stress path triaxial cells generally produced excellent 1-D compression curves during SHANSEP testing that served as the prime data base for determining σ'_p values throughout most of the clay at both test sites.

The SHANSEP triaxial tests also provided excellent K_0 data for both NC clay and as a function of OCR for tests that were rebounded prior to undrained shear. Consequently, less emphasis was placed on the use of MIT's Lateral Stress Oedometer (LSO) that measures the horizontal effective stress (σ'_{hc}) during incremental loading and unloading. However, the triaxial tests did not measure pore pressure gradients during consolidation and thus incremental oedometer and constant rate of strain (CRSC) tests were used to measure flow characteristics, i.e., C_v and k.

2.3.4 Undrained Strength Testing

Parameters from undrained shear testing that are relevant to the CA/T project include the following:

- Undrained shear strength (c_u) as discussed below.
- Stiffness, such as Young's modulus at 50% of the stress increment causing failure (E_{50}).
- Excess pore pressures developed during shearing, which can be obtained from Skempton's A parameter ($A = (\Delta u - \Delta\sigma_3)/(\Delta\sigma_1 - \Delta\sigma_3)$).
- Effective stress failure envelope defined by a cohesion intercept (c') and friction angle (ϕ').

Strength testing issues and types of shear tests

The undrained strength of cohesive soils such as BBC varies with the mode of failure and as a function of the stress history of the soil. Stress history refers both to the initial in situ condition (i.e., the profiles of σ'_{v0} and σ'_p and hence OCR) and how the vertical consolidation stress (σ'_{vc}) may change during construction. Loading problems, such as with embankments, generate positive excess pore pressures during construction and hence drainage will cause strengthening of the foundation soils. In contrast, unloading problems generate negative excess pore pressures during construction and hence drainage (swelling) will cause a reduction in undrained strength. The areal extent and depth of excavations along the CA/T alignment make the latter problem especially important. Moreover, if a failure occurs during construction, such as from bottom instability, the deformations are likely to occur rapidly, i.e., essentially undrained. Consequently, the laboratory strength testing pro gram emphasized development of relationships between c_u/σ'_{vc} and OCR=σ'_p/σ'_{vc}, where σ'_{vc} refers both to the initial in situ σ'_{v0} and changes in the vertical consolidation stress with time.

The strength of soft clays such as BBC has been extensively researched at MIT for the past 25 years. Ladd and Foott (1974) presented a new method for evaluating the

undrained strength of clay foundations : the SHANSEP (Stress History And Normalized Soil Engineering Parameters) technique. Their paper pointed out three of the most important factors affecting the undrained strength and deformation characteristics of cohesive soils: sample disturbance, time effects, and anisotropy. The following discussion of these three topics is abstracted from material presented in Ladd (1991) and Jamiolkowski et al. (1985).

Sample Disturbance and Reconsolidation Techniques

Ladd (1991) states that sample disturbance from conventional tube sampling alters the in situ soil structure, cause internal migration of water, frequently lead to substantial reductions in the effective stress of the sample, and often produces highly variable strengths from unconsolidated-undrained (UU) type testing. He advocates the use of consolidated-undrained (CU) tests to minimize these adverse effects. However, CIU tests are deemed inappropriate since shearing starts from isotropic rather than the in situ K_0 stress conditions. Therefore, CK_0U tests using a consolidation stress ratio, $K_c=\sigma'_{hc}/\sigma'_{vc}$, approximating the in situ K_0 are needed, both to help restore the in situ soil structure, and to give more meaningful stress-strain-strength data. The two distinct reconsolidation techniques used for CK_0U tests, the SHANSEP (Ladd and Foott, 1974) and Recompression (Bjerrum, 1973) methods, are now discussed.

The two techniques are illustrated by Figure 2-6. Hypothetical in situ and laboratory K_0 compression curves for a slightly overconsolidated soft clay are presented. Points 1 and 2 designate the in situ condition and the preshear effective stress for a UU test, respectively (the latter assuming no change in water content during sampling). In the Recompression technique, the test specimen is reconsolidated (ideally at K_0) to $\sigma'_{vc}=\sigma'_{v0}$ shown by point 3. Points A through D correspond to typical stresses used for a SHANSEP test program.

The SHANSEP technique is part of a design procedure for estimating the in situ undrained properties of a clay deposit and involves the following basic steps:

1. Establish the initial stress history (i.e. the profiles of σ'_{v0} and σ'_p) and also possible changes in the σ'_{vc} due to construction, which also determines the range

of OCR value for which data are required.

2. Perform a series of CK_0U shear tests on specimens consolidated well beyond the in situ preconsolidation pressures (to σ'_{vc} greater than 1.5 to 2 times σ'_p) to measure the behavior of normally consolidated clay (points A and B in Figure 2-6), and also on specimens rebounded to varying OCR to measure overconsolidated behavior (points C and D).

3. Express the results in terms of normalized soil parameters (NSP), and establish NSP vs. OCR relationships. e.g., $\log c_u/\sigma'_{vc}$ vs. log OCR to obtain values of S and m in the following equation:

$$c_u/\sigma'_{vc} = S(OCR)^m \tag{2.1}$$

4. Use these NSP relationships and the stress history information to compute profiles of c_u as a function of time.

Much has been debated about the relative merits of the two reconsolidation techniques. Ladd's (1991) opinion can be summarized as follows.

The Recompression technique:

1. Is clearly superior for highly structured deposits (e.g. brittle, sensitive Canadian clays), and for strongly cemented soils.

2. Is preferred whenever block quality samples are available and for testing weathered and highly overconsolidated deposits where SHANSEP is often difficult to apply; and

3. Should always be accompanied by a thorough evaluation of the in situ stress history.

The SHANSEP technique:

1. Is strictly applicable only to mechanically overconsolidated and truly normally consolidated deposits exhibiting normalized behavior.

2. Is probably preferred for testing tube samples from deep deposits of low OCR "ordinary" clays.

3. Has the distinct advantage of forcing the user to assess the in situ history, and of developing normalized stress-strain strength parameters that can be used on subsequent projects.

Very little data exist to compare undrained strength-deformation properties from the SHANSEP and Recompression technique (and none for BBC). H&A's STP therefore specifically addressed this important issue by obtaining both tube and block samples and by running both SHANSEP and Recompression CK_0U tests.

Time Effects

Two types of time effects influence the behavior of CK_0U tests: the time allowed for consolidation prior to shear; and the strain rate (or rate of load application) used during shear. The first type concerns the effects of "aging" at constant effective stress (i.e., secondary compression). Aging increases the stiffness and preconsolidation pressure, and therefore, the undrained strength of low OCR clays. Ladd (1991) recommends a standardized amount of aging to obtain consistent CK_0U data, and suggests one log cycle of time. If $\log(t/t_p)$ is much less than one, significant pore pressures may develop during undrained shear due to preventing secondary compression. More than one log cycle of secondary compression will take too long and the c_u data will need a correction for the increased σ'_p.

The strain rate applied during undrained shearing is known to affect the stress-strain behavior of cohesive materials. Laboratory UU and CU tests show higher strengths with increasing strain rate and hence decreasing time to failure (t_f). Although no rational framework exists for selecting strain rates for CK_0U testing, general experience based on a balance between practicality and limited case histories has resulted in the following practice at MIT: axial strain rate of 0.5%/hr for triaxial tests; and shear strain rate of 5%/hr for direct simple shear tests. In addition, H&A ran its UUC tests at an axial rate of about 0.5%/hr rather than using ASTM's standard

rate of 60%/hr.

Stress Systems for CK_0U Test Programs and Undrained Strength Anisotropy

The differences in the applied stress system for laboratory strength tests can be described by two variables: the relative value of the intermediate principal stress, as defined by b= $(\sigma_2 - \sigma_3)/(\sigma_1 - \sigma_3)$; and the direction of the applied major principal stress relative to the vertical (depositional) direction denoted by the δ angle. Changes in the value of b and δ lead to different stress-strain responses due to the effects of σ_2 and anisotropy, respectively. Ideally, CK_0U testing should shear specimens at representative b values and δ angles. Figure 2-7 illustrates the combinations of b and δ that can be achieved by laboratory shear devices. A detailed discussion of these devices can be found in Jamiolkowski et al. (1985). The text will first define anisotropy and then focus on the types of laboratory shear tests selected for the STP.

There are two kinds of anisotropy: initial and evolving. Jamiolkowski et al. (1985) and Ladd (1991) use initial anisotropy to denote the changes observed in the stress-strain-strength response of a soil with variations in the applied principal stress direction during monotonic shearing. This initial anisotropy has two components: inherent and initial shear stress anisotropy. Inherent anisotropy arises from the "soil structure" developed at the micro-level (preferred particle orientations and interparticle forces) and also at the macro-level for certain soils such as varved glacial-lake deposits. The initial shear stress anisotropy is the directionally dependent undrained strengths exhibited by clays whenever shearing starts from a K_0 different from one condition. Evolving anisotropy denotes the changes in the initial cross anisotropic properties of a K_0 consolidated clay due to plastic strains caused by stresses (both shear and consolidation) applied during construction.

Ladd (1991) describes the methodology for conducting an Undrained Strength Analyses (USA) that has been largely adopted by H&A for assessing stability for the CA/T project. This approach calls for CK_0U tests using either the SHANSEP or Recompression technique. Due to the effects of anisotropy and the intermediate

principal stress, correct estimates of c_u must consider the in situ modes of failure. For bottom stability, which is a prime design concern, the three principal modes are Plane Strain Compression (PSC), Direct Simple Shear (DSS) and Plane Strain Extension (PSE) (see Figure 2-8). Since the PSC/E modes of failure are difficult to model in the lab, they were replaced by triaxial compression (TC) and extension (TE) tests. Ladd et al. (1977) and Ladd (1991) state that triaxial tests will generally underestimate the peak c_u for plane strain problems, e.g., by about 8±5% in compression and by about 18±2% in extension. However, the peak plane strain strengths cannot b e mobilized in situ due to the effects of progressive failure. Based on experience with using the strain compatibility technique (Koutsoftas and Ladd, 1985) to account for this adverse effect, Ladd (personal communication) concluded that these two effects would roughly offset each other. That is, peak strengths from TC and TE tests would approximately equal strengths from PSC and PSE tests treated for strain compatibility. However, Ladd's preliminary conclusion needs to be verified.

Scope of strength testing program

Based on the above strength testing issues and objectives, H&A developed the planned laboratory strength testing program that was presented in Tables 1.3 and 1.4 for SB and EB, respectively. In addition to conventional UUC and CIUC tests by H&A, it includes a very comprehensive set of CK_0U TC,TE and DSS tests that:

- Employ the SHANSEP technique to develop NSP vs. OCR relationships using tube samples from both sites and the SB block samples.
- Employ the Recompression technique to develop NSP vs. OCR relationships, primarily using the SB block samples, but also including some tests on tube samples for comparison (those planned for EB were eliminated due to lack of soil).

More specialized aspects of the overall program also included some:

- CK_0UDSS tests run on "90°" specimens to simulate vertical shear through BBC (i.e., the cut portion in Figure 2-8) and adhesion to diaphragm walls.

- CK_0 triaxial compression tests to simulate installation of diaphragm walls and subsequent excavation.

- K_0 consolidated-drained (CK_0D) unloading tests in TC and TE to simulate drained conditions in the active and passive portion, respectively, of a laterally supported excavation.

2.4 Scope of Testing Program Conducted Under MIT Contract with H&A

Table 2.2 lists the number of "usable" SHANSEP and Recompression CK_0U triaxial tests that are presented in the two SM theses. For the SHANSEP tests, no distinction is made between tests run on tube samples from SB and EB or on the SB block samples since test data do not indicate significant differences in the normalized strength parameters. About 35 SHANSEP tests yielded "Good to Excellent" consolidation data, this meaning reliable estimates of σ'_p, a well defined compression curve and high quality K_0 data (including K_0 versus OCR for the OC tests). About 25 "Fair to Poor" SHANSEP tests provided less reliable and/or incomplete consolidation data. Most of these tests reflected initial problems with the automated control system or internal leakage in one of the cells, as discussed in Section 3.4. About 35 SHANSEP tests gave "Good to Excellent" shear data, meaning reliable stress-strain curves and effective stress paths throughout undrained shear to large strains. And about 20 tests yielded useful, but either less complete or definitive, results.

The Recompression CK_0U program (item B in Table 2.2) encountered fewer experimental problems, with about 32 tests considered "Good to Excellent". The other tests generally had values of K_c that differed from the estimated K_0. About half of the tests were reconsolidated to the effective overburden stress. The other half had σ'_{vc} values less than or greater than σ'_{v0} in order to study the effect of changing OCR on normalized behavior.

Item C in Table 2.2 summarizes the tentative scope of other triaxial tests that are

not included in the two theses.

Finally, MIT conducted nine Lateral Stress Oedometer (LSO) tests in order to check the K_0 versus OCR data obtained from the SHANSEP triaxial tests and to evaluate K_0 during reloading of overconsolidated clay.

Table 2.1: Overview of Consolidation Test Program

Consolidation Test Parameter	Type of Consolidation Test: Planned & Actual Use			
	Standard Incremental Oedometer	Constant Rate of Strain Consolidation (CRSC)	K_o - Triaxial	Incremental Lateral Stress Oedometer (LSO)
Preconsolidation Pressure (σ'_p)	Planned as primary test, but became secondary source of data	Planned = Actual Secondary test	Turned out to be primary source of reliable data	Some supplemental data
Compressibility Parameters (CR, RR & SR)	Same as above, except primary source for SR & RR	Planned = Actual Secondary test	Turned out to be primary source of CR = f (σ'_{vc})	Some supplemental data
Coefficient of Consolidation (c_v)	Planned = Actual primary test for NC c_v	Planned = Actual primary test for continuous c_v data	Not Applicable	Generally not applicable
Coefficient of Permeability vs. Void Ratio (k vs. e)	Supplemental Data	Planned = Actual primary test	Not Applicable	Not Applicable
Coefficient of Earth Pressure at Rest (K_o)	Not Applicable	Not Applicable	Planned = Actual primary test for NC K_o ; Also K_o vs OCR	Planned primary test for K_o vs OCR, but became secondary

Table 2.2: Scope of MIT Triaxial Testing Program (Contract with H&A)

A. SHANSEP CK_oU Triaxial Tests [( ) = # of tests on Block Samples]

Quality and Type of Test	Consolidation Data		Undrained Shear Data	
	OCR ≤ 1.5	OCR = 2-8	OCR ≤ 1.5	OCR = 2-8
1. Good-Excellent				
TC	12	4 (2)	13 (1)	6 (3)
TE	10 (3)	8 (4)	9 (3)	10 (5)
2. Fair-Poor				
TC	10 (1)	4 (2)	10 (1)	2 (1)
TE	5	5 (1)	5	2
3. Number of Useful Tests	37	21	37	20
4. Data not Useful	3 (1)	2	3	3

B. Recompression CK_oU Triaxial Tests (All for SB)

Test Quality	TC		TE	
	Tube	Block	Tube	Block
1. Good-Excellent	8	13	2	9
2. $K_c \neq K_o$ or Leakage	1	6	0	2
3. Number of Useful Tests	9	19	2	11
4. Data not Useful	0	0	0	0

C. Other CU and CD Triaxial Tests

1. Planned SHANSEP CK_oU Tests that provided useful Stress Path data: 3
2. CK_oU C/D Tests: Details still being formulated
3. CK_oDC Tests: Recompression tests planned at OCR = 1.3,2.0,4.0
4. CK_oDE Tests: Recompression tests planned at OCR = 1.3,2.0,4.0

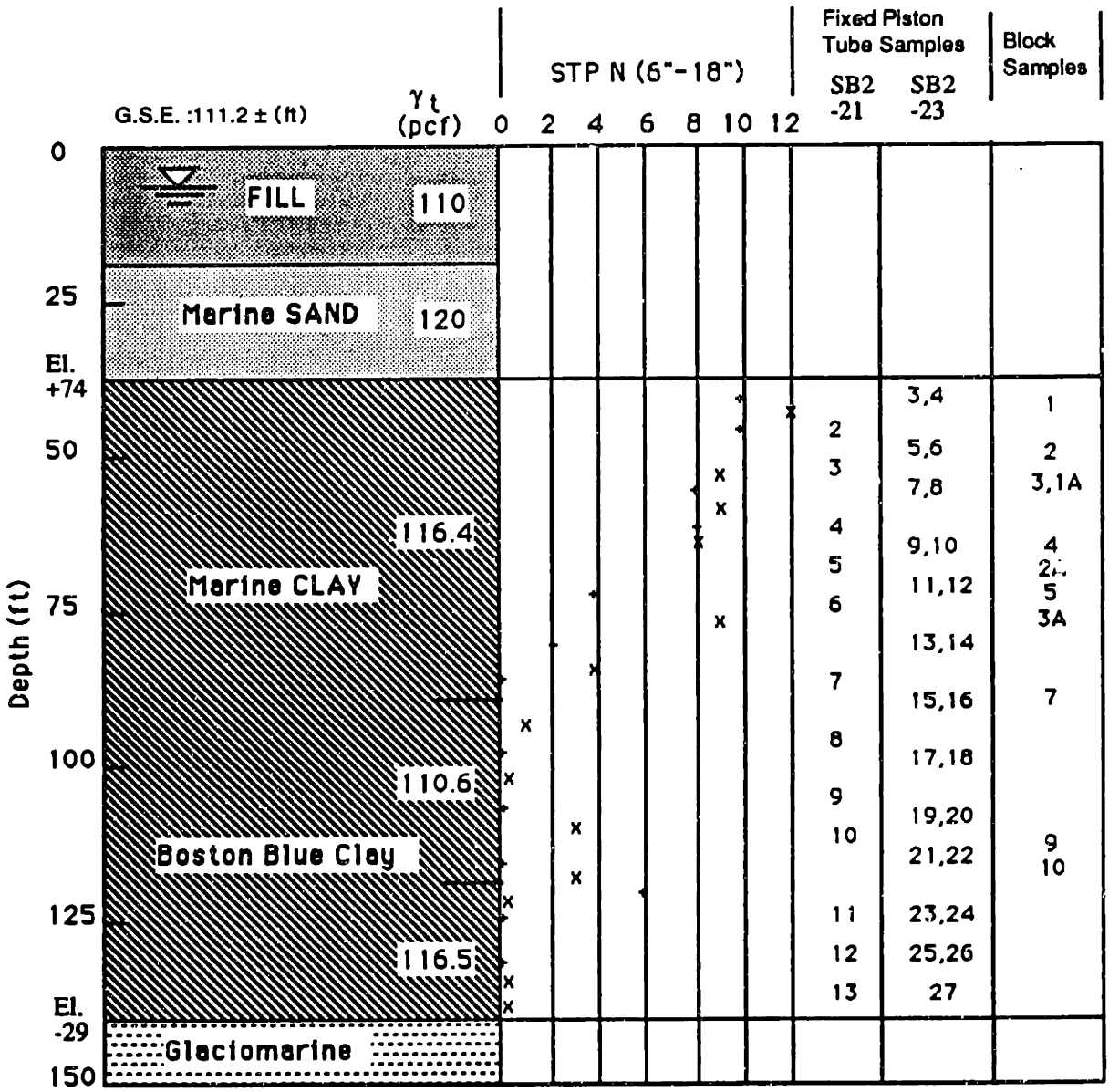

Figure 2-1: Special Test Program: Soil Profile and Sample Locations at South Boston

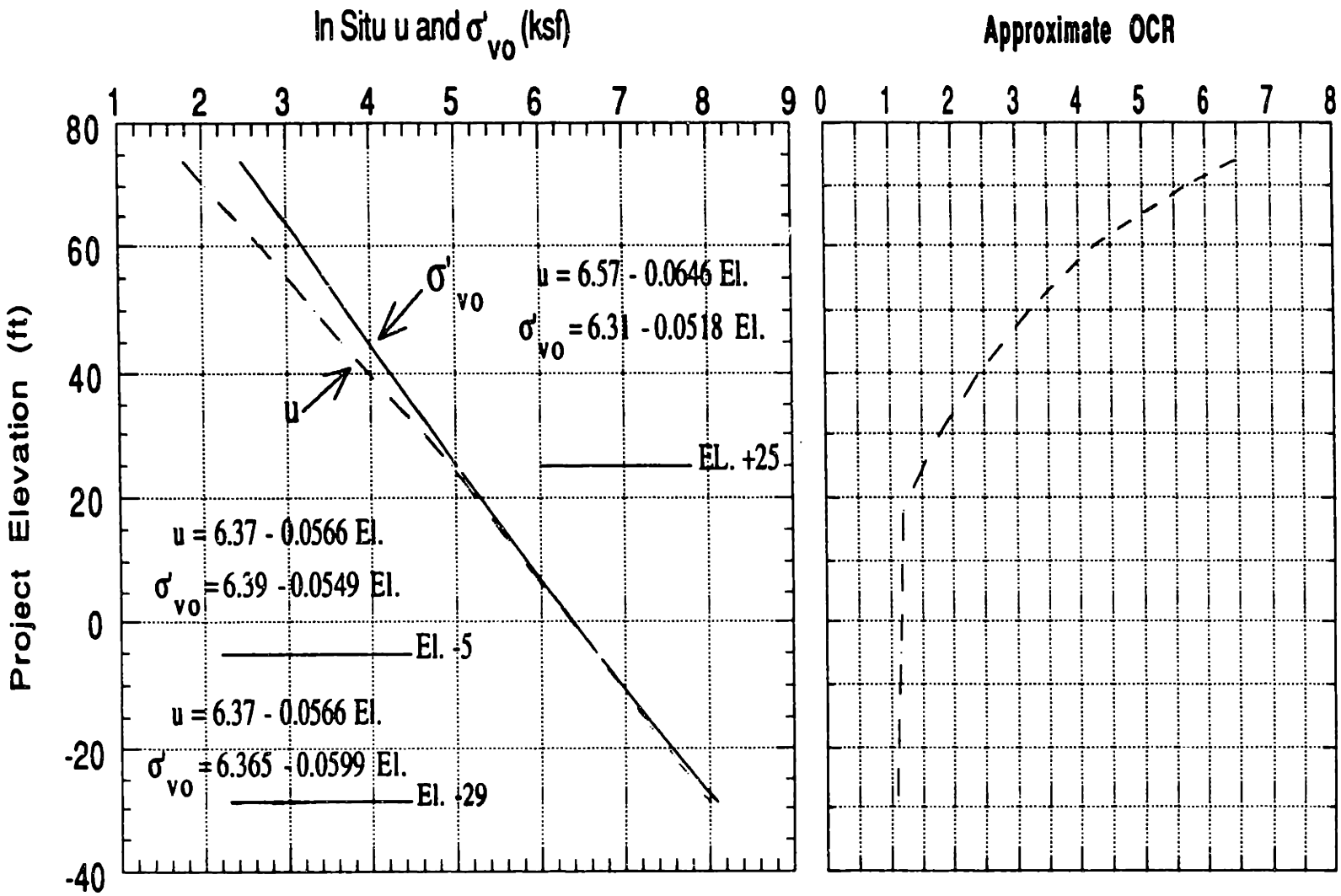

Figure 2-2: Special Test Program: In Situ Stresses and Approximate OCR Profile at South Boston

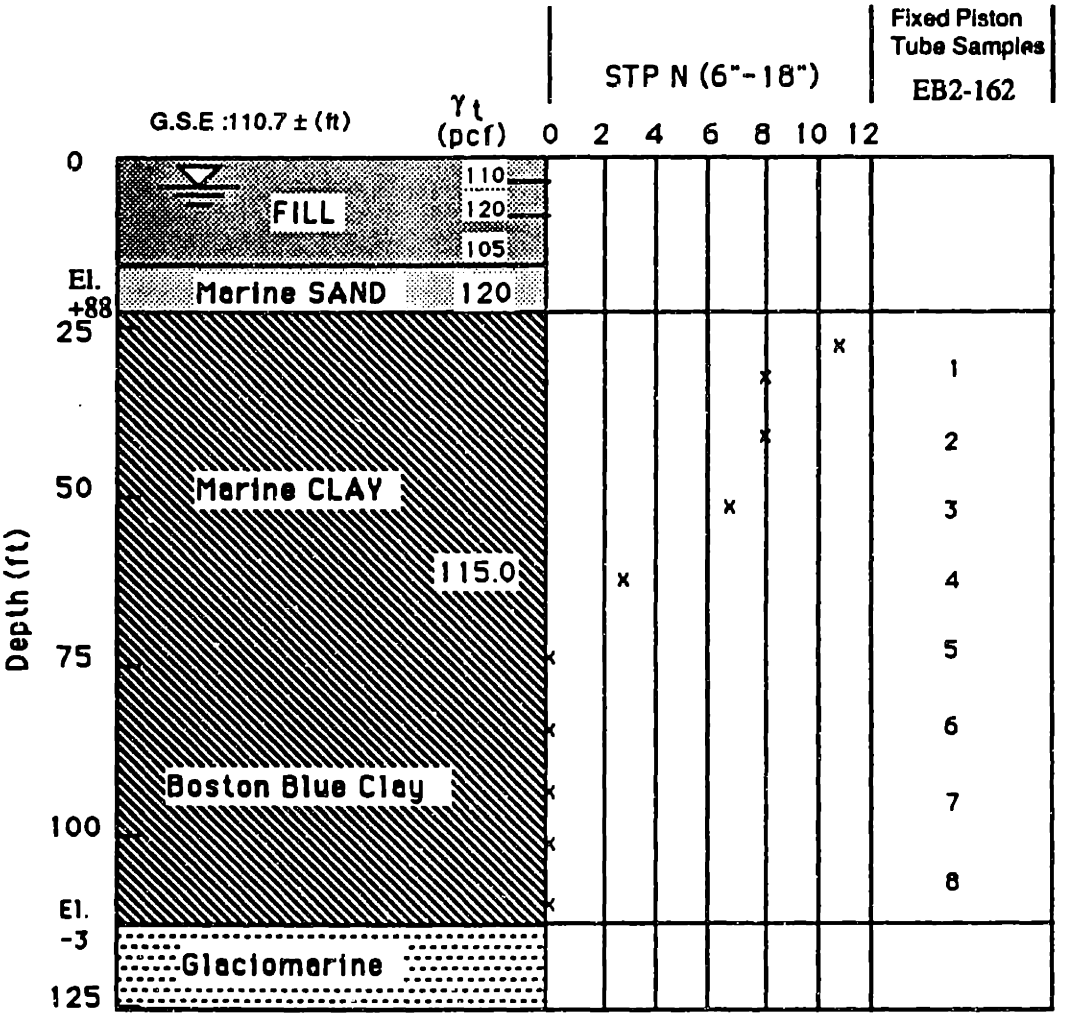

Figure 2-3: Special Test Program: Soil Profile and Sample Locations at East Boston

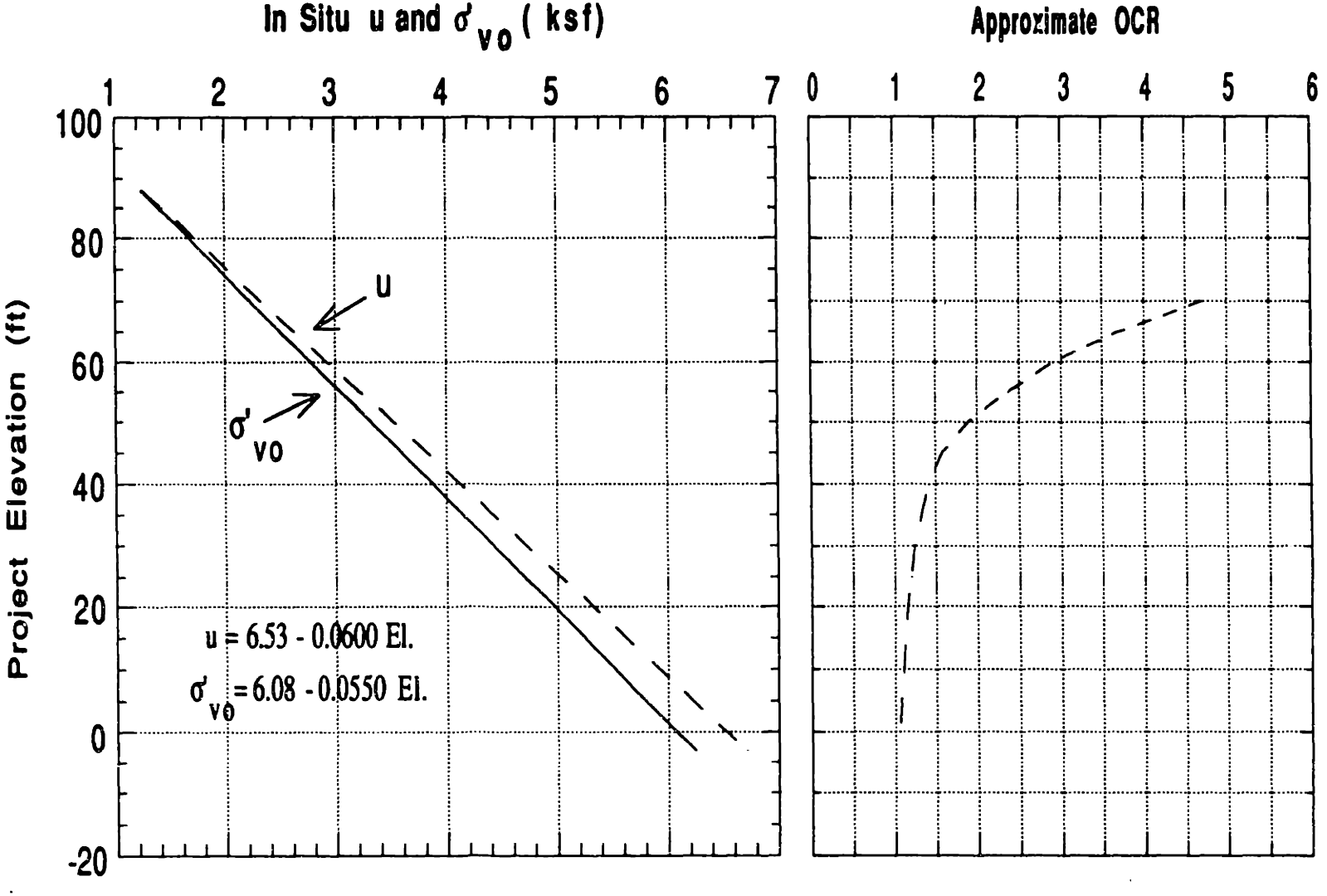

Figure 2-4: Special Test Program: In Situ Stresses and Approximate OCR Profile at East Boston

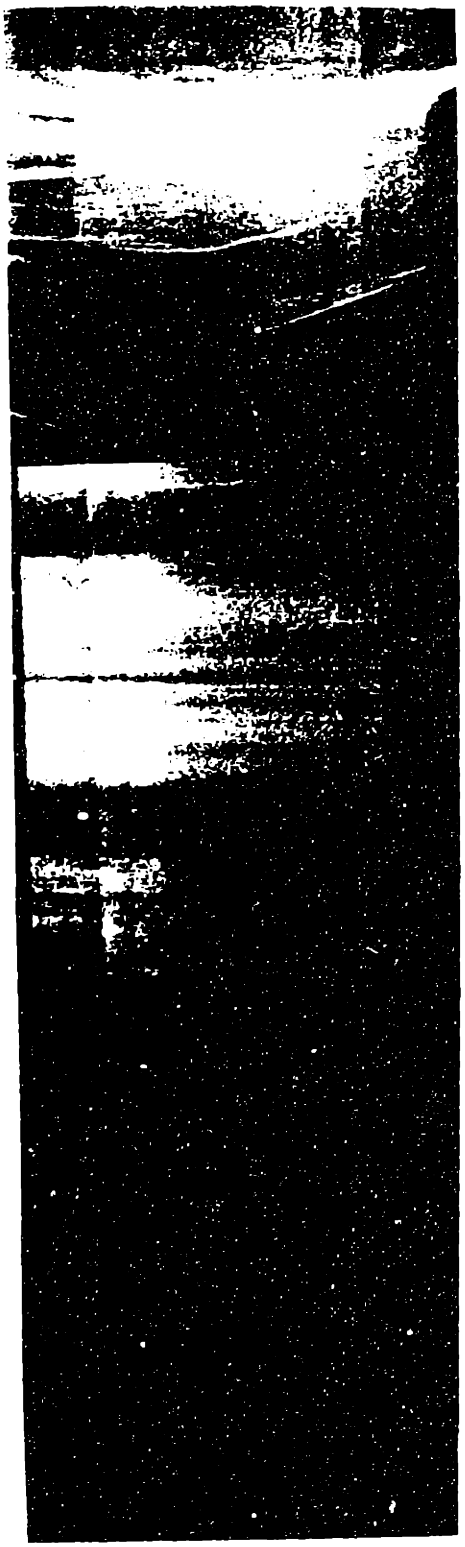

Boring # EB2-162 U4

Disturbed

Boring # SB2-21 U10

Layered

Boring # SB2-21 U10

Uniform

Figure 2-5: Sample Radiographs

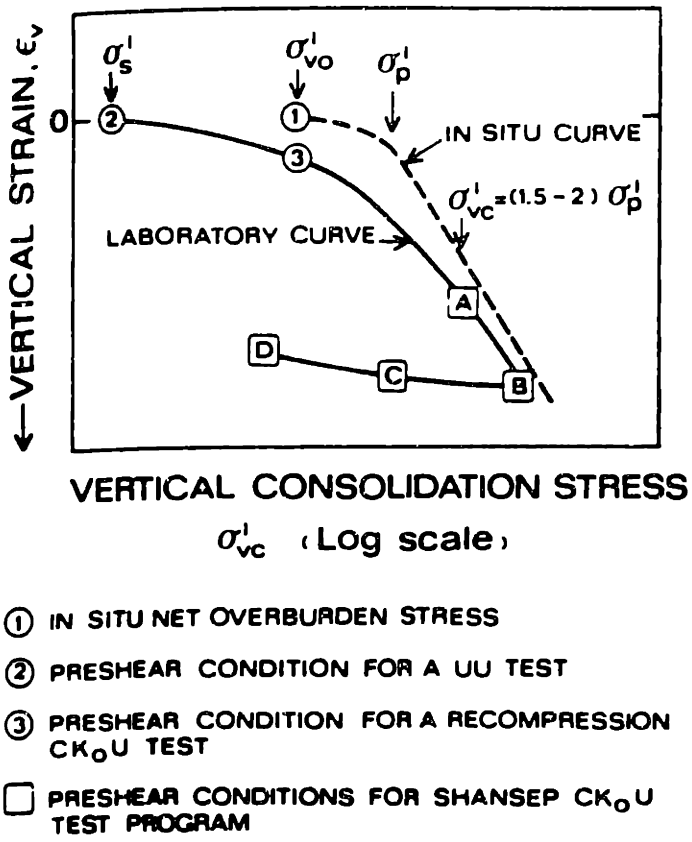

Figure 2-6: Consolidation Procedures for Laboratory CK_0U Testing (after Ladd et al. 1977)

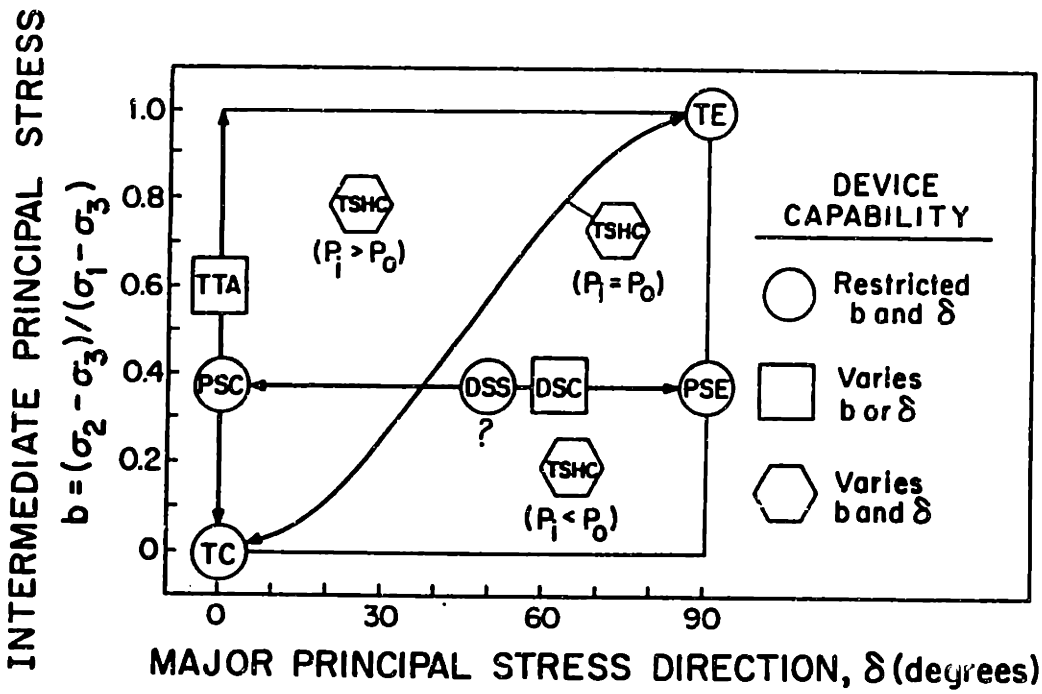

Figure 2-7: Stress Systems Achievable by Shear Devices for CK_0U Testing (modified from Germaine, 1982)

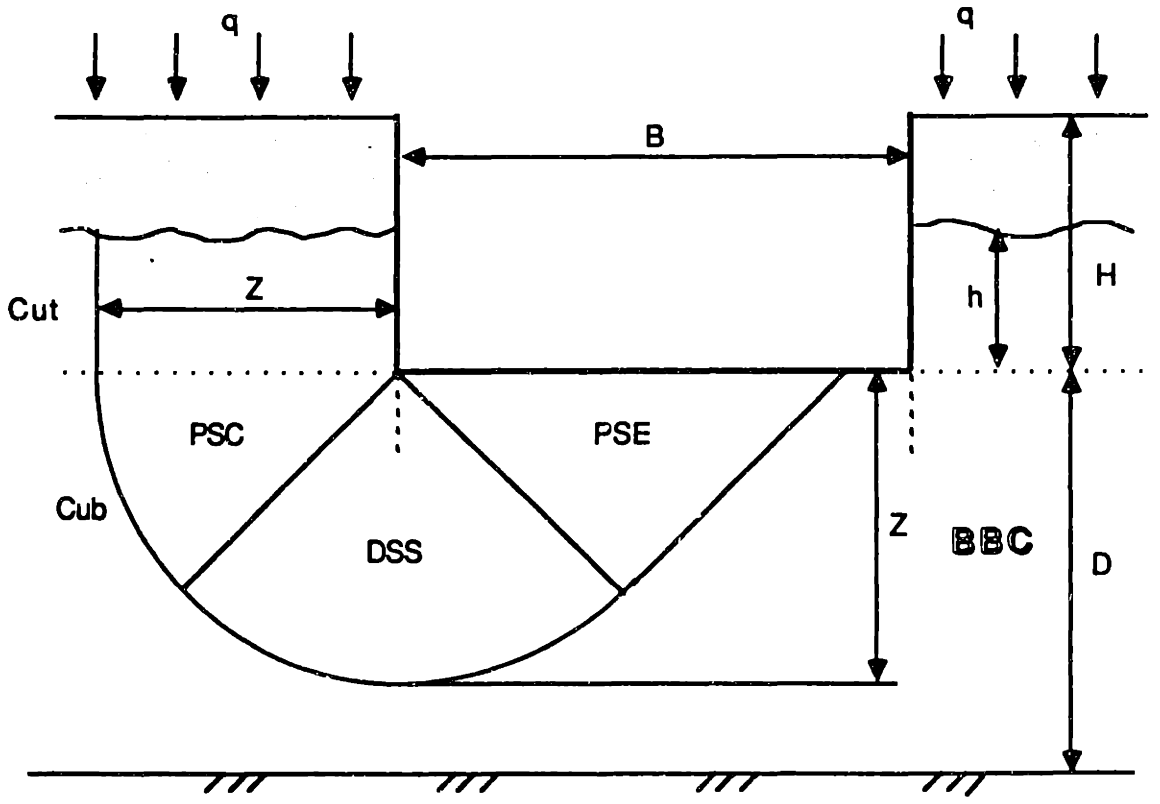

Figure 2-8: Undrained Strength Parameters for Assessing Bottom Stability for Excavations in Boston Blue Clay

Chapter 3

MIT Automated Stress Path Triaxial Apparatus: Equipment and Testing Procedures

In keeping with the goal of running "state-of-the-art" tests during the course of this program, development of improved testing equipment and procedures were an integral part of MIT's participation in this project. Most significantly, new automated stress path triaxial testing capabilities were implemented during the course of the research. Additionally, great emphasis was placed on developing consistent laboratory and data reduction techniques in order to remove as much operator-induced uncertainty in the results as possible. Also, special care was taken in the handling of the samples, to avoid causing additional disturbance, especially in the preparation of the block samples. This chapter describes in very general terms the equipment, testing procedures, and data reduction used for all of the triaxial tests performed at MIT. Specific details are provided in Appendix A.

3.1 Equipment and Software

A significant aspect of the MIT research program was the implementation of four fully automated stress path triaxial testing cells which combined existing MIT testing

equipment with some innovative new components. Figure 3-1 shows a schematic diagram of the testing apparatus.

The existing cells were developed at MIT in the mid-1960's. The bases were made by Wykeham Farrance, with customized features such as linear ball bearing bushings and rolling diaphragms to eliminate piston friction, fixed top cap, and both top and bottom drainage. The cells are mounted on Wykeham Farrance load frames and attached to an external load cell. The cells test cylindrical specimens with approximate volumes of 80 cm^3 (8 cm high and 10 cm^2 cross sectional area). The specimen can be mounted on the pedestal and the piston placed on the specimen before the plexiglass cell chamber is installed, ensuring proper seating.

This basic cell was connected to two new pressure control devices equipped with DC electric servo motors (an improvement on previous automated cells which employed stepper motors). The systems were tied together with a combination of commercially available and MIT-designed electronic components, and control was provided via a personal computer which used new control algorithms tailored to our needs. MIT's Geotechnical Laboratory Director, Dr. Germaine, and Thomas C. Sheahan, a research assistant, created this improved apparatus and greatly enhanced testing capabilities by reducing the number of operator hours required to run sophisticated tests. Section 1 of Appendix A describes the mechanical and electronic equipment required for each of the four cells.

Automated control of the MIT triaxial cells is carried out by a control program written by Mr. Sheahan and Dr. Germaine. The program, written in BASIC, runs on an IBM XT compatable Hyundai personal computer (one dedicated computer per cell). The computer sends signals via a Strawberrytree 12 bit digital to analog converter and an MIT-designed motor control box to three motors. Two motors drive pistons in hydraulic pressure controllers which regulate the pore and cell pressures, and the third motor drives the load frame to regulate either axial load or displacement. Signals from pressure and displacement transducers and the load cell are then converted via an analog to digital converter designed by Mr. Sheahan, read by the computer, and used by the control program to calculate subsequent control signals.

The control program runs at 40 Hz, and is capable of controlling pressures to within 1 kPa ($\approx$ 0.01 ksc) and strains to better than 0.01%.

At regular intervals (predetermined by the tester), transducer readings are also taken by the Hewlett-Packard 3497A Data Acquisition Control Unit which serves as the Central Data Acquisition System for the entire geotechnical laboratory. The resolution of this unit is 0.1 mV for the DCDTs, and approximately 1 μV for the pressure transducers, which translates to resolution of strain to $\approx$ 0.0005%, and pressures to about 0.0001 ksc, which far exceed the sensitivity of the triaxial control program.

The readings are collected into a data file and used to calculate the stresses and strains in the sample with the help of a reduction program (described in Appendix A).

The program is flexible and user-friendly. It performs all phases of a triaxial test: initial application of a cell pressure to establish a positive pore pressure in the specimen; back pressure saturation; B value check; consolidation along any stress path or K_0 consolidation; and shear in either compression or extension. After installing the specimen and inputting initial dimensions and transducer calibration factors and zeros, the operator need only be present to start up each phase of the test and thereafter occasionally check the progress of the test.

An additional benefit is that, throughout the test, the program calculates and displays, on a continuously updated screen, the current progress of the test and current state of the specimen. Information displayed includes not only voltage readings from all transducers and the input channel, but also the corresponding values of axial and volumetric strain (in %), axial load (in kg), and axial, cell and pore pressure (in ksc). Additionally, during timed phases of the test, such as application of saturation increments, the number of minutes elapsed out of the total number of minutes requested are displayed and during the strain controlled portions of the test, such as consolidation and shearing, the target and actual rates of strain are displayed. This continuous display allows the operator to monitor the progress of the test at a glance, and quickly spot any problems.

The control program achieves its versatility by employing one basic motor control

loop for several steps of the test, supplemented by appropriate subroutines. The general operation of the program's main control loop, as well as details of the specific phases of the triaxial test, are described in Section A.2 of Appendix A.

3.2 Testing Procedures

All of the triaxial tests run as part of this program were performed using either the SHANSEP methodology developed by Ladd and Foott (1974), or the Recompression technique formalized by Bjerrum (1973). The reader should refer to the Terzaghi Lecture by Ladd (1991) for detailed explanations of the theory behind the two techniques.

Preliminary steps for each type of test were identical. Tube samples were first radiographed to identify the best areas for testing. Once selected, a portion of the tube was cut off with a band saw and the soil extruded. Alternately, samples of the approximate size needed were cut off the large block samples. The specimens were trimmed in a mitre box and installed in the cell with porous stones, filter strips and two thin membranes. Each specimen was subjected to a small cell pressure (0.5 ksc $\pm$) overnight to establish a positive pore pressure, then back pressure saturated prior to consolidation. These preliminary steps are described in detail in Appendix A. This section will briefly mention the differences between the two methods as they relate to the consolidation phase of triaxial tests.

3.2.1 SHANSEP Tests

The laboratory tests used in a SHANSEP program consist of both CK_0UC and CK_0UE tests. K_0 consolidation is specified to model the one-dimensional consolidation which has occurred during deposition. Tests on normally consolidated specimens were done at different depths, and tests at selected elevations were run with OCRs from 2 to about 6.

Each test consists of two main parts — consolidation and shear — but only the consolidation phase is significantly different from the Recompression type tests. Both

parts are controlled automatically by the computer as mentioned previously. K_0 consolidation is achieved by controlling the amount of water leaving the sample so that the volumetric strain always remains equal to the axial strain, thus maintaining a constant cross-sectional area.

Another requirement of the SHANSEP method is to reconsolidate the sample to two to four times the in situ preconsolidation pressure, σ'_p, which experience has shown, can usually be achieved by straining the specimens at least 10%. The specimen at the end of consolidation, then, is normally consolidated (NC), and the resulting K_0 corresponds to the in-situ, one-dimensionally normally consolidated value. The strain rate used is approximately 0.1%/hr, which results in consolidation times of 4 (NC) to 7 (OC) days. At this point in the test, the specimen is allowed to sit for 24 hours at the final stress state to allow some secondary compression to take place and restore a bit of the structure of the clay which was altered during consolidation. The sample can then either be sheared, or K_0–rebounded to a chosen overconsolidation ratio (OCR), allowed to sit for another 24 hours, and sheared from there. The undrained shearing is done at a rate of 0.5%/hr., and usually takes 1 to 2 days.

3.2.2 Recompression Tests

The Recompression method usually involves consolidating the specimens to the in situ vertical effective stress, σ'_{v0}, before shearing. For this research, some of the tests were also consolidated to lower or higher values of σ'_{vc} (but never exceeding σ'_p) to study the effects of OCR on the shear results. The horizontal consolidation stress, σ'_{hc}, is determined by choosing a value of K_0 which corresponds to either the in-situ OCR of the sample when $\sigma'_{v0} = \sigma'_{vc}$, or the test OCR when $\sigma'_{v0} \neq \sigma'_{vc}$. A major difference between SHANSEP and Recompression consolidation, then, is that prior knowledge of K_0 is required for Recompression, while a K_0 value actually *results* from the SHANSEP test.

In any case, once the final consolidation stresses desired are determined, the stress state is controlled by the computer in such a way that σ'_{vc} and σ'_{hc} are reached by traveling along a straight line stress path. Like the SHANSEP tests, the Recompression

tests are allowed to undergo 24 hours of secondary compression prior to undrained shear.

Aside from the consolidation phase of the test, all other portions, including shearing, are essentially identical to SHANSEP. The procedure used in the laboratory is described further in Section A.3 of Appendix A.

3.3 Data Reduction

The use of a data reduction program written by Mr. Sheahan saves the repetitive calculation of stresses and strains during the consolidation and shear portions of the triaxial tests. The program converts the voltages read by the Central Data Acquisition System into values of stress and strain which are written to a printout and a data file which can be easily imported to Lotus 1-2-3 or similar software program, in order to produce plots.

Inputs to the data reduction program include type of test (drained or undrained, compression or extension), initial dimensions of the specimen, transducer zeros and calibration factors, and information relating to the corrections to be applied (such as filter strip perimeter, number and type of membranes, and area correction to be used). The outputs for a drained test (or the consolidation phase of any test) are: volumetric and axial strain (ϵ_v and ϵ_a), vertical and horizontal effective stress (σ'_v and σ'_h), $q = 0.5(\sigma_v - \sigma_h$, $p' = 0.5(\sigma'_v + \sigma'_h)$, $K_c = \sigma'_h/\sigma'_v$, and cross-sectional area (A). Outputs for the undrained phase of the test (shear), are: ϵ_a, A parameter, friction angle (ϕ'), and normalized values of q (q/σ'_{vc}), p' (p'/σ'_{vc}), Young's modulus (E/σ'_{vc}), and pore pressure ($(\Delta u - \Delta\sigma_3)/\sigma'_{vc}$ for compression tests, $\Delta u/\sigma'_{vc}$ for extension tests). As these calculations are all fairly standard, they are covered briefly in Appendix A, along with the corrections used in the calculations, an explanation of a few changes made to the data file and examples of typical output and plots.

3.4 Comments on Testing Problems and Quality of Test Data

As may be expected for a testing program which utilized new equipment and included such unprecedented numbers of tests, a certain number of problems were encountered. The problems can be roughly categorized as either equipment problems (mechanical or electrical) or procedural problems (including operator errors). Listed below are the primary problems of each type, their effects on the data, and their resolution.

3.4.1 Equipment Problems

Leaks

Leaks are always a concern during triaxial tests, and particularly so for tests which run for extended periods of time, as the SHANSEP CK_0UC/E tests performed at MIT. The two possible types of leaks are internal (i.e., cell fluid leaks into the sample), or external (i.e., pore fluid leaks out of the system, outside of the cell). While there were no detectable external leaks in the cells during the research program, several tests were affected by internal leaks. In particular, several early SHANSEP tests performed on cell MIT04 yielded results inconsistent with tests performed in other cells. Even though precautions are taken to discover the presence of leaks (such as the preshear leak check), at that stage of the project there was inadequate basis for comparison, and the leak went undetected through several tests. Later, as experience increased, a better standard was established, and subsequent leaks were spotted and quickly repaired, with less loss of data. In most cases the degradation of the plastic tubing serving as the top drainage line was the culprit. Ironically, silicon oil, which was used to eliminate internal leakage through the membrane, was "unfriendly" to the plastic tubing, and may have actually *caused* a certain amount of leakage.

Noise

Towards the beginning of the testing program, problems were encountered with "noise" in the electronic systems. Among other things, it was found that the transducer reading was changed when the central data acquisition system took a reading on the specified channel. The control program then tried to compensate for this incorrect reading, leading to generally poor quality stress–strain data, as illustrated in Figure 3-2. By rewiring some of the connections and grounding some of the wires in the motor control and channel switch boxes, Dr. Germaine was able to eliminate most of the noise problems, though subsequent problems with the load motors (described below) may be at least partially attributable to interference or noise in the system.

Erratic Loading Rates

The axial load motors seemed particularly sensitive, and were responsible for loading rates which were more variable than desired. The strain rates specified for consolidation and shear were 0.1%/hr and 0.5%/hr (positive or negative), respectively. Figure 3-3 shows the shear rate for a test with the load motor in good working order, and one for a test when the rate varied. In extreme cases, the load motor sometimes stopped completely. One of the load motors was replaced during the course of the research, which eliminated the problem in that cell.

The other motor which behaved erratically was used through the whole program, with mixed results. Since slow rates were more problematic, the problem was partially alleviated by changing the gear ratio on the load frame to permit the motor to run at a higher rate. Nonetheless, control of the loading rate on cell MIT03 was generally inferior to the other three cells, though still within reasonable limits.

The effect of the variable rate on the test results was probably negligible, except in extreme cases, as shown in Figure 3-4.

Variable Stiffness

As explained in Appendix A, the application of load to the sample is controlled by a "gain" rate which is input into the control program, in engineering unit (e.g., ksc, or %) per volt-second, and which is dependent, among other things, upon the stiffness of the system and the sample. Some problems were encountered during the consolidation phase of the SHANSEP tests, when the stiffness of the sample changed during the course of consolidation, leading to an oversensitive load response, and erratic loading, as illustrated in Figure 3-5. This problem was overcome by entering the control program file and adjusting the gain rate manually until the desired response was achieved. Future improvements to the program will enable one to account for varying stiffness more directly.

3.4.2 Procedural Problems

Extension Test Filter Strips

The first extension tests were performed using 1/4 inch wide, spiral strips of a porous filter paper. Results from these early tests showed unreasonably high values of peak friction angle, ϕ', which was attributed to a strength contribution of the filter strips at large strains. Subsequent extension tests were performed using spiral filter strips $\frac{3}{16}$ inch wide, which eliminated the problem.

Unintentional Overconsolidation

Some of the early SHANSEP tests which were specified to be sheared normally consolidated were actually slightly overconsolidated (OCR $\leq$ 1.2). This was due to a combination of mechanical problems and procedural errors by the testers. What usually occurred in these cases is that, for various reasons, there was a slight unloading during final consolidation or during the 24 hour period of secondary compression. The specimens were then sheared at the lower stresses, leading to slightly overconsolidated tests. The procedure was subsequently changed so that any unloadings were followed by reconsolidation to the virgin compression line.

Incorrect K_c

As described in Appendix A, the stresses input into the computer for stress path consolidation of Recompression type tests are calculated by choosing a σ'_{vc} and an appropriate K_c from which to calculate σ'_{hc}. For tests where $\sigma'_{vc}=\sigma'_{v0}$, the K_c selected is simply the in situ K_0. However, for the tests which were performed with $\sigma'_{vc} \neq \sigma'_{v0}$, the test OCR is different from the in situ OCR, and a different K_c is needed. For several of the early Recompression tests having $\sigma'_{vc} \neq \sigma'_{v0}$, this adjustment in K_c was erroneously neglected by the tester. The interpretation of the resulting data was made more difficult by the use of the incorrect K_c.

3.5 Estimated Success Rate

Despite the problems mentioned above, the overall success rate of the tests was considered reasonable. After the results of each test were plotted and summarized, a judgement on the quality of the test was made and the test was assigned either an Excellent, Good, Fair, or Poor rating (see Section 2.4). For the SHANSEP tests a separate assignation was made for the consolidation and shear phases, while the Recompression tests were given only one rating per test.

For the SHANSEP consolidation phase, approximately 54% of the tests were rated Good to Excellent, 38% were rated Fair to Poor, and 8% were unusable. The large number of tests performed made it possible, for analysis purposes, to exclude all of the Poor tests. For example, a Fair test may have produced a reliable estimate of σ'_p (a very important parameter), but with an incomplete virgin compression curve or erratic K_0 values (less important parameters). In general, most of the consolidation tests were of higher quality than routinely obtained, and thus even the Fair tests, by some standards would by considered Good to Excellent.

For the shear portion of the SHANSEP tests, approximately 59% of the tests were Good to Excellent, 31% were Fair to Poor, and 10% were unusable. The Good to Excellent tests notably *include significant numbers of TE test results, which, until this research program, were notoriously difficult to achieve.*

The success rate of the Recompression testing program benefitted greatly from the lessons learned during the SHANSEP testing, which was done first. Of the Recompression tests performed, 75% were rated Excellent, 9% were rated Very Good, 9% were rated Good, 3% were rated Fair, and a mere 3% (or a single test) was classified as unusable. This phenomenal success rate is not only a function of experience gained during SHANSEP testing, but also an indication that the Recompression tests are less prone to errors because of their reduced testing time (4 - 7 days, as opposed to 8 - 12 days for SHANSEP tests).

3.6 Overall Quality of Test Data

The majority of the data resulting from this test program were of extremely high quality. In particular the 1-D compression curves obtained from the K_0 consolidation phase of the SHANSEP triaxial tests were exceptional. They provided the primary means for estimation of the in situ σ'_p of the deposit at the two sites. The consolidation phase also provided the most extensive and reliable estimates of the K_0 of the samples, an essential input for the Recompression testing program.

The undrained shear data obtained were also, in general, unusually good. The results of the TE tests are particularly pleasing as this marks the first time that Good to Excellent extension data were routinely obtained at varying OCR.

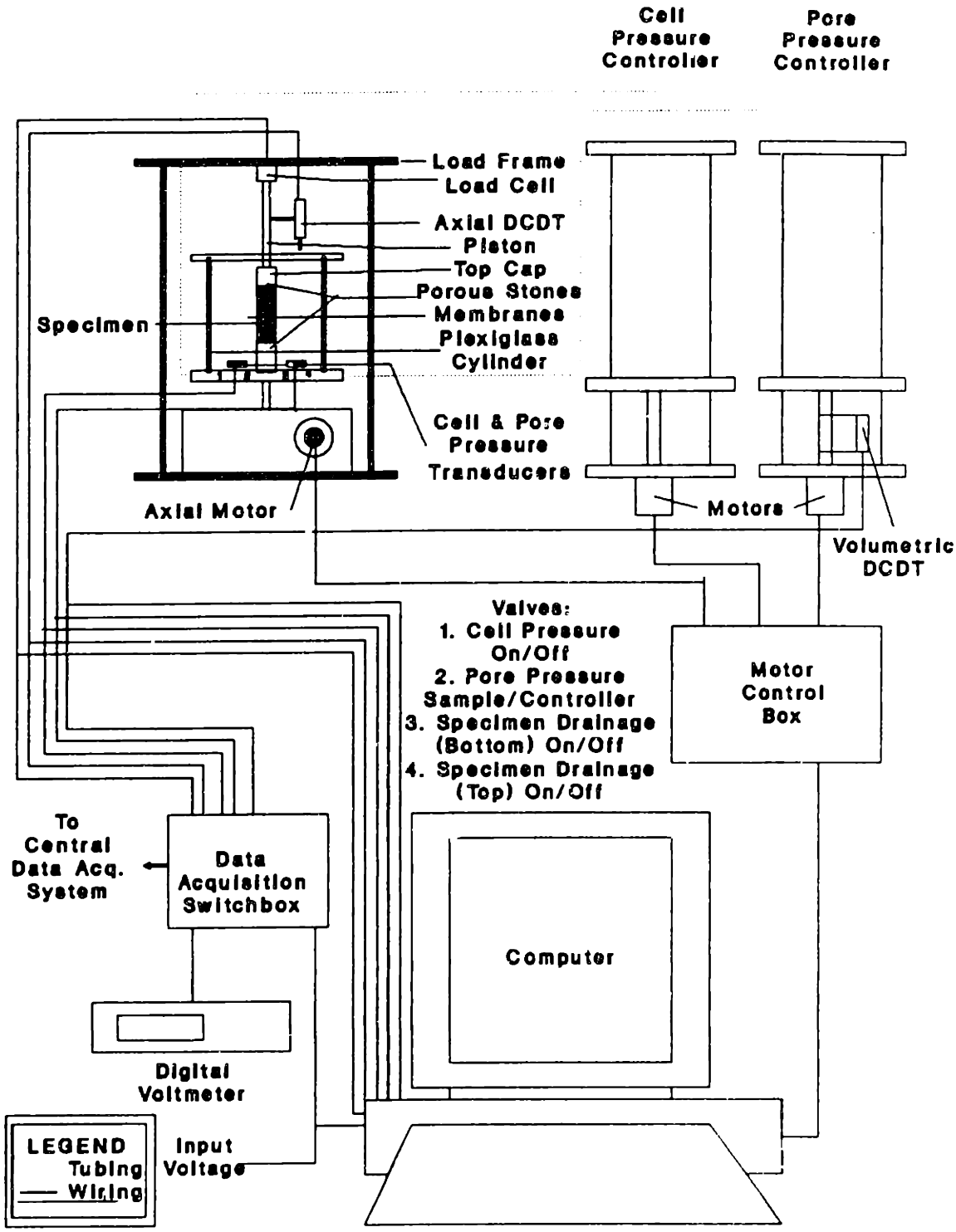

Figure 3-1: Schematic of the MIT Automated Stress Path Triaxial Apparatus

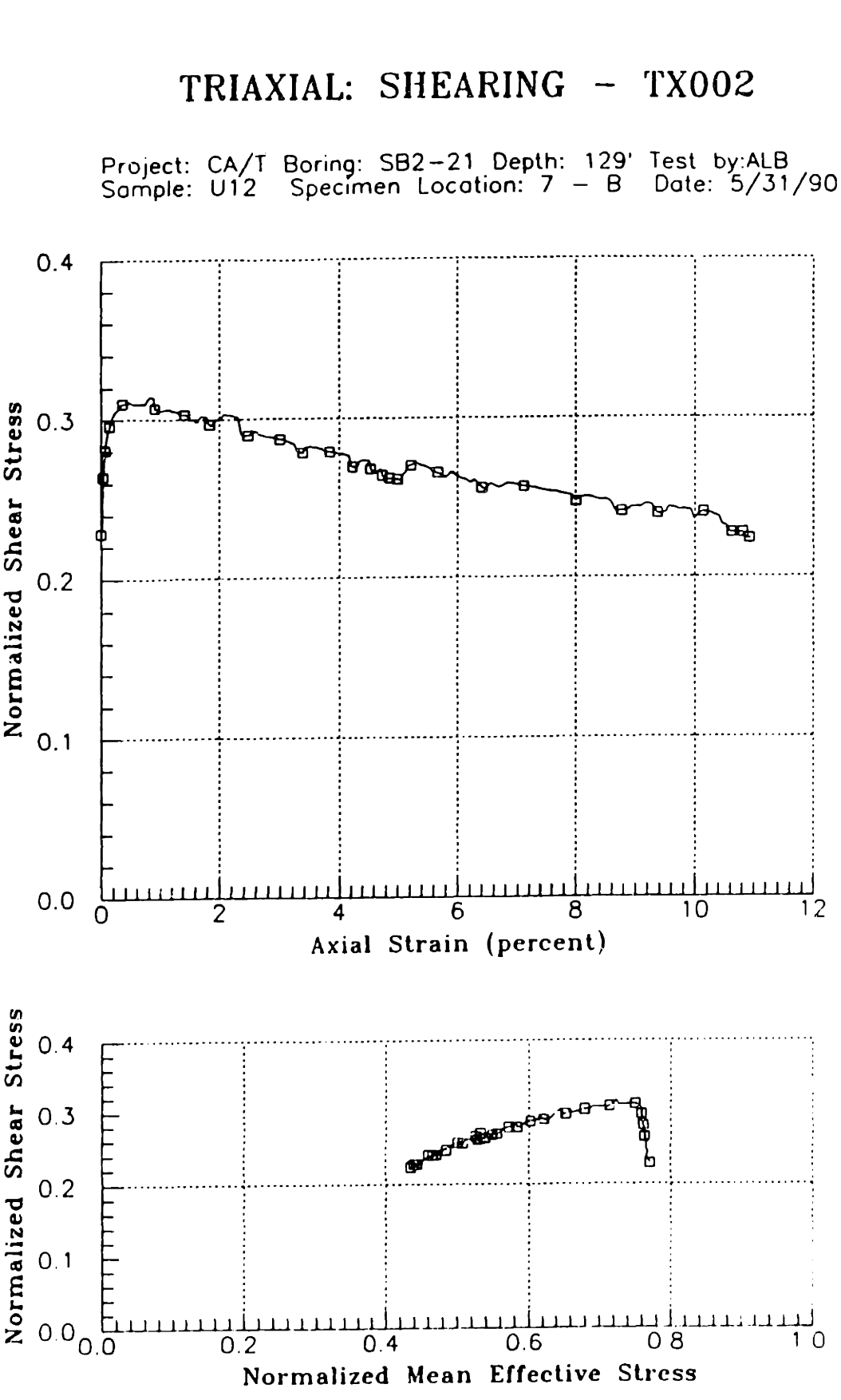

Figure 3-2: Example of Poor Stress Path Affected by System Noise

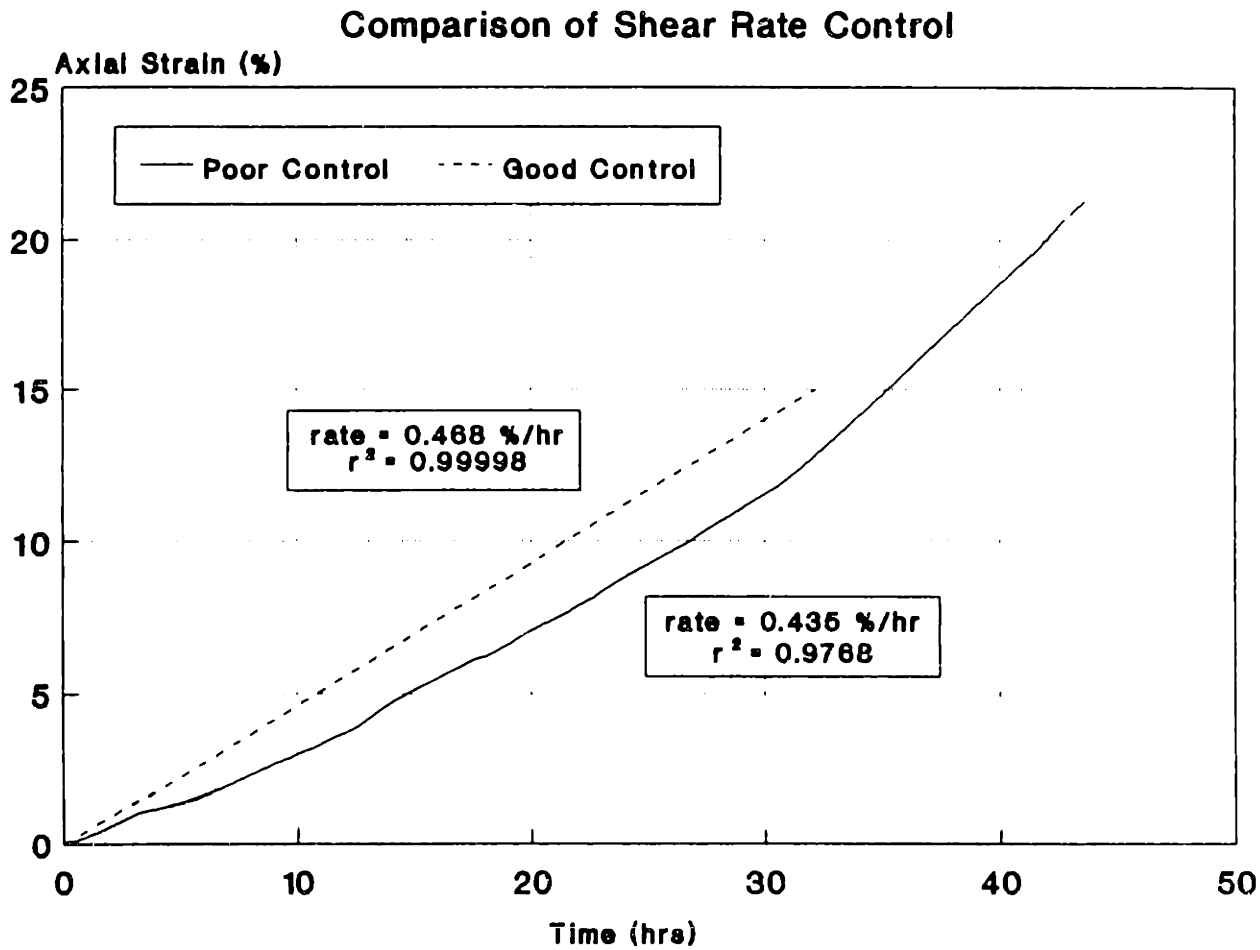

Figure 3-3: Example of Good and Bad Axial Load Rate Control

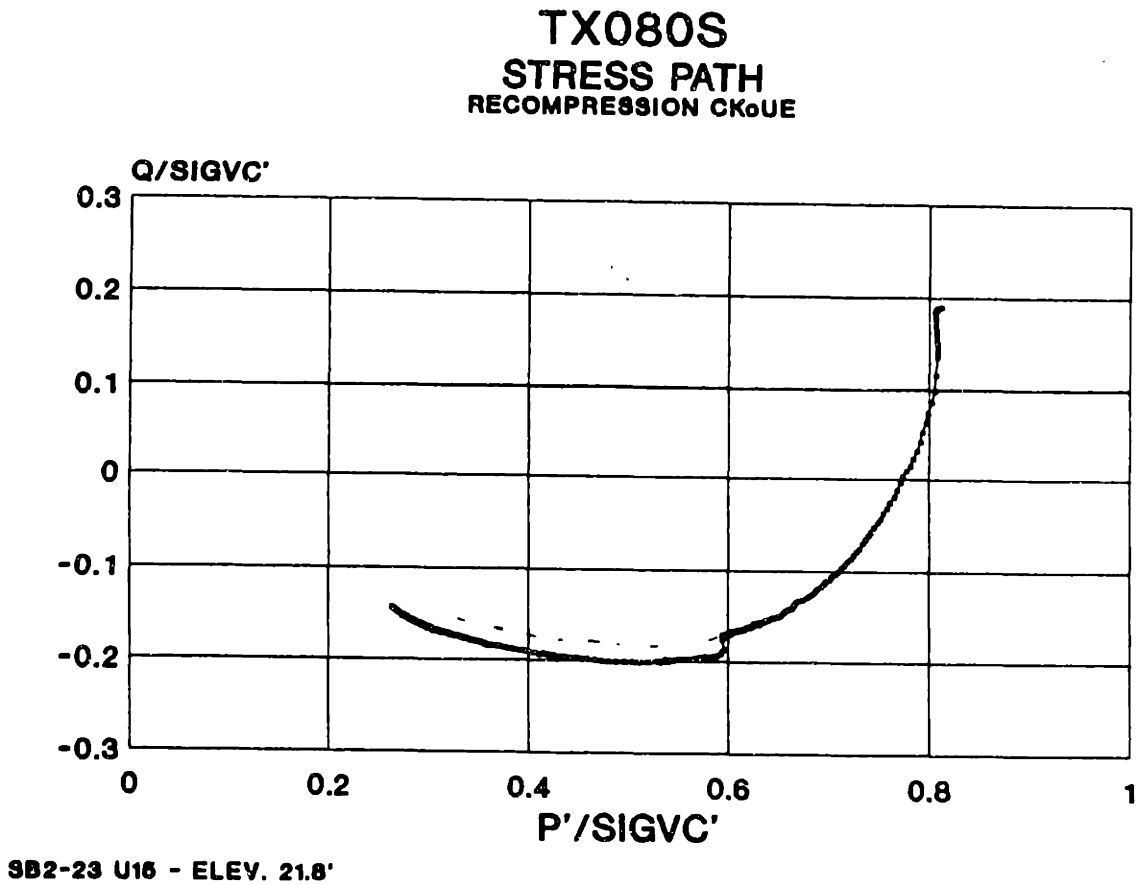

Figure 3-4: Example of Effect on Stress Path of Rate Change (Extreme Case)

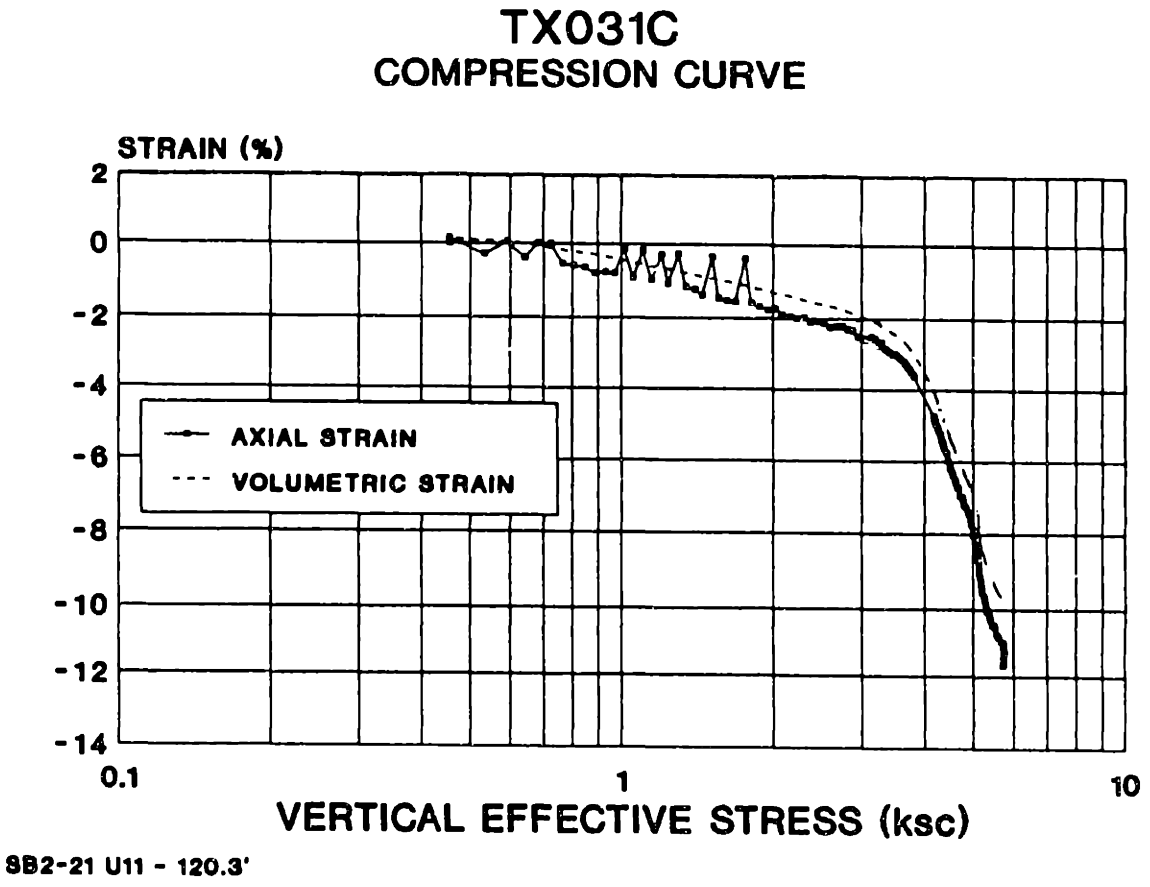

Figure 3-5: Example of Poor Compression Curve Resulting From Incorrect Axial Load Gain Rate

Chapter 4

Sample Characteristics and Distribution of Engineering Tests

4.1 Sample Quality and Macrofabric

The quality and macrofabric of the Boston Blue Clay tube samples are assessed through the use of radiography using the procedures and equipment as described in detail in Sauls et al. (1984). MIT received a total of 45 tube samples for the Special Test Program, all of which were X-rayed 10 inches at a time for a total of 135 radiographs.

The radiographs generally showed clay layers of different density, indicating a certain non-uniformity. Radiographs from the SB and EB borings had essentially the same basic features, with the upper material being fairly uniform, and more pronounced layering being observed with depth. The inclination of the layers ranged from 0 to 10 degrees. The various layers are basically clay type material, occasionally containing very fine lenses of silt or sand (or sand pockets). These lenses were usually visible on the radiograph provided they were approximately perpendicular to the vertical axis of the tube. Upon trimming, additional fine lenses of silt were often observed more or less parallel to the tube's vertical axis. These very fine layers appeared to be a characteristic of the clay as they were apparent in many of the samples from both South and East Boston.

Table 4.1 shows the total recovery and the amount of material available for engineering tests (i.e., of sufficient quality) from the South Boston borings (SB2-21 and 23). The overall quality of the tube sampling at SB was generally excellent. The use of a heavy weight drilling mud ($\gamma_t \approx 70$ pcf) to prevent bottom failure, as recommended by Dr. Ladd, enabled the samples to retain much of their structure, and also resulted in very high recovery ratios. Table 4.2 presents the same information for the East Boston boring (EB2-162).

The SB block sampling analysis is summarized in Table 4.3. From this table, one notices that the quality of the block samples varied and some samples were remolded, apparently the result of the soil being disturbed before the sampling. According to Dr. Lefebvre from Sherbrooke University, for depths of 90 feet or less (above elevation 20), the disturbance was due to the contractor's cleaning bucket and was solved by cleaning the bottom of the hole with Sherbrooke's flat auger. At greater depths no undisturbed soil was obtained. Dr. Lefebvre attributes this problem to bottom failure and claims that, "intact block samples of the highest quality could be obtained if the bottom of the hole can be kept undisturbed and stable" (letter from Dr. Lefebvre to Haley & Aldrich, October 16, 1990).

The block samples were too large to be radiographed. Therefore the quality and quantity of soil available for engineering tests was estimated from direct observations upon opening the samples, and from the field sampling log. After MIT received the samples, they were visually inspected and cut to smaller sizes (approximately 5 inches in height) to facilitate handling. The samples were then waxed to prevent water loss during storage and placed in a humid room. The macrofabric for most of the samples contained some silt and sand layers. Surprisingly a few very distinct shear planes were also observed; a phenomenom not understood and difficult to explain since these were found in very high quality samples of stiff BBC.

4.2 Classification and Index Properties

Following the radiography process, classification and index tests were run on samples from SB2-21 and 23, and EB2-162. The natural water contents and torvane strengths were determined from the ends of each tube, both at MIT and H&A. Additional water contents and torvane strengths were obtained from soil located directly around every sample used for engineering tests. Atterberg limits, grain size analysis and specific gravity tests were also performed on representative samples. Finally, salt concentration, pH and carbonate content tests were run to investigate pore fluid properties and soil composition.

4.2.1 Natural Water Content, Atterberg Limits, Plasticity Chart

Figure 4-1 presents project elevation versus natural water content, plastic and liquid limits for the clay deposit at South Boston and Figure 4-2 does likewise for East Boston. The data are both from standard oedometer testing at H&A and from some MIT triaxial trimmings. The natural water contents generally range from 30 - 40 % within the top 30 feet of the clay, to approximately 40 - 45 % for the remaining clay. The plastic limits are generally around 22%±2% SD throughout the clay deposit, while the liquid limits are more dispersed with values of 50%±6% SD. There is no evidence to indicate any significant difference in these properties from the South Boston (tube or block samples) and the East Boston sites.

Figures 4-3 and 4-4 show both the plasticity index (I_P) and the liquidity index (I_L) variations within the clay. The I_P is fairly consistent, ranging from 20 to 35% with a mean around 28%. The I_L values on the other hand are dispersed, ranging from 0.3 to 0.9. I_L decreases at shallower depths due to increasing preconsolidation pressure.

The plasticity chart is represented in Figure 4-5. The samples plot above the A line, as is typical of marine illitic clays. Once again, there is no difference between the SB and the EB results, and there is also no trend versus elevation.

4.2.2 Strength Index

Figures 4-1 and 4-2 also show the torvane strengths for the clay deposit. The values are very consistent, both for MIT and H&A, generally forming a trend similar to the stress history profile presented in Chapter 5. The strength values start high from 1.5 to 2 ksf at elevation 60, they reach a low of approximately 0.8 at elevation 25, and increase again to about 1 at elevation -20.

4.2.3 Grain Size Distribution and Specific Gravity

Figure 4-6 shows the grain size distribution profile. The grain size analysis obtained from eight hydrometer tests is very consistent throughout the clay and gives approximately 53% clay size (less than 0.002 mm), 44% silt and 3% sand (greater than 0.075 mm). A series of 10 specific gravity tests gave a value of 2.785±.009 SD which is reasonable for BBC (see Figure 4-7). Both series were performed at MIT on clay taken from material around engineering test specimens.

4.2.4 Salt Concentration, Carbonate Content and pH

Figures 4-3 and 4-4 also present the pore (water) fluid salt concentration measured at MIT for tube samples from the three borings. The salt content (expressed as equivalent NaCl concentration in grams per liter) is fairly high at the top elevations, starting at 30 g/l at elevation 70, decreasing to 15 g/l at elevation 55, and reaching a steady value around 12 g/l for the lower portion of the clay.

Figure 4-8 represents the results of carbonate content tests done on soil from boring SB2-23 by Professor DeGroot at the University of Massachusetts at Amherst using the Chittick method. The results are consistent, with dolomite and calcite contents around 3% and 1%, respectively. However, the relatively high carbonate content is rather surprising (Ladd, personal communication).

Figure 4-9 plots elevation versus pH from tests run at MIT. Although most of the values are near seven (neutral), a significant number of tests gave significantly higher values.

4.3 Distribution of Engineering Tests

Tables 4.1 through 4.3 present the distribution of CK_0–Triaxial and lateral stress oedometer tests done at MIT under it's contract with H&A. The tests are listed according to the actual test number used during the program (i.e., TX001-TX104). A total of 33 triaxial tests using the SHANSEP technique (19 Triaxial Compression and 14 Triaxial Extension, TC and TE, respectively) were run on the South Boston tube samples (Table 4.1). An additional six triaxial tests were run using the Recompression technique (four TC and two TE). For the East Boston site (Table 4.2), 11 SHANSEP (six TC and five TE) tests were run, but no Recompression tests were performed due to a lack of soil.

The South Boston block samples were extensively tested with a total of thirteen SHANSEP (five TC and eight TE) tests, and 35 Recompression (24 TC and 11 TE) tests performed (Table 4.3). In addition, a total of nine Lateral Stress Oedometer (LSO) tests were run, four on SB, to on EB and three on block samples.

Table 4.1: Distribution of CK_0-TX and LSO Tests: South Boston Tube Samples
(Page 1 of 3)

Boring & Tube #	Bottom El. (ft)	Recovery (in.)	Available for Eng. Tests (in.)	Remarks	Test Number					
					SHANSEP CK_0U		Recompression CK_0U		CK_0-TX Stress Path	LSO
					TC	TE	TC	TE		
SB2-21	GSE = 111.3									
U2	65.8	17	11	Some Cracks						
U3	57.3	22	18	Inclined Sand Layer						
U4	47.3	21	11	Cracks	TX014					
U5	41.3	23	9	Shear Planes						
U6	32.3	23	18		TX008					LSO11
U7	25.3	23	23		TX011					
U8	17.3	23	18	Void in Middle		TX027				
U9	9.3	23	19							
U10	1.3	21	21		TX001	TX006				LSO10
U11	-10.7	22	19	Stones in Middle		TX031				
U12	-18.7	23	20		TX002 TX007					
U13	-26.7	21	20							

Table 4.1: Distribution of CK_0-TX and LSO Tests: South Boston Tube Samples
(Page 2 of 3)

Boring & Tube #	Bottom El. (ft)	Recovery (in.)	Available for Eng. Tests (in.)	Remarks	Test Number					
					SHANSEP CK_0U		Recompression CK_0U		CK_0-TX Stress Path	LSO
					TC	TE	TC	TE		
SB2-23	GSE = 110.9									
U3	70.7	9	8							
U4	68.7	10	5	Some Cracks						LSO13
U5	61.9	21	8							
U6	59.9	22	11	Cracks	TX032					
U7	53.9	23	19		TX003					
U8	51.9	23	17		TX029					LSO12
U9	45.9	18	11	Cracks		TX012			TX021	
U10	43.9	20	10	Cracks						
U11	37.9	23	19	Cracks	TX034 TX035				TX033	
U12	35.9	22	16	Cracks			TX062			
U13	29.9	22	21		TX004	TX005				
U14	27.9	22	15	Cracks	TX026					

Table 4.1: Distribution of CK_0-TX and LSO Tests: South Boston Tube Samples
(Page 3 of 3)

Boring & Tube #	Bottom El. (ft)	Recovery (in.)	Available for Eng. Tests (in.)	Remarks	Test Number					
					SHANSEP CK_oU		Recompression CK_oU		CK_o-TX Stress Path	LSO
					TC	TE	TC	TE		
SB2-23 U15	20.9	23	15				TX063	TX080		
U16	18.9	22	13		TX009 TX023					
U17	13.9	23	21			TX060				
U18	11.9	23	23		TX028					
U19	5.9	24	23			TX013 TX061				
U20	3.9	24	22		TX017	TX016 TX022				
U21	-2.1	23	23				TX083			
U22	-4.1	23	21					TX096		
U23	-10.1	23	18		TX010 TX030					
U24	-12.1	23	21			TX065				
U25	-18.1	23	21	Stone at Bottom		TX019	TX089			
U26	-21.1	23	19	Stones at Top		TX015 TX020			TX018	
U27	-27.1	22	18	Top Crack						

Table 4.2: Distribution of CK_0-TX and LSO Tests: East Boston Tube Samples

Boring & Tube #	Bottom El. (ft)	Recovery (in.)	Available for Eng. Tests (in.)	Remarks	Test Number					
					SHANSEP CK_oU		Recompression CK_oU		CK_o-TX Stress Path	LSO
					TC	TE	TC	TE		
EB2-162	GSE = 110.7									
U1	75.7	19	13							
U2	65.7	22	21	Some Cracks	TX037 TX038					LSO19
U3	55.7	23	21		TX054					
U4	45.7	23	18	Cracks	TX036 TX040					LSO18
U5	35.7	23	21			TX044				
U6	25.7	24	24			TX041 TX051				
U7	15.7	23	23		TX055	TX039				
U8	5.7	23	20			TX077				

Table 4.3: Distribution of CK_0-TX and LSO Tests: South Boston Block Samples

Caisson Hole # & Block Sample #	Bottom El. (ft)	Recovery (in.)	Available for Eng. Tests (in.)	Remarks	Test Number					
					SHANSEP CK_0U		Recompression CK_0U		CK_0-TX Stress Path	LSO
					TC	TE	TC	TE		
Hole #1	GSE = 111.2						TX040			
B.S. 1	66.9	15	8				TX073			
B.S. 2	59.9	16	14	Top 2" Disturbed			TX050 TX057 TX059 TX078			
B.S. 3	54.9	5	4	Sand Layer in Middle			TX101			
B.S. 4	44.9	4	4			All on B.S. 7	TX042	All on B.S. 7		
B.S. 5	36.2	15	0	Dropped 50' Disturbed		TX067	All on B.S. 7	TX049		
B.S. 7	19.9	15	15	Cracks,possibly remolded at Top	TX076 TX082	TX071 TX072 TX102	TX046 TX064 TX066	TX070 TX074 TX075		LSO17
B.S. 9	-0.1	6	0	Remolded		TX097	TX104	TX093		
B.S. 10	-3.4	6	0	Remolded				TX099		
Hole # 2							TX056 TX079			
B.S. 1A	54.2	10.5	10.5		TX100		TX085	TX084		LSO16
B.S. 2A	41.5	15	15		TX088	TX081	TX047 TX058 TX068 TX069 TX095	TX048 TX087		LSO15
B.S. 3A	33.3	15	15		TX094	TX086 TX092	TX098 TX103 TX052 TX091	TX053 TX090		

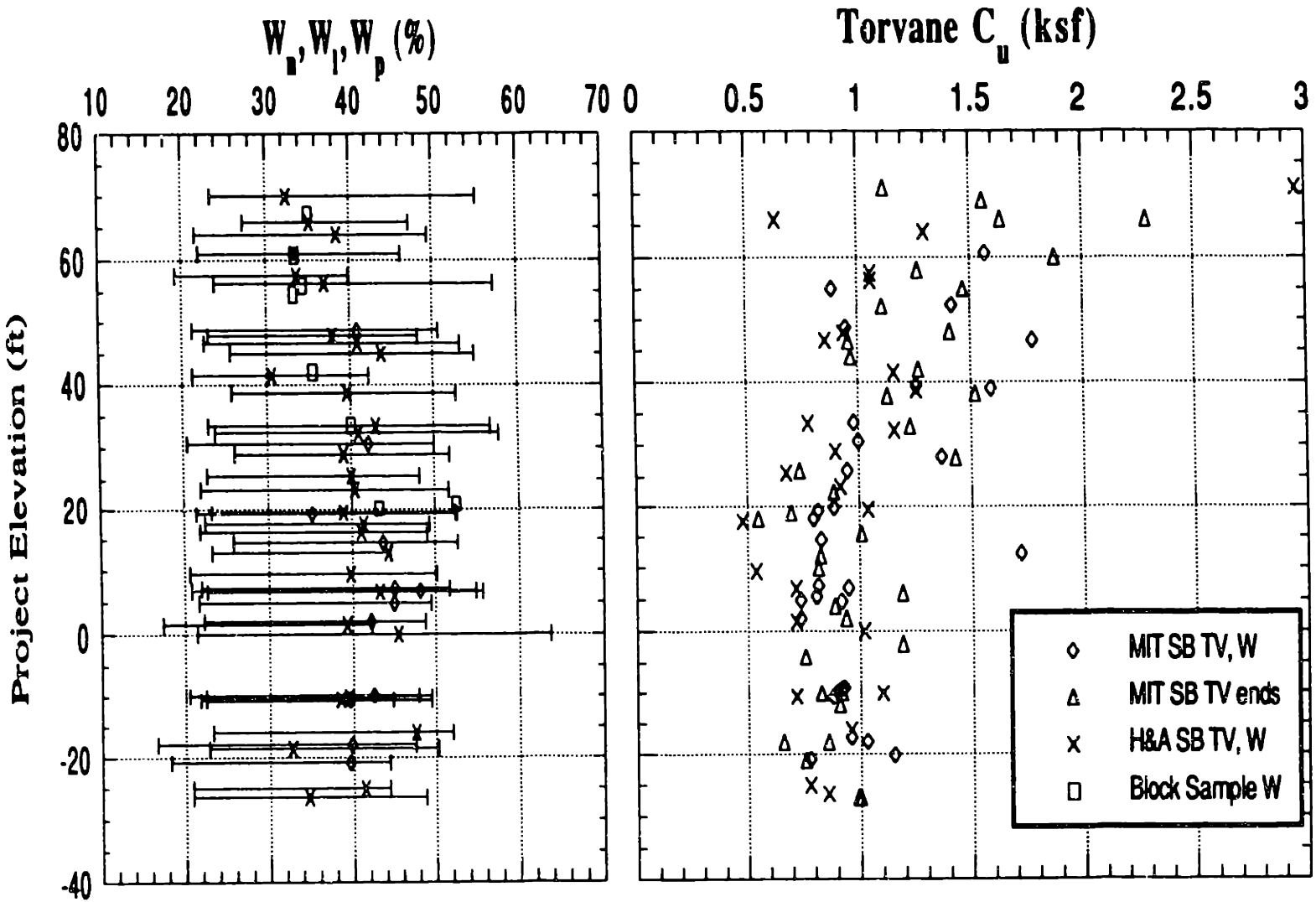

Figure 4-1: South Boston STP: Elevation vs. Water Content and Torvane Strengths

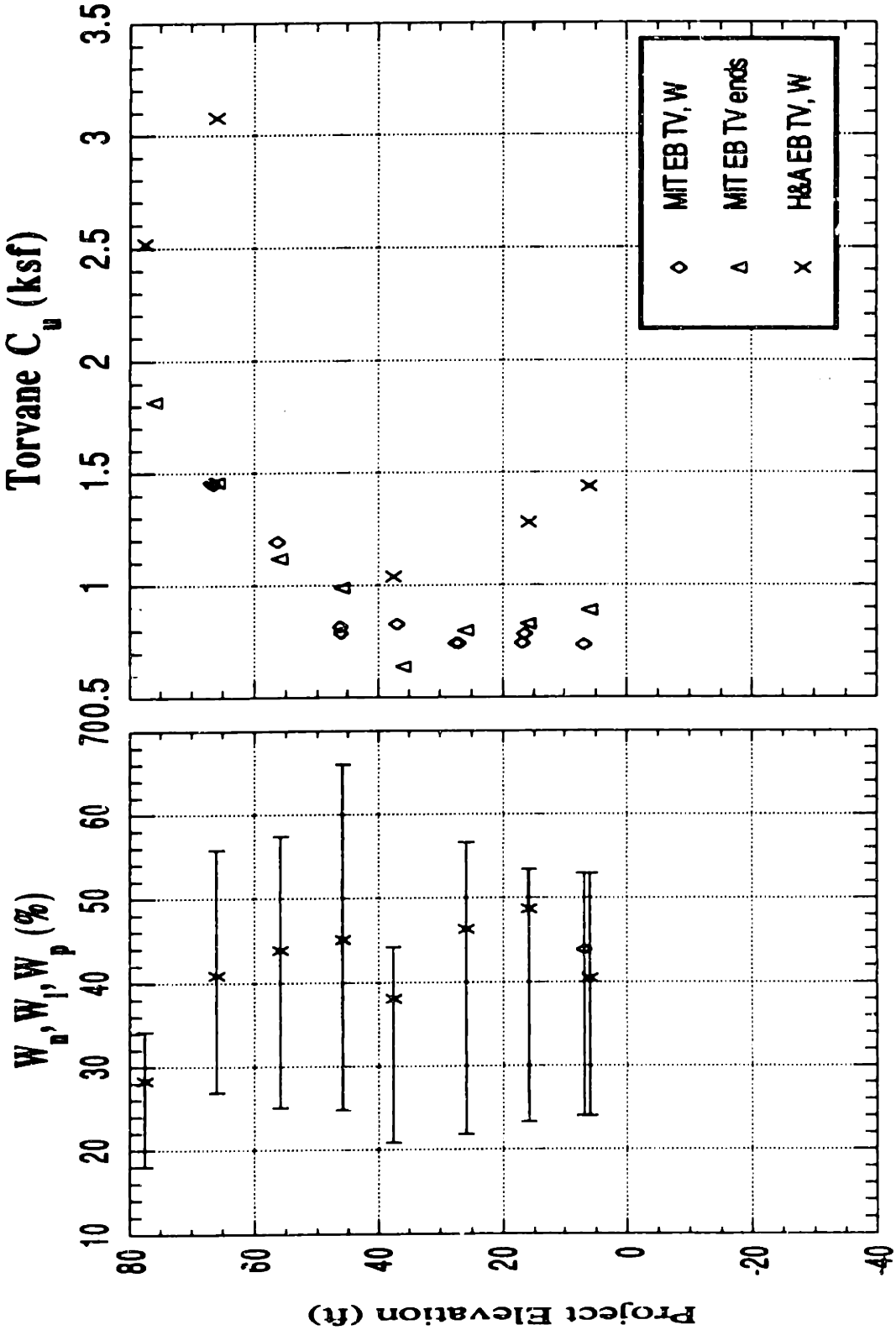

Figure 4-2: East Boston STP: Elevation vs. Water Content and Torvane Strengths

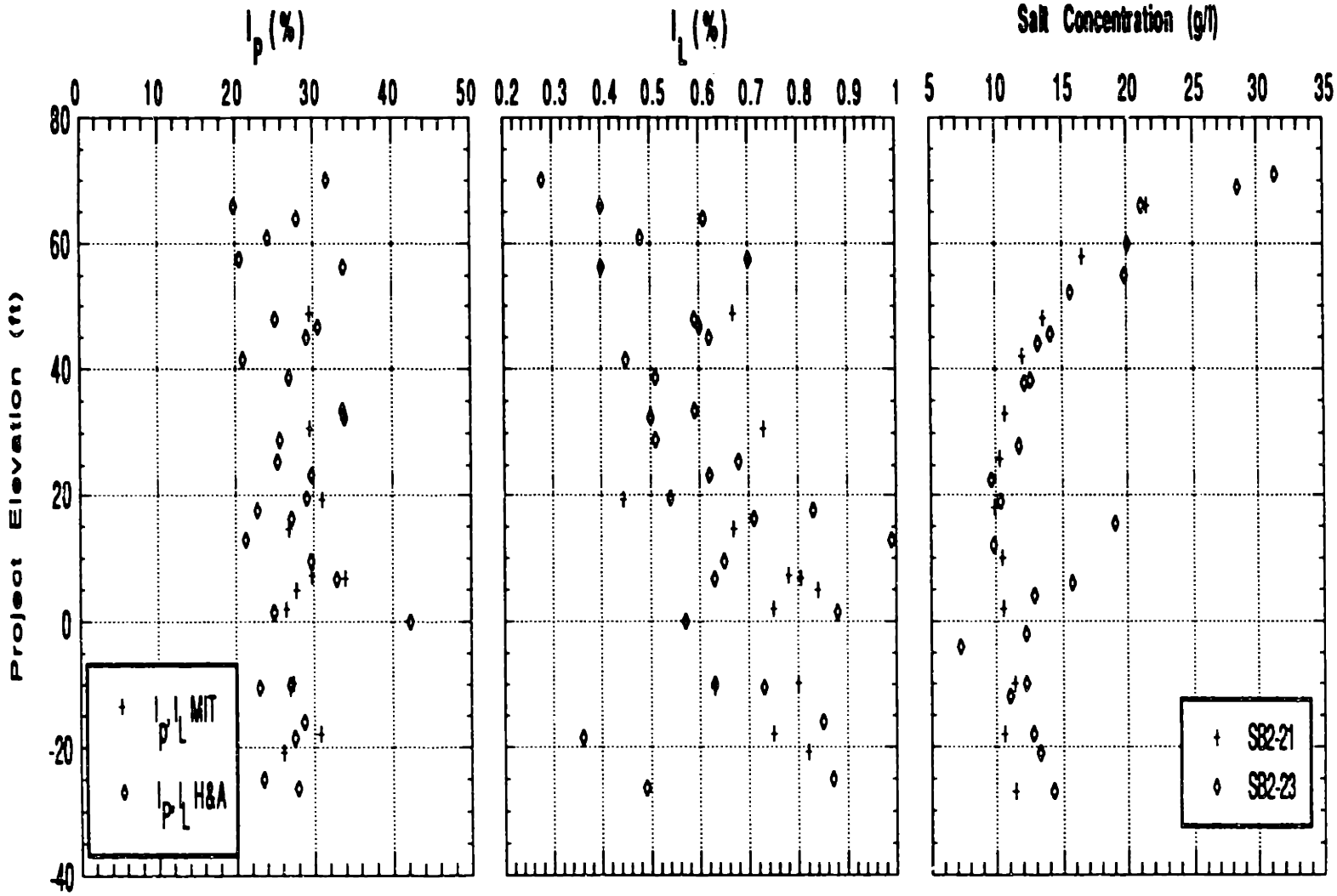

Figure 4-3: South Boston STP: Elevation vs. Plasticity Index, Liquidity Index and Pore Fluid Salt Concentration

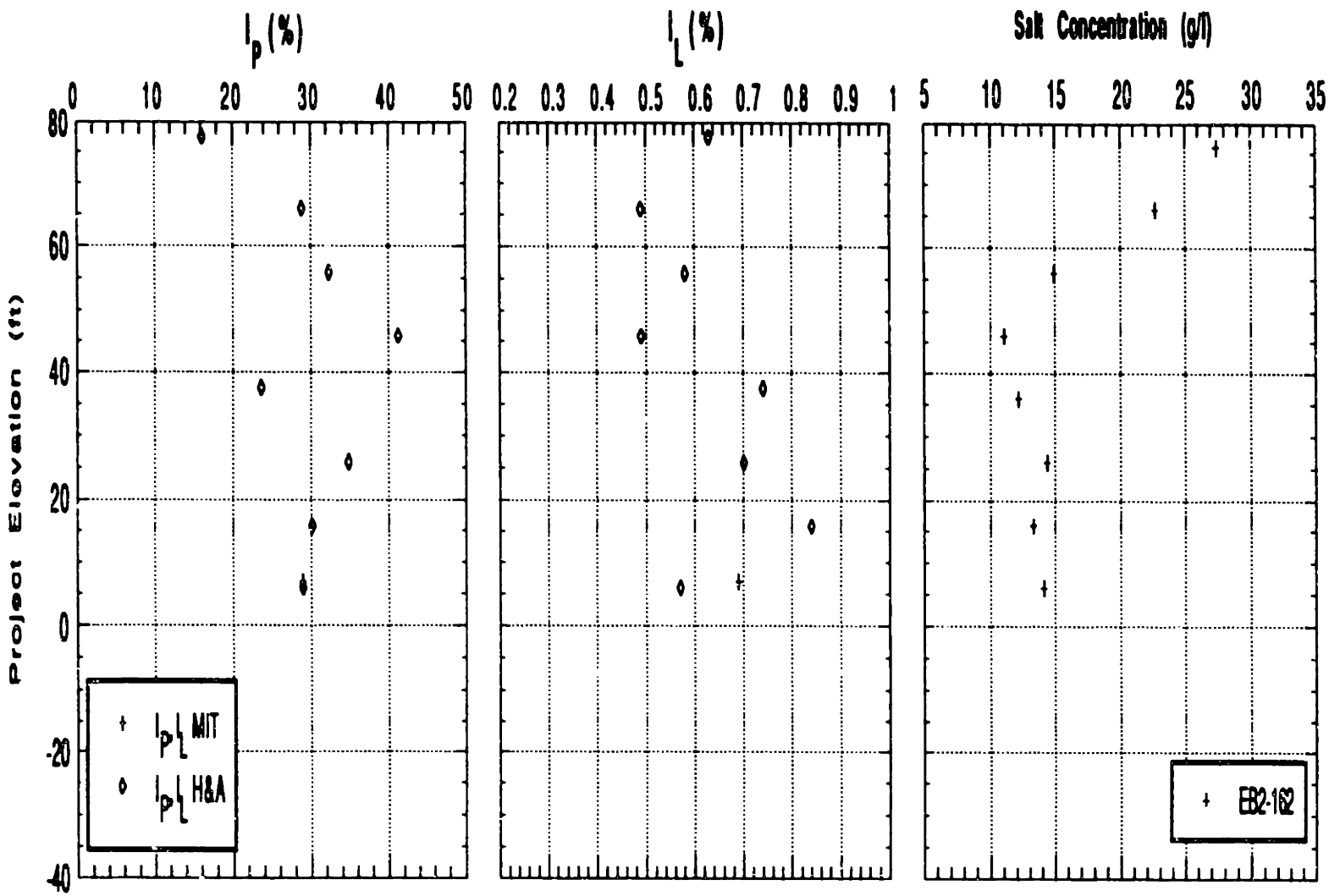

Figure 4-4: East Boston STP: Elevation vs. Plasticity Index, Liquidity Index and Pore Fluid Salt Concentration

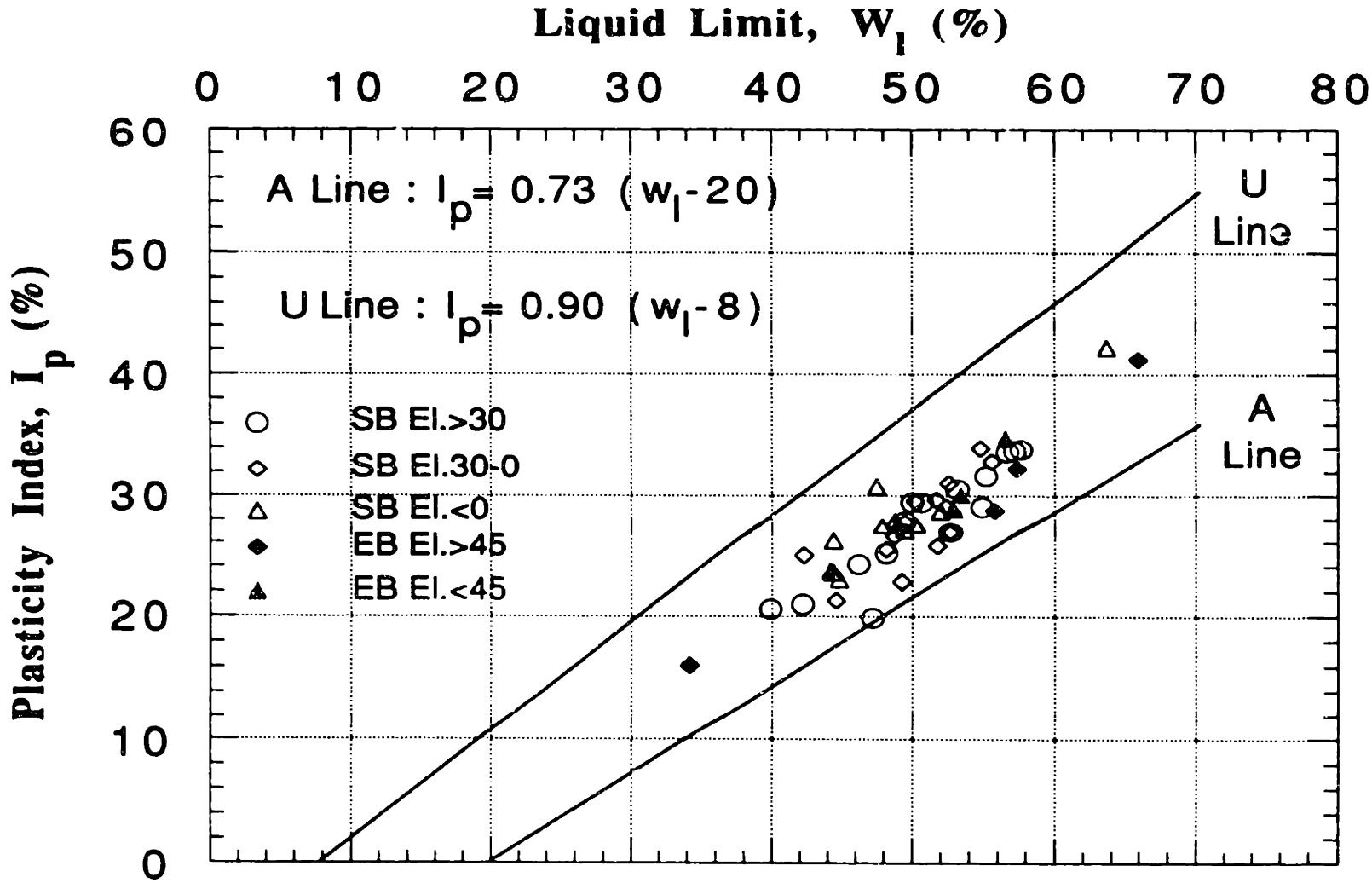

Figure 4-5: South and East Boston STP: Plasticity Chart

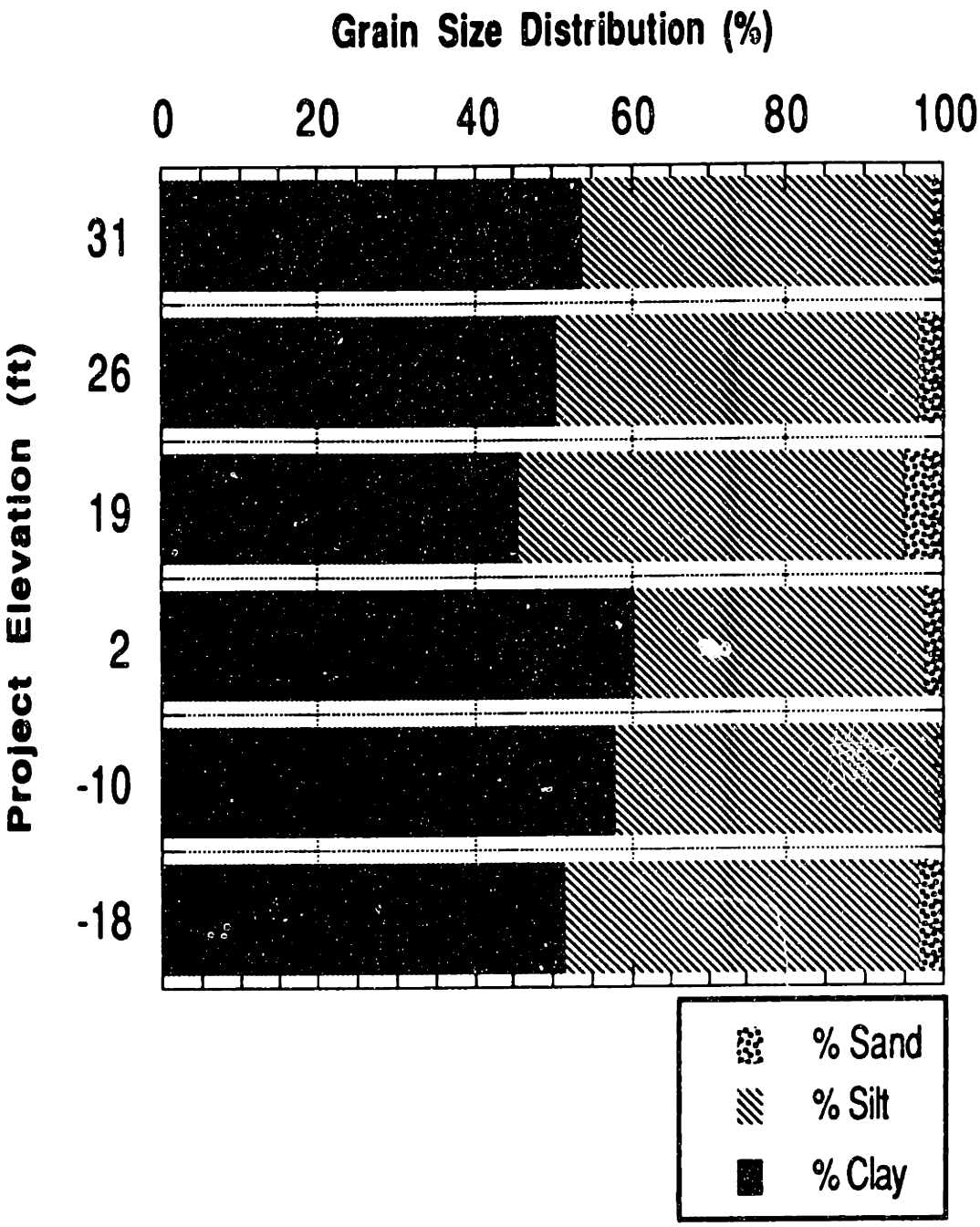

Figure 4-6: South Boston STP: Elevation vs. Grain Size Distribution

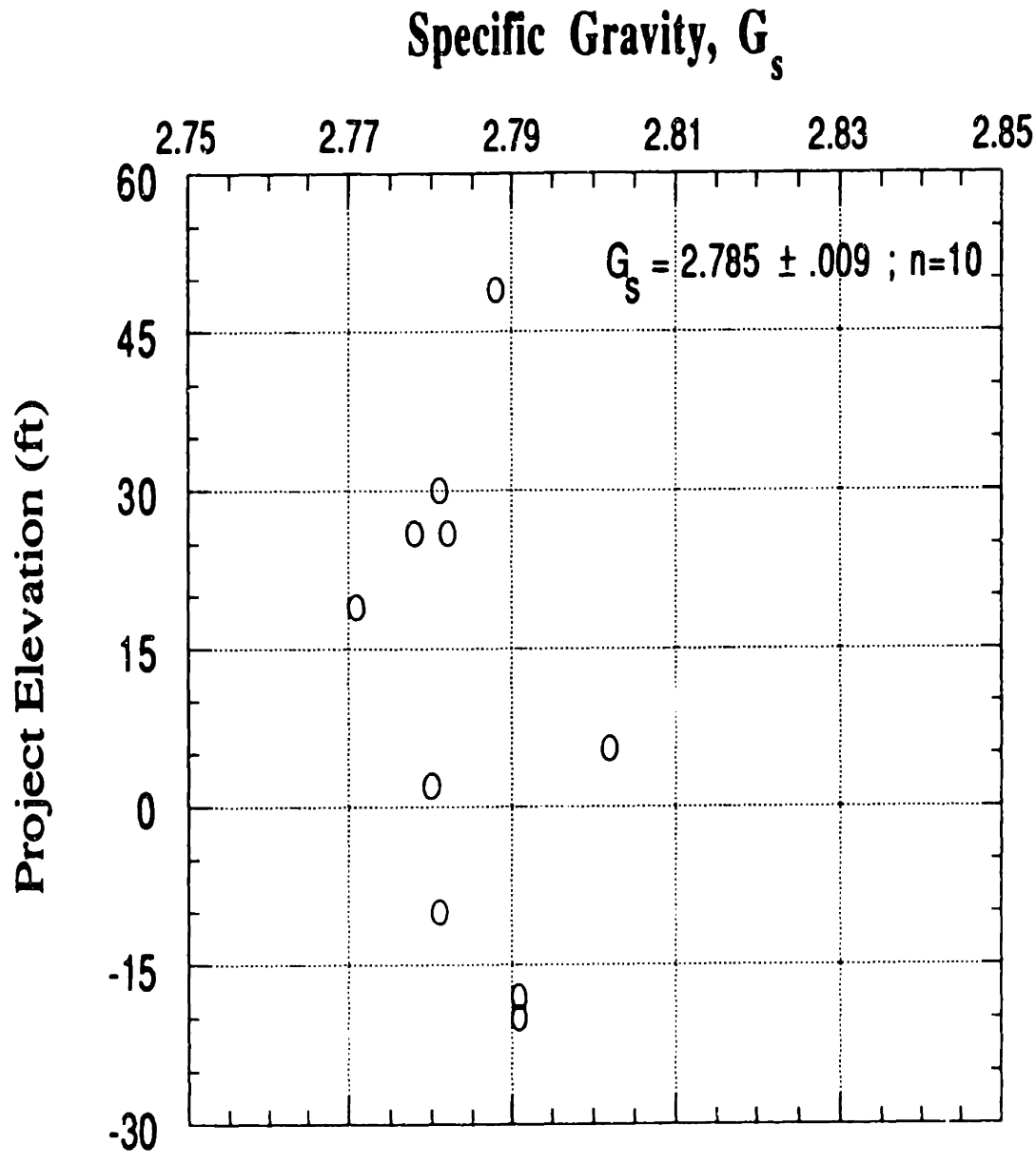

Figure 4-7: South Boston STP: Elevation vs. Specific Gravity

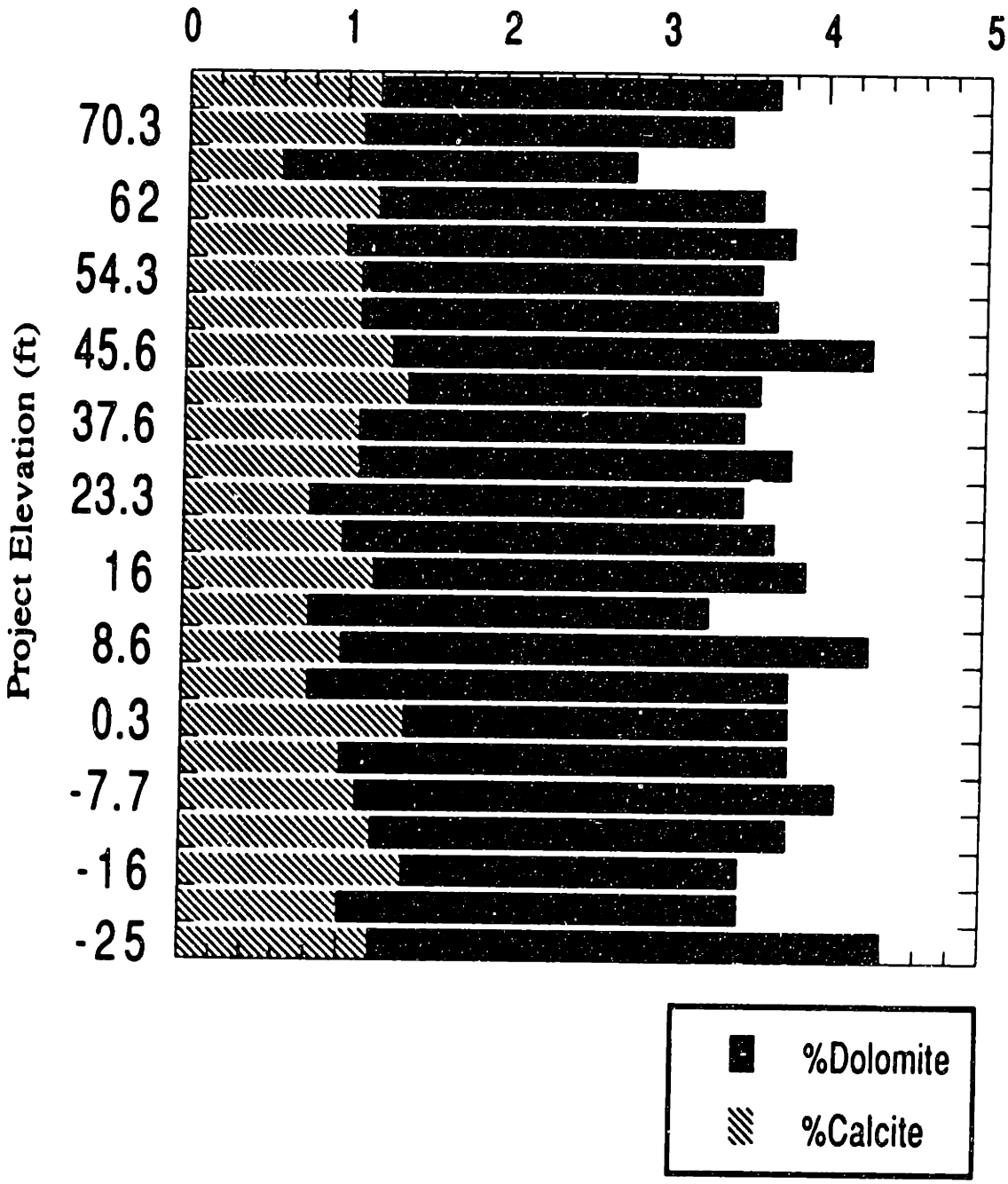

Figure 4-8: South Boston STP: Carbonate Content Profile (by DeGroot, U. Mass., Amherst

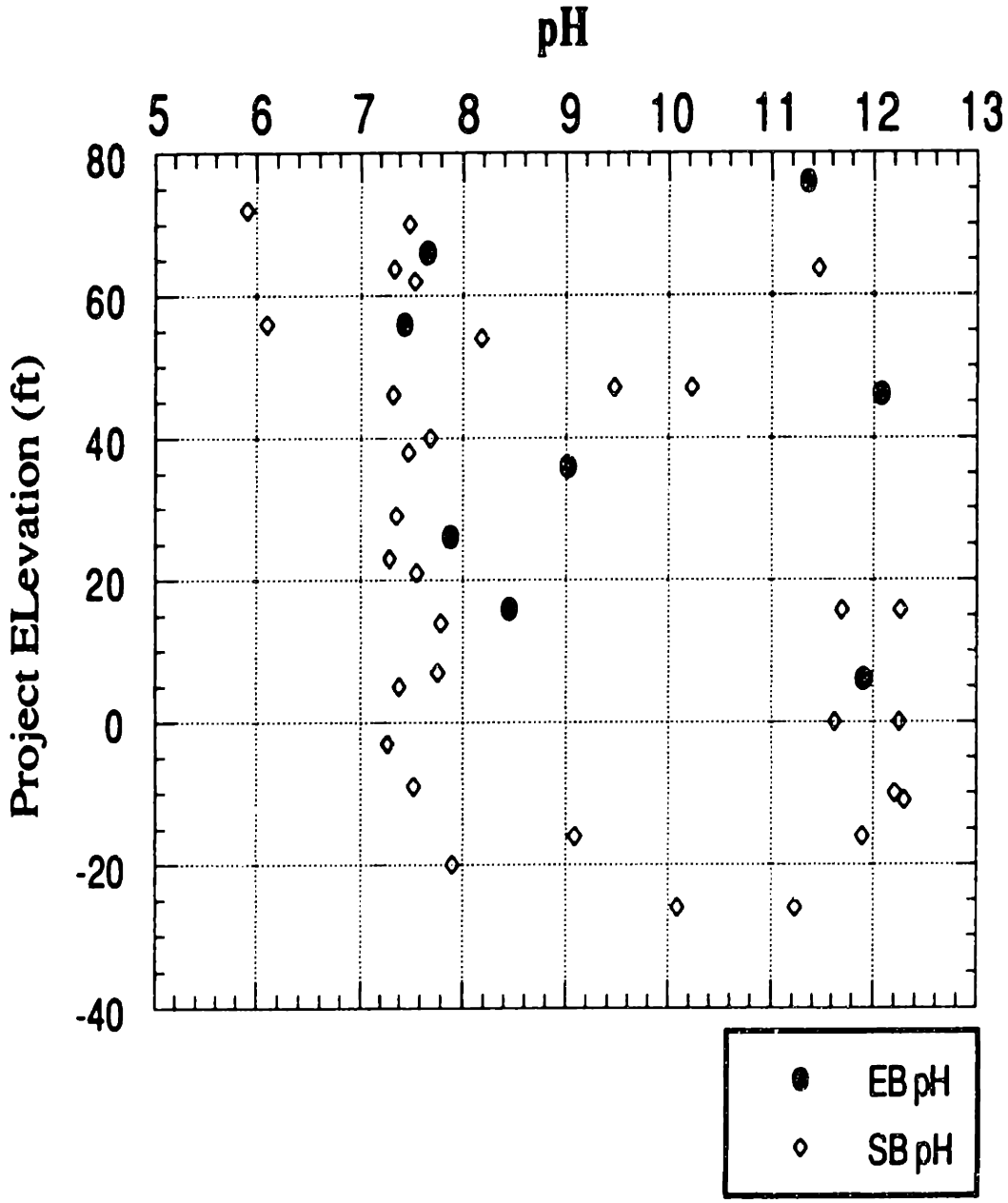

Figure 4-9: South and East Boston STP: Elevation vs. pH

Chapter 5

Evaluation of Stress History and Consolidation Properties

5.1 Introduction

As previously emphasized, establishing the stress history of the sites was an important priority. The bulk of the consolidation data was obtained from the consolidation phase of SHANSEP triaxial tests, but supplemented by standard incremental oedometer tests performed by H&A and several CRSC tests performed at MIT (by Germaine and Associates). The CK_0-TX test also provided information on the K_0 of the soil, with additional data being provided by several LSO tests. This chapter presents a collective summary of consolidation data from all types of tests, as well as some "typical" compression curves and K_0 data. First, however, a few issues relating to the testing technique are covered.

5.1.1 Extrusion Technique

Sample disturbance can severely affect consolidation data. Typically, a disturbed specimen yields a flattened compression curve which results in a higher estimated recompression ratio (RR), a lower estimated virgin compression ratio (CR), and a lower (and/or obscured), preconsolidation pressure (σ'_p). Some of the early results

from H&A's oedometer tests, and MIT's CK_0–TX tests run on South Boston tube samples showed values of σ'_p at the lower elevations that were actually less than the calculated σ'_{v0}. This apparent "underconsolidation" could not be explained by excess pore pressures at the site and was thus attributed to incorrect σ'_p measurements due to sample disturbance.

Specifically, it was felt that the extrusion of the clay from the tubes was causing excessive disturbance, especially for triaxial specimens which were considerably longer (4 inches compared to 1.5 inches) than the oedometer specimens. Accordingly, a new extrusion method, developed by Werner (1991) during a test program on stiff Arctic silt, was adopted. The method consisted of inserting a wire saw into the tube near the edge and cutting around the perimeter of the soil to remove the adhesion between the clay and the tube before attempting to extrude the soil. Subsequent results on samples which did not appear visibly cracked or disturbed were much more reasonable.

5.1.2 Continuous versus Incremental Loading

Another source of ambiguous σ'_p results occurred from the use of incremental loading in the standard oedometer tests. This was especially true for deeper samples that often had slightly S-shaped compression curves. Figure 5-1 illustrates an early oedometer test performed at H&A. Even though the test used a load increment ratio (LIR) of about 0.7 at the higher stresses, the resulting curve is poorly defined in the neighborhood of σ'_p. In fact, the original estimate of $\sigma'_p = 2.4$ ksc was less than the overburden stress of $\sigma'_{v0} = 3.0$ ksc. Figure 5-1 also shows a possible S-shaped compression curve (the dashed line between 2.4 and 4.0 ksc) that would yield a higher and more reasonable value of σ'_p.

Figure 5-2 shows the continuous compression curve from a CK_0–TX test run on a tube sample slightly deeper than used for the oedometer test used in Figure 5-1. This figure illustrates two important points:

1. The deeper BBC often has a highly non-linear, S-shaped virgin compression curve; and

2. Adequate definition of such curves, and hence reliable estimates of σ'_p, will require oedometer tests having very small increments (say a LIR of only 0.1 near σ'_p).

Figure 5-3 shows the curve resulting from a CRSC test. In terms of producing well defined compression curves, the CRSC test is as good as CK_0–TX tests and it has the added advantage of obtaining continuous measurements of permeability (k) and hence coefficient of consolidation (C_v). However, some of the CRSC tests performed on samples taken from the East Boston site gave anomalous results as discussed later. For this reason, and due to problems with the incremental oedometer tests, most of the σ'_p data used to develop stress history profiles at the two test sites came from the numerous compression curves obtained from the SHANSEP tests.

5.1.3 Methods for Estimating σ'_p

Although several methods have been proposed for estimating σ'_p (e.g., Schmertmann, 1955 and Butterfield, 1979). The most widely used is the construction developed by Casagrande (1936). According to the Casagrande technique, σ'_p is defined by the intersection of two lines: 1) the bisector of the angle defined by a horizontal line through the minimum radius of curvature on the curve and a line tangent to the curve at that point, and 2) the extension of the virgin compression line (VCL). An example of this type of construction is shown in Figure 5-4. One disadvantage of this method is that it often requires considerable judgement on the part of the engineer, and different interpretations of the same curve are common.

Recent work by Becker et al. (1987) makes use of strain energy considerations to estimate the preconsolidation pressure. To use the strain energy (SE) method, one plots the strain energy, or work per unit volume of each increment, calculated as:

$$W = \int \sigma'_v d\epsilon_v = \sum(\sigma'_{vc_{ave}} \times \Delta\epsilon_v) \tag{5.1}$$

where $\sigma'_{vc_{ave}}$ is the average vertical effective stress on the specimen during the given increment, and $\Delta\epsilon_v$ is the change in *natural* strain (i.e., $\Delta H/H$) over the increment

versus σ'_{vc}, the final consolidation stress for each increment. The resulting curve resembles an inverted compression curve and σ'_p is defined by the intersection of a line extending the initial "straight line" portion of the curve with the line defining the *maximum* slope of the virgin compression line (VCL),as demonstrated in Figure 5-5.

This new method was applied to most of the high quality compression curves for the upper crust of the two deposits. The results for South Boston are compared with σ'_p estimated via the traditional Casagrande method in Figure 5-6. As shown, there is very good agreement between σ'_p estimated from the two methods, though in general, the strain energy yields slightly lower values as seen in Figure 5-6.

There are advantages to both methods. The strain energy method has a sounder "theoretical" basis, can be easily computerized and probably requires less judgement when applied to curves on stiff clay. But the Casagrande construction is simpler,much more widely used, and has a strong "empirical" basis. For the consolidation tests performed at MIT, the Casagrande construction was used on all of the tests, and the strain energy method on about one third of the tests. When the two methods yielded different estimates of σ'_p, an average of the two values was generally selected.

Table 5.5 summarizes the values of σ'_p used to develop the stress history profile for South Boston that was needed for interpretation of the CK_0U triaxial tests performed with the Recompression technique. The SM thesis by de La Beaumelle presents complete results from the consolidation phase of the SHANSEP triaxial tests at both sites and H&A (1991) does likewise for the oedometer and CRSC tests.

5.2 Typical Results from CK_0–Triaxial Tests

5.2.1 Typical Compression Curves

Figure 5-7 shows triaxial 1-D compression curves from three normally consolidated tests on SB tube samples from different elevations. These curves illustrate the different shapes encountered; linear VCLs, like TX029, or S-shaped like the other two. The curve labeled TX029, from El. 52.4 ft, has a constant virgin compression ratio (CR)

of 0.19 and a preconsolidation pressure (σ'_p) of 6.35 ksc (13.0 ksf). Test TX060, from El. 14.6 feet shows a distinct double curvature and CR decreases from a maximum of about 0.6 near σ'_p = 3.0 ksc, to a minimum of 0.24 at σ'_{vm}. The deepest sample is TX015 at El. -20.8 ft. The CR just beyond σ'_p = 4.2 ksc is about 0.5, decreasing to 0.21 at σ'_{vm}.

Both of the lower curves are distinctly S-shaped. While there's no clear trend of increasing CR_{max} with depth, most of the tests performed on specimens taken below El. 20 (which is just above the bottom of the desiccated crust) at SB yielded S-shaped curves. Similarly, the compression curves of the tests performed at East Boston tend to change from linear to S-shaped at El. 40, corresponding to the bottom of the crust at that site.

5.2.2 Typical K_0 Data

Figure 5-8 shows a K_0 versus log σ'_{vc} plot from a typical, high quality, overconsolidated SHANSEP test. K_0 starts from a value of approximately 1 and decreases during loading to near the preconsolidation pressure. K_0 then increases and remains more or less constant during virgin consolidation (typically about 0.56). When the sample is allowed to swell one-dimensionally to the specified OCR, the K_0 value increases as the OCR increases. Figure 5-9 plots the value of K_0 versus log OCR during this unloading.

Each overconsolidated SHANSEP test yields two important aspects about K_0: the normally consolidated K_0 value, and a relationship between K_0 and OCR. Knowledge of this second relationship is crucial for the performance of Recompression triaxial tests since each test is consolidated to stresses determined by the K_0 corresponding to the OCR selected for each test. Another way to determine this relationship in the laboratory is by using the lateral stress oedometer (LSO), which is covered in Section 5.5 of de La Beaumelle's thesis.

It should be emphasized that one-dimensional reconsolidation of overconsolidated clay to the in situ OCR will result in values of horizontal stress σ'_{hc} that are generally much too low. This is illustrated in Figure 5-8 by the very low values of K_0 during

recompression. This is why Recompression tests require an estimate of the in situ K_0 versus OCR relationship.

5.3 Stress History Profiles

One of the first and most important tasks of the laboratory portion of H&A's STP was to establish reliable stress history profiles at both sites. The stress history of the deposit is needed for at least three important reasons. First, strength of the clay at any point in the deposit is directly related to its in situ OCR via the SHANSEP equation:

$$c_u/\sigma'_{vc} = S(OCR)^m \tag{5.2}$$

Secondly, the in situ OCR an σ'_p are needed both to properly run and to interpret results from Recompression strength test. And thirdly, the same information is essential for evaluation of the various in situ tests conducted as part of the STP.

Thus knowledge of the preconsolidation pressure of the clay at every elevation is vital, and as discussed above, the greatest care was taken to achieve the best possible estimates of σ'_p through use of continuous loading consolidation tests, high quality soil specimens, and different graphical estimation techniques.

As covered in Chapter 2, the Boston Blue Clay found at both the South and East Boston sites is a marine clay deposited after the most recent glaciation of the area. According to Kenney (1964) the clay deposit would be expected to have an eroded and/or weathered top surface, while the lower part of the deposit might be slightly overconsolidated depending upon the amount of erosion and deposition which occurred. As is shown in the following sections, this prediction fits very well with the stress history profiles developed for each site.

5.3.1 South Boston Stress History

Figure 5-10 shows results from CK_0-TX, CRSC and standard oedometer tests performed on both tube and block samples at the South Boston site. The points on this

plot include only the Good or better quality tests with the exception of three Fair quality TX tests, and one Fair oedometer test. The preconsolidation pressures for each type of test and sample are shown with a different symbol. The lines resulting from a linear regression of the points are also shown. Linear regression on 31 tests from El. 18 ft gave

$$\sigma'_p(ksf) = 3.45 + 0.170El.(ft) \tag{5.3}$$

with r^2=0.72 and linear regression on 17 tests from below EL. 15 ft gave

$$\sigma'_p(ksf) = 7.37 - 0.050El.(ft) \tag{5.4}$$

with r^2=0.73. Calculations of σ'_p for use in the Recompression testing program used Eq. 5.3.

As shown in the figure, there is a fairly sharp definition of the bottom of the desiccated crust near El. 20 ft. Below that elevation the clay is very lightly overconsolidated, indicating that over the years, erosion has slightly exceeded deposition in this area.

5.3.2 East Boston Stress History

Figure 5-11 shows the stress history at the East Boston site based on σ'_p data from oedometer and CK_0–TX tests. The profile of σ'_p is similar to South Boston, and fairly well defined despite the fact that there are significantly fewer data points than for the South Boston site. At East Boston El. 30 marks the approximate bottom of the desiccated crust, and results from five SHANSEP triaxial test indicate that the lower clay is slightly overconsolidated.

The reason there are fewer data points for East Boston is mostly due to the organization of the testing program: tests on East Boston were meant to be primarily for confirmation of the more extensive South Boston results, and thus far fewer tube samples and consolidation tests were planned. Moreover, some of the results from tests on East Boston samples are not shown. In particular, several CRSC tests gave

extremely inconsistent results, with values of σ'_p from adjacent specimens in the same tube different by a factor of two in some cases. These differences have not yet been resolved, and thus the results are not presented.

5.4 Compressibility and Flow Properties

In depth discussion of the compressibility and flow properties is beyond the scope of the MIT contract and of this thesis. However, the maximum virgin compression ratio (CR_{max}) and the value at σ'_{vm} ($CR_{\sigma'_{vm}}$) were obtained for each triaxial test and are plotted versus elevation in Figure 5-12 for South Boston, and in Figure 5-13 for East Boston. In these figures, where a single vertical mark is shown, the CR was constant at that value, and where there are two tick marks, they indicate CR_{max} and $CR_{\sigma'_{vm}}$. Thus the longer the horizontal line connecting the two marks, the more pronounced the curvature of the VCL.

As indicated in Figure 5-12, the highest CR_{max} values (hence most pronounced S-shape) occur between El. 20 and 0 ft, approximately. For reference, typical CR values for low OCR sedimentary CL and CH clays are 0.25±0.10 and 0.35±0.10, respectively. Hence the existence of CR_{max} values that frequently exceed 0.4, combined with strong curvature of the VCL suggest that the lower portion of the deposit has a significant "structure" in spite of having a relatively low liquidity index (0.8±0.1 – see Figure 4-3). Most previous tests on soft BBC in South Boston have not shown this "structured" behavior, perhaps because these data came from incremental tests on samples of lower quality.

The East Boston data in Figure 5-13 show a similar increase in CR_{max} and curvature below the crust, though less pronounced than for South Boston. This may reflect either a less structured clay or fewer tests being run on samples of somewhat lower quality.

The next figures present information on measured axial strain at the overburden stress. Figure 5-14 plots data at South Boston from CK_0–TX tests and from typical "Good" and "Disturbed" oedometer tests, and Figure 5-15 does likewise for East

Boston. Four important conclusions can be surmised from these data.

1. There is a consistent trend of increasing strain with depth, as would be expected from the larger stress relief during sampling.

2. The axial (vertical) strains at σ'_{v0} form the oedometer tests are consistently higher than those from the CK_0–TX test. Much of this difference is probably due to the larger specimen size which reduces disturbance due to trimming.

3. "Excessive" strains at the overburden stress is a good indication of excessive sample disturbance that usually gave low σ'_p values. This occasionally occurred for the triaxial tests (specimens taken from high quality zones of the tube based on the radiography records) and more frequently for the oedometer tests (specimens sometimes taken from the ends of the tube to expedite testing).

4. The tube and block samples taken within the crust of the South Boston deposit are both of high quality based on the CK_0 strain data, and the block samples are not significantly stiffer than the tube samples.

Based on preliminary data from oedometer and CRSC tests provided by Ms. Young of H&A, the *normally consolidated* value of the coefficient of consolidation (C_v) at both sites decreases with depth within the crust, and then becomes more or less constant. Typical values of C_v(NC) are:

- Within the crust, $C_v(NC) = 20 \pm 10 \times 10^{-4}$ cm^2/sec
- Below the crust, $C_v(NC) = 7 \pm 3 \times 10^{-4}$ cm^2/sec

For swelling of clay below the crust, C_v values on the order of $50 \pm 20 \times 10^{-}4$ cm^2/sec appear typical.

5.5 Determination of K_0 for Recompression Tests

For Recompression test, one chooses not only the vertical, but also the horizontal effective stress to which the sample is consolidated. The horizontal effective stress is

determined by multiplying σ'_{vc} by K_0. The appropriate K_0 is chosen to correspond to the OCR of the soil. Originally, the idea was to simulate the in situ stresses, and thus σ'_{vc} was set to σ'_{v0} and the in situ K_0 was used to calculate σ'_{hc}. In addition to tests at the in situ stresses, however, tests at varying values of σ'_{vc} (and thus varying OCRs) were also run.

It is possible to measure K_0 in the field by use of various in situ instruments, such as earth pressure cells, but it is even more useful to determine K_0 in the laboratory during unloading and reloading for CK_0–TX of LSO tests, in order to establish a K_0 versus OCR relationship. Then simply knowing the OCR of the sample (e.g., for the stress history profile) enables one to choose K_c, and thus σ'_{hc}.

Such a relationship was established for the soil at the South Boston test site, using CK_0–TX and LSO tests. Section 5.5 of de La Beaumelle's thesis describes in detail how these K_0 measurements were obtained. He presents results from all of the STP tests and compares these results with previously published data and correlations. The reader is referred to Mr. de La Beaumelle's for full coverage of this topic.

Figure 5-16 presents the log-linear K_0 versus OCR relationship which was used to determine the K_c to which the Recompression tests were consolidated. It is based on early results from both CK_0–TX and LSO tests. Based on the elevation of each test, σ'_p and OCR were determined from Equation 5.3 and used with Figure 5-16 to choose K_c.

Table 5.1: Values of σ'_p Used for South Boston Stress History Profile

Oedometer			CK_0-TX			CRSC		
No.	El.(ft)	σ'_p(ksf)	No.	El.(ft)	σ'_p(ksf)	No.	El.(ft)	σ'_p(ksf)
Tube Samples – Elevation≥15 feet								
1	65.9	18.5±1.0	004	30.7	8.7	11	22.6	7.1±0.1
2	57.6	11.2±1	005	30.3	8.7			
3	47.9	8.5±0.5	008	33.6	9.2±0.2			
14	63.4	13.0±0.5	009	19.3	7.1			
15	55.8	14.3±0.5	011	26.0	6.65			
16	46.1	10.3±0.3	012	46.7	12.5±0.2			
17	38.1	9.5±0.3	014	48.8	9.45±0.1			
18	31.8	10.4±0.3	023	19.8	7.3			
19	22.8	6.45	026	28.2	9.5			
			029	52.4	13.0±0.6			
			034	39.4	10.65			
			035	39.0	11.0±0.2			
Tube Samples – Elevation < 15 feet								
12	-26.4	8.4±0.4	001	2.0	7.3	9	-17.5	8.8±0.2
21	6.1	6.6±0.1	002	-17.9	7.9	10	9.8	6.8
			006	3.2	7.6	19	4.0	6.75±0.15
			015	-20.8	8.6			
			016	5.5	7.6			
			018	-20.3	8.3			
			019	-16.4	7.7			
			020	-20.1	9.0			
			022	12.3	6.35			
			030	-9.2	7.4			
			031	-9.0	7.8			
			060	14.6	6.15			
Block Samples								
27	45.0	10.4±0.6	067	20.2	6.6	24	55.1	11.05
28	54.5	15.9±0.5	071	20.2	6.5	30	55.1	11.65
29	41.6	9.0±0.2	072	20.2	6.45			
30	34.3	11.5±0.3	081	41.8	9.7			

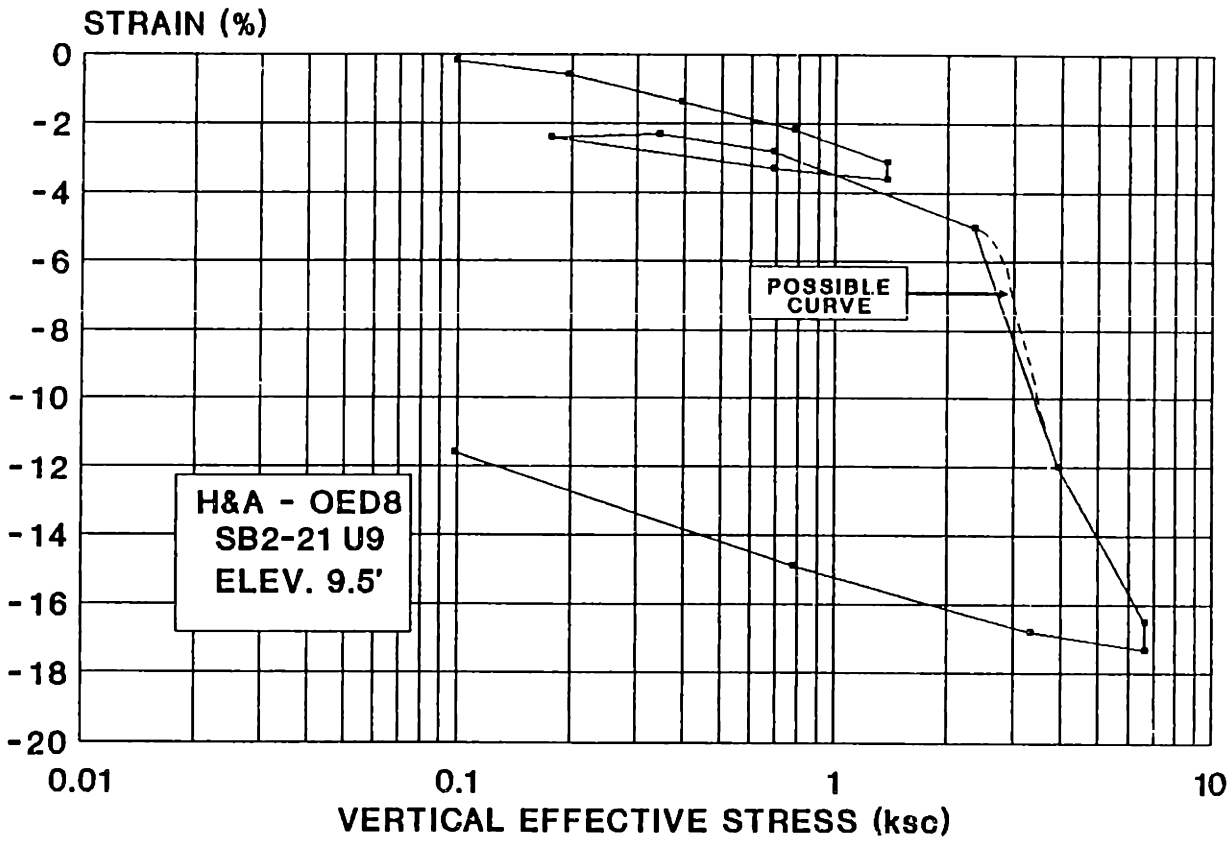

Figure 5-1: Compression Curve from Early Standard Oedometer Test by H&A (Note: End of primary (EOP) strains plotted for test with one day increments)

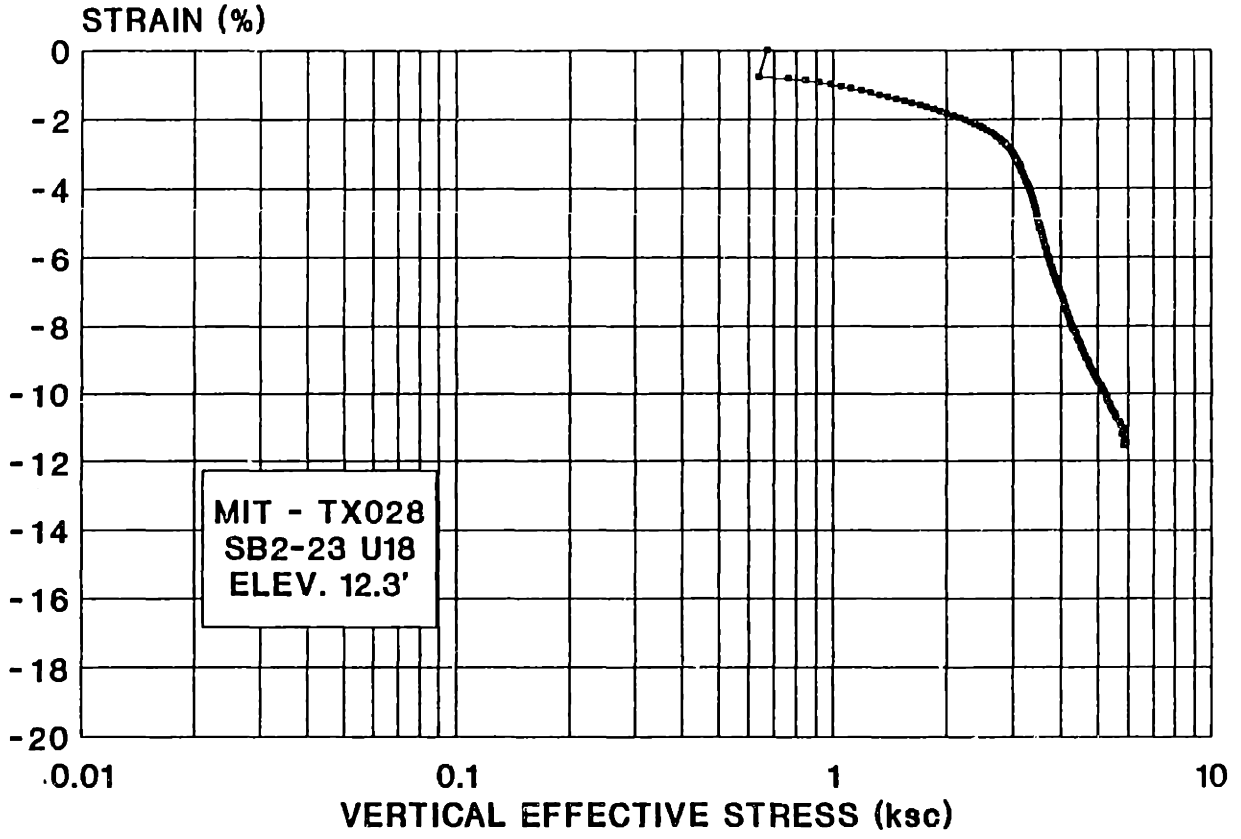

Figure 5-2: Example of Continuous Compression Curve from CK_0–TX Test (σ'_{v0} = 2.79 ksc; σ'_p = 3.1 ksc; OCR = 1.11)

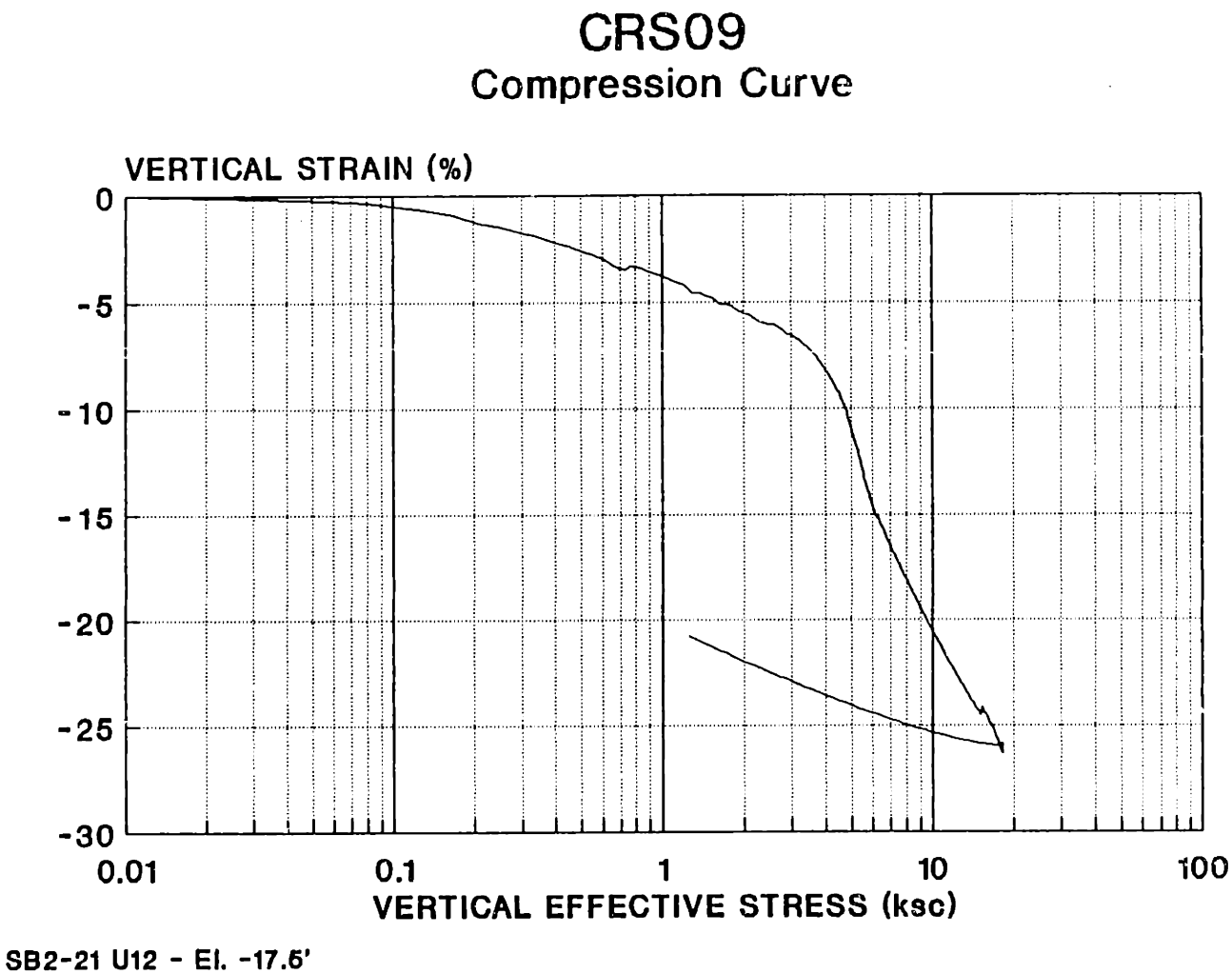

Figure 5-3: Example of Continuous Compression Curve from CRSC Test (σ'_{v0} = 3.62 ksc; σ'_p = 4.3 ksc; OCR = 1.19)

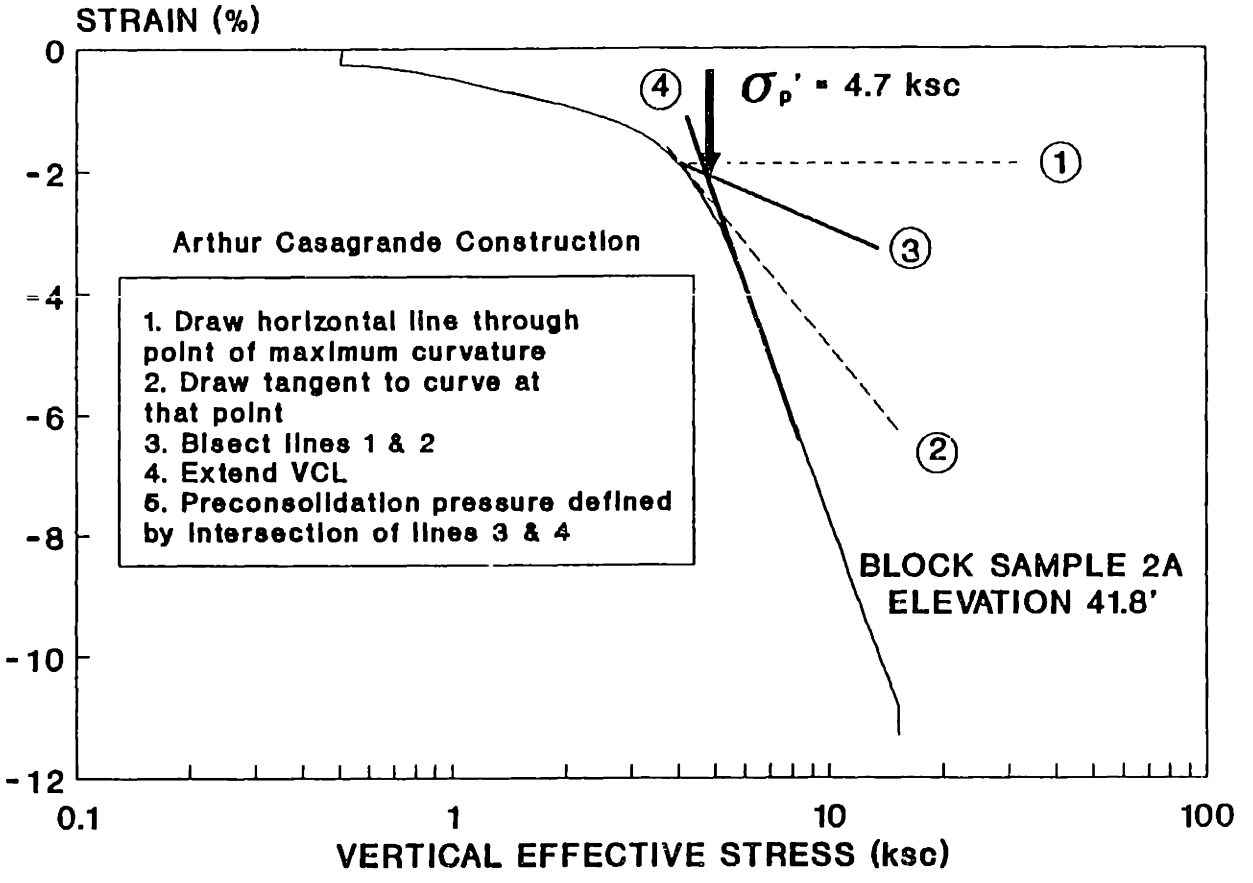

Figure 5-4: Example of Arthur Casagrande σ_p' Construction From CK_0–TX081

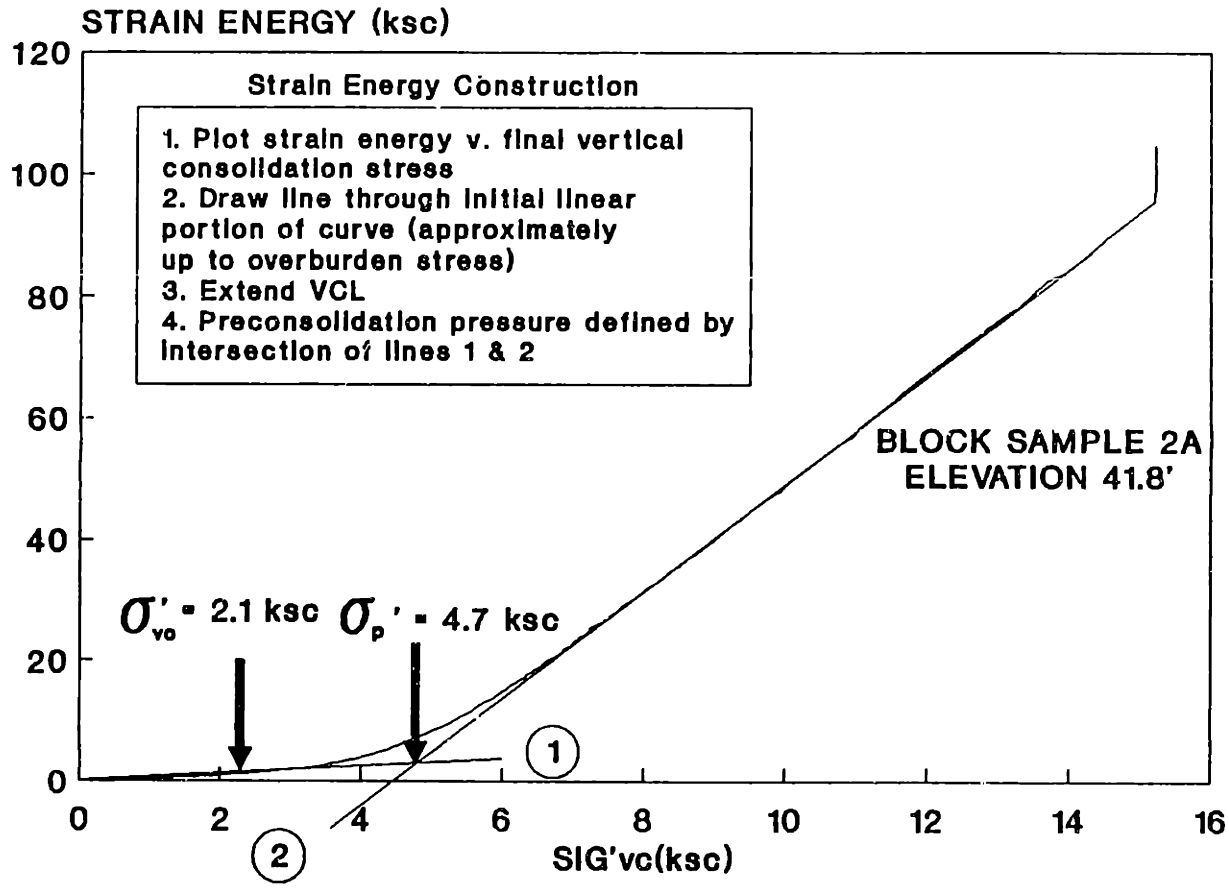

Figure 5-5: Example of Strain Energy σ'_p Construction From CK_0–TX081

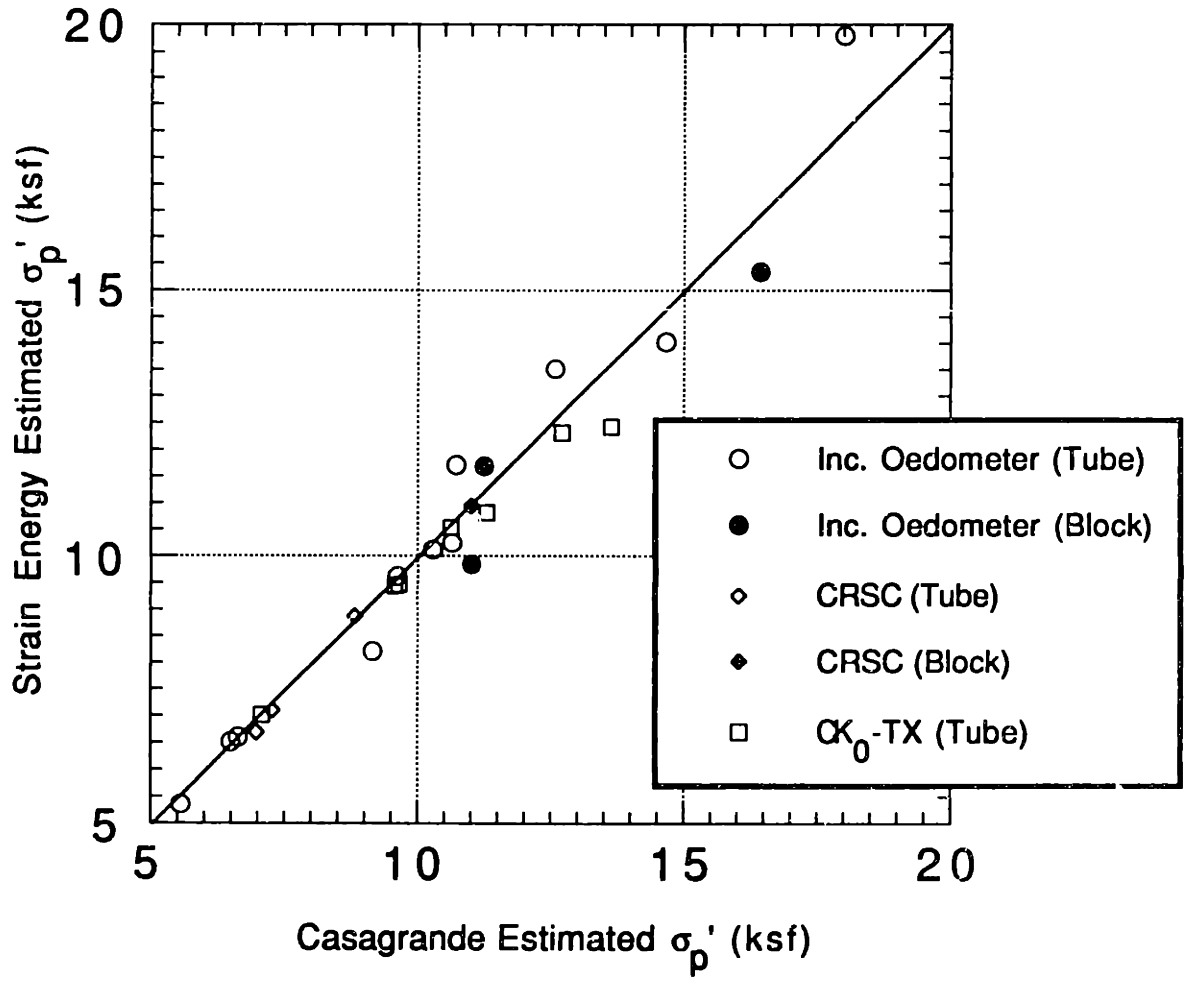

Figure 5-6: Comparison of Estimation of σ'_p from Strain Energy and Casagrande Methods from South Boston Consolidation Tests

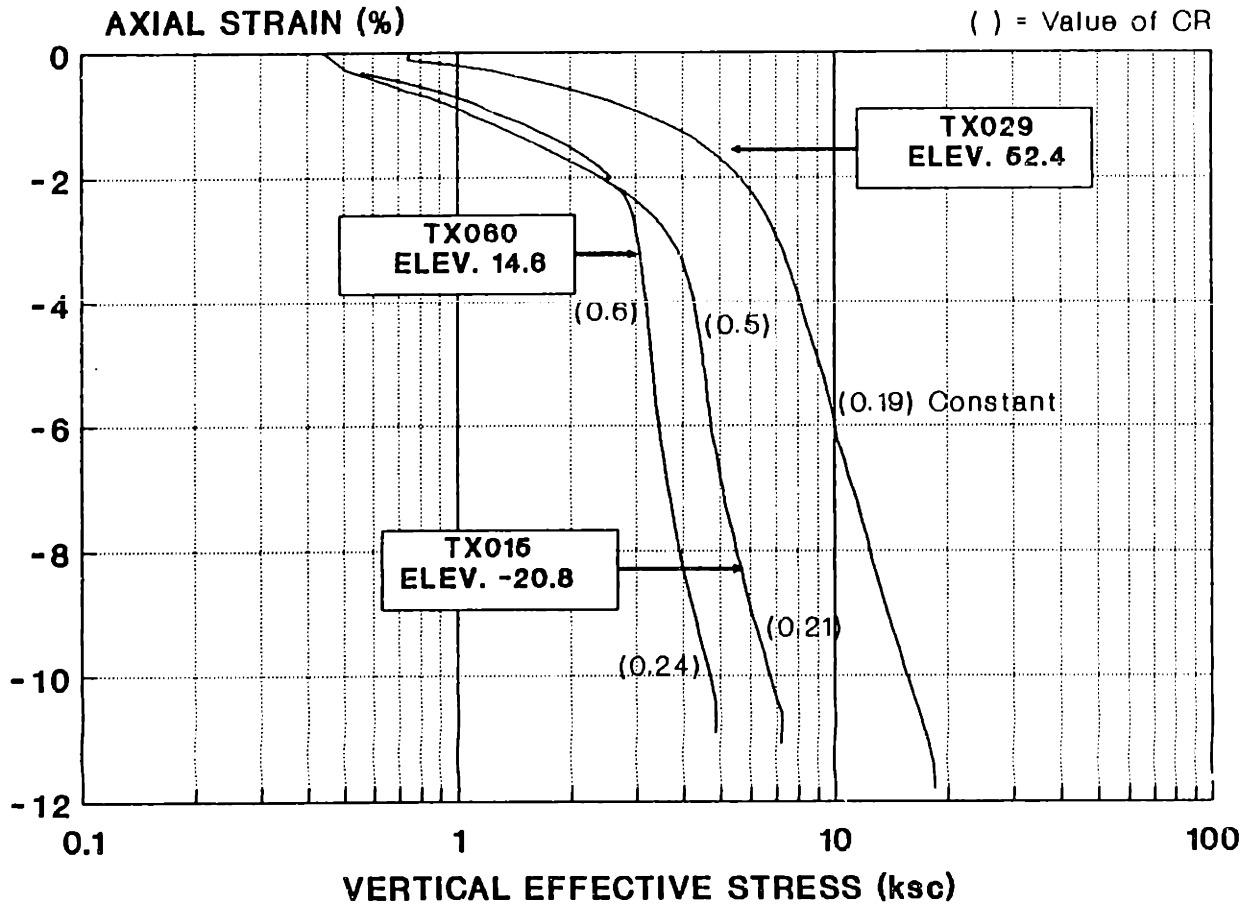

Figure 5-7: Comparison of Compression Curves from South Boston Tube Samples at Different Elevations

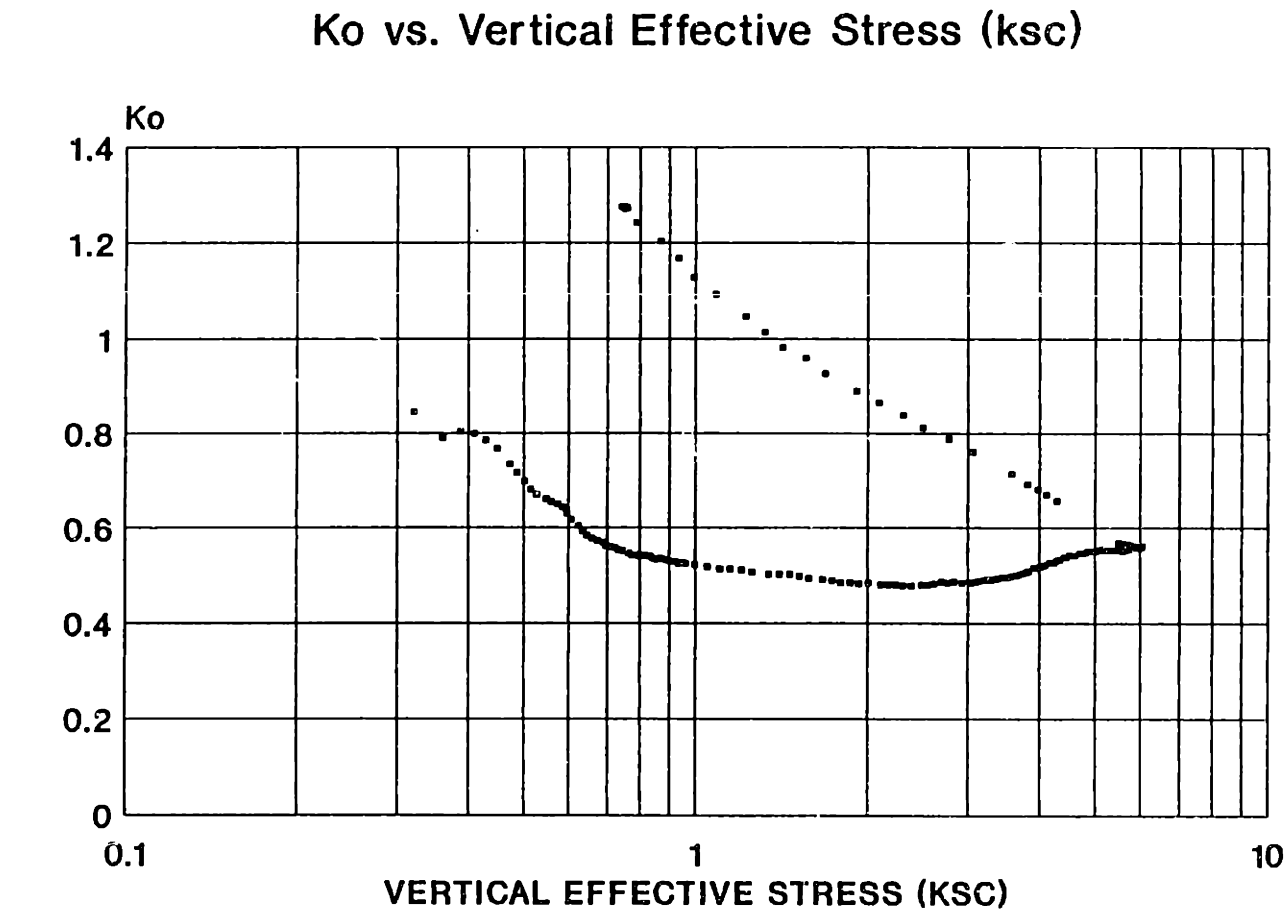

Figure 5-8: Typical K_0 Data from CK_0–TX Test (σ'_{v0} = 3.59 ksc)

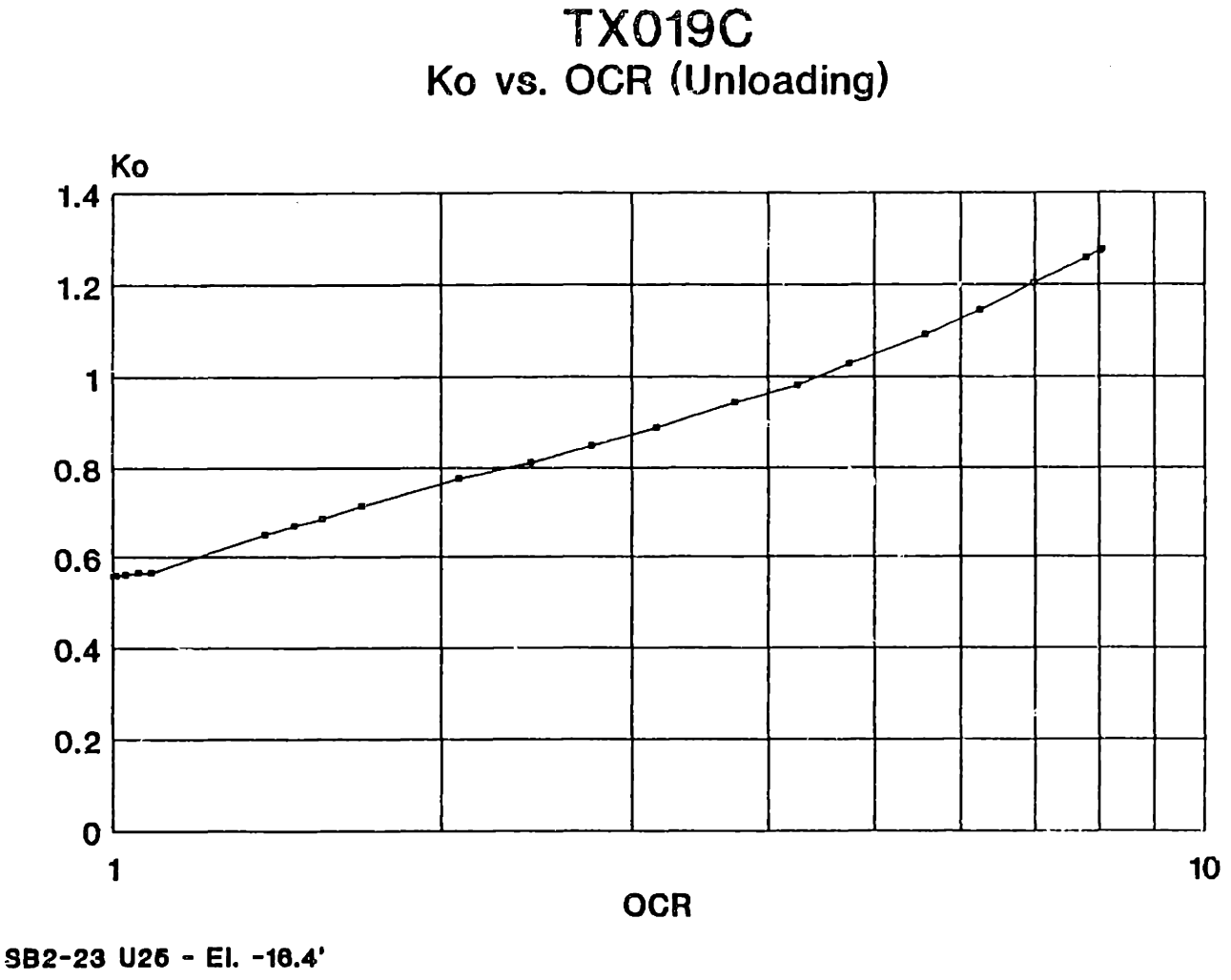

Figure 5-9: Typical K_0 vs. OCR Data from CK_0–TX Test

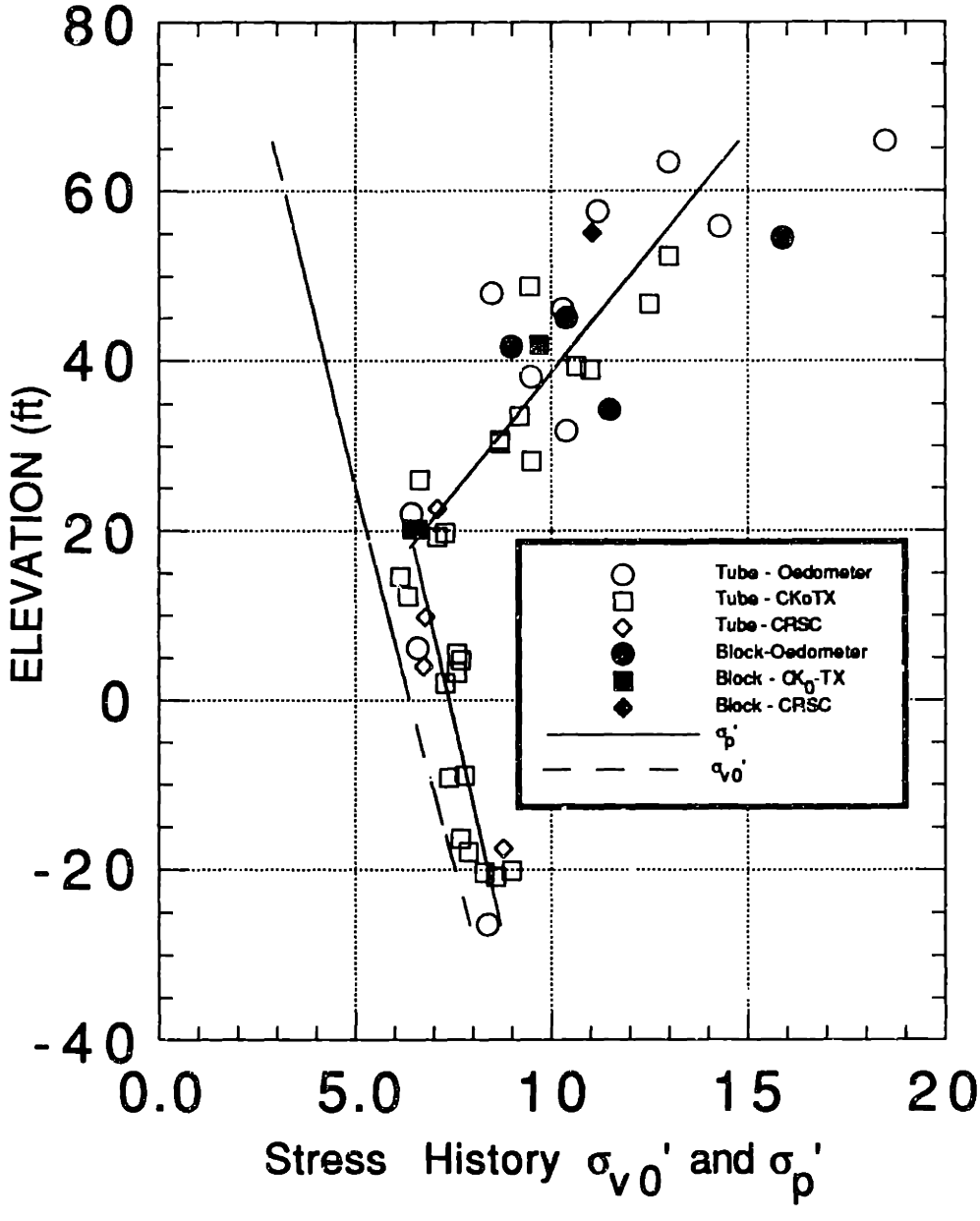

Figure 5-10: South Boston Stress History

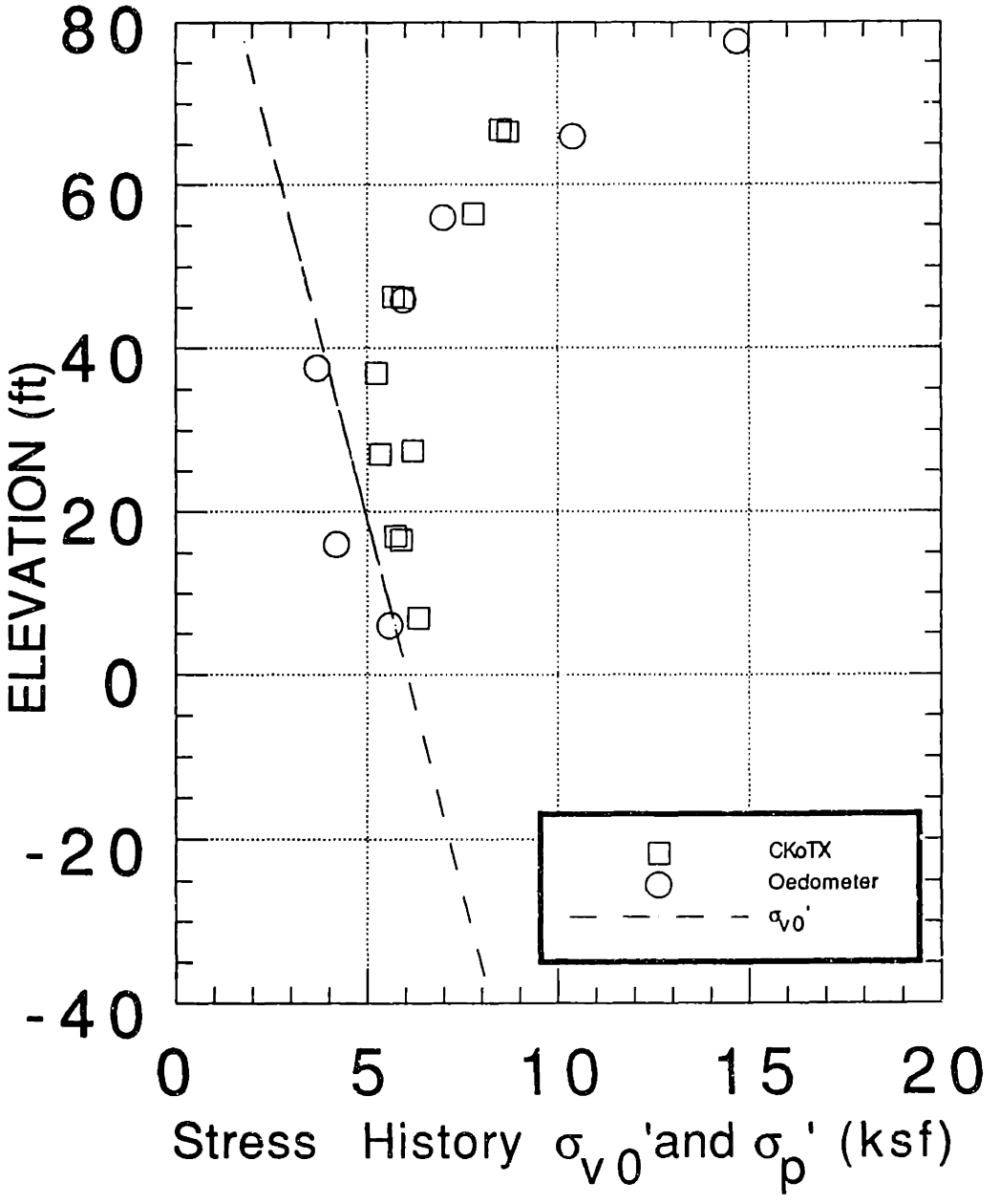

Figure 5-11: East Boston Stress History

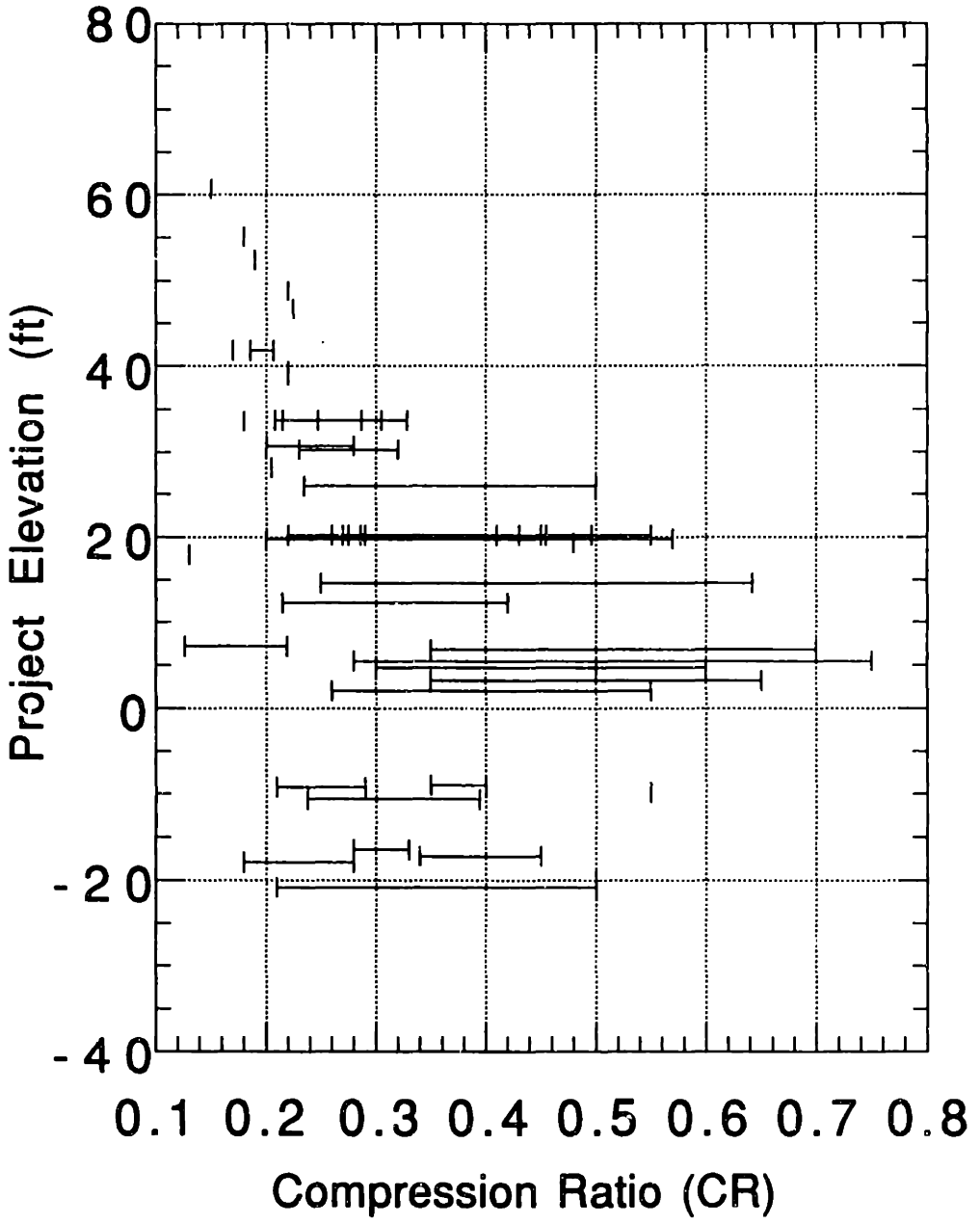

Figure 5-12: South Boston Elevation vs. Virgin Compression Ratio for CK_0–TX Tests

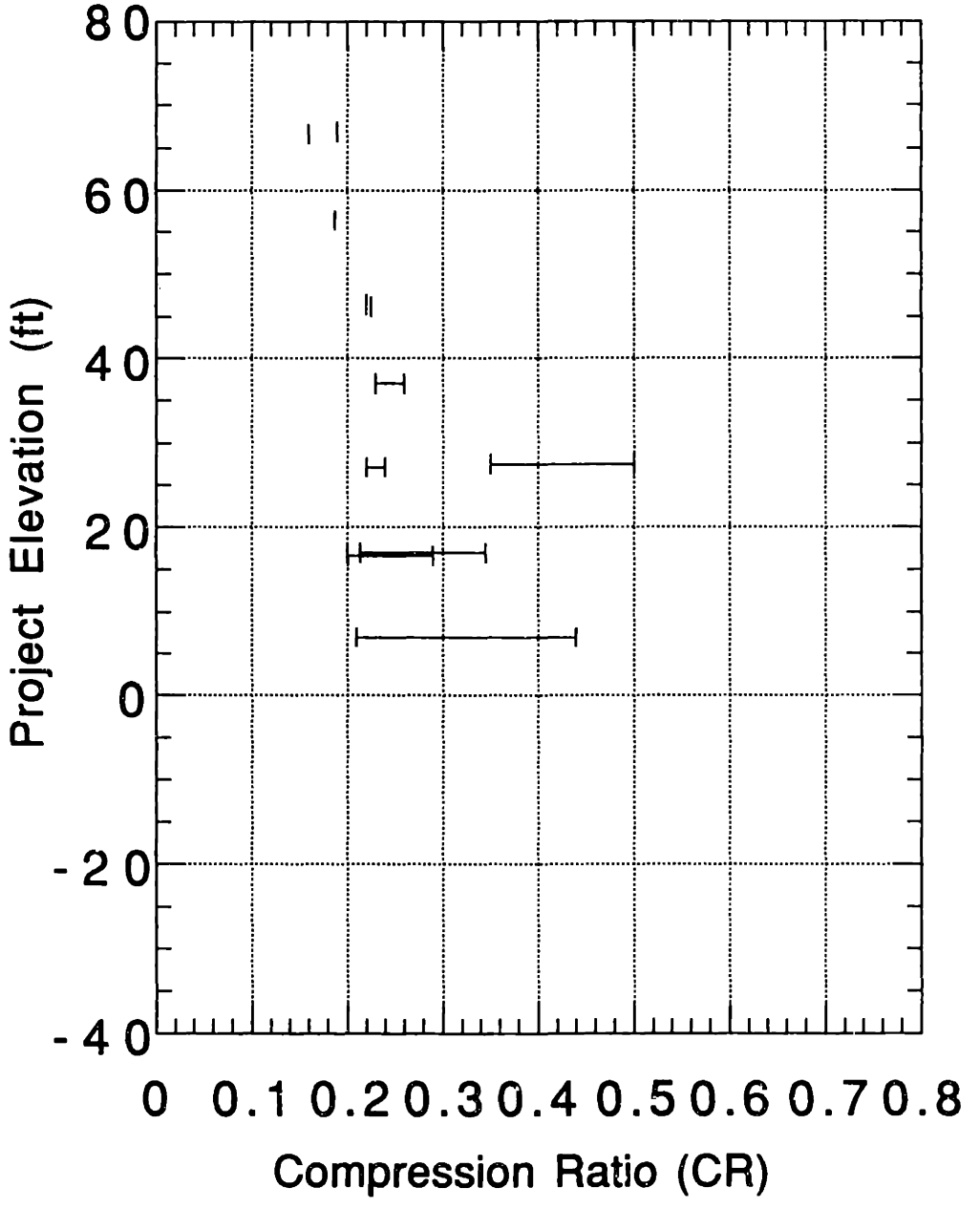

Figure 5-13: East Boston Elevation vs. Virgin Compression Ratio for CK_0-TX Tests

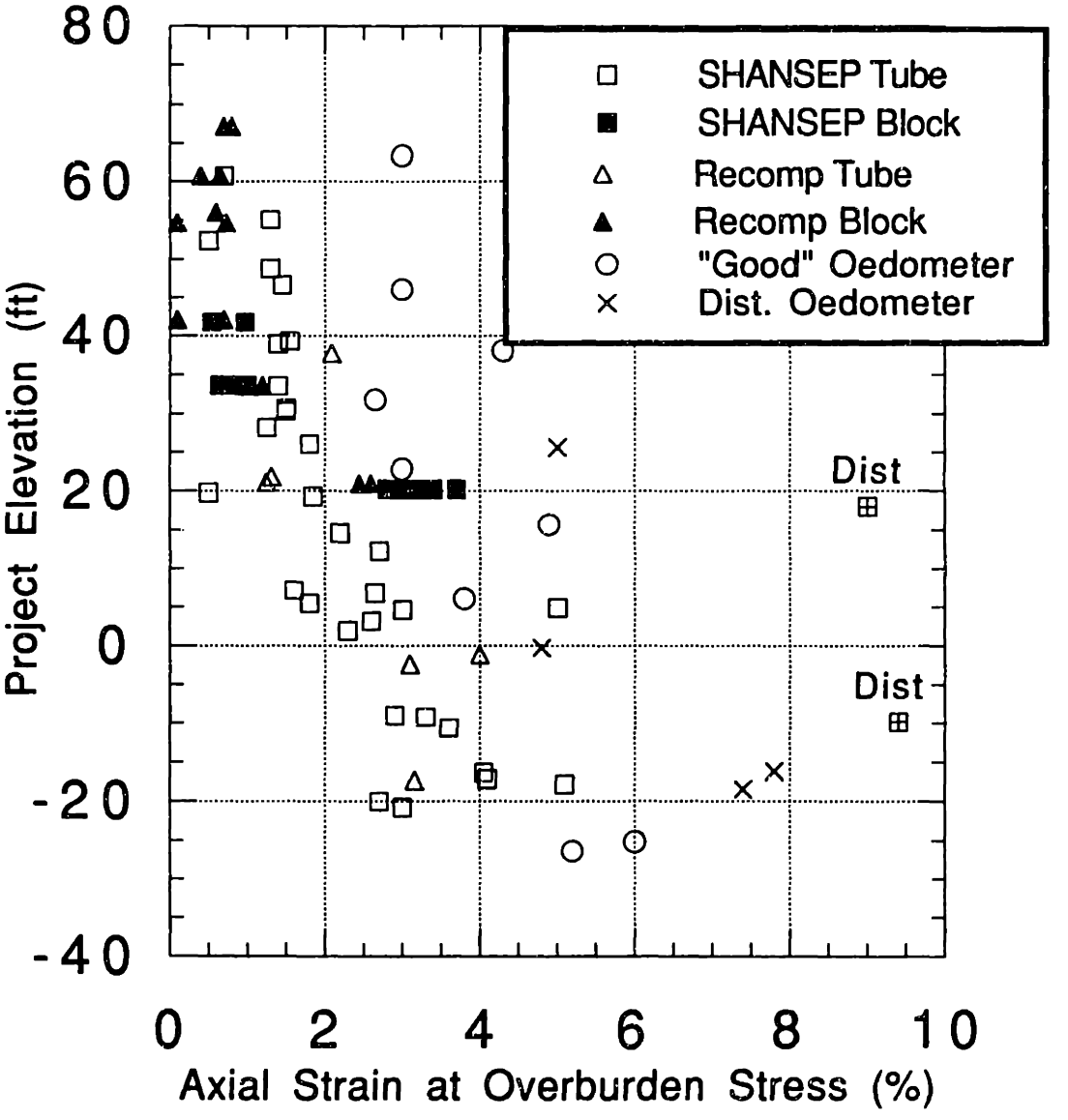

Figure 5-14: South Boston Elevation vs. Axial Strain at Overburden Stress from CK_0 and Typical Oedometer Tests

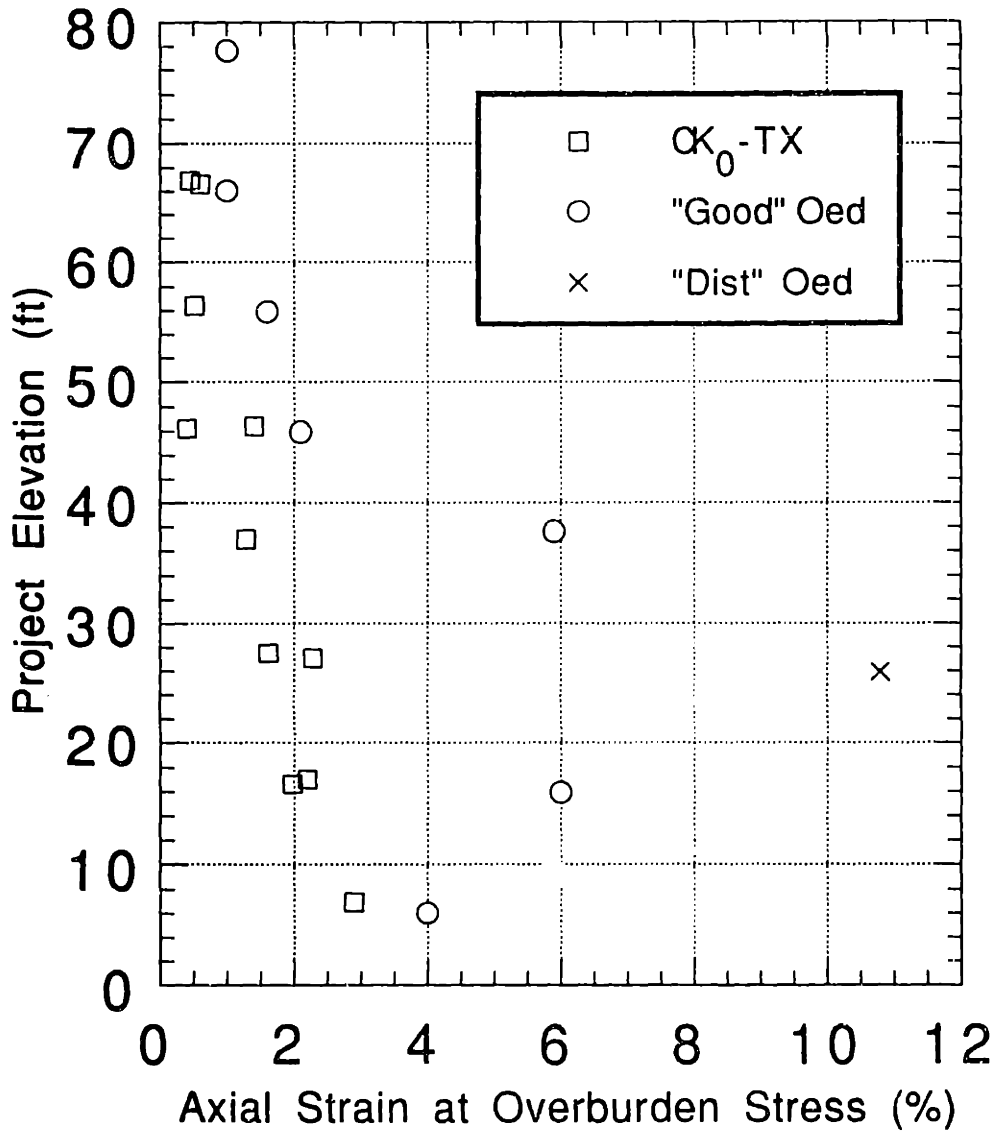

Figure 5-15: East Boston Elevation vs. Axial Strain at Overburden Stress from CK_0 and Incremental Oedometer Tests

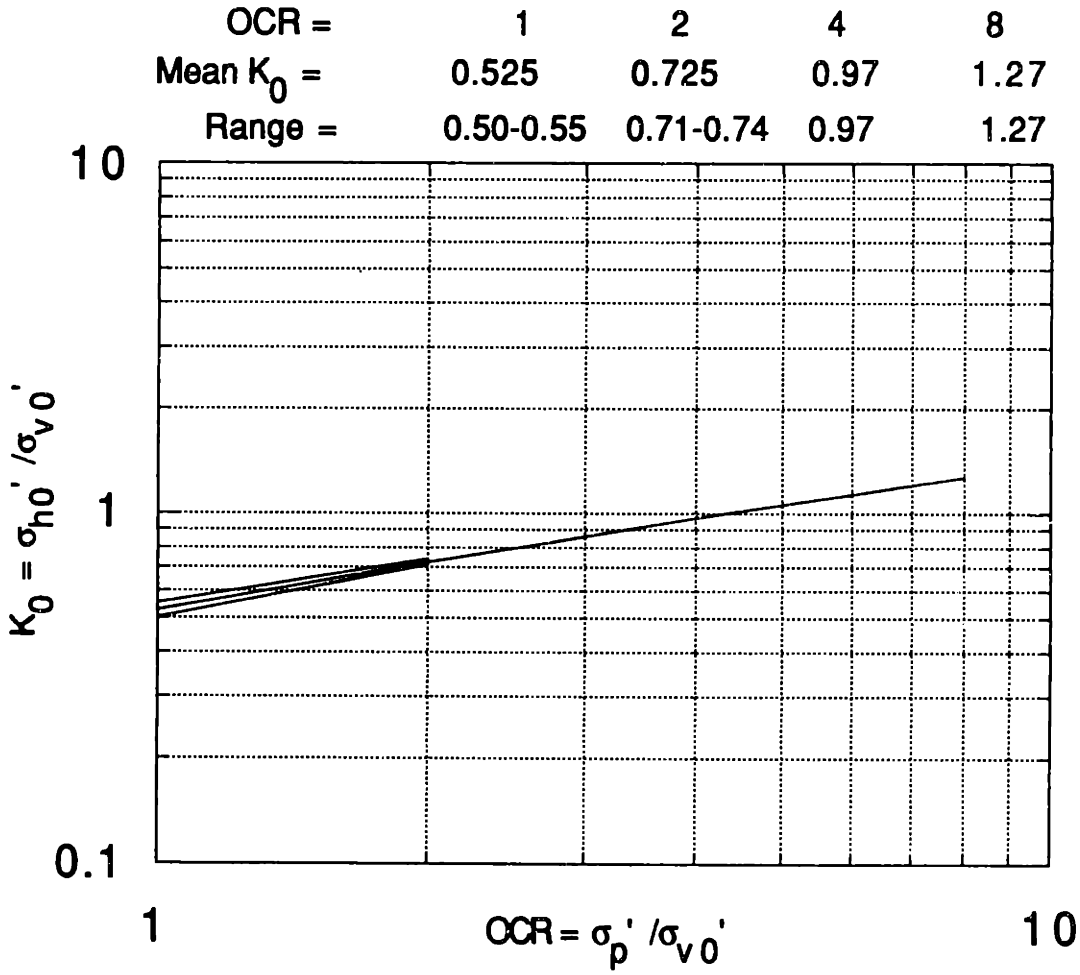

Figure 5-16: K_0 vs. OCR Relationship Used for Determination of Stresses for CK_0U Recompression Tests

Chapter 6

Results of Recompression Triaxial Strength Testing Program

6.1 Introduction

This chapter presents results and discussion of CK_0U triaxial compression and extension tests performed using the Recompression technique. Sections 6.2 and 6.3 cover compression and extension test results, respectively, and Section 6.4 compares these results. The remainder of Section 6.1 discusses the motivations behind the particular testing program undertaken, and the scope of the program.

6.1.1 Objectives of Recompression Testing Program

The first objective of the Recompression testing program was simply to *perform* Recompression tests. Prior to this research program, very few Recompression type tests had been done at MIT, and the few data presented (e.g., Baligh et al. 1987) were for Resedimented BBC. In fact, MIT's basic research on the behavior of cohesive soils has focused almost exclusively on the Resedimented BBC. The last major triaxial testing programs on natural BBC were performed for the I-95 Embankment Study (see Guertin 1967) and the MIT Campus Testing (see Ladd and Luscher 1965). The H&A STP provided a very welcome opportunity to undertake a thorough program of

Recompression tests on undisturbed samples.

As previously mentioned (see Section 2.2), the sampling program provided two types of samples: three inch diameter, fixed piston tube samples, and nine inch diameter Sherbrooke block samples. Recompression tests were performed on both types of samples to investigate the effect, if any, of the sampling method on the strength and deformation properties of the clay. Additionally, the preshear consolidation stress for about half of the tests was changed (i.e., $\sigma'_{vc} \neq \sigma'_{v0}$) in order to further evaluate the effect of the OCR on the shear results.

After the testing was completed, the Recompression results were compared to results from SHANSEP tests run on soil from the same site (both tube and block samples) in an attempt to determine how two very different consolidation techniques affect the shear results. This is a particularly interesting question, as consolidation tests on many of the lower samples indicate a significant structure in the soil (see Chapter 5). As discussed in Section 2.3, this structure may be altered during the consolidation process, affecting the subsequent shear results. Very few detailed comparisons of this type have been made.

Finally, the Recompression results were also compared with CIU and UU triaxial compression tests performed by H&A. As emphasized earlier, the tests performed at MIT are "state-of-the-art" and many consulting firms either do not have the capability to perform such tests, or cannot justify the expense and time required (up to one week per Recompression test, and twice that for SHANSEP). Subsequently, many consulting firms resort to UU and CIU tests which, though generally acknowledged to be inferior to K_0 consolidated tests, have the advantage of being faster and easier to run. By comparing the Recompression results with the CIU and UU results, one can attempt to quantify the difference between the "state-of-the-art" strength testing and the standard practice.

6.1.2 Scope of the Recompression Testing Program

The total number of Recompression tests performed for this program was 41. Of the 41, 28 were sheared in compression, and 13 in extension. As mentioned above,

approximately half of the tests were consolidated to preshear vertical effective stresses different from the overburden stress, in order to examine the effects of OCR on the shear data. The bulk of the tests were performed on block samples; however, six tests on tube samples were also performed (all of the tests on tube samples had $\sigma'_{vc} = \sigma'_{v0}$). Figure 6-1 summarizes the testing program both in tabular form, with the number and type of each test performed (compression or extension, block sample or tube sample, $\sigma'_{vc} = \sigma'_{v0}$ or $\sigma'_{vc} \neq \sigma'_{v0}$) and graphically, with test type and OCR plotted versus elevation.

6.2 Recompression Triaxial Compression Results

6.2.1 Overview

A total of 28 Recompression CK_0UC tests were run. Thirteen of the 28 were run at a stress ratio of 1 (i.e., $\sigma'_{vc} = \sigma'_{v0}$); four of those 13 were from tube samples and nine were from block samples. The remaining 15 tests were run on block samples at stress ratios greater or less than one.

This section first presents a few typical plots for both the consolidation and shear portions of the Recompression triaxial compression tests, summarizes data from the shear portion of all of the Recompression TC tests performed and then discusses specific parameters obtained.

Table 6.1 (5 pages)summarizes data from all 28 Recompression TC tests. Explanations of the data presented follows.

Test Number (Page 1) All triaxial tests, including both SHANSEP and Recompression tests, were numbered consecutively, therefore gaps in the numbering sequence are generally not significant.

Sample Number All samples for Recompression testing were taken from the South Boston test site. Block samples were taken from one of two holes, indicated in the label by the presence or absence of an "A" (e.g., BS-1 is from one hole, BS-1A from the other). All tube samples for Recompression testing were taken

from a single boring (SB2-23), although there is a second borehole at the site.

Depth Depth was calculated by *subtracting* the appropriate amount from the depth to the bottom of the block sample, or by *adding* the appropriate amount to the depth to the top of a tube sample.

Elevation Elevation was calculated by subtracting the depth of the specimen from the elevation of the top of the borehole (111.2 ft for the block samples, 110.9 ft for SB2-23). All elevations are CA/T Project Elevations which are defined as NGVD + 100 ft.

w_n and (SD) The natural water content and standard deviation of the trimmings taken during set up of the specimen. Usually based on three observations.

Specimen data Natural water content, void ratio, and specimen saturation calculated from total and dry weight measurements taken before and after the test. The specific gravity, G_s was assumed to be 2.80 for each calculation.

In situ stresses (Page 2) Vertical effective stresses are calculated using the equations presented in Figure 2-2 derived from the total unit weight of the soil and pore pressure profile as described in Chapter 4. Preconsolidation pressure is calculated using Equation 5.3, $(\sigma'_p(ksf) = 3.45 + 0.170El.(ft))$, based on a linear regression of the measured σ'_p values from various types of consolidation tests (see Section 5.3). In situ OCR is defined as σ'_p/σ'_{v0}.

Test stresses The vertical consolidation stress is taken as the mean value of σ'_{vc} held over the 24 hour period preceding shear. The test OCR is defined as σ'_p/σ'_{vc}. The K_c is defined as $\sigma'_{hc}/\sigma'_{vc}$ and the (K_0) tabulated corresponds to the appropriate K_0 for the test OCR, read from Figure 5-16. As mentioned in Chapter 3, in approximately one-third of the tests K_c was incorrectly chosen, i.e., not equal to K_0. The effect on the shear results of this oversight is discussed below in Section 6.2.

Peak data (Page 3) The peak is defined as the data point where q/σ'_{vc} ($q = \frac{1}{2}(\sigma_v - \sigma_h)$) is maximum. The first column tabulates the axial strain at which the peak occurred (straining during consolidation is considered separately, i.e., the specimen is at zero strain at the beginning of shear). The next two columns, q/σ'_{vc} and p'/σ'_{vc} ($p' = \frac{1}{2}(\sigma'_v + \sigma'_h)$), are automatic outputs of the data reduction program, while q/σ'_p and p'/σ'_p are calculated by dividing q/σ'_{vc} and p'/σ'_{vc} by the test OCR (σ'_p/σ'_{vc}). A_f is the pore pressure parameter at failure and "PHI" (or ϕ') is the friction angle, both of which are automatically calculated by the data reduction program.

Maximum obliquity data (Page 4) The maximum obliquity (σ'_1/σ'_{3max}) is chosen as the highest value of ϕ' reached. The data tabulated for the maximum obliquity are the same as for the peak, with the exception of A_f.

B value (Page 5) This column tabulates the B value of each test at the end of back pressure saturation.

Adjusted q_f The peak q resulting from each test is adjusted to the overburden stress according to the following formula:

$$q_{f_{adj}} = (q_{f_{meas}})(\sigma'_{v0}/\sigma'_{vc})^{(1-m)} \tag{6.1}$$

where m = 0.65 for compression tests (m = 0.85 for extension tests) based on SHANSEP data available at the start of Recompression testing.

E_{50}/σ'_{vc} The Young's modulus is calculated by the data reduction program as the secant modulus. The value tabulated here is taken at half of the maximum incremental stress ($\frac{1}{2}\Delta q_f$) and normalized to σ'_{vc}.

Preshear axial and volumetric strain These columns tabulate the amount of each type of strain that occurred during pressure up, saturation, and consolidation.

Comments The following notation is used in the comments column:

- E (Excellent), VG (Very Good), G (Good), F (Fair) or P (Poor) used to describe overall test quality.
- PSS = preexisting shear surface
- K_c too high or low for test OCR
- Remarks about magnitude of strain rate compared to the standard rate (0.5%/hr), specimen homogeneity, leaks during test, etc.

6.2.2 Typical Consolidation and Shear Data

Consolidation

Figures 6-2 and 6-3 present typical outputs from the consolidation portion of the Recompression tests. The consolidation of Recompression tests is a shorter process than for SHANSEP tests, and does not yield as much information (e.g., no K_0 or σ'_p values)

Figure 6-2 shows a typical compression curve with both volumetric and axial strains plotted versus log vertical effective stress and K_c ($= \sigma'_h/\sigma'_v$) versus log σ'_v. In this particular example, very little secondary compression occurred at σ'_{vc}. One notices that this is not one-dimensional consolidation like SHANSEP tests, because the axial and volumetric strains do not remain equal. As emphasized in Section 5.2.2, one-dimensional reconsolidation of overconsolidated clay to the in situ OCR will result in values of K_c that are generally much to low compared to K_0. Thus to estimate the in situ K_0 for the Recompression tests, the relationship given in Section 5.5 is used. The lower part of the figure shows how K_c typically starts near one and decreases steadily along a smooth curve until it reaches the K_c input into the computer control program. The "preshear" strain data on page 5 of Table 6.1 show that the volu

metric strains exceeded the axial strain in most of the tests.

Figure 6-3 shows the stress path followed by the sample during consolidation. This figure serves mainly to emphasize the quality of control (explained in Appendix A) achieved.

Undrained Shear

Figure 6-4 shows four stress paths, normalized to σ'_p, from typical tests at different OCRs and values of K_c. Figure 6-5 shows the stress-strain (q/σ'_p vs. ϵ_a) plots from the same four tests.

TX083 was done on a tube sample (SB2-23-U21) at El. -1.1 ft and was consolidated to $\sigma'_{vc}/\sigma'_{v0} \approx 1$. This means that the test OCR (=1.175) was approximately the same as the in situ OCR (=1.157). TX052 is from a block sample (BS-3A) at El. 33.6 ft and was also consolidated to the in situ OCR (OCR_{insitu}=2.005, OCR_{test}=2.114). Both of these stress paths have fairly common shapes and resemble SHANSEP stress paths from similarly overconsolidated samples. The stress-strain curves for both are very similar, and exhibit significant strain softening.

TX042 from El. 56.0 is more overconsolidated than the previous two tests (preshear OCR = 4.001 and in situ OCR = 3.804) and has the expected shape for the stress path (i.e., concave to the right). The final curve shown is for test TX073 (BS-1, El. 67.2 ft), which has the highest preshear OCR (5.592) and did not exhibit any strain softening.

Tests with Incorrect K_c

The next figure presented addresses the issue of the effect of K_c on the shear results. As previously mentioned, several of the tests were consolidated to K_c significantly different from the K_0 corresponding to the test OCR. Figure 6-6 shows stress paths normalized to σ'_p for two triaxial compression tests. Both tests are on the same sample, (BS-2), from the same elevation (60.7 ft) and have essentially the same test OCR (TX059 OCR=2.244, TX101 OCR=2.217). But while TX101 has a preshear K_c (=0.74) nearly equal to K_0 (=0.72), TX059 has a much higher K_c (=1.01). The higher average effective stress at consolidation (p'_c) for TX059 was the reason for its higher peak strength since A_f and the peak friction angle did not vary.

Table 6.2 summarizes the tests performed in which the K_c differed from the K_0 by more than 10% (i.e., $K_c/K_0 < 0.9$ or > 1.1). It tabulates values of the parameters which are examined in the following sections, such as the OCR, q_f/σ'_{vc}, A_f, etc, and

notes which tests with incorrect K_c values were repeated.

Strain Softening

Strain softening was a recurrent behavior during the Recompression testing program. Figure 6-7 shows an example of an extreme case, namely TX064 on BS-7, with $\sigma'_{vc}/\sigma'_{v0}$ = .45 and OCR=2.97. A distinct failure surface developed during the rapid decrease in shear stress, followed by more gradual strain softening. In general, the most pronounced strain softening occurred in tests from the deeper samples (particularly BS-7, which was the deepest block sample by about 15 feet). The strain softening in tests on this sample was noticeable regardless of the test OCR. Strain softening is a brittle behavior and usually occurs in "structured" soils. Hence, its observation in the samples from below the crust correlates well with the observation of S-shaped compression curves at these depths (see Section 5.1).

6.2.3 Undrained Strength Ratio

Figure 6-8 plots the Undrained Strength Ratio (USR or q_f/σ'_{vc}) versus test OCR for all 28 compression tests using a log-log scale. A linear regression of such data yields the S and m values used to calculate undrained strength from OCR. Linear regression on all of the points gives the following equation and r^2:

$$q_f/\sigma'_{vc} = 0.305(OCR)^{0.592} \qquad r^2 = 0.7257 \tag{6.2}$$

However, upon inspecting Figure 6-8 one notices several points that are located well below the dashed line representing Eq. 6.2. Three of these low points ($\times$) are from tests where preexisting shear surfaces (PSS) were noted during setup of the specimen. Presence of these surfaces may tend to decrease the peak strength of the soil. The other two tests (+) exhibiting low peak strength were known to have internal leaks. If the tests with PSS and leaks are eliminated from the regression (tests TX040, TX047,

TX050, TX058, and TX095) the correlation becomes much stronger, with

$$q_f/\sigma'_{vc} = 0.298(OCR)^{0.676} \qquad r^2 = 0.9214 \tag{6.3}$$

The standard deviation in log q_f/σ'_{vc} about Eq. 6.3 equals ±0.0475.

As an exercise, tests with a K_c which differed from K_0 by more than 10% were eliminated, and the linear regression repeated. However, the effect on the values of S, m and r^2 was negligible, so these tests were included in this analysis.

There may be a slight effect of having σ'_{vc} <> σ'_{v0} in these tests. Of the eight tests with $\sigma'_{vc}/\sigma'_{v0} < 1$, four fall above the line defined by Eq. 6.3, three fall below the line, and one falls on the line. Of the five tests with $\sigma'_{vc}/\sigma'_{v0} > 1$, one falls above the line, two fall below the line and two fall on the line. This may imply that tests with $\sigma'_{vc} < \sigma'_{v0}$ led to slightly higher undrained strength ratios than tests with $\sigma'_{vc} > \sigma'_{v0}$.

Two of the four tests on tube samples (TX083 and TX089 having the lowest OCR) plot below Eq. 6.3. This was somewhat surprising since Ladd (1991) predicts the opposite trend, i.e., Recompression tests on low OCR tube samples should tend to have strengths that are too high.

6.2.4 Effective Stress Failure Envelope

Figure 6-9 plots the peak and maximum obliquity points normalized to σ'_p for all of the Recompression CK_0UC tests (except for peak values of the two tests with leakage). Also shown are the linear regressions of each set of points which define the peak and maximum obliquity failure envelopes. These envelopes are defined by $q/\sigma'_p = a'/\sigma'_p + \sin\phi' p'/\sigma'_p$ and the Mohr-Coulomb cohesion intercept $c' = a'/\cos\phi'$. The linear regression gave:

Condition	$\sin\phi'$	a'/σ'_p	c'/σ'_p	r^2	SD of q/σ'_p
Peak	0.374	0.072	0.078	0.805	±0.022
Maximum Obliquity	0.484	0.038	0.044	0.885	±0.017

The value of ϕ'_{peak} is 22.0°, which is quite a bit less than $\phi'_{MO} = 28.9°$. Additionally,

there is more scatter in the peak data (SD= ±0.022) than in the M.O. data (SD= ±0.017). The two points plotting the farthest above the mean envelopes are from TX064 that exhibited the most severe strain softening. (Figure 6-7).

Interestingly enough, existence of PSS in the tests had very little effect on these results and removing these points from the linear regression has a negligible effect on the resulting equations and r^2. Similarly, a preshear $K_c \neq K_0$ did not seem to affect the effective stress envelopes.

6.2.5 Stress-Strain Parameters

Figures 6-10 through 6-12 summarize some other important shear parameters from all of the Recompression tests (both TC and TE), excluding the two TC tests with leakage. These figures show dashed and solid curves for the TC and TE data, respectively. These curves represent *approximate* trends from the high quality tests on block samples.

Strain at Failure

Figure 6-10 shows the strain at failure, ϵ_f, versus log OCR for the tests. In general, for the compression tests, ϵ_f seems to remain fairly constant at $\leq$2%, with only a few outlying points. The three tests with the highest ϵ_f (6 to 10%) are from tests with PSS (TX040,TX050) or probable PSS (TX073). Again, the tests with incorrect values of K_c fall well within the scatter of the other points, and no particular relationship between these tests and the others can be discerned.

Pore Pressure Parameter at Failure, A_f

Figure 6-11 plots pore pressure parameter at failure, A_f, for the tests. One notices a trend of decreasing A_f with OCR for the TC tests. The tests with incorrect K_c fall within the range of the "good" tests, though they may be very slightly lower overall. Though not shown in this figure, the tests with leaks showed abnormally high A_f values, as expected. The two tests on tube samples with low OCRs had higher A_f

values than one would expect from block sample tests at similar OCRs, which may have led to the lower USR than predicted by Ladd (1991).

Normalized Young's Modulus

Figure 6-12 shows normalized Young's Modulus, E_{50}/σ'_{vc} versus log OCR. There is a consistent increase in normalized modulus with increasing OCR, with no noticeable effect of tube versus block samples or of having incorrect K_c values.

6.2.6 Discussion

In looking at all of these compression results together, one notices the following points:

1. There is no marked difference between tests performed on block samples and those performed on tube samples, i.e., the data from four tube samples fall within the scatter of the block sample tests. However, the two tests on tube samples at low OCRs (TX083 and TX089) exhibited slightly higher A_f values than the block samples and thus slightly lower q_f/σ'_{vc}. However, the comparison between block and tube samples is incomplete, as no tube samples with OCR>2.5 were taken.

   The similarity in tube results to block sample results is probably due to the exceptional quality of the tube samples. By using a fixed piston sampler and a special heavy-weight drilling mud during sampling and careful handling during specimen preparation (see Chapter 3 for description of extrusion technique), much of the disturbance normally associated with tube samples was successfully eliminated. This has a great practical impact, as the Sherbrooke block samples are prohibitively expensive for most projects. These results indicate that careful tube sampling and handling can produce specimens of comparable quality.

2. Though the data are not comprehensive, there does not appear to be any strong difference in shear behavior between specimens consolidated to the overburden stress and those consolidated to values above or below σ'_{v0}. In other words,

samples with the same test OCR behave similarly regardless of the in situ OCR.

3. Though the example plot shown in Figure 6-6 indicates that K_c definitely affects the stress strain behavior of individual tests during shear, the data presented above (USR, ESE's, and stress-strain parameters) show that the compression tests with incorrect values of K_c exhibit "reasonable" behavior in terms of yielding values that fall within the range of values found for all the tests. In general, though, the higher the mean stress after consolidation, the higher the strength, indicating nearly elastic behavior below the yield envelope.

6.3 Recompression Triaxial Extension Results

6.3.1 Overview

The reader is again referred to Figure 6-1 for a graphic representation of the scope of extension tests performed. In total 13 extension tests, six with $\sigma'_{vc} = \sigma'_{v0}$ and seven with $\sigma'_{vc} \neq \sigma'_{v0}$, were run. Two of the tests were on tube samples (both with consolidation stresses equal to the in-situ stresses) and the remainder on blocks.

This section is organized in the same way as Section 6.2. First, tabulated data are presented with explanatory notes (below), then a few typical plots of stress paths and stress-strain curves are shown, and finally summary plots with USR, effective stress envelopes and stress-strain parameters are presented and commented upon.

Table 6.3 summarizes data from all of the TE tests performed. Most of the same comments apply to these data as to the TC summary, with a few additions.

Axial strain Axial strain tabulated here as positive is actually negative (i.e., in the opposite direction as for TC tests).

q/σ'_{vc}, q/σ'_p, Adjusted q These values are also negative, though tabulated as positive.

6.3.2 Typical Shear Data

Figures 6-13 and 6-14 show stress paths normalized to σ'_p and stress-strain curves for three typical extension tests performed. TX087 is from BS-2A, El. 42.1 feet. Its test OCR was 5.468, while it's in situ OCR was only 2.568. TX075 is from BS-7, El. 20.9. It was consolidated to an OCR of 1.877, which is different from the in situ OCR of 1.336. TX049 is from the same sample with the same in situ OCR, and has been consolidated to approximately the in situ OCR (test OCR = 1.310). The three stress paths display quite a bit of variation in both the peak and M.O. friction angles (e.g., TX087 $\phi_{MO} = 41.7°$, TX075 $\phi_{MO} = 35.7°$ and TX049 $\phi_{MO} = 50.0°$), as well as varied stress path shapes. The three stress-strain curves exhibit a moderate degree of strain softening, but in general, less than was observed for TC tests (especially for tests from BS-7).

Figure 6-15 demonstrates a typical effect of incorrect K_c on high OCR extension test results. As for compression tests, the effective stress envelope does not change. The peak, however, is significantly affected by the low K_c of TX070. The lower K_c causes a lower p′ at consolidation and, since the stress paths have similar shapes, this causes a lower p'_f and hence a lower peak strength.

6.3.3 Undrained Strength Ratio

Figure 6-16 plots q_f/σ'_{vc} versus log OCR for TE tests. The equation resulting from linear regression including all points is:

$$q_f/\sigma'_{vc} = 0.158(OCR)^{0.800} \qquad r^2 = 0.92210 \tag{6.4}$$

with a standard deviation of log $q/\sigma'_{vc} = \pm 0.076$. The two low OCR tests on tube samples fall slightly below this line, but it's difficult to tell whether or not this is a real trend or an artifact of insufficient test results. However, the tests with incorrect values of K_c (both too high and too low) certainly seem to yield lower values of the USR at higher OCRs. When both sets of tests are eliminated, the resulting equation

and r^2 change significantly:

$$q_f/\sigma'_{vc} = 0.144(OCR)^{0.978} \qquad r^2 = 0.9866 \tag{6.5}$$

and SD=±0.030. Finally, if only block sample tests having $\sigma'_{vc} = \sigma'_{v0}$ are included (Tests 48, 49, 53, and 84), one obtains

$$q_f/\sigma'_{vc} = 0.151(OCR)^{0.916} \qquad r^2 = 0.9980 \tag{6.6}$$

and SD=±0.011. Since Equation 6.5 gives similar results and is based on more tests, it will be used as the "best estimate".

Of the three tests with $\sigma'_{vc} < \sigma'_{v0}$, one falls directly on the line for $\sigma'_{vc} = \sigma'_{v0}$, one falls slightly below, and one slightly above. No tests were performed with $\sigma'_{vc} > \sigma'_{v0}$ because the samples at that depth are only very slightly overconsolidated.

Similar to what was observed for TC tests, the tests on tube samples with low OCRs fell below Equation 6.5.

6.3.4 Effective Stress Failure Envelope

Figure 6-17 plots peak and M.O. values for triaxial extension tests. The results of linear regression of each set of points is as follows:

Condition	$\sin\phi'$	a'/σ'_p	c'/σ'_p	r^2	SD of q/σ'_p
Peak	0.225	0.072	0.074	0.612	±0.015
Maximum Obliquity	0.455	0.028	0.031	0.865	±0.010

These results give a $\phi_{peak} = 13.0°$, and $\phi_{MO} = 27.1°$. Again, the M.O. points are considerably less scattered than the peak data.

6.3.5 Stress-Strain Parameters

The reader is referred again to Figures 6-10 to 6-12 which also contain stress-strain parameter summaries for the triaxial extension tests.

Strain at Failure

Figure 6-10 plots ϵ_f versus OCR for both TC and TE tests. The ϵ_f values for TE tests appear to increase slightly with OCR and are generally higher than for TC tests. Tests with $K_c \neq K_0$ show slightly lower ϵ_f than tests which were correctly consolidated. The outlying TE point on this and the following two plots is test number TX093 which, due to poor control during consolidation, was incorrectly consolidated to a much higher OCR=13.8. The two tests on tube samples have higher ϵ_f, which may indicate a certain amount of disturbance, or may be purely coincidental.

Pore Pressure Parameter at Failure, A_f

Figure 6-11 shows A_f versus OCR. Triaxial extension tests follow a similar decreasing trend with OCR as TC tests. Again, the outlying point is for TX093. Otherwise the tests with $K_c \neq K_0$ fall within the scatter of the other data. Similar to what was observed for TC tests, the TE test on a low OCR tube sample displayed a very high A_f value, and a subsequently lower USR (see Figure 6-16).

Normalized Young's Modulus

Figure 6-12 shows normalized Young's Modulus, E_{50}/σ'_{vc}, versus log OCR. Again, TE tests show smoothly increasing E_{50}/σ'_{vc} with log OCR. If the tests with $K_c \neq K_0$ (which gave lower modulus values) are eliminated, the resulting relationship is very well defined, and nearly linear. The two TE tests on tube samples gave slightly lower values of E_{50}.

Overall, the TE data show less scatter than the TC data, and give somewhat lower values for the modulus at higher OCRs.

6.3.6 Discussion

A comprehensive consideration of the TE data leads to the following observations:

1. TE tests are more sensitive to incorrect values of K_c than TC tests. Because the tests have to travel farther in p'-q space before reaching the failure envelope,

small differences in the starting position of the stress path are accentuated. In particular, the equation for the USR vs. OCR relationship was strongly affected by exclusion of tests with $K_c \neq K_0$. Also, the E_{50}/σ'_{vc} values were significantly lower.

2. With only two TE tests on tube samples, it is difficult to draw any conclusions regarding the comparative quality of the samples. Test TX096 however, did exhibit higher A_f and lower USR than typical.

3. As mentioned earlier, strain softening is not as pronounced in the TE tests, even for highly overconsolidated specimens from BS-7.

6.4 Discussion, Summary and Conclusions

Based on consideration of the best quality TC and TE tests, the following conclusions have been drawn:

1. *Undrained Strength Ratio* – The best estimates for S and m are:

   TC S_c=0.298, m_c=0.676, SD log $q_f/\sigma'_{vc} = \pm 0.0475$; Fig. 6-8 and Eq. 6.3

   TE S_e=0.144, m_e=0.978, SD log $q_f/\sigma'_{vc} = \pm 0.030$; Fig. 6-16 and Eq. 6.5

   (a) $K_c \neq K_0$ – As was shown in Figures 6-6 and 6-15 the K_c of a test will effect the stress strain behavior during shear for both TC and TE tests. However, the cumulative result of incorrect K_c values on TC and TE tests is different. For TC tests, the effect of the incorrect K_c values is not systematic, and the results were therefore included in the "best estimate" equation above. For TE tests, the tests with incorrect values of K_c (both too high and too low) gave lower USR values at the higher OCR's, and thus were eliminated from consideration for the "best estimate".

   (b) Tube Samples vs. Block Samples – For both TC and TE, tests performed on tube samples at the lowest OCRs exhibited lower undrained strengths than expected (see Figs. 6-8 and 6-16). This is contrary to what was

predicted by Ladd (1991). In general, however, the tube samples were of extremely high quality.

(c) $\sigma'_{vc} \neq \sigma'_{v0}$ – Though there was a slight indication that TC tests with $\sigma'_{vc} < \sigma'_{v0}$ exhibited higher USRs, in general the effect of different ratios of $\sigma'_{vc}/\sigma'_{v0}$ was negligible. For example, Figure 6-18 shows stress paths and stress strain curves from two tests with the same test OCR, but different in situ OCR's. TX079 has $\sigma'_{vc}/\sigma'_{v0} = 0.70$ and TX091 has $\sigma'_{vc}/\sigma'_{v0} = 0.38$, yet both tests have similarly shaped stress paths and stress-strain relationships, as well as peak values of q/σ'_{vc}, A_f, etc.

2. *Effective Stress Envelope at Maximum Obliquity* – The best estimates for the ESE at MO are:

TC $c'/\sigma'_p = 0.044, \sin\phi' = 0.484(\phi' = 29°)$, SD $q/\sigma'_p = \pm 0.017$; Fig. 6-9

TE $c'/\sigma'_p = 0.031, \sin\phi' = 0.455(\phi' = 27°)$, SD $q/\sigma'_p = \pm 0.010$; Fig. 6-17

(a) $K_c \neq K_0$ – For both TC and TE tests, inclusion of tests with incorrect values of K_c had no effect on the maximum obliquity ESE.

(b) Tube Samples vs. Block Samples – For the MO effective stress envelope, there was no discernible difference between tests performed on tube samples and tests performed on block samples for either the TC or TE tests.

(c) $\sigma'_{vc} \neq \sigma'_{v0}$ – Consolidating specimens to σ'_{vc} different from the overburden stress had no effect on either the TC or TE effective stress envelope at MO.

3. *Other Parameters*

(a) ϵ_f – As shown in Figure 6-10, the strains at failure for TC tests are lower than ϵ_f for TE tests overall. For the TE tests incorrect values of K_c led to lower values of ϵ_f, while for TC tests there was no effect.

(b) A_f – Overall, the pore pressure parameter at failure was lower for TC than for TE tests (Fig. 6-11) TC and TE tests with incorrect K_c values both

:ell within the scatter of the other tests. Tests on tube samples at very low OCRs (both TC and TE) gave higher values of A_f (which contribute to the lower than expected USRs mentioned previously).

(c) E_{50}/σ'_{vc} – In general, TC tests yielded values of E_{50} which were greater than or equal to those from TE tests (see Fig. 6-12). TE tests with $K_c \neq K_0$ showed lower values of E_{50}, but aside from these four tests, the TE results were less scattered than the TC. The tests on tube samples at low OCR yielded lower E_{50} values, both in compression and in extension.

Table 6.1: CA/T SB STP: Recompression CK_0UC Triaxial Test Data (Notes: (1) stresses in ksf, (2) Preshear t_c = 1 day, (3) Shear $\dot{\epsilon}$ = 0.5%/hr unless otherwise noted)–Page 1 of 5

RECOMPRESSION TEST DATA SUMMARY						SPECIMEN			
TEST	SAMPLE	DEPTH (ft)	ELEV. (ft)	Wn (%)	(SD)	Wn (%)	Gs	e	S
40	BS-1	44.0	67.2	35.9	0.8	34.1	2.80	0.968	0.985
42	BS-3	55.2	56.0	34.4	0.1	34.3	2.80	0.928	1.035
46	BS-7	90.3	20.9	52.1	0.8	53.4	2.80	1.495	1.000
47	BS-2A	69.1	42.1	36.1	0.3	37.6	2.80	1.060	0.995
50	BS-2	50.5	60.7	33.7	0.6	33.7	2.80	0.959	0.985
52	BS-3A	77.6	33.6	40.7	0.5	41.4	2.80	1.146	1.010
56	BS-1A	56.5	54.7	32.4	0.9	31.8	2.80	0.910	0.983
57	BS-2	50.5	60.7	33.6	0.5	33.2	2.80	0.930	0.997
58	BS-2A	69.1	42.1	36.5	0.4	35.9	2.80	1.026	0.978
59	BS-2	50.5	60.7	33.6	0.1	33.4	2.80	0.907	1.031
62	SB23-U12	73.1	37.8	40.1	0.5	41.0	2.80	1.130	1.017
63	SB23-U15	89.8	21.1	47.8	0.1	48.0	2.80	1.320	1.015
64	BS-7	90.3	20.9	53.1	0.3	53.8	2.80	1.490	1.013
66	BS-7	90.3	20.9	51.9	0.5	52.4	2.80	1.460	1.002
68	BS-2A	69.1	42.1	34.2	0.8	35.0	2.80	0.984	0.995
69	BS-2A	69.1	42.1	36.7	0.2	38.2	2.80	1.071	0.998
73	BS-1	44.0	67.2	34.2	0.9	33.0	2.80	0.963	0.960
78	BS-2	50.5	60.7	32.9	0.3	32.7	2.80	0.915	1.000
79	BS-1A	56.5	54.7	34.2	0.3	35.0	2.80	0.978	1.002
83	SB23-U21	112.0	-1.1	47.7	0.8	48.6	2.80	1.344	1.013
85	BS-1A	56.5	54.7	33.1	0.4	33.2	2.80	0.932	0.997
89	SB23-U25	128.3	-17.4	40.0	0.2	40.6	2.80	1.124	1.012
91	BS-3A	77.6	33.6	38.7	0.1	41.5	2.80	1.179	0.986
95	BS-2A	69.1	42.1	36.0	0.9	37.3	2.80	1.044	0.999
98	BS-2A	69.1	42.1	37.0	0.7	36.1	2.80	1.017	0.994
101	BS-2	50.5	60.7	33.4	0.3	33.4	2.80	0.918	1.017
103	BS-2A	69.1	42.1	37.3	0.7	38.1	2.80	1.073	0.993
104	BS-7	90.8	20.4	46.0	2.1	45.4	2.80	1.271	1.001

Table 6.1: CA/T SB STP: Recompression CK_0UC Triaxial Test Data (Notes: (1) stresses in ksf, (2) Preshear t_c = 1 day, (3) Shear $\dot{\epsilon}$ = 0.5%/hr unless otherwise noted)–Page 2 of 5

	IN SITU			TEST			
TEST	SIGvo' (ksf)	SIGp' (ksf)	OCR	SIGvc' (ksf)	OCR	Kc	(Ko)
40	2.83	14.874	5.256	3.070	4.845	0.980	1.06
42	3.41	12.970	3.804	3.242	4.001	1.043	0.97
46	5.245	7.003	1.335	5.415	1.293	0.635	0.60
47	4.13	10.607	2.568	4.107	2.583	0.799	0.80
50	3.165	13.769	4.350	3.086	4.462	1.120	1.01
52	4.57	9.162	2.005	4.334	2.114	0.754	0.74
56	3.48	12.749	3.664	3.510	3.632	0.910	0.93
57	3.17	13.769	4.344	3.970	3.468	1.020	0.91
58	4.13	10.607	2.568	1.830	5.796	0.910	1.12
59	3.17	13.769	4.344	6.190	2.224	1.010	0.76
62	4.35	9.876	2.270	4.030	2.451	0.810	0.79
63	5.22	7.037	1.348	4.910	1.433	0.635	0.62
64	5.24	7.003	1.336	2.360	2.967	0.720	0.86
66	5.24	7.003	1.336	3.670	1.908	0.640	0.72
68	4.13	10.607	2.568	2.720	3.900	0.800	0.96
69	4.13	10.607	2.568	6.870	1.544	0.810	0.63
73	2.83	14.874	5.256	2.660	5.592	1.120	1.11
78	3.17	13.769	4.344	2.990	4.605	1.060	1.05
79	3.48	12.749	3.664	2.420	5.268	1.080	1.08
83	6.45	7.460	1.157	6.350	1.175	0.580	0.58
85	3.48	12.749	3.664	6.045	2.109	0.730	0.75
89	7.41	9.160	1.236	7.430	1.233	0.540	0.58
91	4.57	9.162	2.005	1.720	5.327	1.090	1.09
95	4.13	10.607	2.568	6.820	1.555	0.650	0.64
98	4.13	10.607	2.568	2.257	4.700	1.22	0.94
101	3.17	13.769	4.344	6.210	2.217	0.74	0.72
103	4.13	10.607	2.568	1.820	5.828	1.19	1.08
104	5.27	6.918	1.313	2.450	2.824	0.835	0.81

Table 6.1: CA/T SB STP: Recompression CK_0UC Triaxial Test Data (Notes: (1) stresses in ksf, (2) Preshear t_e = 1 day, (3) Shear $\dot{\epsilon}$ = 0.5%/hr unless otherwise noted)–Page 3 of 5

	PEAK						
TEST	ΔX STRN (%)	q/SIGvc'	p'/SIGvc'	q/SIGp'	p'/SIGp'	A f	PHI' (deg)
40	6.10	0.609	1.079	0.126	0.223	0.425	34.3
42	2.00	0.771	1.317	0.193	0.329	0.315	35.9
46	0.90	0.395	0.769	0.305	0.595	0.615	30.8
47	1.28	0.454	0.863	0.176	0.334	0.550	31.7
50	9.90	0.539	1.009	0.121	0.226	0.540	32.3
52	0.74	0.468	0.862	0.221	0.408	0.500	32.9
56	1.47	0.757	1.255	0.208	0.346	0.290	37.1
57	1.65	0.633	1.079	0.183	0.311	0.446	35.9
58	0.57	0.467	0.619	0.081	0.107	0.898	49.0
59	1.24	0.598	1.062	0.269	0.477	0.454	34.3
62	4.00	0.522	0.879	0.213	0.359	0.531	36.4
63	0.68	0.396	0.778	0.276	0.543	0.594	30.6
64	1.03	0.754	1.005	0.254	0.339	0.381	48.7
66	0.73	0.460	0.802	0.241	0.420	0.530	35.0
68	0.89	0.718	1.113	0.184	0.285	0.327	40.2
69	1.30	0.371	0.739	0.240	0.479	0.801	30.2
73	9.50	0.858	1.467	0.153	0.262	0.277	35.8
78	1.07	0.927	1.443	0.201	0.313	0.270	40.0
79	0.92	1.134	1.613	0.215	0.306	0.255	44.7
83	0.72	0.307	0.676	0.261	0.575	1.090	27.0
85	0.76	0.510	0.924	0.242	0.438	0.422	33.5
89	0.49	0.303	0.685	0.246	0.556	1.080	26.3
91	0.74	1.000	1.340	0.188	0.252	0.357	48.2
95	0.89	0.306	0.636	0.197	0.409	1.220	28.8
98	1.55	0.772	1.256	0.164	0.267	0.417	37.9
101	2.71	0.496	0.894	0.224	0.403	0.467	33.6
103	0.67	0.820	1.242	0.141	0.213	0.420	41.3
104	0.98	0.632	1.001	0.224	0.355	0.424	39.2

Table 6.1: CA/T SB STP: Recompression CK_0UC Triaxial Test Data (Notes: (1) stresses in ksf, (2) Preshear t_c = 1 day, (3) Shear $\dot{\epsilon}$ = 0.5%/hr unless otherwise noted)–Page 4 of 5

	MAXIMUM OBLIQUITY					
TEST	AX STRN (%)	q/SIGvc'	p'/SIGvc'	q/SIGp'	p'/SIGp'	PHI' (deg)
40	1.1	0.573	0.960	0.118	0.198	36.7
42	1.2	0.760	1.272	0.190	0.318	36.7
46	0.9	0.386	0.747	0.298	0.578	31.1
47	10.5	0.370	0.634	0.143	0.245	35.7
50	4.3	0.526	0.955	0.118	0.214	33.4
52	4.3	0.407	0.685	0.193	0.324	36.5
56	1.5	0.757	1.255	0.208	0.346	37.1
57	2.1	0.631	1.073	0.182	0.309	36.0
58	0.9	0.439	0.580	0.076	0.100	49.1
59	10.1	0.490	0.856	0.220	0.385	34.9
62	4.0	0.522	0.879	0.213	0.359	36.4
63	6.1	0.234	0.419	0.163	0.292	34.0
64	0.8	0.727	0.949	0.245	0.320	50.0
66	0.7	0.460	0.802	0.241	0.420	35.0
68	1.0	0.717	1.108	0.184	0.284	40.3
69	11.6	0.271	0.473	0.176	0.306	35.0
73	1.2	0.797	1.204	0.143	0.215	41.5
78	0.8	0.910	1.404	0.198	0.305	40.4
79	0.6	1.090	1.521	0.207	0.289	45.8
83	12.6	0.163	0.253	0.139	0.215	40.1
85	4.1	0.457	0.804	0.217	0.381	34.6
89	16.1	0.156	0.243	0.127	0.197	40.0
91	0.6	0.981	1.292	0.184	0.243	49.4
95	8.9	0.227	0.322	0.146	0.207	44.9
98	1.6	0.772	1.256	0.164	0.267	37.9
101	5.4	0.481	0.852	0.217	0.384	34.4
103	0.7	0.820	1.242	0.141	0.213	41.3
104	1.0	0.632	1.001	0.224	0.355	39.2

Table 6.1: CA/T SB STP: Recompression CK_0UC Triaxial Test Data (Notes: (1) stresses in ksf, (2) Preshear t_c = 1 day, (3) Shear $\dot{\epsilon}$ = 0.5%/hr unless otherwise noted)–Page 5 of 5

				PRE SHEAR		
TEST	B (%)	ADJ. qf (ksf)	E50/SIGvc'	AX STRN (%)	VOL STRN (%)	Comments
40	97	1.816	495	0.70	0.85	E, probable PSS
42	105	2.544	319	0.60	1.35	E
46	90	2.113	197	2.45	2.70	E
47	91	1.866	335	0.70	1.61	E, prominent PSS, high strain rate
50	93	1.678	400	0.65	1.05	VG, PSS
52	89	2.066	320	1.20	1.55	E, high strain rate
56	100	2.649	630	0.10	0.71	E, high strain rate
57	96	2.323	472	0.56	1.82	E, high strain rate
58	103	1.136	1283	0.12	8.60	P,leak, Kc too low, delete qf
59	98	2.929	370	0.34	1.40	E, but Kc too high
62	95	2.161	196	2.09	2.75	F, v. high strain rate
63	96	1.986	240	1.25	1.39	VG
64	96	2.353	34	1.61	1.78	G, but Kc too low
66	87	1.912	225	2.00	2.55	VG, but Kc bit low
68	97	2.260	508	0.52	1.24	E, but Kc too low
69	92	2.133	301	1.20	2.10	E, but Kc too high
73	94	2.332	611	0.80	0.99	E, loose silty parting, probable PSS
78	100	2.829	530	0.40	0.77	E
79	99	3.116	788	0.24	0.38	E
83	95	1.960	142	3.97	4.05	VG, high strain rate
85	100	2.541	396	0.90	1.40	E
89	104	2.249	120	3.16	4.02	E, small stone in specimen
91	100	2.421	665	0.18	0.19	G
95	100	1.751	218	2.70	5.40	F, leak, PSS, delete qf
98	97	2.153	406	0.48	1.74	VG, prominent PSS, Kc too high
101	97	2.434	142	-0.12	1.89	G, unsteady strain rate
103	101	1.988	683	0.401	0.984	E, but Kc bit high
104	99	2.024	279	1.424	2.096	E, low strain rate

Table 6.2: Summary of Recompression Tests with K_c Different from $K_0 \geq 10\%$

			PEAK					M Q			Repeat
TEST	OCR	Kc/Ko	Failure Strn (%)	q/SIGvc'	q/SIGp'	p'/SIGp'	Af	q/SIGp'	p'/SIGp'	E50/SIGvc'	Test Number
Compression Tests											
50	4.462	1.11	9.90	0.539	0.121	0.226	0.540	0.118	0.214	400	
57	3.468	1.12	1.65	0.633	0.183	0.311	0.446	0.182	0.309	472	
58	5.796	0.81	0.57	0.467	0.081	0.107	0.898	0.076	0.100	1283	103
59	2.224	1.33	1.24	0.598	0.269	0.477	0.454	0.220	0.385	370	101
64	2.967	0.84	1.03	0.754	0.254	0.339	0.381	0.245	0.320	340	104
66	1.908	0.89	0.73	0.46	0.241	0.420	0.530	0.241	0.420	225	
68	3.900	0.83	0.89	0.718	0.184	0.285	0.327	0.184	0.284	508	98
69	1.544	1.29	1.30	0.371	0.240	0.479	0.801	0.176	0.306	301	95
98	4.700	1.30	1.55	0.772	0.164	0.267	0.417	0.164	0.267	406	
Extension Tests											
70	4.638	0.68	1.60	0.529	0.114	0.198	0.450	0.079	0.130	340	99
74	2.955	0.76	1.40	0.371	0.126	0.265	0.541	0.091	0.149	297	
93	13.813	?	3.40	0.923	0.067	0.092	0.526	0.067	0.092	441	
99	4.580	1.14	1.12	0.568	0.124	0.235	0.481	0.095	0.158	421	

Table 6.3: CA/T SB STP: Recompression CK_0UE Triaxial Test Data (Notes: (1) stresses in ksf, (2) Preshear t_c = 1 day, (3) Shear $\dot{\epsilon}$ = 0.5%/hr unless otherwise noted)–Page 1 of 5

RECOMPRESSION TEST DATA SUMMARY						SPECIMEN			
TEST	SAMPLE	DEPTH (ft)	ELEV. (ft)	Wn (%)	(SD)	Wn (%)	Gs	e	S
46	BS-2A	69.1	42.1	36.9	0.5	37.0	2.80	1.039	0.995
49	BS-7	90.3	20.9	53.1	0.2	53.6	2.80	1.509	0.995
53	BS-3A	77.6	33.6	40.9	0.3	41.3	2.80	1.150	1.010
70	BS-7	90.3	20.9	53.5	0.1	53.7	2.80	1.490	1.009
74	BS-7	90.3	20.9	51.3	1.1	53.8	2.80	1.489	1.011
75	BS-7	90.3	20.9	52.7	0.2	53.8	2.80	1.499	1.005
80	SB23-U15	89.1	21.8	50.3	0.2	50.4	2.80	1.418	0.995
84	BS-1A	56.5	54.7	33	0.9	32.6	2.80	0.919	0.994
87	BS-2A	69.1	42.1	36.15	1.1	38.6	2.80	1.090	0.991
90	BS-3A	77.6	33.6	39.8		41.8	2.80	1.167	1.004
93	BS-7	90.3	20.9	41.8	1.1	42.8	2.80	1.189	1.009
96	SB23-U22	113.2	-2.3	45.3	0.3	45.3	2.80	1.260	1.007
99	BS-7	90.3	20.9	52.05	0.2	52.6	2.80	1.472	1.000

Table 6.3: CA/T SB STP: Recompression CK_0UE Triaxial Test Data (Notes: (1) stresses in ksf, (2) Preshear t_c = 1 day, (3) Shear $\dot{\epsilon}$ = 0.5%/hr unless otherwise noted)–Page 2 of 5

	IN SITU			TEST			
TEST	SIGvo' (ksf)	SIGp' (ksf)	OCR	SIGvc' (ksf)	OCR	Kc	(Ko)
48	4.13	10.607	2.568	4.233	2.506	0.858	0.79
49	5.245	7.003	1.335	5.347	1.310	0.578	0.60
53	4.56	9.162	2.009	4.531	2.022	0.794	0.73
70	5.24	7.003	1.336	1.510	4.638	0.700	1.03
74	5.24	7.003	1.336	2.370	2.955	0.650	0.86
75	5.24	7.003	1.336	3.730	1.877	0.720	0.72
80	5.19	7.156	1.379	4.980	1.437	0.620	0.62
84	3.48	12.749	3.664	3.250	3.923	0.980	0.96
87	4.13	10.607	2.568	1.940	5.468	1.170	1.10
90	4.57	9.162	2.005	2.060	4.448	1.070	1.03
93	5.24	7.003	1.336	0.507	13.813	1.610	
96	6.52	7.515	1.153	6.260	1.200	0.580	0.56
99	5.24	7.003	1.336	1.529	4.580	1.110	0.97

Table 6.3: CA/T SB STP: Recompression CK_0UE Triaxial Test Data (Notes: (1) stresses in ksf, (2) Preshear t_c = 1 day, (3) Shear $\dot{\epsilon}$ = 0.5%/hr unless otherwise noted)–Page 3 of 5

	PEAK						
TEST	AX STRN (%)	q/SIGvc'	p'/SIGvc'	q/SIGp'	p'/SIGp'	Af	PHI' (deg)
48	2.93	0.340	0.597	0.135	0.238	0.905	34.7
49	1.90	0.194	0.471	0.148	0.360	0.895	24.3
53	1.89	0.290	0.610	0.143	0.302	0.865	28.4
70	1.60	0.529	0.916	0.114	0.198	0.450	35.3
74	1.40	0.371	0.782	0.126	0.265	0.541	28.3
75	1.40	0.260	0.677	0.138	0.361	0.733	22.6
80	2.15	0.203	0.519	0.141	0.361	0.874	23.0
84	3.43	0.534	0.840	0.136	0.214	0.639	39.4
87	2.45	0.720	1.104	0.132	0.202	0.483	40.7
90	1.20	0.699	1.199	0.157	0.270	0.375	35.7
93	3.40	0.923	1.272	0.067	0.092	0.526	46.5
96	5.30	0.142	0.276	0.118	0.230	1.230	31.0
99	1.12	0.568	1.075	0.124	0.235	0.481	31.9

Table 6.3: CA/T SB STP: Recompression CK_0UE Triaxial Test Data (Notes: (1) stresses in ksf, (2) Preshear t_c = 1 day, (3) Shear $\dot{\epsilon}$ = 0.5%/hr unless otherwise noted)–Page 4 of 5

	MAXIMUM OBLIQUITY					
TEST	AX STRN (%)	q/SIGvc'	p'/SIGvc'	q/SIGp'	p'/SIGp'	PHI' (deg)
48	2.9	0.340	0.597	0.135	0.238	34.7
49	9.5	0.152	0.199	0.116	0.152	50.0
53	4.4	0.281	0.541	0.139	0.268	31.3
70	10.0	0.367	0.604	0.079	0.130	37.4
73	1.2	0.797	1.204	0.143	0.215	41.5
74	8.9	0.270	0.440	0.091	0.149	37.8
75	9.3	0.191	0.327	0.102	0.174	35.7
80	10.3	0.164	0.290	0.114	0.202	34.3
84	1.5	0.496	0.752	0.126	0.192	41.3
87	1.2	0.696	1.048	0.127	0.192	41.7
90	0.9	0.681	1.163	0.153	0.261	35.8
93	3.4	0.923	1.272	0.067	0.092	46.5
96	8.0	0.134	0.233	0.112	0.194	35.0
99	5.7	0.433	0.722	0.095	0.158	36.8

Table 6.3: CA/T SB STP: Recompression CK_0UE Triaxial Test Data (Notes: (1) stresses in ksf, (2) Preshear t_c = 1 day, (3) Shear $\dot{\epsilon}$ = 0.5%/hr unless otherwise noted)–Page 5 of 5

				PRE SHEAR		
TEST	B (%)	E50/SIGvc'	ADJ. qf (ksf)	AX STRN (%)	VOL STRN (%)	Comments
48	94	299	1.432	0.10	1.85	VG
49	100	200	1.032	2.60	3.30	E, slightly high strain rate
53	94	300	1.315	1.00	1.40	E, low strain rate
70	98	340	0.963	0.70	1.00	G, but Kc too low
74	96	297	0.990	1.65	1.80	E, but Kc too low
75	100	282	1.021	1.76	2.01	E
80	96	164	1.017	1.32	1.52	G, unsteady strain rate
84	100	440	1.753	0.73	0.96	E
87	101	538	1.564	0.74	0.80	E
90	95	473	1.623	0.30	0.49	E
93	98	441	0.664	0.23	0.53	F, OCR too high
96	100	133	0.894	3.1	4.5	E
99	101	421	1.045	0.92	1	E, but Kc too high

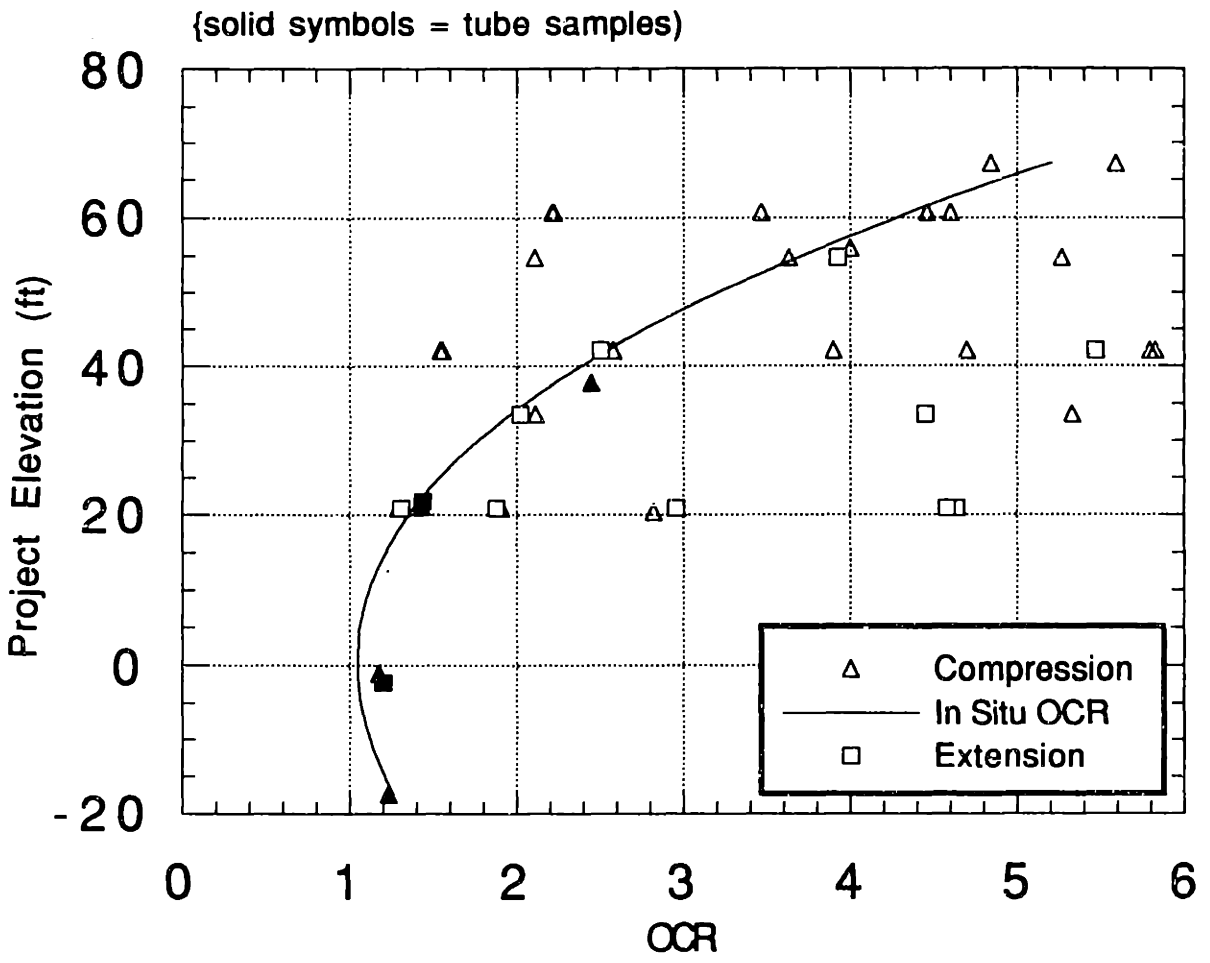

Stress Ratio	Number of Tests on Blocks (Tubes)		
	Compression	Extension	Total
$\sigma'_{vc} = \sigma'_{vo}$	9 (4)	4 (2)	13 (6)
$\sigma'_{vc} \neq \sigma'_{v0}$	15 (0)	7 (0)	22 (0)
Total	28	13	41

Figure 6-1: Elevation vs. Test OCR for Recompression CK_0UC/E Tests on SB Tube and Block Samples

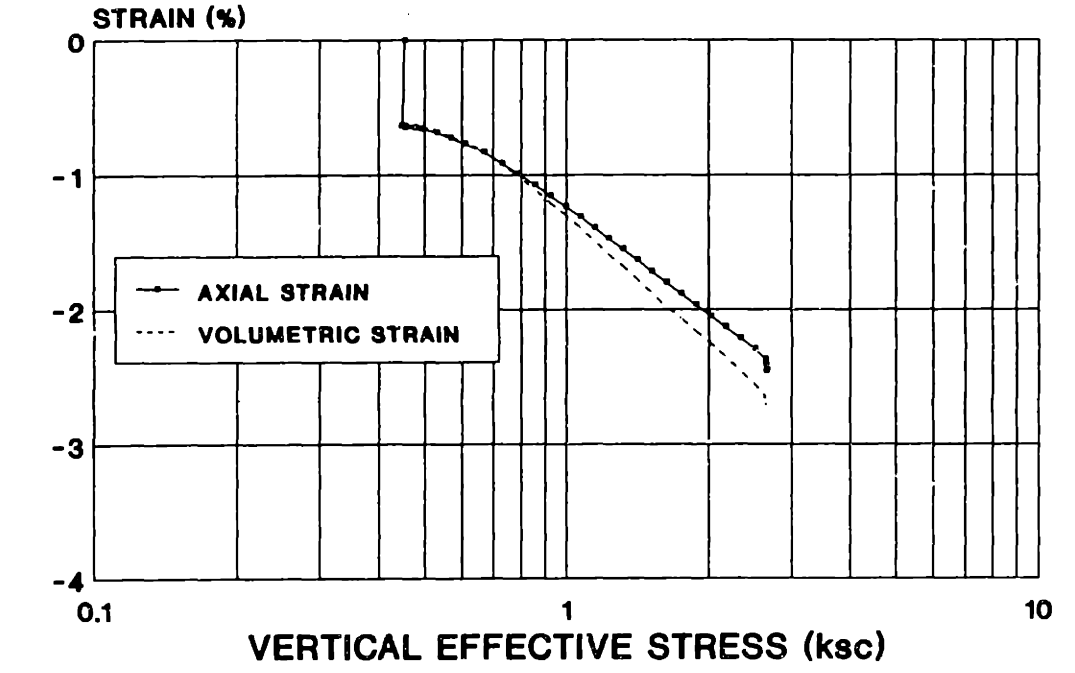

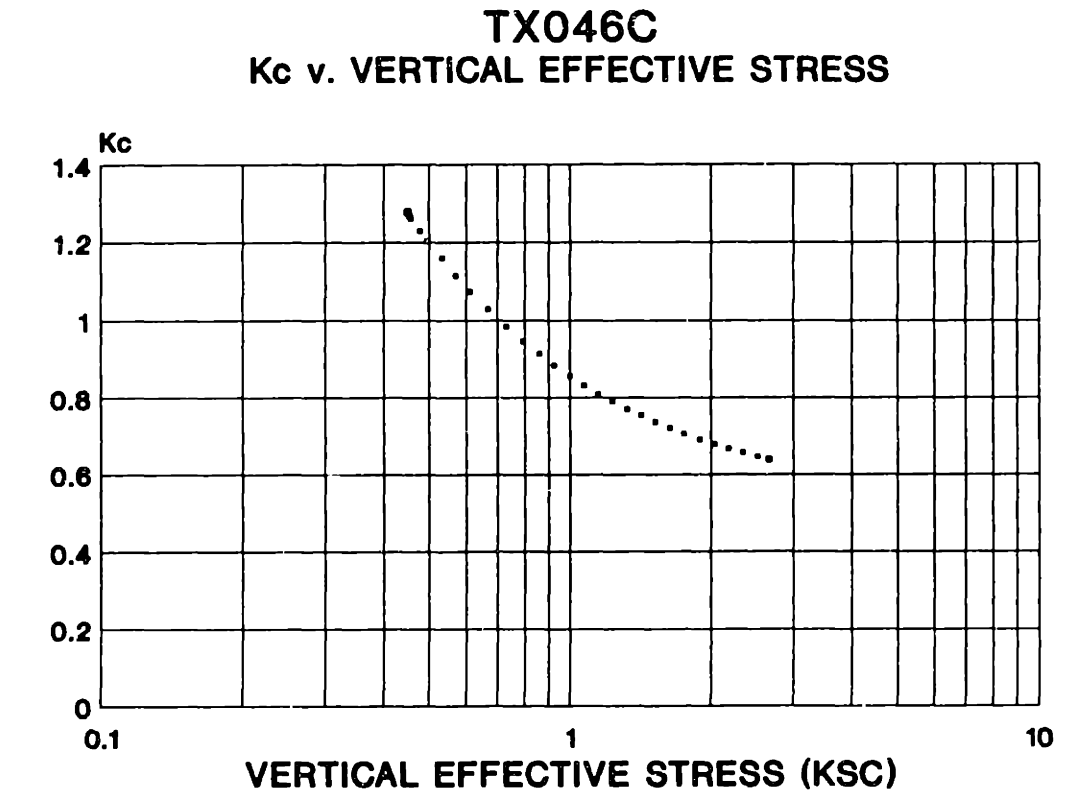

Figure 6-2: Typical Compression Curve and K_0 vs. σ'_{vc} plot from Recompression Test TX046 (σ'_{v0} = 5.245 ksf, σ'_p =7.003 ksf; ksf=2.048×ksc)

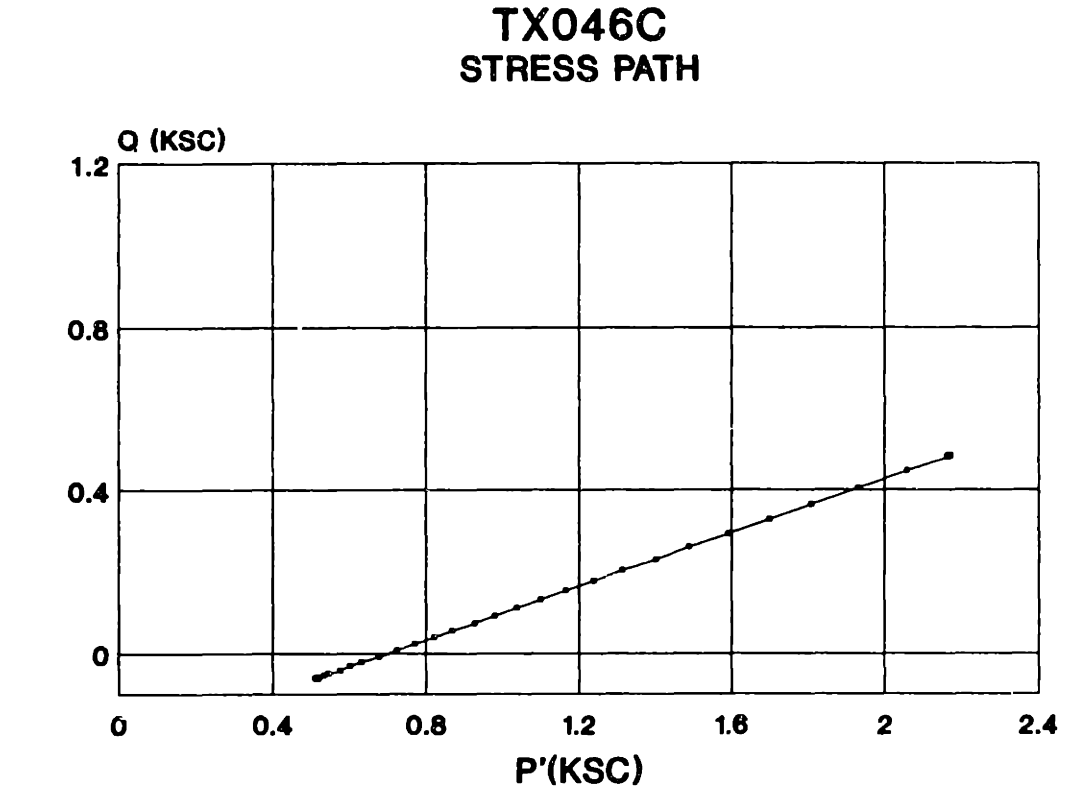

Figure 6-3: Typical Consolidation Stress Path from Recompression Test TX046 (σ'_{v0} = 5.245 ksf, σ'_p =7.003 ksf; ksf=2.048×ksc)

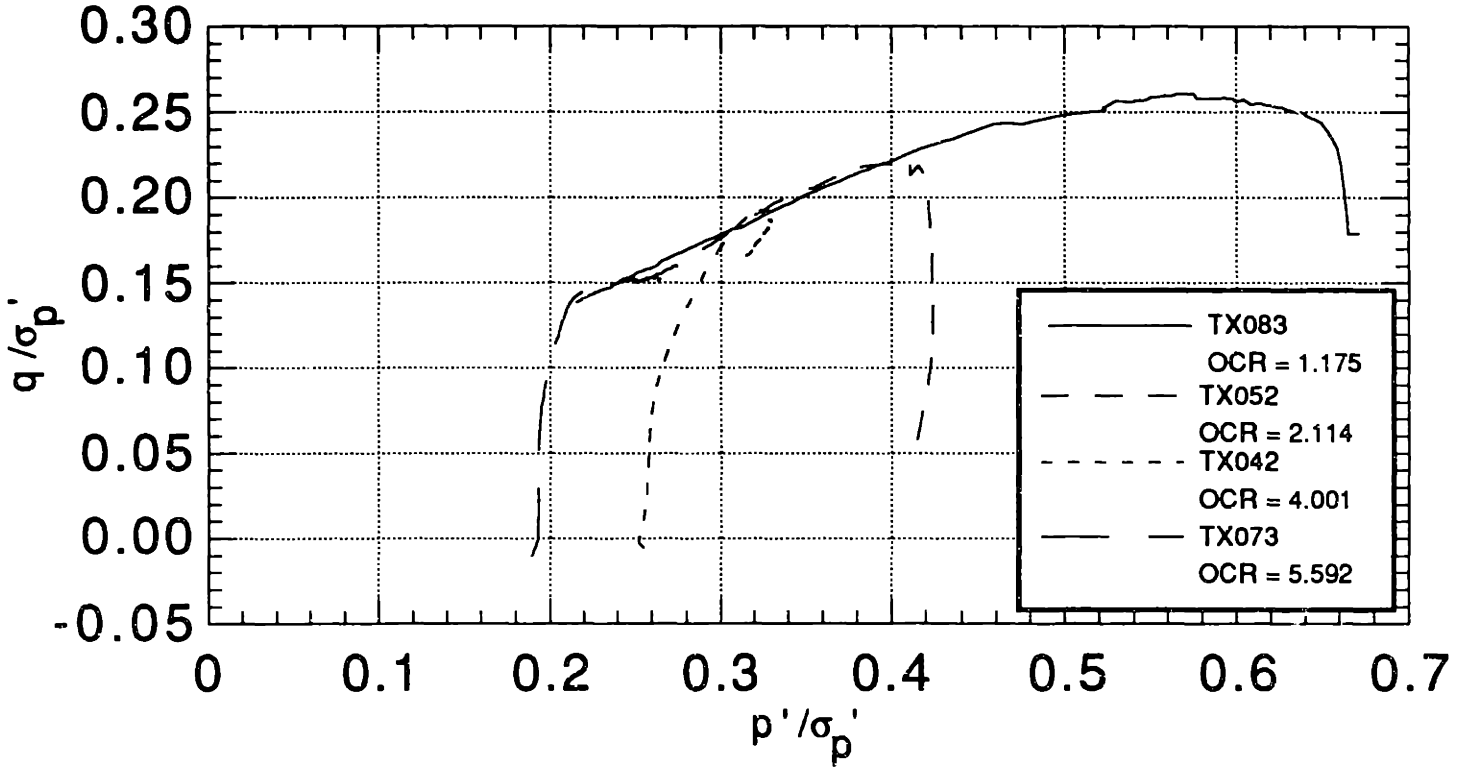

Figure 6-4: Comparison of Typical Normalized Stress Paths from Recompression TC Tests

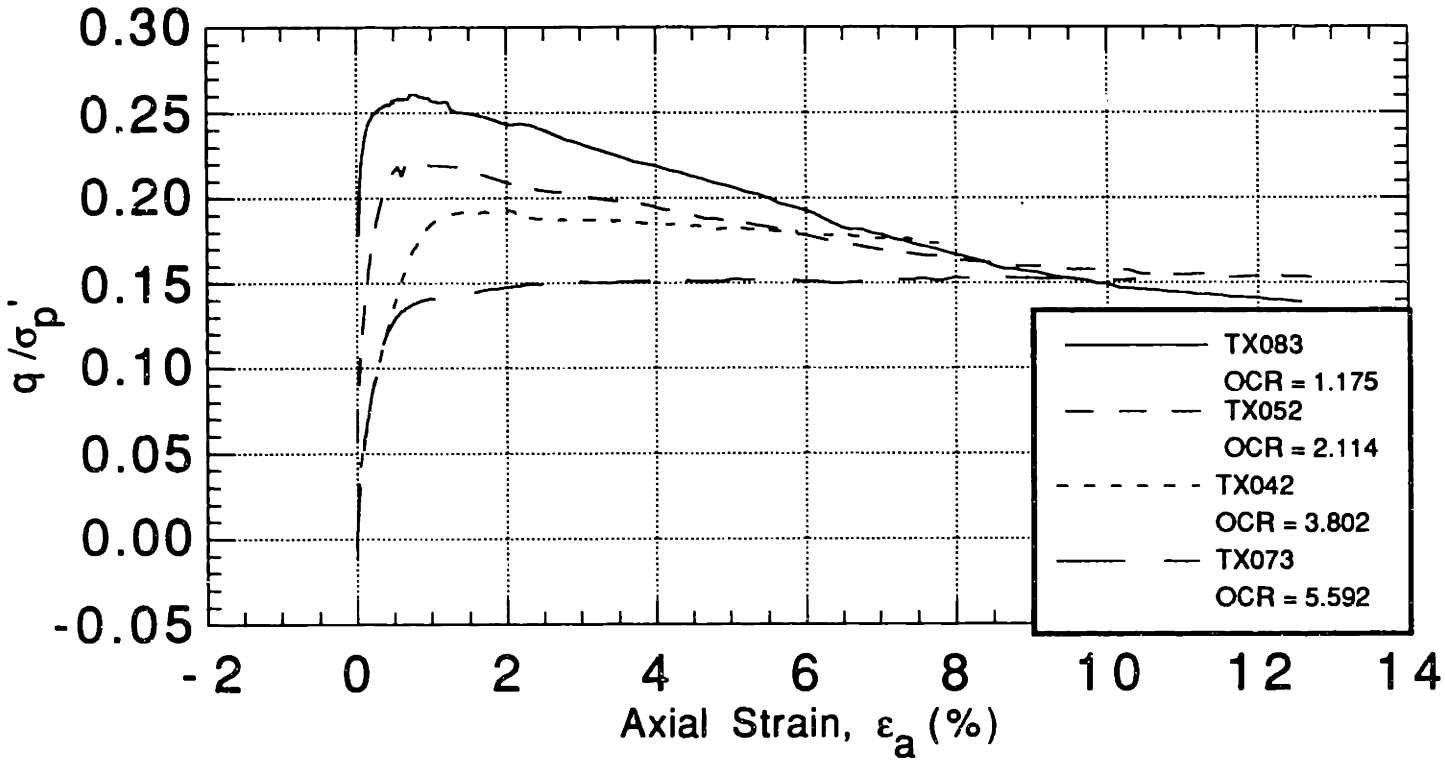

Figure 6-5: Comparison of Typical Stress-Strain Curves from Recompression TC Tests

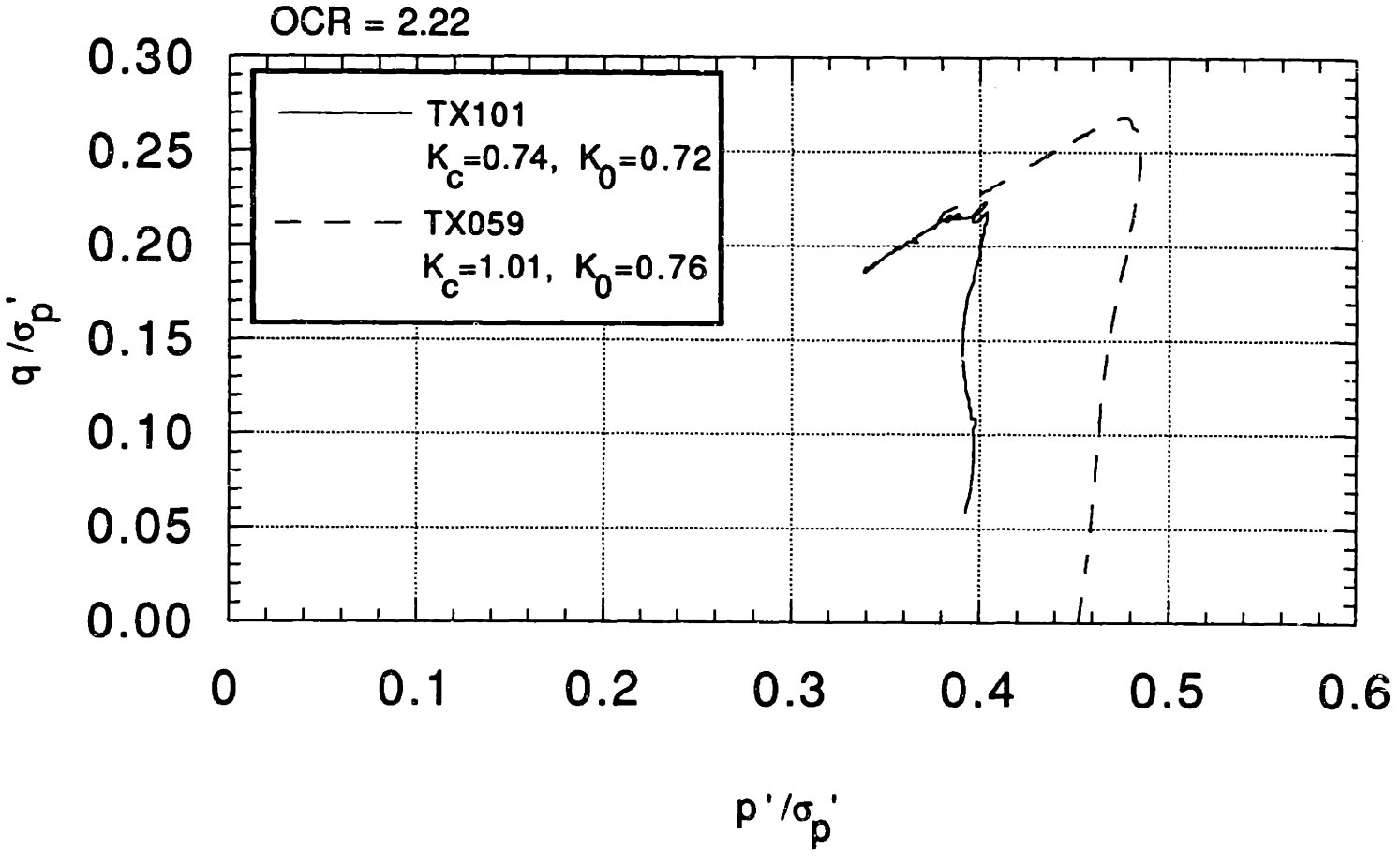

Figure 6-6: Comparison of Recompression TC Stress Paths (OCR = 2.22) with Good and Bad K_c

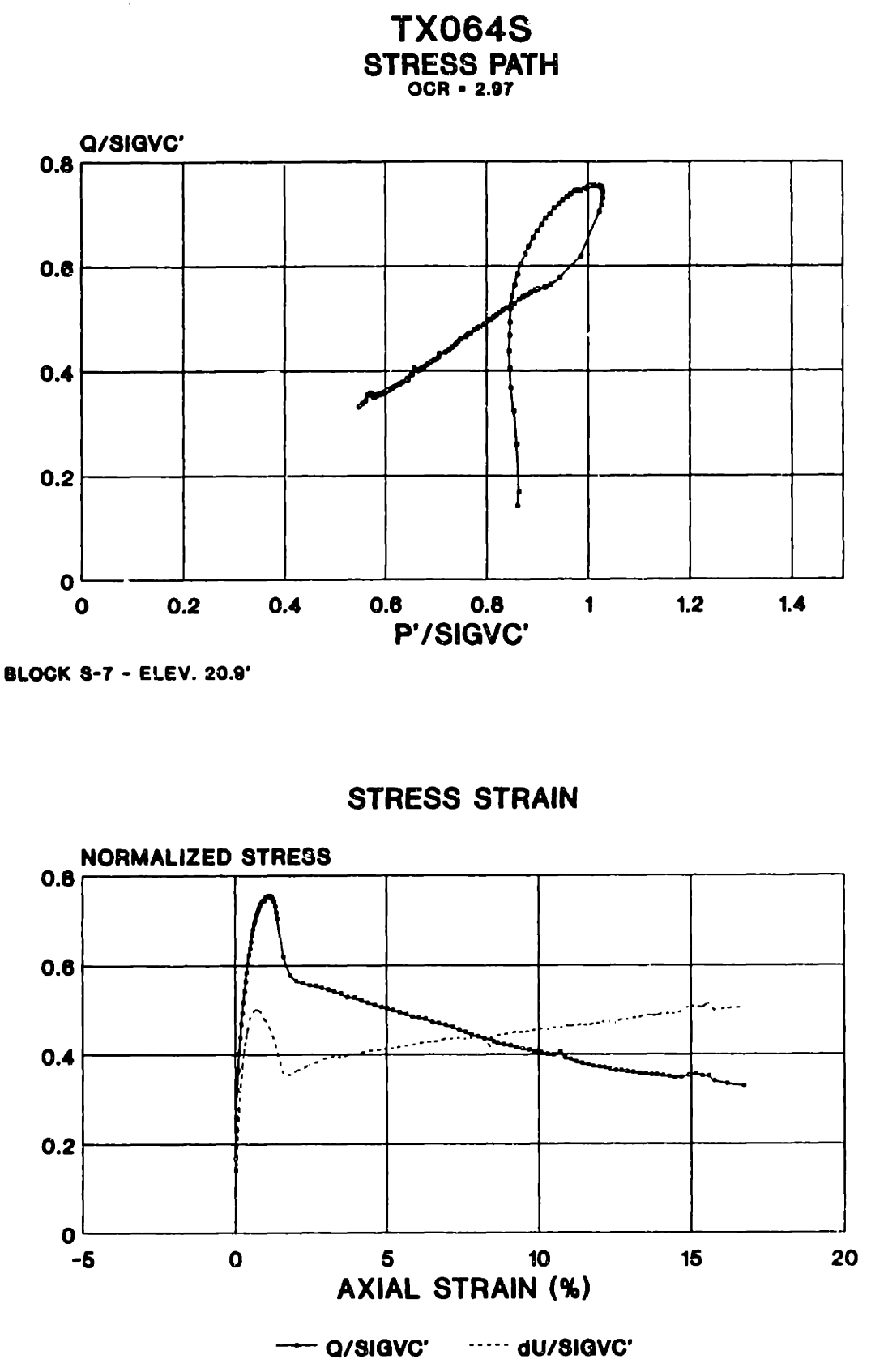

Figure 6-7: Example of Extreme Case of Strain Softening in TC (OCR=2.97)

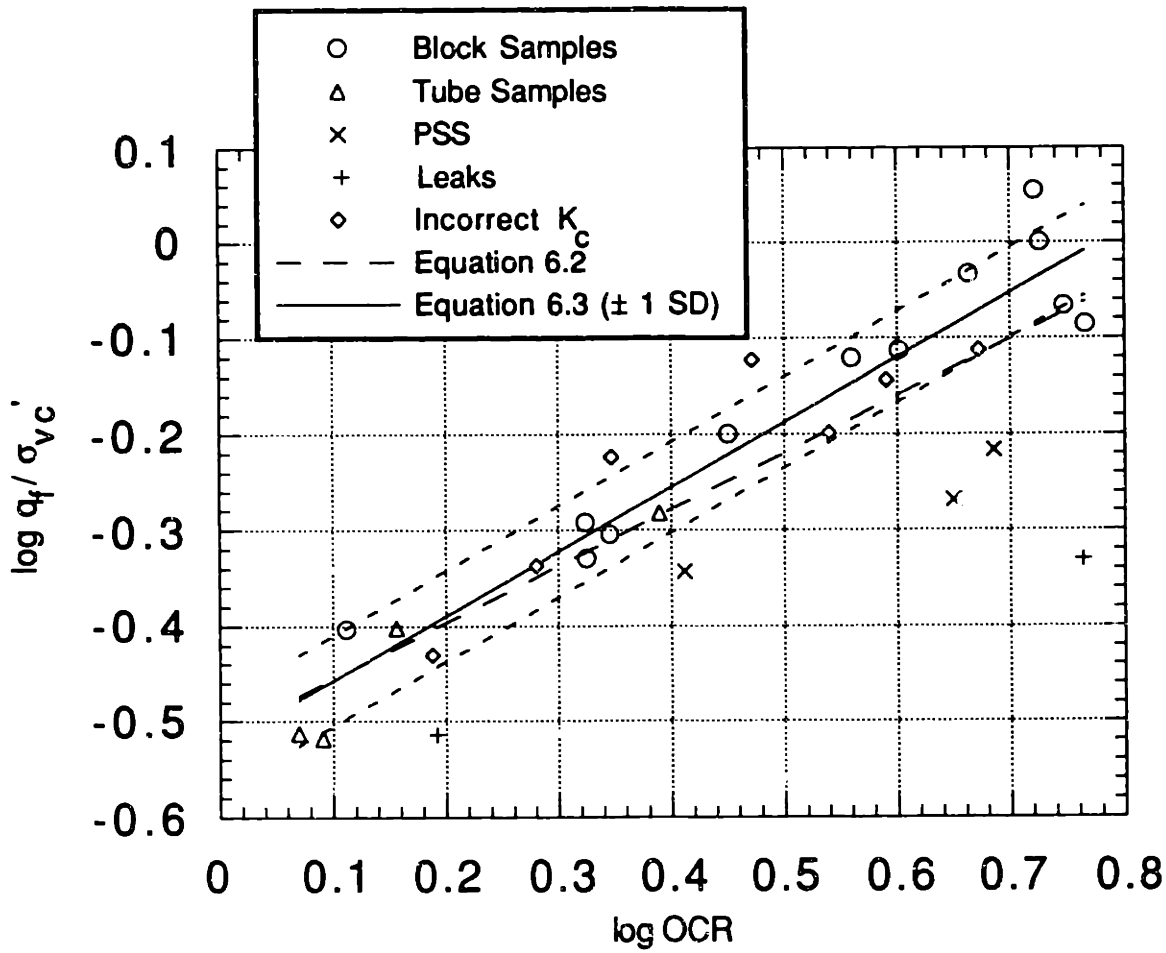

Figure 6-8: Undrained Strength Ratio versus OCR from Recompression CK_0UC Triaxial Tests

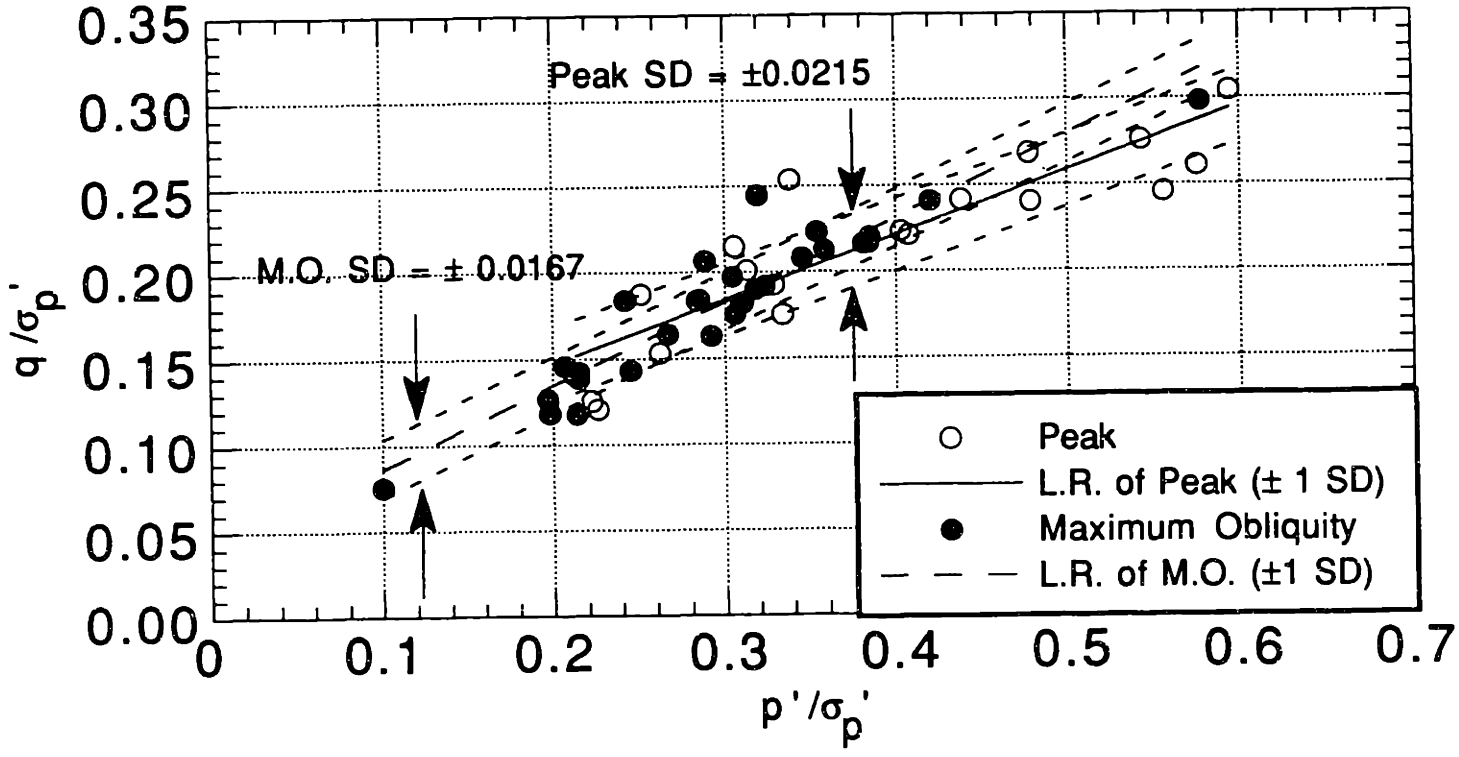

Figure 6-9: Normalized Stresses at Peak and Maximum Obliquity from Recompression CK_0UC Triaxial Tests

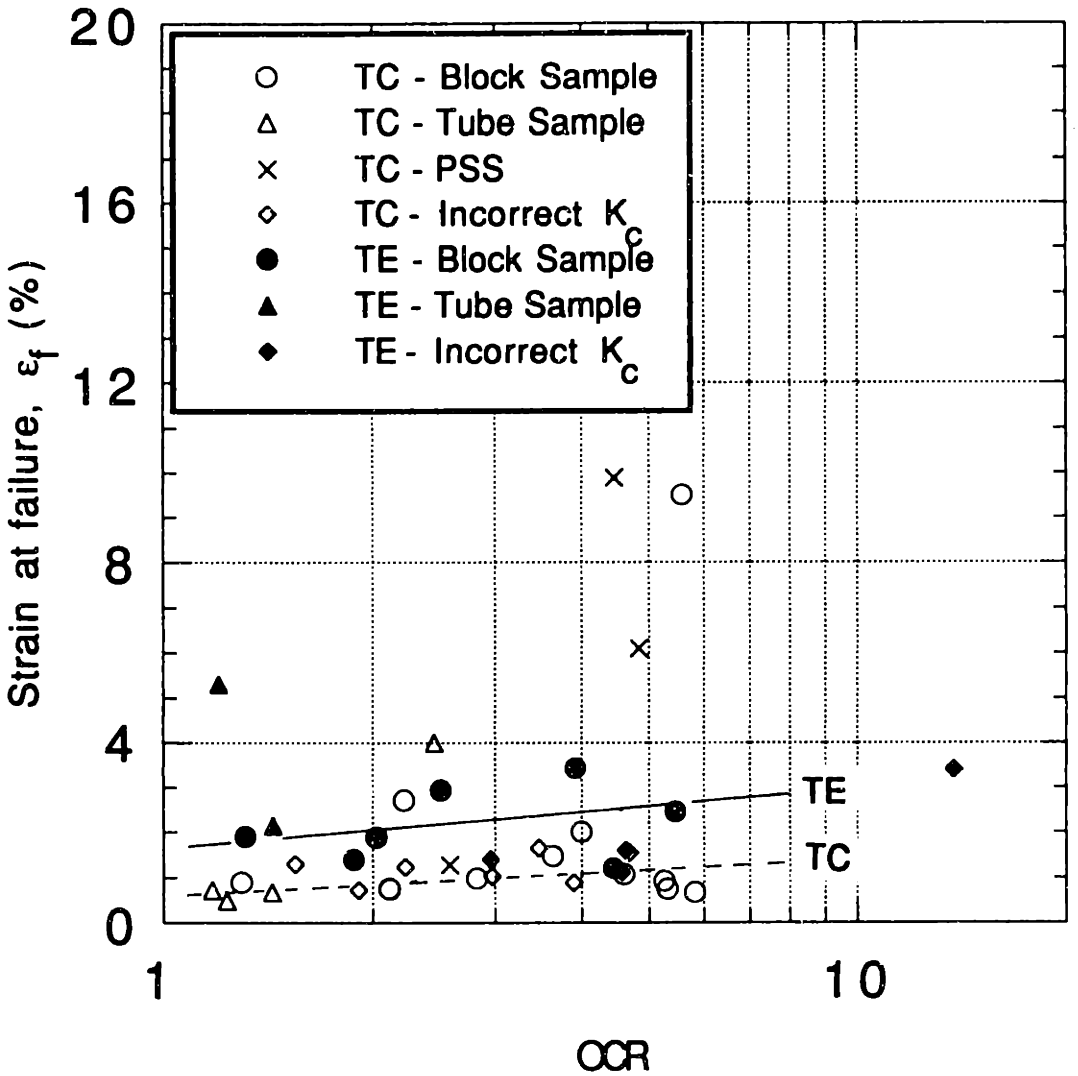

Figure 6-10: Strain at Failure vs. OCR from Recompression CK_0UC and CK_0UE Triaxial Tests

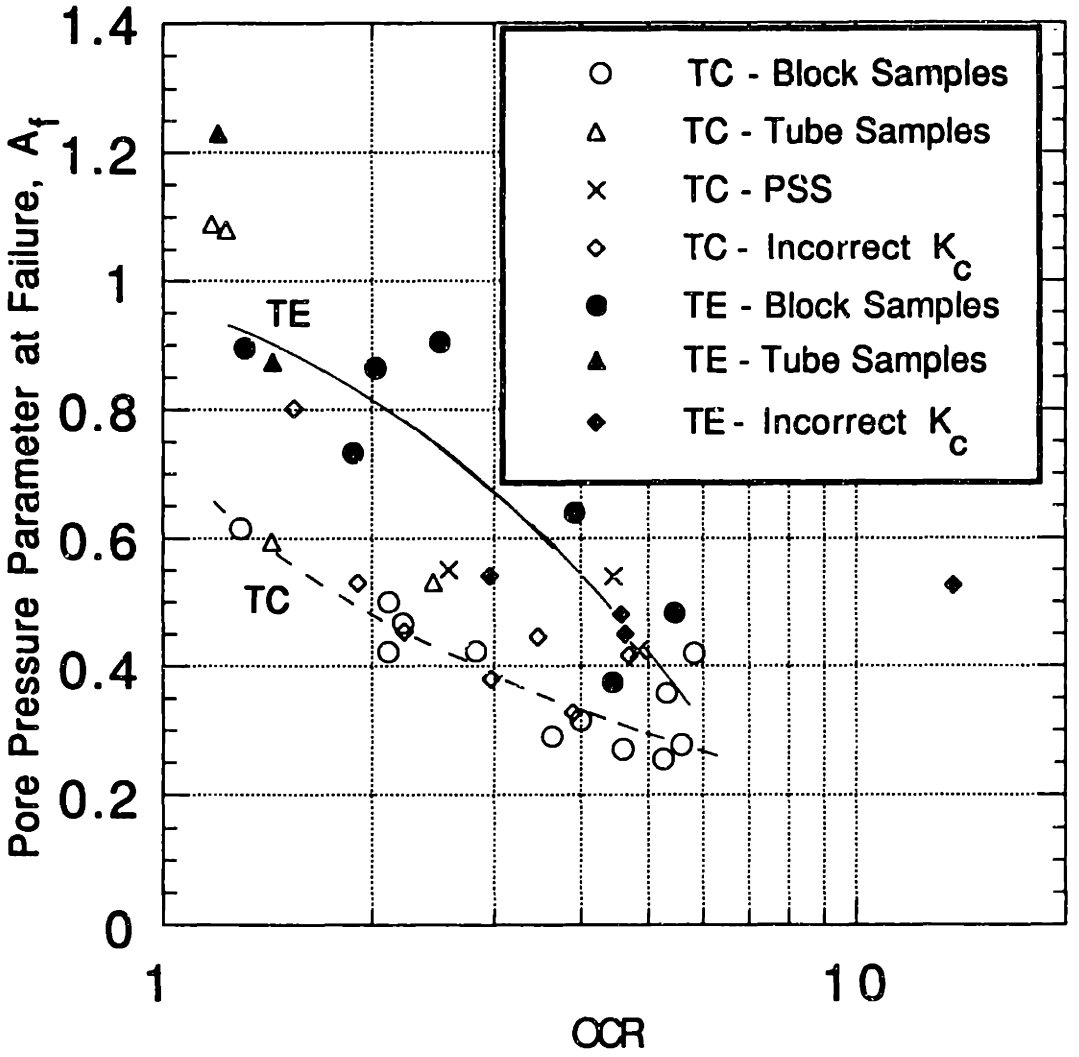

Figure 6-11: A_f vs. OCR from Recompression CK_0UC and CK_0UE Triaxial Tests

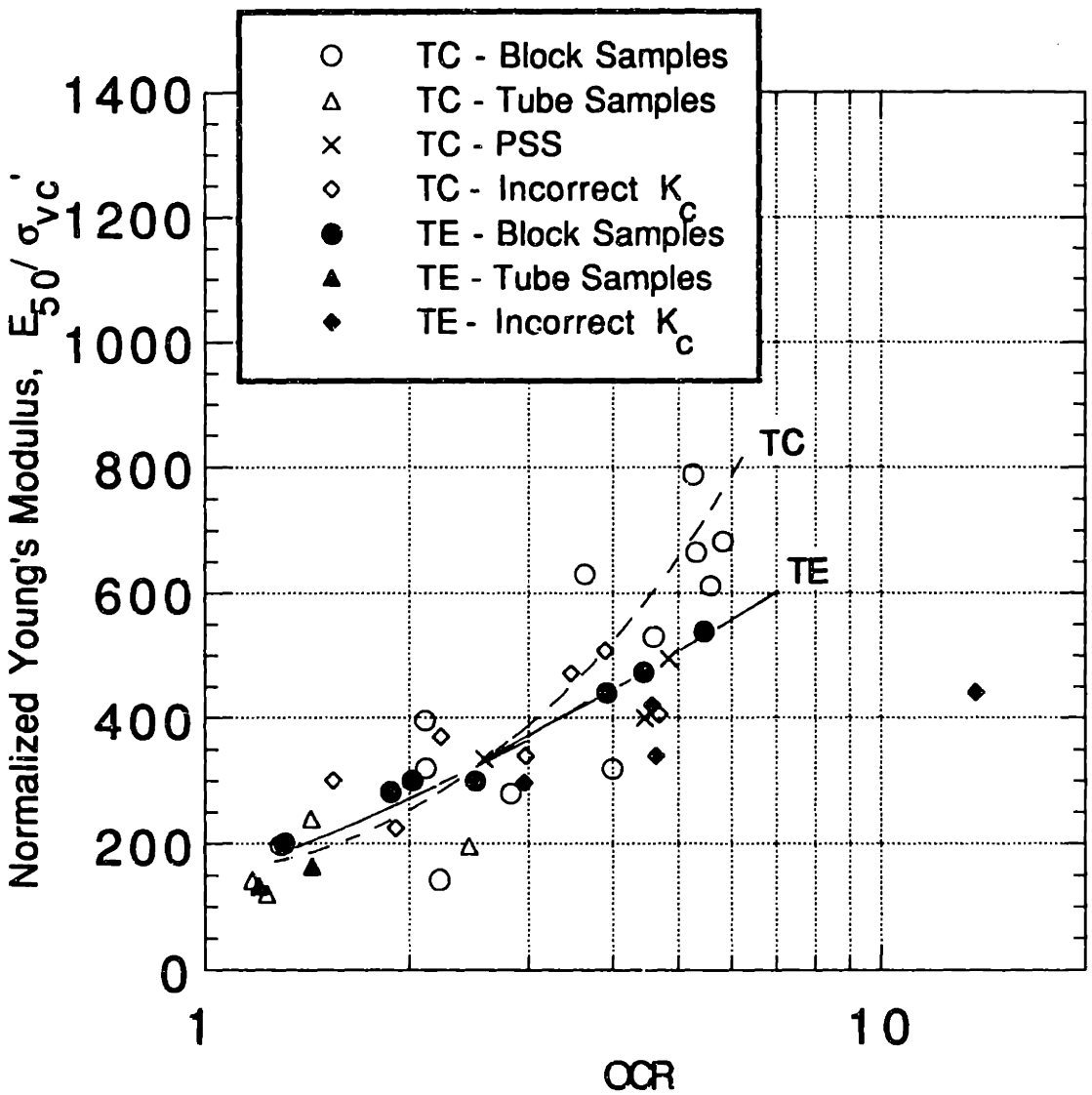

Figure 6-12: $E_{50}/\sigma_{vc'}$ vs. OCR from Recompression CK_0UC and CK_0UE Triaxial Tests

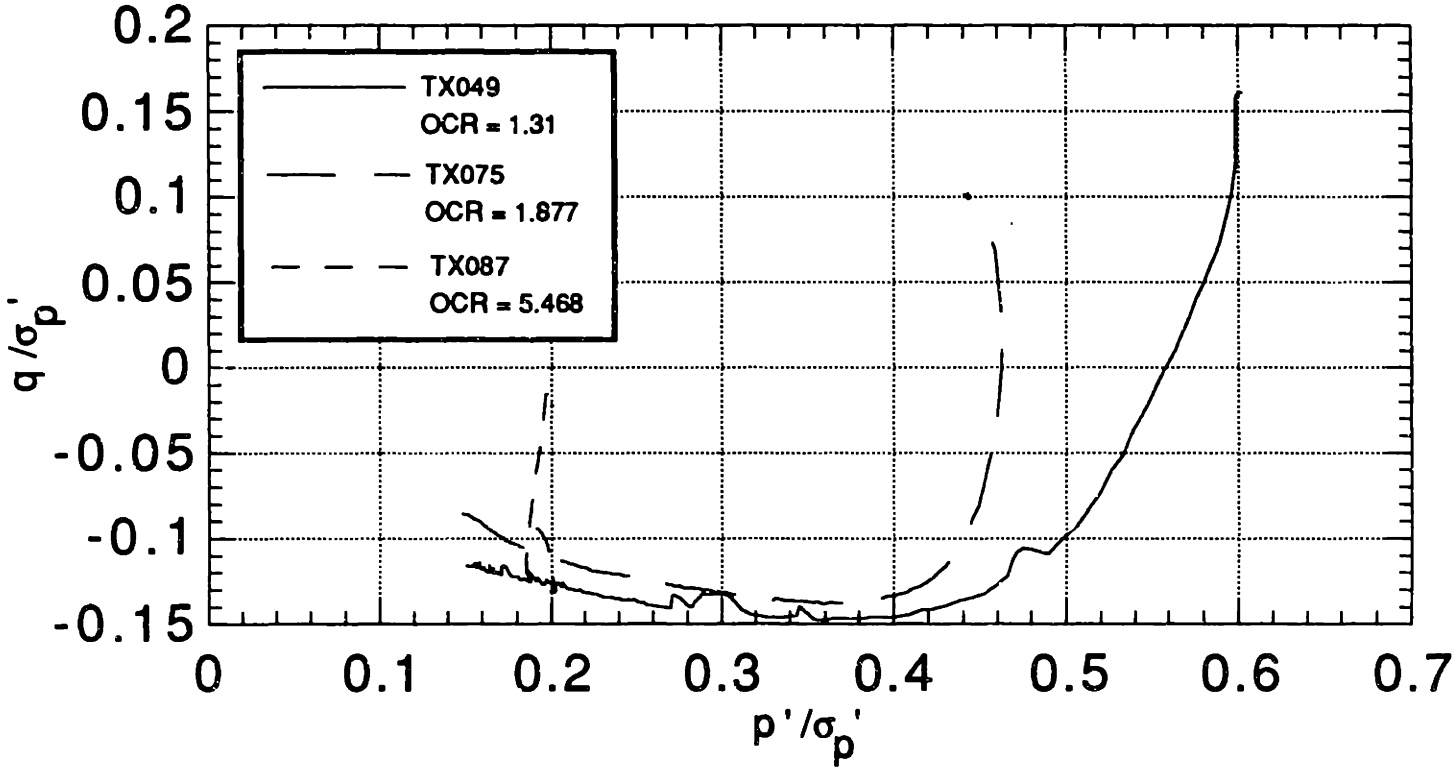

Figure 6-13: Comparison of Typical Normalized Stress Paths from Recompression TE Tests

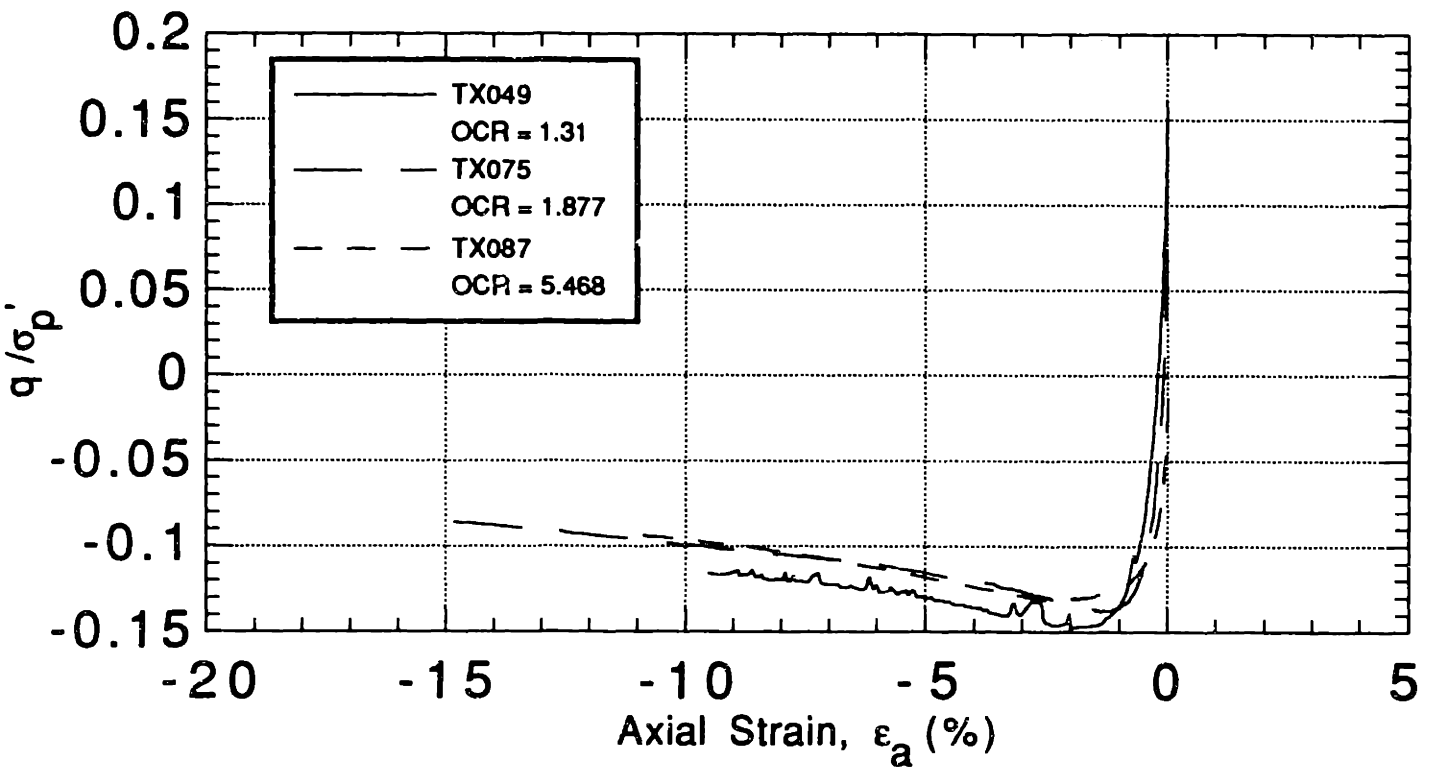

Figure 6-14: Comparison of Typical Stress-Strain Curves from Recompression TE Tests

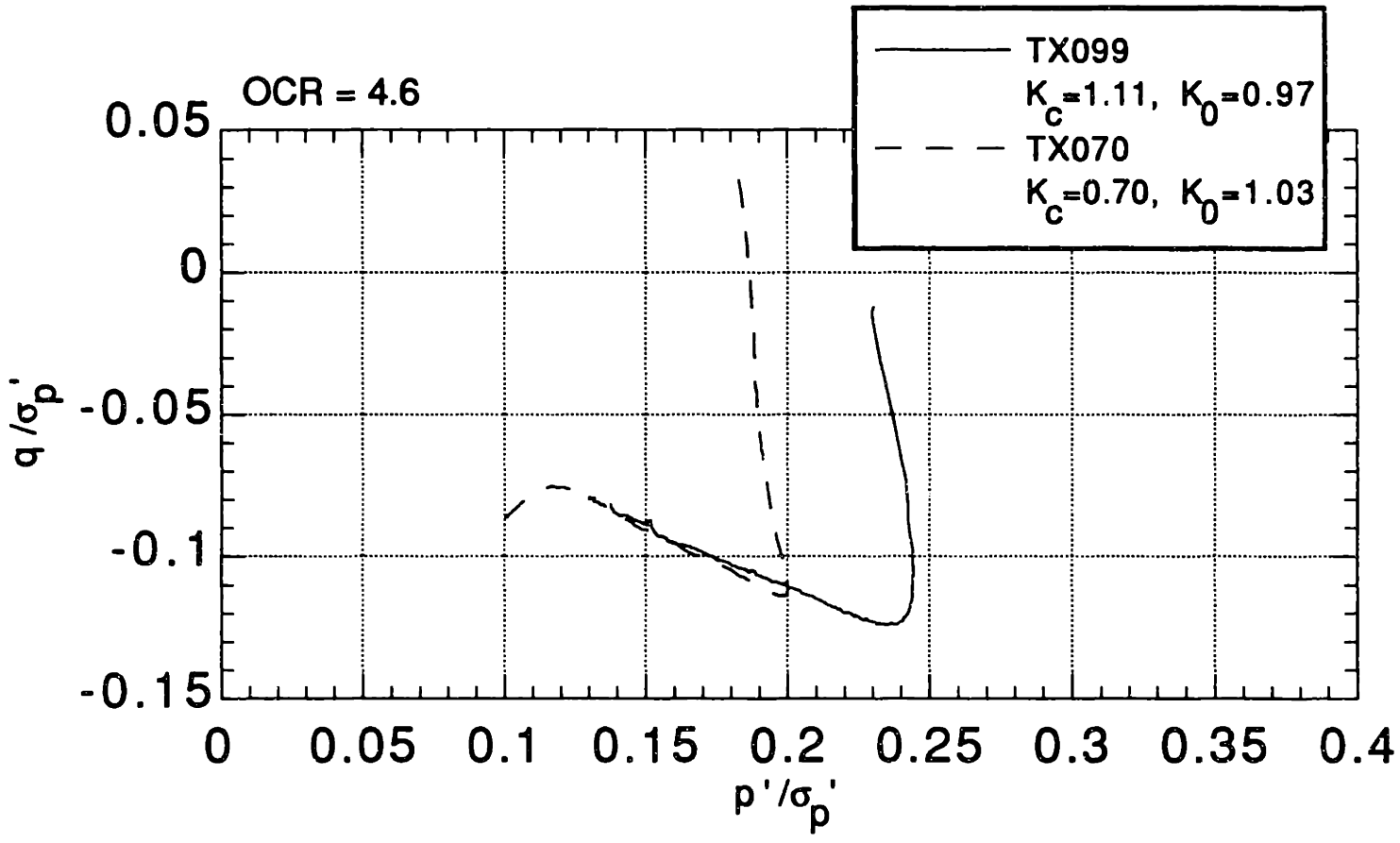

Figure 6-15: Comparison of Recompression TE Stress Paths with Good and Bad K_c

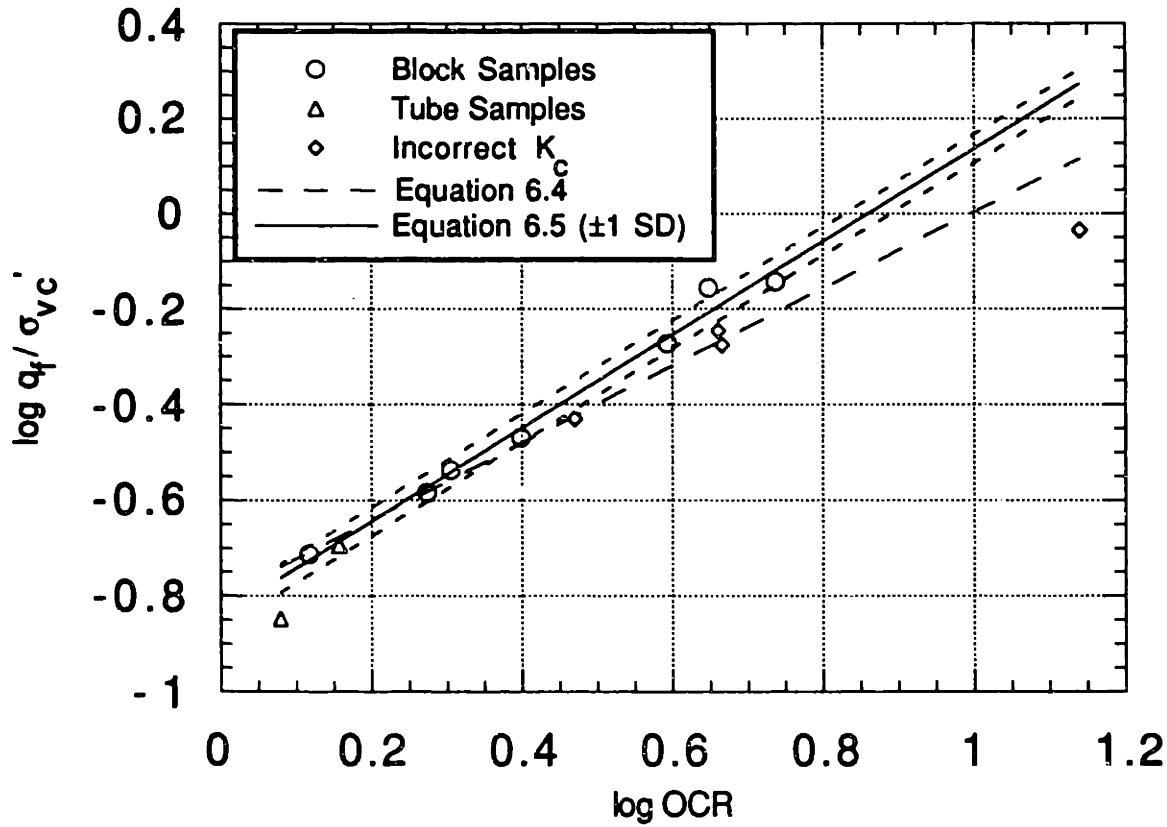

Figure 6-16: Undrained Strength Ratio versus OCR from Recompression CK_0UE Triaxial Tests

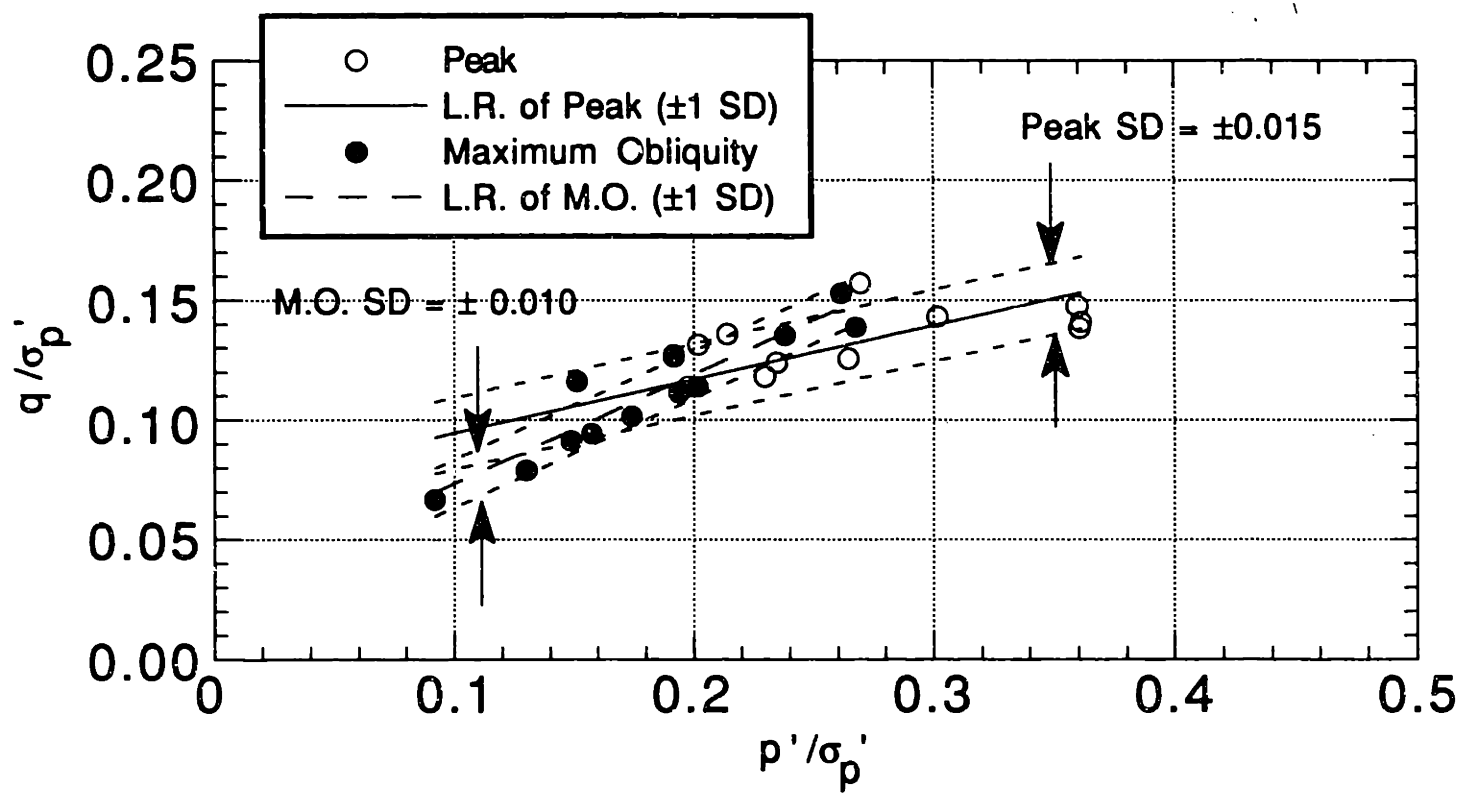

Figure 6-17: Normalized Stresses at Peak and Maximum Obliquity from Recompression CK_0UE Triaxial Tests

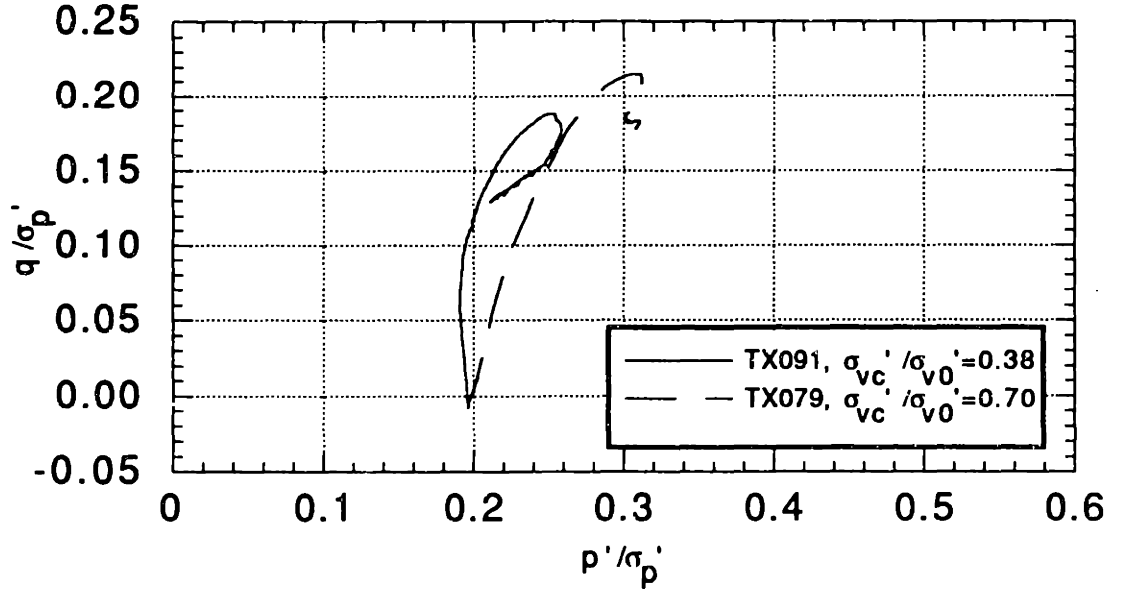

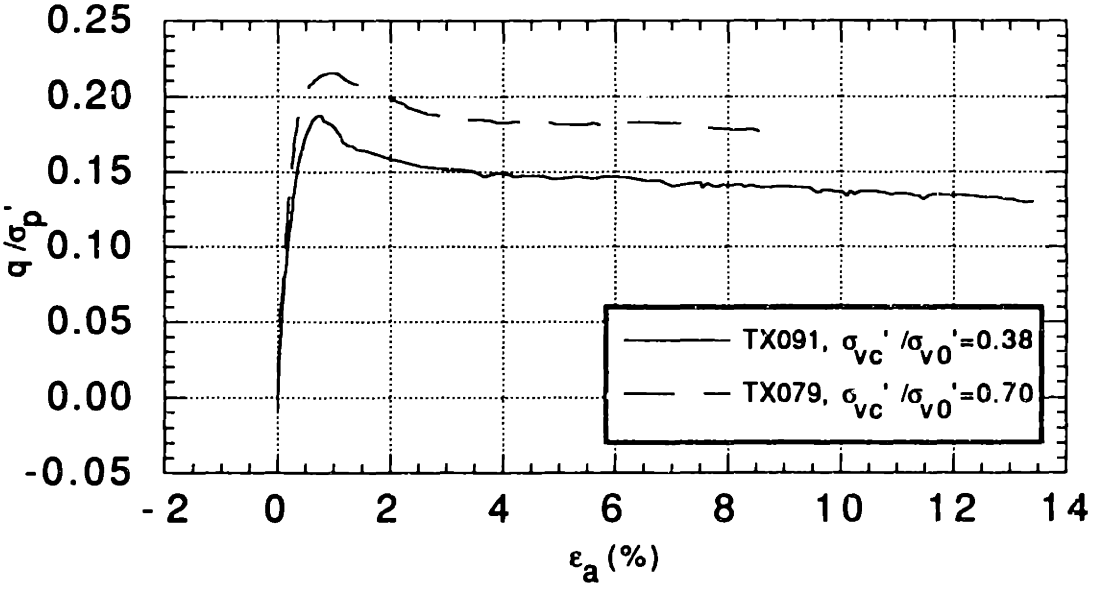

Figure 6-18: Example of Effect of Consolidation Stress on Stress Path

Chapter 7

Comparison of Recompression Test Results with SHANSEP and CIUC/UUC Test Results

7.1 Introduction

This chapter compares results from Recompression CK_0UC and CK_0UE tests with those obtained from SHANSEP CK_0UC/E and CIUC/UUC tests on BBC at the South Boston site. The introduction section discusses some possible questions that comparison of these data might answer. Section 7.2 covers the SHANSEP comparison, and Section 7.3 the comparison with H&A's UUC and CIUC data.

Ladd (1991) outlines the advantages and disadvantages of the Recompression versus SHANSEP methods. His recommendations are summarized in Section 2.3, but are abstracted here. In particular, he mentions that Recompression is superior for highly structured or cemented soils, and is preferred when block samples are available, and in highly overconsolidated crusts, but should always be accompanied by a thorough evaluation of the stress history. The SHANSEP method, on the other hand, is strictly applicable only to mechanically overconsolidated or truly normally consolidated deposits of soils exhibiting normalized behavior, but is still probably preferred for deep deposits of low OCR "ordinary" clays and has the advantage of *forcing* one

to evaluate the stress history of the site.

Comparison of these test results on BBC will evaluate Ladd's opinions in several important ways.

1. All of the Recompression test specimens are overconsolidated by mechanisms acting on the deposit, which, as described in Chapter 2, are thought to be desiccation and mechanical unloading due to erosion. The overconsolidated SHANSEP tests, in contrast, are strictly mechanically overconsolidated in the laboratory. The two issues to be considered are: a) whether overconsolidation by means other than mechanical (e.g., desiccation) leads to some sort of inherent difference in the soil structure, and b) whether reaching the preconsolidation pressure by *loading* (as in Recompression tests) or *unloading* (as in SHANSEP tests) will affect shear behavior as the result of the typical hysteresis observed in unload/reload cycles. Thus Recompression and SHANSEP tests run at the same OCR may yield different stress-strain-strength parameters due to different overconsolidation methods.

2. Comparing test results may help highlight the importance of "structure" in the soil. Ladd (1991) makes the distinction that Recompression testing is superior for highly structured, brittle clays, such as those typical of eastern Canada, while SHANSEP is more appropriate for "ordinary" clays. However, early observations (such as S-shaped compression curves – see Section 5.2) indicate that the lower BBC samples obtained for the STP have a significant structure, perhaps somewhere between "highly structured" and "ordinary". How much this structure affects the undrained shear behavior of the clay, and the degree to which this structure is altered by the SHANSEP consolidation process are both issues one might hope to address through comparison of the Recompression and SHANSEP results.

3. It is acknowledged that sample disturbance will have a greater effect on Recompression results than SHANSEP results, and thus the recommendation that Recompression tests are "clearly preferred" if block samples are available. How-

ever, as covered in the previous chapter, the tube samples obtained by H&A on this project were of excellent quality, and tests run on them generally gave results which fell within the scatter of the block sample tests. On the other hand, the SHANSEP procedure of consolidating the specimen well beyond the preconsolidation pressure is intended to minimize sampling disturbance effects (based on the concept of normalized behavior). Though the subject of sample disturbance is extremely complex, an examination of the results of these two testing programs may lead to at least qualitative conclusions on the effect of sample disturbance on the undrained stress-strain-strength parameters of BBC.

The second half of this chapter compares Recompression results with CIUC and UUC tests performed by H&A. The inaccuracies associated with these types of tests are numerous. UUC tests are affected by several factors: sampling disturbance which decreases the effective stress in the specimen and thus decreases strength; a fast strain rate (ASTM standard is 1%/minute) which tends to increase strength; and shear in compression ($\delta = 0$) which also tends to increase strength. As a result of these compensating errors, UUC can yield reasonable, though often highly variable, results. But they can also give mean strengths that are significantly too high or too low depending on soil type, sample quality, etc. The advantages of UUC tests are that they are quick, easy and inexpensive, and hence are frequently used in practice.

CIUC test results may be less variable, but are in many cases *unsafe* due to neglect of strength anisotropy and larger consolidation strains from using K_c=1. Their use can be justified to measure triaxial compression behavior for moderately overconsolidated (OCR $\approx$ 4) samples for which $K_0 \approx 1$. Again, however, they are widely used in practice.

Since these testing practices are still common, it would be valuable to quantify the effects that standard tests have on shear results by comparing them with more reliable data, i.e., from Recompression or SHANSEP tests.

In both of the following sections, only results from "reliable" Recompression tests are used for comparison. In particular, the two tests with internal leaks are not considered at all. When the existence of PSS, use of incorrect K_c values, or use of

tube samples rather than block samples, were thought to affect the results (as covered in Chapter 6), these tests were shown with different symbols.

7.2 Comparison with SHANSEP CK_0U Results

7.2.1 Triaxial Compression Tests

Overview

The organization of this chapter is similar to Chapter 6. Typical plots comparing Recompression and SHANSEP stress paths and stress-strain curves are presented first, then a comparison is made between the USR-OCR relationship obtained for each type of test and the effective stress envelopes at peak and maximum obliquity that results from each, and finally, the stress-strain parameters (ϵ_f, A_f, and E_{50}/σ'_{vc}) are examined.

The reader is referred to Chapter 4 for a description of the scope of the SHANSEP testing program. For the comparisons presented here, only "reliable" results (based on analyses performed by de La Beaumelle) were used, which generally meant tests with leaks or rated "Poor" for other reasons were not included. SHANSEP data from both South and East Boston sites are used since they gave essentially the same results. The TC peak strength data are based on 13 normally consolidated tests and 11 overconsolidated tests (OCR = 1.1 to 5.8).

Typical Plots

Figures 7-1 through 7-3 show normalized stress paths and stress-strain curves for three pairs of good quality compression tests. For all of these plots the stresses have been normalized to σ'_p (calculated from Eq. 5.3) for the Recompression tests and σ'_{vm} for SHANSEP tests. Each figure represents a specific OCR and contains both Recompression and SHANSEP test data at that OCR. The point on each stress path and stress-strain curve represents the peak.

Figure 7-1 shows Recompression test TX083 on tube sample SB2-23 U21 at El.

-1.1 ft, with test OCR≈1.2 and SHANSEP test TX002 on SB2-21 U12 at El. -17.9 ft and OCR = 1.22. Both of these tests (as well as all of the typical plots presented hereafter) were rated very good or excellent. The Recompression test has a slightly higher peak, gives a higher effective stress envelope, and more strain softening.

Figure 7-2 shows two tests with OCR = 2.8. The Recompression test, TX104, is from BS-7 at El. 20.4, while the SHANSEP TX035 is from SB2-23 U11 at El. 39.0. Here the ESEs defined by the stress paths are significantly different and the Recompression test shows a higher, more pronounced peak and significant strain softening.

The final figure in the series, Figure 7-3, shows more highly overconsolidated samples. Recompression test TX073 is from BS-1 at El. 67.2 and sheared at OCR = 5.6. The SHANSEP test, TX034, is from SB2-23 U11 at El. 39.4 and OCR = 5.8. As in the previous two figures, the Recompression ESE is higher than the SHANSEP ESE (though peak values are approximately the same). The shape of the stress paths is somewhat interesting. The Recompression test stress path is concave to the right, reflecting a decrease in pore pressure after peak, while the SHANSEP test's sharp hook to the left reflects increasing pore pressures after peak (for plots showing both stress and pore pressure during shear, the reader is referred to Appendix B which contains stress path and stress-strain plots for all Recompression tests).

Undrained Strength Ratio

Figure 7-4 compares q_f/σ'_{vc}, the undrained strength ratio, versus OCR relationships obtained from the two types of tests. The dashed line shown is a linear regression of 24 SB and EB SHANSEP TC tests, including both tubes and blocks. The Recompression points shown include tests on blocks and tubes, and include tests sheared at incorrect values of K_c , but do not include the two tests with leaks (see explanation in Section 6.3). The L.R. of the SHANSEP data yields the following equation (SD = standard deviation of log q/σ'_{vc}):

$$q_f/\sigma'_{vc} = 0.280(OCR)^{0.682} \qquad SD = \pm 0.020 \qquad (7.1)$$

With very few exceptions, the Recompression data lie above this line. Recall that the L.R. of Recompression data from Chapter 6 (Eq. 6.3) gave

$$q_f/\sigma'_{vc} = 0.298(OCR)^{0.376} \qquad SD = \pm 0.047 \tag{7.2}$$

(excluding points with PSS) which is a line nearly parallel to the SHANSEP line, but about 6% higher. The scatter in the Recompression is significantly larger, however.

Effective Stress Envelopes

Figures 7-5 and 7-6 compare the effective stress envelopes for SHANSEP and Recompression tests at peak and maximum obliquity, respectively. For the peak SHANSEP data (Figure 7-5) two lines are shown. The solid line is the normally consolidated ESE, which yields $\phi'_f = 22.2°$. The square point shown on the solid line is the mean p'_f and q_f from the NC SHANSEP tests. The dashed line is the overconsolidated (OCR>2) ESE with $\phi' = 19.6°$, $c'/\sigma'_{vm} = 0.0604$, and SD = ± 0.005. Most of the Recompression test data lie above the SHANSEP ESE, and linear regression (also shown on Figure 7-5) on these peak values gives both a higher friction angle ($\phi' = 22.0°$) and cohesion (c'/σ'_p=0.078), but with much larger scatter (SD=$\pm$0.022).

For clarity, the TC maximum obliquity data are presented separately in Figure 7-6. In this case, the SHANSEP NC ESE has $\phi'_m = 30.1°$ (square symbol) and the OC ESE (dashed line) yields $\phi' = 28.5°$ and $c'/\sigma'_{vm} = 0.015$, with SD= ± 0.006. As before, most Recompression tests lie above the SHANSEP envelope. Linear regression on the Recompression points gives $\phi' = 28.9°$ and $c'/\sigma'_p = 0.044$, with SD= ± 0.017. This is a similar result as for the peak data; slightly higher ϕ' and c'/σ'_p which yields a higher envelope overall, but large scatter.

Stress-Strain Parameters

In the next three figures, the solid and dashed curves shown represent *approximate* trends for the Recompression TE and TC parameters respectively, as determined in Chapter 6.

Figure 7-7 plots Recompression and SHANSEP ϵ_f values (i.e., at peak strength) versus OCR for both TC and TE, tube and block samples. The SHANSEP TC point plotted at OCR = 1 represents the mean $\epsilon_f = 0.35\% \pm 0.15$SD. The SHANSEP ϵ_f data show a steady increase from OCR 1 to OCR 6. The Recompression TC data show no such trend with ϵ_f being generally much smaller than SHANSEP at high OCRs.

The next figure in the series, Figure 7-8, plots the pore pressure parameter at failure, A_f versus OCR. The OCR=1 TC point shown is a mean of the SHANSEP tests (0.85±0.1SD). The TC data from both types of tests follow a clear decreasing trend with OCR, as expected, though the SHANSEP A_f is consistently lower than the Recompression data at higher OCRs. This is somewhat surprising because, as previously noted, the Recompression tests yield higher peak strengths. This implies that the higher ESE of the Recompression tests more than offsets lower A_f values in the SHANSEP tests, to give an overall increase in USR.

The final figure in this section, Figure 7-9 plots E_{50}/σ'_{vc} versus OCR for the two types of tests. The values from SHANSEP compression tests remain fairly constant with OCR in a range of approximately 200 to 300 (at OCR = 1, mean E_{50}/σ'_{vc} = 275±50SD). In contrast, the Recompression tests show a marked increase in E_{50}/σ'_{vc} with increasing OCR. Thus the Recompression tests at higher OCRs give a much "stiffer" response, i.e., lower ϵ_f and higher modulus.

Discussion

To summarize the main observations of the preceding section:

1. Recompression TC tests (for specimens without preexisting shear surfaces) yield consistently higher peak undrained strength ratios than SHANSEP tests, though there is larger scatter in the data (see Fig. 7-4). Linear regression of both sets of points yielded two approximately parallel lines, with the Recompression line about 6% higher than the SHANSEP line.

2. Both the peak and MO ESEs are higher for Recompression than SHANSEP tests due to both slightly higher values of ϕ' and higher cohesion intercepts (Figures 7-5 and 7-6).

3. This increase in the effective stress envelope more than offsets slightly lower values of A_f for the SHANSEP tests (see Fig. 7-8).

4. Lower strains at failure and higher E_{50}/σ'_{vc} values reflect the steeper initial stress-strain curves observed in the Recompression tests, especially at high OCRs (Fig. 7-9).

These observations tend to support the hypothesis that some sort of structure in the BBC enhances the strength and furthermore, that this strength contribution is diminished during the SHANSEP consolidation process. This is a very interesting finding as the BBC does not fit the description of "highly structured or sensitive". These results indicate that even slightly structured soils are sensitive to the testing technique employed.

7.2.2 Triaxial Extension Results

Overview

As for TC results in the previous section, only the most reliable of the SHANSEP TE results are used in this comparison. These results include both tube and block samples, both South and East Boston, but exclude various leaky or "Poor" tests, as determined by de La Beaumelle. The TE peak strength data are based on 11 normally consolidated tests and 11 overconsolidated tests (OCR = 2 to 8).

Typical Plots

The first of the TE plots, Figure 7-10, shows two OCR = 2 tests on the same block sample. The Recompression test, TX053, was at El. 33.6, in BS-3A and the SHANSEP test, TX092, at El. 33.7. The Recompression test shows a higher peak, a much smaller strain at failure, and a correspondingly higher E_{50}/σ'_{vc} than SHANSEP.

Next, Figure 7-11 shows two tests with OCR≈ 3. The Recompression test, TX074, has OCR = 2.956 and is from BS-7 at El. 20.9. The SHANSEP test has OCR = 2.93 and is TX016 from SB2-23 U20 at El. 5.5. Both tests have about the same peak strength, though it takes much larger strains for the SHANSEP test to mobilize this strength. While the Recompression test shows moderate strain softening, the SHANSEP test did not exhibit such behavior. Note that TX074 is one of the Recompression tests sheared with a value of K_c that was too low (K_c=0.65, K_0=0.86) which would have the effect of lowering the peak strength.

Finally, Figure 7-12 shows two extension tests with higher OCRs. Recompression test TX087 is from BS-2A at El. 42.1, and has OCR = 5.468. TX067, a SHANSEP test also from a block sample (BS-7) was from El. 20.2 and sheared at OCR = 5.78. The Recompression test in this comparison exhibits both higher peak and ESE than the SHANSEP test. As in the previous two figures, the stress-strain curve is much steeper for the Recompression test, and the peak much more pronounced. The Recompression test also shows significant strain softening, which is somewhat surprising given that results in Chapter 6 indicate that the deeper samples (in this case, the SHANSEP test on BS-7) have more of a propensity for this behavior. At high OCR, it appears that while the Recompression tests reach an early peak strength and then soften towards a "residual" stress level, the SHANSEP tests seem to harden continuously towards a peak strength which is very close to the "residual" strength of the Recompression tests.

Undrained Strength Ratio

Figure 7-13 is similar to Fig. 7-4 but shows TE data. Two linear regressions are shown for SHANSEP data. The first is for tests above El. 25 (i.e., in the crust) and yields the following equation:

$$q_f/\sigma'_{vc} = 0.151(OCR)^{0.860} \tag{7.3}$$

No standard deviation was calculated for this equation, as it is based on only 3 tests. The second L.R. for SHANSEP is for 17 tests below El. 25 and gives:

$$q_f/\sigma'_{vc} = 0.142(OCR)^{0.830} \qquad SD = \pm 0.031 \tag{7.4}$$

Recompression data from tests on block samples with correct values of K_c lie above both SHANSEP lines. The tests with incorrect K_c and tests on tube samples are lower and were not included in the L.R. of the Recompression data. The remaining seven tests yielded

$$q_f/\sigma'_{vc} = 0.144(OCR)^{0.978} \qquad SD = \pm 0.030 \tag{7.5}$$

While the S parameter is approximately the same for the two types of tests, the exponent m is significantly higher for the Recompression tests. Both have the same degree of scatter.

Effective Stress Envelope

Figure 7-14 presents triaxial extension data for SHANSEP and Recompression tests. For SHANSEP TE tests, the peak and MO occurred nearly simultaneously, thus only the MO data are presented here. The SHANSEP line shown includes all reliable tests from SB and EB, tube and block samples, and all in situ OCRs. This L.R. gave $\phi' = 21.8°$, $c'/\sigma'_{vm} = 0.044$, and SD= ± 0.010. Another SHANSEP L.R. (which is not shown on Fig. 7-14 for clarity) which included only tests with in situ OCRs less than 1.5 (i.e., samples below the upper crust), gave a lower envelope, with $\phi' = 18.8°$, $c'/\sigma'_{vm} = 0.052$, and SD= ± 0.010. Also shown is the Recompression ESE at MO, with $\phi' = 27.1°$, $c'/\sigma'_p = 0.028$, and SD= ± 0.010. Though the Recompression ϕ' is quite a bit larger than for SHANSEP, the cohesion intercept is smaller. In any case, the MO values for the Recompression tests fall within the ± 1 SD of the SHANSEP envelope.

Stress-Strain Parameters

The reader is again referred to Figures 7-7 through 7-9, which also contain TE data.

Figure 7-7 shows strain at failure, ϵ_f. There is a remarkable difference between the ϵ_f values for SHANSEP and Recompression tests. The Recompression tests all have $\epsilon_f < 6\%$, and generally less than 4%, while the SHANSEP tests all have $\epsilon_f > 9\%$ (at OCR = 1, mean $\epsilon_f = 12.7\% \pm 3.4$SD), and generally greater than 12%. The typical plots presented earlier in this section demonstrate this rather clearly, with the SHANSEP stress-strain curves consistently flatter than the Recompression curves. This also ties in with the fact that, for most of the SHANSEP tests, peak and MO were the same.

Figure 7-8 shows A_f versus OCR. Contrary to the TC tests, the SHANSEP TE tests generally had higher A_f values than Recompression tests (at OCR = 1, $A_f = 1.19 \pm 0.06$SD).

The final figure in this section, Figure 7-9 plots E_{50}/σ'_{vc} versus OCR. As expected, the modulus values for SHANSEP (at OCR = 1, $E_{50}/\sigma'_{vc} = 109 \pm 18$SD) are not only much lower than Recompression values, but also essentially constant (or possibly even slightly decreasing) with OCR. While the SHANSEP TC values are two to three times higher than SHANSEP TE values, the Recompression tests gave essentially the same values of E_{50}/σ'_{vc} in compression and extension.

Discussion

The conclusions from comparison of Recompression and SHANSEP TE results are very similar to those made for TC tests, and can be summarized as follows:

1. Recompression and SHANSEP test data in Figure 7-13 gave values of S which were approximately equal ($S \approx 0.14$–0.15), but the value of the exponent, m, is significantly higher for Recompression tests than SHANSEP tests (m=0.98 for Recompression, m=0.83–0.86 for SHANSEP).

2. A higher ϕ' but lower c'/σ'_p for the mean Recompression ESE result in MO normalized stresses which are comparable to the SHANSEP ESE ± 1 SD in the

range of OCRs considered, as shown in Figure 7-14.

3. The Recompression stress-strain curves exhibit steep initial slopes leading to much lower strains at failure and higher values of normalized modulus than SHANSEP (Figures 7-7 and 7-9). Recompression tests also gave lower values of A_f (Fig. 7-8). Additionally, they often undergo significant strain softening compared to the SHANSEP tests (e.g., Figs. 7-11 and 7-12).

7.3 Comparison of Recompression CK_0UC Data with UUC/CIUC Data

7.3.1 Overview

Haley & Aldrich performed nine UUC and five CIUC tests as part of the South Boston STP. The UUC tests were all done on tube samples, at elevations varying from about -9 to 62 ft. Pore pressures were measured during shear, and in order to get reasonable readings, the shear rate was decreased from the ASTM standard of 1%/minute to approximately 5%/hr. One disadvantage of these UU tests was that the specimens were typically not saturated during shear. For example, the B values for these tests varied between 25% and 85%.

Since there is no consolidation stress for UUC tests, one comparison of normalized stresses was made by normalizing the UUC data to p'_0, the value of p' at the beginning of shear. This p'_0 is analagous to σ'_s, and is thus a measure of sample disturbance. This is only possible because pore pressure measurements were made for these tests. Additionally, since it is common practice to normalize UUC test results to the effective overburden stress, this was also done.

The CIUC tests (all on tube samples) varied in elevation from El. 29 to 70 ft. The specimens were back pressure saturated to values of B exceeding 96%, then consolidated isotropically to $\sigma'_{vc} \approx \sigma'_{v0}$, which resulted in OCR = 1.76 to 5.49. The standard shear rate for the CIUC tests was 0.5%/hour, or the same rate used for the SHANSEP and Recompression tests. The CIUC tests then, were run in essentially the

same manner as the Recompression tests on samples with higher OCRs (i.e., $K_0 \approx 1$).

The following sections compare both types of tests simultaneously to the Recompression CK_0U triaxial compression test data.

7.3.2 General Comparison

Figure 7-15 compares values of q_f (adjusted to the overburden stress – see Section 6.2.1) from Recompression tests with unadjusted q_f values from the UUC and CIUC tests, plotted versus elevation. Also shown is a line depicting the TC q_f calculated from the SHANSEP equation using σ'_{v0}, the best estimate for the SB σ'_p (Fig. 5-10), and choosing S=0.28 and m=0.68. Additionally, σ'_s is plotted for the UUC tests. Three of the UUC tests from lower elevations had preexisting shear planes or cracks, which are noted on the plot. These three tests gave very low strengths; however, two other tests on "intact" samples (El. 20 and 30) gave similar results. One other UUC test showed a very high q_f (3 ksf), and the remaining three fell fairly close to the SHANSEP line, and within the scatter of the Recompression data. One can clearly see that the scatter for UUC tests is much larger, as expected, and that q_f is very closely tied to σ'_s, i.e., a low σ'_s (more disturbance), leads to a low q_f. The CIUC tests are more tightly clustered around the SHANSEP line, however, they remain essentially constant with depth.

Figure 7-16 compares ϵ_f and normalized E_{50} versus depth for the three types of tests. No differentiation is made here between tests on block samples and tests on tube samples, but only Recompression tests with $\sigma'_{vc} \approx \sigma'_{v0}$ are shown. The Recompression ϵ_f values follow a clear trend, in general, decreasing with depth, with values for the most part less than 3%. The CIUC ϵ_f also decreases with depth, but the values are much higher overall. The UUC tests exhibit ϵ_f values ranging from about 1.5% to 9.5%, with no discernible trend with elevation and tremendous scatter.

The right hand side of Figure 7-16 plots the Young's modulus, normalized to either σ'_{vc} for Recompression and CIUC tests or σ'_{v0} for UUC tests. The Recompression values of E_{50}/σ'_{vc} generally decrease with depth. The UUC tests, which are normalized to σ_{v0}, give much lower values of modulus, especially at depth. The CIUC

values are constant with depth, and surprisingly, much lower than values from the Recompression tests at the higher elevations.

7.3.3 Undrained Strength Ratio

Figure 7-17 shows the linear regression of the q_f/σ'_{vc} versus OCR relationship for all Recompression tests with the exception of tests with leaks or PSS. Also plotted are the results from the UUC and CIUC tests. Note that for the UUC tests q_f is normalized both to σ'_s and σ'_{v0}. Most of the UUC tests normalized to σ'_s (and with OCR $= \sigma'_p/\sigma'_s$) fall within or very close to ± 1 SD of the Recompression, including the three tests with cracks or PSS. This close agreement shows the value of measuring σ'_s since the resulting q_f/σ'_s versus σ'_p/σ'_s relationship could be used to calculate corrected UUC strengths if one knows the in situ OCR profile. However, the UUC results normalized to σ'_{v0} (and with OCR $= \sigma'_p/\sigma'_{v0}$), as commonly done in practice, mostly plot far below the other data. The CIUC test strengths are very close to the Recompression line below OCR$\approx$4 (log OCR = 0.6), but are slightly lower at the higher OCRs.

7.3.4 Effective Stress Failure Envelope

Figure 7-18 compares the peak effective stress envelope for the Recompression tests (plotted mean with $\pm$ 1 SD) with the peak values from the UUC and CIUC tests (all normalized to σ'_p). Somewhat surprisingly, there appears to be a very good correlation between the envelope defined by the Recompression tests, and the data from the UUC and CIUC tests. Nearly all of the UUC and CIUC points fall within one standard deviation of the Recompression line, though most of them are on the low side.

Figure 7-19 compares the ESE at maximum obliquity with the UUC and CIUC points. Again, the result is similar, with the UUC and CIUC points falling on or slightly below the L.R of the Recompression tests.

7.3.5 Stress-Strain Parameters

Figure 7-20 is the familiar ϵ_f versus OCR plot. For both this figure and Fig. 7-21, the UUC OCR is defined as σ'_p/σ'_s, and not as σ'_p/σ'_{v0}. While the Recompression test ϵ_f values remain more or less constant with OCR, both the CIUC and UUC data show increasing trends with OCR. In particular, the CIUC form a smooth, well defined, upward curve. The UUC data are more scattered, and give lower strains than CIUC tests at higher OCRs. However, if the UUC data were plotted versus OCR $= \sigma'_p/\sigma'_{v0}$, the results would all move to the left, i.e., to much lower values of OCR.

In Figure 7-21, A_f is again plotted versus OCR for the Recompression tests, this time including the UUC and CIUC tests as well. All of the tests follow the same trend, very little distinction can be made between the different test types. Both the UUC and CIUC points fall within the range of the Recompression points. But again, the UUC data would plot very differently if based on OCR $= \sigma'_p/\sigma'_{v0}$.

The final figure, Fig. 7-22 plots the normalized modulus versus OCR. The Recompression tests show a marked increase in E_{50}/σ'_{vc} with OCR. As noticed in Figure 7-16, the CIUC tests gave very low values which remain constant with OCR. The UUC values are also extremely low.

7.3.6 Discussion

The following conclusions can be made from the comparison of these results:

1. In terms of strength, both the UUC and CIUC tests gave reasonable results at some elevations, but were less consistent overall, especially for the deep UUC tests (see Figure 7-15).

   The CIUC tests with OCRs between 1.8 and 3.7 gave q_f very near to the values predicted by SHANSEP. At the higher OCRs the values were lower than both SHANSEP and Recompression q_f values, the latter being especially surprising as the testing method was nearly identical.

   The UUC test gave reasonable results in the upper part of the crust, but below El. 20±, the strengths were drastically lower. This may be partly due to sample

disturbance; the low OCR samples at depth are more prone to disturbance, and since there is no mechanism for overcoming this disturbance in UU tests (i.e., consolidation), the lower samples are severely affected. The initial stress, σ'_s, is a qualitative indicator of the amount of sample disturbance, and in most cases, σ'_s is lower for the lower samples (see Fig. 7-15).

2. USR versus OCR values from the CIUC tests on specimens with OCRs between two and four were reasonably similar to the Recompression L.R. At higher OCRs the USR was lower, as noted above. The UUC tests normalized to σ'_s were also surprisingly close to the Recompression line. The UUC values normalized to σ'_{v0}, however, were much lower. This suggests that if UUC tests must be used, pore pressure measurements should be made, and σ'_s used for normalization.

3. In terms of deformability properties, neither test appears to be very reliable. Both types of tests yield high strains to failure and very low values of modulus. In particular, the UUC tests exhibit excessive scatter. This is due to the nature of UUC tests which are highly dependent on the degree of sample disturbance. The fact that the CIUC ϵ_f and E_{50}/σ'_{vc} values are so different from the Recompression values at high OCR's is surprising, since differences in K_c at moderate to high OCRs were not shown to have much of an effect on Recompression test results in Chapter 6. This leads one to believe that these differences are the result of different sampling methods, as the Recompression CK_0UC tests were done mostly on block samples and the CIUC tests on tube samples only.

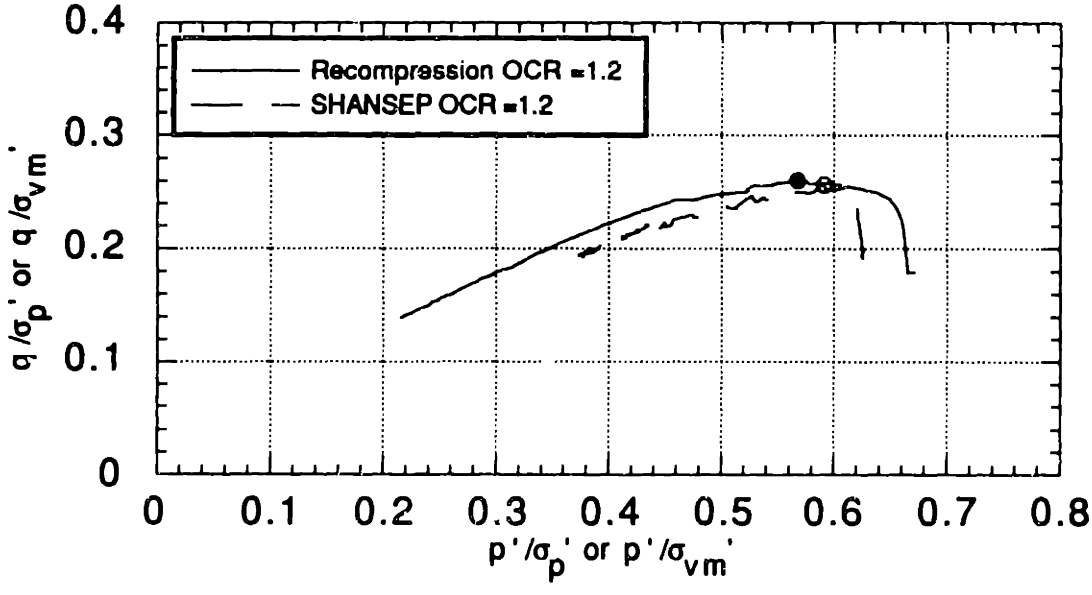

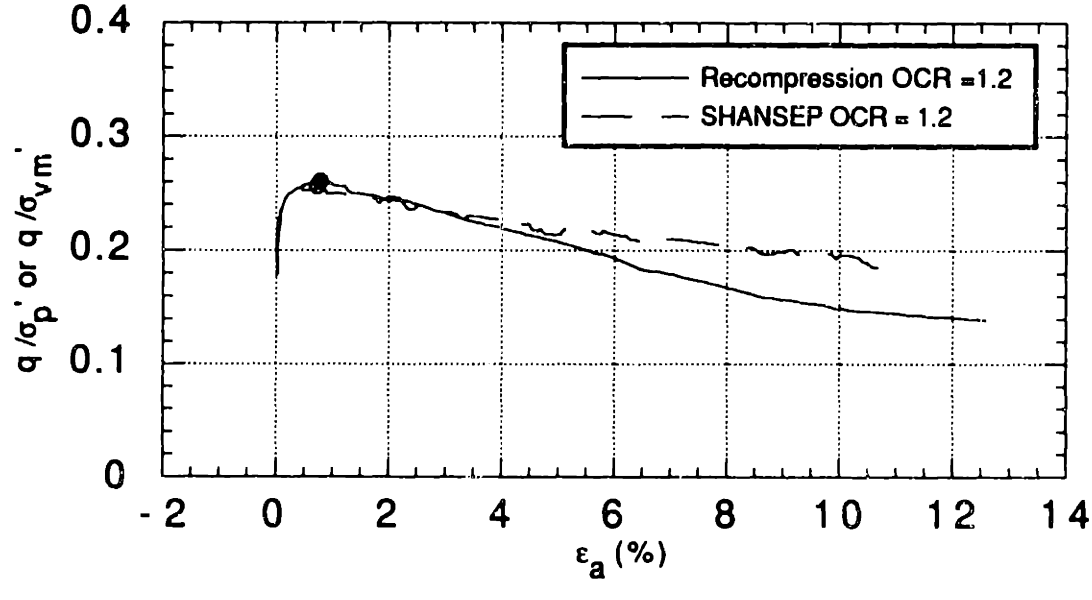

Figure 7-1: Comparison of SHANSEP and Recompression Triaxial Compression Test Stress Paths and Stress-Strain Curves at Low OCR

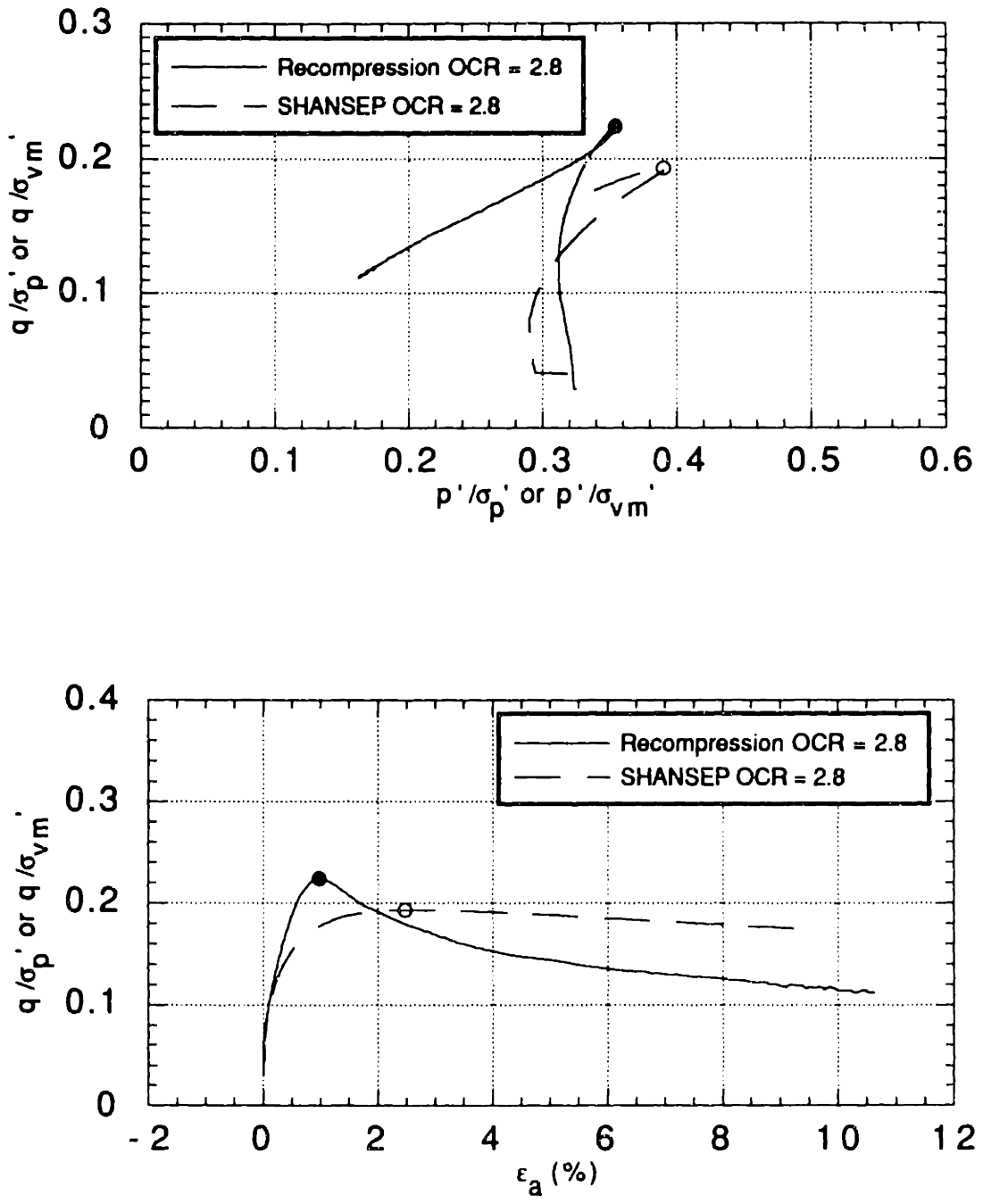

Figure 7-2: Comparison of SHANSEP and Recompression Triaxial Compression Test Stress Paths and Stress-Strain Curves at Moderate OCR

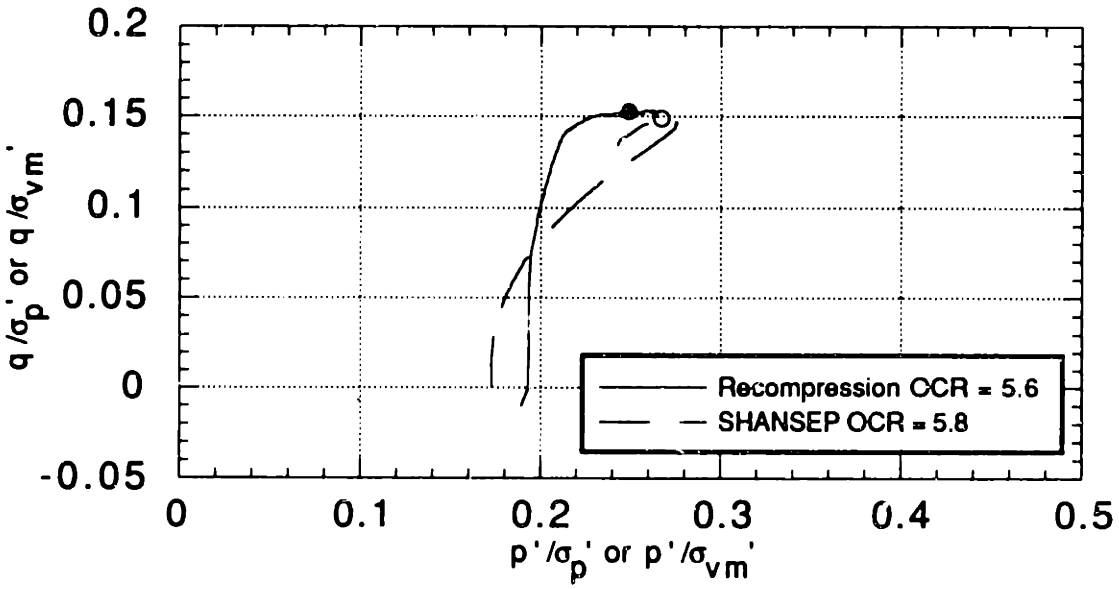

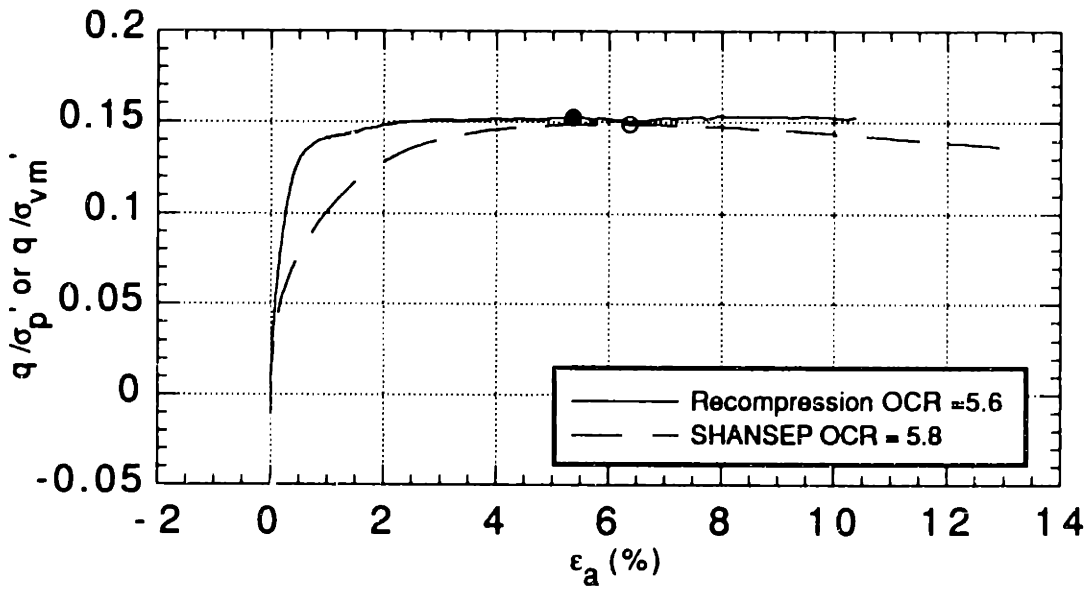

Figure 7-3: Comparison of SHANSEP and Recompression Triaxial Compression Test Stress Paths and Stress-Strain Curves at High OCR

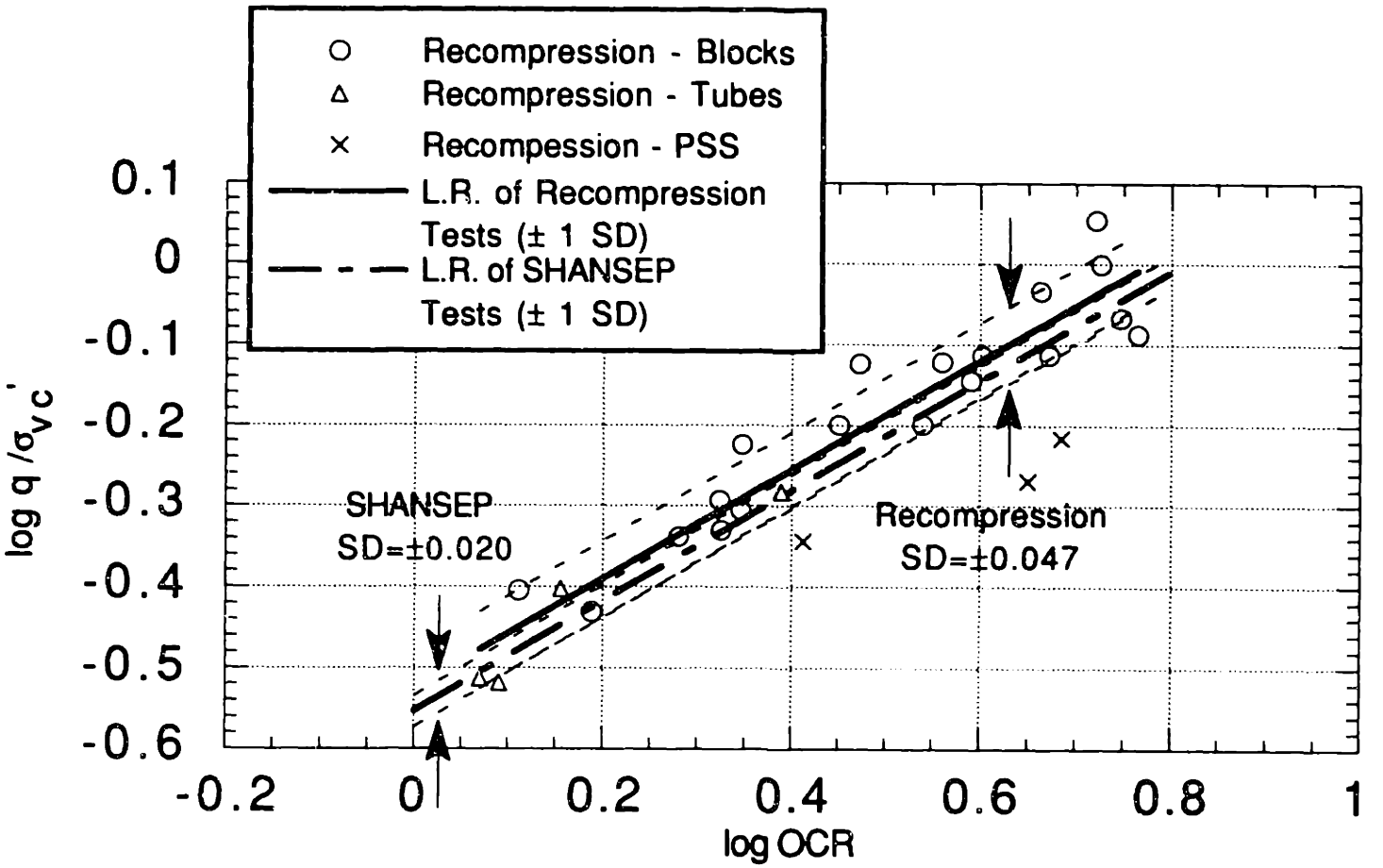

Figure 7-4: Undrained Strength Ratio vs. OCR Comparison of SHANSEP and Recompression Triaxial Compression Tests

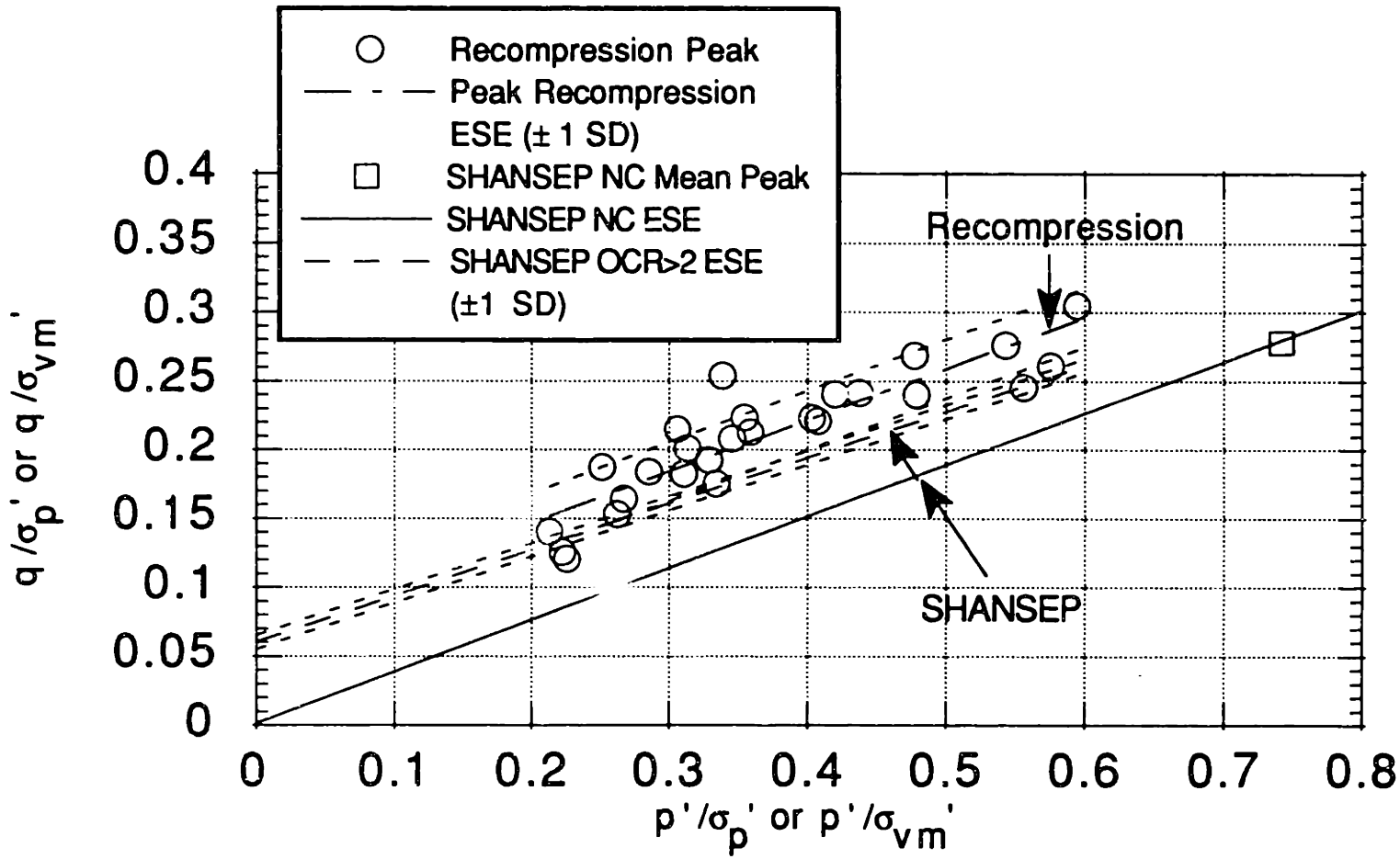

Figure 7-5: Effective Stress Envelope at Peak for SHANSEP and Recompression TC Tests

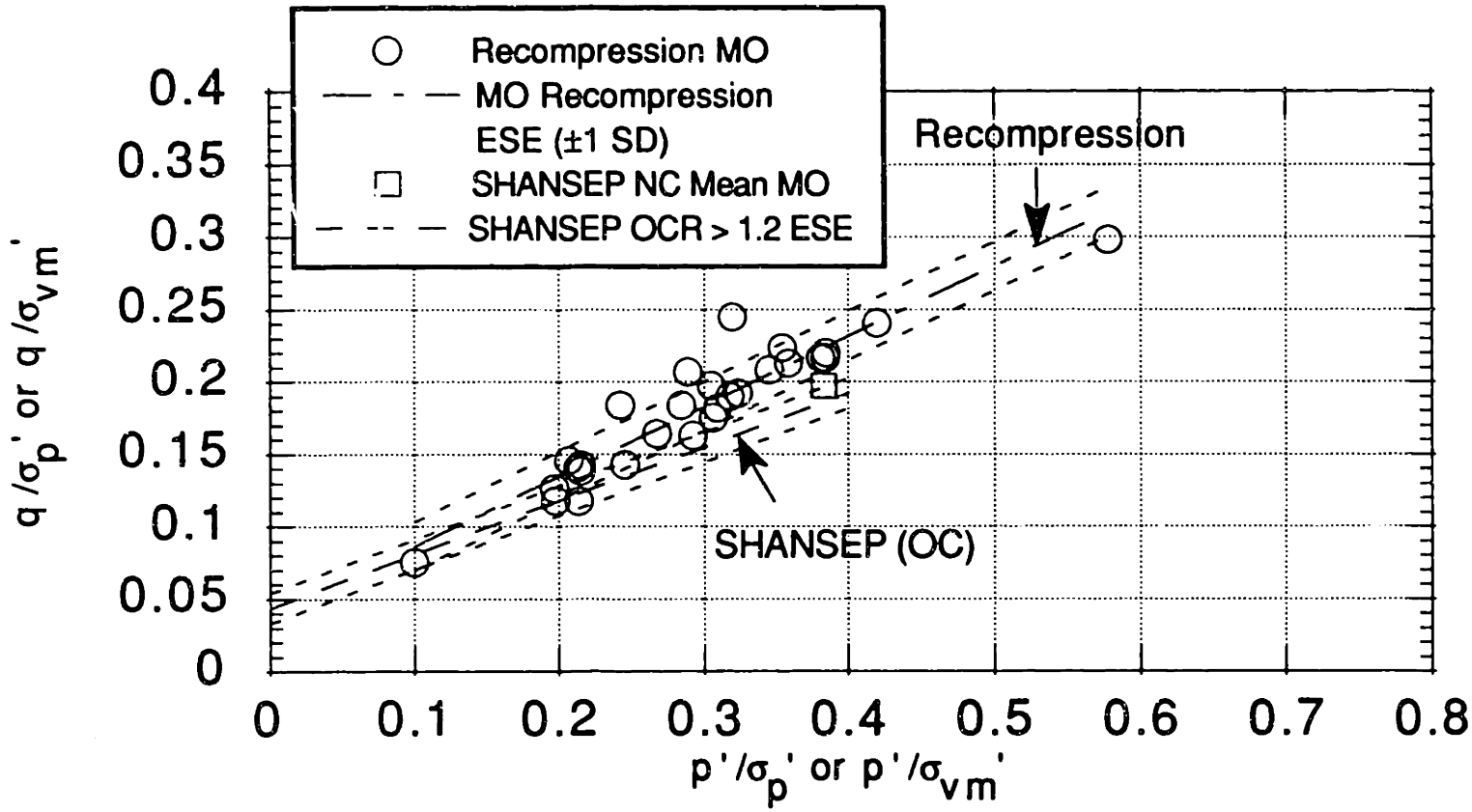

Figure 7-6: Effective Stress Envelope at Maximum Obliquity for SHANSEP and Recompression TC Tests

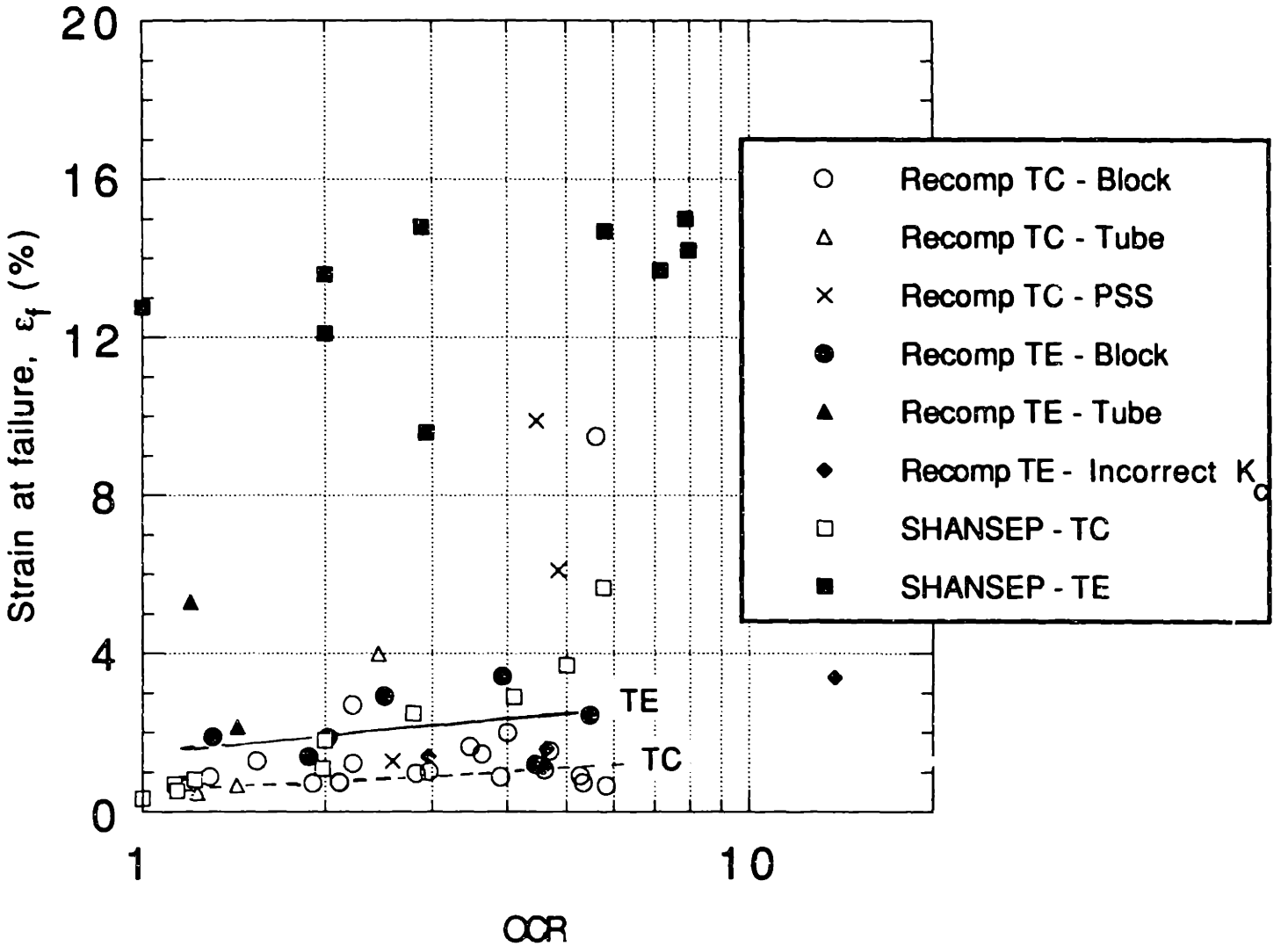

Figure 7-7: Strain at Failure vs. OCR for SHANSEP and Recompression Triaxial Compression and Extension Tests on Tube and Block Samples

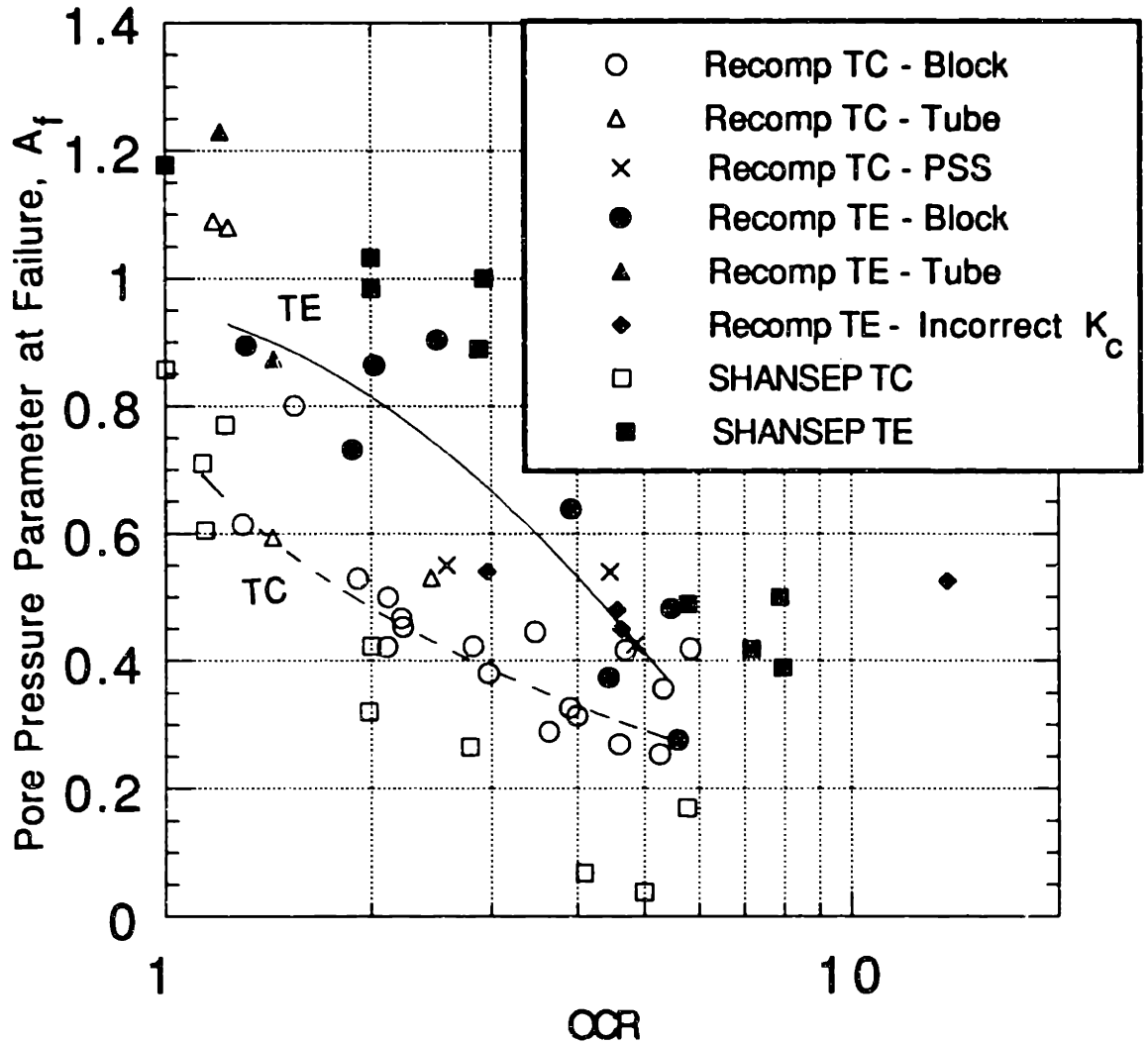

Figure 7-8: Pore Pressure Parameter at Failure vs. OCR for SHANSEP and Recompression Triaxial Compression and Extension Tests on Tube and Block Samples

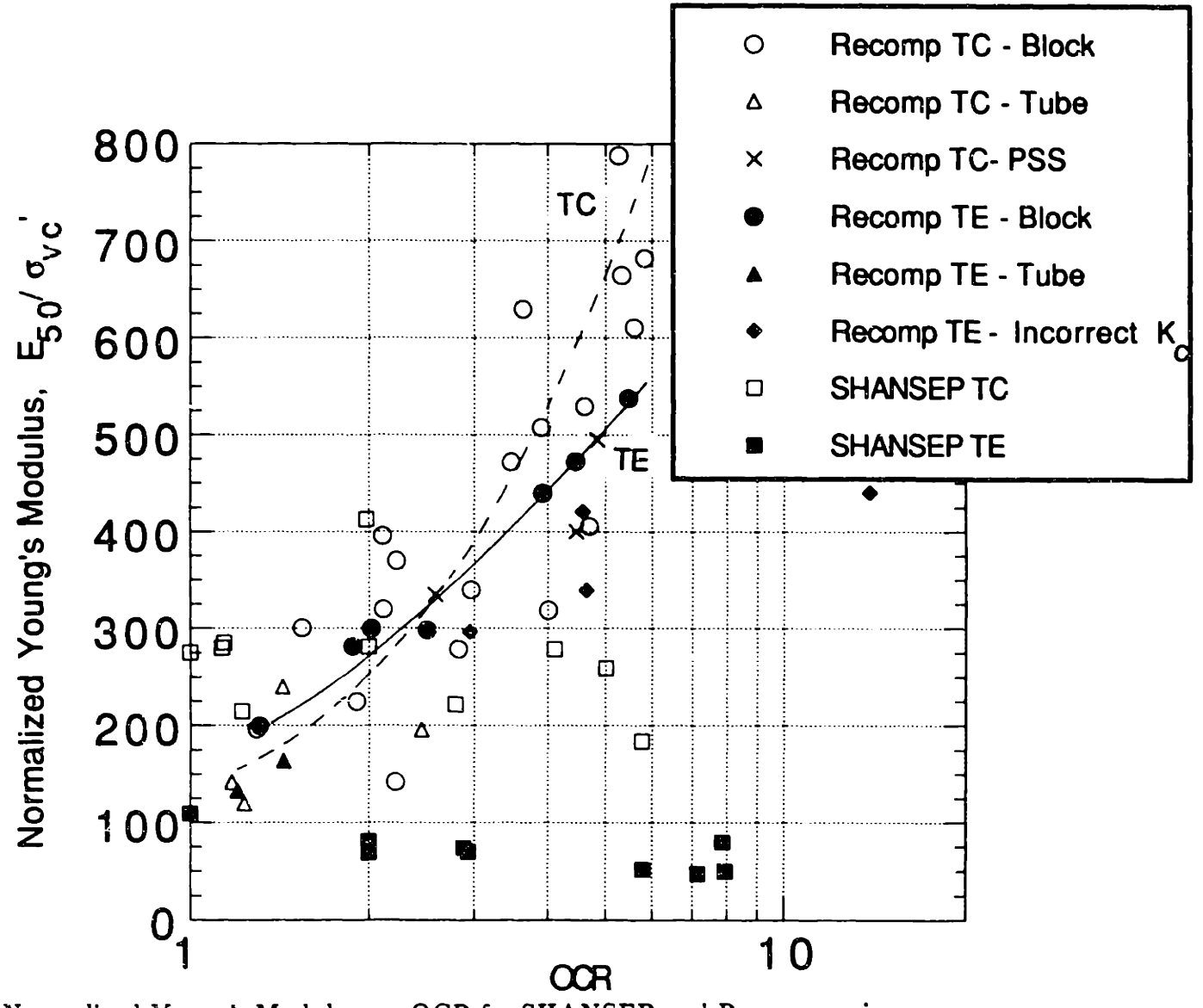

Figure 7-9: Normalized Young's Modulus vs. OCR for SHANSEP and Recompression Triaxial Compression and Extension Tests on Tube and Block Samples

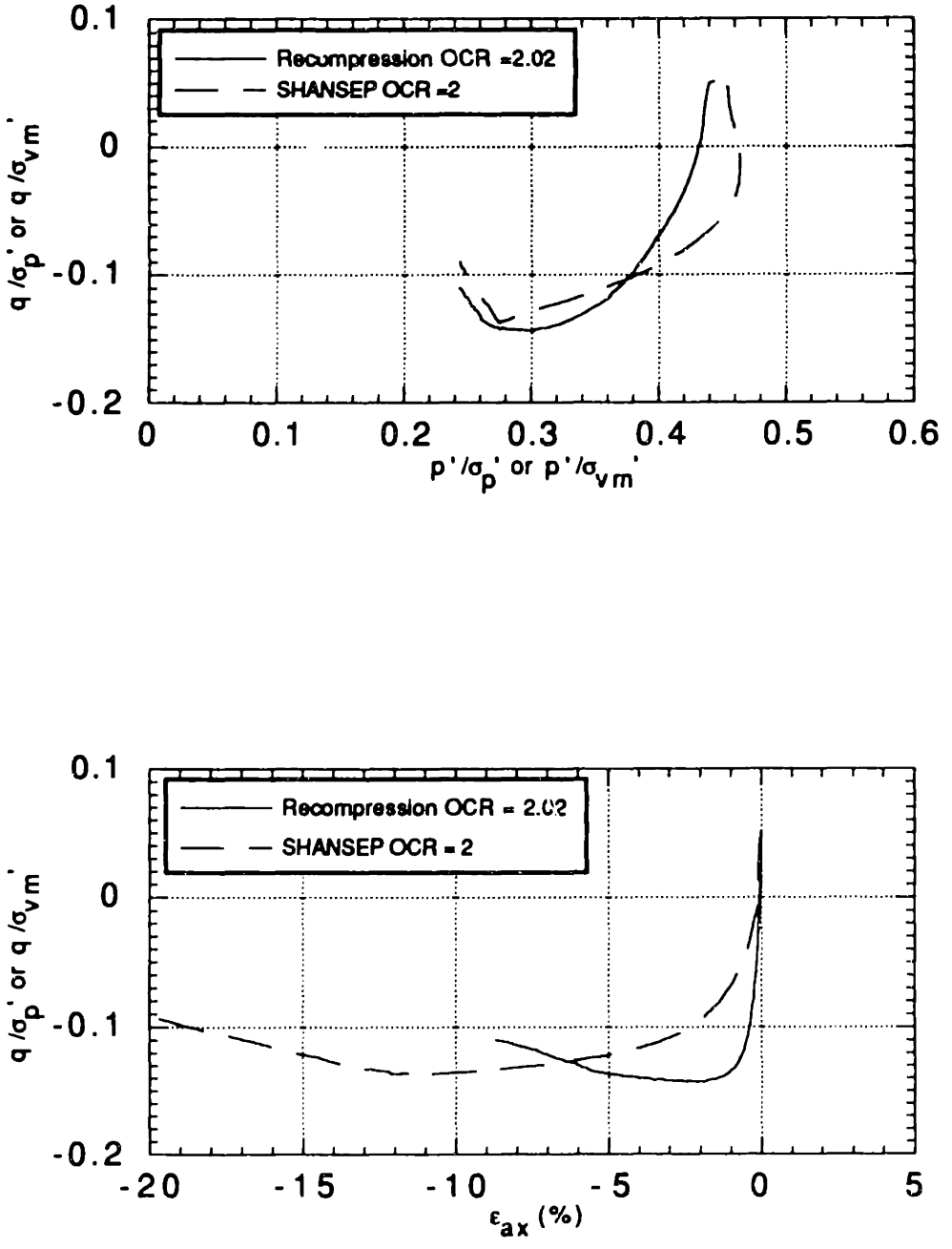

Figure 7-10: Comparison of SHANSEP and Recompression Triaxial Extension Test Stress Paths and Stress-Strain Curves at Low OCR

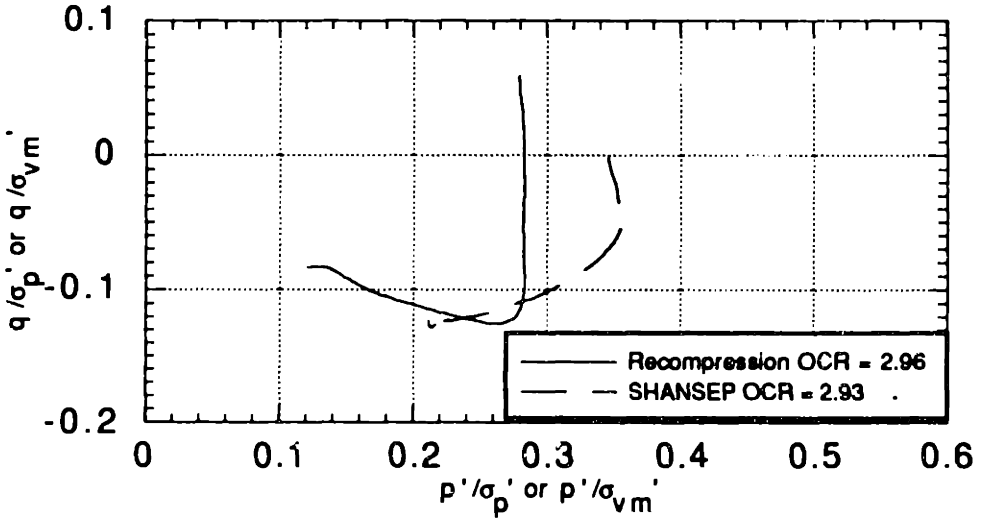

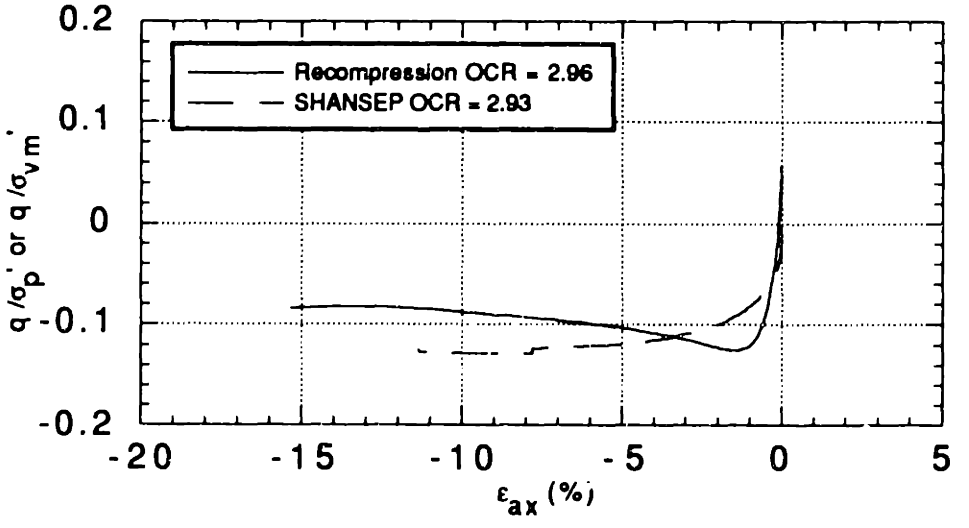

Figure 7-11: Comparison of SHANSEP and Recompression Triaxial Extension Test Stress Paths and Stress-Strain Curves at Moderate OCR

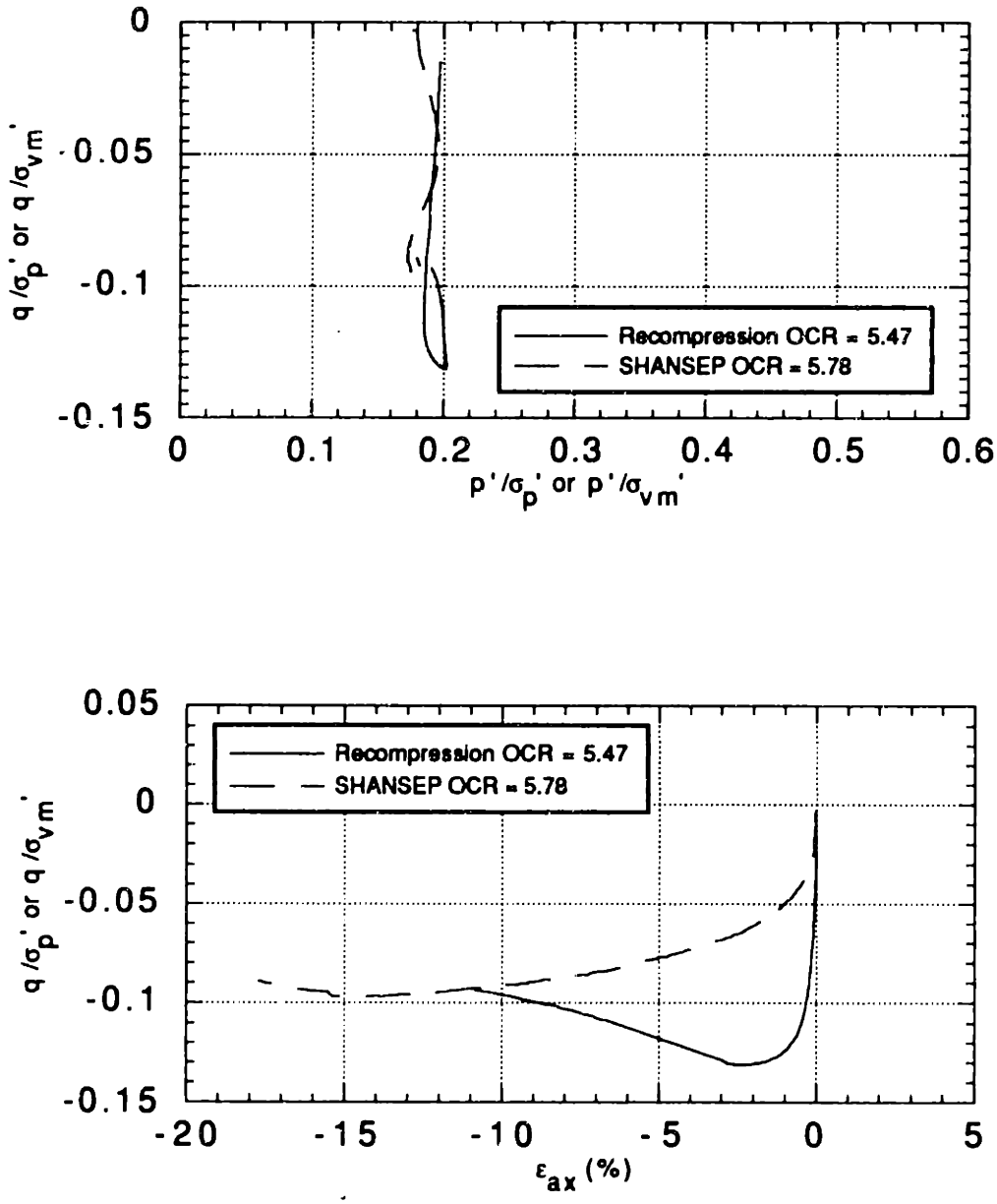

Figure 7-12: Comparison of SHANSEP and Recompression Triaxial Extension Test Stress Paths and Stress-Strain Curves at High OCR

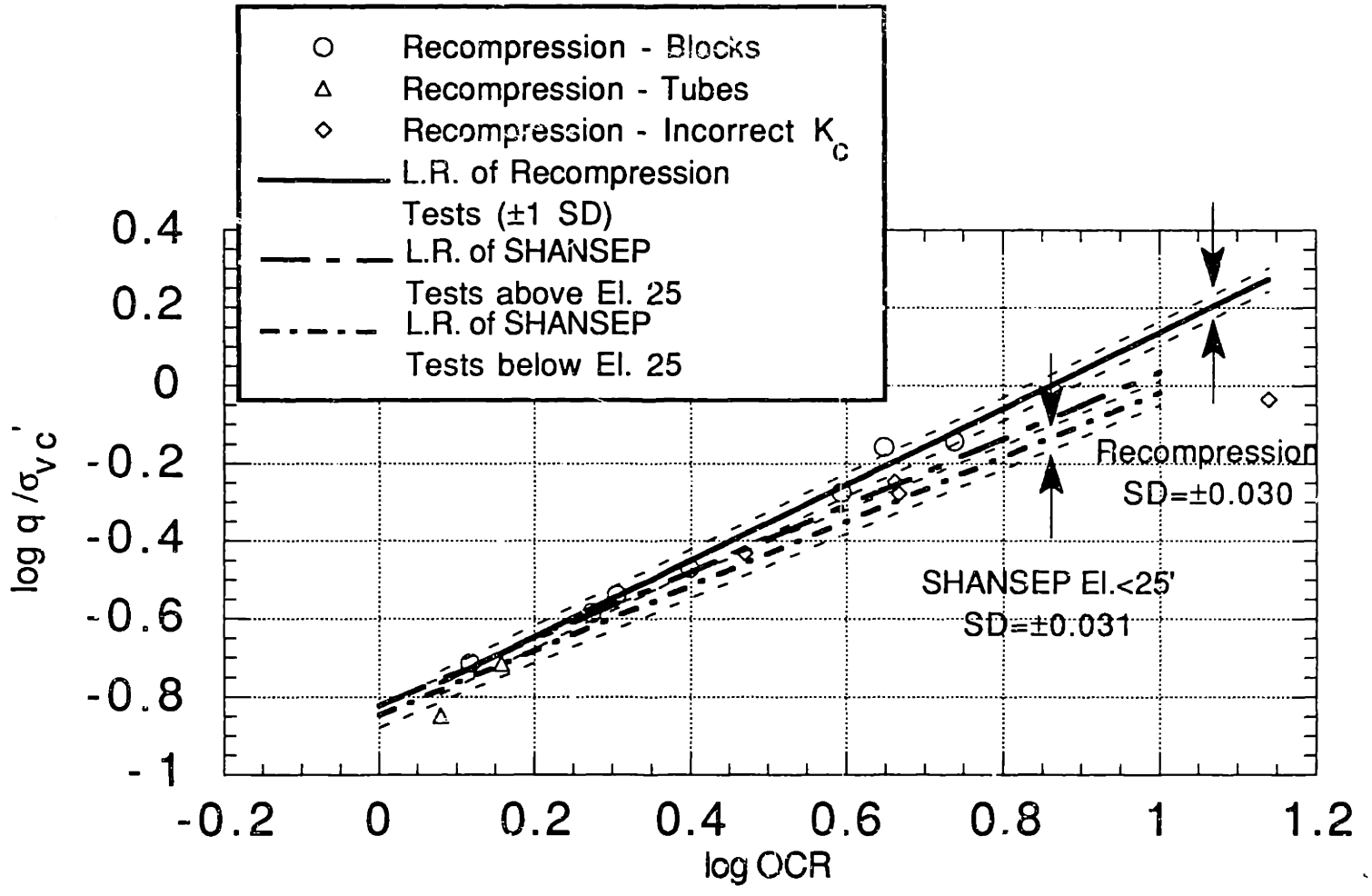

Figure 7-13: Undrained Strength Ratio vs. OCR Comparison of SHANSEP and Recompression Triaxial Extension Tests

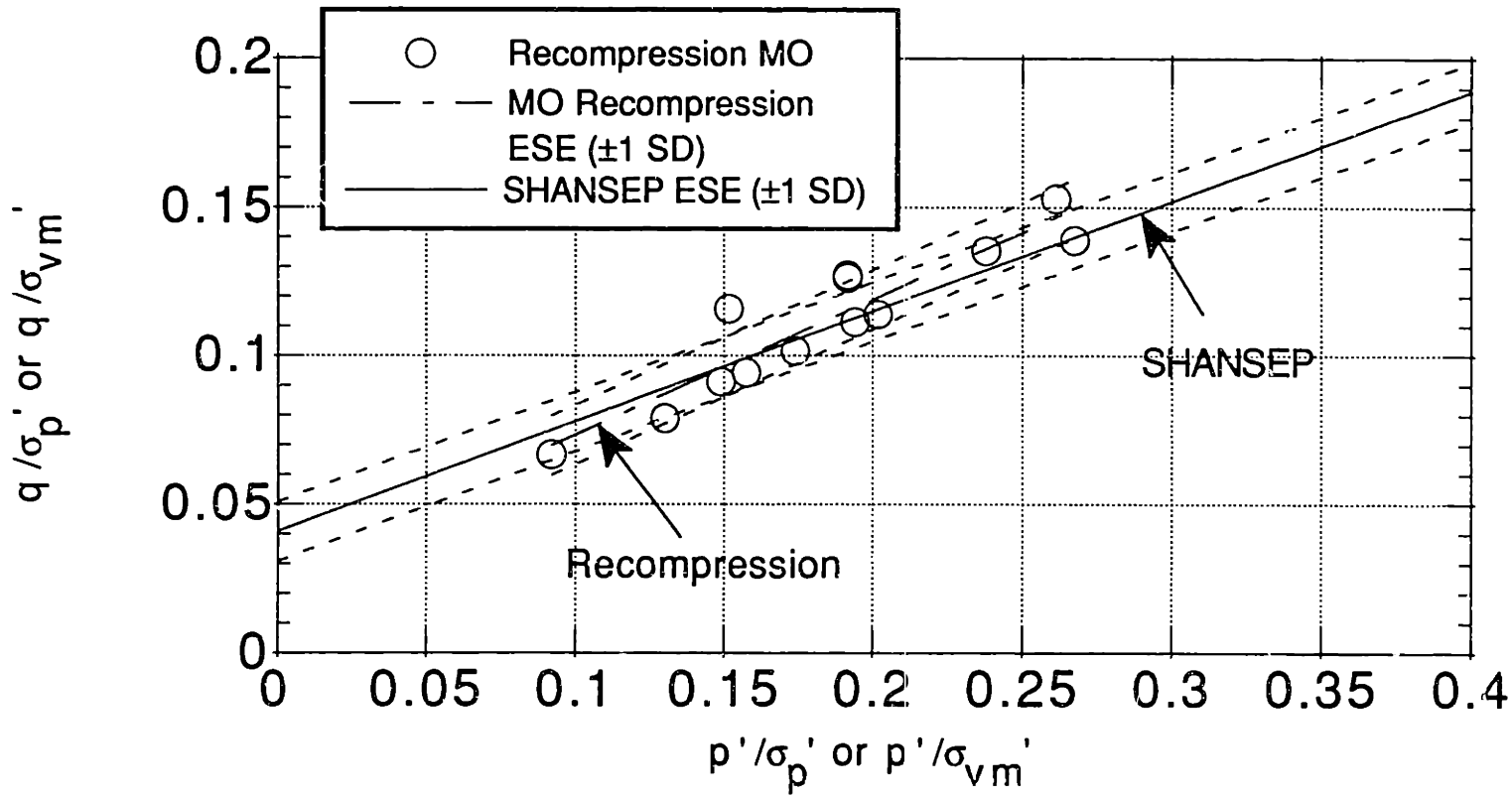

Figure 7-14: Effective Stress Envelope at Maximum Obliquity for SHANSEP and Recompression TE Tests

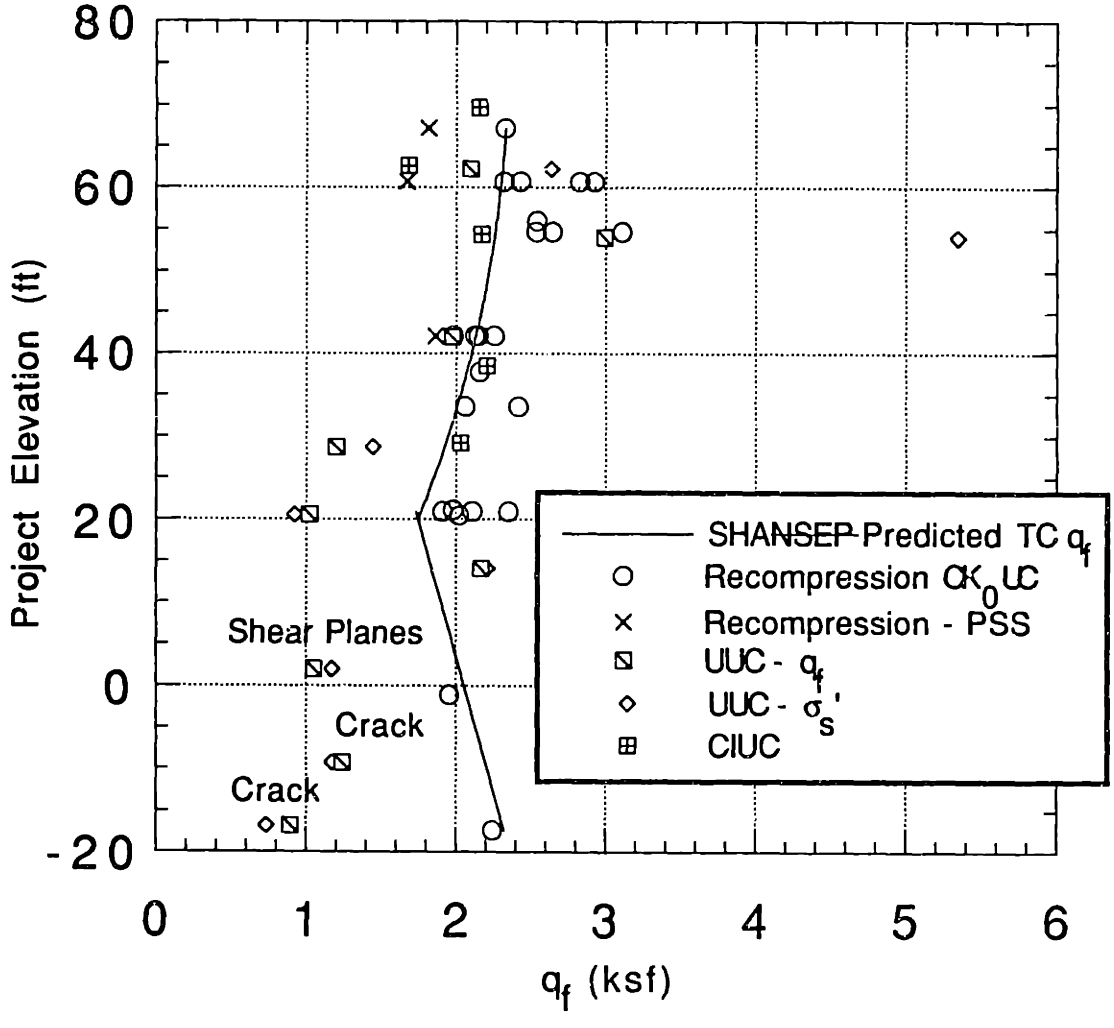

Figure 7-15: Comparison of Recompression CK_0UC and SHANSEP CK_0UC q_f with UUC and CIUC q_f versus Elevation

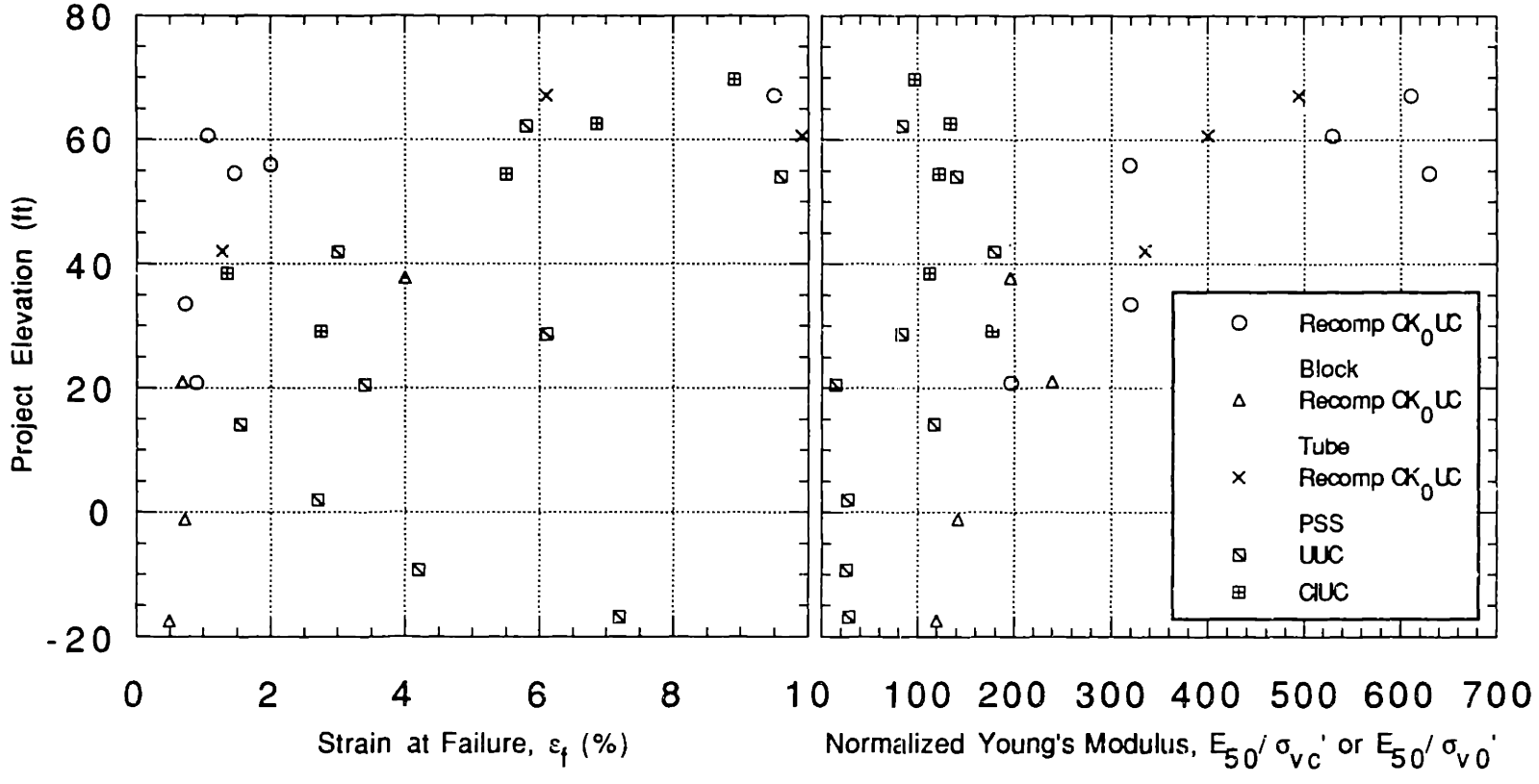

Figure 7-16: Strain at Failure and Normalized Young's Modulus versus Elevation for Recompression CK_0UC, UUC and CIUC Tests

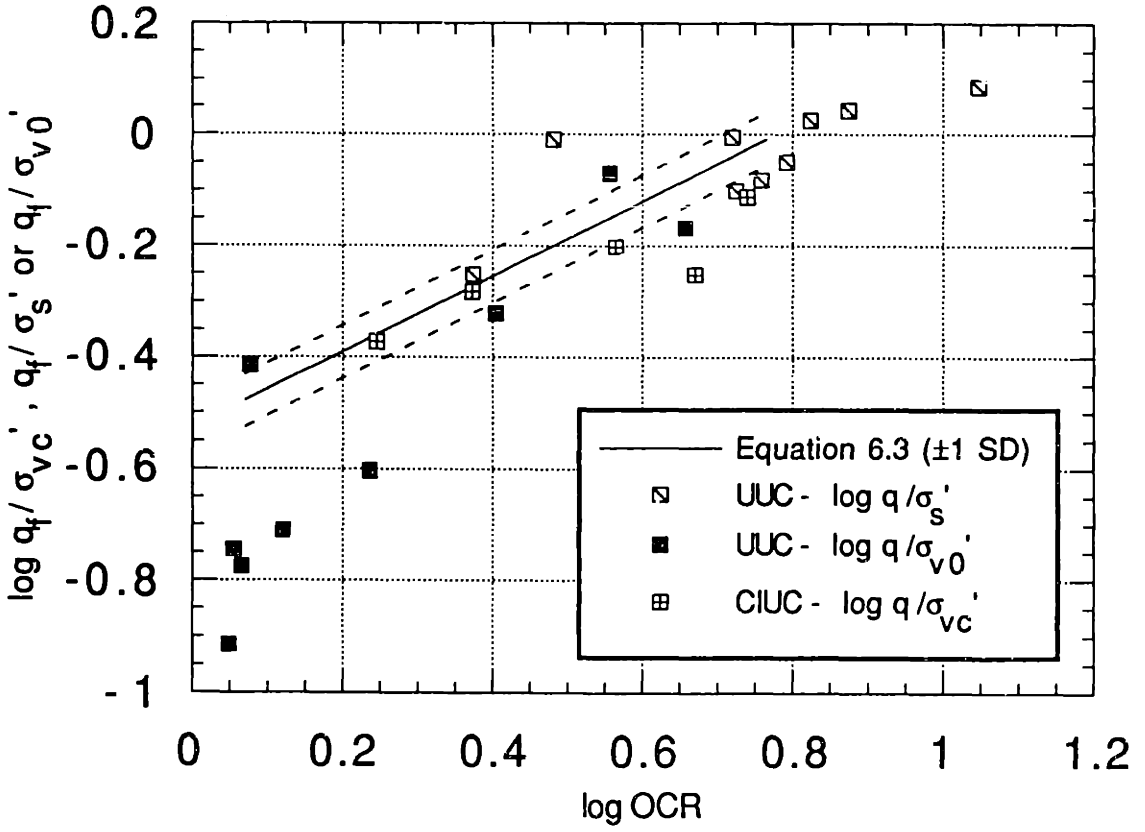

Figure 7-17: Undrained Strength Ratio versus OCR for Recompression CK_0UC, UUC and CIUC Tests

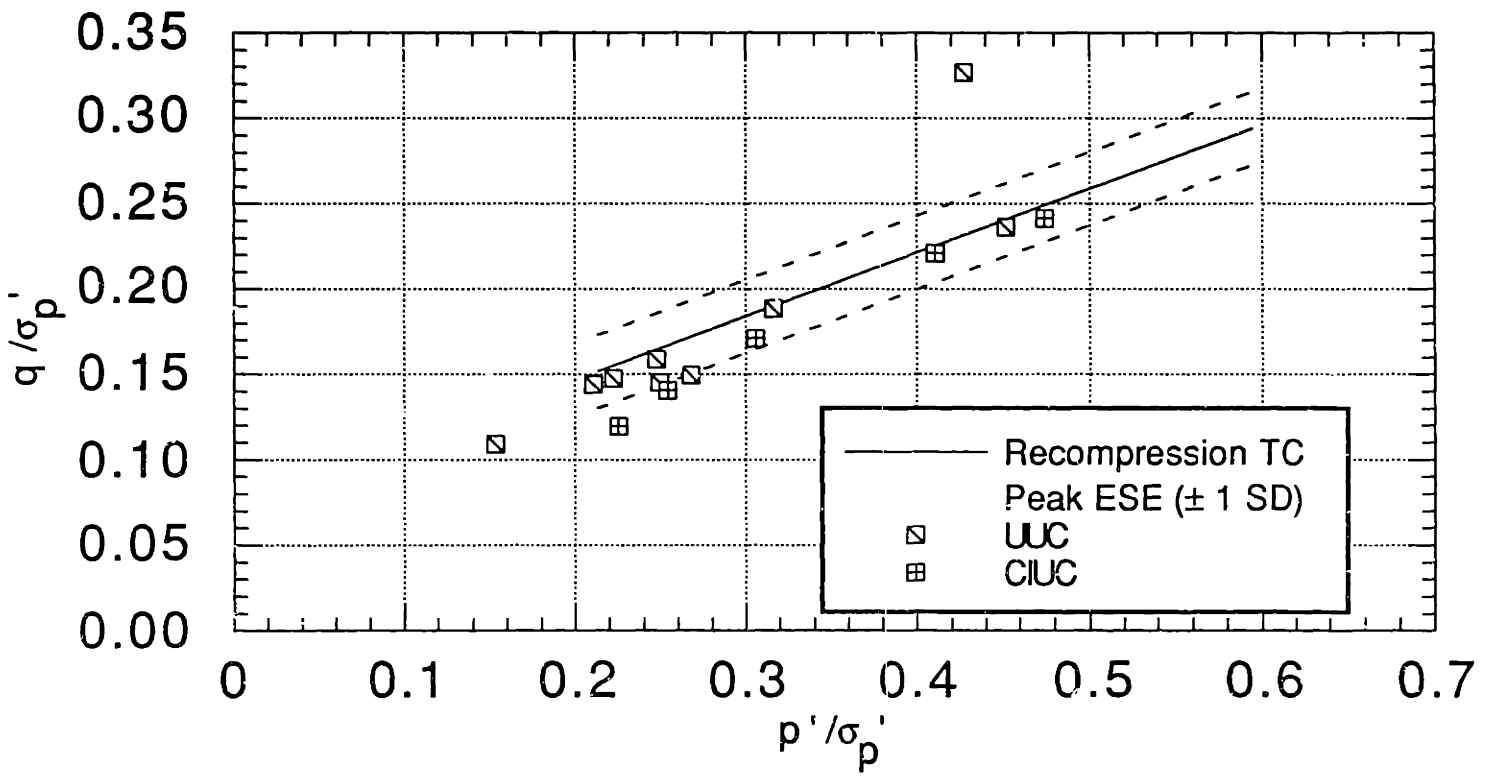

Figure 7-18: Peak Effective Stress Envelope for Recompression CK_0 UC, UUC, and CIUC Tests

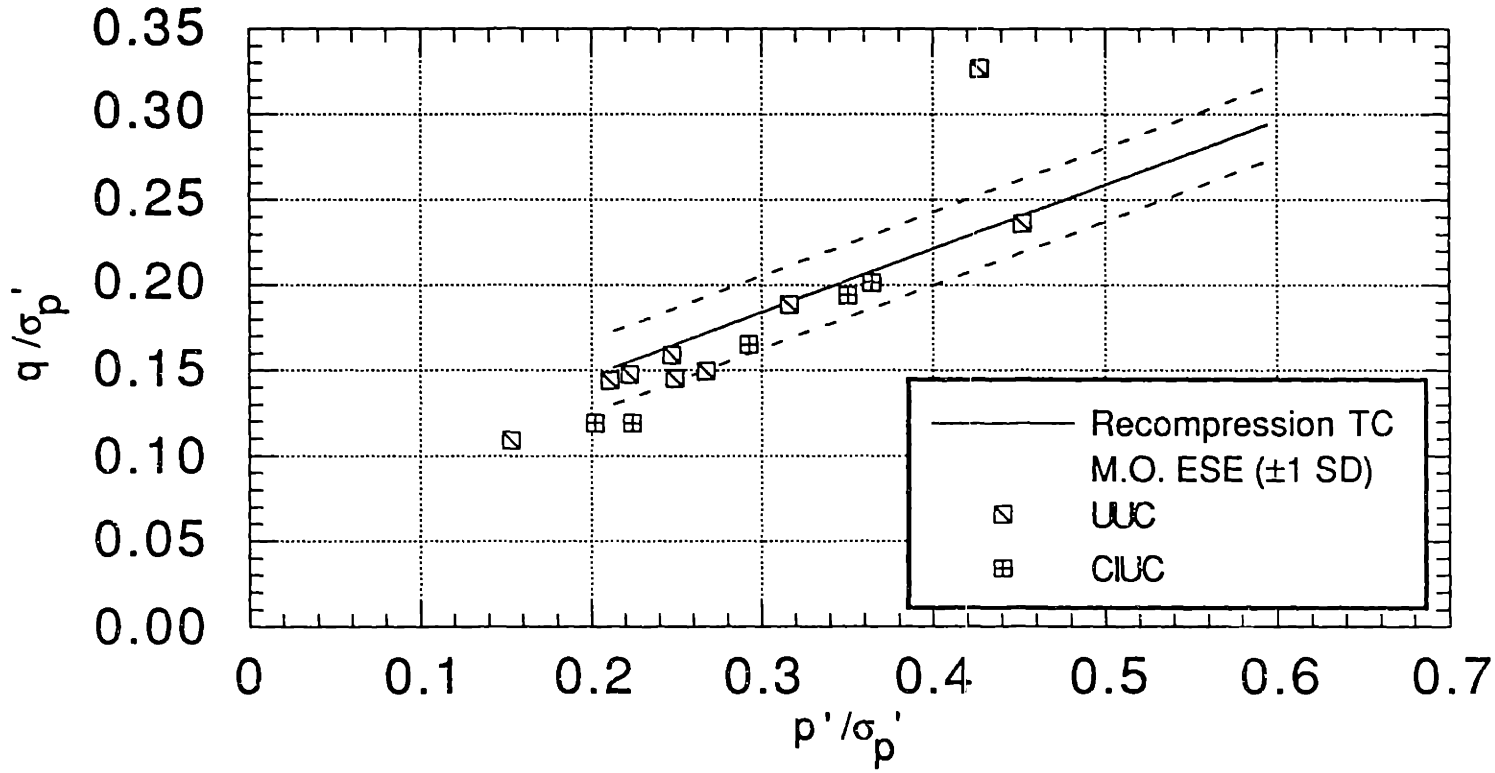

Figure 7-19: Maximum Obliquity Effective Stress Envelope for Recompression CK_0UC, UUC, and CIUC Tests

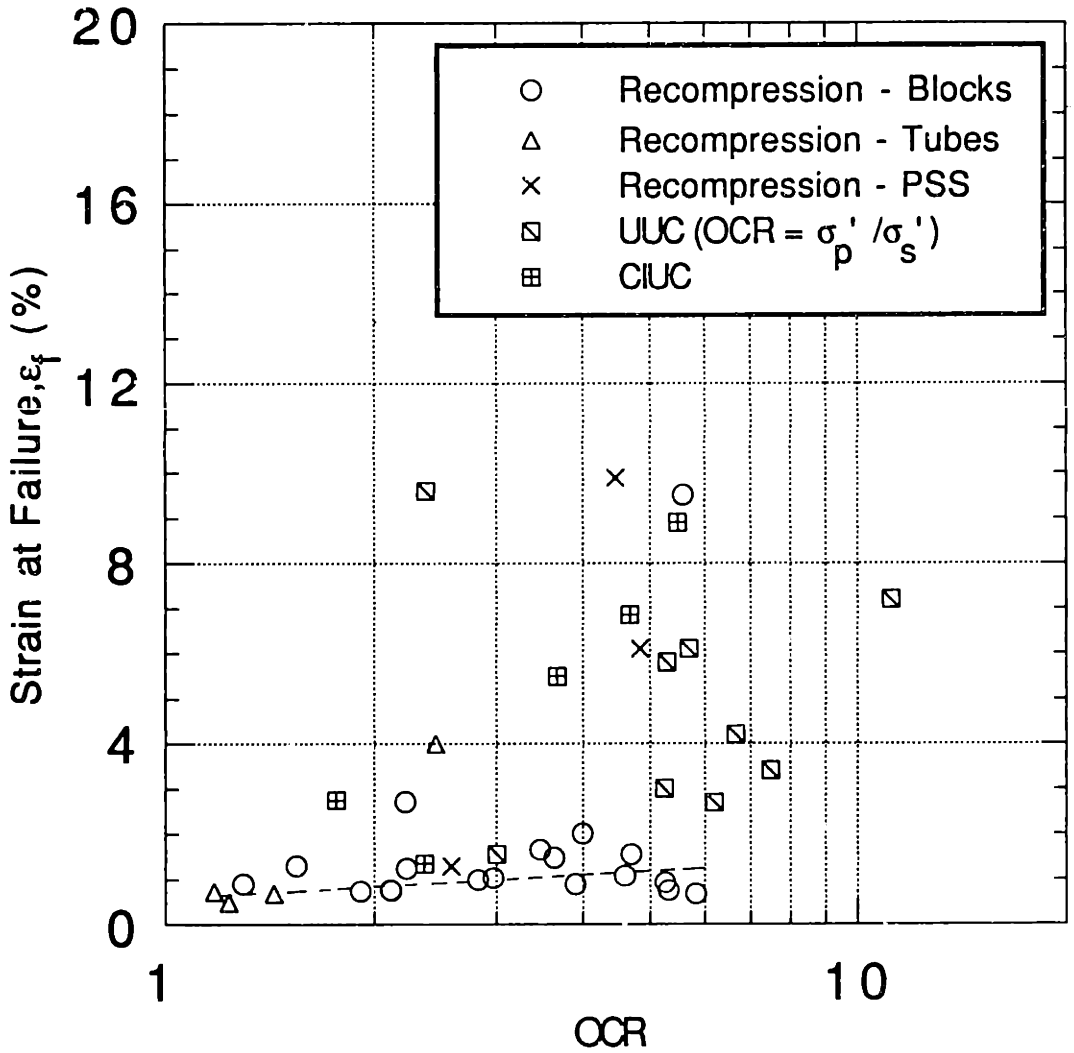

Figure 7-20: Strain at Failure versus OCR for Recompression CK_0UC, UUC, and CIUC Tests

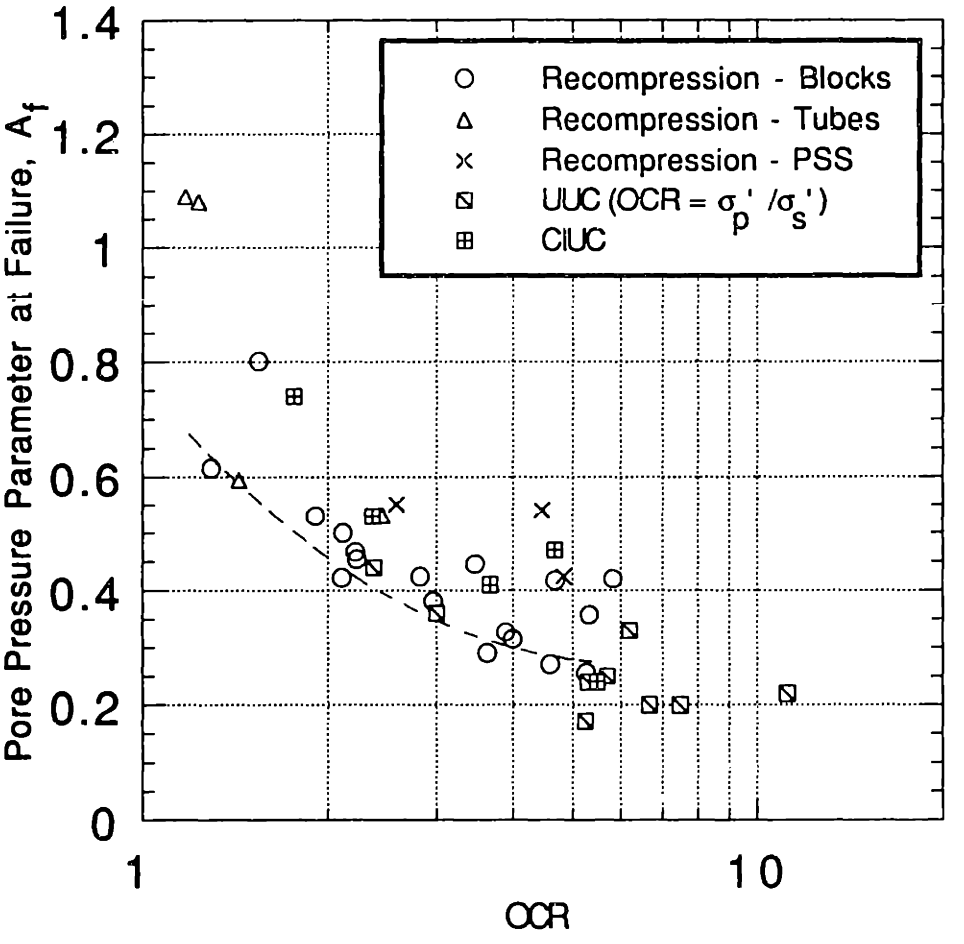

Figure 7-21: Pore Pressure Parameter at Failure versus OCR for Recompression CK_0UC, UUC, and CIUC Tests

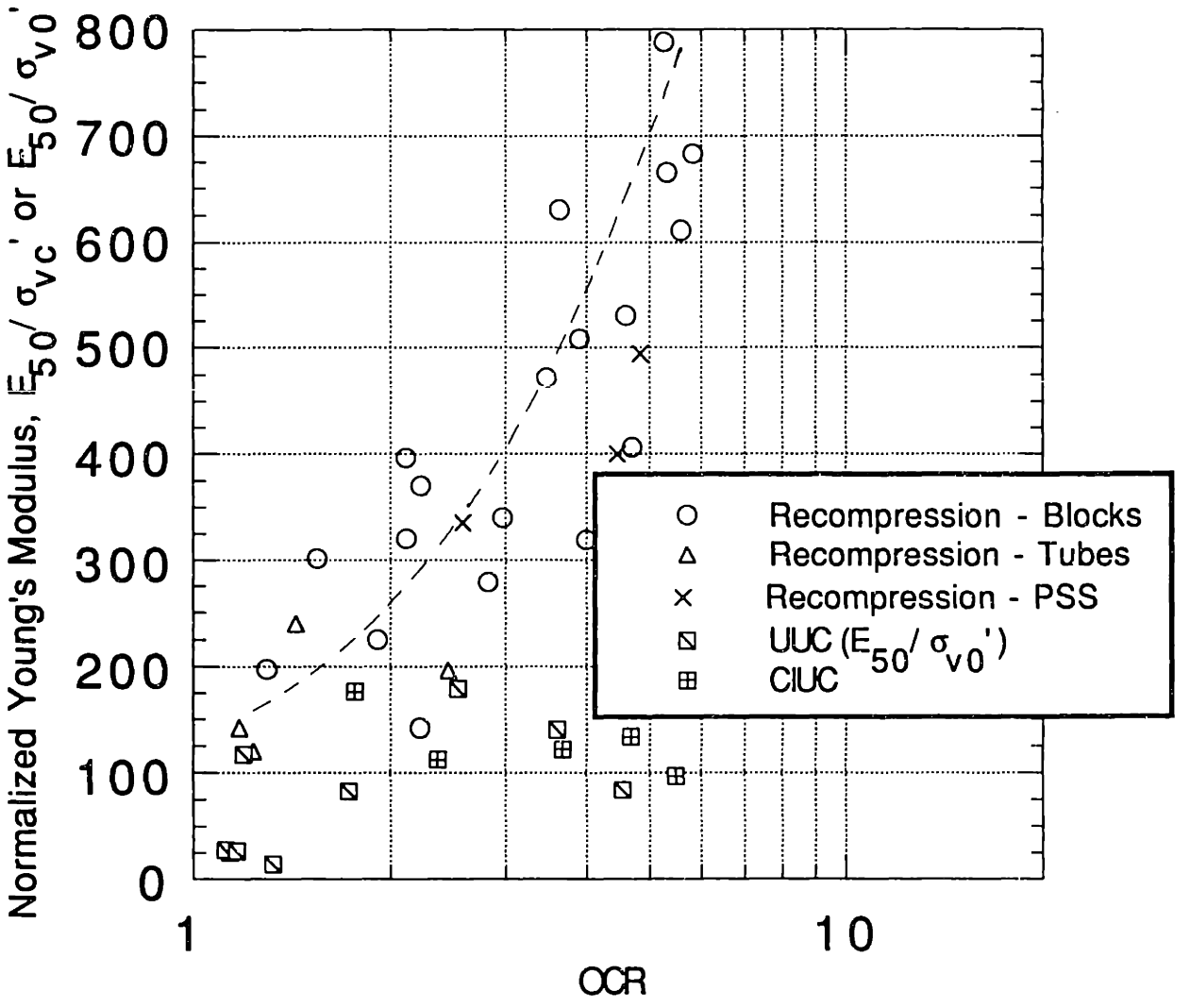

Figure 7-22: Normalized Young's Modulus versus OCR for Recompression CK_0UC, UUC, and CIUC Tests

Chapter 8

Summary, Conclusions, and Recommendations

8.1 Summary and Conclusions

8.1.1 Background

The CA/T Project and STP

The multi-year, multi-billion dollar Central Artery and Third Harbor Tunnel Project is now starting construction. The scope of the work on this project demands thorough knowledge of the properties of the Boston blue clay (BBC) which underlies not only the project alignment, but much of the Boston basin as well. Preliminary geotechnical investigations have already been performed by local geotechnical consulting firms, including Haley & Aldrich. As part of its investigations, H&A developed the Special Testing Program (STP) to try to improve the body of knowledge of the BBC.

H&A outlined several specific objectives for the STP:

1. Measure the engineering properties of the BBC using both Recompression and SHANSEP testing methods to develop Normalized Soil Properties (NSP) correlations using very high quality samples.

2. Attempt to develop correlations between engineering properties obtained from

state-of-the-art laboratory testing on very high quality samples and properties obtained from more routine tests on conventional piston tube samples.

3. Attempt to develop correlations between clay engineering properties determined from laboratory and in situ tests.

These objectives were carried out via an extensive program of field testing and sampling at two sites (South Boston and East Boston), and laboratory testing carried out by H&A, J.T. Germaine & Associates, and MIT. The objectives of the MIT research, which was conducted under an OSP contract with H&A, were:

1. Conduct K_0 consolidated-undrained triaxial compression and extension (CK_0UC and CK_0UE) tests using the SHANSEP technique to obtain undrained stress-strain-strength parameters as a function of overconsolidation ratio (OCR). These tests would provide data showing how Normalized Soil Properties (NSP) varied as a function of: type of shearing (compression or extension); type of sample (tube versus block); depth within BBC; and site location (South Boston versus East Boston). The results would also be compared to prior data obtained at MIT on Resedimented BBC and with data from conventional UU and CIU triaxial compression tests.

2. Conduct CK_0UC/E tests using the Recompression technique in order to compare these NSP v. OCR relationships with those obtained from the SHANSEP test program and from conventional strength tests.

3. Conduct several K_0 consolidated-drained triaxial compression and extension tests (CK_0DC and CK_0DE) using both the SHANSEP and Recompression techniques in order to determine the effects of drainage on stress-strain-strength behavior. Some special stress path tests would also be run to simulate conditions during installation of diaphragm walls and subsequent excavation.

4. Perform tests using MIT's newly developed automated stress path triaxial cells and/or MIT's Lateral Stress Oedometer (LSO) to estimate the in situ K_0 and how K_0 varies with overconsolidation ratio.

Tables 1.3 and 1.4 summarize the extent of the laboratory testing undertaken. This thesis presents the data from the Recompression tests performed, then compares these results with SHANSEP CK_0UC/E tests and UUC and CIUC tests performed by H&A. Table 1.5 summarizes the content of the companion thesis by de La Beaumelle.

General Site Characteristics and Laboratory Testing Program

Figure 1-1 shows the location of the test sites. Haley & Aldrich (1990) describes the area stratigraphy as follows: "the subsurface soil conditions along the proposed roadway alignment vary, but are dominated by glacial and marine deposits having combined thicknesses which exceed 200 feet locally. Subsurface conditions along much of the alignment in Geotechnical work areas 01 and 02 consist of 15–40 feet of fill and organic deposits overlying up to 100 feet of marine 'Boston Blue Clay' (BBC). Glacial till and Argillite bedrock typically underlie the clay". Figures 2-1 and 2-3 are representations of the soil profile at the SB and EB sites, respectively, and also outline the sampling program at each site.

The laboratory testing program included: radiography, classification and index testing, consolidation testing and triaxial testing, with the most time being devoted to the last two. Because issues such as anisotropy, sample disturbance, and time effects cannot be properly accounted for in conventional triaxial testing, a program of CK_0UC/E triaxial testing was undertaken, using both the SHANSEP and Recompression testing techniques. Tables 2.1 and 2.2 summarize the scope of the consolidation and strength testing programs, respectively.

8.1.2 Equipment and Procedures

A major portion of the initial research by MIT involved automating four of MIT's existing triaxial cells. Figure 3-1 shows a schematic diagram of the apparatus which includes: the triaxial cell and load frame, two pressure control cylinders to control cell and back pressure, three electric motors to drive the pressure controllers and the load frame, a control box containing a motor drive unit, and a personal computer equipped with A/D and D/A converters, upon which the customized control software runs. A

detailed description of the automated triaxial apparatus is included in Appendix A.

With the help of the automated equipment, over one hundred triaxial tests were performed. The quality of the results was generally outstanding, and included unprecedented numbers of successful extension tests.

8.1.3 Sample Characteristics and Distribution of Tests

The first phase of the lab testing program involved radiography of all tube samples, followed by classification and index tests to characterize the general nature of the clay. Tests performed included natural water content, Atterberg Limits, torvanes, grain size analysis, specific gravity, salt content and pH. Results of the first three types of test are summarized in Figures 4-1 and 4-2 for SB and EB, respectively.

Tables 4.1 to 4.3 summarize the distribution of CK_0-TX tests on South Boston tube samples, East Boston tube samples, and South Boston Block Samples.

8.1.4 Stress History and Consolidation Properties

Establishment of reliable stress history profiles at the South Boston site was a very high priority. Some of the issues addressed during this experimental work included the merits of continuous versus incremental loading, the reduction of sample disturbance through development of a new extrusion technique, and the use of the strain energy as well as the Casagrande method to estimate σ'_p. The resulting stress history profiles are shown in Figures 5-10 (SB) and 5-11 (EB).

Most of the reliable consolidation data came from the K_0-consolidation portion of the SHANSEP tests. The high quality S-shaped compression curves resulting from the SHANSEP tests were the first indication that the soil might be " structured". Additionally, SHANSEP consolidation also yielded valuable K_0 information, such as the K_0 versus OCR relationship shown in Figure 5-16 that was used for determination of the K_c used for the Recompression tests.

8.1.5 Recompression CK_0U Test Results

Tables 6.1 and 6.3 summarize shear data from 28 Recompression TC and 13 Recompression TE tests done on both block and tube samples from the South Boston site. Additionally, Appendix B presents a set of plots for each test, and MIT Research Report R91-10 presents the computer printout of the data reduction program for each test.

Based on consideration of the best quality CK_0U TC and TE tests, the following conclusions were drawn in Chapter 6. It should be emphasized that all of these conclusions depended upon a reliable estimate of the in situ preconsolidation pressure (σ'_p) at the South Boston test site. Figure 5-10 shows the measured σ'_p data and the linear regression σ'_p that was used to calculate the OCR = σ'_p/σ'_{vc} for all Recompression CK_0U tests.

1. *Undrained Strength Ratio* – The "best estimates" for S and m to use in the SHANSEP undrained strength equation are:

   TC S_c=0.298, m_c=0.676, SD log q_f/σ'_{vc} = ±0.0475 ; see Fig. 6-8

   TE S_e=0.144, m_e=0.978, SD log q_f/σ'_{vc} = ±0.030 ; see Fig. 6-16

   Based on these relationships, the degree of undrained strength anisotropy decreases with increasing OCR. For example, q_f(TE)/q_f(TC) equals about 0.6 at OCR = 2 and equals about 0.8 at OCR = 5.

   (a) $K_c \neq K_0$ – Some of the tests were not reconsolidated to the estimated K_0 for the test OCR, i.e., K_c was not equal to K_0. As shown in Figures 6-6 and 6-15, the K_c of a test will effect the stress strain behavior during shear for both TC and TE tests. However, the cumulative result of incorrect K_c values on TC and TE tests is different. For TC tests, the effect of the incorrect K_c values is not systematic, and the results were therefore included in the "best estimate" equation above. For TE tests, the tests with incorrect values of K_c (both too high and too low) gave lower USR

values at the higher OCR's, and thus were eliminated from consideration for the "best estimate".

(b) Tube Samples vs. Block Samples - For both TC and TE, tests performed on tube samples at the lowest OCRs exhibited lower undrained strengths than expected (see Figs. 6-8 and 6-16). This is contrary to what was predicted by Ladd (1991). In general, however, the tube samples were of extremely high quality.

(c) $\sigma'_{vc} \neq \sigma'_{v0}$ - Many of the Recompression tests were consolidated to stresses either less than or greater than the in situ σ'_{v0} in order to further study the effect of OCR on undrained shear behavior. Though there was a slight indication that TC tests with $\sigma'_{vc} < \sigma'_{v0}$ exhibited higher USRs, in general the effect of different ratios of $\sigma'_{vc}/\sigma'_{v0}$ was negligible. In other words, samples with the same test OCR behave similarly regardless of the in situ OCR.

2. *Effective Stress Envelope at Maximum Obliquity* - The best estimates for the ESE at MO, which should also apply to drained shear conditions, are:

TC $c'/\sigma'_p = 0.044, \sin\phi' = 0.484(\phi' = 29°)$, SD $q/\sigma'_p = \pm 0.017$; see Fig. 6-9

TE $c'/\sigma'_p = 0.031, \sin\phi' = 0.455(\phi' = 27°)$, SD $a/\sigma'_p = \pm 0.010$; see Fig. 6-17

(a) $K_c \neq K_0$ - For both TC and TE tests, inclusion of tests with incorrect values of K_c had no effect on the maximum obliquity ESE.

(b) Tube Samples vs. Block Samples - For the MO effective stress envelope, there was no discernible difference between tests performed on tube samples and tests performed on block samples for either the TC or TE tests.

(c) $\sigma'_{vc} \neq \sigma'_{v0}$ - Consolidating specimens to σ'_{vc} different from the overburden stress had no effect on either the TC or TE effective stress envelope at MO.

3. *Other Parameters*

(a) ϵ_f – As shown in Figure 6-10, the strains at failure for TC tests are lower than ϵ_f for TE tests overall. The higher than typical values of ϵ_f generally came from TC tests with a preexisting shear surface (PSS) and from tests run on tube samples. For the TE tests incorrect values of K_c led to lower values of ϵ_f, while for TC tests there was no effect.

(b) A_f – Overall, the pore pressure parameter at failure was lower for TC than for TE tests (Fig. 6-11). TC and TE tests with incorrect K_c values both fell within the scatter of the other tests. Tests on tube samples at very low OCRs (both TC and TE) gave higher values of A_f (which contribute to the lower than expected USRs mentioned previously).

(c) E_{50}/σ'_{vc} – In general, TC tests yielded values of E_{50} which were greater than or equal to those from TE tests (see Fig. 6-12). TE tests with $K_c \neq K_0$ showed lower values of E_{50}, but aside from these four tests, the TE results were less scattered than the TC. The tests on tube samples at low OCR yielded lower E_{50} values, both in compression and in extension.

8.1.6 Comparison of Recompression Results with SHANSEP and UUC/ CIUC

Comparison of the Recompression and SHANSEP and Recompression and UUC/CIUC tests was done in three main categories; undrained strength ratio, effective stress envelopes, and stress-strain parameters.

From comparison of Recompression and SHANSEP TC results, the findings were as follows:

1. Recompression TC tests (for specimens without preexisting shear surfaces) yield consistently higher peak undrained strength ratios than SHANSEP tests, though there is larger scatter in the data (see Fig. 7-4). Linear regression of both sets of points yielded two approximately parallel lines, with the Recompression line about 6% higher than the SHANSEP line.

2. Both the peak and MO ESEs are higher for Recompression than SHANSEP tests due to both slightly higher values of ϕ' and higher cohesion intercepts (Figures 7-5 and 7-6).

3. This increase in the effective stress envelope more than offsets slightly lower values of A_f for the SHANSEP tests (see Fig. 7-8).

4. Lower strains at failure and higher E_{50}/σ'_{vc} values reflect the steeper initial stress-strain curves observed in the Recompression tests, especially at high OCRs (Fig. 7-9).

The conclusions from comparison of Recompression and SHANSEP TE results are very similar to those made for TC tests, and can be summarized as follows:

1. Recompression and SHANSEP test data in Figure 7-13 gave values of S which were approximately equal ($S \approx 0.14$–0.15), but the value of the exponent, m, is significantly higher for Recompression tests than SHANSEP tests (m=0.98 for Recompression, m=0.83–0.86 for SHANSEP).

2. A higher ϕ' but lower c'/σ'_p for the mean Recompression ESE result in MO normalized stresses which are comparable to the SHANSEP ESE ± 1 SD in the range of OCRs considered, as shown in Figure 7-14.

3. The Recompression stress-strain curves exhibit steep initial slopes leading to much lower strains at failure and higher values of normalized modulus than SHANSEP (Figures 7-7 and 7-9). Recompression tests also gave lower values of A_f (Fig. 7-8). Additionally, they often undergo significant strain softening compared to the SHANSEP tests (e.g., Figs. 7-11 and 7-12).

These observations tend to support the hypothesis that some sort of structure in the BBC enhances the strength and furthermore, that this strength contribution is diminished during the SHANSEP consolidation process. This is a very interesting finding as the BBC does not fit the description of "highly structured or sensitive".

These results indicate that even slightly structured soils are sensitive to the testing technique employed.

Observations from comparison with UUC/CIUC tests include:

1. In terms of strength, both the UUC and CIUC tests gave reasonable results at some elevations, but were less consistent overall, especially for the deep UUC tests (see Figure 7-15).

   The CIUC tests with OCRs between 1.8 and 3.7 gave q_f very near to the values predicted by SHANSEP. At the higher OCRs the values were lower than both SHANSEP and Recompression q_f values, the latter being especially surprising as the testing method was nearly identical.

   The UUC tests gave reasonable results in the upper part of the crust, but below El. 20±, the strengths were drastically lower. This may be partly due to sample disturbance; the low OCR samples at depth are more prone to disturbance, and since there is no mechanism for overcoming this disturbance in UU tests (i.e., consolidation), the lower samples are severely affected. The initial stress, σ'_s, is a qualitative indicator of the amount of sample disturbance, and in most cases, σ'_s is lower for the lower samples (see Fig. 7-15).

2. USR versus OCR values from the CIUC tests on specimens with OCRs between two and four were reasonably similar to the Recompression linear regression. At higher OCRs the USR was lower, as noted above. The UUC tests normalized to σ'_s were also surprisingly close to the Recompression line. The UUC values normalized to σ'_{v0}, however, were much lower. This suggests that if UUC tests must be used, pore pressure measurements should be made, and σ'_s used for normalization.

3. In terms of deformability properties, neither test appears to be very reliable. Both types of tests yield high strains to failure and very low values of modulus. In particular, the UUC tests exhibit excessive scatter. This is due to the nature of UUC tests which are highly sensitive to the level of sample disturbance. The

fact that the CIUC ϵ_f and E_{50}/σ'_{vc} values are so different from the Recompression values at high OCR's is surprising, since differences in K_c at moderate to high OCRs were not shown to have much of an effect on Recompression test results in Chapter 6. This leads one to believe that these differences are the result of different sampling methods, as the Recompression CK_0UC tests were done mostly on block samples and the CIUC tests on tube samples only.

8.2 Recommendations Regarding Types of Undrained Strength Tests

After examining the results of the Recompression testing program, and comparing them with the SHANSEP and UUC/CIUC test results, the author has developed the following conclusions and recommendations on each type of test.

8.2.1 Recompression Tests

Recompression tests should give the truest measure of the stress-strain-strength parameters of the Boston Blue Clay *when very high quality samples are available.* A distinct advantage of Recompression tests is that they take only about half the time to perform as SHANSEP tests. However, on the "negative" side, Recompression tests do not give vital information regarding the in situ preconsolidation pressure (and hence OCR) needed both to define the stress history of the site and to properly evaluate Recompression strength-deformation parameters.

8.2.2 SHANSEP Tests

It is clear that the SHANSEP consolidation technique alters the undrained stress-strain-strength parameters of the moderately structured BBC. In particular SHANSEP tests tend to give lower peak strengths, higher ϵ_f and lower E_{50}/σ'_{vc}, and to mask strain softening behavior. This latter behavior is an important consideration for stability analyses for which the strain compatibility technique is used (see Ladd 1991).

The major advantage that SHANSEP testing has over Recompression testing is that valuable consolidation data (i.e., σ'_p, CR, RR) and K_0 data are obtained during the consolidation phase of the test. So, even though the test takes longer, it may be cost effective to get the extra information.

8.2.3 UUC/CIUC Tests

There are far too many variables in UUC tests to recommend them for determination of undrained stress-strain-strength parameters. It is acknowledged, however, that they are widely used, and if they must be used, they should be used only in the overconsolidated crust, and not in the deeper, normally or slightly overconsolidated strata where they give very low strengths due to sample disturbance. Also, pore pressure measurements should be made in order to determine a value of σ'_3 to which stresses can be normalized (rather than σ'_{v0}). In general, however, UUC should not be relied upon for determination of stress-strain parameters.

CIUC tests should only be used for OCRs between 2 and 4 (where $K_0 \approx 1$), and then cautiously. CIUC tests on tube samples are also unreliable for determination of stress-strain parameters.

8.3 Further Recommendations

8.3.1 Further Testing

The information provided by this research program has answered many questions regarding the nature of the BBC samples as well as strength testing techniques, but points out several questions which might be addressed with the help of further tests.

1. CIUC tests gave peak strength values which were consistent with the Recompression values at OCRs between 2 and 4. It is expected that CIUC on samples with lower OCRs will overpredict the peak strength due to a K_c (and hence p'_c) which is too high. It would be useful to perform several CIUC tests on samples with OCR<2 to check this prediction.

2. Though the CIUC tests at moderate to high OCRs gave strength values which were consistent with Recompression tests, they gave much higher strains to failure and lower values of normalized modulus, possibly due to the fact that they were performed on tube samples rather than block samples. It would be valuable to perform a CIUC test on a block sample with OCR>3 (El. > 10 ft).

3. Recompression TC and TE tests on tube samples with low OCRs (OCR≈1.1-1.2) gave lower peak strengths and higher A_f values (based on two tests of each type at the low OCRs). More Recompression tests on tube samples at the lower elevations would be required to determine whether or not this is a consistent trend.

4. Determination of whether or not a soil exhibits normalized behavior is a pre-requisite for the use of the SHANSEP testing method. From past experience with Resedimented BBC, it was assumed that the STP BBC samples would also exhibit normalized behavior, however, this was never formally established during the testing program. In light of the observations of "structure" in the clay, it is possible that the BBC samples do not strictly adhere to normalized behavior, and therefore it would be useful to test the assumption using the method suggested by Ladd and Foott (1974), i.e., consolidating the specimen to 1.5, 2 and 4 times σ'_p, and verifying that S_u/σ'_{vc} remains constant.

8.3.2 Further Analysis

Data from the STP will provide valuable information for many more analyses than are covered here. In particular, the following areas of additional analysis are suggested:

- A more thorough consideration of the compressibility (RR, SR, and CR) of the BBC.

- An analysis of the Recompression and SHANSEP undrained strength data in terms of strain compatibility (Ladd 1991), i.e., evaluation of q/σ'_{vc} at various strain levels.

- Quantification of the degree of sample disturbance in tube samples versus block samples, through tabulation and comparison of σ'_s values for Recompression and SHANSEP tests on blocks and tubes.

Chapter 9

List of References

1. Baligh, M.M., Azzouz, A.S., and Chin, C.-T.(1987). "Disturbance due to 'ideal' tube sampling." *Journal of Geotechnical Engineering*, ASCE, 113(7), 739–757.

2. Becker, D.E., Crooks, J.H.A., Been, K., and Jefferies, M.G.(1987). "Work as a criterion for determining in situ and yield stresses in clays." *Canadian Geotechnical Journal*, 24(4), 549–564.

3. Bishop, A.W., and Henkel, D.J.(1962). *The Measurement of Soil Properties in the Triaxial Test.* 2nd Ed., Edward Arnold Ltd., London.

4. Bjerrum, L.(1973). "Problems of soil mechanics and construction on soft clays: SOA report." *Proceedings of the 8th International Conference on Soil Mechanics and Foundation Engineering*, Moscow, U.S.S.R., 3, 111–159.

5. Butterfield, R.(1979). "A natural compression law for soils (an advance on $e - \log p'$)." *Geotechnique*, 29(4).

6. Casagrande, A.(1936). "The determination of the pre-consolidation load and its practical significance." *Proceedings of the 1st International Conference on Soil Mechanics and Foundation Engineering*, Cambridge, MA, 3, 60–64.

7. Germaine, J.T., and Ladd, C.C.(1988). "Triaxial testing of saturated cohesive soils: SOA paper." *Advanced Triaxial Testing of Soil and Rock*, ASTM STP 977, 421–459.

8. Guertin, J.D.(1967). "Stability and settlement analyses of an embankment on clay," thesis presented to MIT, Cambridge, MA, in partial fulfillment of the requirements for the degree of Master of Science.

9. Haley & Aldrich (1990). "Overview of planned special lab and field testing program for the Central Artery/Tunnel Project, Geotechnical Areas 01 and 02, Boston, Massachusetts", prepared for the Massachusetts Department of Public Works.

10. Jamiolkowski, M., Ladd, C.C., Germaine, J.T., and Lancellotta, R.(1985). "New developments in field and laboratory testing of soils: Theme Lecture 2." *Proceedings of the 11th International Conference on Soil Mechanics and Foundation Engineering*, San Francisco, 1, 57–153.

11. Kenney, T.C.(1964). "Sea level movements and the geologic histories of the post-glacial marine soils at Boston, Nicolet, and Oslo." *Geotechnique*, 14(3), 203–227.

12. Lacasse, S., and Berre, T.(1988). "Triaxial testing methods for soils: SOA paper." *Advanced Triaxial Testing of Soil and Rock*, ASTM STP 977, 264–289.

13. Ladd, C.C.(1991). "Stability evaluation during staged construction." *Journal of Geotechnical Engineering*, ASCE, 117(4), 542–615.

14. Ladd, C.C., and Foott, R.(1974). "New design procedure for stability of soft clays." *Journal of Geotechnical Engineering Division*, ASCE, 100(7), 763–786.

15. Ladd, C.C., and Luscher, U.(1965). "Engineering properties of the soils underlying the MIT campus," *Research Report R65-11, No. 177*, Department of Civil Engineering, MIT, Cambridge, MA.

16. Sauls, D.P., Germaine, J.T., and Ladd, C.C.(1984). "Strength deformation properties of Harrison Bay Arctic Silts," *Research Report R84-18, No. 773*, Department of Civil Engineering, MIT, Cambridge, MA, 318 pages.

17. Sheahan, T.C.(1988). "Modification and implementation of a computer controlled triaxial apparatus," thesis presented to MIT, at Cambridge, MA, in partial fulfillment of the requirements for the degree of Master of Science.

18. Sheahan, T.C., Germaine, J.T., and Ladd, C.C.(1990). "Automated testing of soft clays: and upgraded commercial system." *Geotechnical Testing Journal*, ASTM, 13(3), 153-163.

19. Werner, R.J.(1991). "The influence of load history on the response of Arctic Silt to undrained cyclic and monotonic direct simple shear," thesis presented to MIT, at Cambridge, MA, in partial fulfillment of the requirements for the degree of Master of Science.

Appendix A

Equipment and Procedures

A.1 Components of the MIT Automated Stress Path Triaxial Apparatus

The MIT automated triaxial system was developed by Dr. Germaine and Thomas C. Sheahan. The evaluation of a commercially available computer controlled triaxial apparatus was the topic of Mr. Sheahan's thesis (Sheahan, 1988; Sheahan et al. 1990). Mr. Sheahan then developed new software and electromechanical control devices that were used to automate two of MIT's "standard" triaxial cell-load frames (MIT01-02) for his doctoral thesis research on "rate effects" of Resedimented BBC. The design of the four automated triaxial devices (MIT03–06) constructed for this research is an extension of Mr. Sheahan's work. Hence Appendix A will only briefly describe the major components of the system, their role and their mutual interaction, referring the reader to Mr. Sheahan's thesis for a more thorough explanation.

A schematic diagram of MIT's Automated Stress Path Triaxial Apparatus is shown in Figure 3-1. The diagram can be separated into five main components: the triaxial cell and pressure control cylinders, the three control motors, the motor control box, the personal computer, and the Central Data Acquisition Control Unit.

A.1.1 Triaxial Cell and Pressure Control Cylinders

The triaxial cells were manufactured by Wykeham Farrance (England) and modified at MIT in the mid-1960's to facilitate operation and to better fit its research needs. Figure A-1 shows the cell in more detail. The chamber consists of the load piston to which the top cap is fixed to facilitate specimen set up, a base pedestal upon which the specimen is fitted, a plexiglass tube which surrounds the chamber and a stainless steel cover and base. The cell is connected to the control system by four valves and is monitered by a load cell, two pressure transducers and a direct current displacement transducer (DCDT).

The load piston is a linear ball bearing bushing type which maintains alignment and eliminates friction. A frictionless rolling diaphragm is connected at its bottom and provides an impermeable seal between the piston and cell chamber. The load cell, located on the load frame outside the cell directly above the piston, registers the force acting on the piston. In addition, some accessories are connected to the piston such as a long arm in contact with the axial DCDT, connecting rods which permit extension tests, and a steel ball or "bullet" to produce a point load with no eccentricity on the top of the specimen. The top cap is designed to provide an internal connection for the drainage line.

Double drainage is provided by copper tubing connected to both the base pedestal and top cap. Each drainage line is controlled by a valve to allow various drainage configurations. Another valve allows one to isolate the pore pressure transducer in order to measure pressures either in the lines or in the specimen when drainage is closed.

The remaining valve connects the cell to the cell pressure controller and another pressure transducer is used to measure the cell pressure. Each pressure transducer is installed next to the chamber which makes for a more rigid system.

The triaxial cell is placed upon a load frame which can be moved up or down to cause vertical deformations. A load cell and DCDT connected to the pistonallow one to conduct tests with either stress or strain control.

The pressure controllers consist of two hydraulic cylinders, one containing silicon

oil and one containing distilled, deaired water, connected by plastic tubing to the cell chamber and copper specimen drainage lines, respectively. A second DCDT is attached to the pore pressure controller to measure volumetric strains in the specimen.

The cell and the pressure controllers are enclosed in an insulated case equipped with a device which automatically maintains a constant temperature over the course of the test.

A.1.2 Control Motors

The three motors are manufactured by Robbins & Myers Electro-Craft Servo Products. They are direct current servo motors with a gear box. For the pore and cell pressures, the motors drive a piston into a cylinder full of fluid. The third motor controls the vertical strain by raising or lowering the load frame. The motors are connected to the control motor box which serves as the nerve center of the system.

A.1.3 Motor Control Box

This component is the indispensable relay between the personal computer and the motors. Depending on the required stress or strain change requested by the computer, digital signals in binary mode are converted to analog signals and relayed to the control box which then regulates the motor rates.

A.1.4 Personal Computer

A Hyundai Super 16TE computer is used with each triaxial unit, and with the use of a digital to analog (D/A) card, manufactured by Strawberry Tree Incorporated, and Mr. Sheahan's A/D card, sends signals to the motors. The computer receives voltage signals from the pressure transducers, DCDTs and load cell, converts them to digital signals using the A/D converter card. Using the different software programs installed, these binary codes are then converted to engineering units. These engineering units are compared to target values calculated by the program, and the difference is is used to calculate digital correction signals, converted to analog signals by the Strawberry

Tree D/A card, and transmitted to the control box which then creates the signal to the motors. The computer uses programs written by Dr. Germaine and Mr. Sheahan and provides the users with the ability to monitor and control the triaxial tests.

A.1.5 Central Data Acquisition Control Unit

Throughout the test, the voltage signals from the transducers, DCDTs and load cell are also periodically sent directly to the Hewlett-Packard 3497A Data Acquisition Control Unit. Each sensor is hooked to a 6 channel switch box with each channel comprised of 12 pins, 10 pins for the sensors (5 for the Central Data Acquisition System, 5 for the personal computer) and two for the power supply. The data acquisition unit has a reading rate of one second and a resolution of 0.1 mV on the DCDT's and 1 μV on the pressure transducers. The readings from the various channels are stored in a data file at the Data Acquisition Control Unit. The file can then be retrieved and used for generating results and plots.

A.2 Control Algorithm

A.2.1 General Operation

Before beginning a test, the operator must type some basic data into a setup file. The data required includes physical information about the test, such as the initial dimensions of the specimen (height and cross sectional area), filter strip perimeter, membrane type, and type of area correction. Additionally, zeros and calibration factors for each of the pressure transducers, direct current displacement transducers (DCDT's), and load cell, are entered. After filling out the input file the data are read automatically by the control program and used for converting voltage readings to engineering units.

The other important input to the control program are "gain" rates. These are written directly into the code and are equipment specific, so generally do not need to be changed from test to test. The gain rate is input in engineering units (e.g.,

kg, cm, or ksc) per volt-second and used by the program to calculate the amount of voltage which needs to be sent to the motor for a specified time period (1 second) to achieve the required change. For example, a gain rate of 0.1 kg/volt-sec on the axial load motor signifies that one volt applied for one second will result in an increase of one-tenth of a kilogram of load on the specimen. The axial motor and pressure controllers require two gain rates each; one for the stress controlled parts of the test (pressure up, saturation and B check), and one for the strain controlled parts of the test (consolidation and shear).

The motor control loop takes readings from the transducers or load cell and converts these to engineering units. This current reading is subtracted from a target value and this difference is divided by the gain rate. The signal is sent in one-second bursts to the control motors which increase or decrease the pressures or load accordingly. The system frequency is 40 Hz, the pressures are controlled to within 0.01 ksc ($\approx$ 1 kPa), and the strains to better than 0.01%.

The target values sought by the control program are determined differently for different phases of the test, as outlined below.

A.2.2 Pressure Up

The "pressure up" phase is the first performed in each test and consists of applying a small cell pressure to the specimen (with drainage valves closed) and allowing it to sit for approximately twelve hours in order to induce a pore pressure greater than zero. The control of this phase of the test is straight forward; the operator inputs directly the cell pressure required (usually 0.5 to 0.75 ksc) and a deviator load (usually 0.1 kg) to provide a slight seating load, and the control program uses these values as "target values", invoking the motor control loop repeatedly until they are achieved.

A.2.3 Back Pressure Saturation

After the pore pressure has stabilized in the "pressure up" phase, the specimen is saturated by increasing the cell pressure and back pressure equally to maintain a

constant effective stress. In this phase of the test, the tester inputs a cell pressure, a pore pressure, and a holding time. In this manner the specimen can be back pressured in small increments spread out over several hours; the tester need not be physically present in order to increase the pressures.

The control program reads the values input and uses these to calculate the pressure increment required. This large increment is then divided by ten to yield small increments which are applied to the specimen by the cell and pore pressure controller motors. After each small increment is applied, the compliance of the pressures to the intermediate target value is checked. Only when both the cell pressure and the pore pressure are within 0.01 ksc (approximately 1 kPa) of the intermediate target value, and the axial load is equal to zero (plus or minus 0.10 kg), will the next small increment be applied, ensuring that the effective stress in the specimen never deviates from the intended value by more than 1 or 2 kPa.

After the ten intermediate steps have been applied, and compliance with the final incremental target value is achieved, a prompt appears that enables one to check the B value of the specimen. If the B value check (described below) is not chosen within one minute, the program holds the current stress state for the specified time, and then begins automatically to apply the next increment of stress. After the last increment has been applied, the program holds the stresses indefinitely.

A.2.4 B value Check

Skempton's B value ($B = \Delta u/\Delta\sigma_c$) is used to determine whether the specimen is saturated. As mentioned above, the B value can be checked at the end of each increment, or at any other time during the test. To check the degree of saturation, the operator either chooses the B value check item from the main menu or simply pushes "Enter" on the keyboard at the B value check prompt. The computer then prompts the operator to input a cell pressure increment (usually 0.2 - 0.5 ksc) and close the drainage valves to the specimen before restarting the program by hitting "Enter" on the keyboard. The control program takes an initial set of readings, and then calls the motor control loop to apply the cell pressure increment. Pore and cell

pressure readings are taken and the B value is automatically calculated and displayed on the computer screen continuously for two minutes; the final value is recorded and used to check the degree of saturation. After the final B value is displayed, the control program returns the pressures to their original values, and the operator opens the drainage valves and chooses the next phase of the test (either continued saturation or consolidation).

A.2.5 Consolidation

This control program provides automated control for two types of consolidation: K_0 consolidation or stress path consolidation. Both portions of the program can also be used to control swelling of the specimen simply by inputting a negative strain rate. Each type of consolidation is described in more detail below.

Stress Path Consolidation

This phase of the control program consolidates the specimen along a straight line between the point representing the current stress state and the final stress state input by the operator. The axial motor is strain controlled, while both pressure controllers are stress controlled. At the beginning of consolidation the tester chooses an axial strain rate (typically 0.1%/hr) and values for the final vertical and horizontal effective stresses. The first thing the program does is convert the effective stresses to total stresses, then it calculates a gradient, β:

$$\beta = \frac{\Delta\sigma_v}{\Delta\sigma_h} = \frac{\sigma_{vf} - \sigma_{vi}}{\sigma_{hf} - \sigma_{hi}} \tag{A.1}$$

and a horizontal reference stress, σ_{hr}:

$$\sigma_{hr} = \sigma_h - \sigma_v\beta \tag{A.2}$$

to use in the following control equation:

$$\sigma_h = \sigma_{hr} + \beta\sigma_v \tag{A.3}$$

where σ_{hi} and σ_{vi} are the initial values of stress after back pressure saturation and σ_{hf} and σ_{vf} are the target values of stress.

The program strains the sample at a constant rate, thus slowly increasing (or decreasing if unloading) the axial load, maintains a constant back pressure, and adjusts the cell pressure to increase the horizontal effective stress according to the preceding control equation. Once the target stresses are reached the program switches automatically to the hold stress subroutine, and will maintain the stresses until the operator chooses the next phase of the test.

K_0 Consolidation

Two of the inputs for the K_0 consolidation phase are identical to the stress path consolidation; axial strain rate and final vertical effective stress. In this case however, the final horizontal effective stress is determinedby the control program as it consolidates the specimen maintaining a zero lateral strain condition. In this phase of the test both the axial motor and the pore pressure controller are strain controlled.

K_0 consolidation is achieved by controlling the volumetric strain so that it is always equal to the axial strain, ensuring that there is no radial strain (i.e., the cross-sectional area remains constant throughout). The axial motor receives a constant signal and strains at a steady rate, and the back pressure is held constant to within 0.01 ksc of the value at the end of back pressure saturation. The control signal to the cell pressure controller is calculated by dividing the change in volume (Area$\times\Delta$Height) by a volume gain rate. This signal causes the cell pressure controller to push oil into the cell chamber, displacing more volume, and causing pore water to flow out of the specimen. Compliance with the final axial stress is checked continuously, and when it is reached the program jumps to the "hold stress" loop described below. This feature is especially useful for SHANSEP type tests during which the specimen is consolidated

beyond the in situ preconsolidation pressure and rebounded to a specified OCR.

A.2.6 K_0 Swelling

For SHANSEP tests on overconsolidated specimens it is necessary at the end of K_0 consolidation to allow the specimen to rebound to a specified vertical effective stress. The control of this portion of the test is essentially identical to K_0 consolidation, the only difference being that a negative axial strain rate is input. This causes the axial strain to decrease, and the computer responds by moving the volumetric strain controller so that water flows into the specimen, rather than out as during consolidation.

A.2.7 Hold Stress

During several phases of the test it is necessary at times to hold the existing state of stress in the specimen constant. For instance, at the end of the application of a saturation increment stresses are held for some specified period of time to allow the air in the specimen to dissolve into solution, and at the end of K_0 consolidation the final consolidation stresses are held for one log cycle of time (or 24 hours) to allow the specimen to undergo secondary compression.

In both of these cases the "hold stress" loop is called by the program when compliance with a final state of stress is achieved. For the saturation phase of the test a timer is invoked so that the stresses are held for a specified period before the next saturation increment is applied. For the consolidation phase of the test the stresses are held indefinitely until the tester chooses the next phase of the test.

When the hold stress subroutine is called, the computer first takes a set of readings, and these stresses become the target values. The program then maintains these values by continuously calculating the difference between the subsequent readings and the target values, dividing the differences by the cell pressure, pore pressure and axial load gain rates, and sending the appropriate signals to the control motors.

A.2.8 Shear

The final phase of the test is shearing. The specimen can be sheared in compression or in extension, using the same portion of the control program, simply by specifying a positive or negative strain rate. This portion of the program, as it is currently written, is limited to only two total stress paths; triaxial compression loading (TC(L)) or triaxial extension unloading (TE(U)). However, it is possible, by using the stress path consolidation portion (see Section A.2.5) of the program and inputting final values of σ'_v and σ'_h well beyond the failure envelope, to control stresses along any stress path, including TC(U) and TE(L) for *drained* shear. This is, in fact, how the CK_0DC/E tests were performed during this research program.

For undrained shearing, the control program simply maintains a constant cell pressure, and applies a steady axial strain rate. The pore pressure is not controlled, and the motor is generally turned off entirely to prevent drift. The operator also inputs a final axial stress, though for the shear phase this is usually merely a safeguard against overloading the load cell.

A.3 Triaxial Testing Procedure

A.3.1 Specimen Preparation and Setup

For tests run on tube samples, each tube's radiographic record is first reviewed to find high quality "undisturbed" sections. Once the decision is made, a 4 inch portion of the tube is cut with a band saw. Torvane strengths are taken from one of the tube's extremities, and the remaining portion of the tube is sealed using wax and a layer of plastic wrap. Before extruding the soil sample, a wire is inserted through the soil near the edge of the tube, attached to a wire saw handle, and drawn around the perimeter of the tube in order to diminish the adhesion between the soil and the metal tube. The soil is then pushed out and taken to the humid room for trimming.

The block samples arrived in the MIT laboratory covered with a thick layer of wax and gauze and packed in individual crates full of sawdust or straw. The first task

in the preparation of the block samples was to remove the protective coating. Next, the outermost layer of clay, which is imbedded with sand and gravel picked up during the sampling process, is scraped off to reveal the natural clay underneath. At this point, photographs and notes are taken to try to quantify any visible disturbance of the sample. The larger samples were then cut into more manageable sizes. This is a delicate process involving making one side of the cylindrical sample flat, carefully laying the block on its flat side on a wax paper-covered glass plate, and slicing the block into two to three 4 inch – 6 inch layers. Each layer is then typically cut in half vertically, and these semi-circular pieces are labelled, tightly covered with paraffin and plastic wrap, and stored in the humid room for future use. In all steps of the preparation process, the greatest care is taken not to squeeze or jolt the sample, and thus cause disturbance. Figures A-2 to A-11 show steps in the preparation of the block samples.

When a test is specified on the block samples, a piece is cut off of the waxed soil block to the minimum dimensions needed for the test (about 9 cm × 4 cm × 4 cm for triaxial tests), then the remainder of the block is rewaxed and returned to storage. Figure A-12 shows how the semicircular pieces are divided up to yield specimens for triaxial, oedometer, or DSS tests.

The sample is then trimmed with a wire saw to final dimensions of approximately 8 cm in height and 3.55 cm in diameter using a mitre box. The exact measurements of diameter and height are obtained using an optical device. The trimmings are used for water content measurements while the excess is kept in a jar in the humid room for possible future testing (e.g., Atterberg limits).

The prepared specimen is weighed and then placed on the base pedestal with filter paper and a porous stone covering each end. The porous stone and filter paper had previously been boiled in distilled water for cleansing and deairing while system compliance was checked and pressure and displacement transducer and load cell zeros were recorded.

Filter strips are then installed on the surface of the specimen to increase the rate of consolidation and to equilibrate pore pressures during shear. For triaxial compression

tests, eight vertical strips 1/4 inch wide are used. For extension tests five or six 1/4 inch strips, spiralled around the sample so as to allow them to stretch without tearing during the shearing process, were initially used, but the width of each strip was later reduced to $\frac{3}{16}$ inch when early extension tests yielded unrealistically high values of ϕ'. The filter strips are connected at both ends to the porous stones by sliding them underneath the rubber sleeve used to protect the membranes from the contact with the stones. Two prophylactics are used as thin membranes, and are sealed using three rubber o-rings and vacuum grease at top and bottom. The plexiglass cylinder is then slid over the sample, the top plate installed, the cell chamber filled with silicon oil and the test begins. Photographs of various steps of the setup process are shown in Figures A-13 through A-18.

A.3.2 Pressure up

The first task is to inform the computer program of initial conditions : 1) height and area of the specimen, 2) zeros and calibration factors for the pressure transducers, DCDTs and load cell. Following this step, an initial cell pressure is applied while the drainage lines are closed and the pressure transducer is reading the pressure inside the specimen, in order to monitor the pore pressure response as described in Section A.2.2. The magnitude of the cell pressure is considered high enough when positive pore pressures are measured after at least 12 hours (when they have equilibrated). The value of the cell pressure was usually betweem 0.5 and 0.75 ksc, but occasionally be higher for stiffer specimens. During the whole process, the deviatoric load is maintained constant at a low value (around 0.1 kg). The initial effective stresses (σ'_v and σ'_h) are recorded and the second part of the process begins.

A.3.3 Saturation and B value

The pore pressure transducer is connected with the pore pressure controller and the system's back pressure is equilibrated with the specimen's pore pressure before opening the drainage lines. In order to saturate the specimen, the back pressure is in-

creased by increments of 0.2 ksc while maintaining the same initial effective stress as described in Section A.2.3. B values are measured every 0.4 ksc or so and are obtained by closing the drainage lines, increasing the cell pressure and measuring the pore pressure response (see Section A.2.4). The saturation process is repeated until a B value of 0.95 or above is obtained which indicates adequate saturation of the specimen.

A.3.4 Consolidation

Before beginning stress path consolidation for Recompression tests, a final vertical effective stress, σ'_{vc}, is chosen (often equal to the in situ vertical stress, σ'_{v0}, but sometimes higher or lower as outlined in Section 1.2), and depending upon the OCR of the specimen, an appropriate K_0 is used to calculate σ'_{hc}. These stresses are calculated with the help of a worksheet shown in Figure A-23 and input into the computer for control of the test. Additionally, for both K_0 (for SHANSEP tests) and stress path (for Recompression tests) consolidation, the volumetric DCDT zero is changed in the setup file so that the volumetric strain equals the axial strain. This enables the computer to ignore the small amounts of strain which occur during pressure up and saturation, and begin control of the consolidation phase with the two strains equal (see Section A.4 for an explanation of how this is accounted for during the reduction of the test data).

An axial strain rate of 0.1%/hr is used for both the SHANSEP and Recompression tests. Primary consolidation is usually stopped around 10% vertical strain for SHANSEP tests and as required to achieve the proper stresses for Recompression tests (typically between 1% and 5%). The sample is then held at the same stress state for 24 hours to allow secondary compression to occur as described in Section A.2.5. For an overconsolidated SHANSEP test, swelling is allowed after the secondary compression (see Section A.2.6). Throughout the process, the computer displays current values of stress and strain, which allows the operator to monitor the progress of the test by producing a manual plot of the compression curve.

A.3.5 Shearing

Undrained

When shearing undrained, the drainage lines are closed and a leak test is performed. The pore pressure changes are monitored while maintaining the state of stress constant for 30 minutes. If the pore pressure difference is less than 0.03 ksc, there is no indication of a leak. For shearing, the drainage lines are kept closed and an axial strain rate of 0.5%/hr is applied by the computer. The test is stopped when failure planes are noticed in compression tests or necking occurs in extension tests, which usually requires an additonal 10% vertical strain after consolidation.

Drained

The stress path consolidation algorithm is used for drained shear. Final vertical and horizontal effective stresses well beyond the failure envelope are input, the drainage lines are kept open, and a rate of 0.10%/hr is applied until the specimen fails.

A.3.6 Takedown

Once the test is finished, the computer program is turned off, and the cell pressure and load are decreased manually while drainage lines to the specimen remain closed. The cell fluid is then drained and the cell disassembled. The sample is photographed and weighed, final height and area are measured, and the soil is split into four sections and oven dried for final water content and dry weight measurements. The cell is cleaned and drainage lines are emptied partially to look for oil (indication of an internal leak) in preparation for the installation of another specimen.

A.4 Data Reduction

A.4.1 Calculations

Table A.1 lists the formulae used by the data reduction program to calculate the various parameters which are obtained from each test.

A.4.2 Corrections

Area Correction

The first type of correction used in the data reduction is an area correction. During the consolidation phase the specimen is assumed to remain cylindrical, and the area is corrected according to the following formula (Germaine and Ladd, 1988):

$$A_c = \frac{A_0(1 - \Delta V/V_0)}{1 - \Delta L/L_0} \tag{A.4}$$

where A_c is the corrected area, A_0 is the initial area (at the beginning of the test), ΔV and ΔL are the change in volume and length respectively, and V_0 and L_0 are the initial volume and height of the specimen. The corrected area is then used in calculation of the axial stress and change in volume ($\Delta V = A_c \times \Delta H$) for the K_0 consolidation control program.

During undrained shear in compression, the specimen is assumed to deform parabolically and the equation used is the following (Germaine and Ladd, 1988):

$$A_c = A_0\{-\frac{1}{4} + \frac{\sqrt{25 - 20\frac{\Delta L}{L_0} - 5(\frac{\Delta L}{L_0})^2}}{4(1 - \frac{\Delta L}{L_0})}\}^2 \tag{A.5}$$

For undrained extension tests, the cylindrical correction is used, i.e. $A_c = A_0/(1 - \Delta L/L_0$.

Filter Strip Correction

The second type of correction used is for the increase in axial stress due to the load carried by the filter strips during the consolidation and undrained shear phases of compression tests. The equation used to calculate the stress increase is:

$$\Delta\sigma_{fs} = K_{fp}\frac{P_{fp}}{A_c} \tag{A.6}$$

where K_{fp} is a correction factor which varies between 0.13 and 0.19 kg/cm (0.16 was selected), P_{fp} is the filter strip perimeter, calculated as the number of strips times the width of the strip (typically $8 \times 1/4$ inch = 5.08 cm), and A_c is the cross sectional area of the sample. The value of σ_{fs} calculated is the maximum correction applied. The actual correction applied increases linearly from zero to σ_{fs} as the axial strain increases from 0 to 2%, as shown in Figure A-19. After 2% axial strain the filter strips are assumed to buckle and their load contribution remains constant. The filter strip correction is as recommended by Bishop and Henkel (1962) in their book on triaxial testing procedures.

For extension tests, spiral filter strips are used, and no correction is applied during consolidation or shear.

Membrane Correction

The next correction to the stresses is a membrane correction. All of the tests were performed using two prophylactics as thin membranes. The membranes contribute additional axial stress and radial stress. The corrections for membranes are based on shell theory as follows (Germaine and Ladd, 1988):

$$\Delta\sigma_a = \frac{4tE_r}{D_i}(\epsilon_a + \frac{2}{3}\epsilon_v) \tag{A.7}$$

$$\Delta\sigma_r = \frac{4tE_r}{D_i}(\frac{\epsilon_v}{3}) \tag{A.8}$$

where E_r is the modulus of the rubber, t is the thickness of the rubber, and D_i is the initial sample diameter. If the diameter of the membrane is less than the diameter of the specimen, $\Delta\sigma_r$ should be increased by the following amount:

$$\Delta\sigma_{ri} = 2tE_r(\frac{D_i - D_m}{D_m D_i})$$

where D_m is the initial diameter of the membrane. In this program, however, the diameter of the specimen and membrane are essentially equal and this adjustment is neglected. These membrane corrections are suggested by Lacasse and Berre (1986).

The net result of these formulae is a constant membrane correction factor for undrained shear of 1.942 ksc/100% axial strain for the two prophylactics used on all of our tests. Again, this correction is automatically applied by the data reduction program.

Piston Correction

The final correction applied to the vertical stress is to account for the area of the piston and the weight of the piston and the attached accessories. The weight of the piston plus accessories (W_p) is added to the load registered by the load cell to get the total point load acting on the top of the sample. In addition, the cell pressure contributes to the axial load by acting over the area of the top cap (A_t) minus the area of the piston (A_p) to which it is attached. Typically W_p equals 0.8 to 1.0 kg, A_p is about 3.6 cm^3, and A_t is taken to be the same as the initial cross sectional area of the specimen (A_0), or about 10 cm^3.

A.4.3 Changes to Input File

The voltage readings from the Central Data Acquisition System are read directly by the data reduction program, but one additional line is input manually by the operator for both the consolidation and shear portions of the program.

Small amounts of axial and volumetric strain occur during the pressure-up and saturation phases of the test. The volumetric strain is typically between -0.5 and -2%

and is a combination of water flowing into the sample and air dissolving into solution during saturation. The axial strain is typically less than +0.5% and is due to initial application of a seating load during pressure-up. To remove these small strains from the consolidation results from each test, a first line is input which forces the axial and volumetric strains to equal zero on the first line, and to equal each other on the second line. The zero recorded for the axial DCDT is input into the initial information file as well as on the first line of data read by the reduction program, effectively forcing the axial strain to equal zero. The operator then converts the difference between the axial DCDT zero recorded during the setup of the test and the first DCDT reading taken by the data acquisition system into an axial strain, and back calculates a voltage reading which will give an equivalent amount of volumetric strain. This voltage is entered into the initial information file as the zero for the volumetric strain DCDT, and is also inserted in the first line of data in the data acquisition file.

In a similar manner, a first line of data is inserted into the shear data file. In this case, however, the object is to ensure that the initial vertical and horizontal effective stresses are equal to the average values held over the 24-hour secondary compression portion of the consolidation phase. The value of the initial vertical stress reading during shear is particularly important as it is taken as the vertical consolidation stress (σ'_{vc}) to which the stresses calculated during undrained shear are normalized. Inputting a mean value as we do gives a more accurate vertical effective stress and K_c value, eliminating the effects of small pressure fluctuations during the pre-shear leak.

A.4.4 Plotting of Results

The output from the data reduction program consists of printed file containing a heading summarizing the input information and the list of data and an ASCII file containing only the data which is saved on a floppy disk. This ASCII file has the advantage of versatility in that it can be easily imported to almost any spreadsheet or graphics program, either on IBM or Macintosh systems.

For each test a standard set of plots was produced to aid in analysis of the data.

These plots included:

for consolidation – the compression curve (ϵ_a and ϵ_v v. log σ'_{vc}), K_0 v. log σ'_{vc}, stress path (q – p' diagram), and for overconsolidated SHANSEP tests, K_0 v. log OCR

for shear – the normalized stress path (q/σ'_{vc} v. p'/σ'_{vc}), normalized stress and pore pressure (q/σ'_{vc} and u/σ'_{vc} for TE or $\Delta u - \Delta\sigma'_3/\sigma'_{vc}$ for TC), A parameter, and friction angle (ϕ') v. axial strain (ϵ_a) , log normalized modulus v. log axial strain (log E_s/σ'_{vc} v. log σ'_{vc}), and log normalized modulus v. differential load ratio (log E_s/σ'_{vc} v. log dq/dq_m).

These plots were produced by first importing the data reduction results file into Lotus 1-2-3 and then using templates created on Harvard Graphics to produce final copies. Examples of both the printed data output and the standard plots produced are included in the following section which covers documentation. Additional plots, such as those used to calculate the preconsolidation pressure by the Strain Energy (SE) method, were produced using Lotus 1-2-3 directly, and some of the plots included in this thesis were produced on the Macintosh, using the KaleidaGraph software.

A.5 Documentation of Tests

In order to standardize the tests and obtain as much information as possible from each, a set of data sheets was developed to use during each test. An example of a set of completed data sheets, along with the printed data output and the standard plots from a typical Recompression test are included in Figures A-20 through A-45. Except for the worksheet labelled "Recompression Test Stress Worksheet" (Figure A-23), the data sheets and plots presented are identical for SHANSEP tests.

Table A.1: Formulae Used in Data Reduction Program

Basic conversion from volts to engineering units	$(\frac{reading}{V_{in}} - \frac{zero}{V_{in}}) \times calibration\,factor$	reading = transducer reading zero = initial transducer zero V_{in} = input voltage
Axial strain	$\epsilon_a = L/L_0 \times 100\%$	L = current specimen height L_0 = initial specimen height (different for consol. and shear)
Volumetric strain	$\epsilon_v = V/V_0 \times 100\%$	V = current specimen volume V_0 = initial specimen volume (different for consol. and shear)
Area	$A = \frac{V_0 - \Delta V}{L_0 - \Delta L}$	ΔV = change in volume from beginning of test ΔL = change in height from beginning of test
Horizontal Effective Stress	$\sigma'_h = \sigma_c - u + \Delta\sigma_r$	σ_c = cell pressure u = pore pressure $\Delta\sigma_r$ = radial membrane correction
Vertical Effective Stress	$\sigma'_v = \frac{P + W_p + (A - A_p) \times \sigma_c}{A_c} - u$ $-\Delta\sigma_{fs} - \Delta\sigma_a$	P = load (from load cell) W_p = weight of piston A_p = area of piston $\Delta\sigma_{fs}$ = filter strip correction $\Delta\sigma_a$ = axial membrane correction
Shear stress	$q = \frac{\sigma'_v - \sigma'_h}{2}$	
Ave. effective stress	$p' = \frac{\sigma'_v + \sigma'_h}{2}$	
Lateral stress ratio	$K_c = \sigma'_h/\sigma'_v$	
Friction Angle	$\phi = \sin^{-1}(\frac{q}{p'})$	
A parameter	$A = \frac{\Delta u - \Delta\sigma_3}{\Delta\sigma_1 - \Delta\sigma_3}$	$\Delta\sigma_1$ = change in major principal stress* $\Delta\sigma_3$ = change in minor principal stress*
Normalized pore pressure	$\frac{\Delta u - \Delta\sigma_3}{\sigma'_{vc}}$	σ'_{vc} = vertical preshear consolidation stress
Normalized q	q/σ'_{vc}	
Normalized p'	p'/σ'_{vc}	
Normalized secant modulus	$\frac{(\Delta\sigma_1 - \Delta\sigma_3)/\epsilon_a}{\sigma'_{vc}}$	

* For TC, $\Delta\sigma_1 = \Delta\sigma_v$, $\Delta\sigma_3 = \Delta\sigma_h$ For TE, $\Delta\sigma_1 = \Delta\sigma_h$, $\Delta\sigma_3 = \Delta\sigma_v$

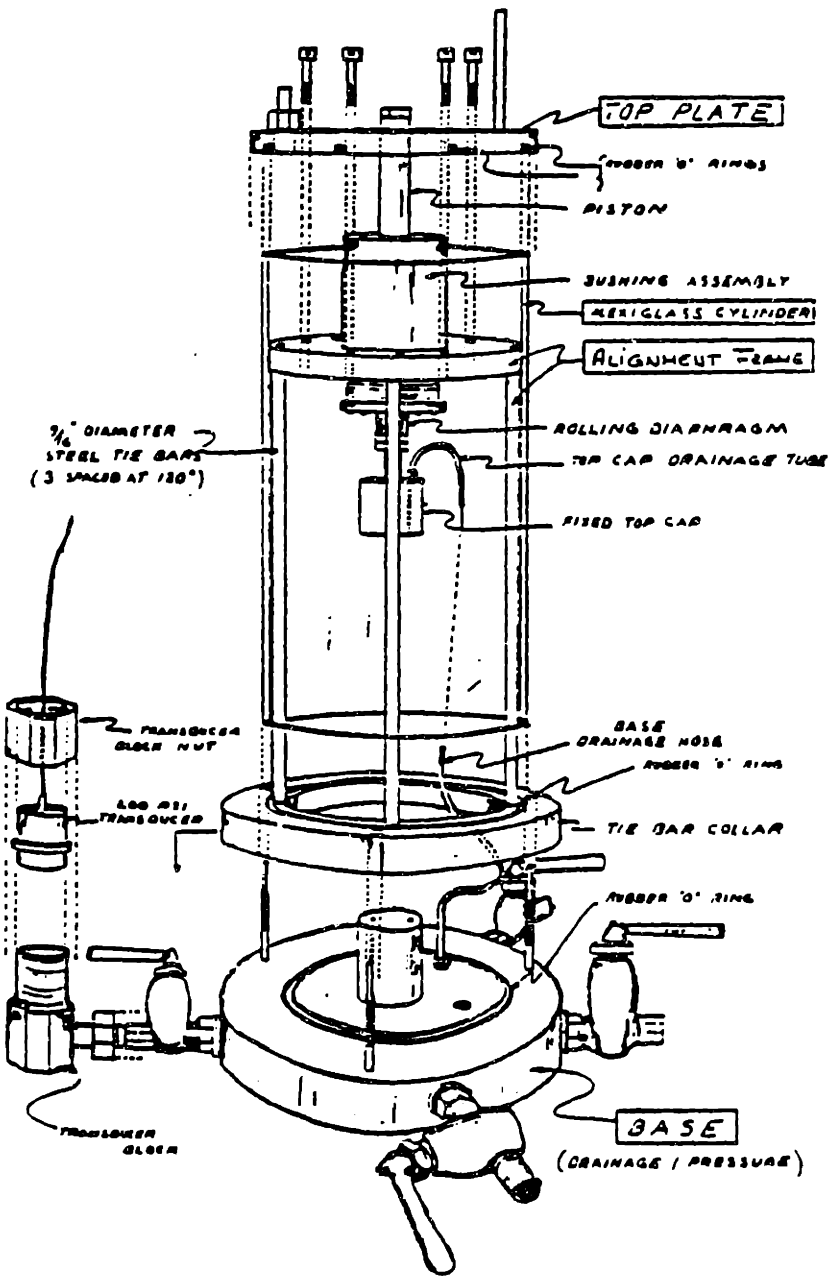

Figure A-1: Detail of MIT Triaxial Cell

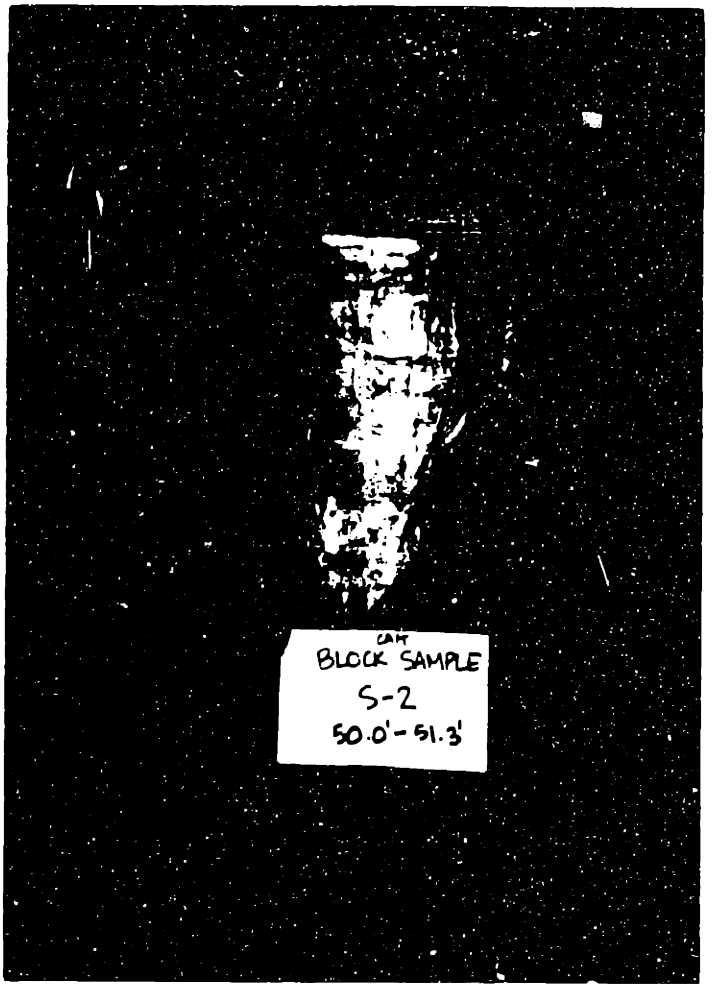

Figure A-2: Preparation of Block Samples – Block Sample in Protective Cover

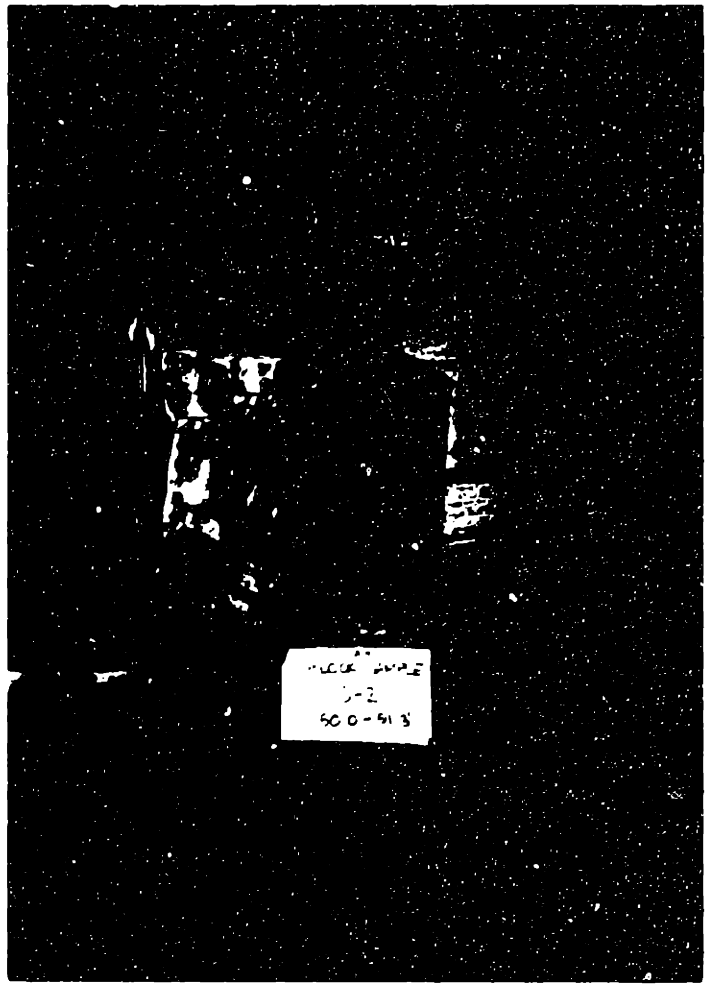

Figure A-3: Preparation of Block Samples – Removal of Protective Cover

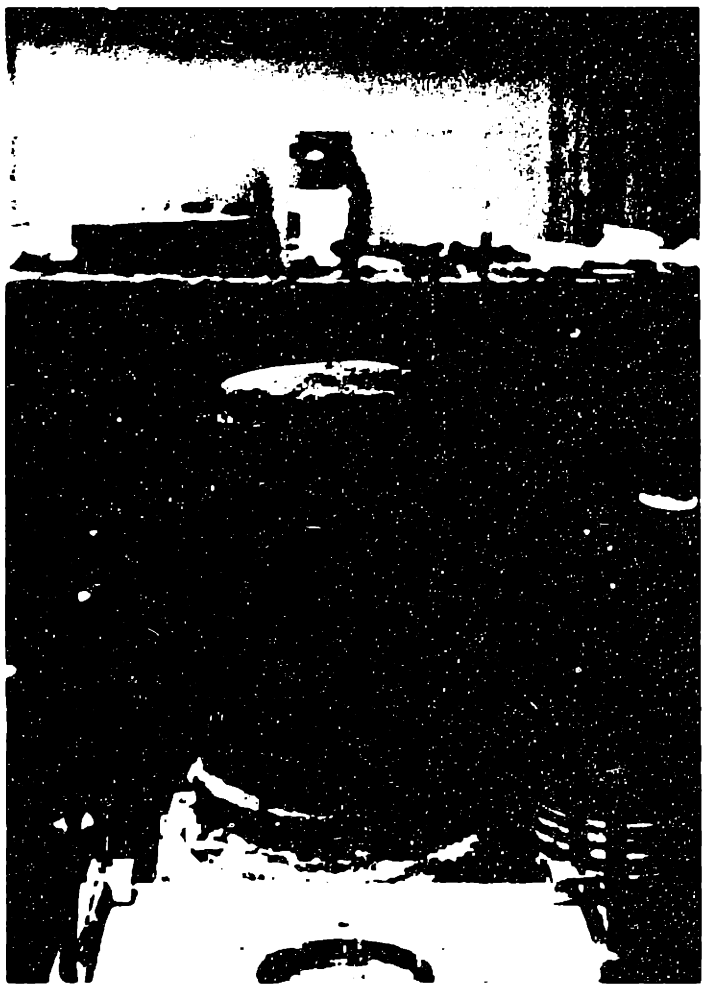

Figure A-4: Preparation of Block Samples – Outermost layer scraped off; one side flattened

Figure A-5: Preparation of Block Samples – Wax paper on flat surface; preparing to lay sample down

Figure A-6: Preparation of Block Samples - Laying Block Down

Figure A-7: Preparation of Block Samples - Slicing off one layer

Figure A-8: Preparation of Block Samples – Removing top layer

Figure A-9: Preparation of Block Samples – Halving layer

Figure A-10: Preparation of Block Samples - Covering block with wax and plastic wrap

Figure A-11: Preparation of Block Samples – Evidence of disturbance

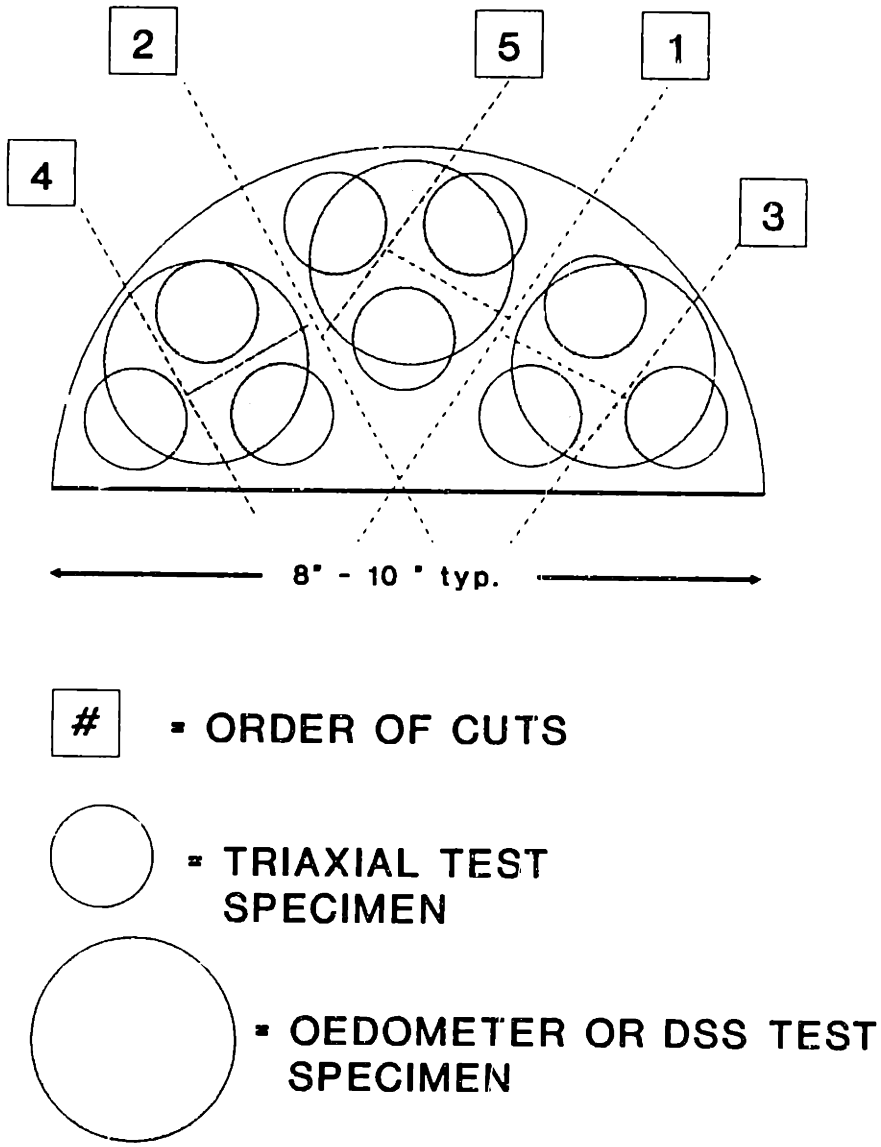

Figure A-12: Diagram of Specimens Cut from Block Sample

Figure A-13: Setup of Triaxial Specimen - Trimming specimen in mitre box

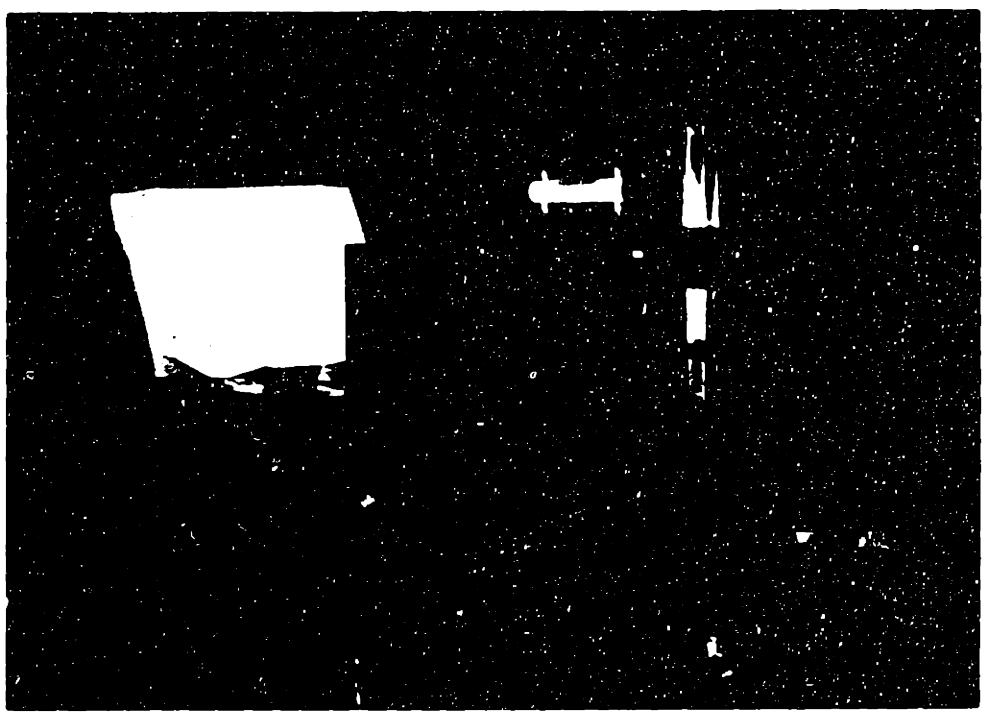

Figure A-14: Setup of Triaxial Specimen – Measuring diameter of specimen

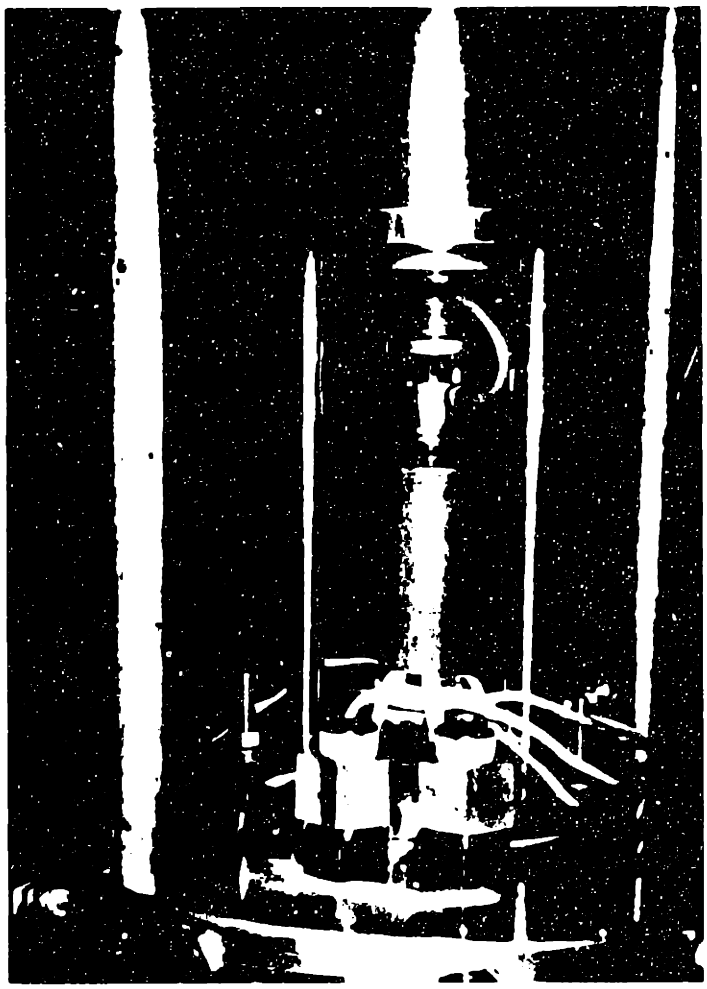

Figure A-15: Setup of Triaxial Specimen – Specimen installed on pedestal

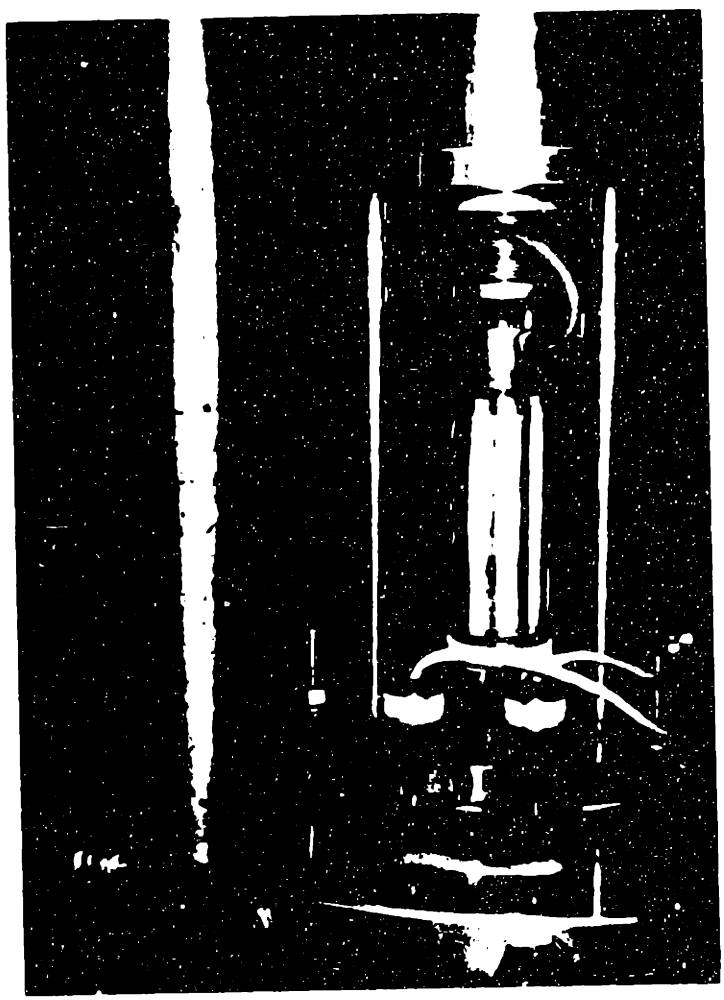

Figure A-16: Setup of Triaxial Specimen – Filter strips in place

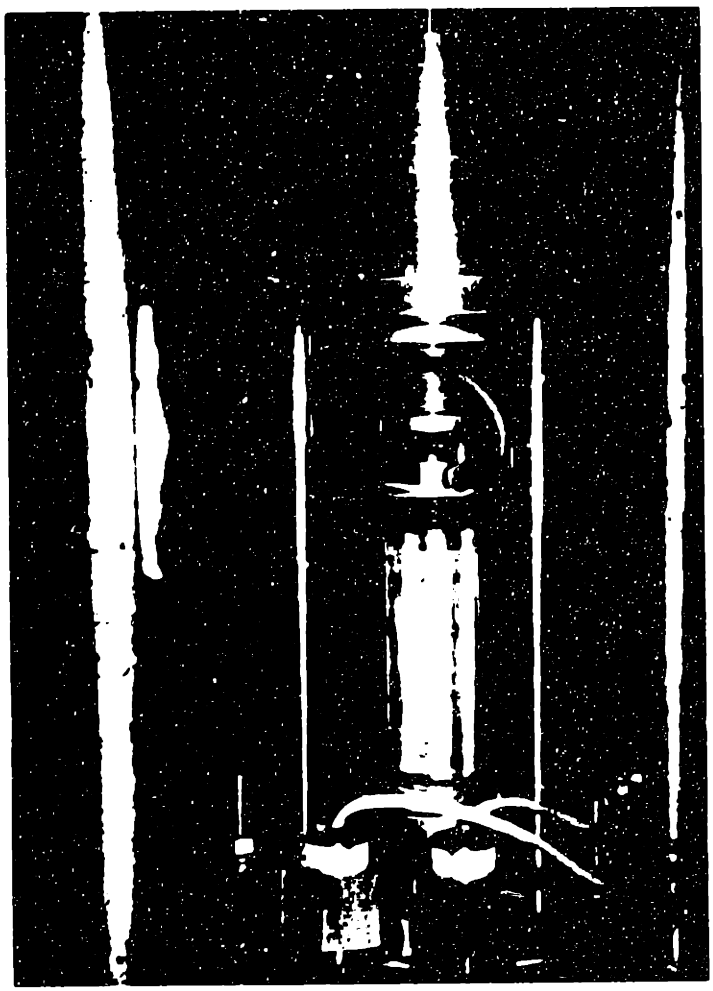

Figure A-17: Setup of Triaxial Specimen - Membranes in place

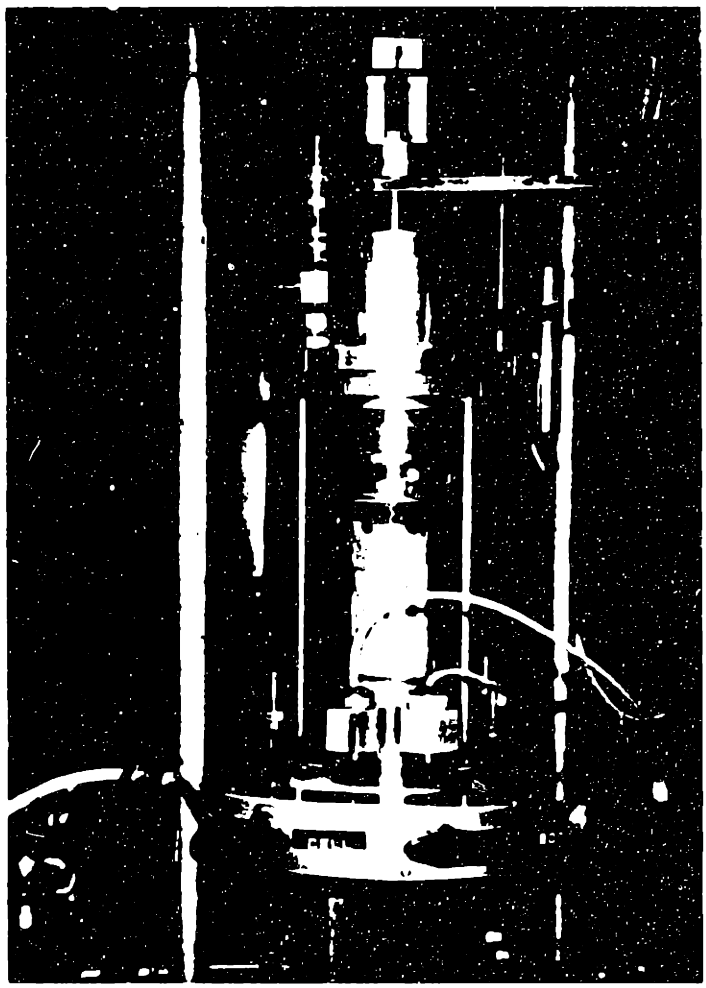

Figure A-18: Setup of Triaxial Specimen - Cell filled with oil - test begins

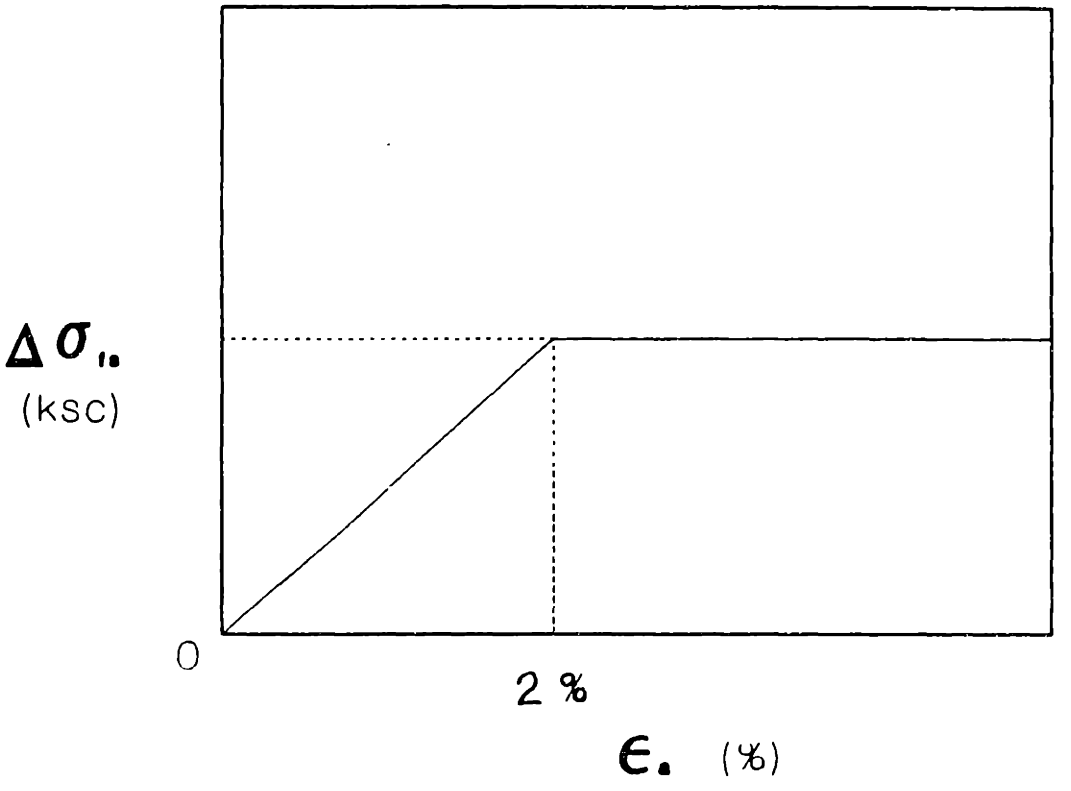

Figure A-19: Application of Filter Strip Correction for Triaxial Compression Tests

MIT
GEOTECHNICAL LABORATORY
TRIAXIAL TESTING REFERENCE DATA SHEET

Project CA/T Boring SOUTH BOSTON Depth 56.5' Test by/date AHE 3/5/91
Test No. TX085 Sample BS-1A Specimen Loc Bottom 1/3 Test Type Recomp. TC OCR

*2

1. INSTRUMENTS	Make/No.	Calib Factor	Zero at Start	Zero at Finish
PP Transducer	D10342	703.2 psi/V/V	0.15 mV v_{in} = 5.542V	v_{in} =
CP Transducer	D10343	688.7 "	0.60 mV v_{in} = 5.542V	v_{in} =
Load Cell	B0386	7844 kg/V/V	-0.18 mV v_{in} = 5.542V	v_{in} =
Axial DCDT	A90	-2.433 cm/V/V	2.025 V v_{in} = 5.542V	v_{in} =
Vol DCDT	L9	-9.263 cm³/V/V	0.565V v_{in} = 5.542V	v_{in} =

Cell No. MIT03 Weight of Accessories - DCDT Arm //
Piston Area(A_p) 36 cm² Extension
Piston Weight(w_p) 0.48 kg Moment break //
$W_o = W_p + W_a$ = 0.901 kg Total (W_a) 0.421 kg

System Compliance (to 2 ksc) Compliance = $\frac{\Delta DCDT \times DCDTCF}{\Delta PP \times PPCF}$ = 0.024 cc/ksc

	START	FINISH
Vol. DCDT	-0.302	-0.238
PP Trans	+0.34	+35.00

PP response to push = 12 mv

Filter Paper 8 x 1/4" = 5.08 cm T_{FP} 0.012" Cell Fluid Si OIL
Membranes 2 thin T_m 0.016" Pore Fluid DISTILLED H_2O

2. SPECIMEN DATA	Weights and Measures				
Location	TRIMMINGS	TRIMMINGS	TRIMMINGS		
Tare No.	J25	38	B		
Tare & Wet Soil	25.31	31.62	28.41		
Tare & Dry Soil	21.77	26.74	24.38	AVE:	
Tare	11.08	12.17	12.08		
W_c (%)	33.12	33.49	32.76	⇒ 33.12 ± 0.36	
Torvane (ksc)	—	—	—	—	

z_3 w/Dummy, Stones, FP
1 2.375"
2 2.377"
3 2.376"
Ave(Z_d) 2.376" = 6.035 cm

z_3 w/specimen
1 2.421"
2 2.421"
3 2.420"
Ave(Z_s) 6.138 cm

Specimen Diameter
Top 4.095 = 1.398
Mid 4.088 = 1.396
Bot 4.100 = 1.404
Ave(d_i) 1.399"

Tare+Specimen 155.66
Tare 0.48
Specimen(W_{Ti}) 155.18

Dummy Ht(H_d) 8.002 cm
after membranes Yes or (No)
If Yes $T_{cor} = T_m + T_{FP}$
if No $T_{cor} = 0$

3. CALCULATIONS

$H_i = H_d - z_d + z_s$ = 8.105 cm	$A_i = \pi D_i^2/4$ = 9.92 cm²	$\gamma_{wet} = W_{Ti}/V_i$ = 1.93 %
$D_i = d_i - T_{cor}$ = 3.554 cm	$V_i = H_i \times A_i$ = 80.40 cm³	σ'_{vo} est = 1.70 ksc

4. SPECIMEN DESCRIPTION & NOTES

Figure A-20: Example of Typical Triaxial Test Data Sheet - Page 1 of 3

MIT
GEOTECHNICAL LABORATORY
TRIAXIAL TESTING REFERENCE DATA SHEET

5. PROCESS DOCUMENTATION

Test TX085

	DAP Chn'l	Local Chn'l	Values at the End of ... (A) SETUP DVM	(A) SETUP Computer Volts	(A) SETUP Computer Eng	(B) PRESSURE UP DVM	(B) PRESSURE UP Computer Volts	(B) PRESSURE UP Computer Eng	(C) SATURATE DVM	(C) SATURATE Computer Volts	(C) SATURATE Computer Eng
Axial DCDT	106	1	2.025	2.026	-0.01 %	1.945	1.946	0.44%	1.938	1.940	0.49%
Cell Pres	105	2	0.79	0.72	0.02 ksc	8.75	8.74	1.00 ksc	28.10	28.07	3.40 ksc
Load Cell	104	3	-1.31	-1.22	-0.48 kg/	1.67	1.82	0.13 kg/	7.71	7.82	0.02 kg/
Pore Pres	103	4	-1.03	-0.95	-0.03 ksc	-1.67	-1.60	1.02 ksc	20.48	20.50	3.40 ksc
Vol DCDT	102	5	0.565	0.565	0.01 ksc	0.566	0.566	0.00 ksc	1.003	1.008	2.49 ksc
V in.	107	6	5.541	5.543	0%	5.552	5.553	0%	5.556	5.558	-0.07%
Date			3/5			3/6			3/7		
Time			3:00			8:30			8:30		

Saturation Check

Date/Time	Back Pressure	Pressure Increment	B value	Vol. Strain
3/6 4:00	1.40	0.20	0.78	-0.76
3/6 5:45	2.10	0.20	0.94	- 0.83
3/7 8:30	2.48	0.20	1.00	- 0.92

	Values at the End of ... (D) CONSOLIDATION DVM	(D) CONSOLIDATION Computer Volts	(D) CONSOLIDATION Computer Eng	(E) SWELLING DVM	(E) SWELLING Computer Volts	(E) SWELLING Computer Eng	(F) SHEARING DVM	(F) SHEARING Computer Volts	(F) SHEARING Computer Eng
Axial DCDT	1.814	1.815	0.93%				-0.810	-0.810	15.15%
Cell Pres	37.81	37.84	4.72 ksc				40.28	40.28	4.71 ksc
Load Cell	16.67	16.80	8.45 kg/				31.67	32.10	27.70 kg/
Pore Pres	19.90	20.03	5.57 ksc				31.61	31.71	7.11 ksc
Vol DCDT	0.542	0.542	2.48 ksc				0.587	0.587	3.74 ksc
V in.	5.420	5.430	1.43%				5.788	5.791	1.42%
Date	3/8						3/10		
Time	10:45						9:00		

6. DATA ACQUISITION FILES

File Name	Time	Date	Process	Remarks
TX085i	3:10	3/5	pressure up	
TX085b	8:45	3/6	back pressure	
TX085c	0:45	3/7	consolidation	
TX085l	11:00	3/8	leak check	
TX085s	11:30	3/8	shear	

TXϕϕϕψ77

TX - Triaxial
ϕϕϕ- Test number (sequential)
77 - sequence number

ψ = I - Pressure up
B - Back Pressure
C - Consolidation
S - Shear
P - Preshear
L - Leak Check

Figure A-21: Example of Typical Triaxial Test Data Sheet – Page 2 of 3

MIT
GEOTECHNICAL LABORATORY
TRIAXIAL TESTING REFERENCE DATA SHEET

7. SPECIAL NOTES — Test TX085

@ B compute initial effective stress $\sigma'_i = \sigma_c - u_i$ = 0.90

@ C change vol DCDT zero to have $\epsilon_a = \epsilon_{vol}$

New Zero = Zero+ $(\epsilon_a - \epsilon_{vol}) \times V_i/100/$Vol CF = 0.2243

@ D for SHANSEP test be sure

$\epsilon_a > 10\%$

σ'_{vmax} is on for 24 hrs prior to unload (for OC test) or shear

@ D or E prior to undrained shear

close drain line for 30 min and monitor P.P.

P.P. open 2.48 P.P. closed 2.48 P.P. 30 min 2.49

8. POST SHEAR MEASUREMENTS

	Weights & Measures				
Location	A4	66	ELSO 21	DONALD	Σ
Tare No.					
Tare & wet soil	48.29	53.25	48.17	53.11	202.82
Tare & dry soil	39.37	38.88	42.91	43.47	164.63
Tare	12.04	12.01	12.22	12.12	48.39 *
W_c (%)					

z_3 w/specimen	Specimen Diameter	
1. 2.000	Top ____ - ____ = ____	T_{ave}+Specimen 193.87
2. 2.002	Mid ____ - ____ = ____	T_{ave} 32.10
3. 2.003	Bot ____ - ____ = ____	Specimen(W_{Tf}) 154.77
Ave Z_s 2.002" = 5.084cm	Ave(d_f) = ____	
	with membranes see other sheet Yes or No	

Radiograph Yes or (No) Picture Yes or (No)

Description:

see other sheet

* ΣW_{TF} = 154.43

ΣW_{SF} = 110.24

Front Side

9. CALCULATIONS

$H_f = H_d - Z_d + Z_s$ = 7.051 cm	$A_f = \pi D_f^2/4$ = ____ cm^2	$\gamma_{wet} = W_{T_f}/V_f$ = ____ g/cc
$D_f = d_f - T_{cor}$ = ____ cm	$V_f = H_f \times A_f$ = ____ cm^3	W_s = ____ g

Figure A-22: Example of Typical Triaxial Test Data Sheet – Page 3 of 3

TEST TXCBS | BOREHOLE/SAMPLE/... BY: EHE
z 56.5' ELEV 547'. | BS-1A Bottom 1/3 | DATE: 3/5/91

RECOMPRESSION TX TEST STRESS WORKSHEET

1. SAMPLE/SPECIMEN STRESS HISTORY

σ'_{vo} = 3.48 ksf = 1.70 ksc OCR = 3.66

σ'_{ho} = 2.23 ksf = 1.58 ksc K_o = 0.93

σ'_p = 12.75 ksf = 6.23 ksc

q_c = 0.06 ksc p_c = 1.64 ksc

- IF PLANNED $\sigma'_{vc} \neq \sigma'_{vo}$:

$\sigma'_{hc}/\sigma'_{vo}$ = 1.83

σ'_{vc} = 6.375 ksf = 3.11 ksc OCR = 2

σ'_{hc} = 4.59 ksf = 2.24 ksc K_o = 0.72

2. ADJUSTED q_f (TC → m = 0.65, TE → m = 0.55)

- ACTUAL PRESHEAR σ'_{vc} = 6.045 ksf = 2.952 ksc
- MEASURED q_f = 3.083 ksf = 1.505 ksc m = 0.65
- (IN-SITU σ'_{vo})/(TEST σ'_{vc}) = (3.48)/(6.045) = 0.576
- ADJUSTED q_f = (MEAS q_f)$(\sigma'_{vo}/\sigma'_{vc})^{1-m}$

= (3.083)(0.576)$^{0.35}$

= 2.541 ksf = 1.241 ksc

3. COMMENTS ON TEST

Test OCR = 2.11

Figure A-23: Example of Typical Recompression Triaxial Test Worksheet – Page 1 of 3

TEST KOBE BOREHOLE/SAMPLE/LOC. BY AHE

E 565 ELEV. 54.7 BK-1A Bottom 1/3 DATE 3-12-91

Initial State of Specimen Worksheet

1. Input Data

1.1 Initial Specimen

L_o 8.105 cm x A_o 9.92 cm^2

W_{To} = 155.18 g = V_{To} 80.40 cm^3

$\gamma_t = W_{To}/V_{To}$ = 1.93 g/cc

1.2 Final Specimen

W_{Tf} = 154.77 g

ΣW_{Tf} = 154.43 g

ΣW_s = 116.24 g

$\Rightarrow \Sigma W_{Tf} - \Sigma W_s = \Sigma W_{wf}$ = 38.19 g

$\Delta W_{Tf} = W_{Tf} - \Sigma W_{Tf}$ = 0.34

$w_f = \Sigma W_{wf}/\Sigma W_s$ = 32.85

Initial $W_s = \Sigma W_s + \frac{\Delta W_{Tf}}{(1+w_f)}$ = 116.24 + 0.34/(1+.3285)

= 116.50

1.3 G_s

G_s = 2.80 (assumed)

2 Specimen w_n, e, S

2.1 Phase Diagram

WEIGHTS (g)		VOLUMES (cc)
	AIR	$V_V = V_A + V_W$ = 0.11 + 38.68 = 38.78
W_w = 38.68	WATER	
W_s = 116.50	SOLIDS	V_s = 41.61

$W_{WC} = W_{To} - W_s$ = 155.18 − 116.50

= 38.68 g = V_{Wi}

$V_s = W_s/G_s$ = 116.50 g / 2.80 g/cc = 41.61 cc

$V_A = V_T - V_W - V_s$ = 80.40 − 38.68 − 41.61

2.2 Computations:

$w_n = W_w/W_s$ = 38.68 / 116.50

w_n = 33.20 %

$e = V_V/V_s$ = 38.78 cc / 41.61 cc

e = 0.932

$S = V_W/V_V$ = 38.68 / 38.78 cc

S = 99.74 %

check $S = G_s w_n/e$ ✓

Figure A-24: Example of Typical Triaxial Test Worksheet – Page 2 of 3

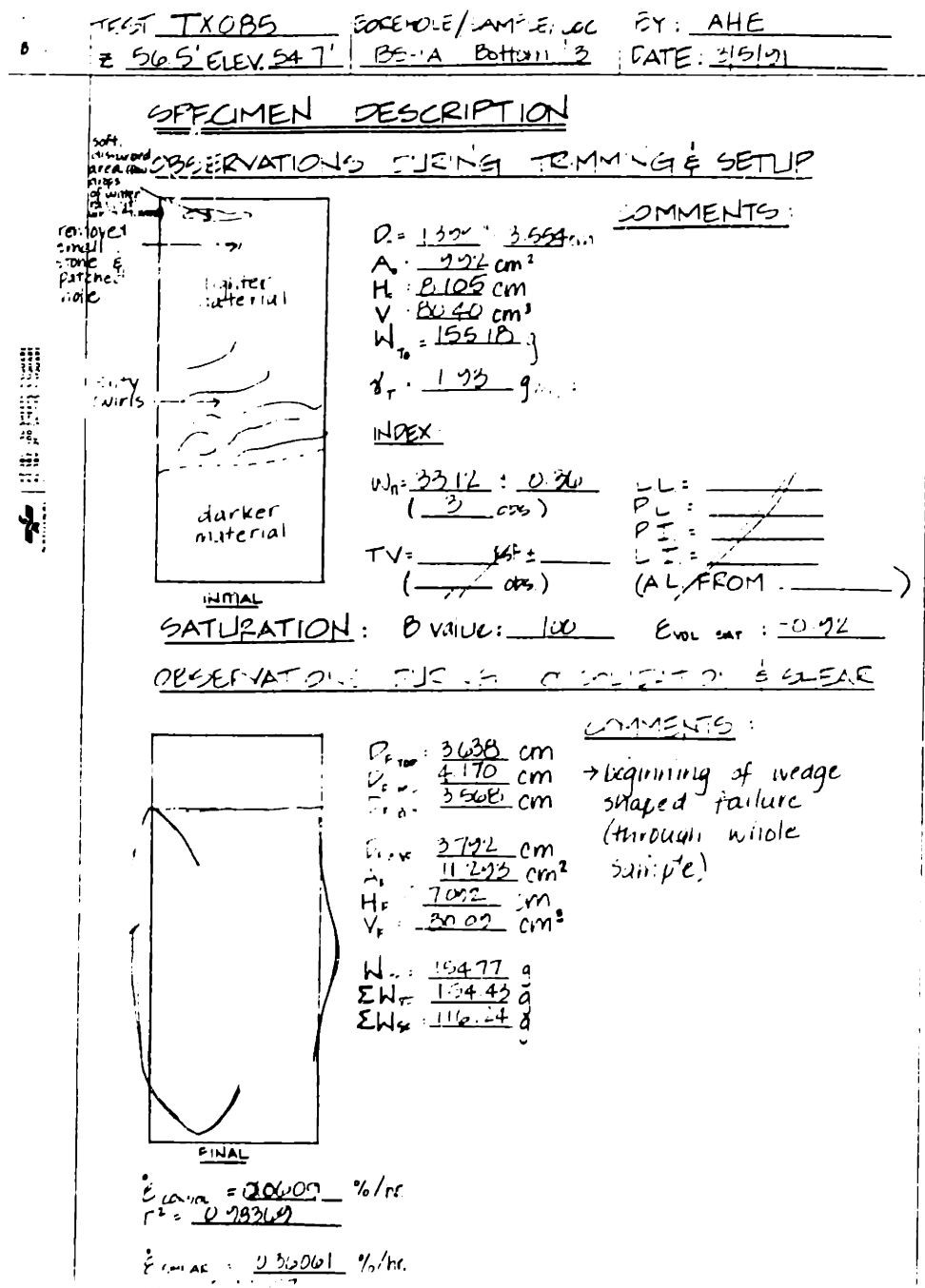

Figure A-25: Example of Typical Triaxial Test Worksheet – Page 3 of 3

```
**********************************************************************
              RESULTS OF TRIAXIAL REDUCTION PROGRAM
                      MIT GEOTECHNICAL LAB
**********************************************************************

                DATA FILENAME : triax\tx085c.dat
            (Reduction program : TXRED3.BAS)
  ------------------  ***********  ----------------------
                       REDUCTION DATA

     DATE :3-11-91                INITIALS :AHE
     DRAINAGE :D                TYPE :C
     INIT HEIGHT : 8.105         INIT AREA : 9.92
     PISTON AREA: 3.6            PIST/HANGER WT : .901
 TRANSDUCER ZEROS AND CALIBRATION FACTORS
     LC ZERO : .00018            LC CALIBRATION :-7844.042
     DCDT ZERO :-2.025           DCDT CALIBRATION : 2.433
     2nd DCDT ZERO : 0
     CPT ZERO :-.00068           CPT CALIBRATION :-688.7
     PPT ZERO :-.00015           PPT CALIBRATION :-703.2
     VOL CHANGE ZERO :-1.2326
     VOL CHANGE CALIBRATION : 9.262999
 CORRECTIONS
     AREA CORRECTION :  RIGHT CYLINDER
     MEMBRANE CORRECTION :  1.942
     FILTER STRIP CORRECTION :  .16
     UNDRAINED SHEAR STRENGTH:  0



 ----------------------------------------------------------

INITIAL CONDITIONS:
SIGBARVC=  .8077542 ,SIGBARHC=  .8321341
 VERTSTRO      Q         P'        SIGV'     SIGH'     Ko       VOLSTR      AREA

    0.000     -0.012    0.820     0.808     0.832     1.030     0.000      9.920
    0.457     -0.022    0.810     0.787     0.832     1.057     0.457      9.920
    0.457     -0.024    0.806     0.783     0.830     1.060     0.464      9.919
    0.455     -0.022    0.809     0.787     0.831     1.056     0.463      9.919
```

Figure A-26: Example of Typical Triaxial Test Consolidation Output - Page 1 of 4

0.458	-0.012	0.847	0.835	0.859	1.030	0.468	9.919
0.463	-0.004	0.880	0.876	0.884	1.009	0.476	9.919
0.467	0.003	0.914	0.917	0.911	0.993	0.483	9.918
0.472	0.011	0.940	0.951	0.930	0.978	0.492	9.918
0.476	0.017	0.970	0.987	0.952	0.965	0.500	9.918
0.480	0.024	0.994	1.018	0.970	0.954	0.509	9.917
0.485	0.029	1.020	1.049	0.991	0.945	0.515	9.917
0.488	0.036	1.044	1.080	1.009	0.934	0.527	9.916
0.492	0.041	1.066	1.107	1.024	0.925	0.536	9.916
0.498	0.048	1.096	1.143	1.048	0.917	0.547	9.915
0.505	0.053	1.118	1.172	1.065	0.909	0.560	9.915
0.509	0.059	1.144	1.203	1.085	0.902	0.563	9.915
0.514	0.065	1.166	1.231	1.102	0.895	0.582	9.913
0.520	0.072	1.191	1.263	1.119	0.886	0.594	9.913
0.525	0.080	1.227	1.307	1.148	0.878	0.608	9.912
0.531	0.089	1.258	1.347	1.169	0.868	0.623	9.911
0.534	0.092	1.279	1.371	1.186	0.865	0.631	9.910
0.550	0.114	1.364	1.478	1.249	0.845	0.675	9.907
0.570	0.140	1.471	1.611	1.331	0.826	0.730	9.904
0.607	0.162	1.558	1.720	1.395	0.811	0.781	9.903
0.625	0.178	1.635	1.813	1.457	0.804	0.817	9.901
0.645	0.206	1.734	1.940	1.529	0.788	0.861	9.898
0.666	0.225	1.824	2.049	1.599	0.781	0.901	9.896
0.684	0.251	1.916	2.167	1.666	0.769	0.950	9.893
0.659	0.281	2.036	2.316	1.755	0.757	0.997	9.886
0.666	0.304	2.129	2.433	1.825	0.750	1.051	9.882
0.694	0.323	2.213	2.536	1.890	0.745	1.104	9.879
0.717	0.343	2.298	2.641	1.955	0.740	1.144	9.877
0.725	0.365	2.383	2.748	2.019	0.735	1.187	9.874
0.744	0.388	2.487	2.874	2.099	0.730	1.242	9.870
0.769	0.406	2.560	2.966	2.155	0.727	1.297	9.867
0.791	0.405	2.560	2.966	2.155	0.727	1.324	9.867
0.805	0.404	2.560	2.965	2.156	0.727	1.339	9.867
0.804	0.405	2.559	2.964	2.154	0.727	1.344	9.866
0.801	0.406	2.562	2.968	2.156	0.726	1.344	9.866
0.822	0.409	2.564	2.973	2.155	0.725	1.365	9.866
0.848	0.403	2.561	2.963	2.158	0.728	1.378	9.867
0.829	0.403	2.564	2.967	2.160	0.728	1.387	9.864
0.872	0.401	2.562	2.963	2.161	0.729	1.401	9.867
0.873	0.403	2.560	2.963	2.157	0.728	1.406	9.867
0.873	0.402	2.556	2.958	2.154	0.728	1.413	9.866
0.873	0.402	2.559	2.962	2.157	0.728	1.417	9.866
0.875	0.402	2.562	2.963	2.160	0.729	1.420	9.865
0.876	0.403	2.560	2.963	2.158	0.728	1.422	9.865
0.877	0.402	2.559	2.961	2.157	0.729	1.424	9.865

Figure A-27: Example of Typical Triaxial Test Consolidation Output - Page 2 of 4

0.877	0.403	2.560	2.963	2.157	0.728	1.427	9.865
0.877	0.402	2.560	2.962	2.158	0.729	1.430	9.865
0.878	0.402	2.563	2.965	2.161	0.729	1.432	9.865
0.880	0.402	2.559	2.961	2.158	0.729	1.434	9.865
0.880	0.403	2.559	2.961	2.156	0.728	1.436	9.864
0.881	0.403	2.562	2.965	2.159	0.728	1.437	9.864
0.882	0.402	2.559	2.962	2.157	0.728	1.438	9.864
0.882	0.402	2.560	2.962	2.158	0.729	1.439	9.864
0.883	0.402	2.560	2.962	2.158	0.729	1.439	9.864
0.883	0.402	2.560	2.961	2.158	0.729	1.439	9.864
0.883	0.402	2.559	2.961	2.157	0.729	1.439	9.864
0.883	0.402	2.559	2.961	2.157	0.728	1.439	9.864
0.885	0.400	2.557	2.957	2.157	0.729	1.438	9.865
0.884	0.401	2.560	2.962	2.159	0.729	1.437	9.865
0.883	0.403	2.554	2.957	2.151	0.727	1.435	9.865
0.885	0.402	2.557	2.960	2.155	0.728	1.434	9.865
0.885	0.400	2.567	2.967	2.167	0.730	1.433	9.865
0.885	0.401	2.559	2.960	2.159	0.729	1.432	9.865
0.885	0.402	2.560	2.961	2.158	0.729	1.431	9.865
0.885	0.402	2.555	2.957	2.152	0.728	1.429	9.866
0.885	0.400	2.552	2.952	2.152	0.729	1.428	9.866
0.885	0.400	2.557	2.957	2.156	0.729	1.426	9.866
0.886	0.401	2.561	2.962	2.160	0.729	1.425	9.866
0.885	0.402	2.559	2.960	2.157	0.729	1.423	9.866
0.887	0.401	2.559	2.960	2.158	0.729	1.423	9.866
0.889	0.402	2.558	2.960	2.155	0.728	1.424	9.866
0.889	0.402	2.562	2.964	2.160	0.729	1.429	9.866
0.890	0.403	2.558	2.961	2.156	0.728	1.432	9.866
0.891	0.402	2.561	2.963	2.158	0.728	1.435	9.866
0.890	0.402	2.561	2.963	2.160	0.729	1.436	9.865
0.890	0.403	2.561	2.964	2.159	0.728	1.437	9.865
0.892	0.402	2.559	2.961	2.157	0.729	1.437	9.865
0.890	0.401	2.559	2.961	2.158	0.729	1.438	9.865
0.892	0.402	2.560	2.962	2.158	0.729	1.438	9.865
0.892	0.402	2.555	2.957	2.153	0.728	1.438	9.865
0.892	0.402	2.562	2.964	2.159	0.728	1.438	9.865
0.892	0.402	2.560	2.962	2.158	0.728	1.435	9.866
0.892	0.401	2.560	2.962	2.159	0.729	1.435	9.866
0.893	0.400	2.560	2.960	2.160	0.730	1.436	9.866
0.894	0.402	2.559	2.961	2.157	0.728	1.437	9.866
0.894	0.400	2.561	2.960	2.161	0.730	1.438	9.866
0.894	0.401	2.560	2.962	2.159	0.729	1.438	9.865
0.894	0.401	2.559	2.960	2.158	0.729	1.438	9.866
0.894	0.400	2.557	2.957	2.157	0.729	1.436	9.866
0.895	0.403	2.561	2.963	2.158	0.728	1.431	9.866

Figure A-28: Example of Typical Triaxial Test Consolidation Output – Page 3 of 4

0.894	0.403	2.560	2.963	2.157	0.728	1.435	9.866
0.895	0.402	2.561	2.963	2.159	0.729	1.434	9.866
0.894	0.404	2.561	2.965	2.158	0.728	1.434	9.866
0.894	0.403	2.559	2.962	2.155	0.728	1.433	9.866
0.895	0.403	2.561	2.964	2.158	0.728	1.432	9.866
0.895	0.402	2.561	2.963	2.159	0.728	1.431	9.866
0.895	0.401	2.560	2.961	2.159	0.729	1.430	9.866
0.895	0.401	2.560	2.961	2.159	0.729	1.429	9.867
0.895	0.402	2.561	2.964	2.159	0.728	1.426	9.867
0.895	0.402	2.561	2.963	2.159	0.729	1.425	9.867
0.895	0.402	2.562	2.964	2.160	0.729	1.423	9.867
0.895	0.402	2.558	2.961	2.156	0.728	1.422	9.867
0.895	0.402	2.559	2.961	2.157	0.728	1.421	9.867
0.895	0.402	2.561	2.962	2.159	0.729	1.419	9.868
0.895	0.401	2.559	2.960	2.157	0.729	1.417	9.868
0.895	0.401	2.558	2.959	2.157	0.729	1.415	9.868
0.895	0.401	2.561	2.962	2.160	0.729	1.411	9.868
0.895	0.401	2.560	2.961	2.158	0.729	1.411	9.868
0.895	0.401	2.560	2.961	2.159	0.729	1.406	9.869
0.895	0.400	2.555	2.955	2.155	0.729	1.404	9.869
0.894	0.401	2.560	2.961	2.160	0.729	1.402	9.869
0.894	0.401	2.558	2.959	2.157	0.729	1.399	9.870
0.894	0.401	2.557	2.958	2.157	0.729	1.395	9.870
0.894	0.400	2.559	2.960	2.159	0.729	1.393	9.870
0.894	0.402	2.558	2.961	2.156	0.728	1.390	9.870
0.894	0.401	2.561	2.962	2.160	0.729	1.388	9.871
0.894	0.401	2.560	2.961	2.159	0.729	1.381	9.871
0.895	0.402	2.558	2.960	2.156	0.729	1.386	9.871
0.897	0.402	2.562	2.964	2.160	0.729	1.390	9.871
0.896	0.403	2.563	2.966	2.159	0.728	1.394	9.870
0.897	0.402	2.560	2.962	2.157	0.728	1.397	9.870
0.898	0.402	2.561	2.963	2.159	0.729	1.401	9.870
0.898	0.402	2.562	2.965	2.160	0.729	1.403	9.870
0.896	0.403	2.560	2.963	2.157	0.728	1.400	9.870

FINAL AREA = 9.869569

Figure A-29: Example of Typical Triaxial Test Consolidation Output - Page 4 of 4

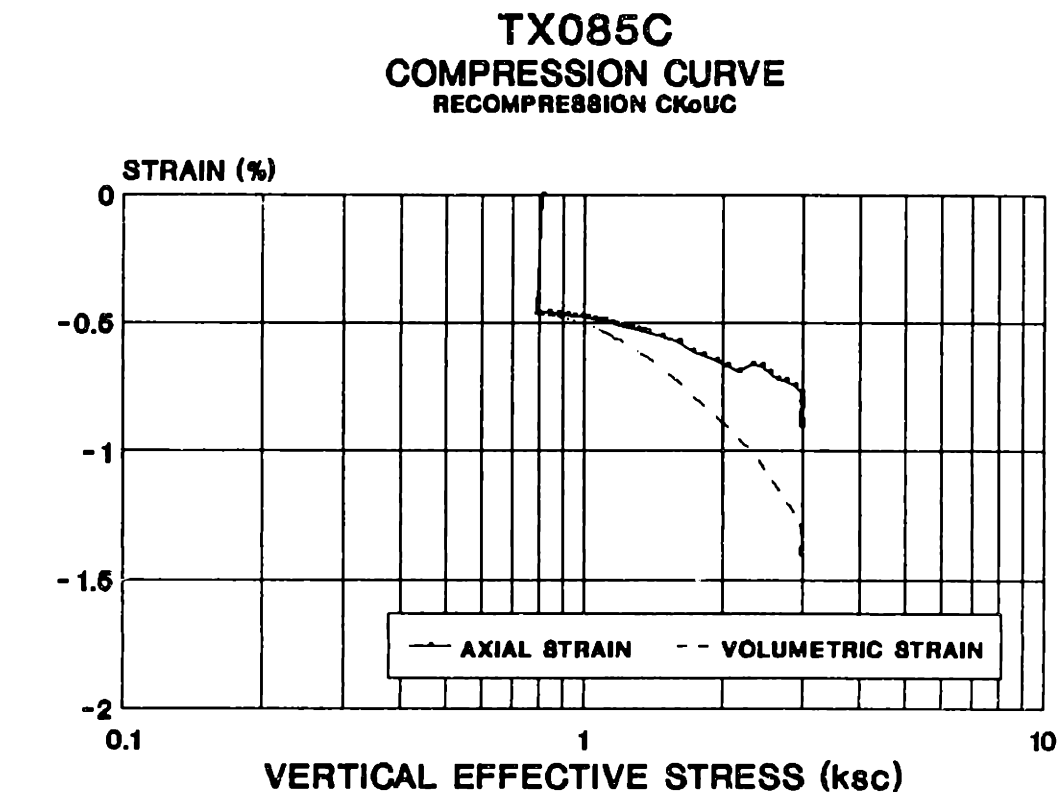

Figure A-30: Example of Typical Triaxial Test Consolidation Plot - 1 of 3

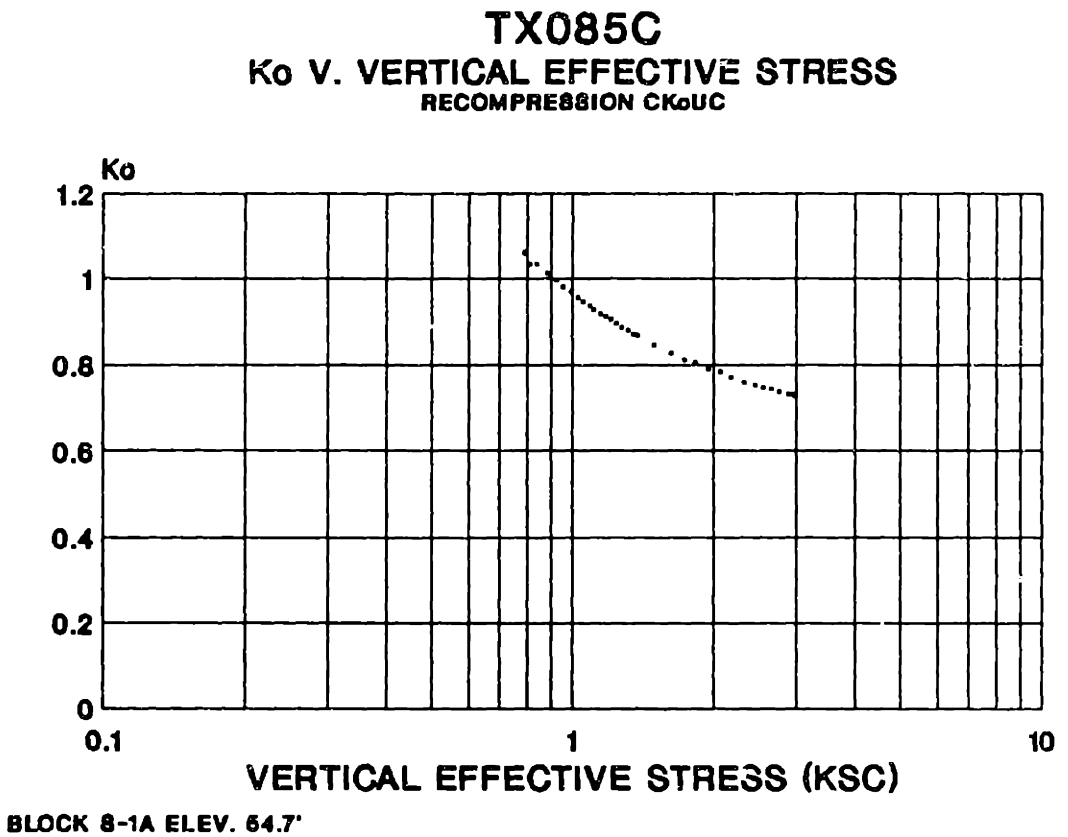

Figure A-31: Example of Typical Triaxial Test Consolidation Plot – 2 of 3

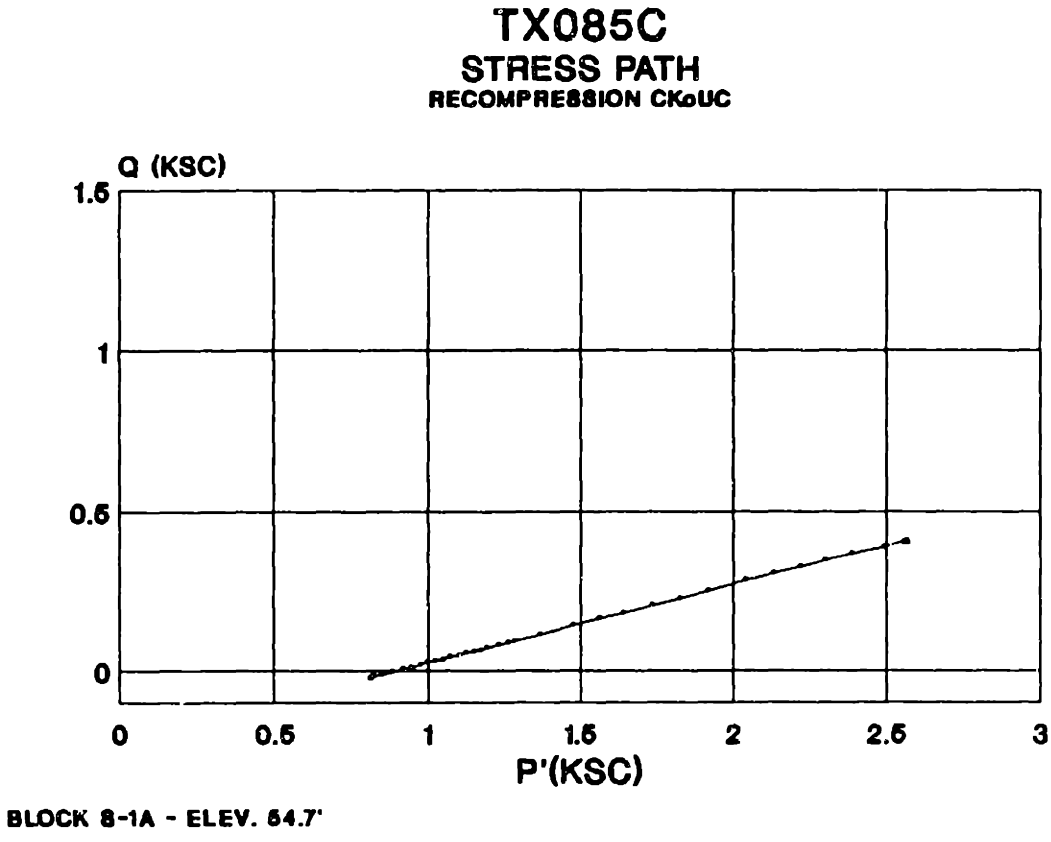

Figure A-32: Example of Typical Triaxial Test Consolidation Plot – 3 of 3

```
**********************************************************************
              RESULTS OF TRIAXIAL REDUCTION PROGRAM
                      MIT GEOTECHNICAL LAB
**********************************************************************

                DATA FILENAME : triax\tx085s.dat
             (Reduction program : TXRED3.BAS)
   -------------------   ***********  ----------------------
                       REDUCTION DATA

     DATE :3-11-91                INITIALS :AHE
     DRAINAGE :U                TYPE :C
     INIT HEIGHT : 8.032        INIT AREA : 9.87
     PISTON AREA: 3.6           PIST/HANGER WT : .901
 TRANSDUCER ZEROS AND CALIBRATION FACTORS
     LC ZERO : .00018           LC CALIBRATION :-7844.042
     DCDT ZERO :-2.025           DCDT CALIBRATION : 2.433
     2nd DCDT ZERO : 0
     CPT ZERO :-.00068          CPT CALIBRATION :-688.7
     PPT ZERO :-.00015          PPT CALIBRATION :-703.2
     VOL CHANGE ZERO :-1.2326
     VOL CHANGE CALIBRATION : 9.262999
 CORRECTIONS
     AREA CORRECTION :  PARABOLIC
     MEMBRANE CORRECTION :  1.942
     FILTER STRIP CORRECTION :  .16
     UNDRAINED SHEAR STRENGTH:  1.506817


 ----------------------------------------------------------

INITIAL CONDITIONS:
SIGBARVC=  2.95179 ,SIGBARHC=  2.155275
 VERTSTR    Q/SIGV'    P/SIGV'    dU/SIGV    dQ/dQm    Esec/SIGV   A   #2dU/SIGV  phi

   0.000      0.135      0.865      0.000      0.000      0.000     0.000      0.000      8.973
   0.002      0.134      0.865     -0.003     -0.002    -74.034     0.536      0.000      8.921
```

Figure A-33: Example of Typical Triaxial Test Shear Output - Page 1 of 7

0.002	0.134	0.864	-0.004	-0.002	-73.345	-0.102	0.000	8.939
0.003	0.151	0.873	0.006	0.043	959.511	0.267	0.000	9.964
0.009	0.171	0.881	0.017	0.096	821.853	0.279	0.000	11.182
0.014	0.188	0.887	0.029	0.142	776.542	0.297	0.000	12.264
0.019	0.204	0.893	0.040	0.183	710.516	0.298	0.000	13.183
0.025	0.217	0.896	0.049	0.218	665.993	0.313	0.000	14.000
0.030	0.229	0.898	0.056	0.250	626.802	0.324	0.000	14.756
0.035	0.240	0.902	0.065	0.279	595.913	0.326	0.000	15.417
0.041	0.250	0.904	0.072	0.305	563.055	0.332	0.000	16.034
0.046	0.259	0.907	0.080	0.329	534.374	0.331	0.000	16.570
0.051	0.267	0.908	0.086	0.353	516.197	0.338	0.000	17.127
0.057	0.276	0.910	0.093	0.375	493.628	0.340	0.000	17.641
0.063	0.284	0.912	0.099	0.398	476.652	0.342	0.000	18.159
0.069	0.292	0.915	0.105	0.419	457.356	0.342	0.000	18.635
0.075	0.300	0.916	0.111	0.439	437.924	0.345	0.000	19.104
0.081	0.307	0.918	0.117	0.459	424.938	0.346	0.000	19.545
0.087	0.314	0.919	0.122	0.477	410.150	0.349	0.000	19.986
0.093	0.321	0.921	0.126	0.495	399.450	0.351	0.000	20.385
0.099	0.327	0.922	0.131	0.511	387.636	0.352	0.000	20.757
0.105	0.333	0.923	0.136	0.526	376.989	0.354	0.000	21.125
0.111	0.338	0.925	0.141	0.541	366.447	0.352	0.000	21.427
0.116	0.343	0.925	0.145	0.554	358.303	0.356	0.000	21.772
0.122	0.348	0.926	0.149	0.567	348.831	0.357	0.000	22.073
0.128	0.353	0.927	0.153	0.581	341.011	0.358	0.000	22.386
0.134	0.358	0.929	0.157	0.595	333.310	0.358	0.000	22.704
0.140	0.364	0.929	0.161	0.609	327.063	0.360	0.000	23.036
0.146	0.369	0.930	0.165	0.622	320.119	0.361	0.000	23.344
0.152	0.373	0.931	0.169	0.635	313.547	0.361	0.000	23.635
0.159	0.378	0.933	0.173	0.647	305.983	0.361	0.000	23.902
0.165	0.382	0.933	0.176	0.659	300.119	0.362	0.000	24.192
0.171	0.387	0.935	0.179	0.671	294.337	0.362	0.000	24.446
0.177	0.391	0.935	0.183	0.681	288.636	0.363	0.000	24.698
0.183	0.395	0.936	0.185	0.692	283.798	0.364	0.000	24.967
0.189	0.399	0.936	0.188	0.702	278.874	0.365	0.000	25.202
0.195	0.402	0.937	0.191	0.712	273.475	0.366	0.000	25.425
0.201	0.405	0.938	0.195	0.720	268.646	0.366	0.000	25.620
0.207	0.409	0.938	0.198	0.730	264.400	0.367	0.000	25.853
0.214	0.413	0.938	0.199	0.740	260.051	0.369	0.000	26.108
0.220	0.416	0.938	0.204	0.749	255.635	0.370	0.000	26.341
0.227	0.419	0.940	0.207	0.758	251.223	0.369	0.000	26.513
0.233	0.423	0.941	0.210	0.766	247.114	0.369	0.000	26.696
0.239	0.426	0.940	0.212	0.774	243.474	0.371	0.000	26.913
0.245	0.429	0.941	0.214	0.783	239.900	0.372	0.000	27.134
0.251	0.432	0.942	0.217	0.790	236.233	0.371	0.000	27.290
0.257	0.435	0.942	0.220	0.798	233.031	0.372	0.000	27.476

Figure A-34: Example of Typical Triaxial Test Shear Output - Page 2 of 7

0.264	0.438	0.942	0.221	0.806	229.475	0.372	0.000	27.667
0.270	0.440	0.942	0.224	0.813	226.083	0.373	0.000	27.844
0.276	0.442	0.943	0.227	0.818	222.829	0.373	0.000	27.956
0.283	0.445	0.942	0.229	0.825	219.437	0.375	0.000	28.169
0.289	0.446	0.942	0.230	0.829	215.510	0.376	0.000	28.274
0.295	0.450	0.943	0.233	0.839	213.665	0.376	0.000	28.490
0.301	0.447	0.939	0.234	0.830	207.171	0.381	0.000	28.403
0.307	0.452	0.941	0.237	0.843	206.441	0.380	0.000	28.663
0.313	0.455	0.942	0.240	0.851	204.557	0.380	0.000	28.864
0.319	0.457	0.944	0.242	0.858	201.811	0.378	0.000	28.969
0.326	0.460	0.943	0.244	0.865	199.604	0.380	0.000	29.184
0.333	0.462	0.943	0.246	0.871	196.699	0.380	0.000	29.336
0.339	0.465	0.944	0.247	0.878	194.283	0.381	0.000	29.493
0.346	0.467	0.944	0.250	0.883	191.603	0.381	0.000	29.619
0.352	0.468	0.945	0.252	0.888	189.283	0.381	0.000	29.732
0.359	0.470	0.944	0.253	0.893	187.035	0.382	0.000	29.868
0.365	0.472	0.944	0.254	0.898	184.667	0.383	0.000	29.995
0.372	0.474	0.945	0.256	0.903	182.436	0.383	0.000	30.114
0.378	0.476	0.944	0.257	0.908	180.214	0.384	0.000	30.253
0.386	0.474	0.943	0.258	0.902	175.732	0.385	0.000	30.143
0.392	0.477	0.943	0.261	0.911	174.759	0.386	0.000	30.396
0.398	0.479	0.943	0.263	0.917	172.972	0.387	0.000	30.547
0.405	0.481	0.943	0.265	0.922	171.098	0.387	0.000	30.669
0.411	0.483	0.944	0.266	0.927	169.226	0.387	0.000	30.782
0.418	0.484	0.944	0.268	0.931	167.090	0.387	0.000	30.875
0.426	0.486	0.944	0.269	0.935	164.994	0.388	0.000	30.989
0.432	0.487	0.944	0.270	0.938	163.299	0.389	0.000	31.092
0.438	0.488	0.943	0.271	0.940	161.314	0.389	0.000	31.161
0.442	0.489	0.943	0.273	0.942	160.063	0.389	0.000	31.204
0.493	0.497	0.942	0.282	0.965	147.057	0.394	0.000	31.871
0.544	0.503	0.940	0.290	0.980	135.197	0.398	0.000	32.324
0.595	0.506	0.936	0.297	0.989	124.728	0.405	0.000	32.751
0.649	0.509	0.932	0.304	0.996	115.234	0.411	0.000	33.104
0.703	0.510	0.929	0.309	0.998	106.689	0.415	0.000	33.299
0.757	0.510	0.924	0.312	1.000	99.205	0.422	0.000	33.537 Peak
0.814	0.510	0.920	0.316	1.000	92.299	0.427	0.000	33.709
0.870	0.510	0.918	0.320	0.998	86.243	0.430	0.000	33.761
0.928	0.509	0.913	0.324	0.997	80.672	0.436	0.000	33.917
0.986	0.509	0.909	0.326	0.995	75.785	0.441	0.000	34.026
1.047	0.508	0.906	0.329	0.994	71.343	0.445	0.000	34.130
1.108	0.507	0.902	0.331	0.990	67.059	0.451	0.000	34.186
1.172	0.505	0.899	0.333	0.985	63.129	0.455	0.000	34.178
1.236	0.504	0.895	0.335	0.982	59.665	0.459	0.000	34.241
1.297	0.501	0.891	0.336	0.974	56.400	0.465	0.000	34.217
1.356	0.498	0.886	0.337	0.966	53.488	0.471	0.000	34.173

Figure A-35: Example of Typical Triaxial Test Shear Output – Page 3 of 7

1.417	0.497	0.884	0.339	0.965	51.167	0.474	0.000	34.245
1.478	0.497	0.882	0.341	0.964	48.969	0.477	0.000	34.295
1.543	0.496	0.880	0.343	0.963	46.872	0.480	0.000	34.355
1.606	0.495	0.877	0.344	0.957	44.784	0.484	0.000	34.338
1.669	0.492	0.875	0.345	0.951	42.805	0.486	0.000	34.231
1.732	0.492	0.871	0.346	0.950	41.200	0.491	0.000	34.356
1.795	0.490	0.868	0.347	0.947	39.616	0.495	0.000	34.389
1.858	0.489	0.867	0.350	0.944	38.149	0.498	0.000	34.377
1.920	0.487	0.864	0.350	0.939	36.727	0.502	0.000	34.344
1.981	0.487	0.862	0.351	0.937	35.550	0.504	0.000	34.400
2.045	0.486	0.860	0.353	0.935	34.325	0.507	0.000	34.390
2.095	0.480	0.854	0.352	0.920	32.968	0.516	0.000	34.230
2.146	0.480	0.852	0.354	0.918	32.134	0.518	0.000	34.242
2.200	0.481	0.852	0.355	0.922	31.457	0.519	0.000	34.364
2.260	0.481	0.851	0.356	0.922	30.657	0.520	0.000	34.419
2.322	0.481	0.850	0.356	0.921	29.784	0.521	0.000	34.415
2.388	0.480	0.849	0.357	0.918	28.862	0.523	0.000	34.377
2.456	0.478	0.847	0.358	0.913	27.931	0.527	0.000	34.370
2.511	0.476	0.843	0.360	0.907	27.124	0.532	0.000	34.338
2.575	0.478	0.844	0.360	0.913	26.618	0.531	0.000	34.471
2.639	0.476	0.841	0.360	0.908	25.836	0.536	0.000	34.466
2.704	0.475	0.840	0.361	0.905	25.133	0.537	0.000	34.412
2.772	0.474	0.837	0.362	0.902	24.438	0.541	0.000	34.437
2.844	0.473	0.838	0.362	0.901	23.790	0.540	0.000	34.375
2.915	0.473	0.836	0.363	0.899	23.168	0.543	0.000	34.431
2.989	0.472	0.835	0.364	0.898	22.565	0.545	0.000	34.459
3.060	0.471	0.831	0.365	0.895	21.974	0.550	0.000	34.516
3.135	0.470	0.831	0.366	0.893	21.391	0.551	0.000	34.475
3.196	0.466	0.826	0.367	0.882	20.724	0.559	0.000	34.348
3.257	0.463	0.822	0.366	0.873	20.126	0.566	0.000	34.251
3.308	0.462	0.820	0.368	0.870	19.763	0.569	0.000	34.265
3.366	0.464	0.820	0.369	0.875	19.534	0.568	0.000	34.429
3.422	0.463	0.819	0.370	0.872	19.149	0.571	0.000	34.403
3.485	0.464	0.821	0.371	0.877	18.906	0.567	0.000	34.457
3.536	0.460	0.816	0.369	0.867	18.414	0.575	0.000	34.328
3.585	0.459	0.813	0.371	0.862	18.063	0.580	0.000	34.331
3.633	0.458	0.812	0.372	0.861	17.803	0.582	0.000	34.352
3.679	0.458	0.811	0.373	0.859	17.544	0.584	0.000	34.343
3.732	0.457	0.810	0.375	0.857	17.249	0.586	0.000	34.344
3.785	0.456	0.807	0.374	0.854	16.947	0.590	0.000	34.370
3.839	0.455	0.808	0.375	0.854	16.699	0.589	0.000	34.325
3.895	0.456	0.807	0.374	0.854	16.476	0.591	0.000	34.399
3.954	0.456	0.807	0.375	0.855	16.247	0.591	0.000	34.432
4.007	0.456	0.807	0.376	0.856	16.045	0.591	0.000	34.453
4.067	0.458	0.808	0.375	0.860	15.892	0.589	0.000	34.560

Figure A-36: Example of Typical Triaxial Test Shear Output – Page 4 of 7

4.128	0.457	0.804	0.377	0.856	15.579	0.594	0.000	34.577
4.198	0.456	0.806	0.377	0.855	15.302	0.592	0.000	34.476
4.270	0.456	0.805	0.377	0.855	15.043	0.594	0.000	34.533
4.355	0.458	0.806	0.377	0.859	14.820	0.591	0.000	34.574
4.437	0.455	0.803	0.377	0.853	14.436	0.596	0.000	34.513
4.518	0.455	0.804	0.378	0.852	14.166	0.596	0.000	34.484
4.616	0.456	0.803	0.378	0.854	13.895	0.596	0.000	34.551
4.717	0.455	0.802	0.378	0.851	13.559	0.598	0.000	34.530
4.799	0.446	0.794	0.380	0.827	12.945	0.615	0.000	34.145
4.885	0.452	0.796	0.383	0.843	12.964	0.609	0.000	34.565
4.984	0.449	0.793	0.381	0.837	12.611	0.614	0.000	34.482
5.087	0.450	0.794	0.383	0.839	12.387	0.613	0.000	34.528
5.173	0.448	0.790	0.384	0.833	12.095	0.620	0.000	34.512
5.276	0.446	0.788	0.385	0.829	11.799	0.624	0.000	34.483
5.376	0.443	0.785	0.386	0.821	11.473	0.631	0.000	34.408
5.469	0.443	0.782	0.387	0.820	11.265	0.634	0.000	34.480
5.550	0.443	0.781	0.388	0.821	11.105	0.636	0.000	34.553
5.655	0.440	0.780	0.388	0.814	10.805	0.640	0.000	34.402
5.759	0.440	0.778	0.390	0.814	10.613	0.642	0.000	34.466
5.866	0.440	0.776	0.390	0.812	10.403	0.645	0.000	34.526
5.963	0.436	0.772	0.390	0.801	10.090	0.655	0.000	34.370
6.057	0.436	0.771	0.392	0.802	9.945	0.656	0.000	34.445
6.146	0.435	0.769	0.392	0.800	9.775	0.660	0.000	34.465
6.242	0.434	0.768	0.392	0.796	9.576	0.663	0.000	34.401
6.342	0.434	0.767	0.394	0.797	9.439	0.663	0.000	34.461
6.439	0.433	0.766	0.395	0.793	9.250	0.666	0.000	34.395
6.534	0.430	0.763	0.394	0.786	9.032	0.673	0.000	34.298
6.627	0.428	0.760	0.394	0.781	8.847	0.679	0.000	34.290
6.718	0.429	0.759	0.396	0.782	8.741	0.681	0.000	34.372
6.751	0.428	0.758	0.396	0.781	8.686	0.683	0.000	34.384
6.844	0.426	0.756	0.396	0.776	8.512	0.687	0.000	34.300
6.938	0.427	0.756	0.397	0.776	8.407	0.688	0.000	34.364
7.037	0.426	0.755	0.398	0.776	8.283	0.689	0.000	34.383
7.137	0.424	0.752	0.397	0.770	8.108	0.695	0.000	34.318
7.209	0.414	0.743	0.399	0.743	7.743	0.718	0.000	33.849
7.256	0.414	0.740	0.401	0.743	7.691	0.724	0.000	34.021
7.323	0.418	0.743	0.402	0.755	7.739	0.715	0.000	34.241
7.416	0.422	0.747	0.402	0.765	7.753	0.706	0.000	34.436
7.513	0.422	0.746	0.401	0.763	7.633	0.707	0.000	34.390
7.615	0.420	0.745	0.402	0.759	7.483	0.710	0.000	34.286
7.719	0.420	0.744	0.402	0.759	7.386	0.712	0.000	34.360
7.826	0.419	0.743	0.403	0.756	7.255	0.714	0.000	34.289
7.925	0.416	0.740	0.404	0.749	7.098	0.723	0.000	34.237
8.024	0.417	0.739	0.403	0.750	7.020	0.724	0.000	34.319
8.123	0.414	0.736	0.404	0.743	6.870	0.731	0.000	34.219

M.O.

Figure A-37: Example of Typical Triaxial Test Shear Output - Page 5 of 7

8.217	0.414	0.736	0.406	0.743	6.787	0.732	0.000	34.231
8.321	0.413	0.735	0.404	0.740	6.678	0.735	0.000	34.191
8.414	0.411	0.732	0.406	0.736	6.567	0.742	0.000	34.198
8.508	0.411	0.731	0.407	0.736	6.499	0.743	0.000	34.269
8.604	0.410	0.729	0.408	0.732	6.391	0.748	0.000	34.210
8.702	0.410	0.729	0.409	0.733	6.331	0.748	0.000	34.284
8.804	0.408	0.726	0.408	0.727	6.205	0.754	0.000	34.192
8.912	0.408	0.726	0.409	0.728	6.136	0.755	0.000	34.241
9.013	0.407	0.724	0.410	0.725	6.040	0.760	0.000	34.233
9.127	0.406	0.724	0.411	0.722	5.946	0.761	0.000	34.153
9.237	0.403	0.719	0.410	0.713	5.801	0.773	0.000	34.096
9.340	0.403	0.718	0.410	0.714	5.740	0.774	0.000	34.139
9.446	0.401	0.716	0.412	0.708	5.626	0.781	0.000	34.032
9.535	0.401	0.715	0.412	0.709	5.589	0.781	0.000	34.128
9.644	0.399	0.713	0.413	0.703	5.475	0.788	0.000	34.009
9.748	0.399	0.712	0.414	0.703	5.417	0.790	0.000	34.068
9.862	0.399	0.712	0.413	0.702	5.346	0.791	0.000	34.050
9.978	0.397	0.710	0.416	0.698	5.258	0.795	0.000	34.010
10.052	0.387	0.700	0.414	0.672	5.019	0.828	0.000	33.597
10.123	0.393	0.702	0.417	0.686	5.091	0.816	0.000	33.980
10.219	0.390	0.702	0.414	0.680	4.997	0.820	0.000	33.799
10.274	0.386	0.695	0.417	0.669	4.891	0.838	0.000	33.733
10.368	0.393	0.701	0.418	0.686	4.972	0.817	0.000	34.046
10.473	0.393	0.702	0.417	0.687	4.927	0.816	0.000	34.044
10.556	0.391	0.698	0.417	0.681	4.845	0.826	0.000	34.016
10.663	0.389	0.698	0.417	0.676	4.761	0.829	0.000	33.850
10.768	0.389	0.698	0.418	0.677	4.722	0.829	0.000	33.897
10.889	0.388	0.696	0.419	0.675	4.654	0.834	0.000	33.926
10.999	0.388	0.696	0.418	0.675	4.608	0.834	0.000	33.914
11.081	0.383	0.691	0.418	0.660	4.475	0.852	0.000	33.671
11.153	0.384	0.690	0.420	0.664	4.472	0.850	0.000	33.825
11.242	0.380	0.688	0.420	0.652	4.359	0.861	0.000	33.516
11.315	0.384	0.689	0.420	0.664	4.406	0.853	0.000	33.900
11.414	0.384	0.690	0.420	0.664	4.371	0.851	0.000	33.862
11.505	0.382	0.688	0.420	0.658	4.296	0.857	0.000	33.706
11.609	0.382	0.687	0.420	0.657	4.251	0.860	0.000	33.725
11.688	0.375	0.682	0.420	0.638	4.103	0.882	0.000	33.327
11.763	0.379	0.683	0.422	0.650	4.151	0.873	0.000	33.700
11.851	0.378	0.683	0.420	0.649	4.111	0.875	0.000	33.678
11.945	0.378	0.683	0.421	0.648	4.075	0.875	0.000	33.663
12.039	0.379	0.683	0.422	0.649	4.052	0.873	0.000	33.694
12.127	0.378	0.681	0.422	0.647	4.006	0.878	0.000	33.674
12.222	0.376	0.680	0.422	0.642	3.946	0.884	0.000	33.574
12.319	0.377	0.680	0.423	0.645	3.932	0.881	0.000	33.653
12.419	0.376	0.679	0.422	0.642	3.883	0.885	0.000	33.611

Figure A-38: Example of Typical Triaxial Test Shear Output – Page 6 of 7

12.513	0.376	0.678	0.424	0.643	3.860	0.886	0.000	33.699
12.615	0.376	0.678	0.424	0.641	3.818	0.888	0.000	33.650
12.699	0.374	0.675	0.424	0.636	3.760	0.898	0.000	33.613
12.801	0.374	0.675	0.423	0.638	3.742	0.896	0.000	33.677
12.887	0.375	0.676	0.425	0.639	3.724	0.893	0.000	33.656
13.008	0.375	0.677	0.424	0.640	3.698	0.892	0.000	33.710
13.107	0.377	0.678	0.426	0.643	3.688	0.888	0.000	33.769
13.189	0.368	0.670	0.425	0.621	3.538	0.919	0.000	33.358
13.275	0.374	0.674	0.426	0.637	3.605	0.900	0.000	33.736
13.380	0.373	0.673	0.426	0.635	3.566	0.902	0.000	33.681
13.489	0.373	0.672	0.426	0.633	3.524	0.906	0.000	33.661
13.592	0.365	0.666	0.425	0.613	3.388	0.931	0.000	33.223
13.682	0.370	0.668	0.427	0.626	3.437	0.919	0.000	33.640
13.794	0.369	0.668	0.428	0.623	3.395	0.920	0.000	33.515
13.896	0.363	0.664	0.425	0.608	3.285	0.941	0.000	33.184
13.996	0.367	0.665	0.429	0.618	3.315	0.931	0.000	33.487
14.064	0.360	0.657	0.428	0.599	3.198	0.964	0.000	33.230
14.144	0.364	0.659	0.428	0.611	3.243	0.948	0.000	33.532
14.243	0.364	0.660	0.430	0.609	3.212	0.949	0.000	33.462
14.336	0.362	0.658	0.430	0.604	3.164	0.957	0.000	33.371
14.357	0.363	0.659	0.432	0.607	3.174	0.953	0.000	33.414

FINAL AREA = 12.38029

Figure A-39: Example of Typical Triaxial Test Shear Output - Page 7 of 7

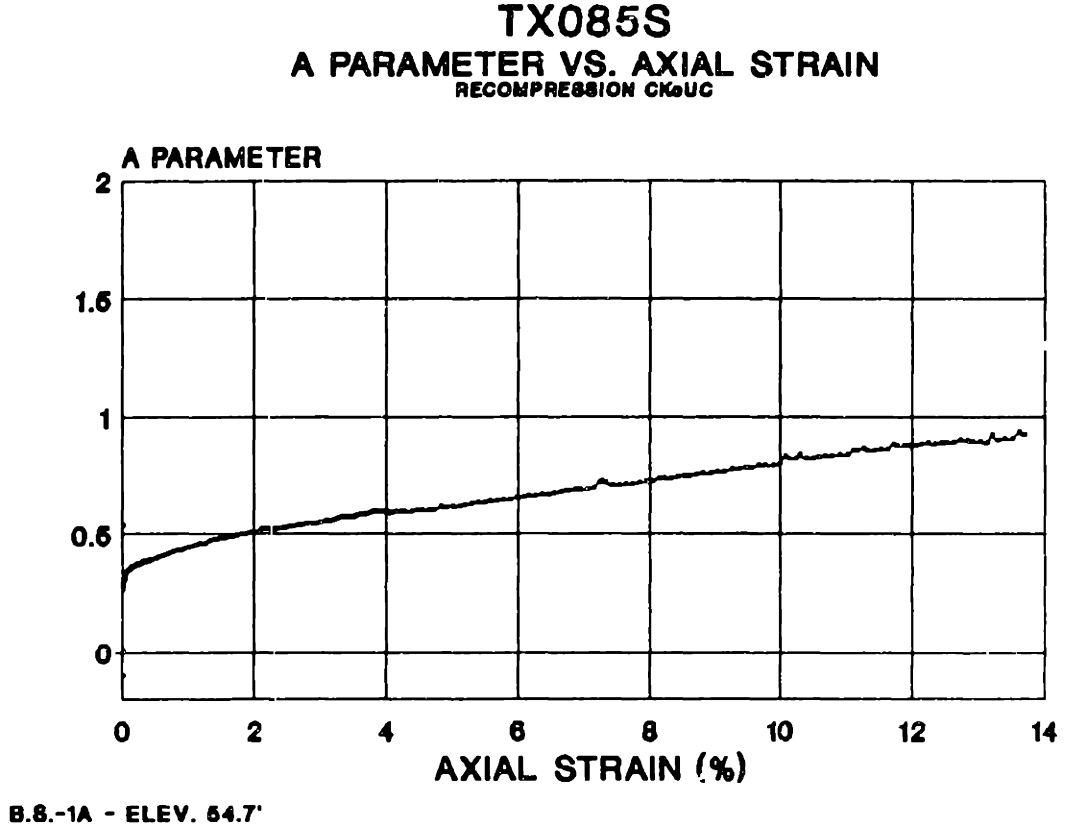

Figure A-40: Example of Typical Triaxial Test Shear Plot – 1 of 6

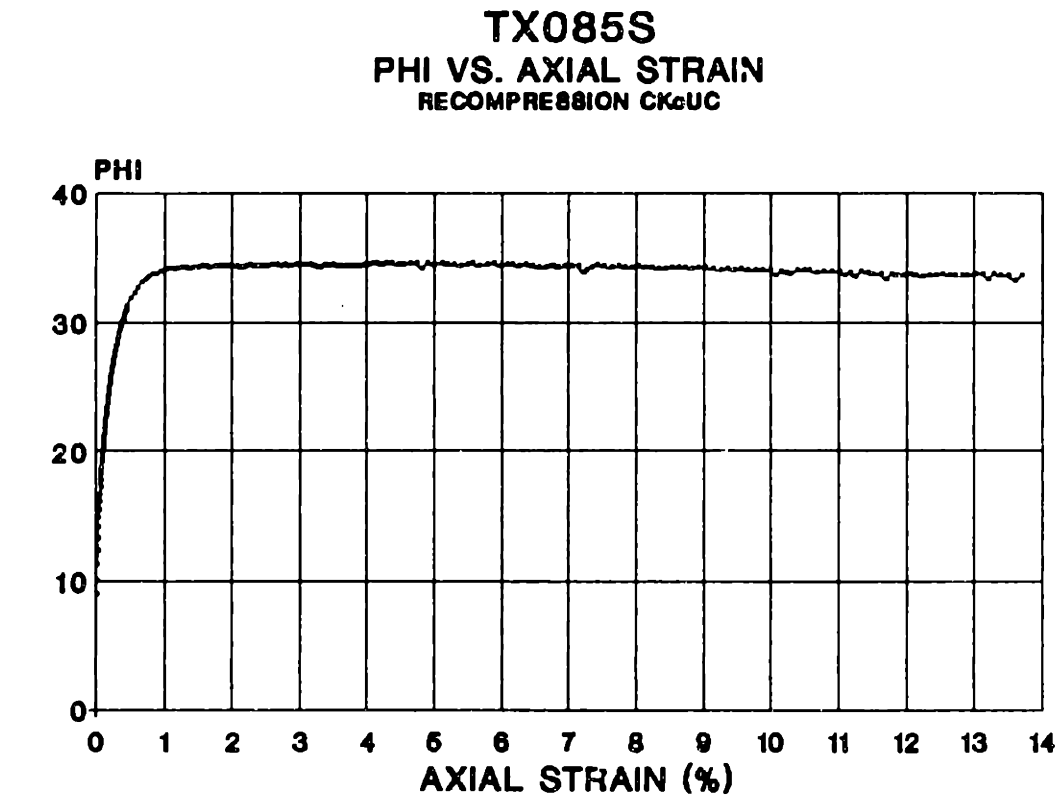

Figure A-41: Example of Typical Triaxial Test Shear Plot - 2 of 6

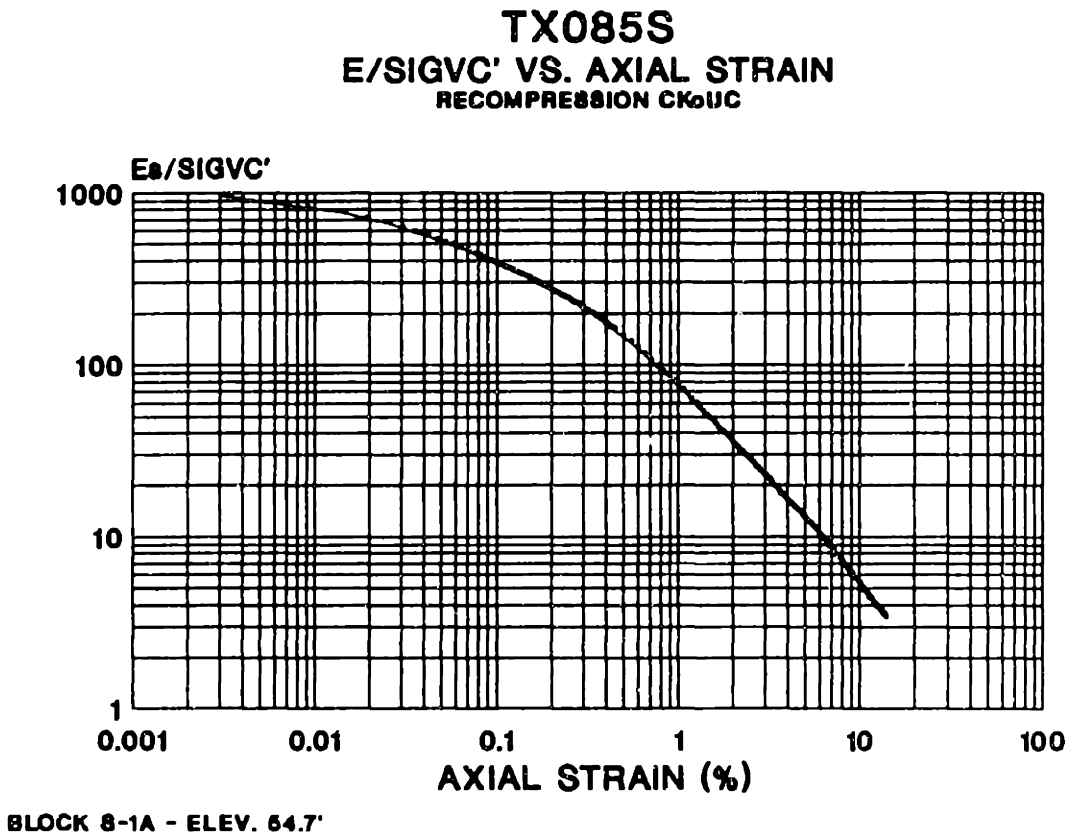

Figure A-42: Example of Typical Triaxial Test Shear Plot - 3 of 6

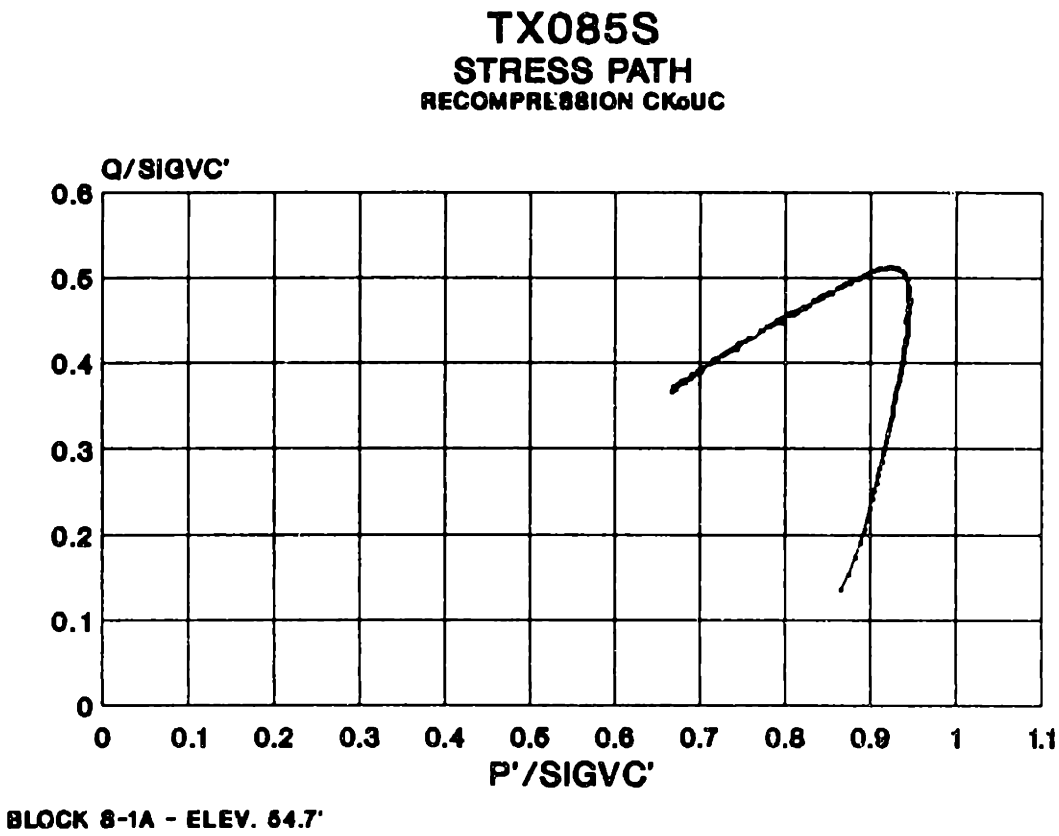

Figure A-43: Example of Typical Triaxial Test Shear Plot - 4 of 6

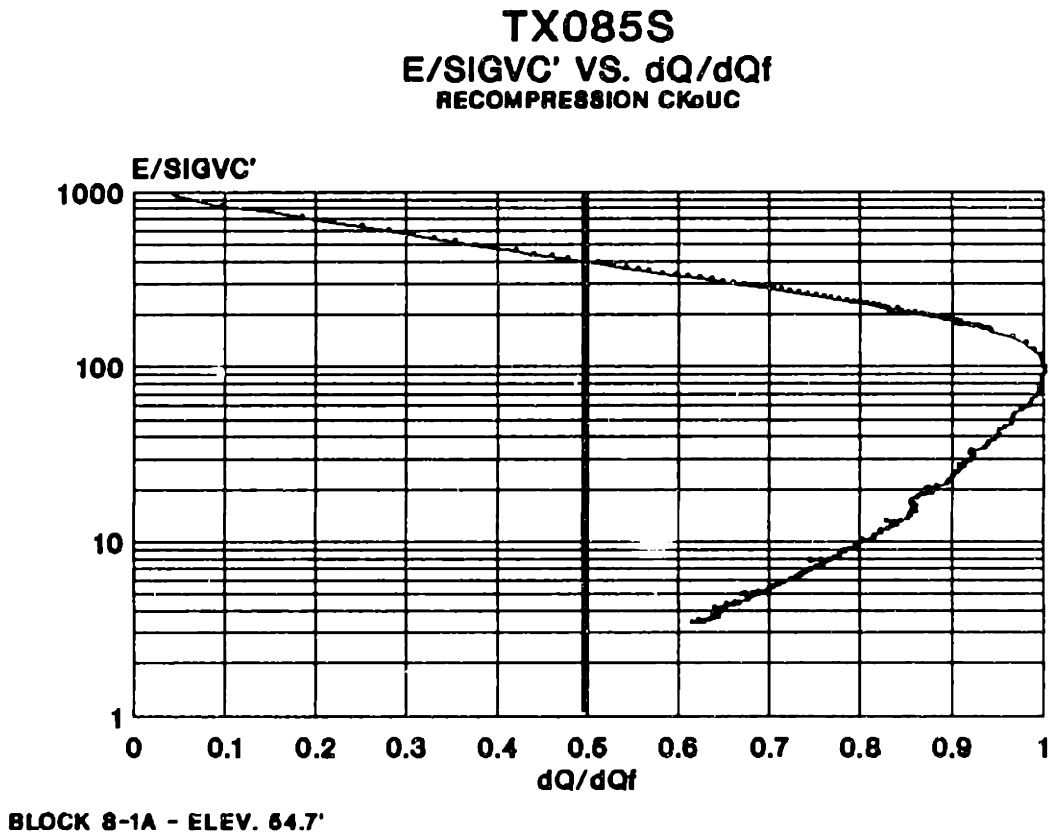

Figure A-44: Example of Typical Triaxial Test Shear Plot - 5 of 6

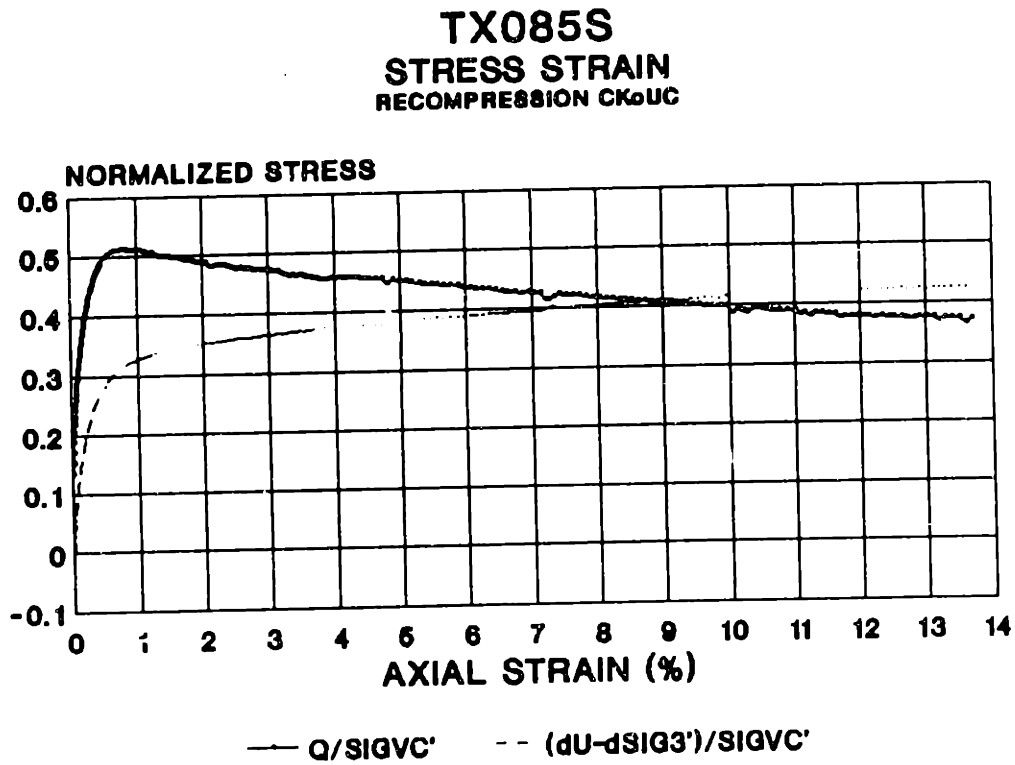

Figure A-45: Example of Typical Triaxial Test Shear Plot - 6 of 6

Appendix B

Plots from Recompression Tests

The following pages present plots from all Recompression tests performed. Each test is represented by four plots: the stress path (normalized to σ'_{vc}, the stress-strain curve (q/σ'_{vc} versus ϵ_a), and pore pressure parameter (A_f) and friction angle (ϕ') versus axial strain. The tests are arranged in numerical order. The reader is referred to Tables 6.1 and 6.3 for summaries of pertinent engineering parameters for each test, and to MIT research report R91-10 for the tabulated data used to generate these plots.

TX040S
STRESS PATH

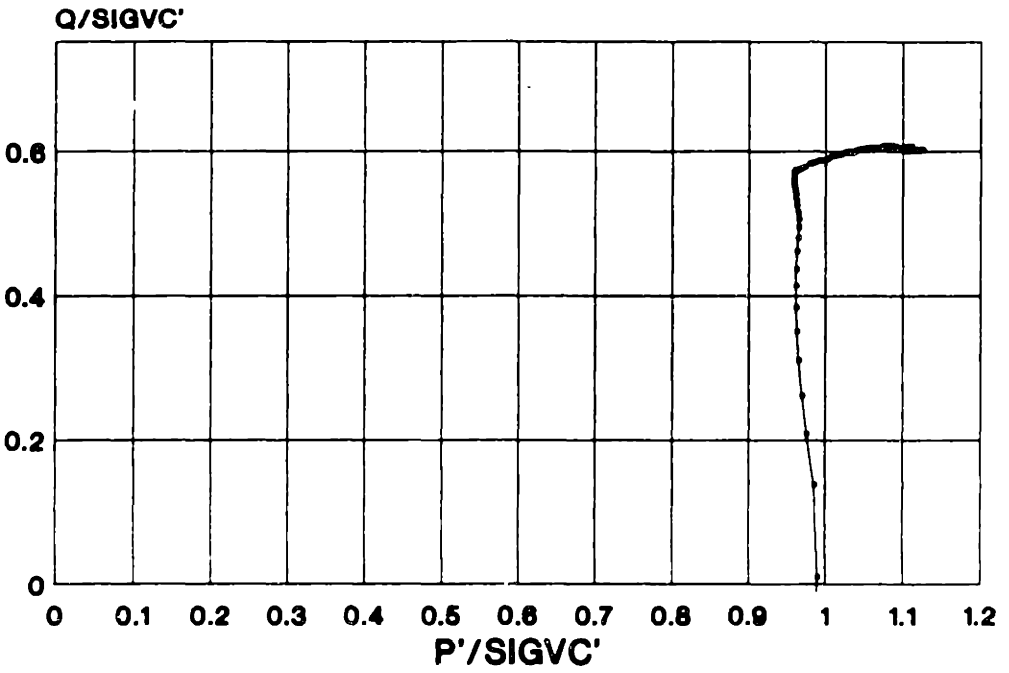

BLOCK S-1 - 43.5'

TX040S
STRESS STRAIN

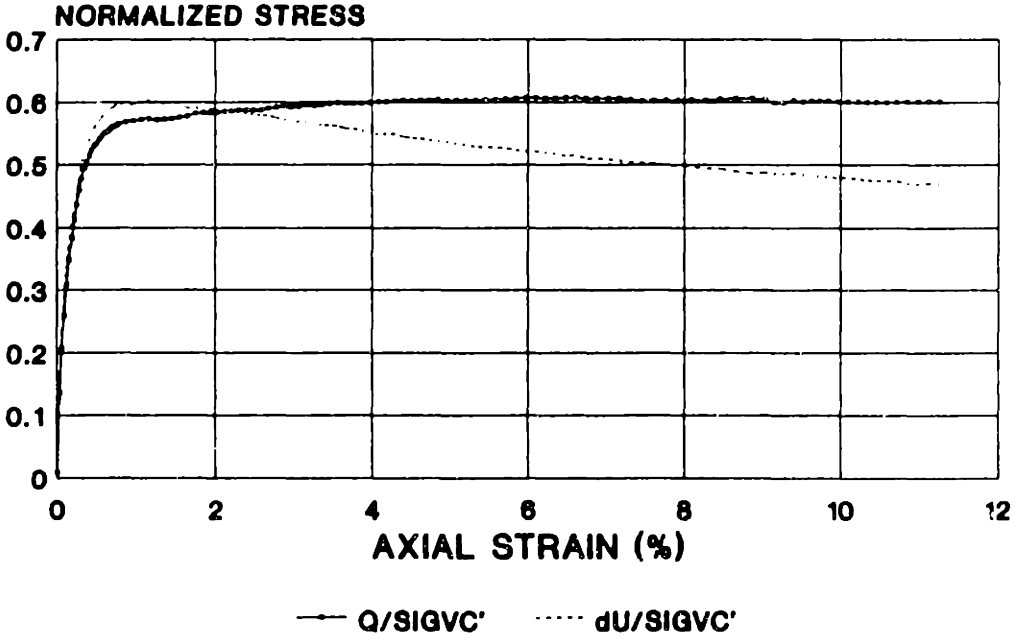

BLOCK S-1 - 43.5'

TX040S
A PARAMETER VS. AXIAL STRAIN

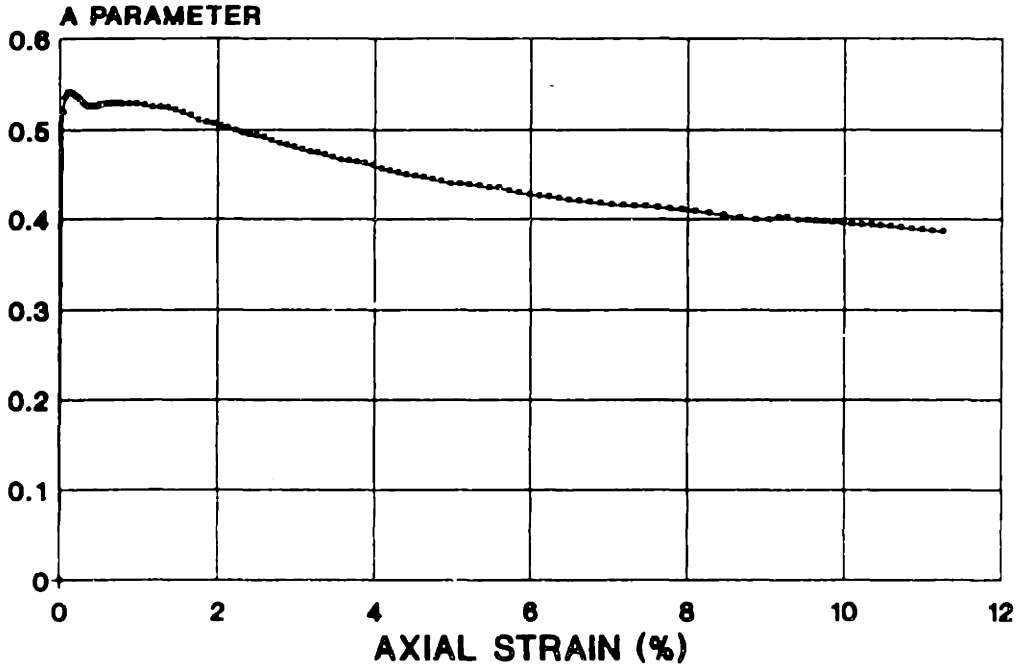

BLOCK S-1 - 43.5'

TX040S
PHI VS. AXIAL STRAIN

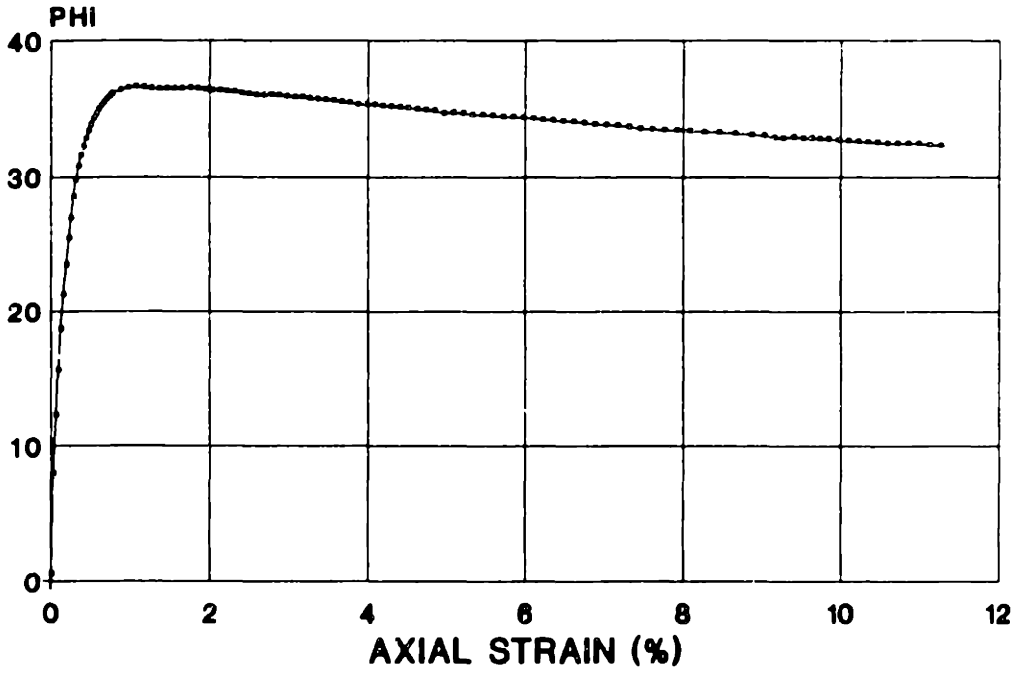

BLOCK S-1 - 43.5'

TX042S
STRESS PATH

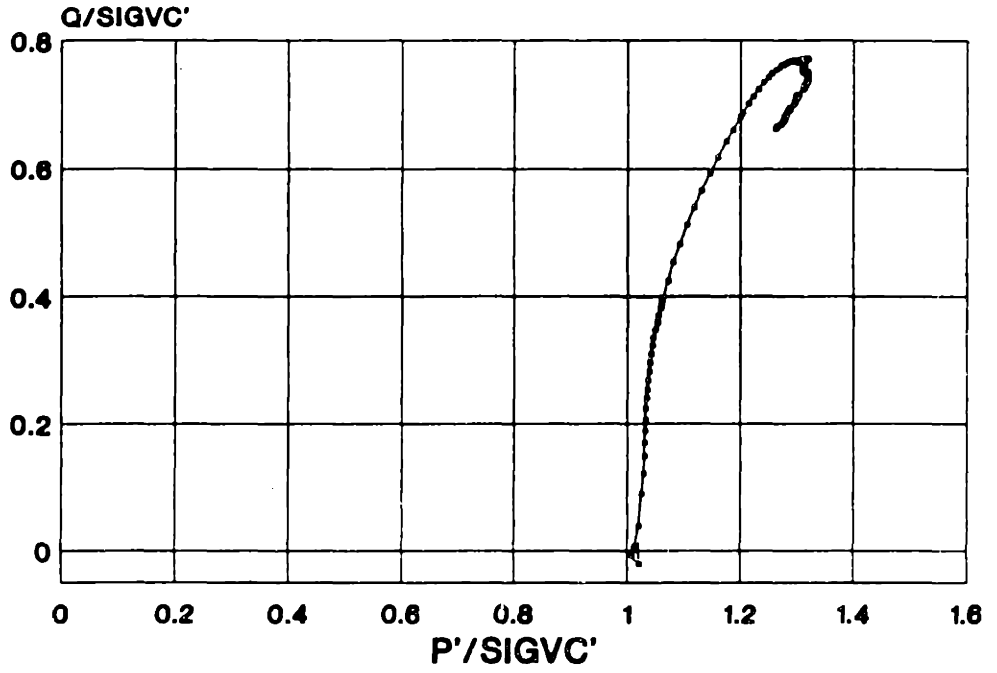

BLOCK S-3 - ELEV. 56.0'

TX042S
STRESS STRAIN

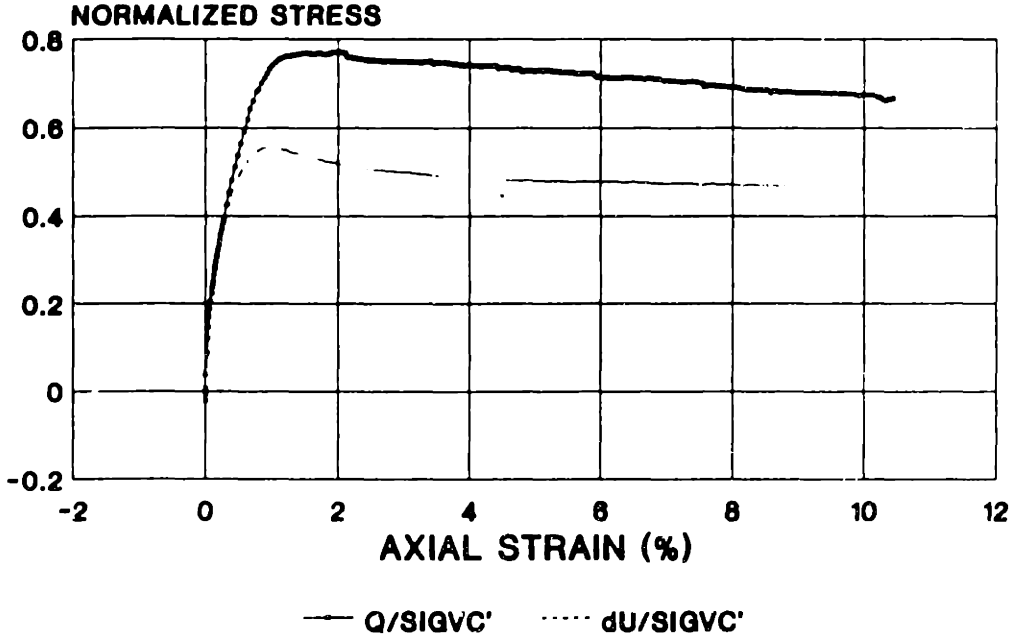

BLOCK S-3 -ELEV. 56.0'

TX042S
A PARAMETER VS. AXIAL STRAIN

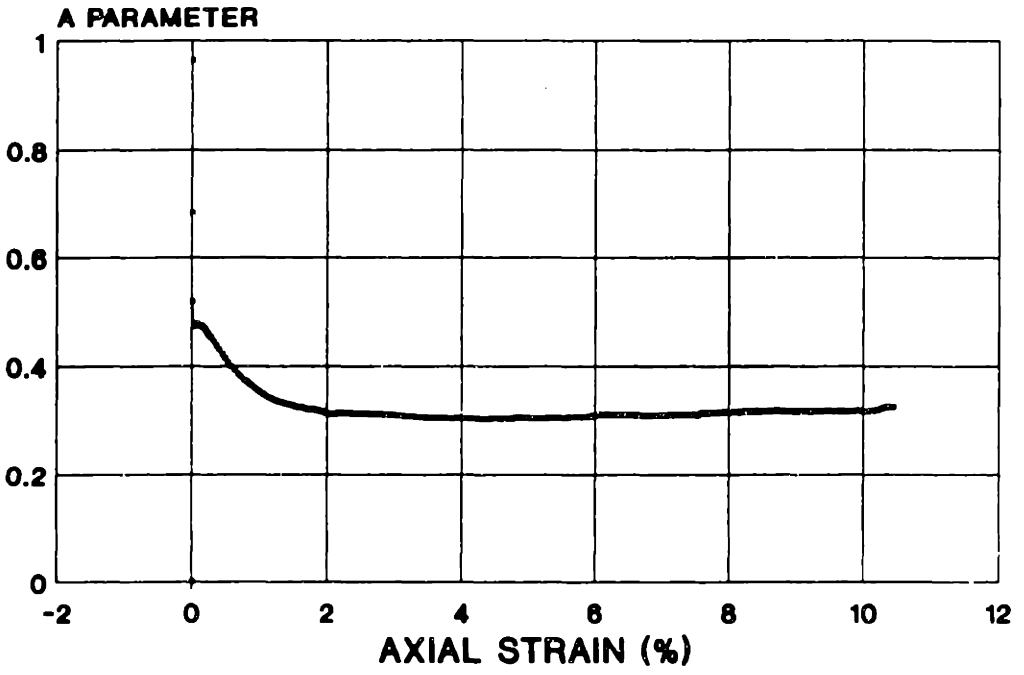

BLOCK S-3 - ELEV. 56.0'

TX042S
PHI VS. AXIAL STRAIN

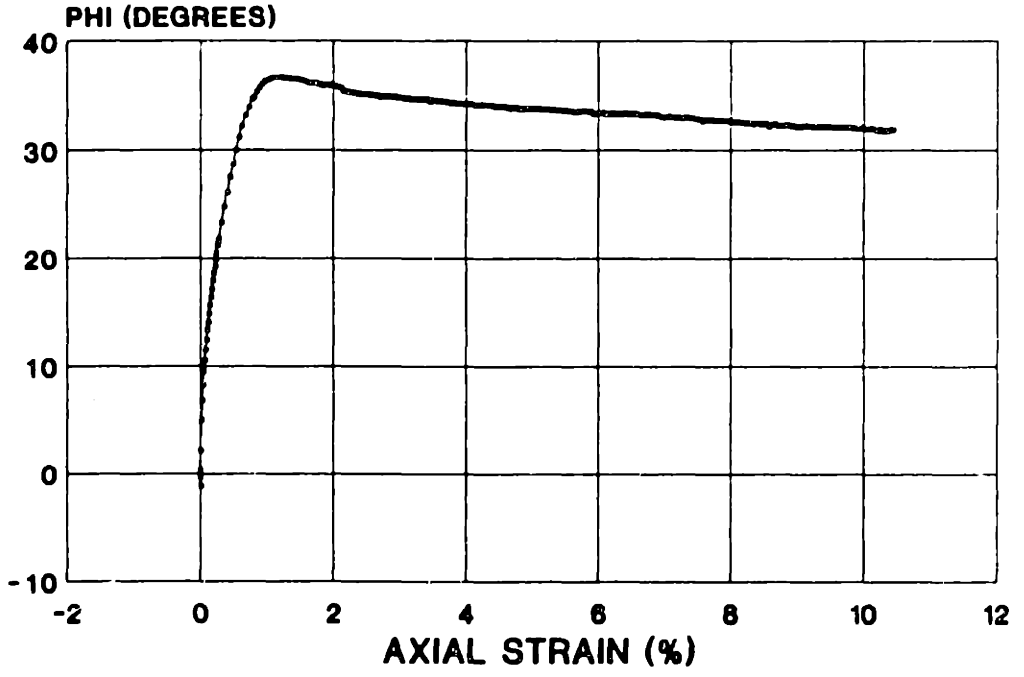

BLOCK S-3 - ELEV. 56.0'

TX046S
STRESS PATH

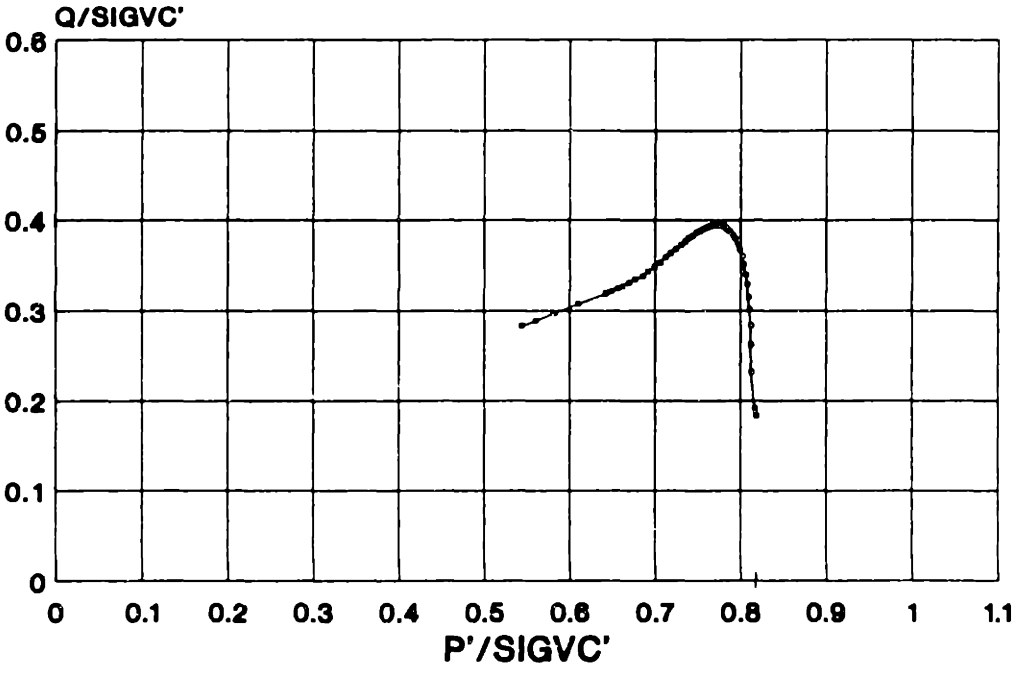

BLOCK S-7 - ELEV. 20.9'

TX046S
STRESS STRAIN

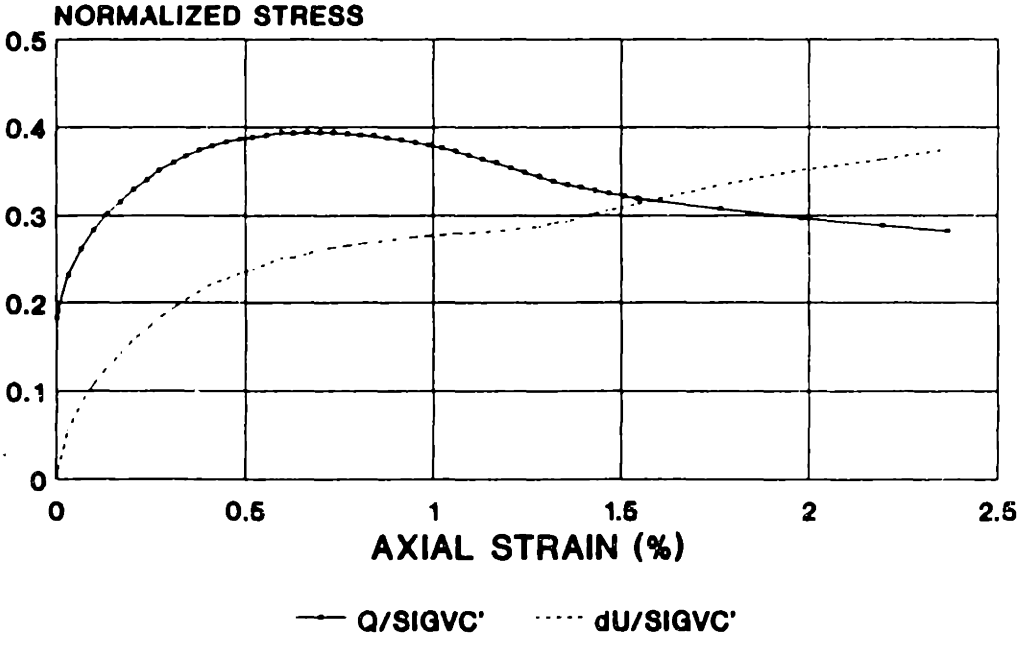

BLOCK S-7 - ELEV. 20.9'

TX046S
A PARAMETER VS. AXIAL STRAIN

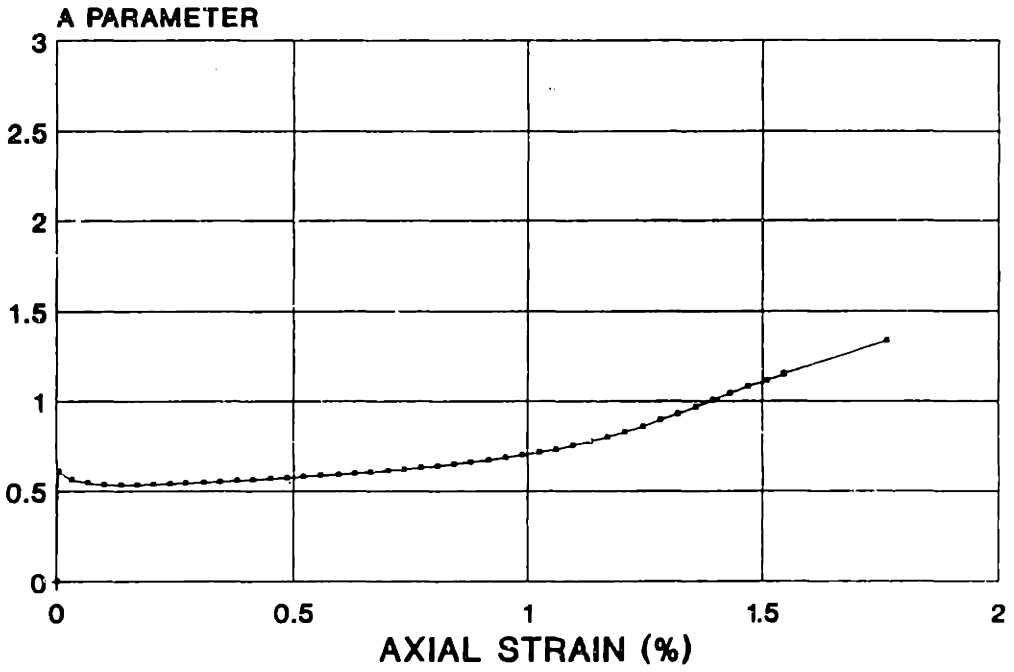

BLOCK S-7 - ELEV. 20.9'

TX046S
PHI VS. AXIAL STRAIN

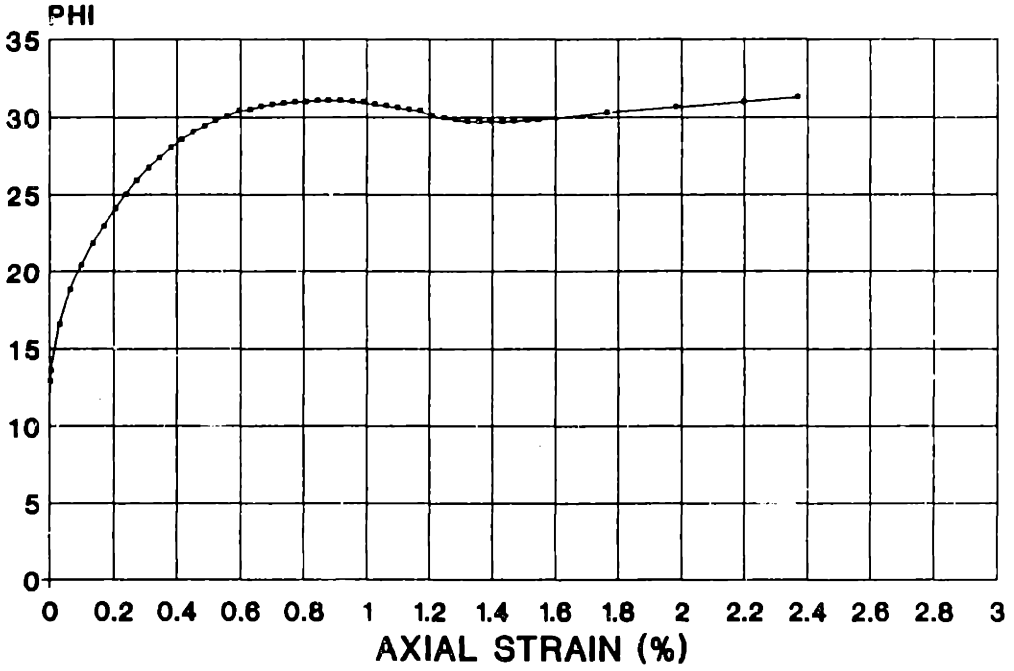

BLOCK S-7 - ELEV. 20.9'

TX047S
STRESS PATH

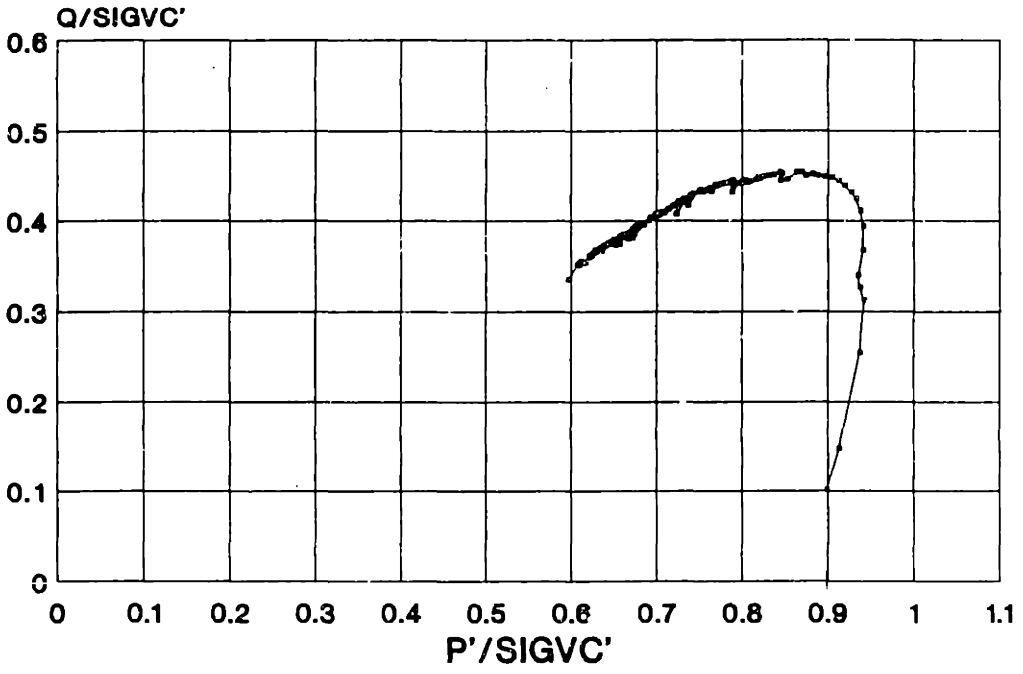

BLOCK S-2A - ELEV. 42.1'

TX047S
STRESS STRAIN

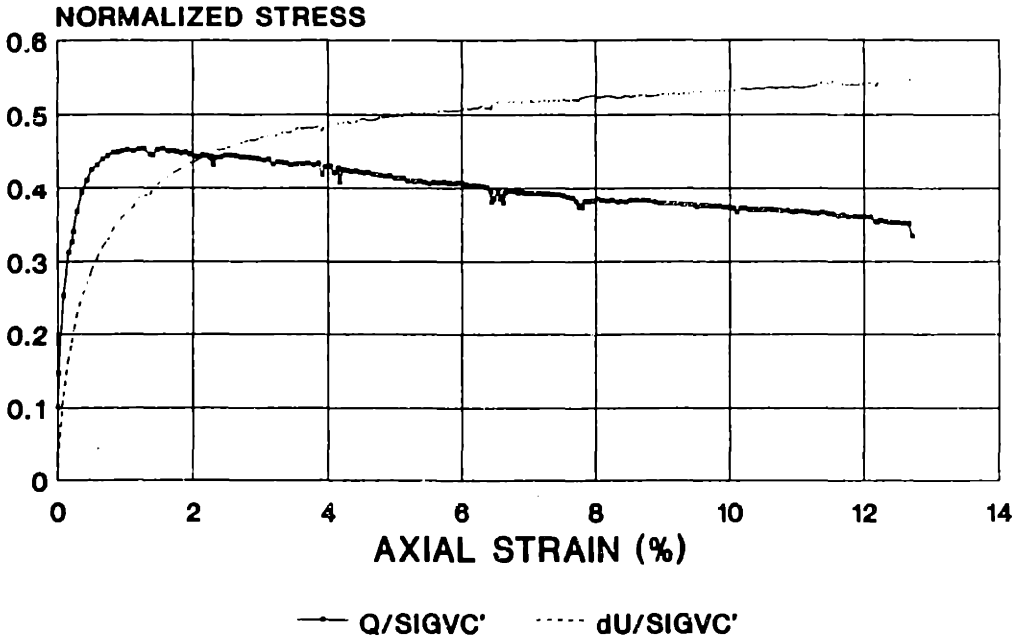

BLOCK S-2A - ELEV. 42.1'

TX047S
A PARAMETER VS. AXIAL STRAIN

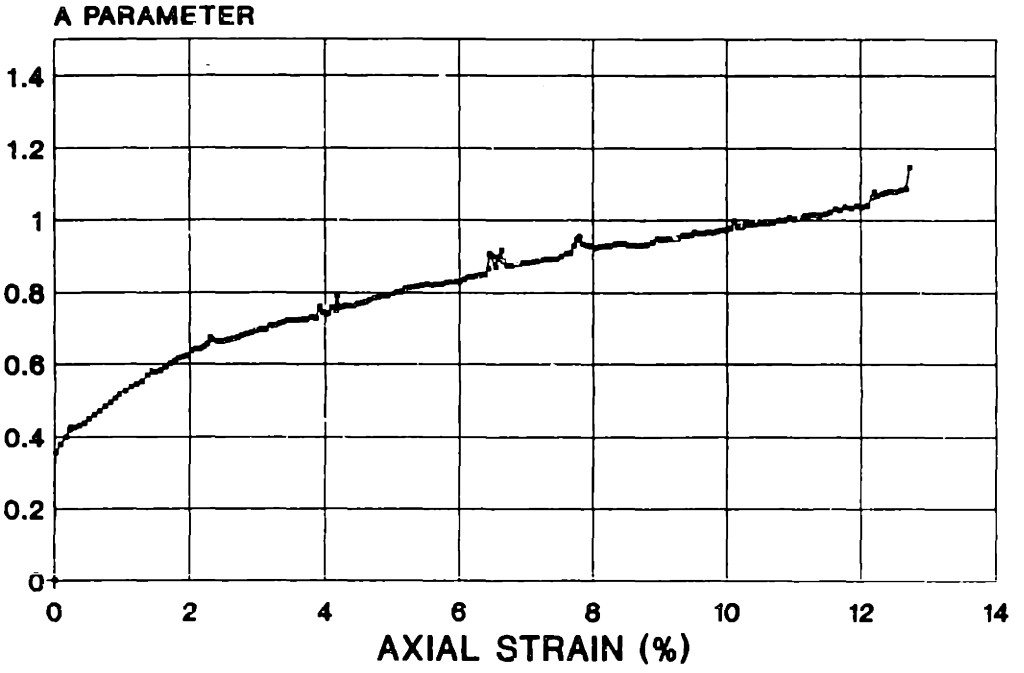

BLOCK S-2A - ELEV. 42.1'

TX047S
PHI VS. AXIAL STRAIN

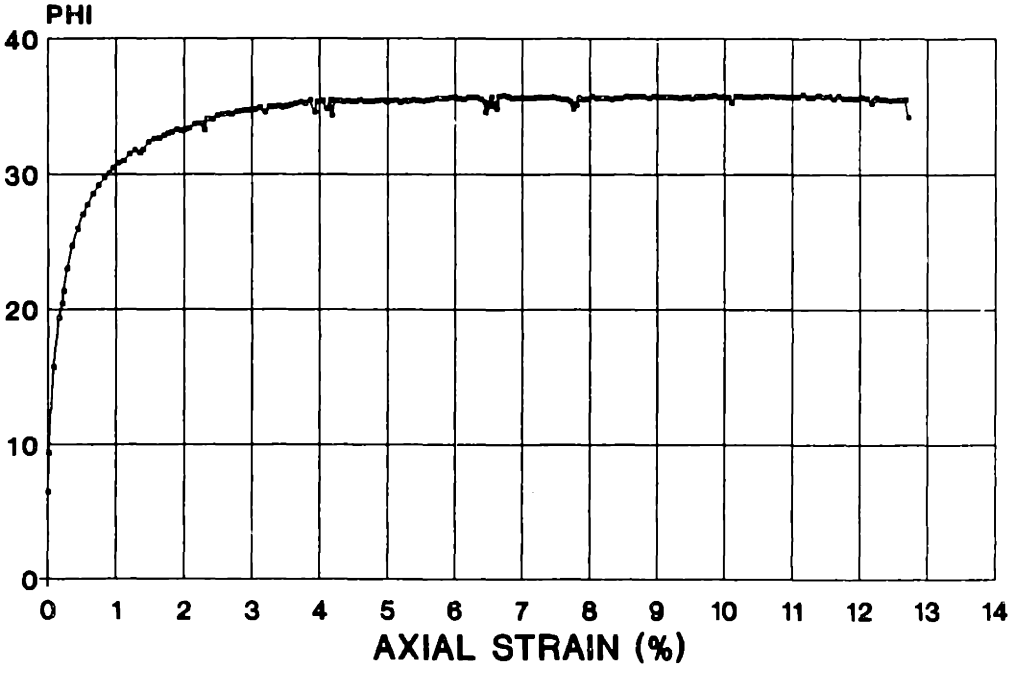

BLOCK S-2A - ELEV. 42.1'

TX048S
A PARAMETER VS. AXIAL STRAIN

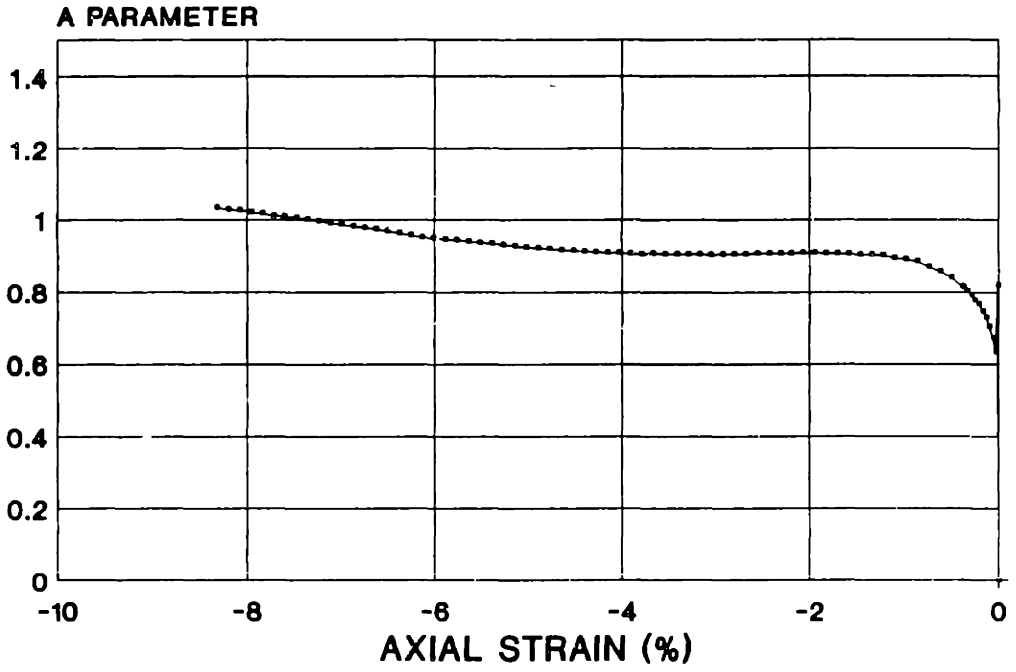

BLOCK S-2A - ELEV. 42.1'

TX048S
PHI VS. AXIAL STRAIN

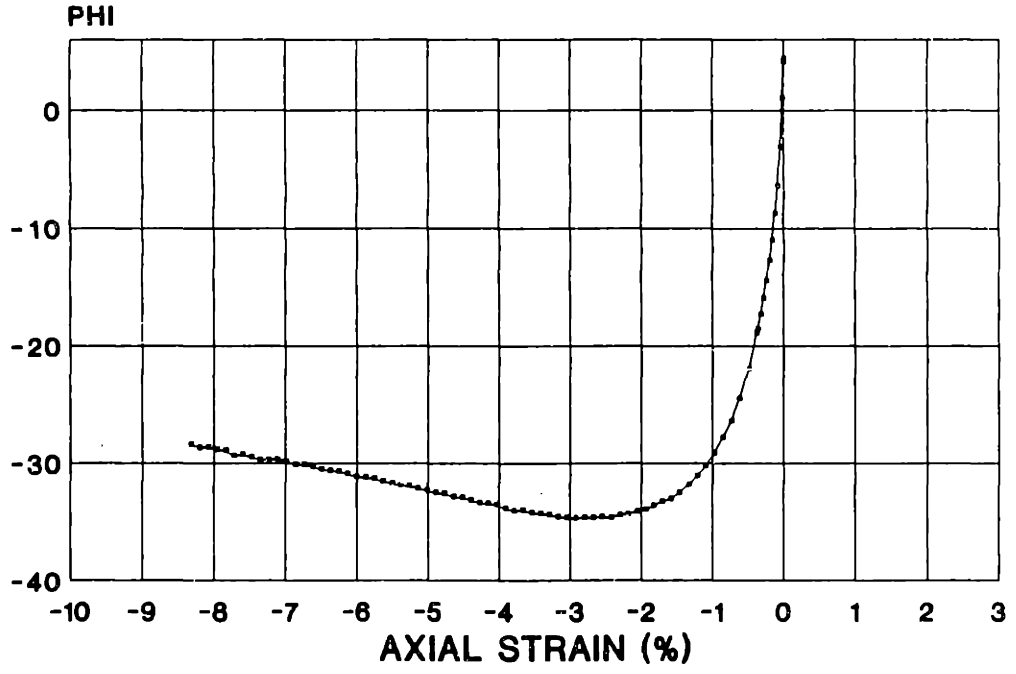

BLOCK S-2A - ELEV. 42.1'

TX048S
STRESS PATH

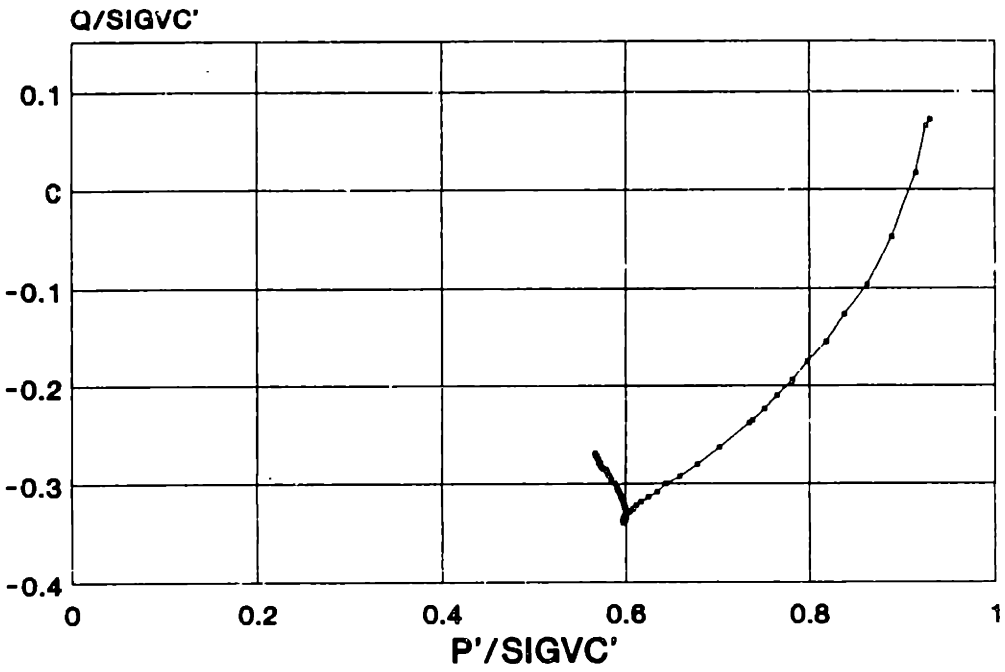

BLOCK S-2A - ELEV. 42.1'

TX048S
STRESS STRAIN
RECOMPRESSION CKoUC

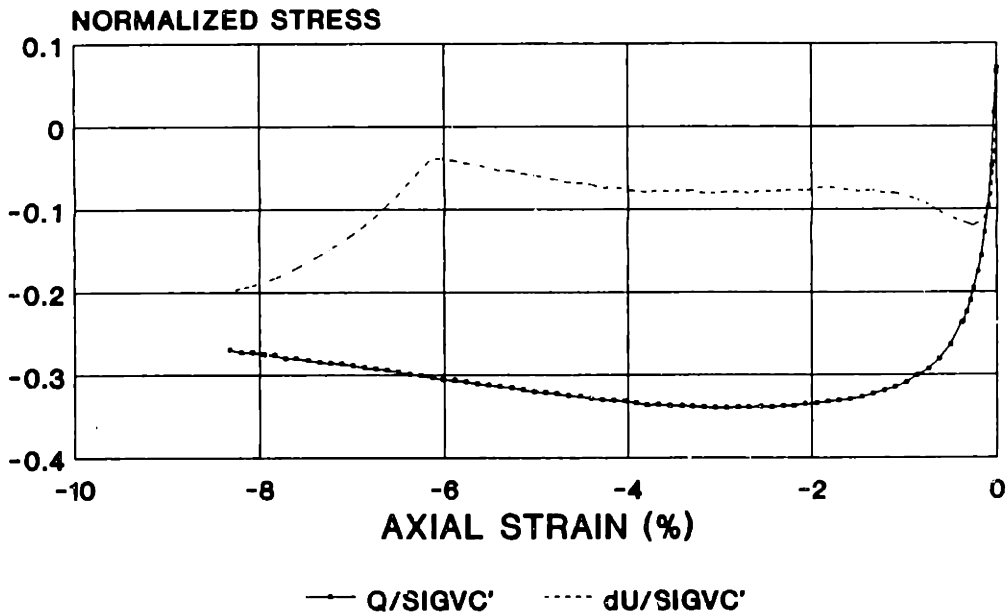

BLOCK S-2A - ELEV. 42.1'

TX049S
STRESS PATH

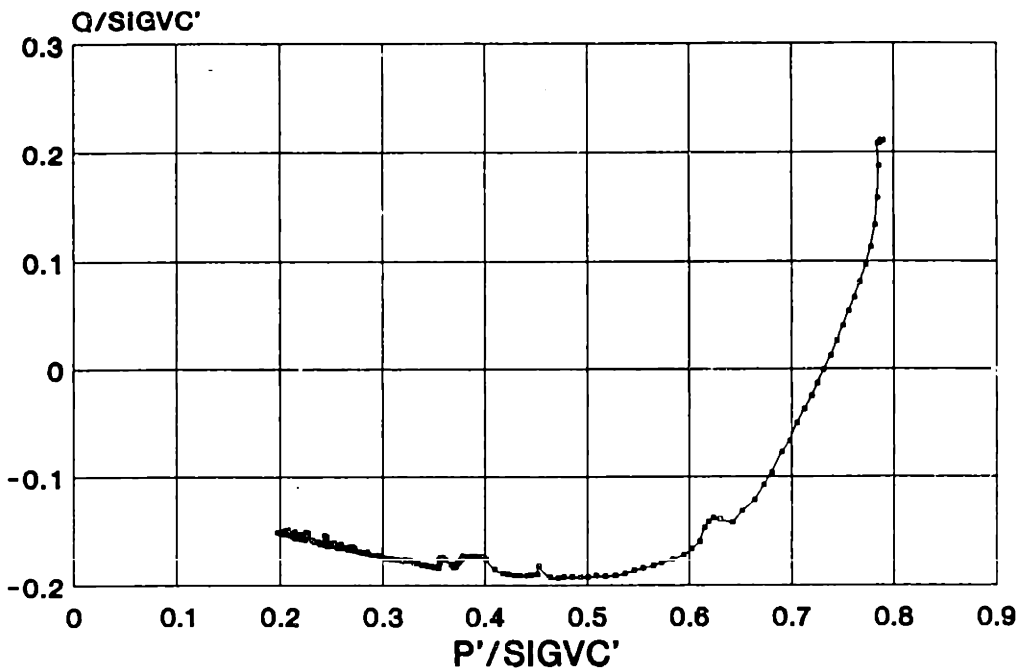

BLOCK S-7 - ELEV. 20.9'

TX049S
STRESS STRAIN

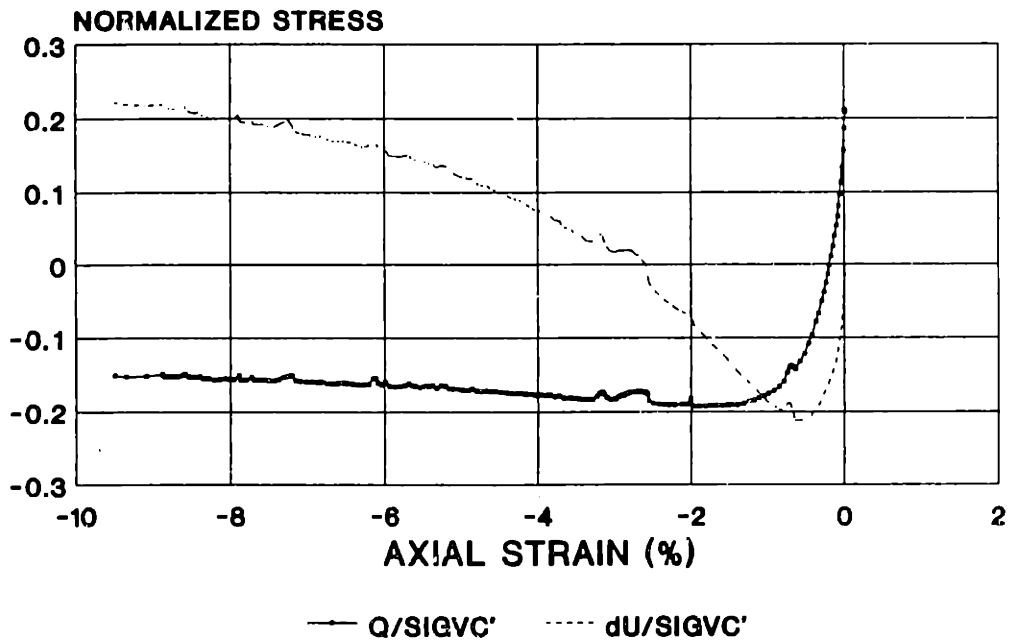

BLOCK S-7 - ELEV. 20.9'

TX049S
A PARAMETER VS. AXIAL STRAIN

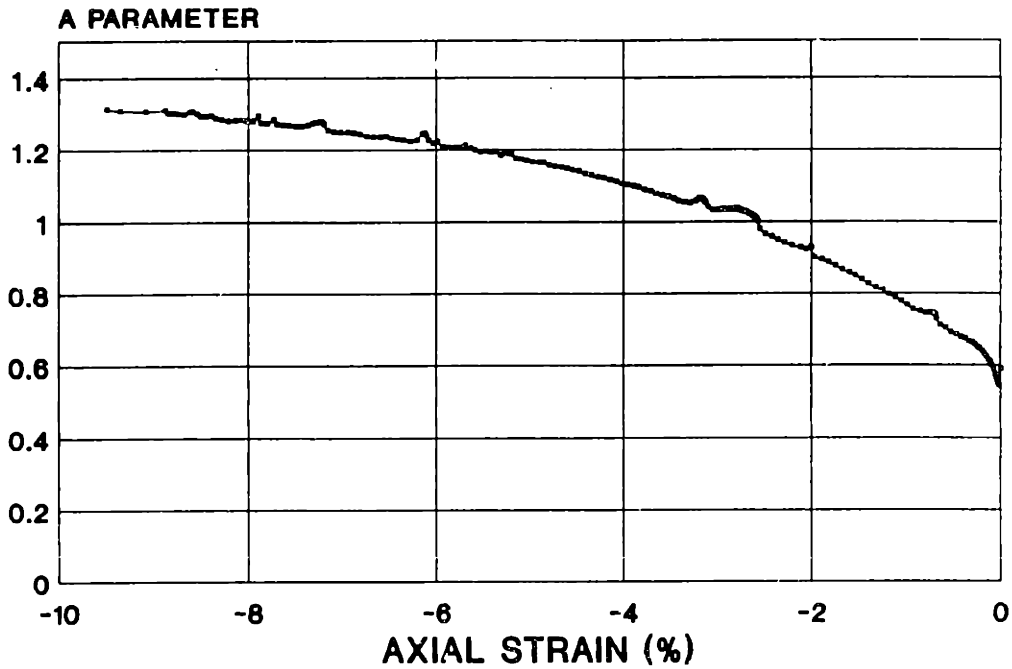

BLOCK S-7 - ELEV. 20.9'

TX049S
PHI VS. AXIAL STRAIN

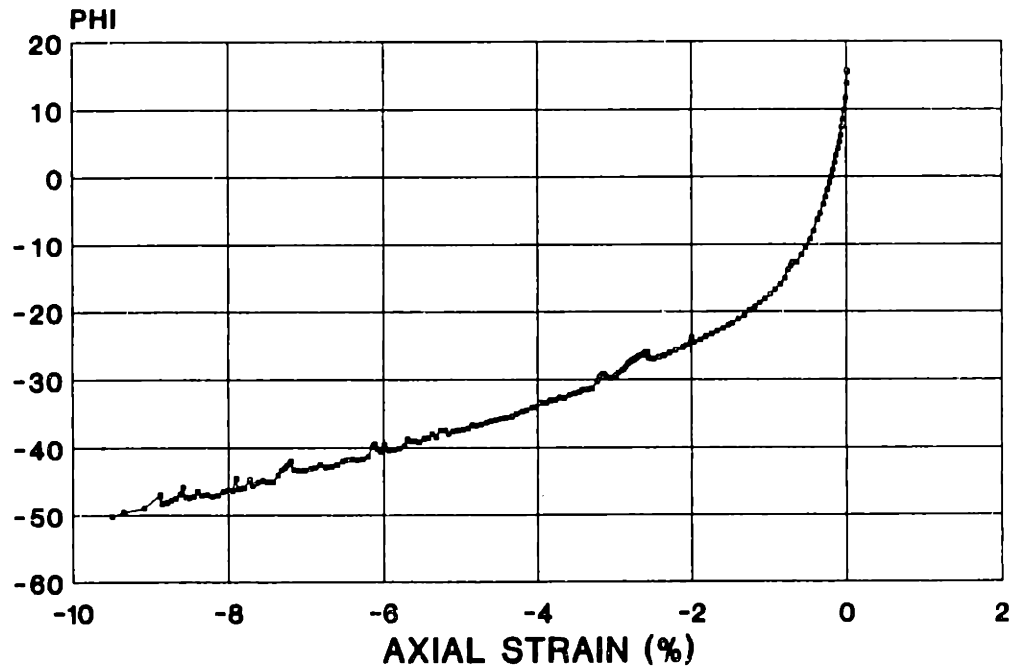

BLOCK S-7 - ELEV. 20.9'

TX050S
STRESS PATH

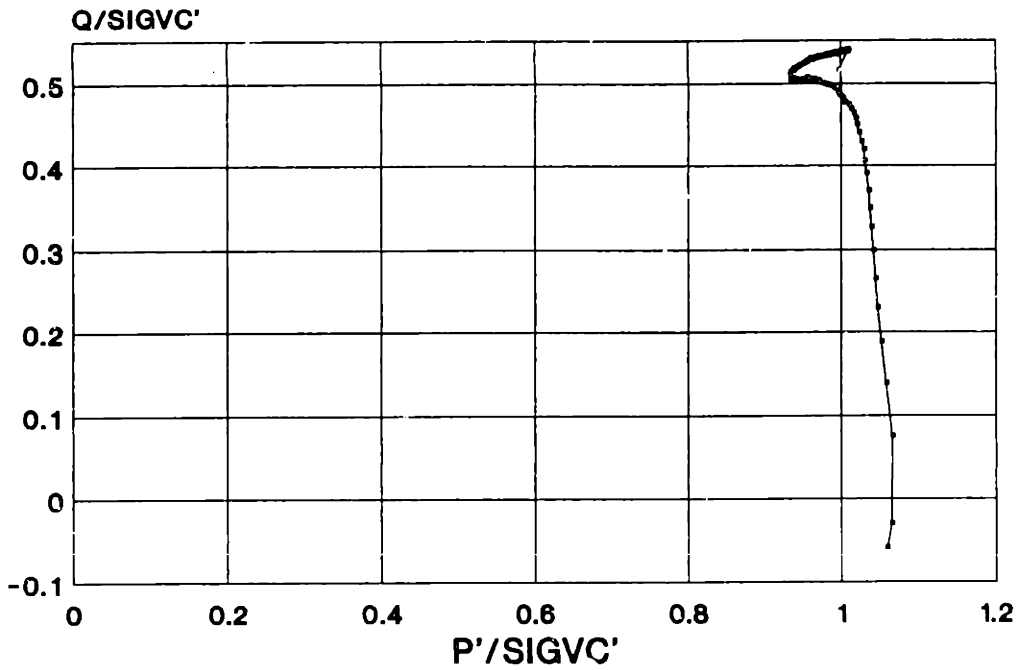

BLOCK S-2 - ELEV. 60.7'

TX050S
STRESS STRAIN

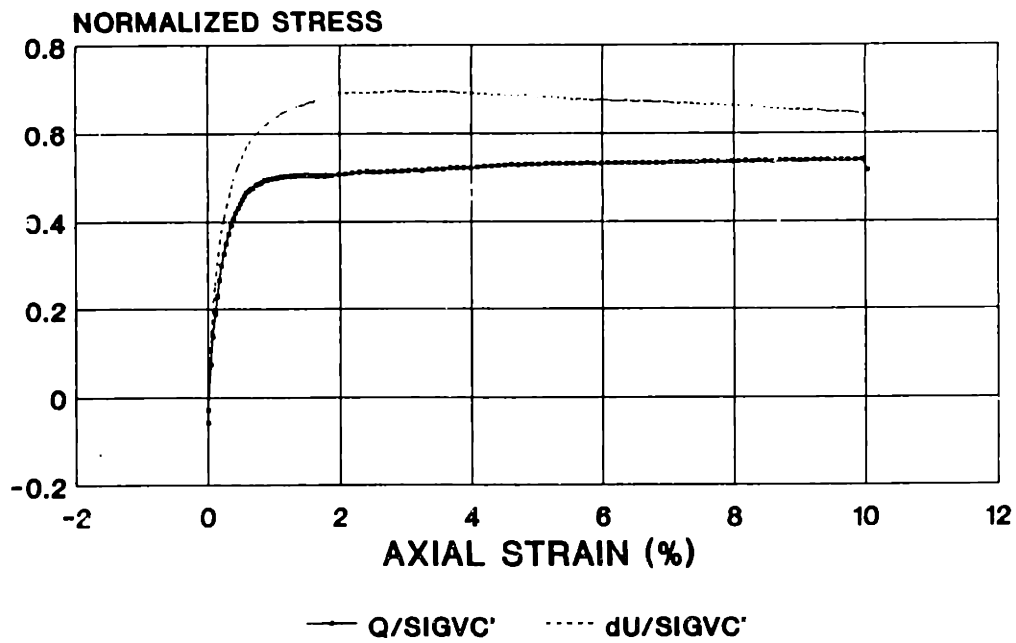

BLOCK S-2 - ELEV. 60.7'

TX050S
A PARAMETER VS. AXIAL STRAIN

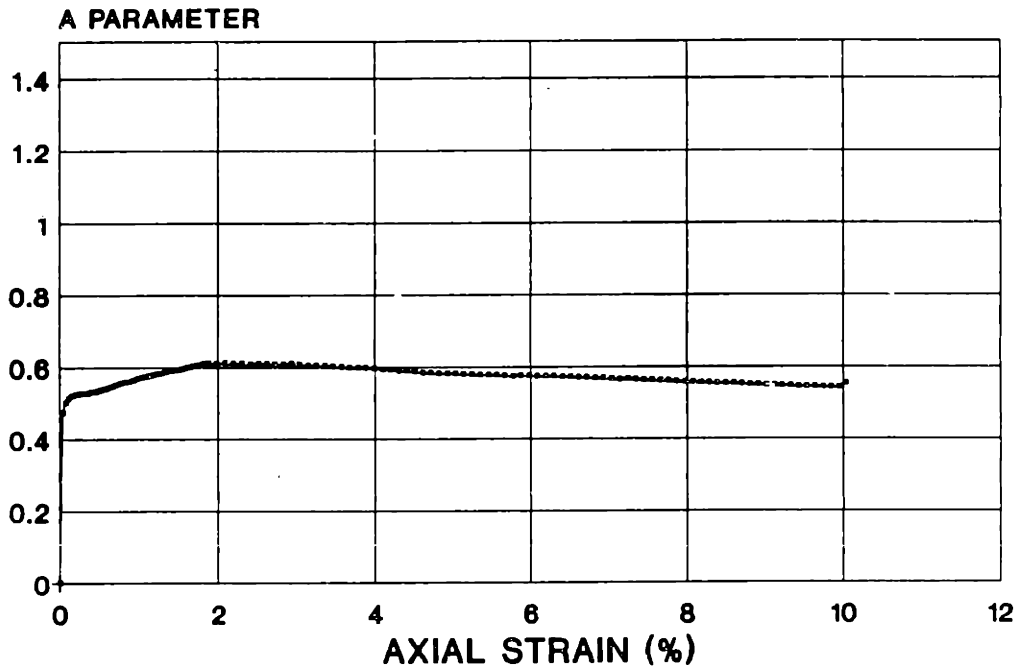

BLOCK S-2 - ELEV. 60.7

TX050S
PHI VS. AXIAL STRAIN

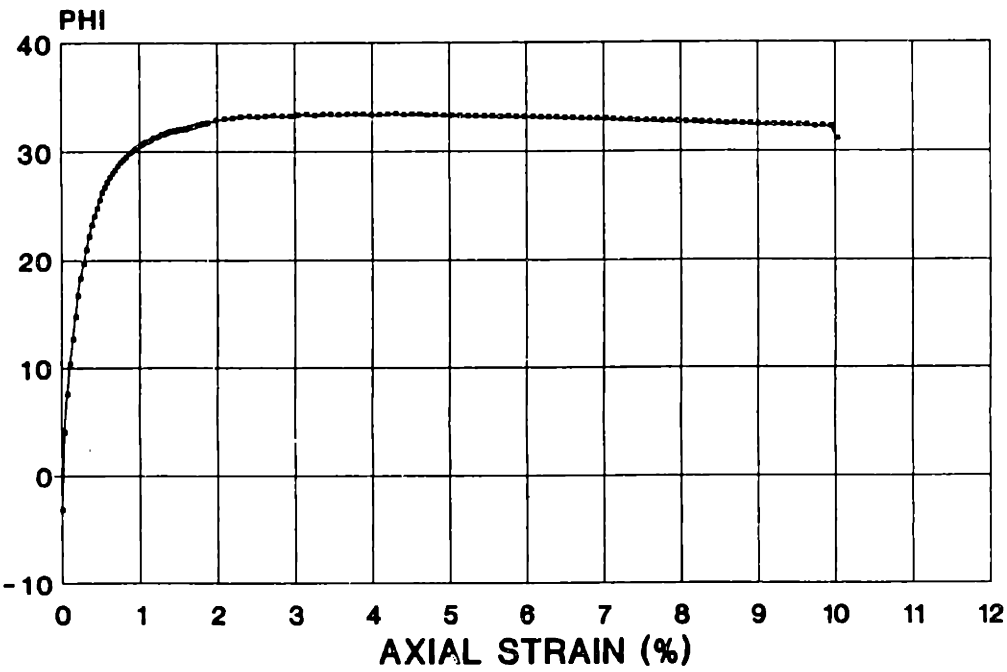

BLOCK S-2 - ELEV. 60.7'

TX052S
STRESS PATH

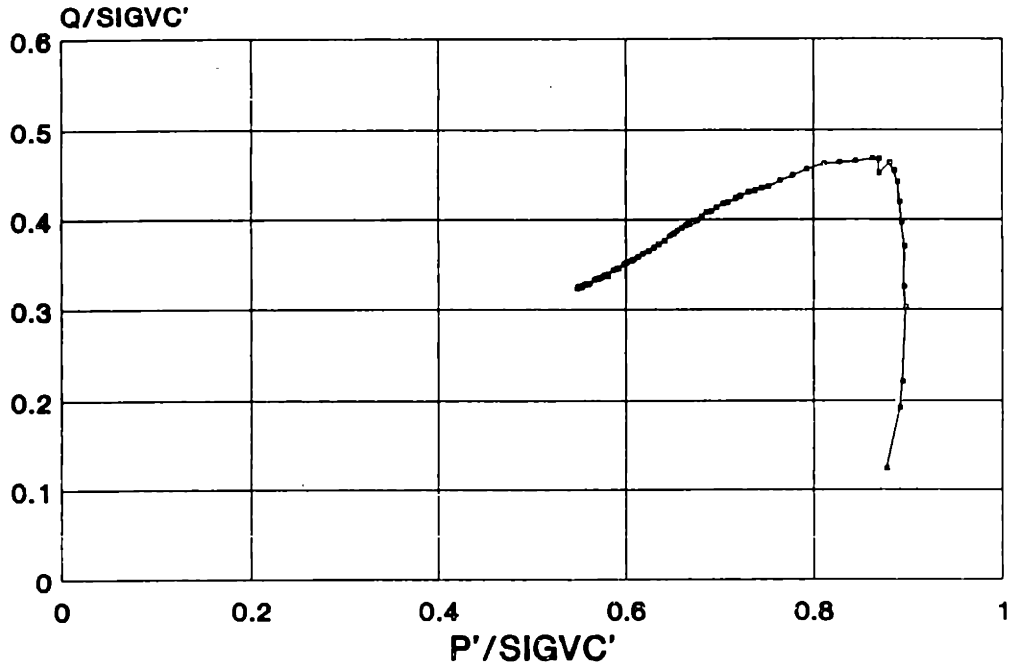

BLOCK S-3A - ELEV. 33.6'

TX052S
STRESS STRAIN

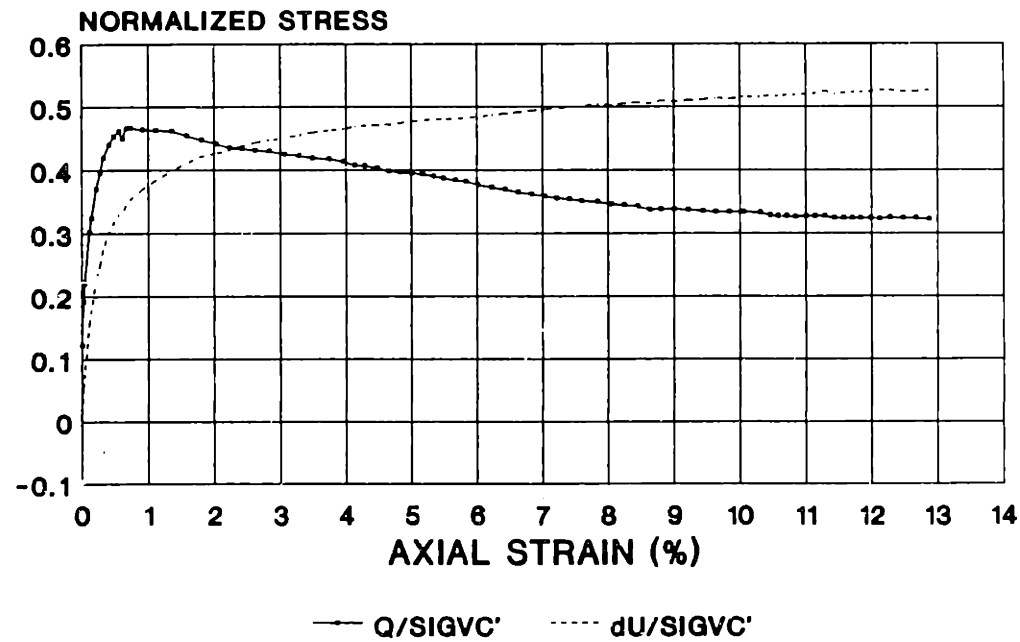

BLOCK S-3A - ELEV. 33.6'

TX052S
A PARAMETER VS. AXIAL STRAIN

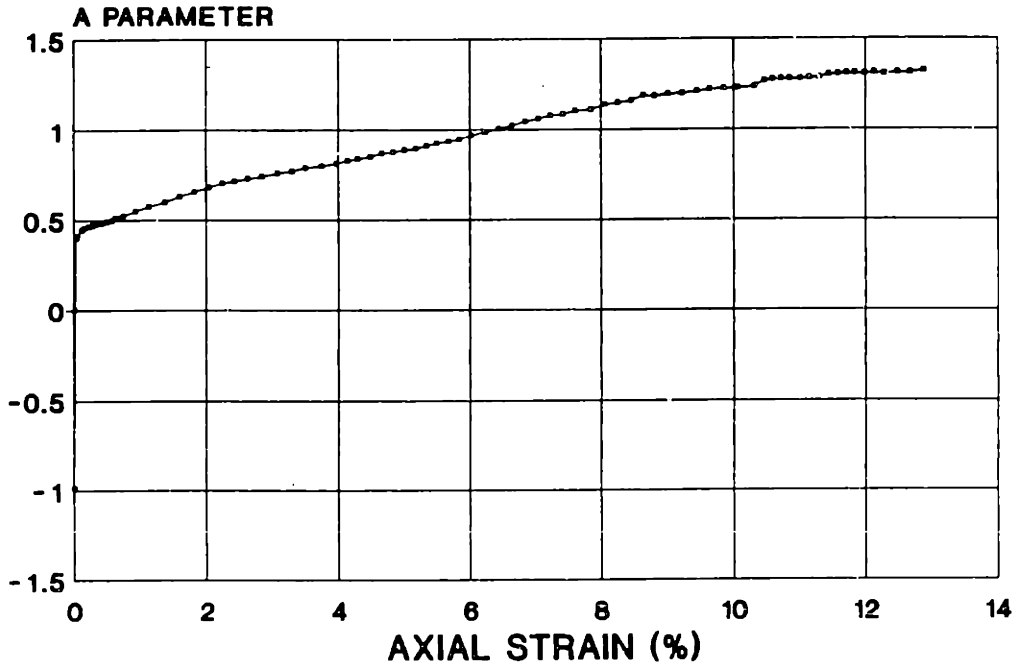

BLOCK S-3A - ELEV. 33.6'

TX052S
PHI VS. AXIAL STRAIN

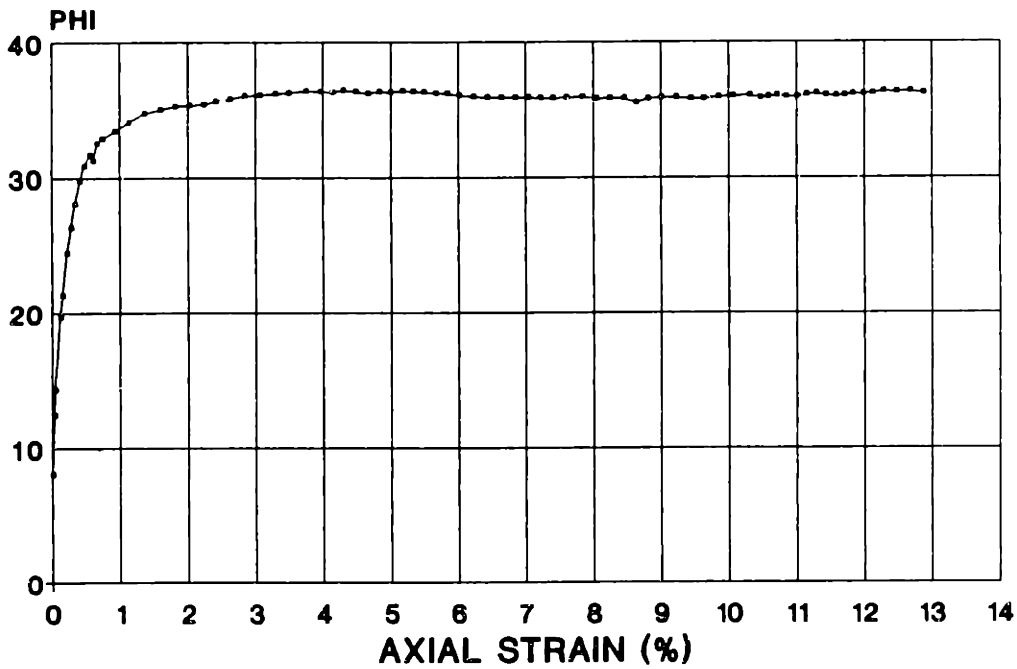

BLOCK S-3A - ELEV. 33.6'

TX053S
STRESS PATH

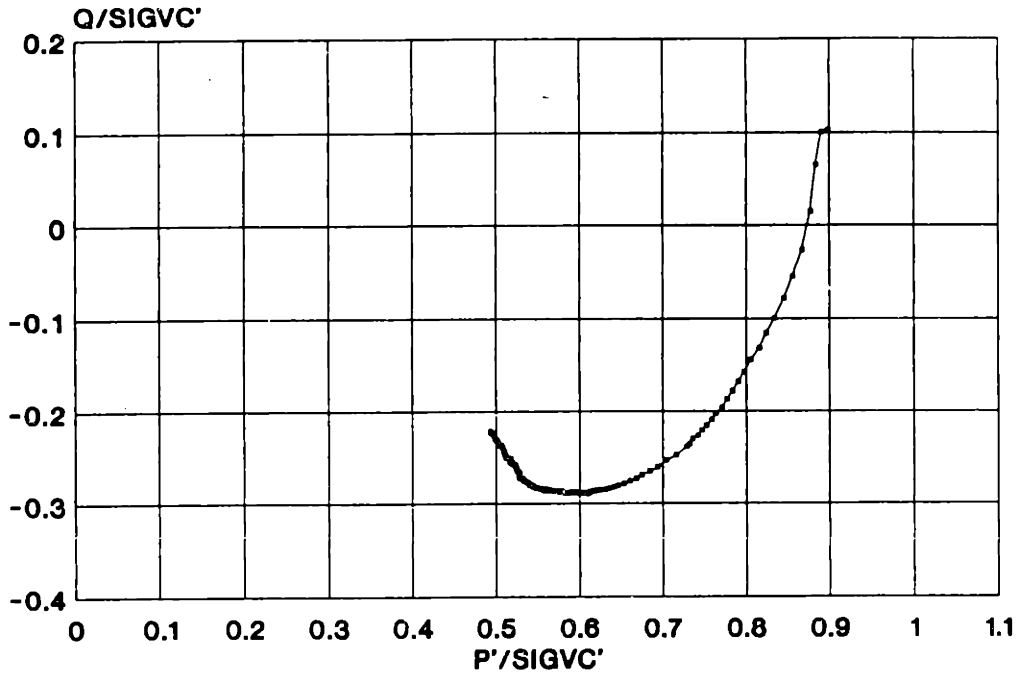

BLOCK S-3A - ELEV. 33.6'

TX053S
STRESS STRAIN

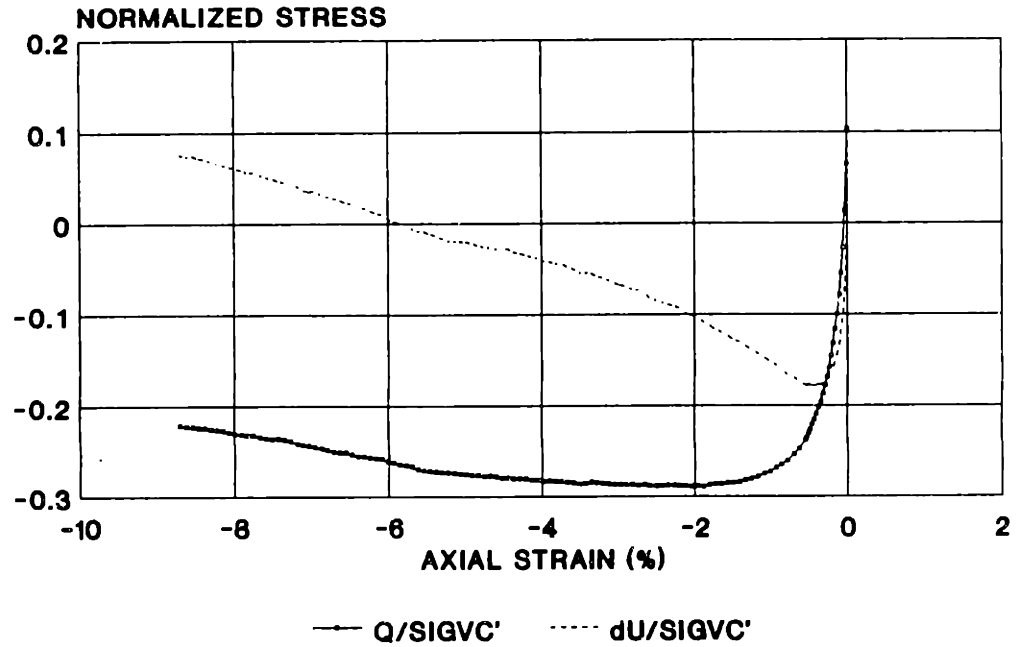

BLOCK S-3A - ELEV. 33.6'

TX053S
A PARAMETER VS. AXIAL STRAIN

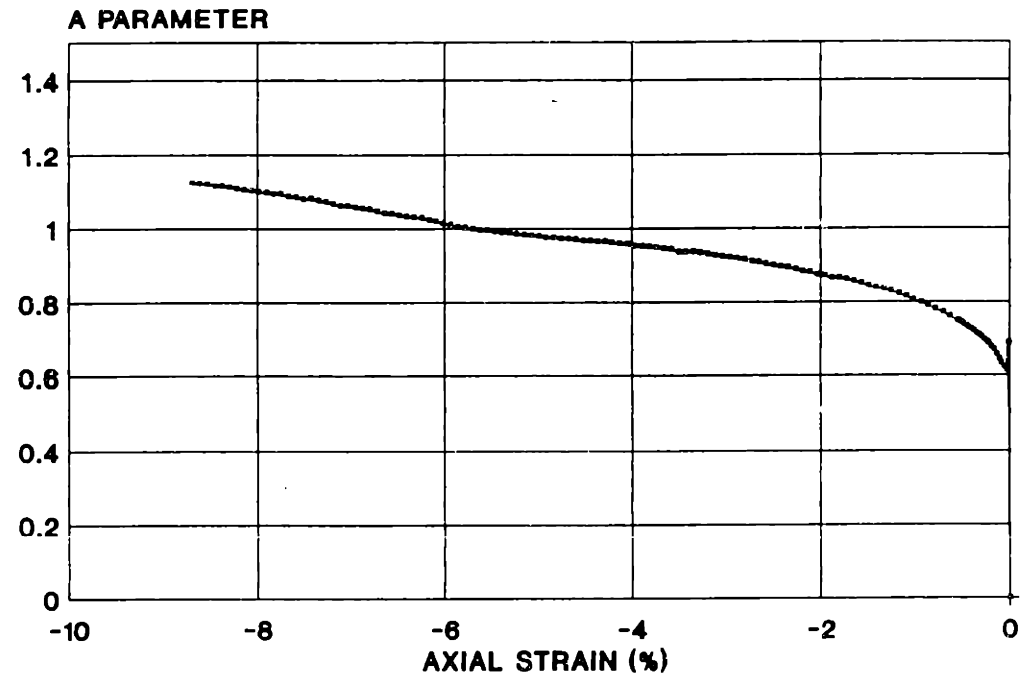

BLOCK S-3A - ELEV. 33.6'

TX053S
PHI VS. AXIAL STRAIN

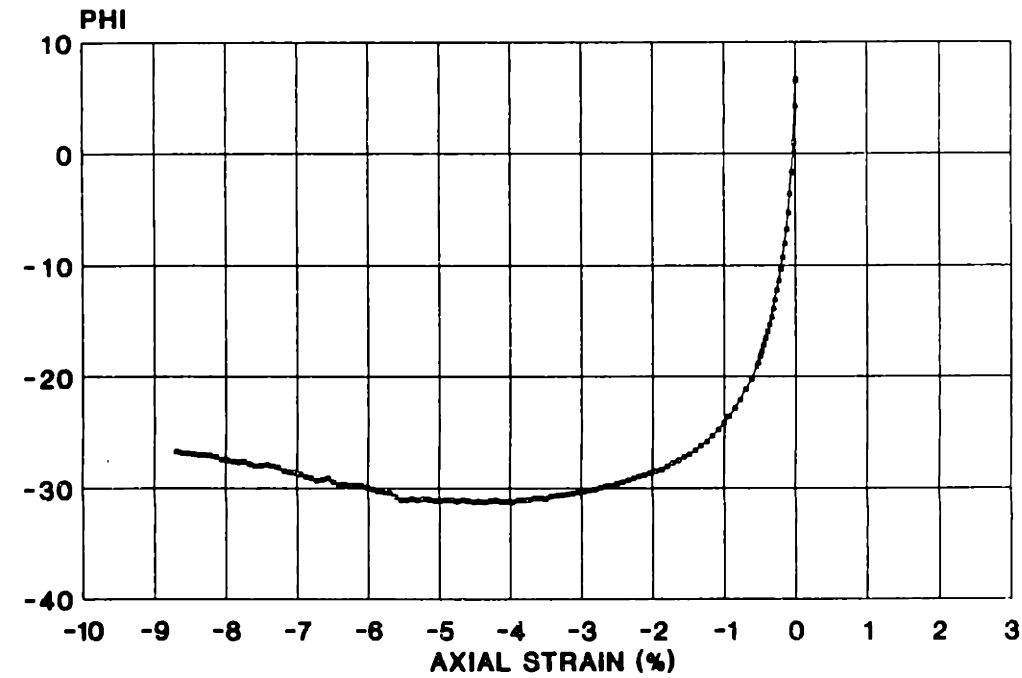

BLOCK S-3A - ELEV. 33.6'

TX056S
STRESS PATH
RECOMPRESSION CKoUC

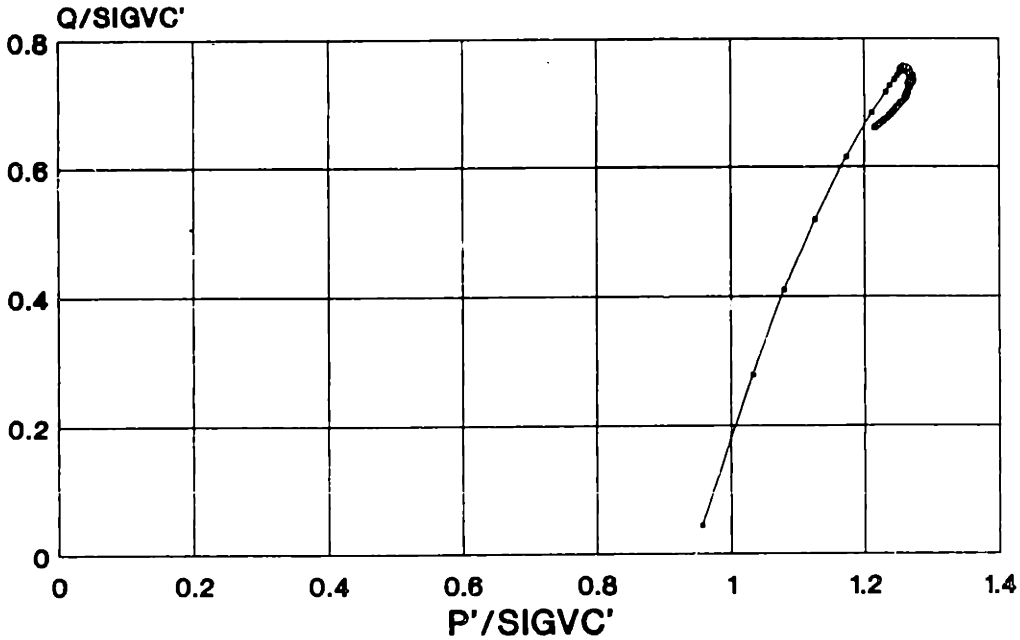

BLOCK S-1A - ELEV. 54.7'

TX056S
STRESS STRAIN
RECOMPRESSION CKoUC

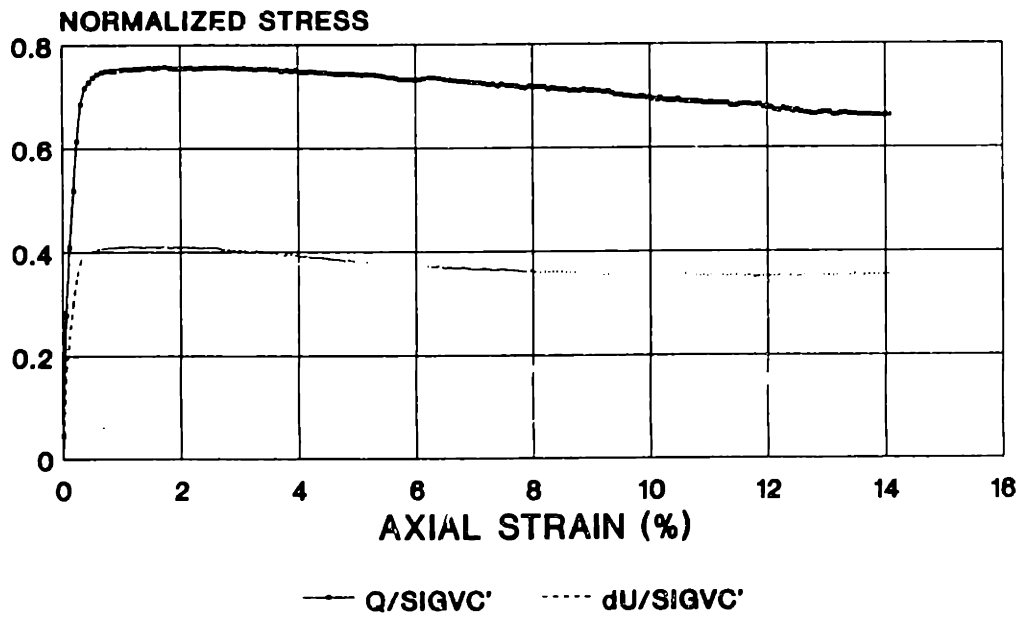

BLOCK S-1A - ELEV. 54.7'

TX056S
A PARAMETER VS. AXIAL STRAIN
RECOMPRESSION CKoUC

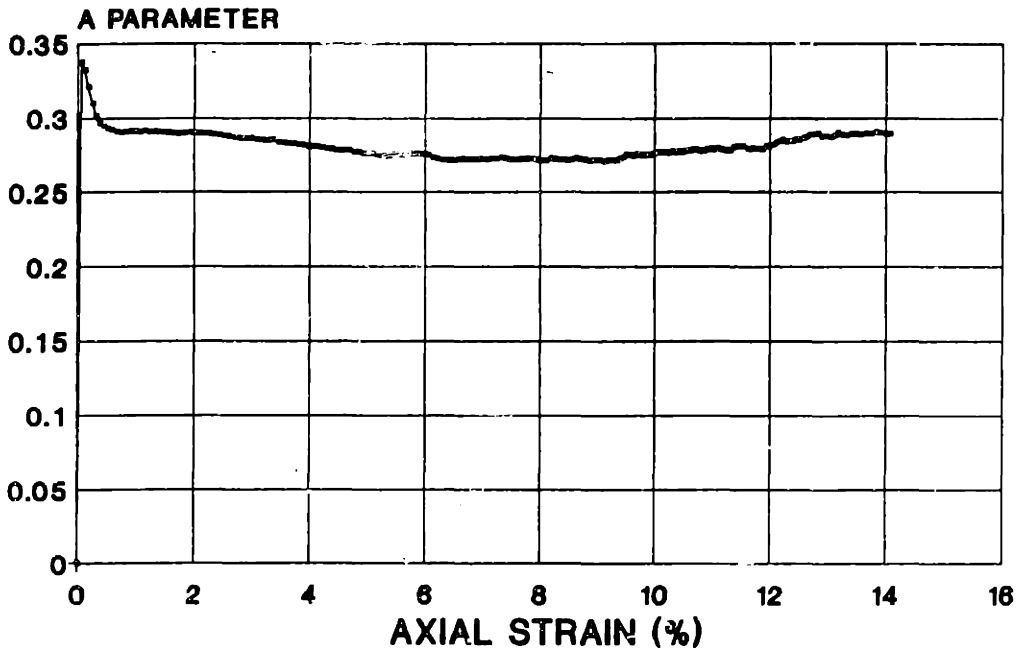

B.S.-1A - ELEV. 54.7

TX056S
PHI VS. AXIAL STRAIN
RECOMPRESSION CKoUC

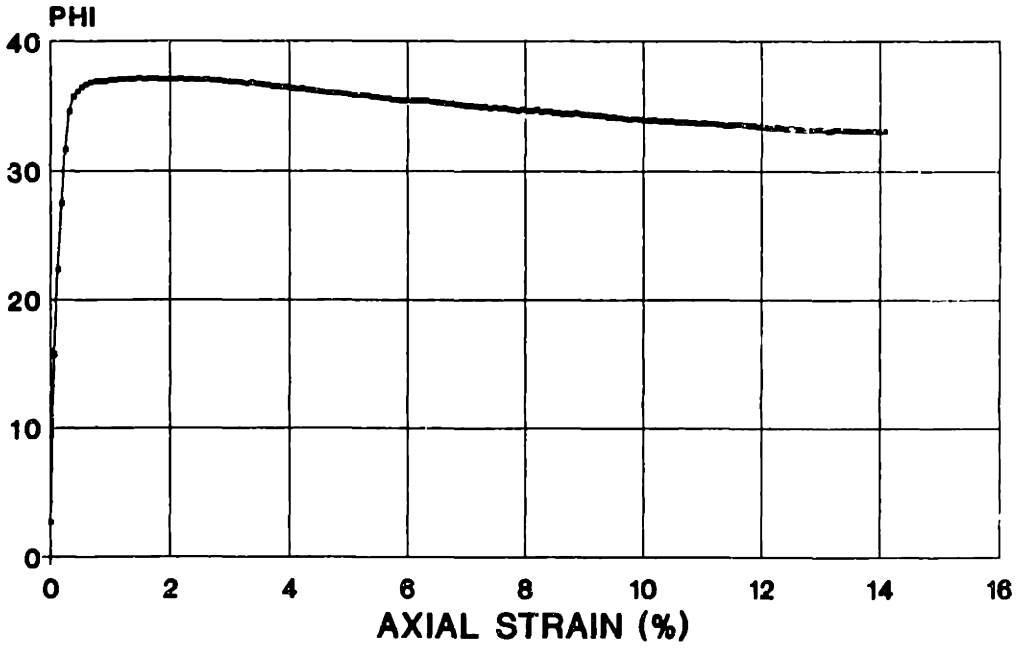

BLOCK S-1A - ELEV. 54.7'

TX057S
STRESS PATH
RECOMPRESSION CKoUC

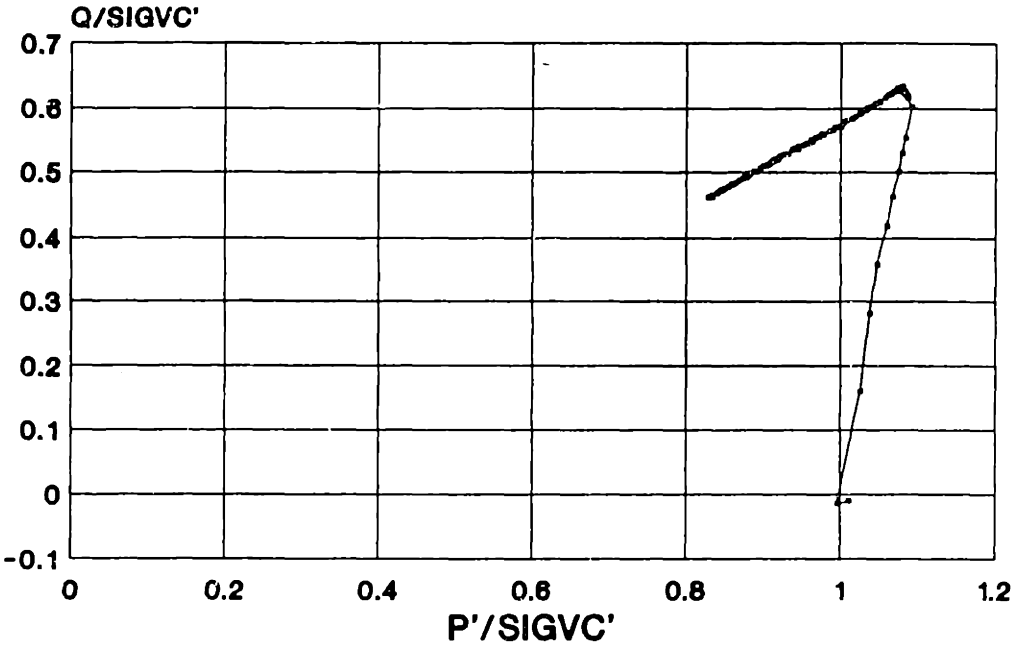

BLOCK S-2 - ELEV. 60.7'

TX057S
STRESS STRAIN
RECOMPRESSION CKoUC

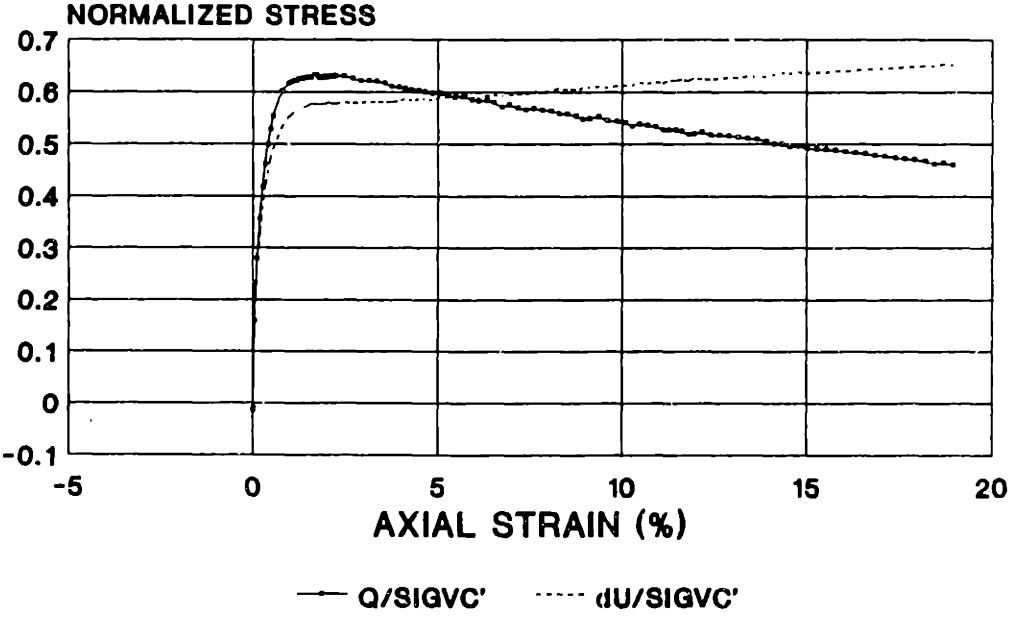

BLOCK S-2 - ELEV. 50.7'

TX057S
A PARAMETER VS. AXIAL STRAIN
RECOMPRESSION CKoUC

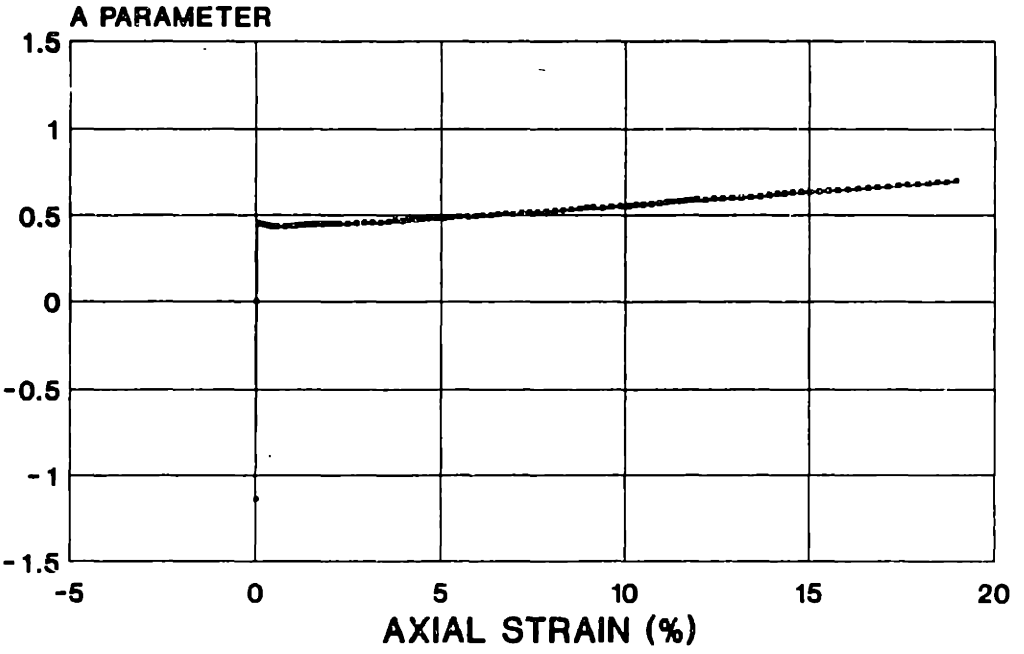

B.S.- 2 ELEV. 60.7

TX057S
PHI VS. AXIAL STRAIN
RECOMPRESSION CKoUC

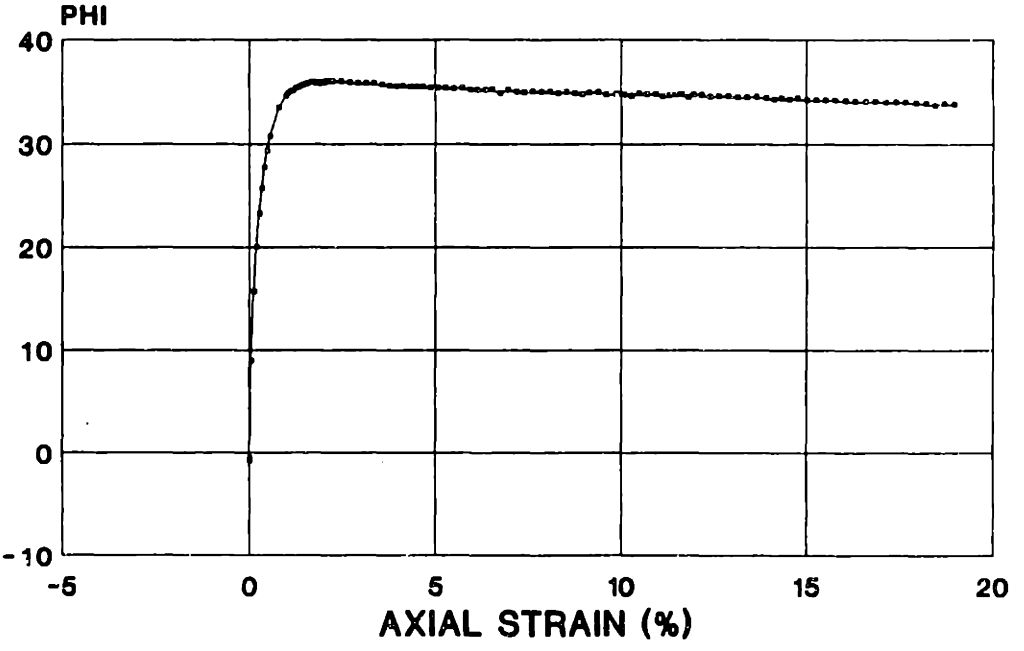

BLOCK S-2 - ELEV. 60.7'

TX058S
STRESS PATH
RECOMPRESSION CKoUC

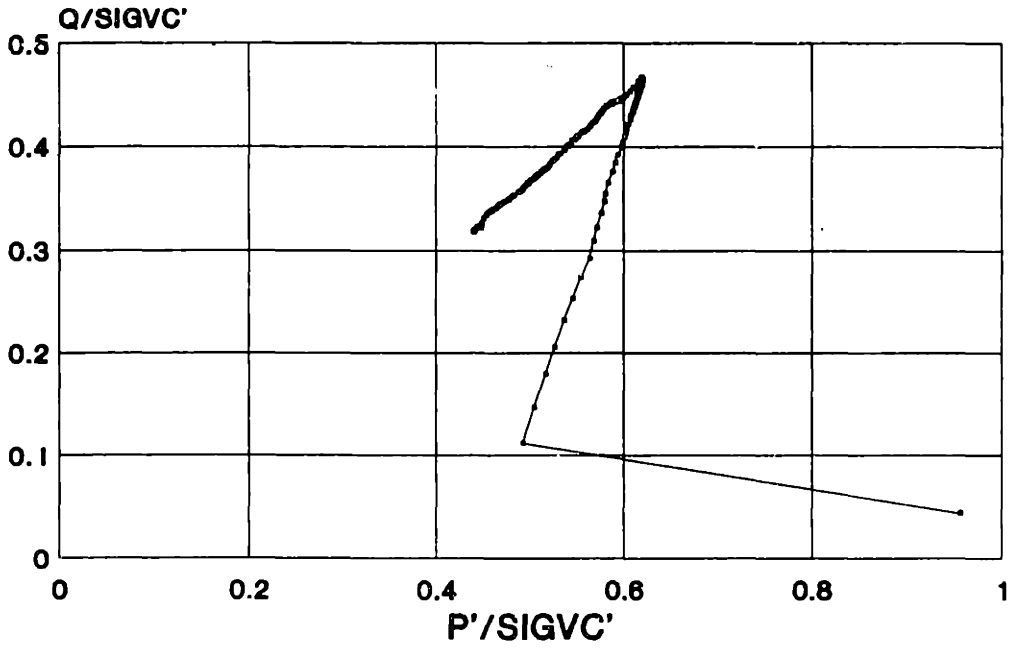

BLOCK S-2A - ELEV. 42.1'

TX058S
STRESS STRAIN
RECOMPRESSION CKoUC

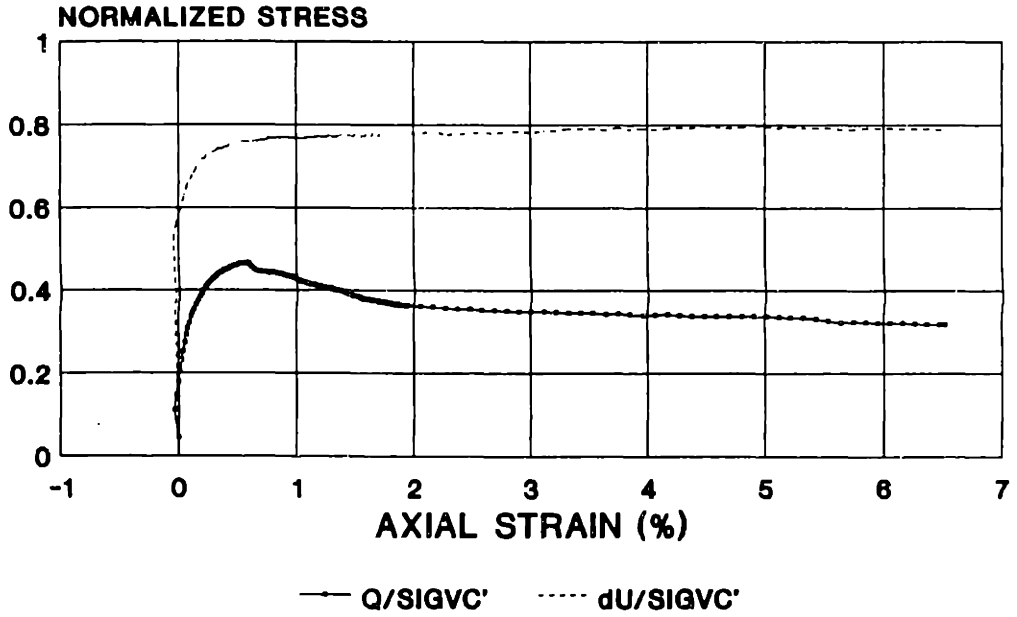

BLOCK S-2A - ELEV. 42.1'

TX058S
A PARAMETER VS. AXIAL STRAIN
RECOMPRESSION CKoUC

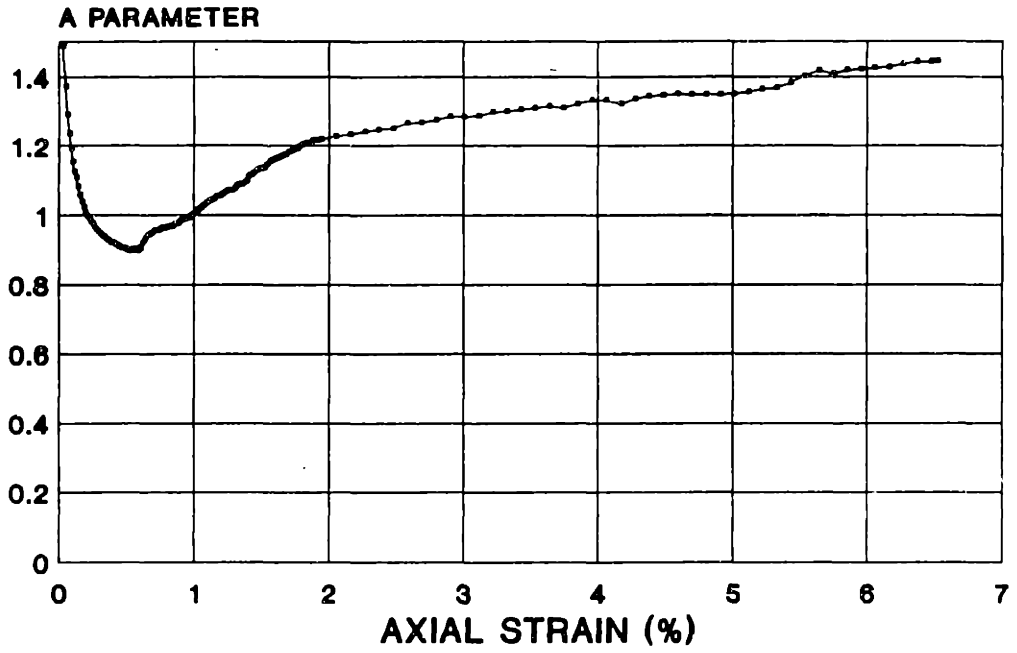

B.S.-2A - ELEV. 42.1

TX058S
PHI VS. AXIAL STRAIN
RECOMPRESSION CKoUC

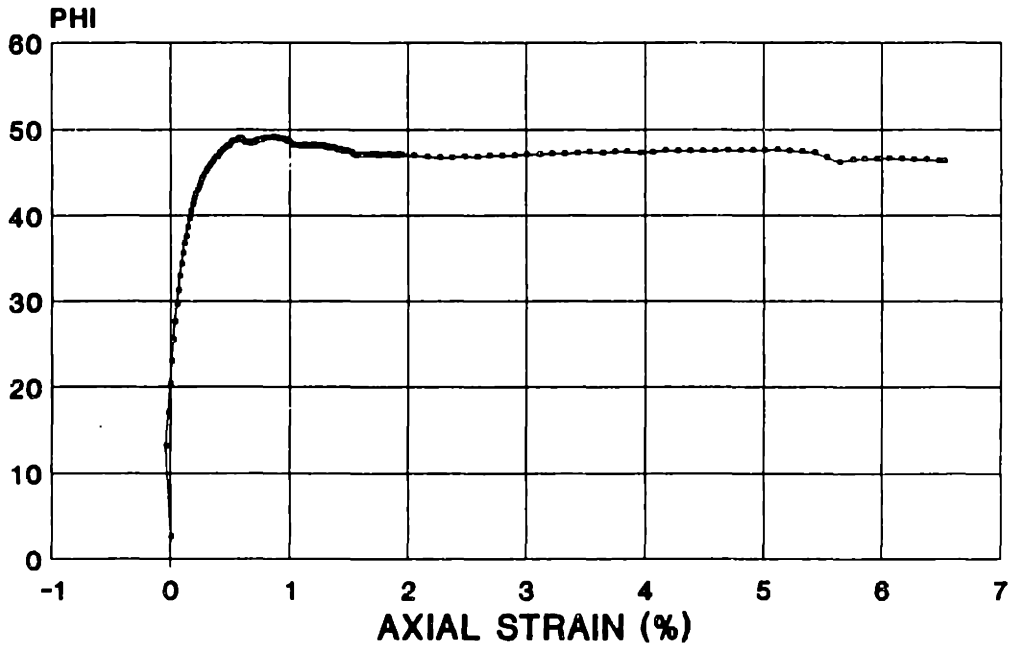

BLOCK S-2A - ELEV. 42.1'

TX059S
STRESS PATH
RECOMPRESSION CKoUC

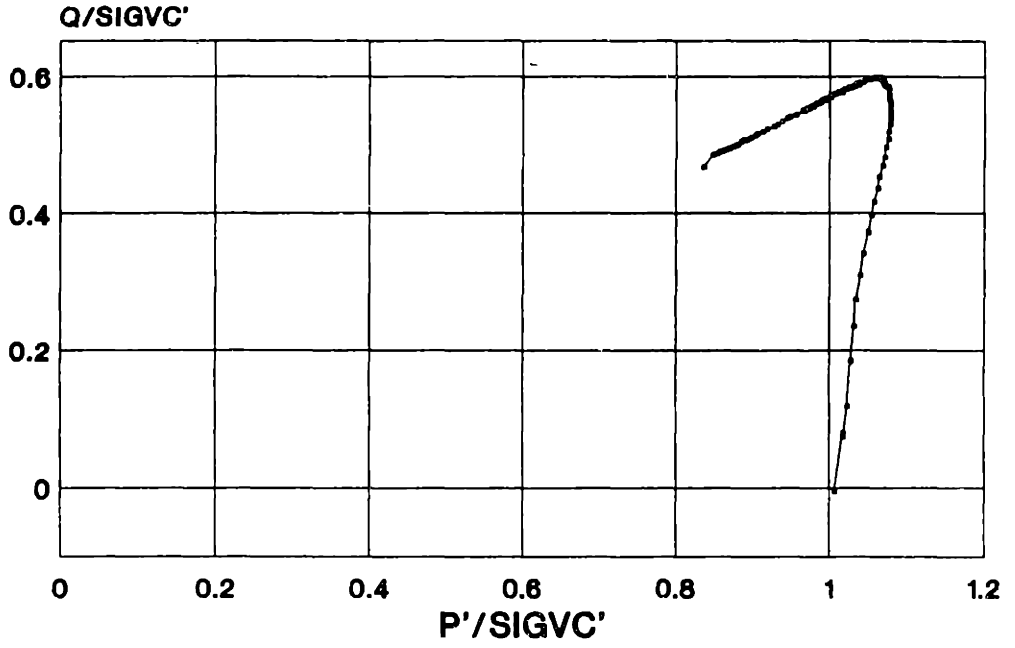

BLOCK S-2 - ELEV. 60.7'

TX059S
STRESS STRAIN
RECOMPRESSION CKoUC

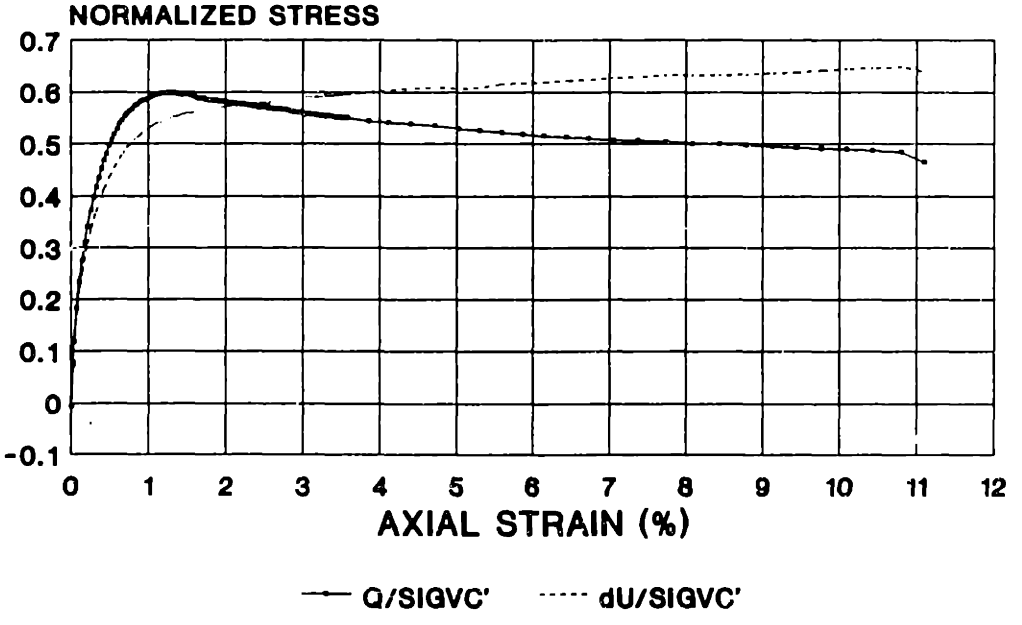

BLOCK S-2 - ELEV. 60.7'

TX059S
A PARAMETER VS. AXIAL STRAIN
RECOMPRESSION CKoUC

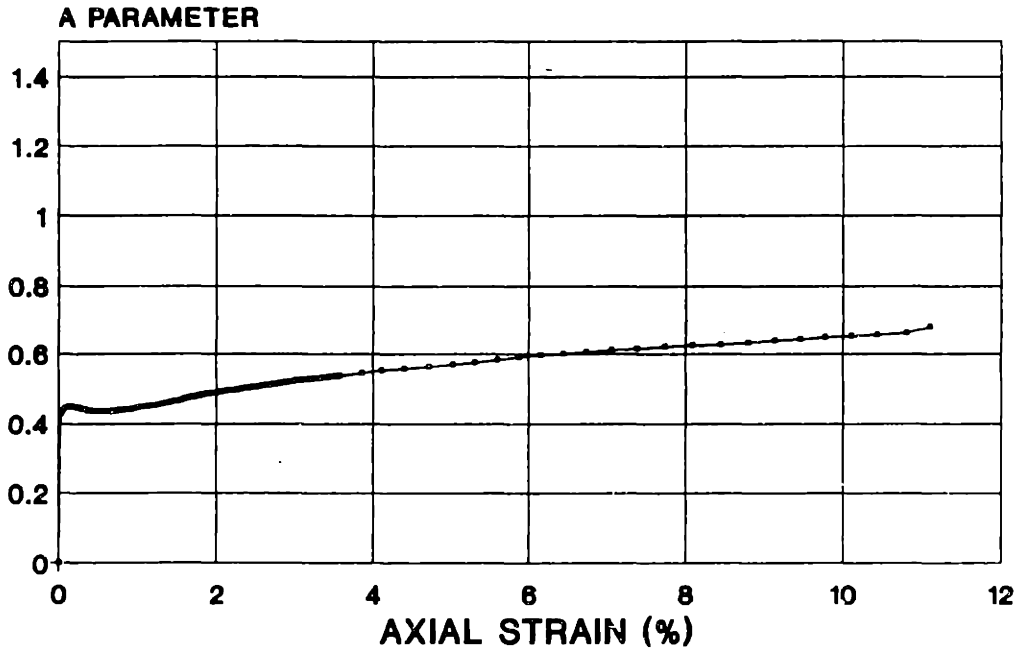

BLOCK S-2 - ELEV. 60.7'

TX059S
PHI VS. AXIAL STRAIN
RECOMPRESSION CKoUC

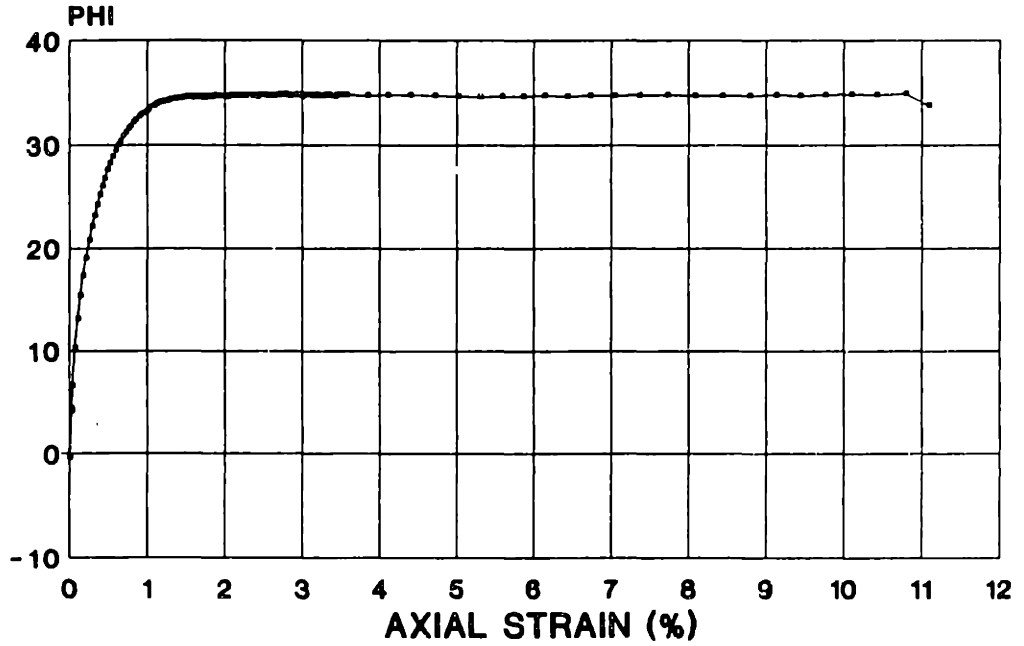

BLOCK S-2 - ELEV. 60.7'

TX062S
STRESS PATH
RECOMPRESSION CKoUC

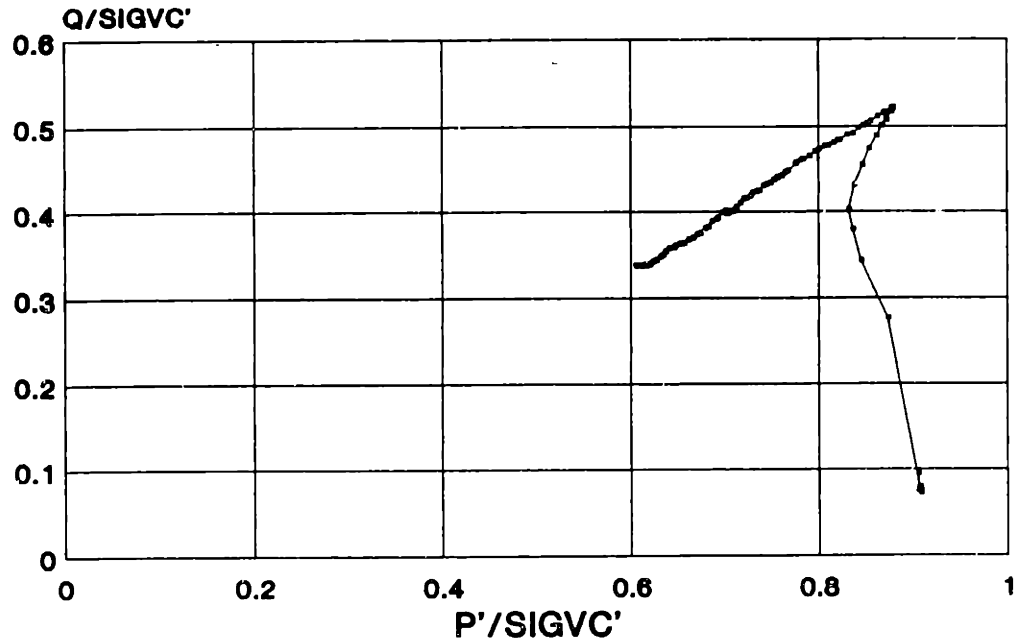

SB2-23 U12 - ELEV. 37.8'

TX062S
STRESS STRAIN
RECOMPRESSION CKoUC

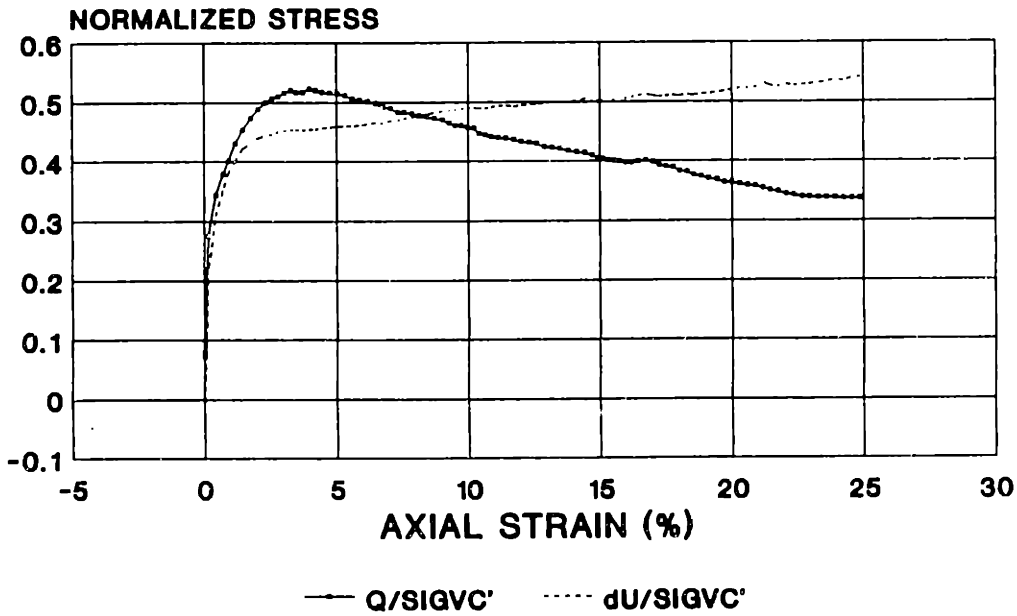

SB2-23 U12 - ELEV. 37.8'

TX062S
A PARAMETER VS. AXIAL STRAIN
RECOMPRESSION CKoUC

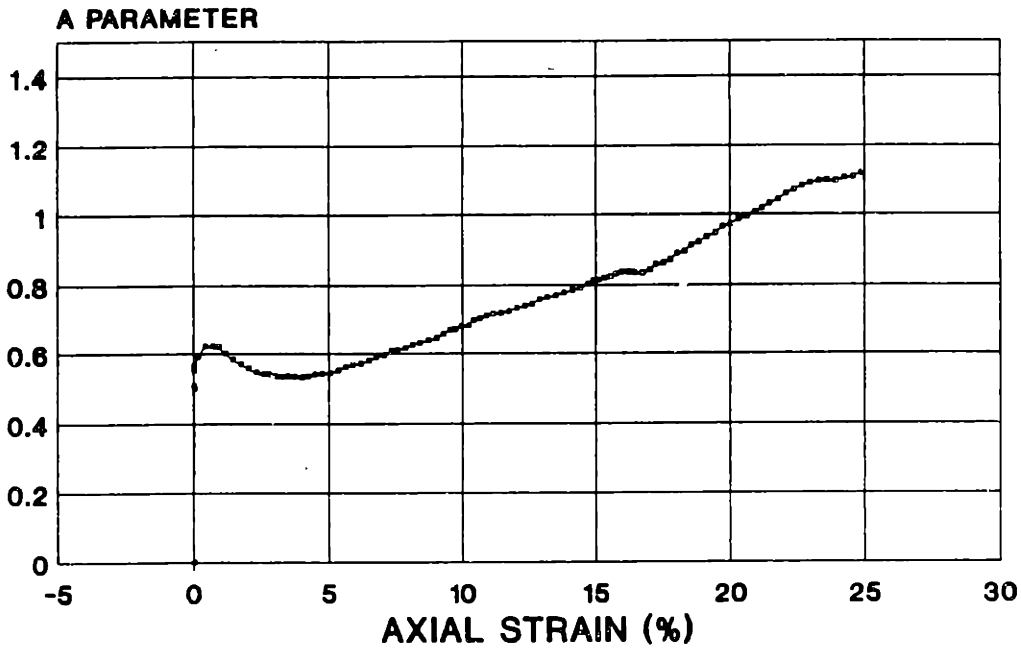

SB2-23 U12 ELEV. 37.8'

TX062S
PHI VS. AXIAL STRAIN
RECOMPRESSION CKoUC

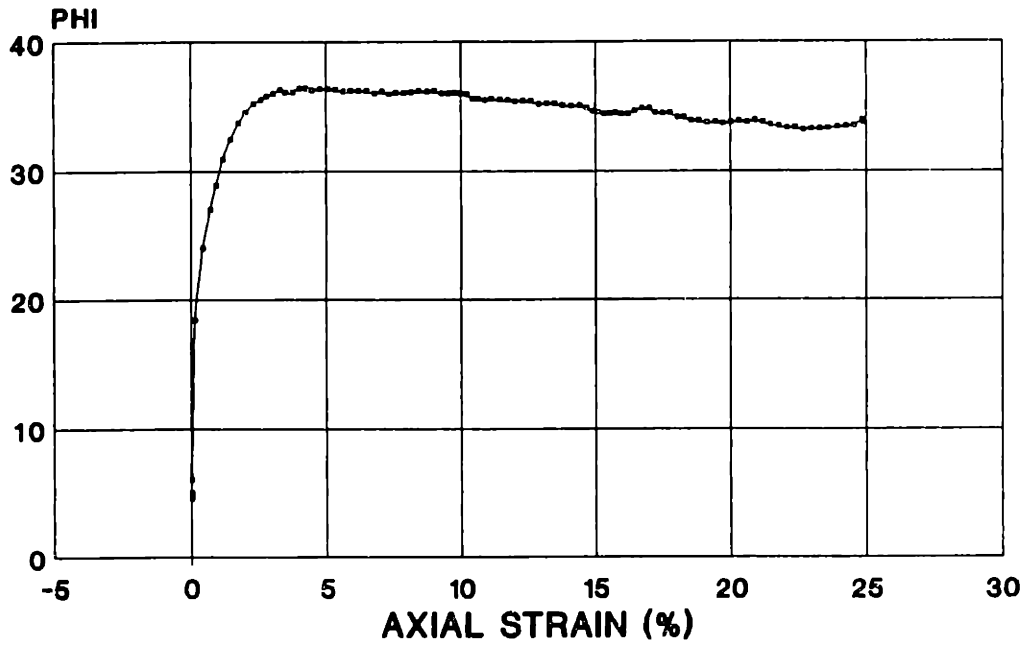

SB2-23 U12 - ELEV. 37.8'

TX063S
STRESS PATH
RECOMPRESSION CKoUC

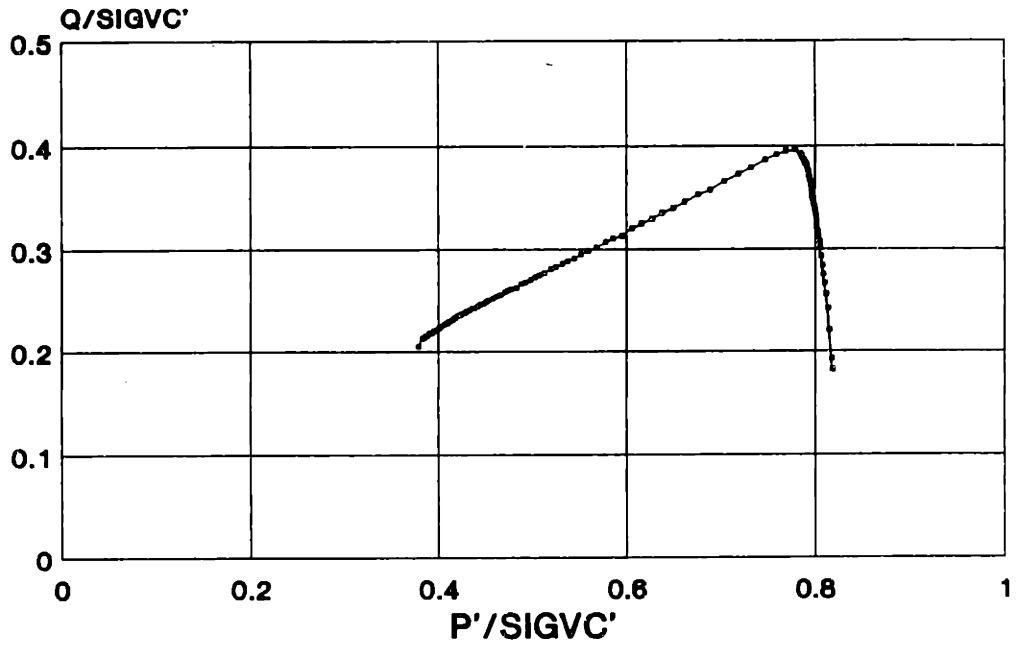

SB2-23 U15 - ELEV. 21.1'

TX063S
STRESS STRAIN
RECOMPRESSION CKoUC

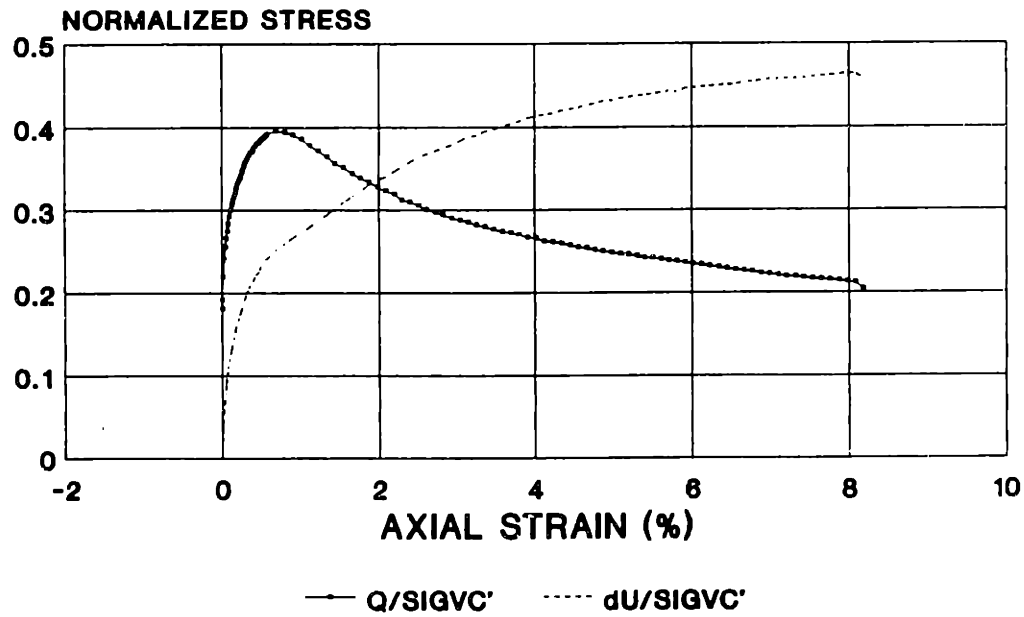

SB2-23 U15 - ELEV. 21.1'

TX063S
A PARAMETER VS. AXIAL STRAIN
RECOMPRESSION CKoUC

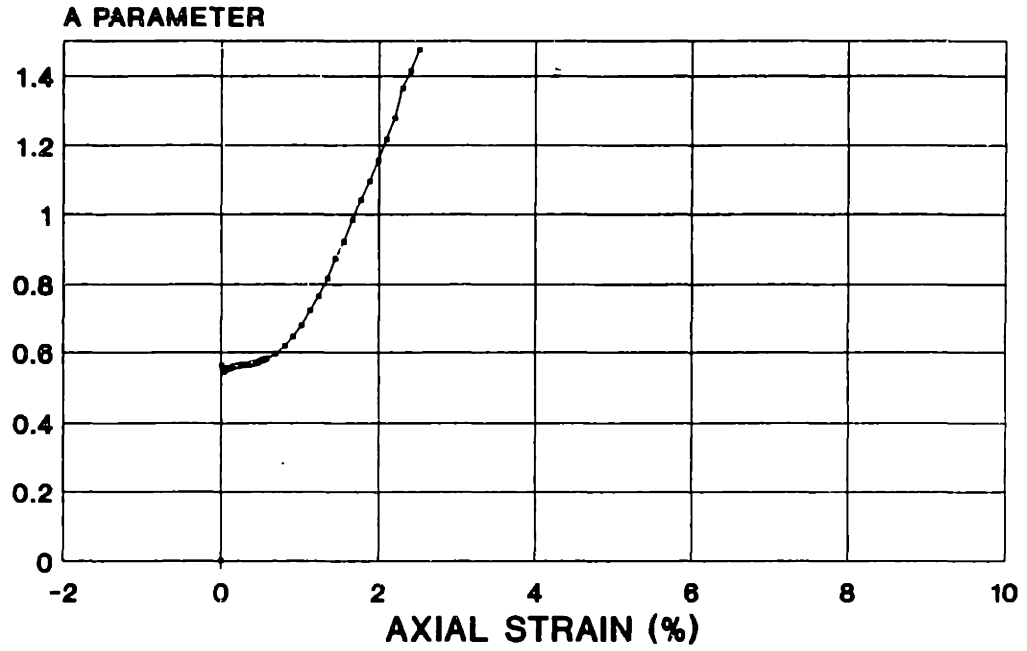

SB2-23 U16 ELEV. 21.1'

TX063S
PHI VS. AXIAL STRAIN
RECOMPRESSION CKoUC

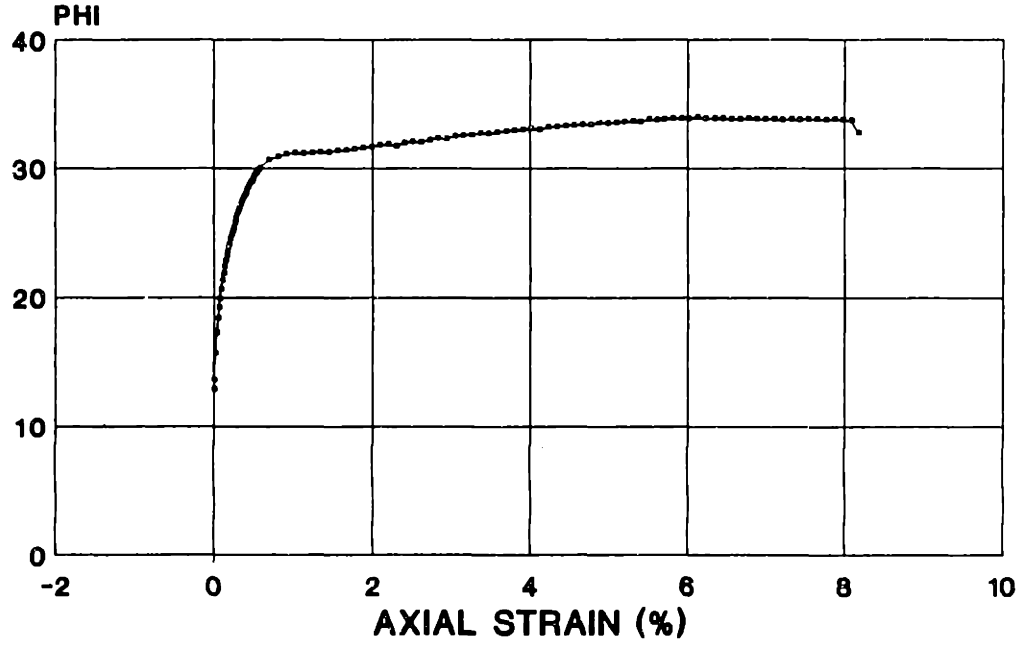

SB2-23 U15 - ELEV. 21.1'

TX064S
STRESS PATH
RECOMPRESSION CKoUC

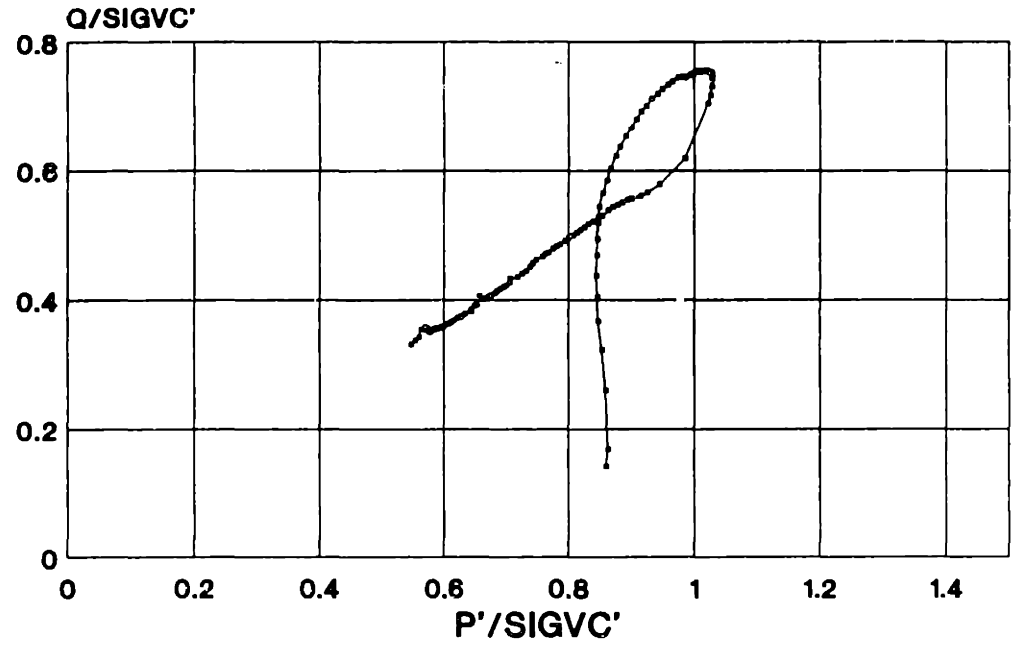

BLOCK S-7 - ELEV. 20.9'

TX064S
STRESS STRAIN
RECOMPRESSION CKoUC

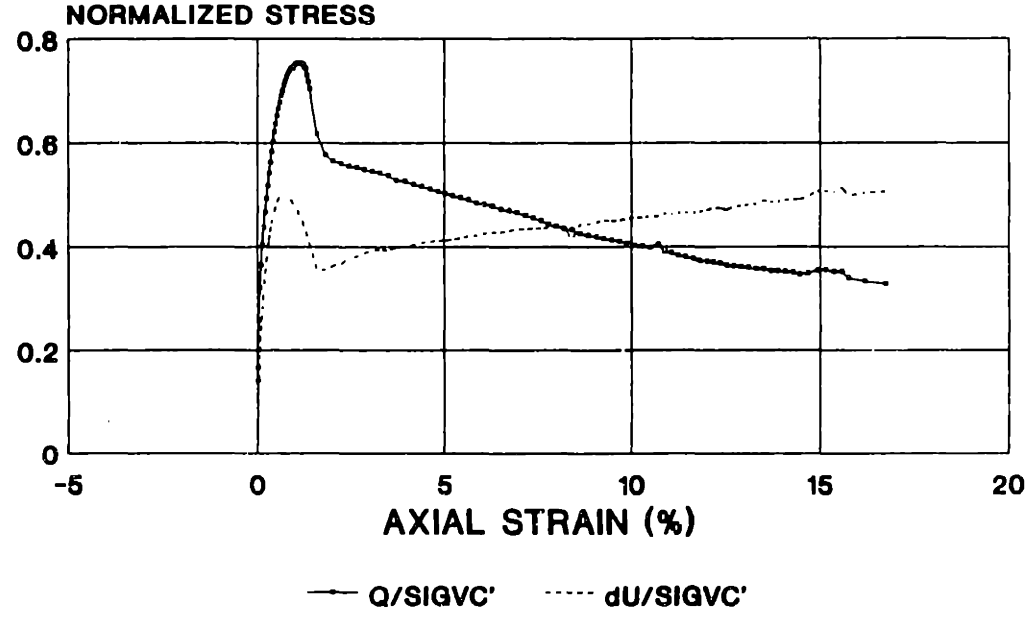

BLOCK S-7 - ELEV. 20.9'

TX064S
A PARAMETER VS. AXIAL STRAIN
RECOMPRESSION CKoUC

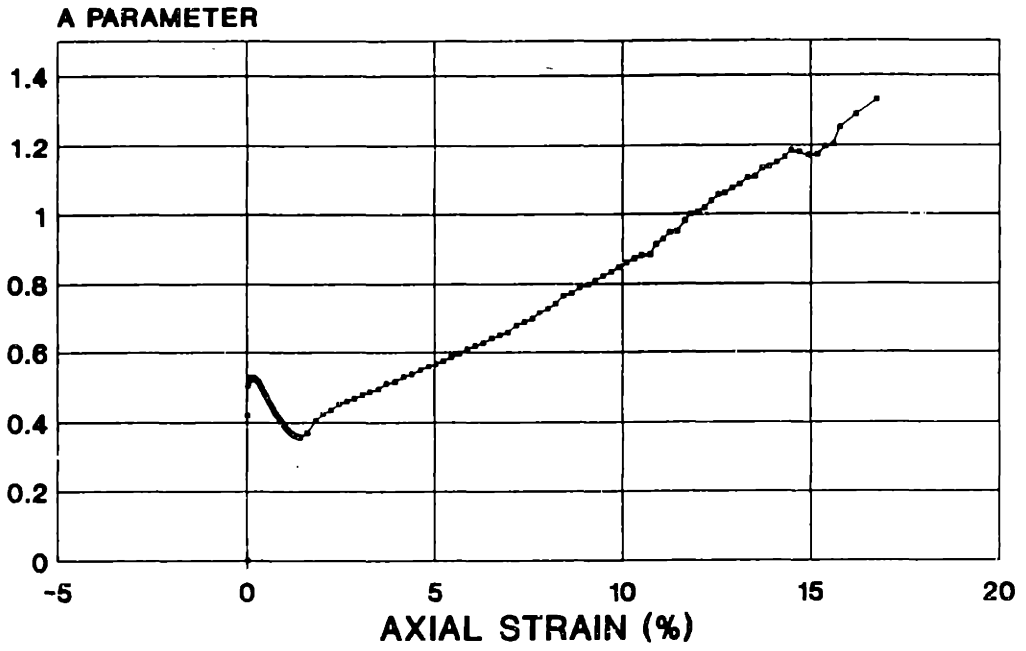

B.S.-7 - ELEV. 20.9'

TX064S
PHI VS. AXIAL STRAIN
RECOMPRESSION CKoUC

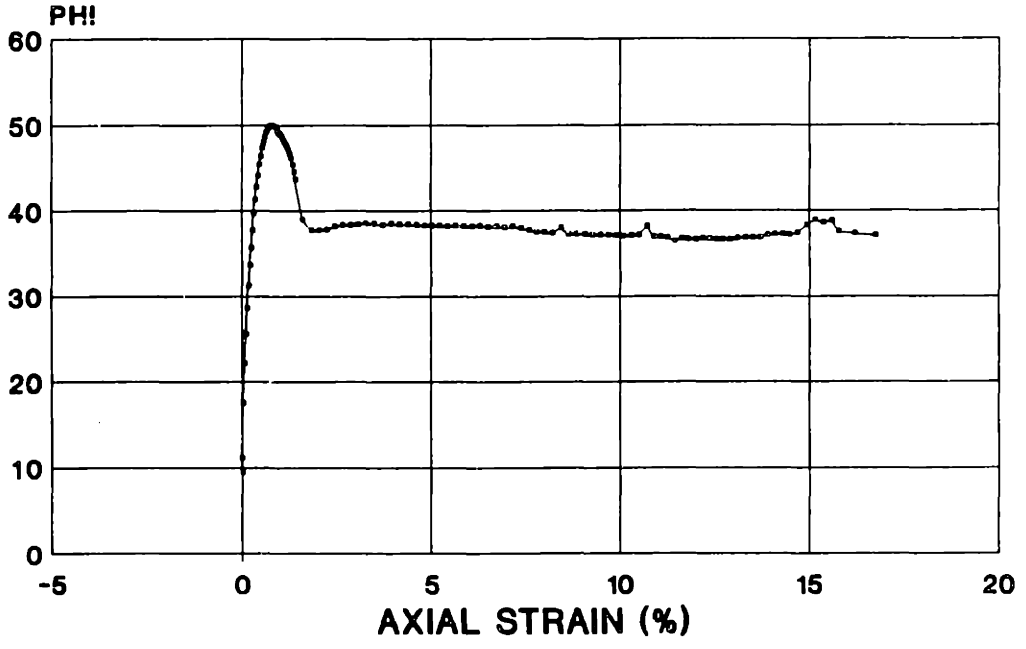

BLOCK S-7 - ELEV. 20.9'

TX066S
STRESS PATH
RECOMPRESSION CKoUC

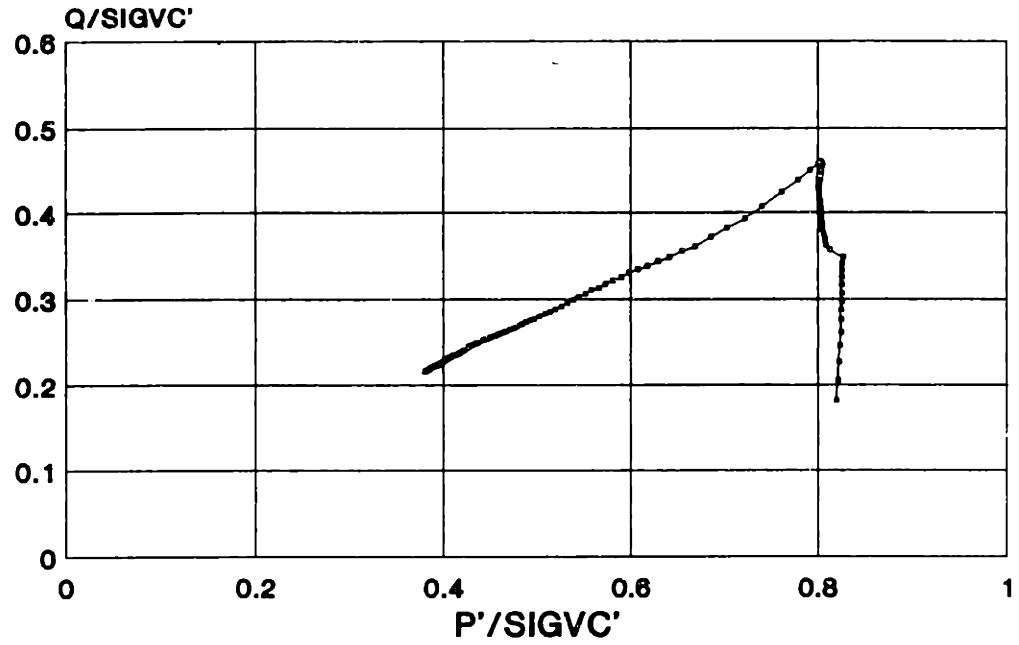

BLOCK S-7 - ELEV. 20.9'

TX066S
STRESS STRAIN
RECOMPRESSION CKoUC

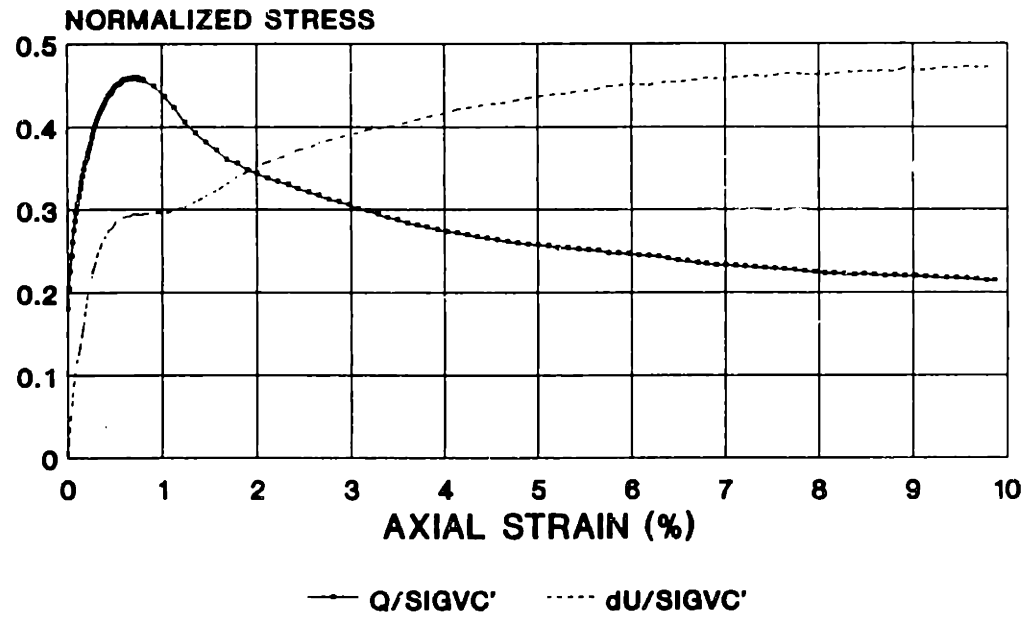

BLOCK S-7 - ELEV. 20.9'

TX066S
A PARAMETER VS. AXIAL STRAIN
RECOMPRESSION CKoUC

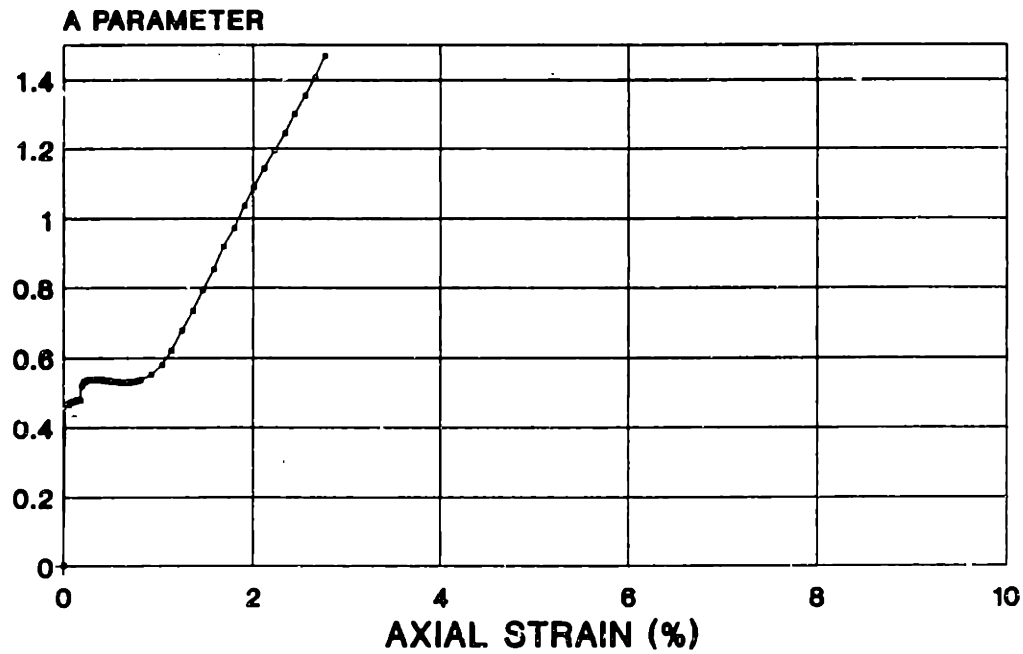

B.S.-7 - ELEV. 20.9'

TX066S
PHI VS. AXIAL STRAIN
RECOMPRESSION CKoUC

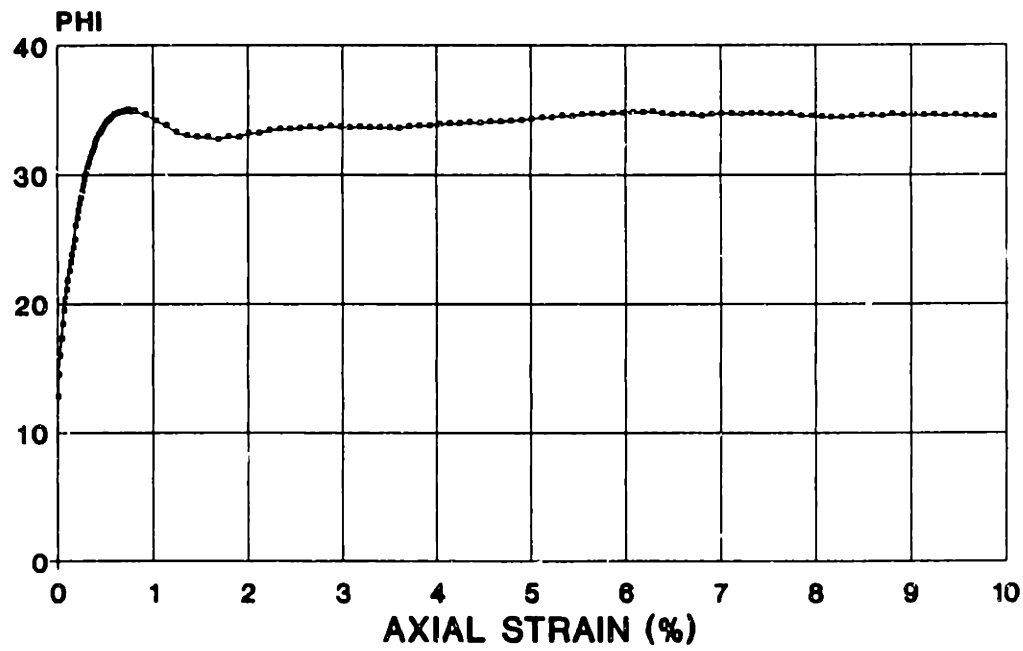

BLOCK S-7 - ELEV. 20.9'

TX068S
STRESS PATH
RECOMPRESSION CKoUC

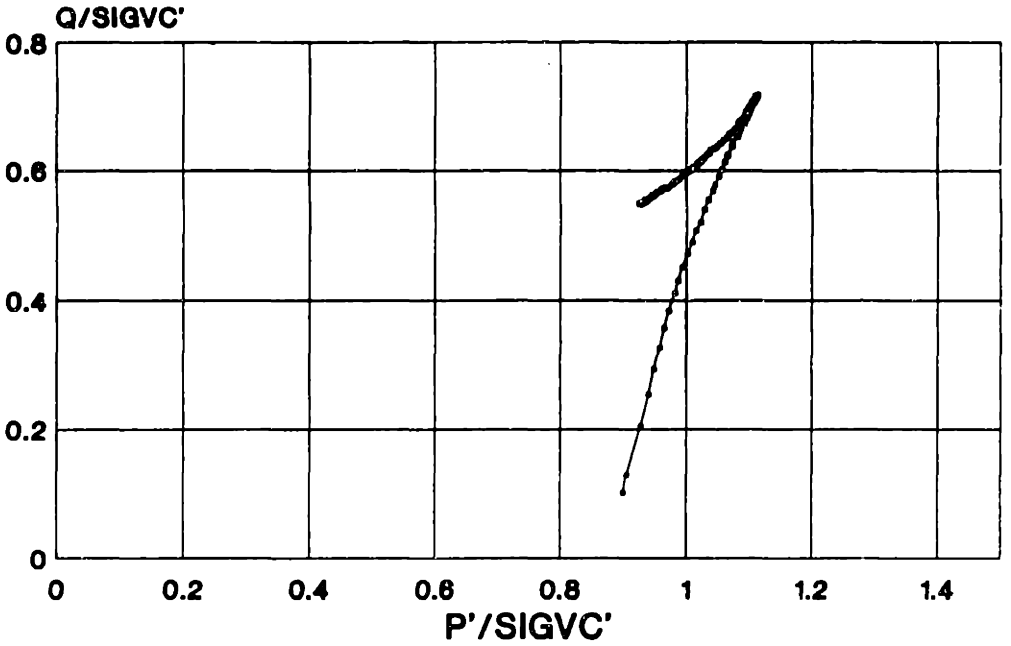

BLOCK S-2A - ELEV. 42.1'

TX068S
STRESS STRAIN
RECOMPRESSION CKoUC

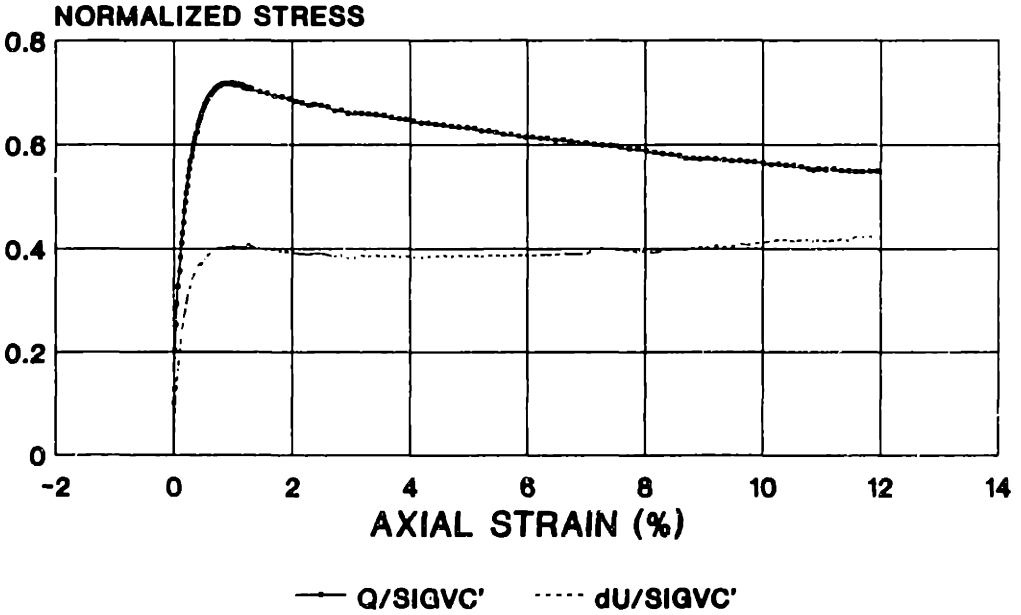

BLOCK S-2A - ELEV. 42.1'

TX068S
A PARAMETER VS. AXIAL STRAIN
RECOMPRESSION CKoUC

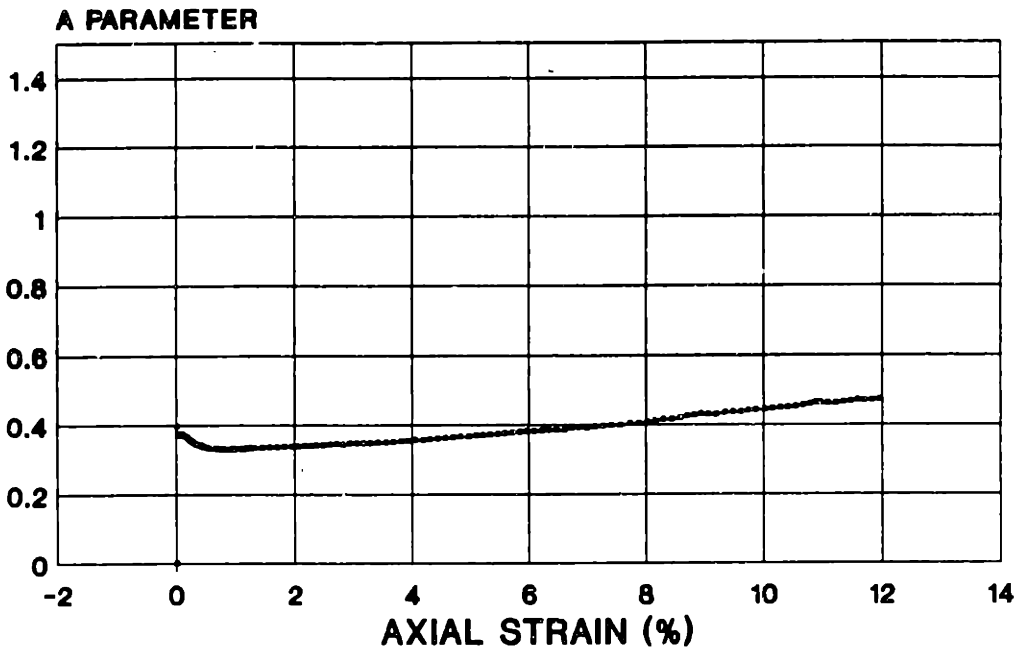

BLOCK-2A - ELEV. 42.1'

TX068S
PHI VS. AXIAL STRAIN
RECOMPRESSION CKoUC

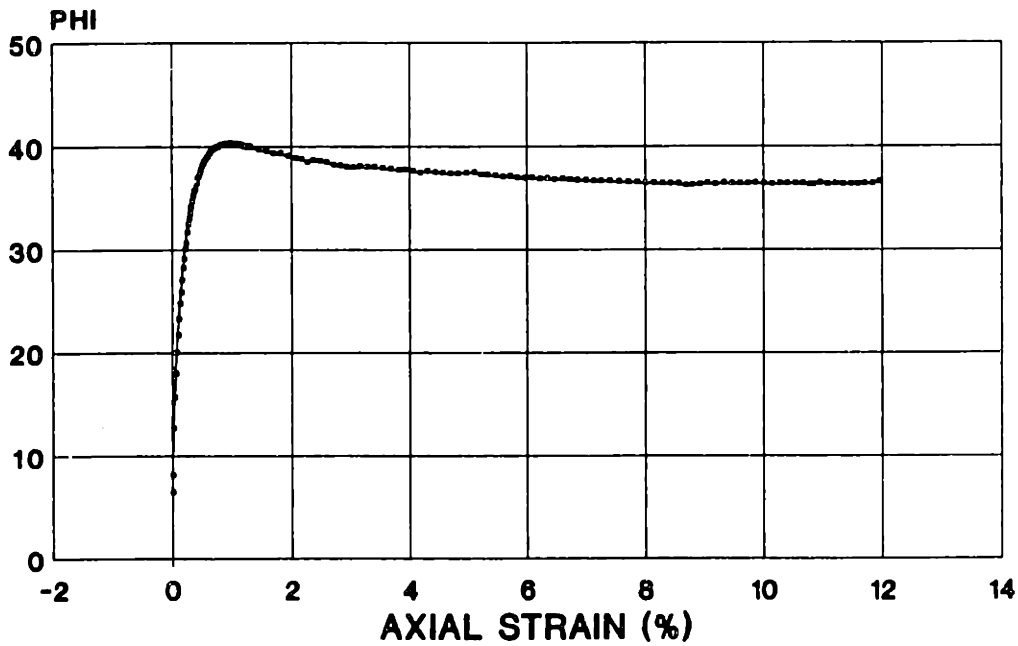

BLOCK S-2A - ELEV. 42.1'

TX069S
STRESS PATH
RECOMPRESSION CKoUC

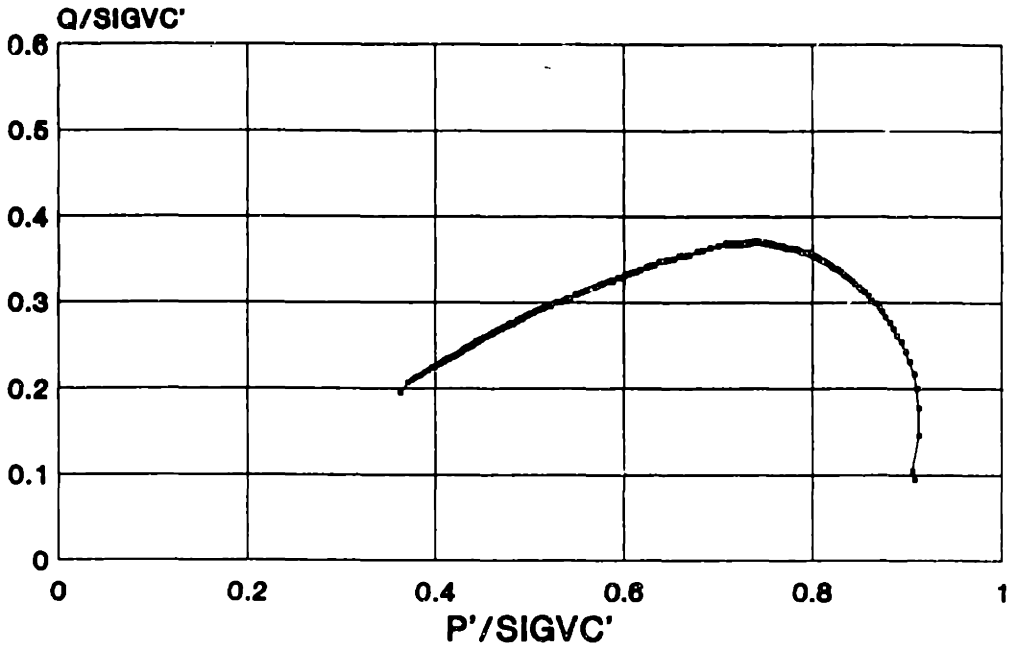

BLOCK S-2A - ELEV. 42.1'

TX069S
STRESS STRAIN
RECOMPRESSION CKoUC

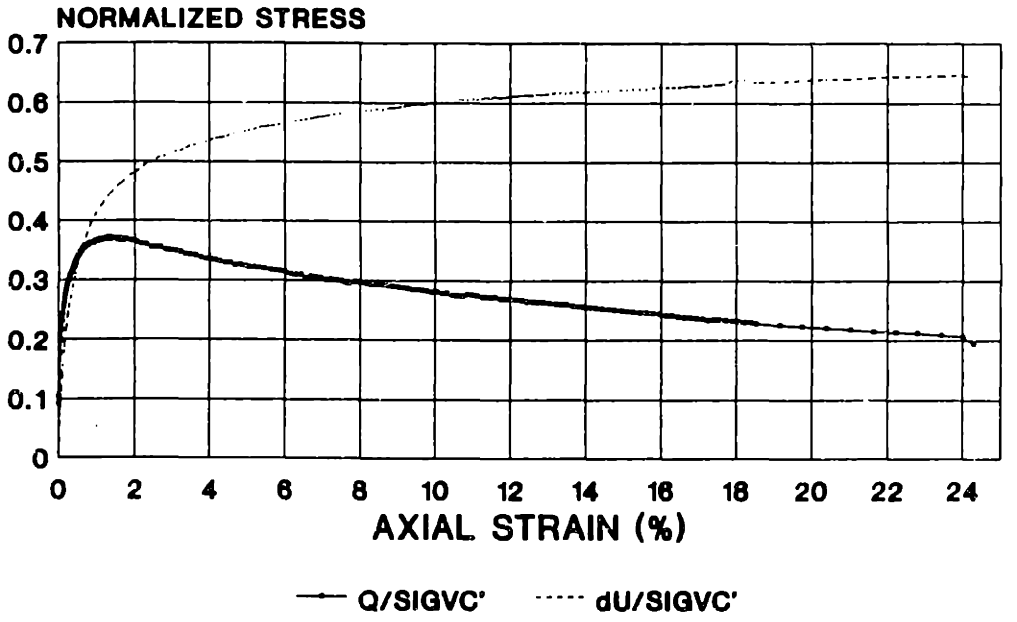

BLOCK S-2A - ELEV. 42.1'

TX069S
A PARAMETER VS. AXIAL STRAIN
RECOMPRESSION CKoUC

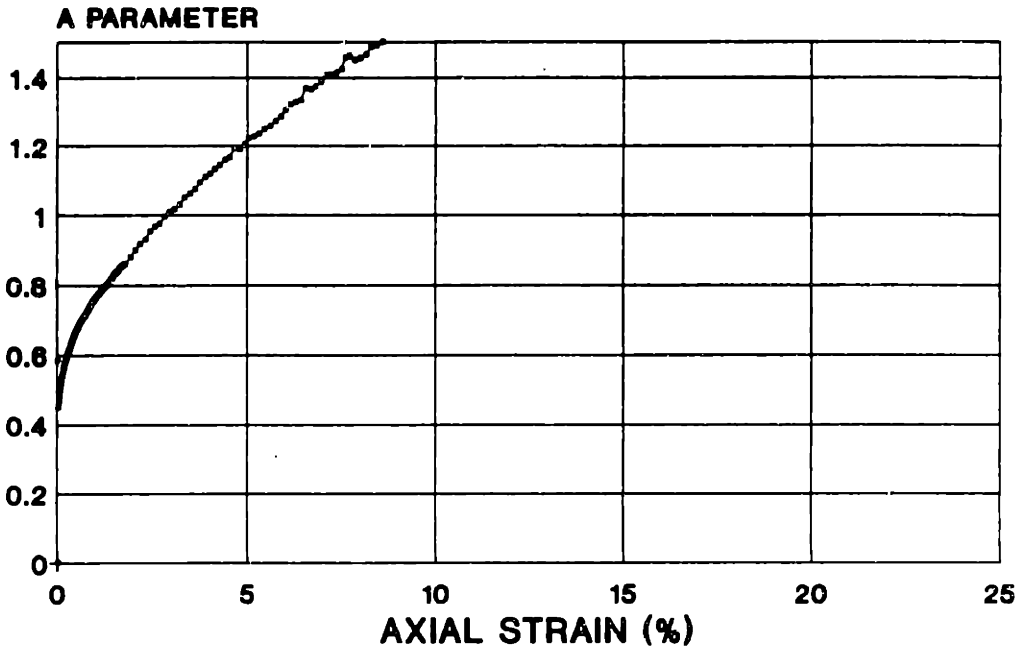

B.S.-2A - ELEV. 42.1'

TX069S
PHI VS. AXIAL STRAIN
RECOMPRESSION CKoUC

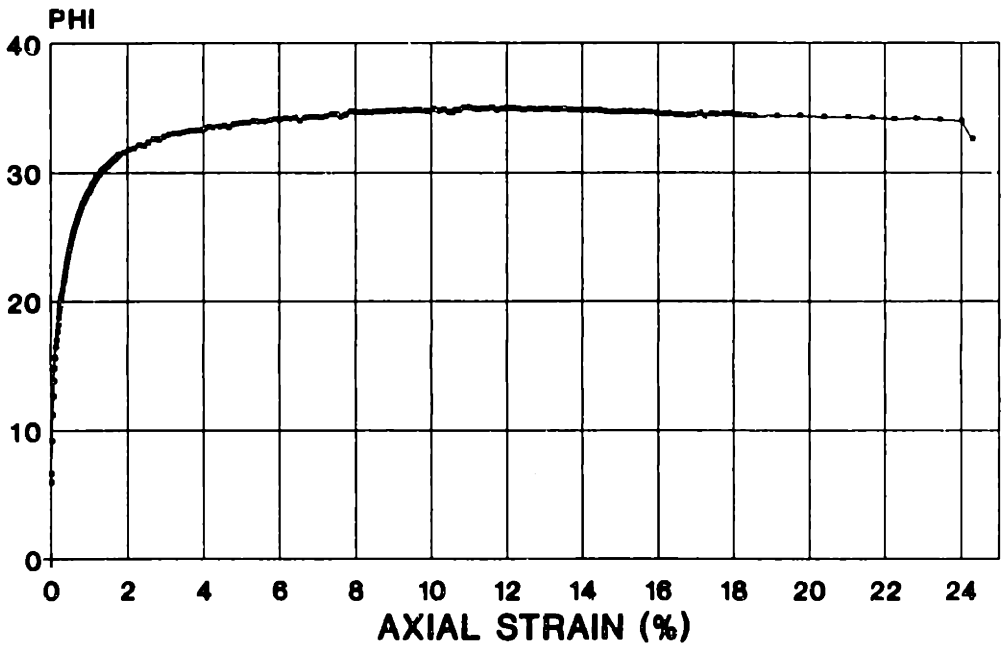

BLOCK S-2A - ELEV. 54.7'

TX070S
STRESS PATH
RECOMPRESSION CKoUE

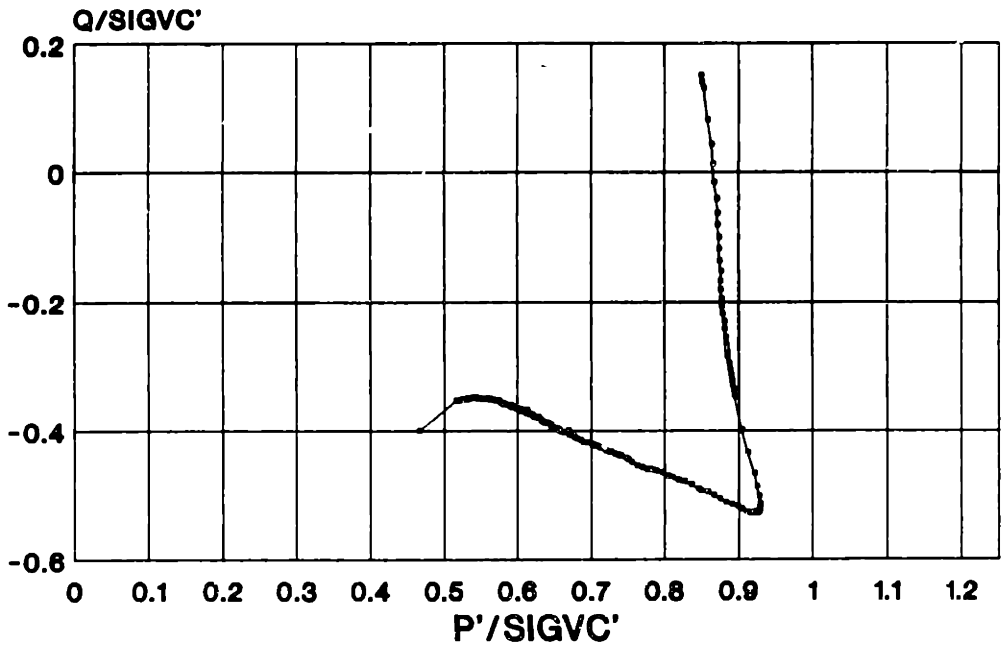

BLOCK S-7 - ELEV. 20.9'

TX070S
STRESS STRAIN
RECOMPRESSION CKoUE

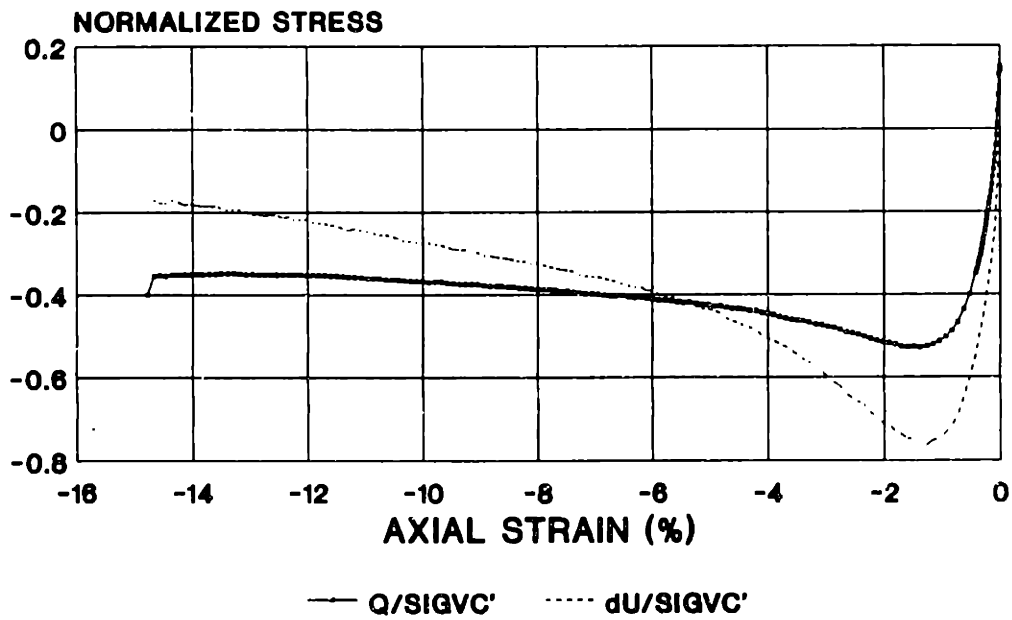

BLOCK S-7 - ELEV. 20.9'

TX070S
A PARAMETER VS. AXIAL STRAIN
RECOMPRESSION CKoUE

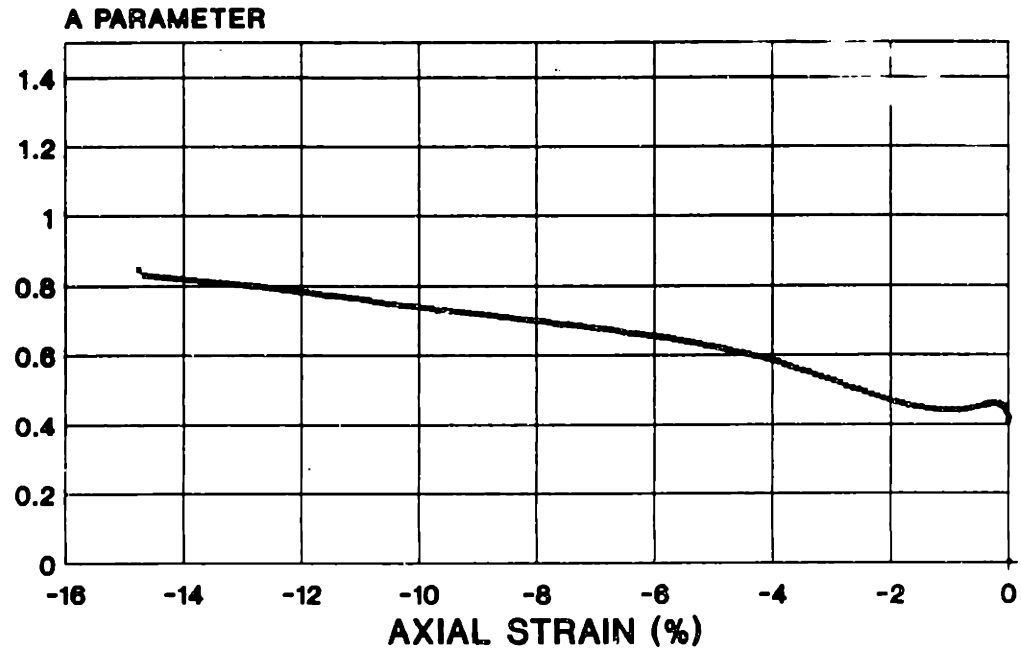

B.S.-7 - ELEV. 20.9'

TX070S
PHI VS. AXIAL STRAIN
RECOMPRESSION CKoUE

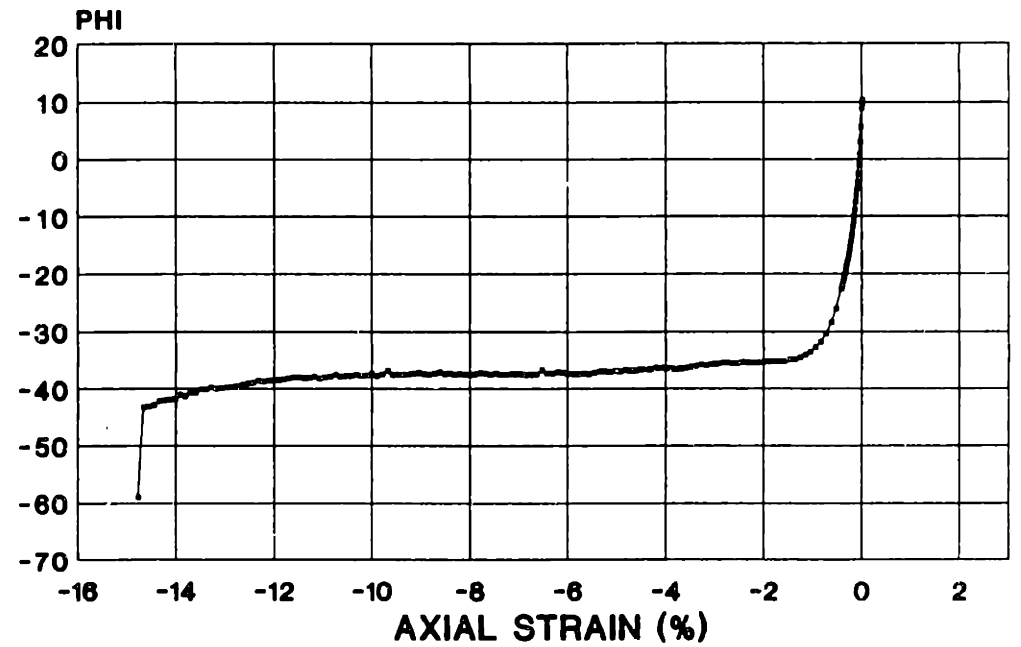

BLOCK S-7 - ELEV. 20.9'

TX073S
STRESS PATH
RECOMPRESSION CKoUC

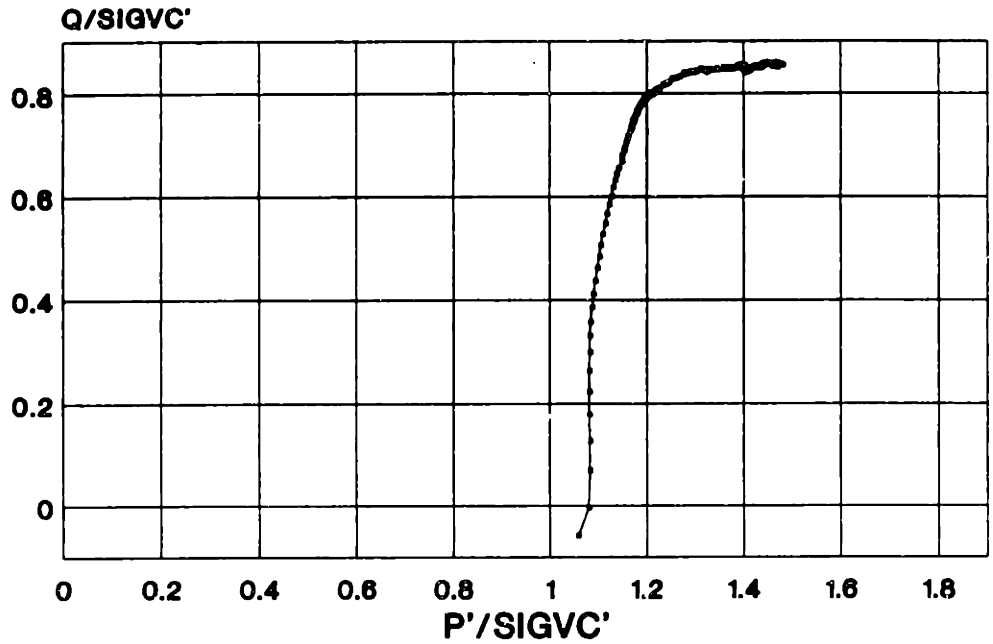

BLOCK S-1 - ELEV. 67.2'

TX073S
STRESS STRAIN
RECOMPRESSION CKoUC

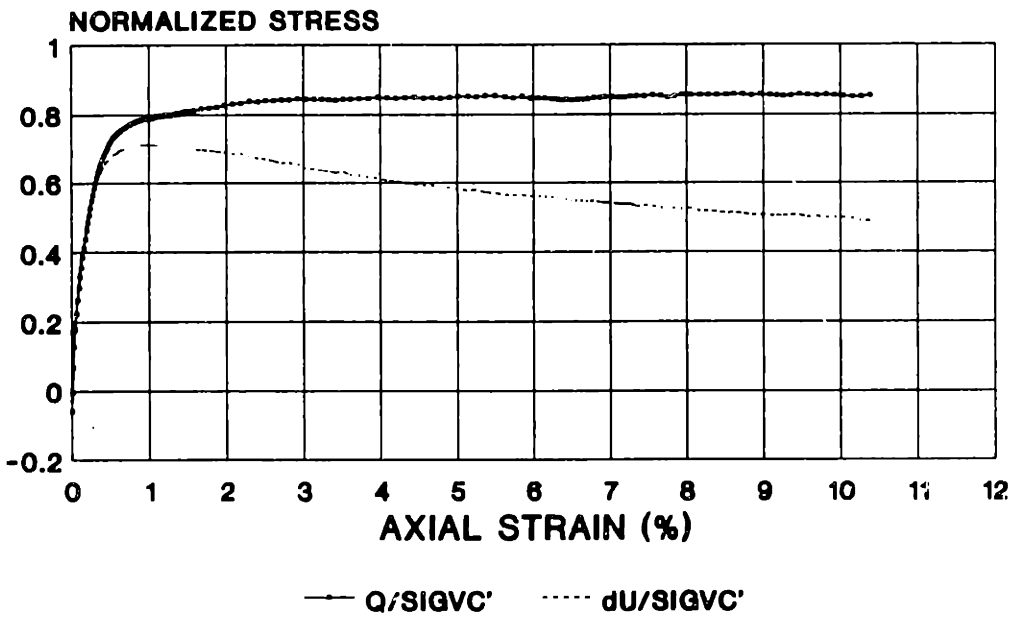

BLOCK S-1 - ELEV. 67.2'

TX073S
A PARAMETER VS. AXIAL STRAIN
RECOMPRESSION CKoUC

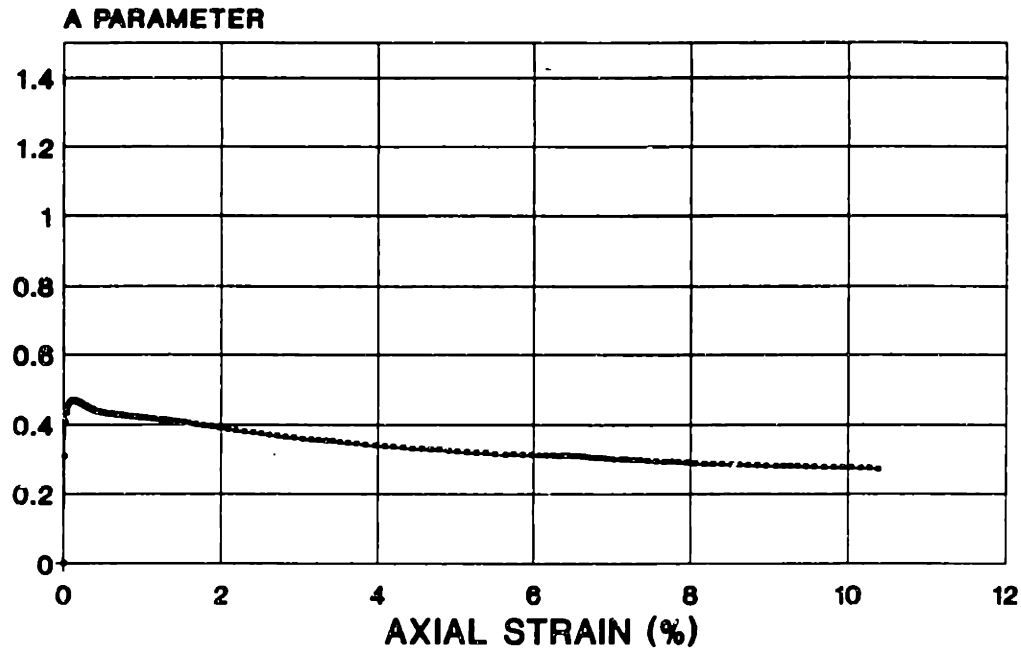

B.S.-1 - ELEV. 67.2'

TX073S
PHI VS. AXIAL STRAIN
RECOMPRESSION CKoUC

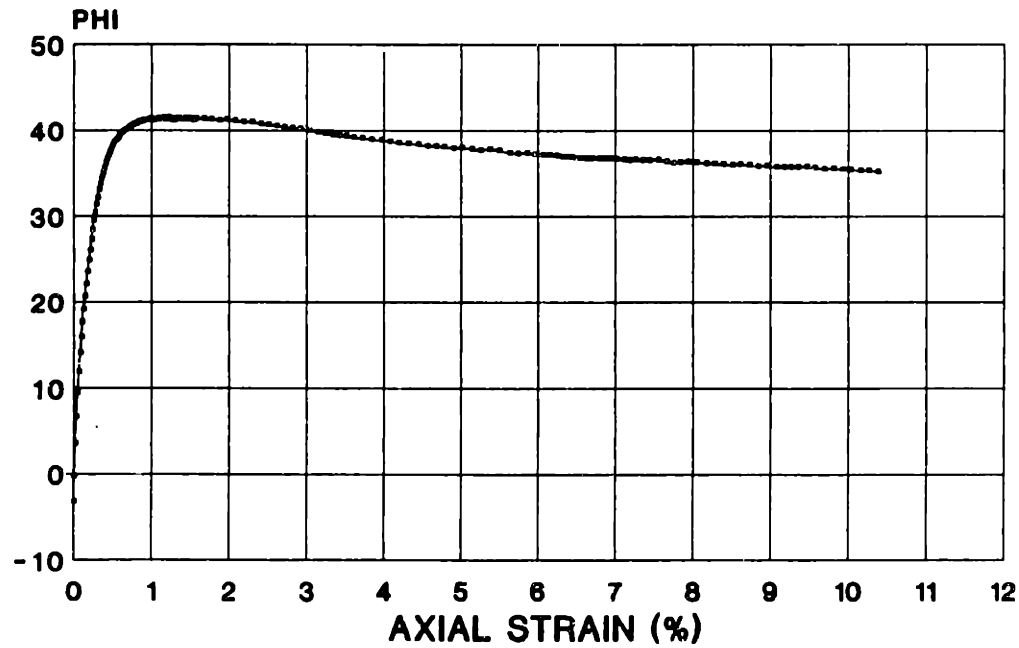

BLOCK S-1 - ELEV. 67.2'

TX074S
STRESS PATH
RECOMPRESSION CKoUE

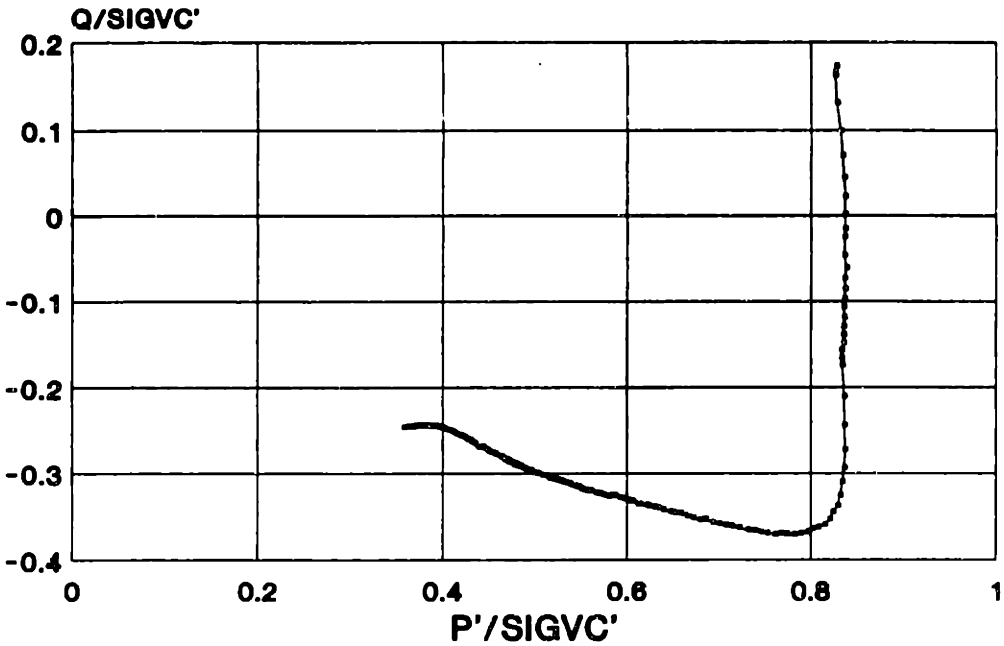

BLOCK S-7 - ELEV. 20.9'

TX074S
STRESS STRAIN
RECOMPRESSION CKoUE

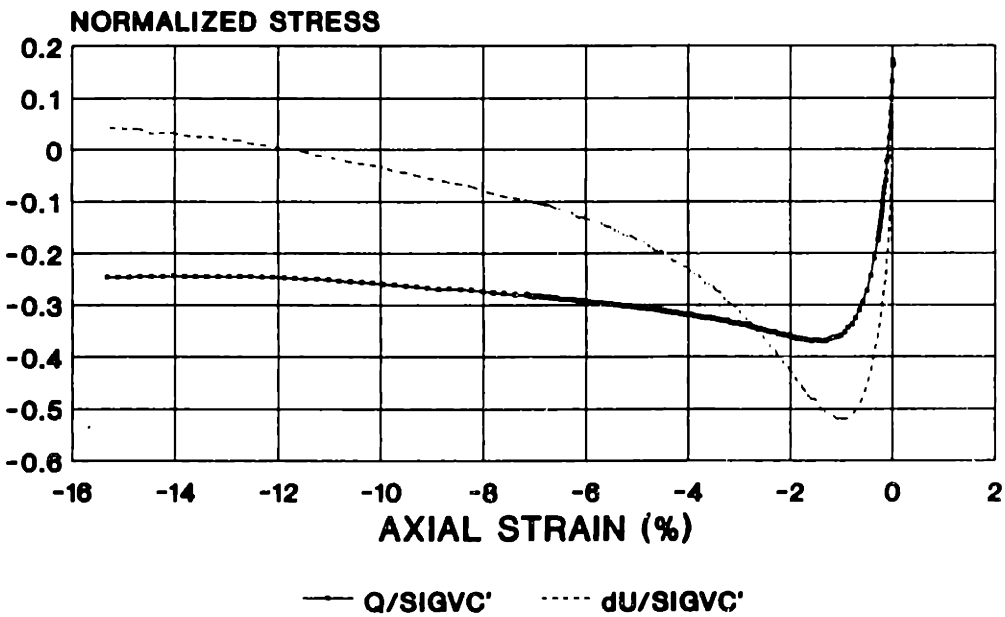

BLOCK S-7 - ELEV. 20.9'

TX074S
A PARAMETER VS. AXIAL STRAIN
RECOMPRESSION CKoUE

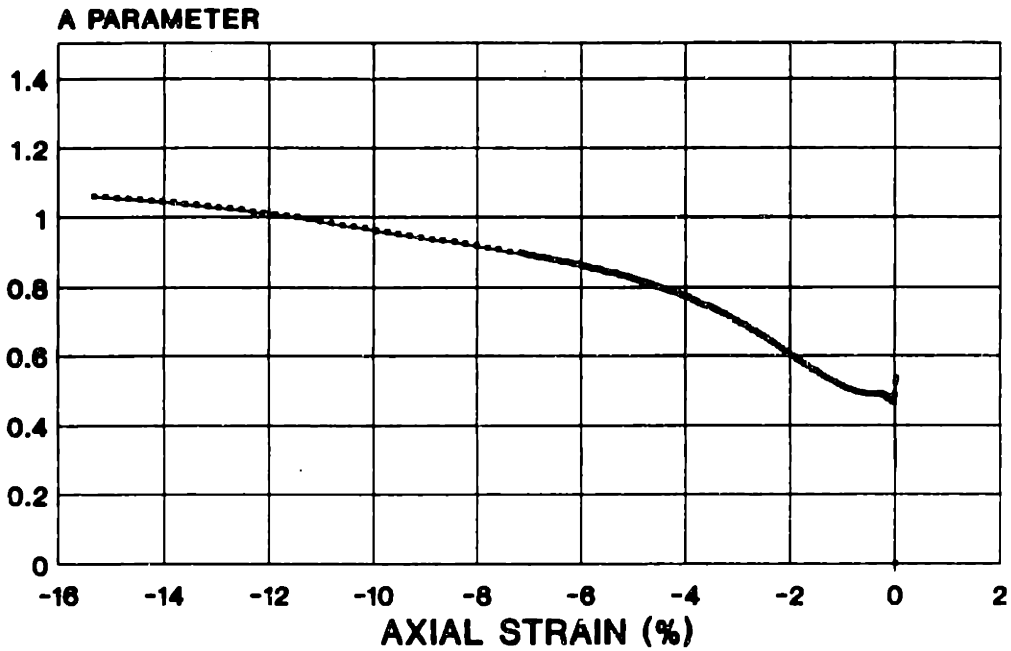

B.S.-7 - ELEV. 20.9

TX074S
PHI VS. AXIAL STRAIN
RECOMPRESSION CKoUE

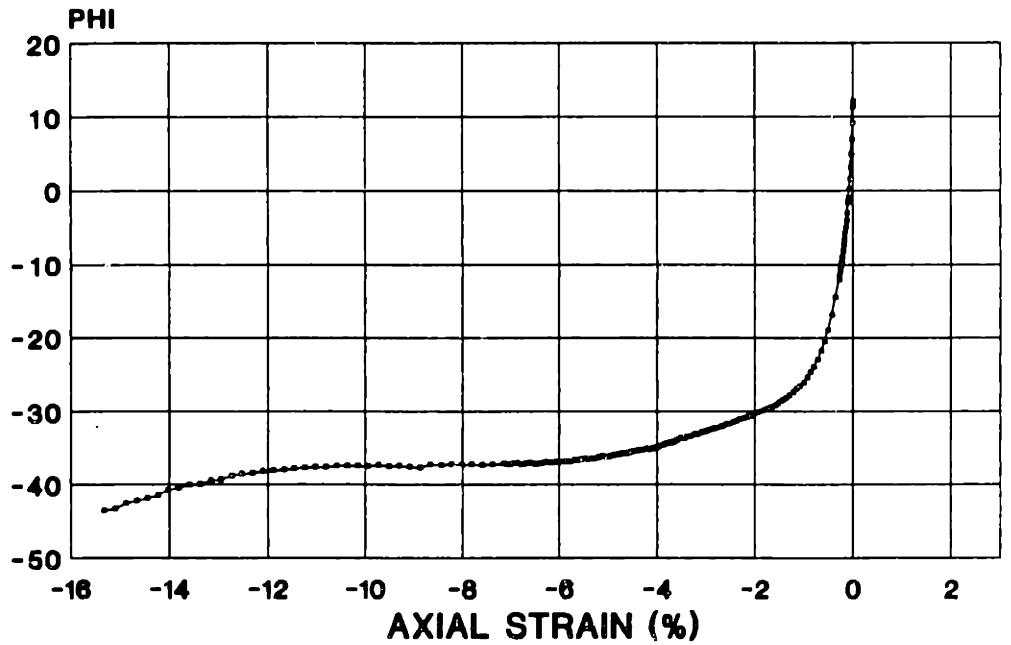

BLOCK S-7 - ELEV. 20.9'

TX075S
STRESS PATH
RECOMPRESSION CKoUE

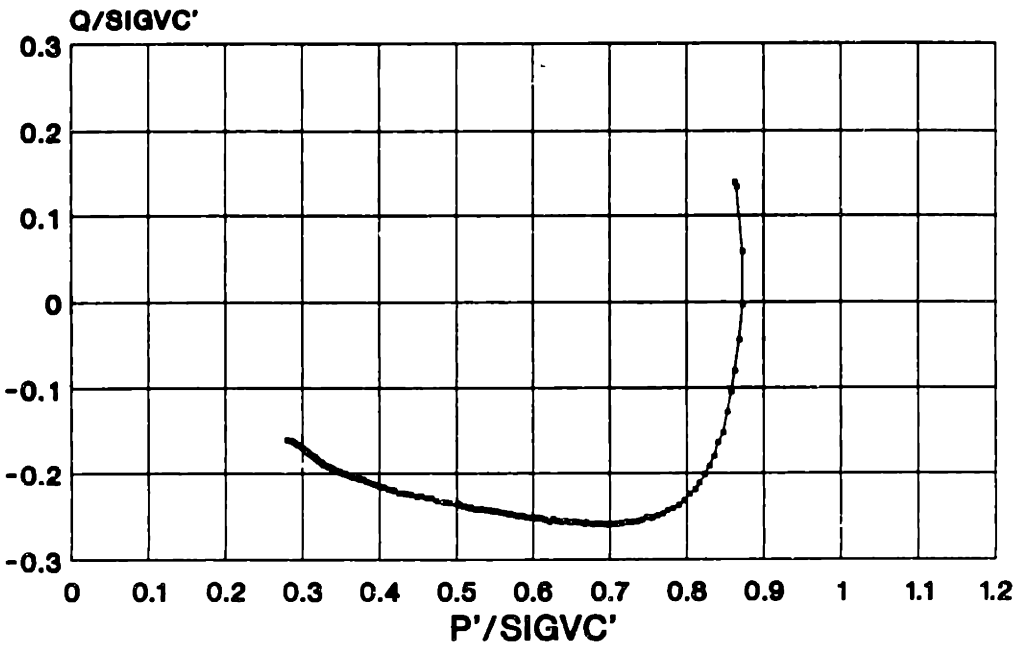

BLOCK S-7 - ELEV. 20.9'

TX075S
STRESS STRAIN
RECOMPRESSION CKoUE

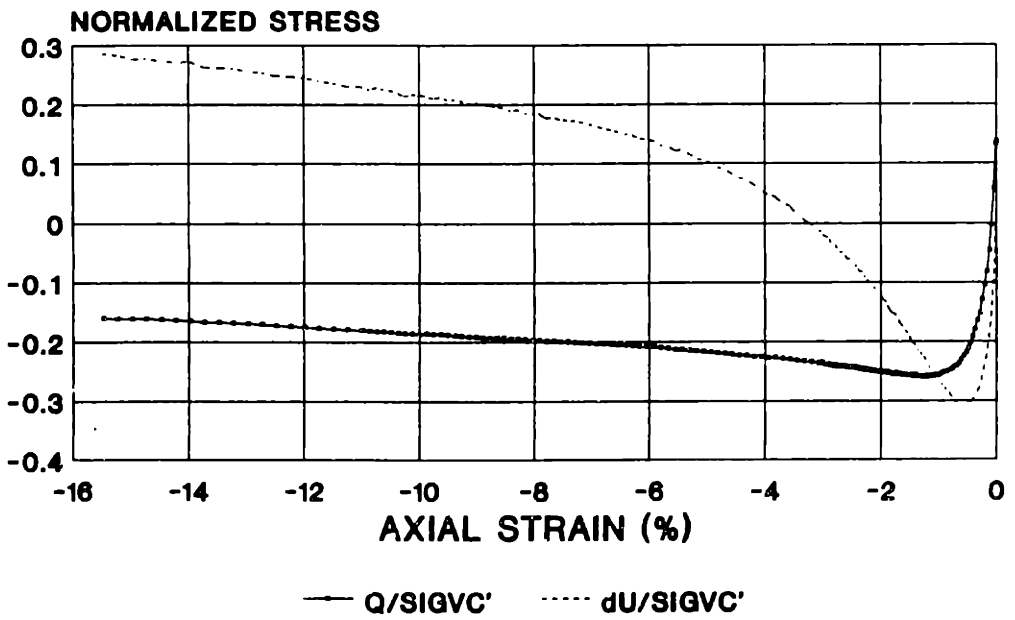

BLOCK S-7 - ELEV. 20.9'

TX075S
A PARAMETER VS. AXIAL STRAIN
RECOMPRESSION CKoUE

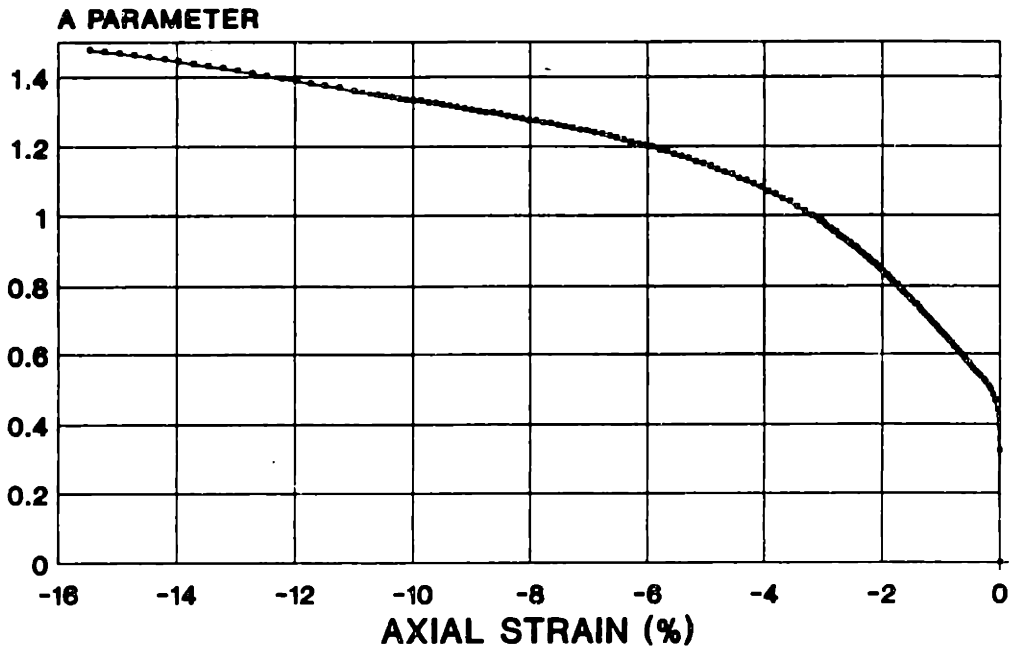

B.S.-7 - ELEV. 20.9

TX075S
PHI VS. AXIAL STRAIN
RECOMPRESSION CKoUE

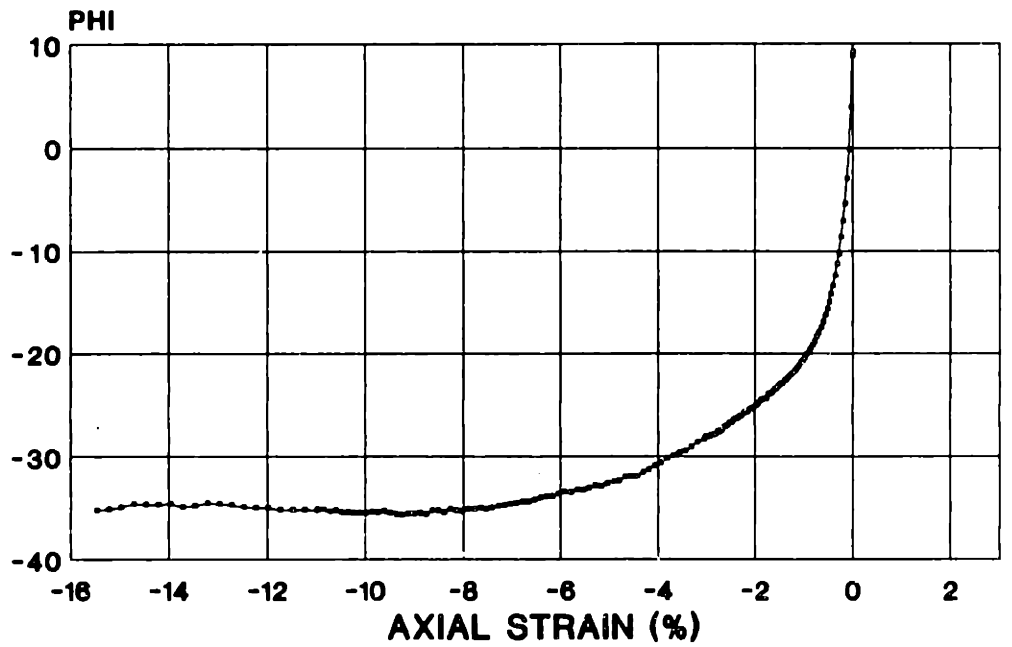

BLOCK S-7 - ELEV. 20.9'

TX078S
STRESS PATH
RECOMPRESSION CKoUC

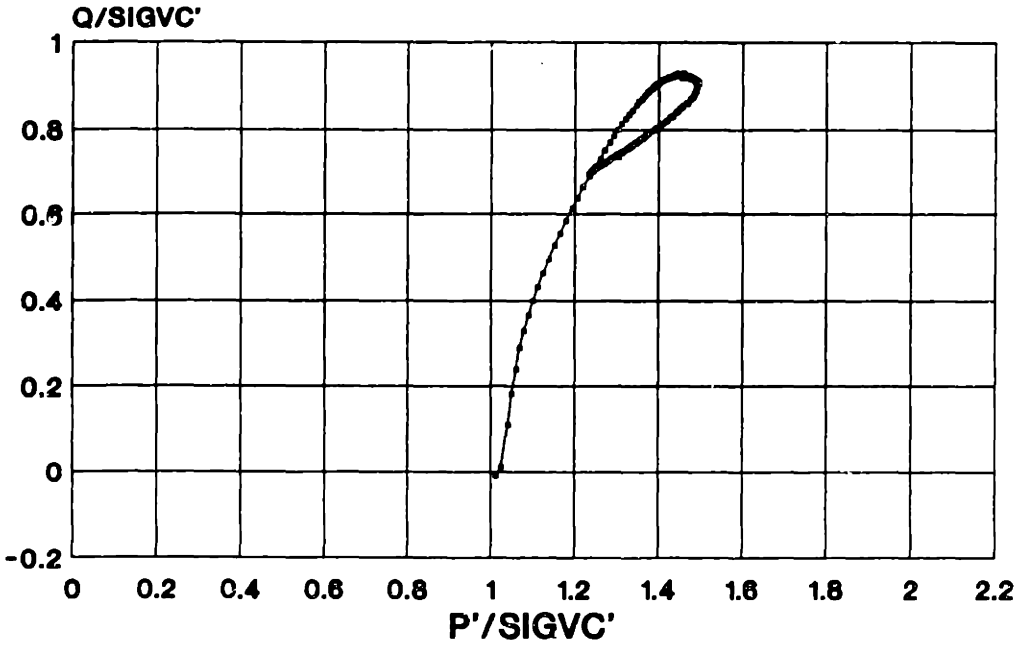

BLOCK S-2 - ELEV. 60.7'

TX078S
STRESS STRAIN
RECOMPRESSION CKoUC

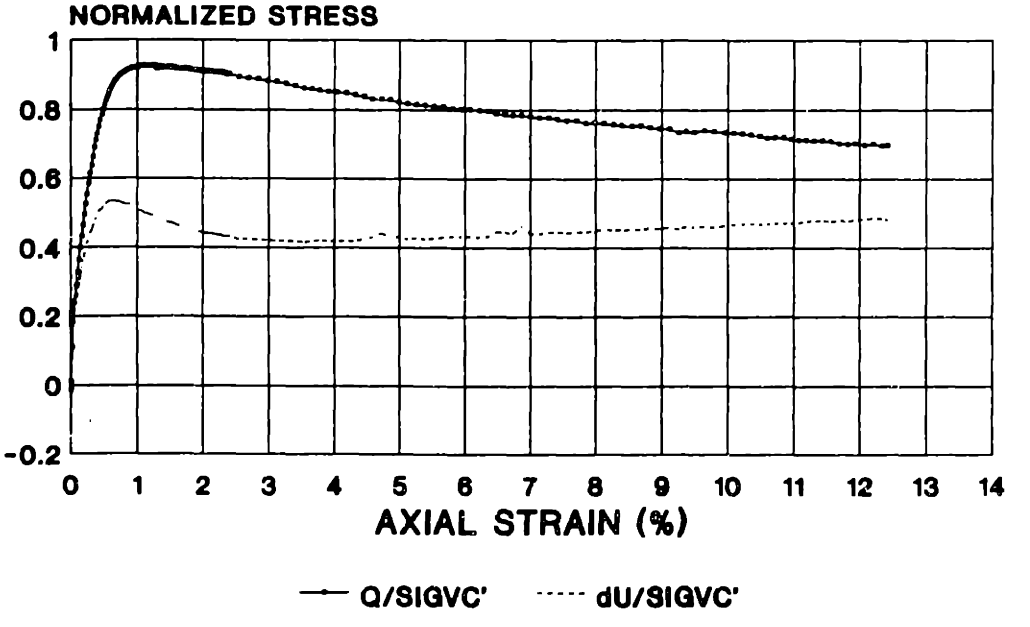

BLOCK S-2 - ELEV. 60.7'

TX078S
A PARAMETER VS. AXIAL STRAIN
RECOMPRESSION CKoUC

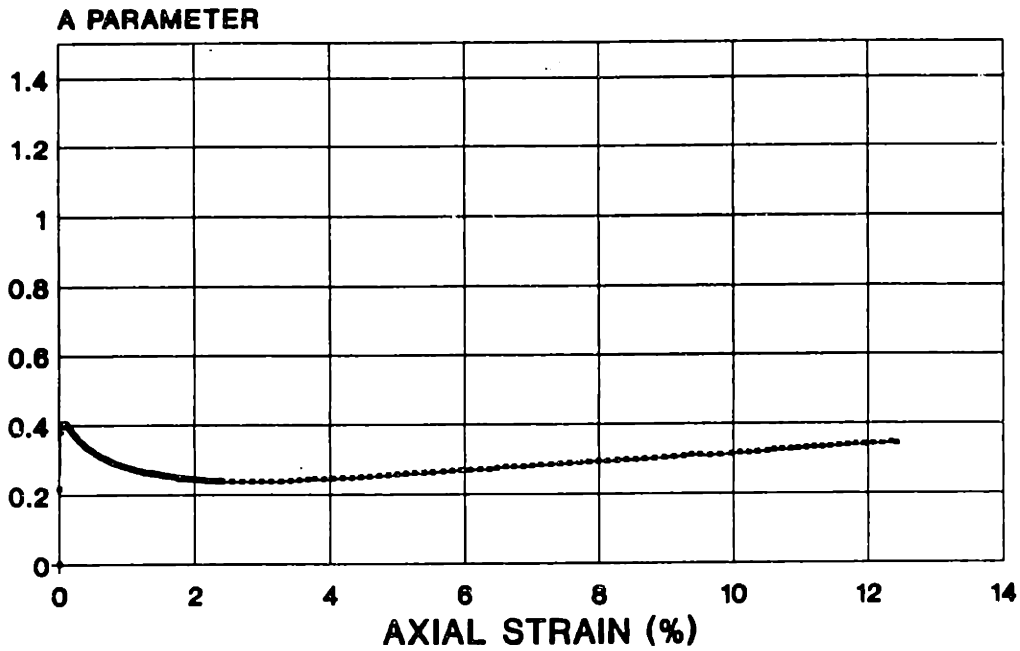

B.S.-2 - ELEV. 60.7'

TX078S
PHI VS. AXIAL STRAIN
RECOMPRESSION CKoUC

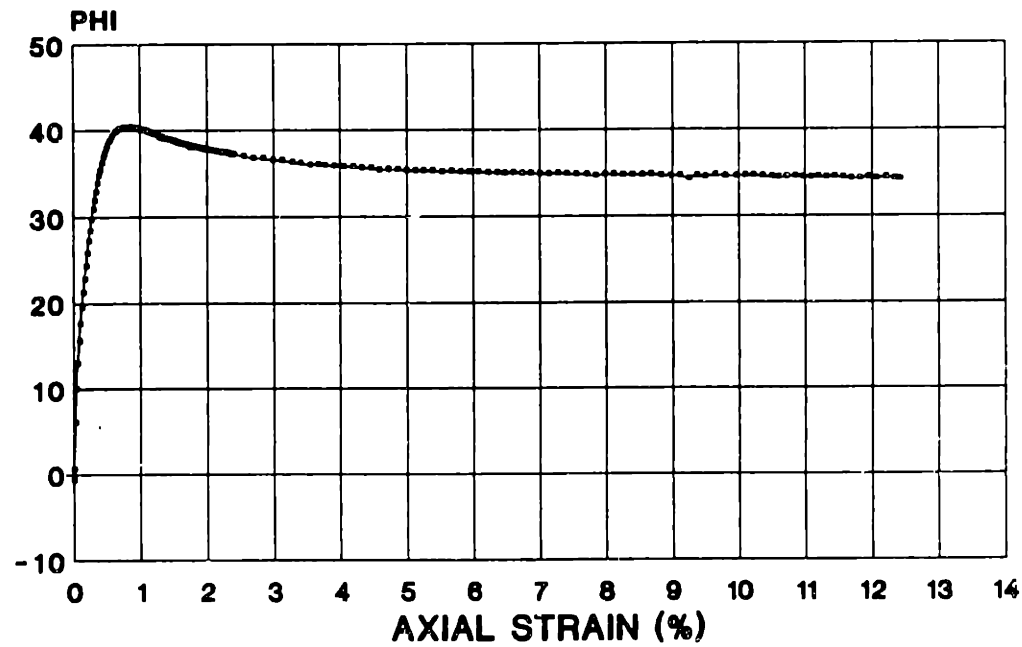

BLOCK S-2 - ELEV. 60.7'

TX079S
STRESS PATH
RECOMPRESSION CKoUC

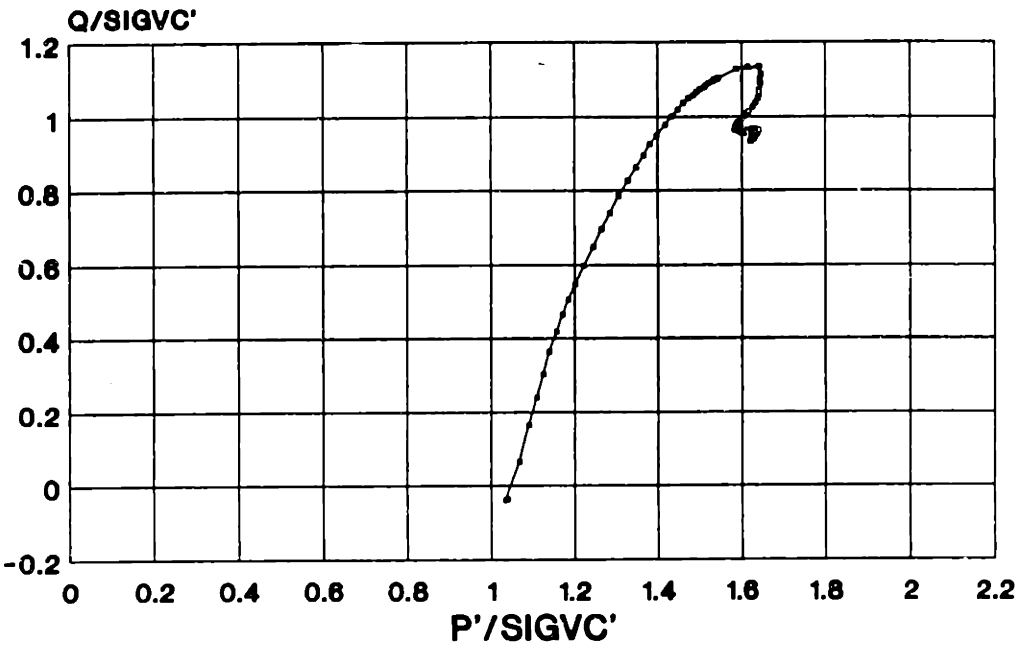

BLOCK S-1A - ELEV. 54.7'

TX079S
STRESS STRAIN
RECOMPRESSION CKoUC

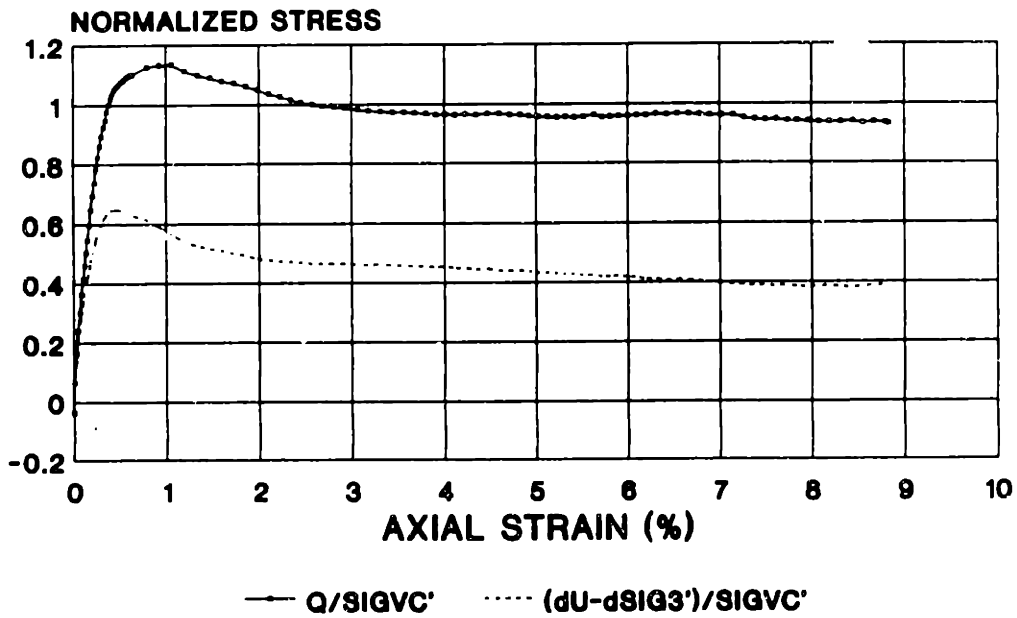

BLOCK S-1A - ELEV. 54.7'

TX079S
A PARAMETER VS. AXIAL STRAIN
RECOMPRESSION CKoUC

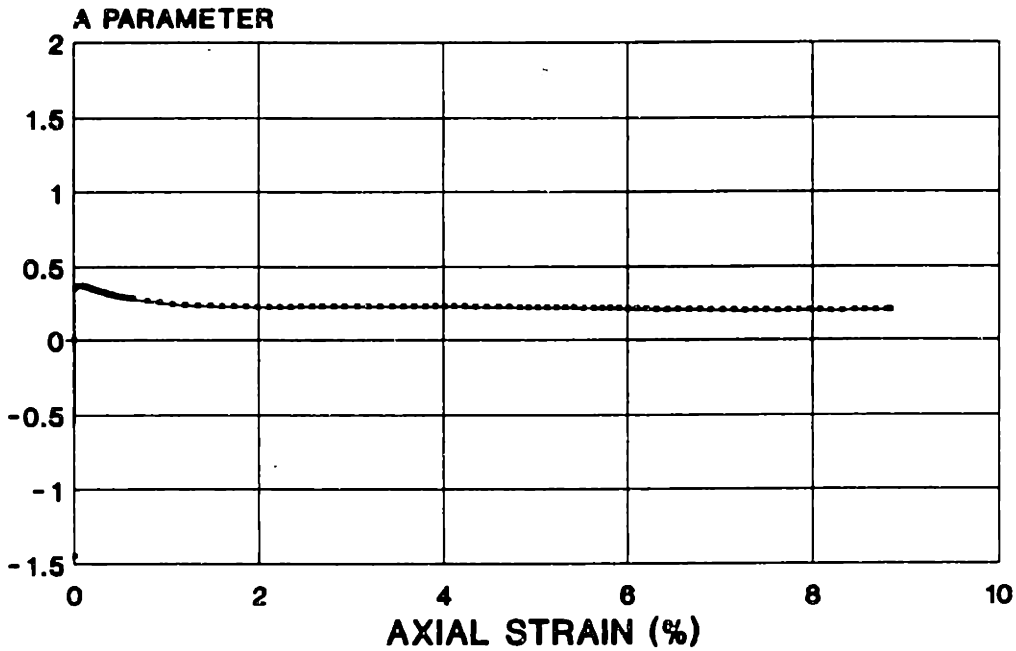

B.S.-1A - ELEV. 54.7

TX079S
PHI VS. AXIAL STRAIN
RECOMPRESSION CKoUC

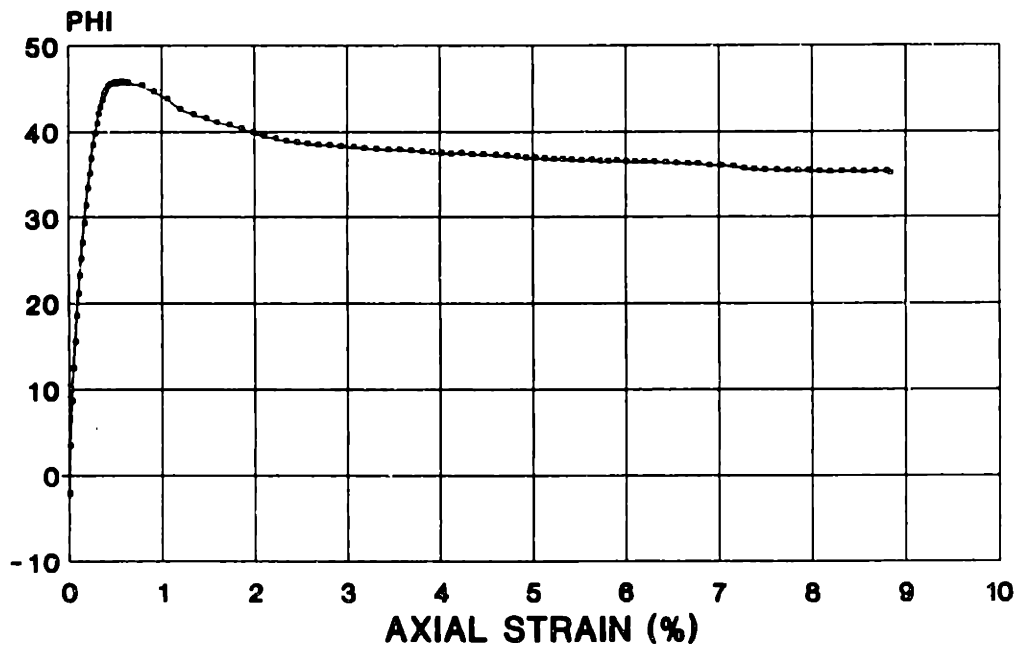

BLOCK S-1A - ELEV. 54.7'

TX080S
STRESS PATH
RECOMPRESSION CKoUE

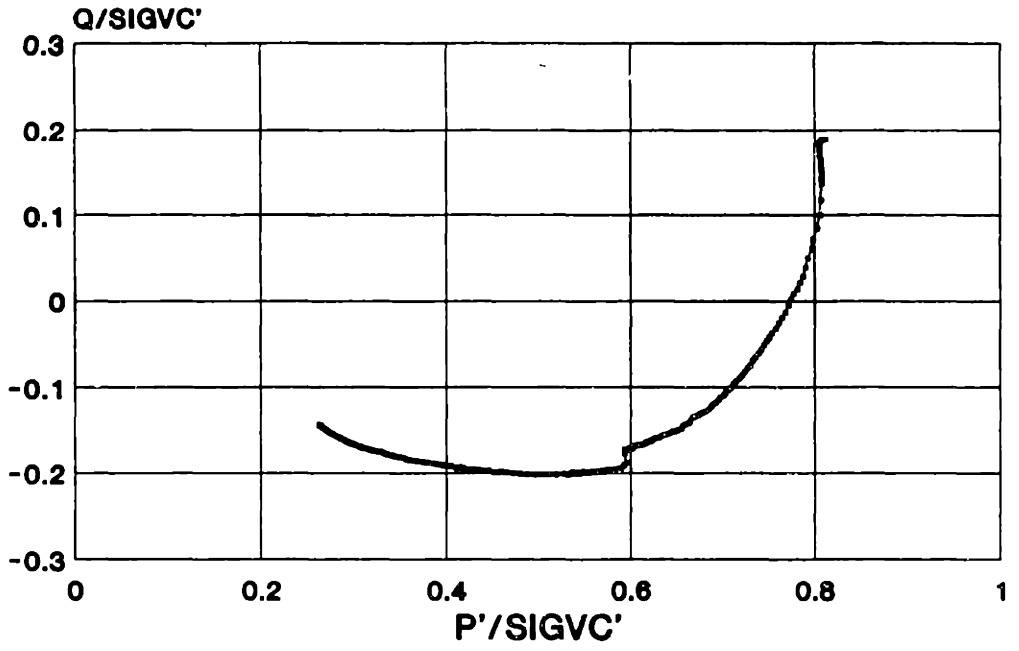

SB2-23 U15 - ELEV. 21.8'

TX080S
STRESS STRAIN
RECOMPRESSION CKoUE

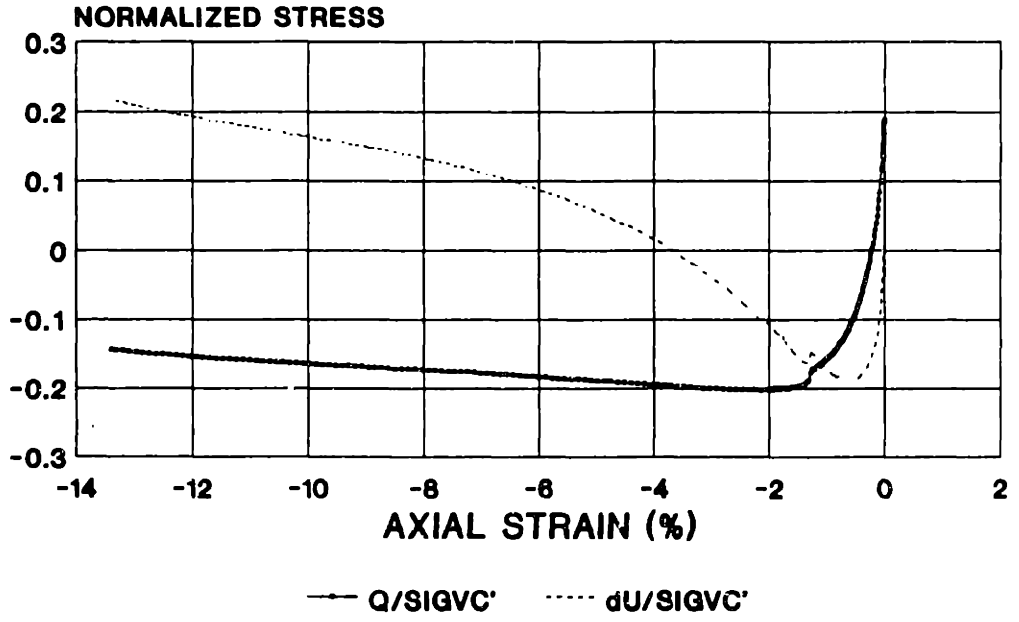

SB2-23 U15 - ELEV. 21.8'

TX080S
A PARAMETER VS. AXIAL STRAIN
RECOMPRESSION CKoUE

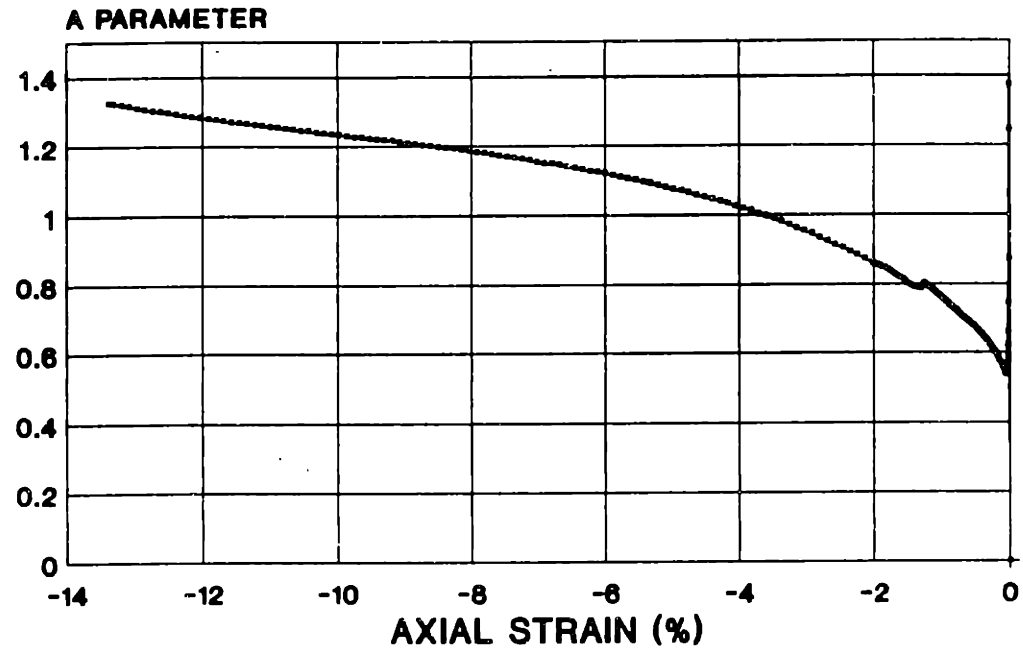

SB2-23 U15 - ELEV. 21.8'

TX080S
PHI VS. AXIAL STRAIN
RECOMPRESSION CKoUE

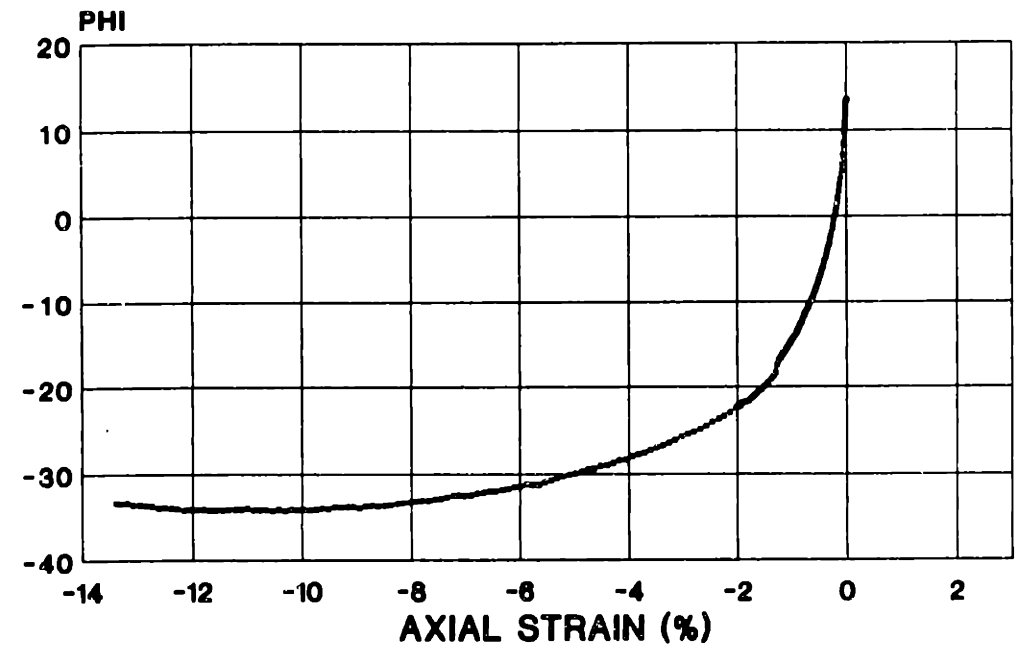

SB2-23 U15 - ELEV. 21.8'

TX083S
STRESS PATH
RECOMPRESSION CKoUC

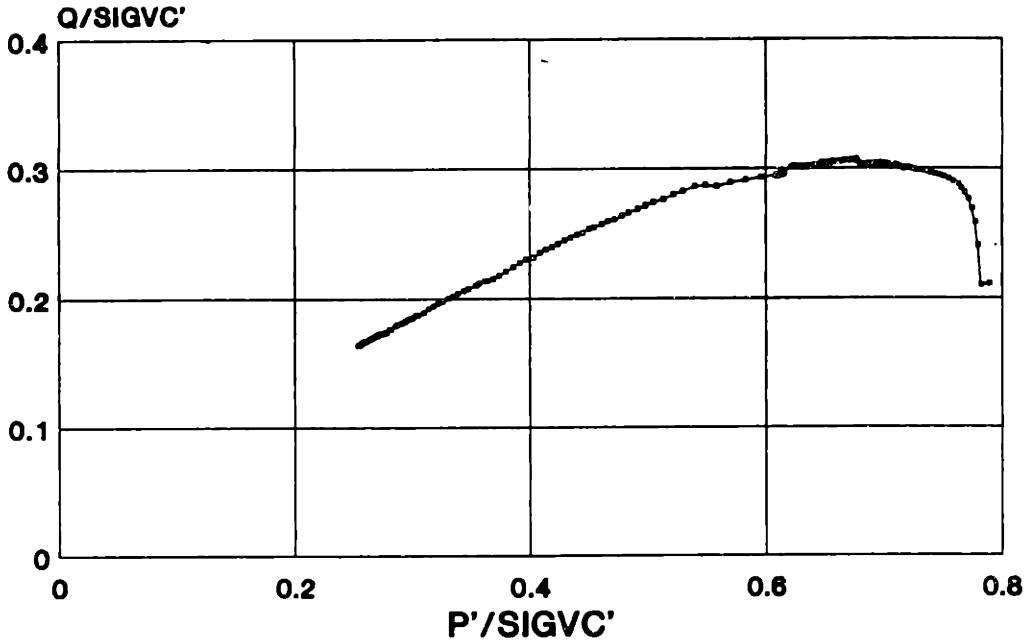

BLOCK S-1A - ELEV. 54.7'

TX083S
STRESS STRAIN
RECOMPRESSION CKoUC

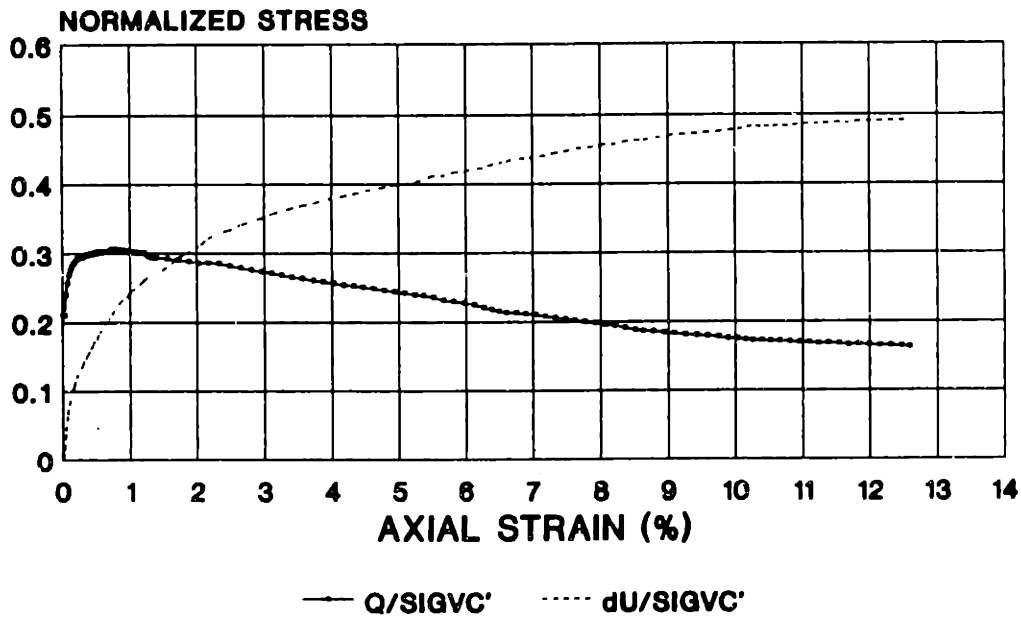

BLOCK S-1A - ELEV. 54.7'

TX083S
A PARAMETER VS. AXIAL STRAIN
RECOMPRESSION CKoUC

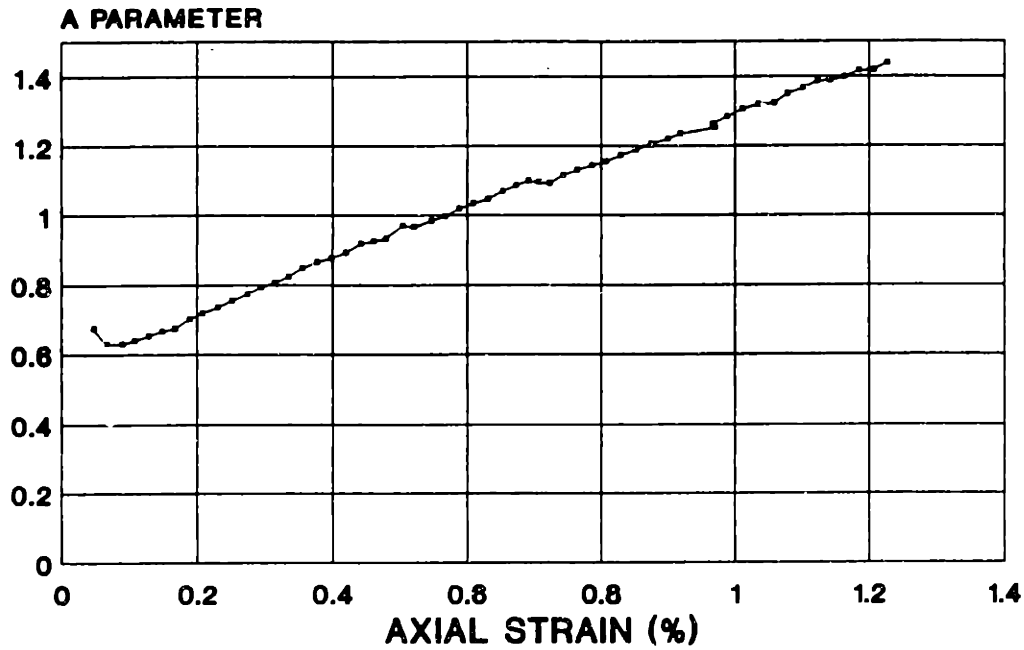

B.S.-1A - ELEV. 54.7'

TX083S
PHI VS. AXIAL STRAIN
RECOMPRESSION CKoUC

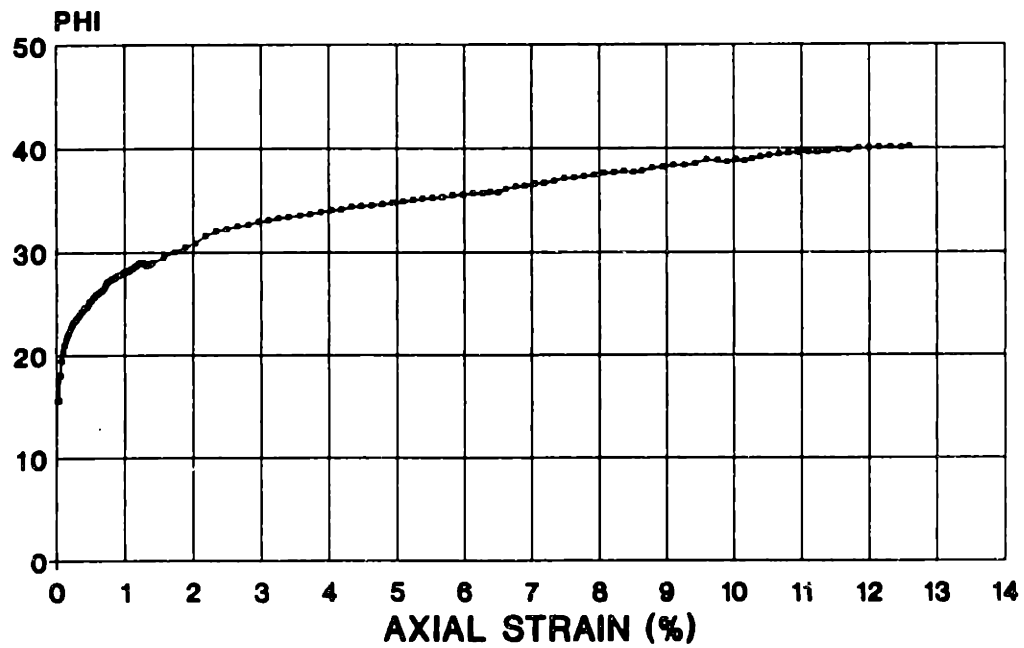

BLOCK S-1A - ELEV. 54.7'

TX084S
STRESS PATH
RECOMPRESSION CKoUE

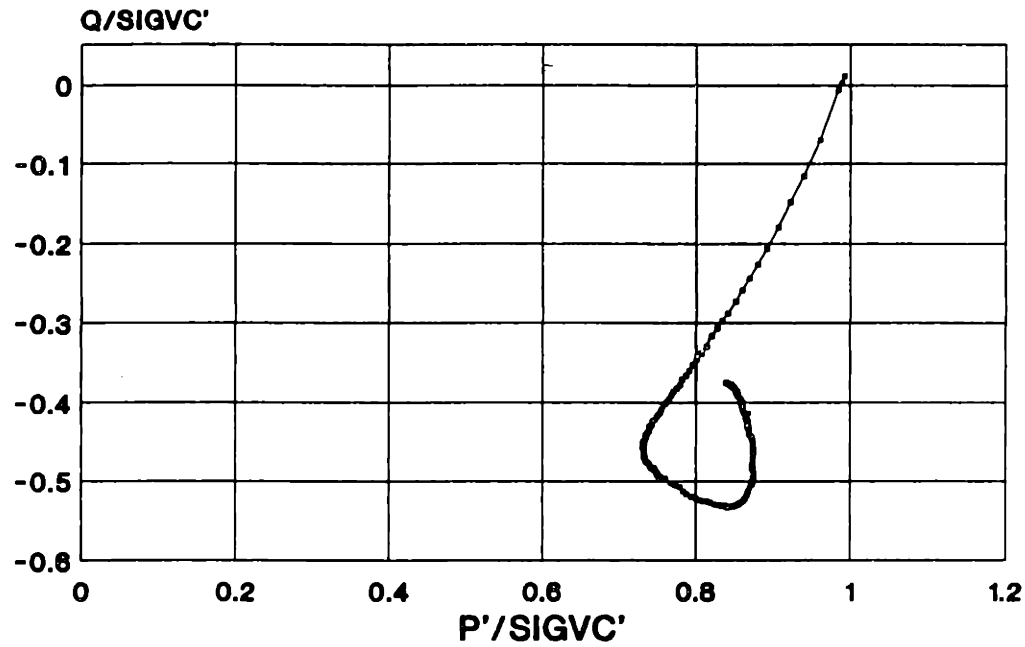

BLOCK S-1A - ELEV. 54.7'

TX084S
STRESS STRAIN
RECOMPRESSION CKoUE

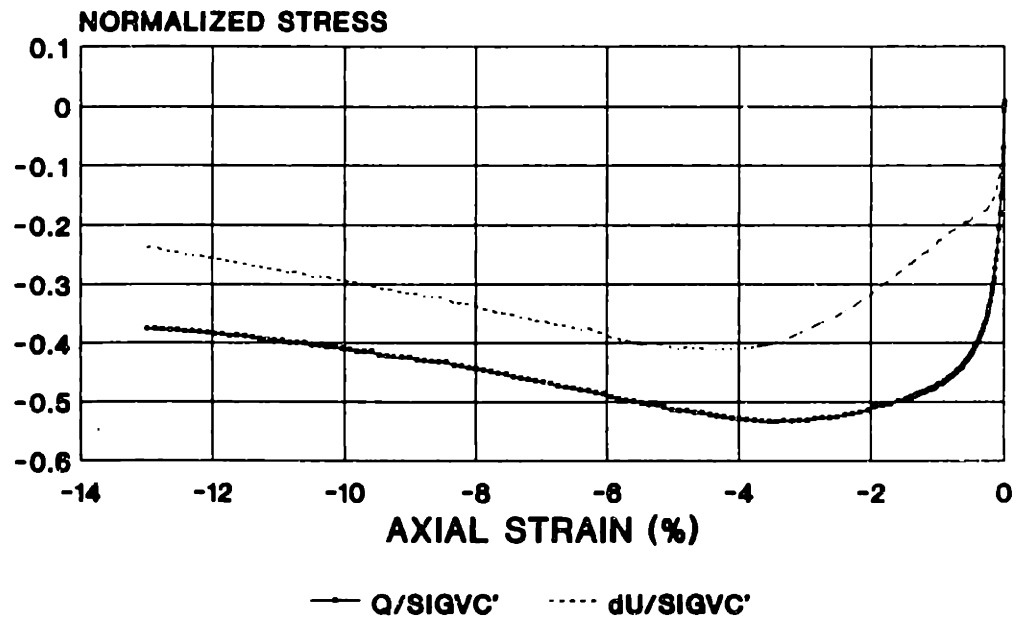

BLOCK S-1A - ELEV. 54.7'

TX084S
A PARAMETER VS. AXIAL STRAIN
RECOMPRESSION CKoUE

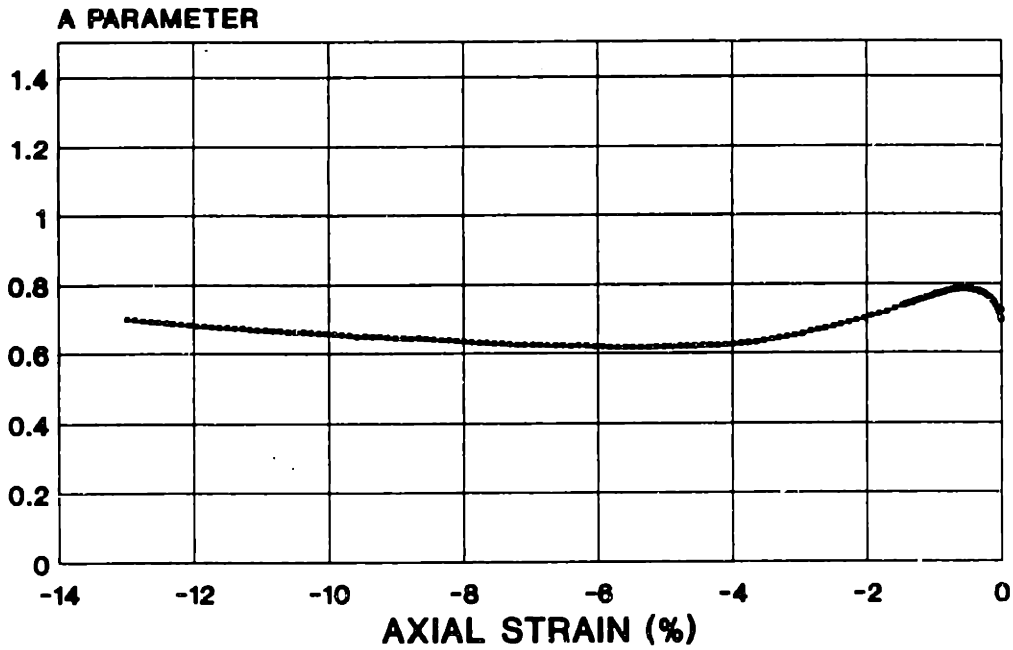

B.S.-1A - ELEV. 54.7'

TX084S
PHI VS. AXIAL STRAIN
RECOMPRESSION CKoUE

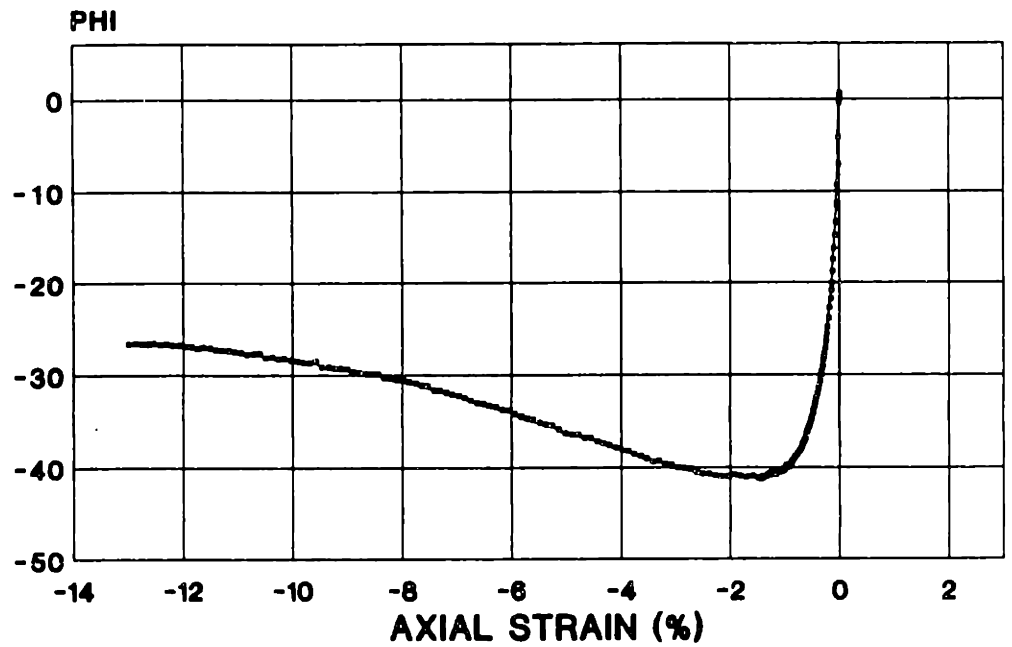

BLOCK S-1A - ELEV. 54.7'

TX085S
STRESS PATH
RECOMPRESSION CKoUC

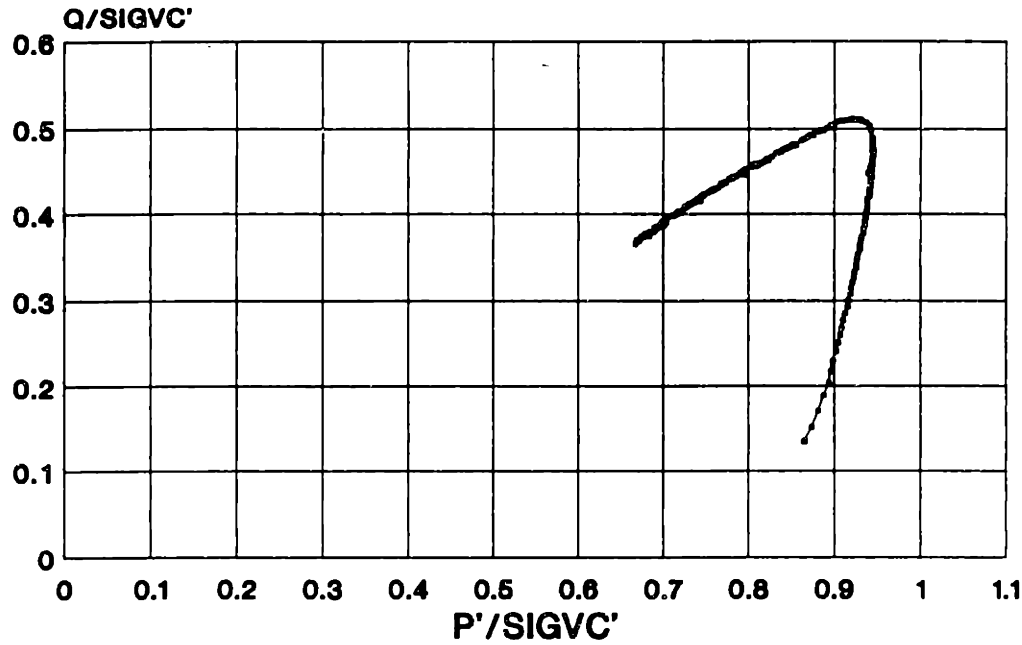

BLOCK S-1A - ELEV. 54.7'

TX085S
STRESS STRAIN
RECOMPRESSION CKoUC

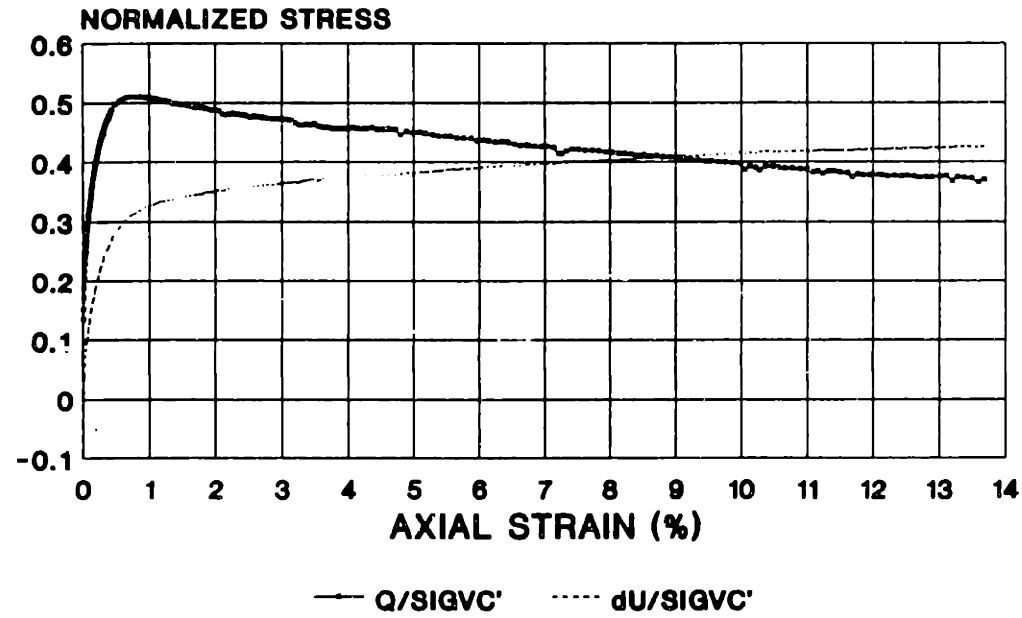

BLOCK S-1A - ELEV. 54.7'

TX085S
A PARAMETER VS. AXIAL STRAIN
RECOMPRESSION CKoUC

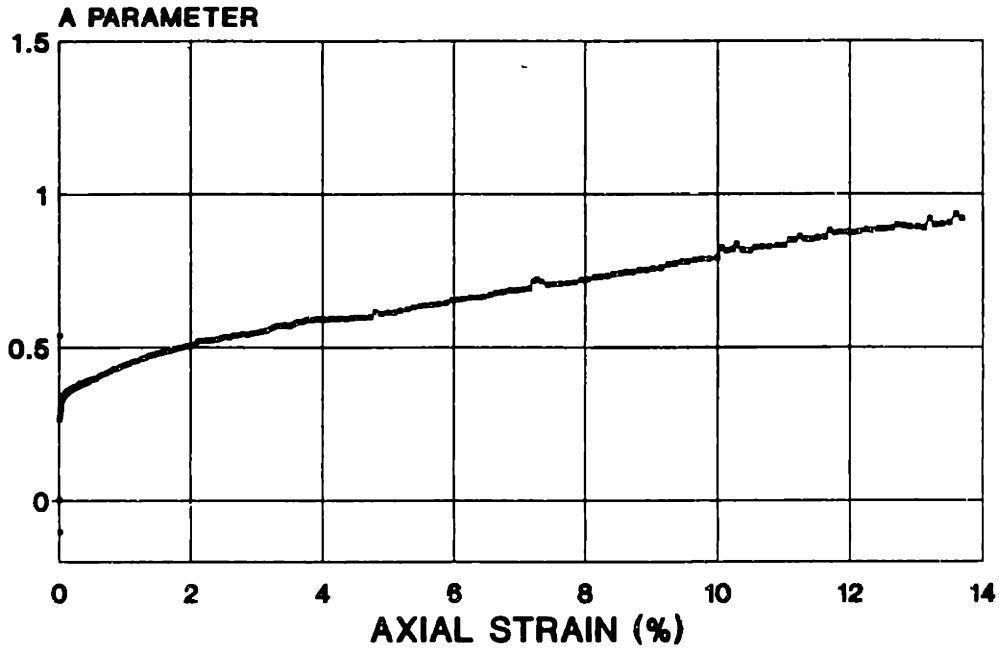

B.S.-1A - ELEV. 54.7'

TX085S
PHI VS. AXIAL STRAIN
RECOMPRESSION CKoUC

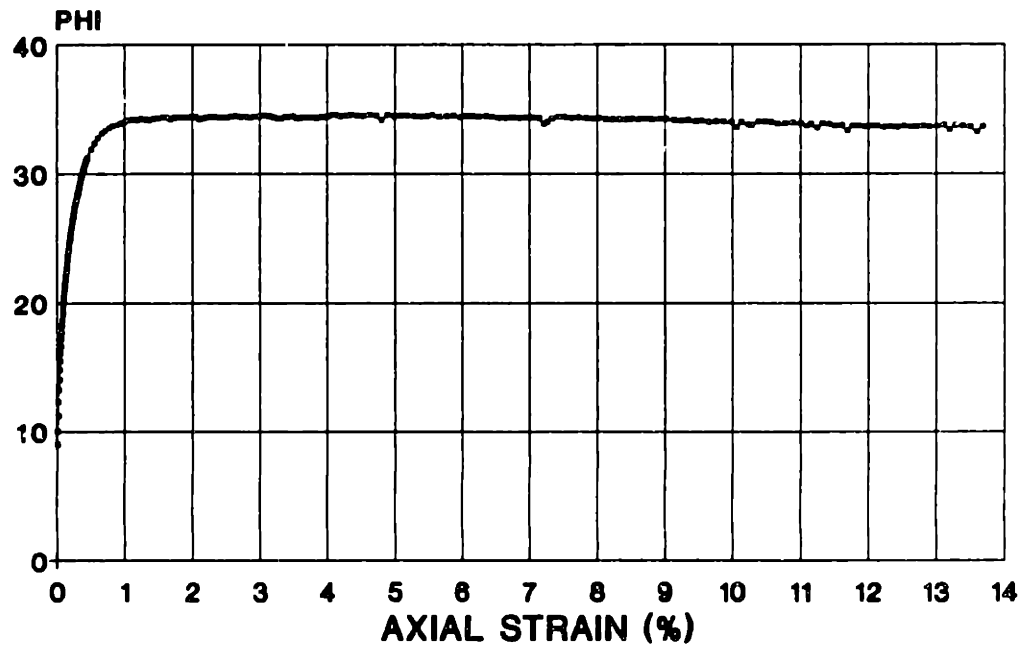

BLOCK S-1A - ELEV. 54.7'

TX087S
STRESS PATH
RECOMPRESSION CKoUE

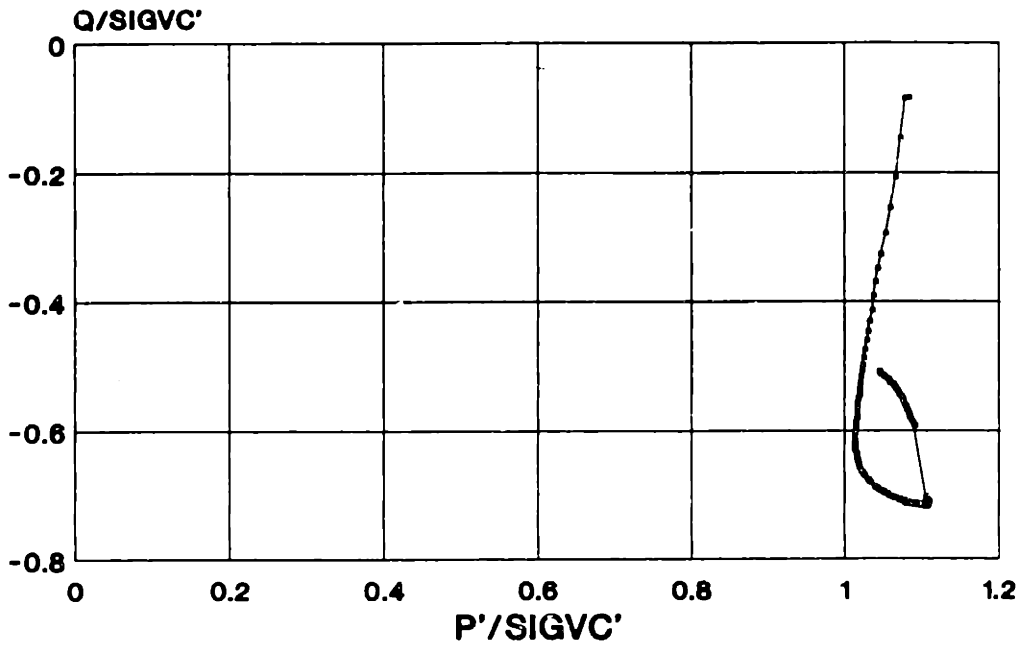

BLOCK S-2A - ELEV. 42.1'

TX087S
STRESS STRAIN
RECOMPRESSION CKoUE

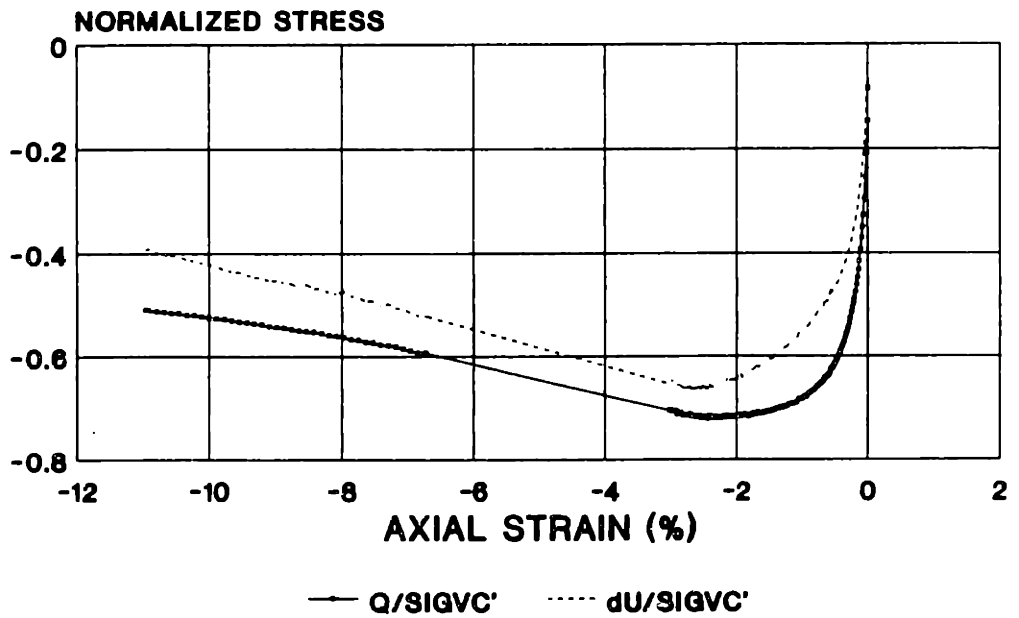

BLOCK S-2A - ELEV. 42.1'

TX087S
A PARAMETER VS. AXIAL STRAIN
RECOMPRESSION CKoUE

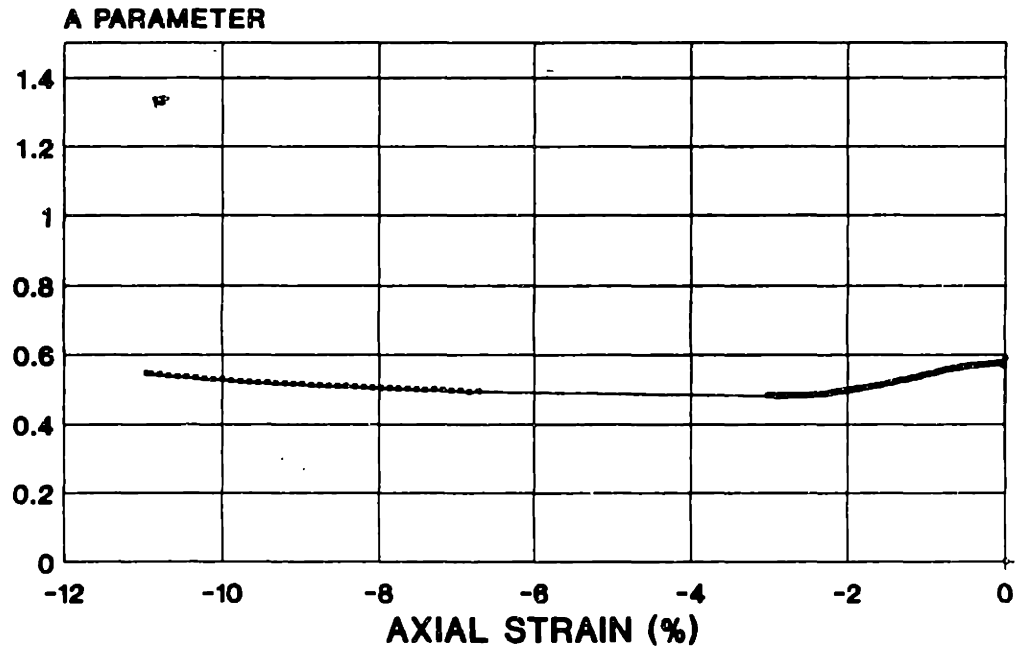

B.S.-2A - ELEV. 42.1'

TX087S
PHI VS. AXIAL STRAIN
RECOMPRESSION CKoUE

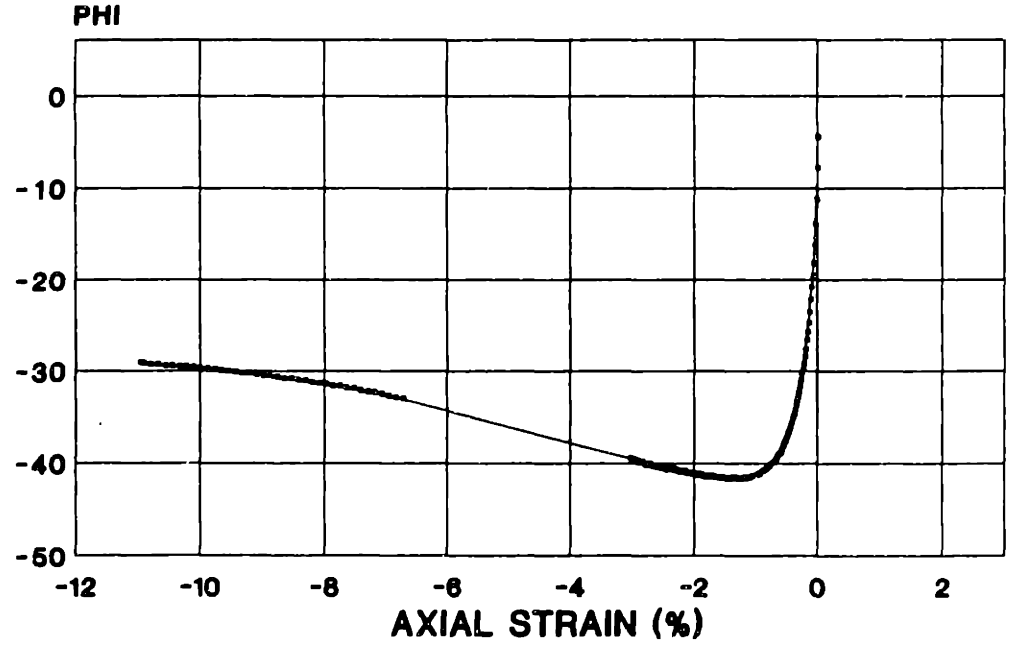

BLOCK S-2A - ELEV. 42.1'

TX089S
STRESS PATH
RECOMPRESSION CKoUC

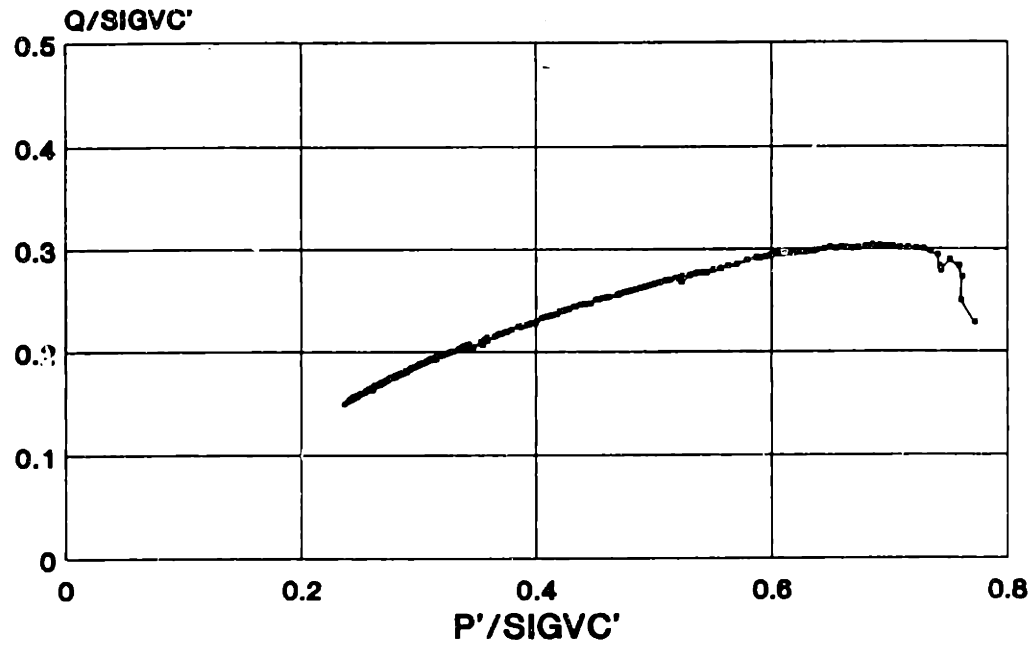

SB2-23 U25 - ELEV. -17.4'

TX089S
STRESS STRAIN
RECOMPRESSION CKoUC

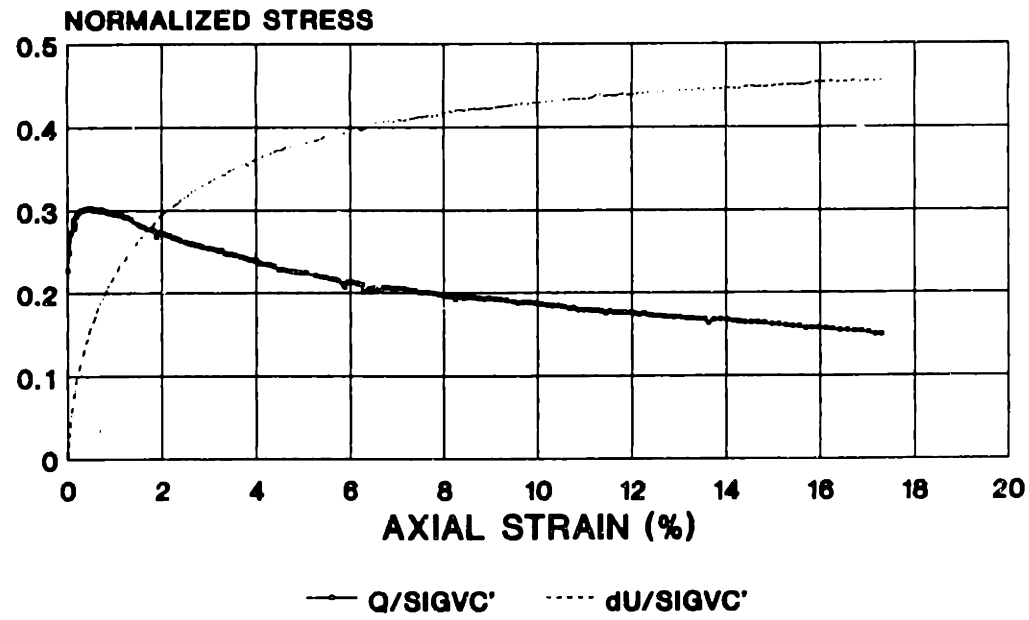

SB2-23 U25 - ELEV. -17.4'

TX089S
A PARAMETER VS. AXIAL STRAIN
RECOMPRESSION CKoUC

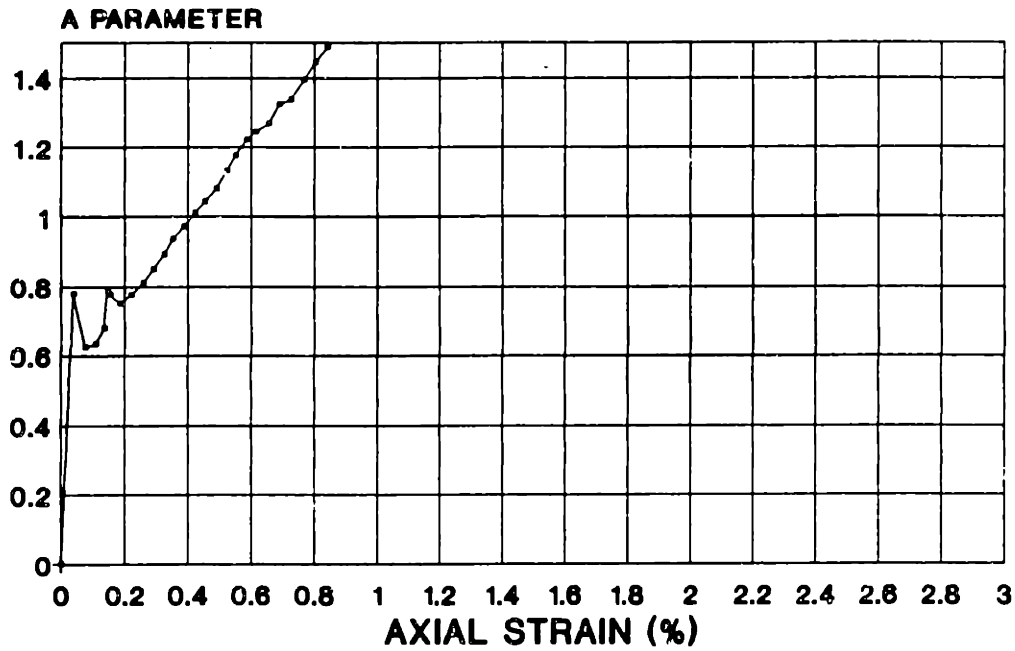

SB2-23 U25 - ELEV. -17.4'

TX089S
PHI VS. AXIAL STRAIN
RECOMPRESSION CKoUC

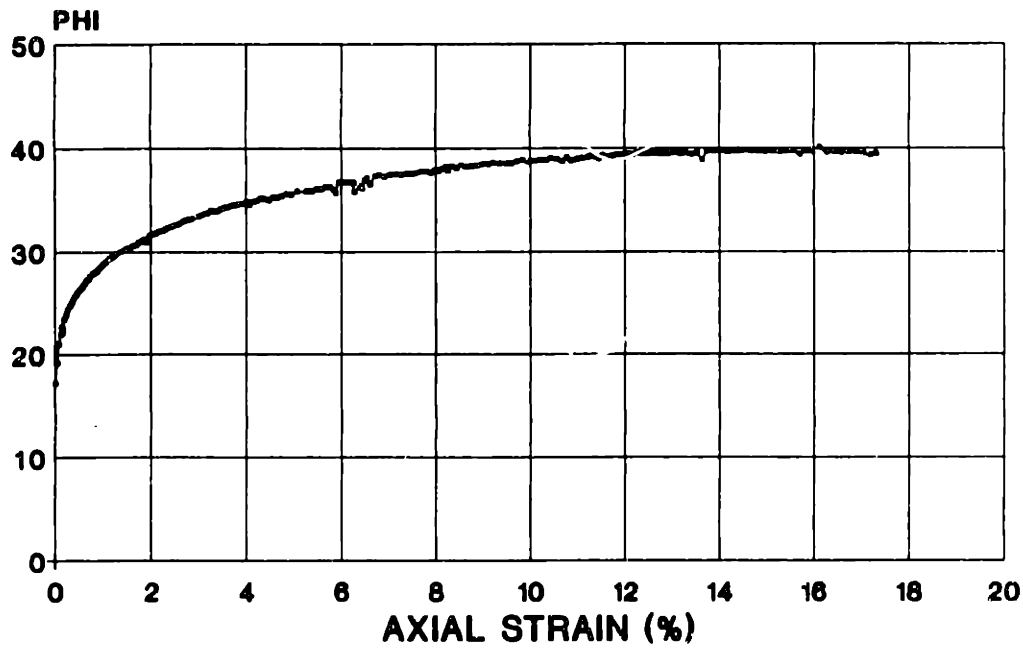

SB2-23 U25 - ELEV. -17.4'

TX090S
STRESS PATH
RECOMPRESSION CKoUE

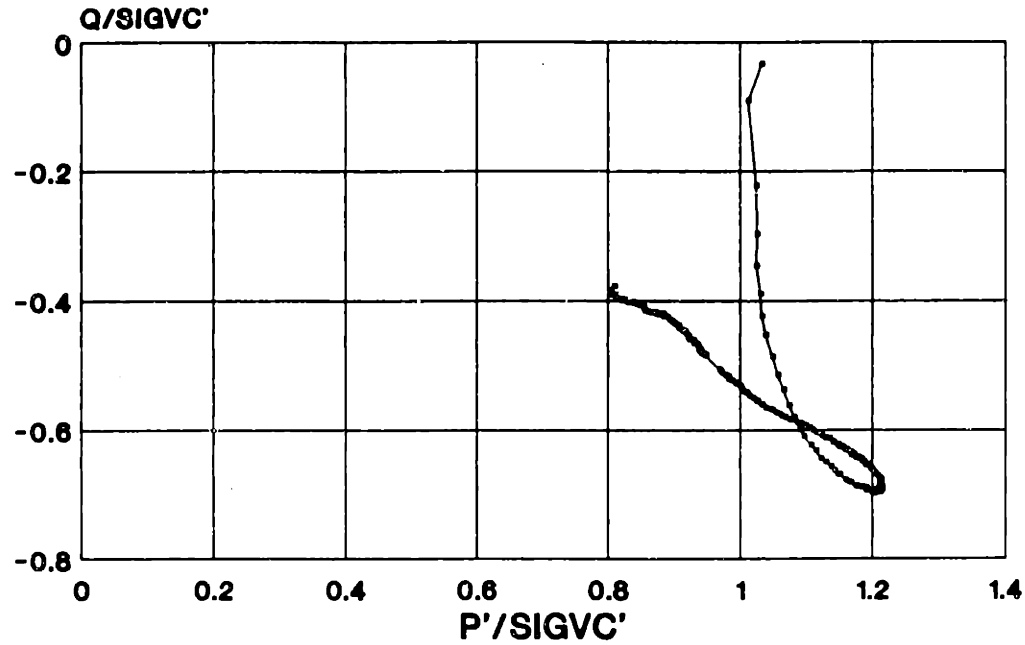

BLOCK S-3A - ELEV. 33.6'

TX090S
STRESS STRAIN
RECOMPRESSION CKoUE

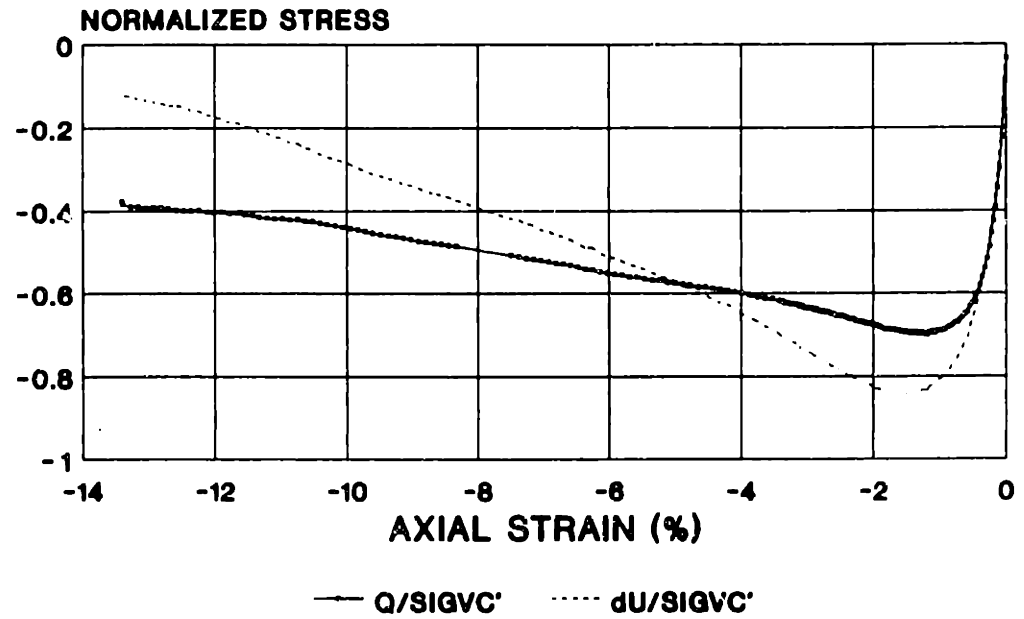

BLOCK S-3A - ELEV. 33.6'

TX090S
A PARAMETER VS. AXIAL STRAIN
RECOMPRESSION CKoUE

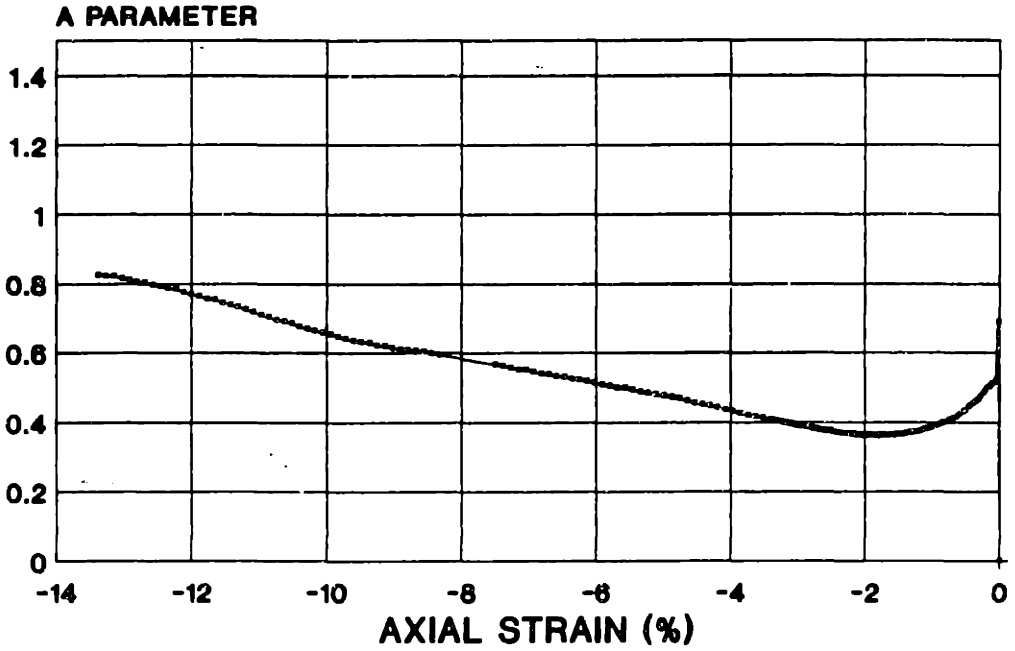

B.S.-3A - ELEV. 33.6'

TX090S
PHI VS. AXIAL STRAIN
RECOMPRESSION CKoUE

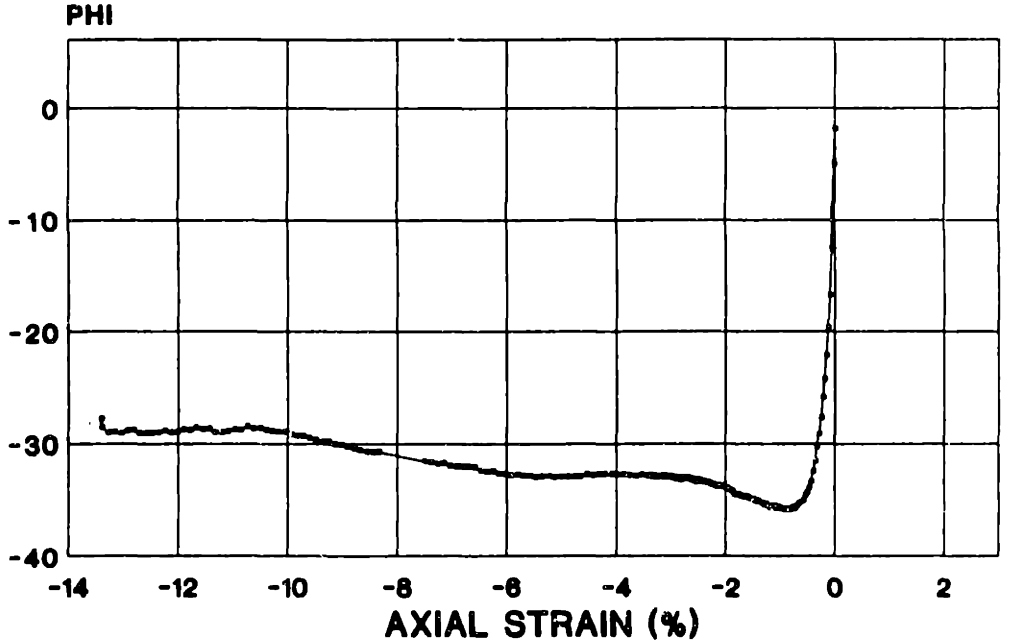

BLOCK S-3A - ELEV. 33.6'

TX091S
STRESS PATH
RECOMPRESSION CKoUC

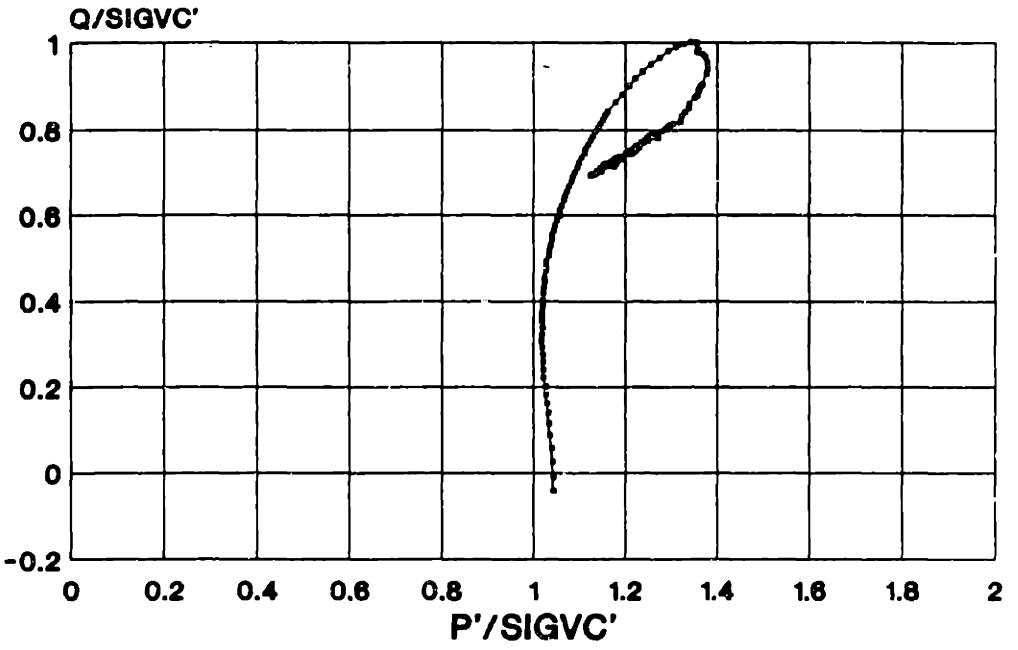

BLOCK S-3A - ELEV. 33.6'

TX091S
STRESS STRAIN
RECOMPRESSION CKoUC

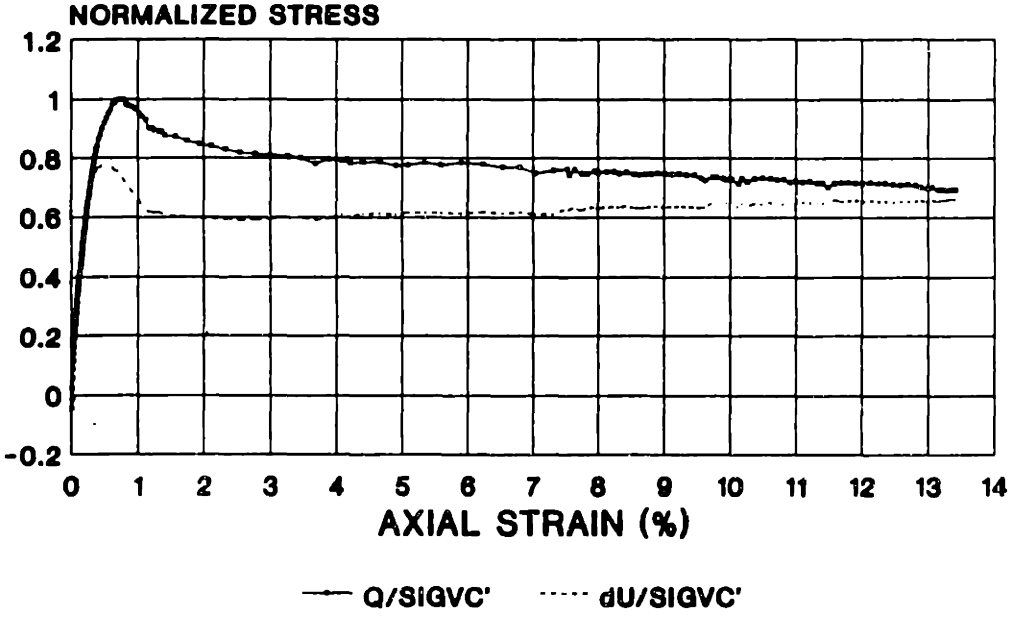

BLOCK S-3A - ELEV. 33.6'

TX091S
A PARAMETER VS. AXIAL STRAIN
RECOMPRESSION CKoUC

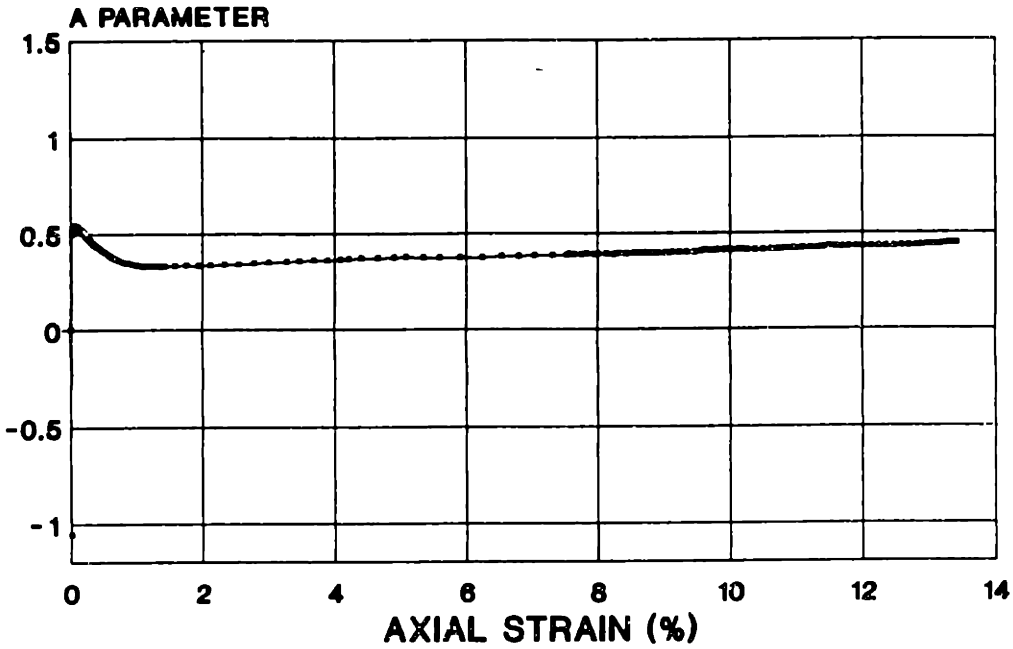

B.S.-3A - ELEV. 33.6'

TX091S
PHI VS. AXIAL STRAIN
RECOMPRESSION CKoUC

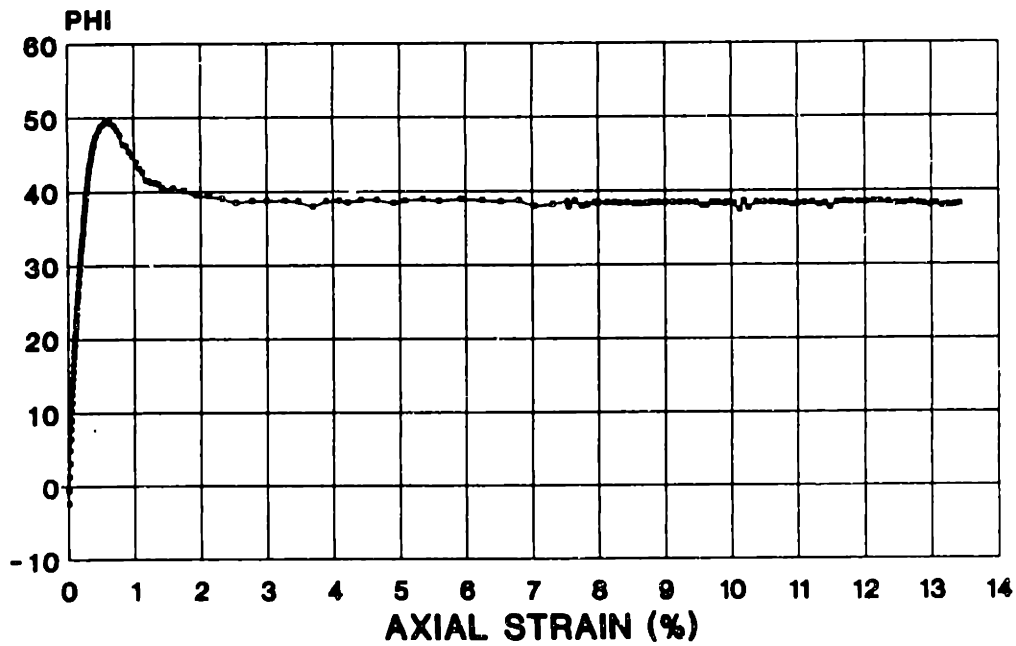

BLOCK S-3A - ELEV. 33.6'

TX093S
STRESS PATH
RECOMPRESSION CKoUE

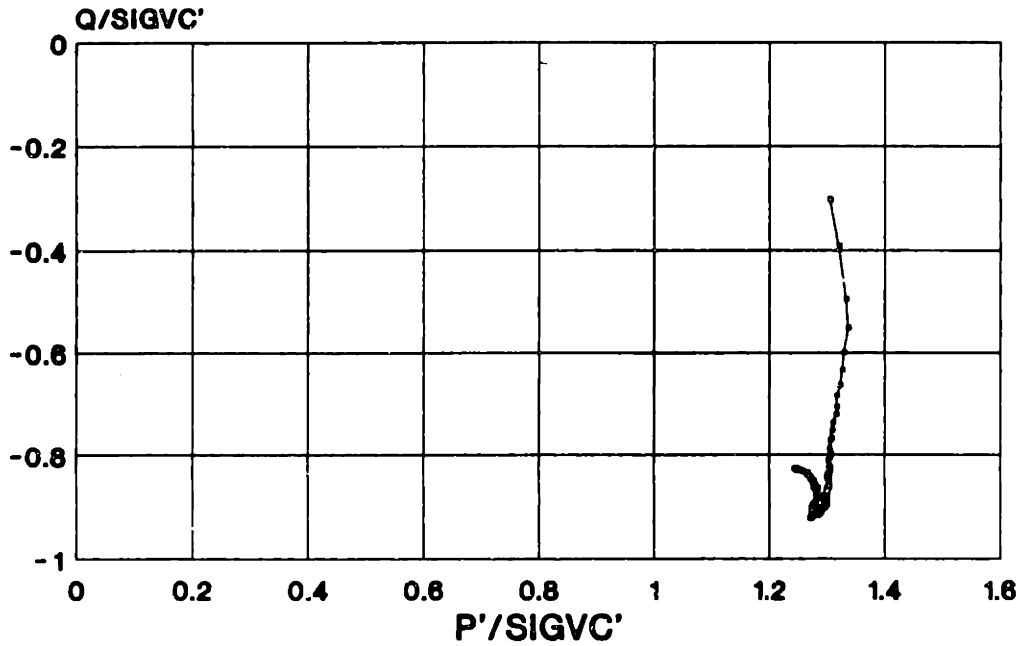

BLOCK S-7 - ELEV. 20.9'

TX093S
STRESS STRAIN
RECOMPRESSION CKoUE

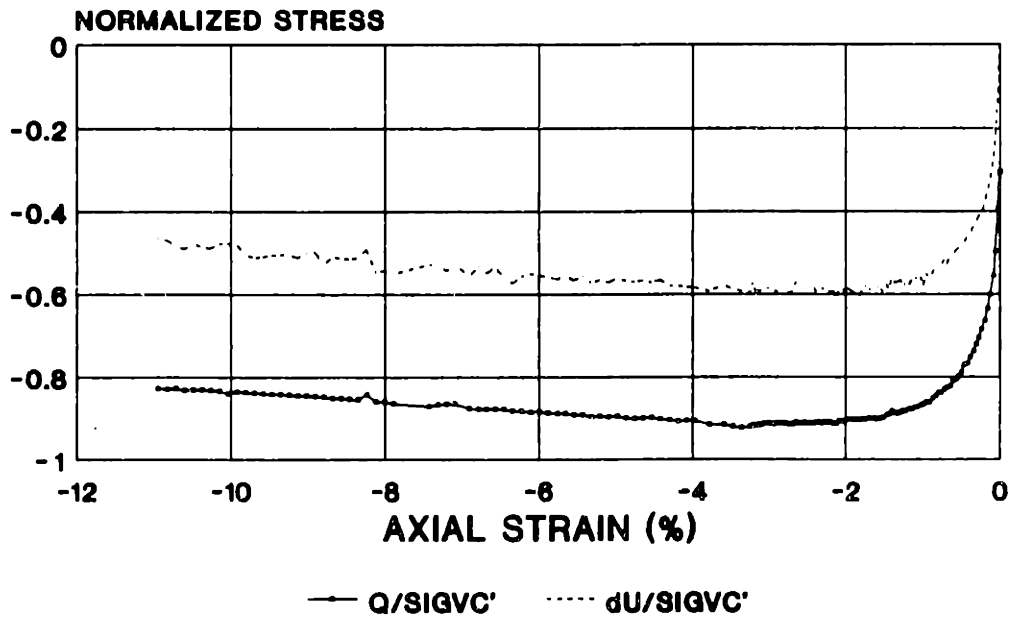

BLOCK S-7 - ELEV. 20.9'

TX093S
A PARAMETER VS. AXIAL STRAIN
RECOMPRESSION CKoUE

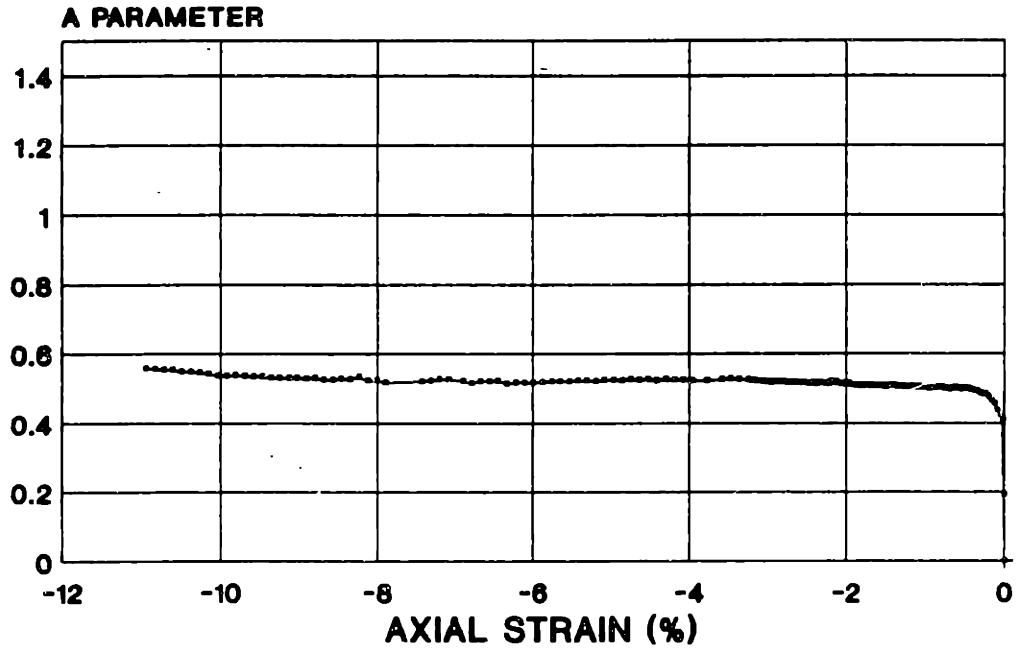

B.S.-7 - ELEV. 20.9

TX093S
PHI VS. AXIAL STRAIN
RECOMPRESSION CKoUE

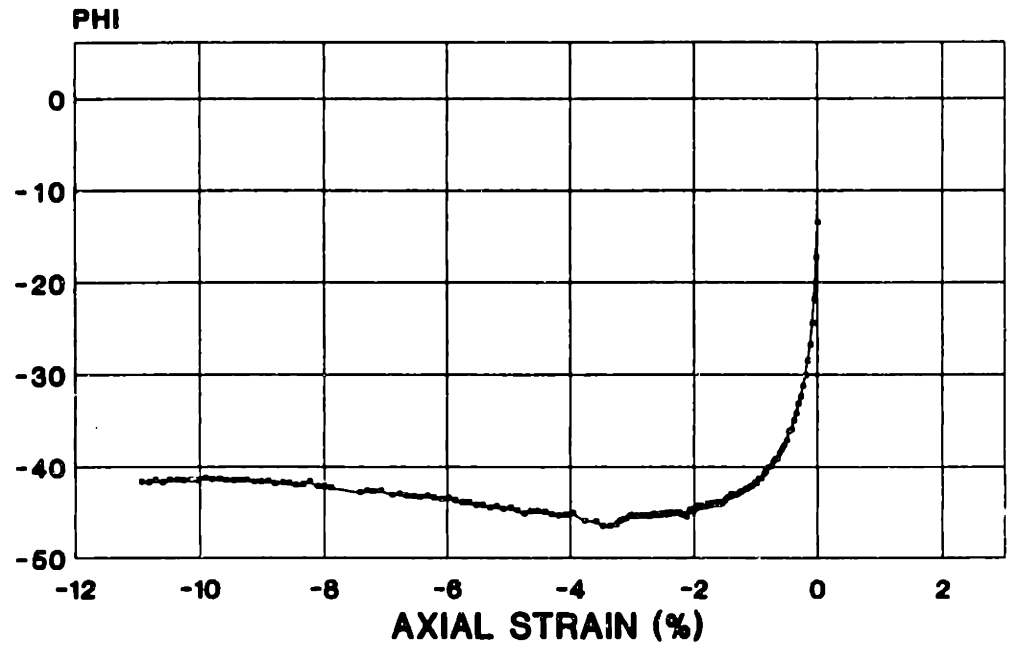

BLOCK S-7 - ELEV. 20.9'

TX095S
STRESS PATH
RECOMPRESSION CKoUC

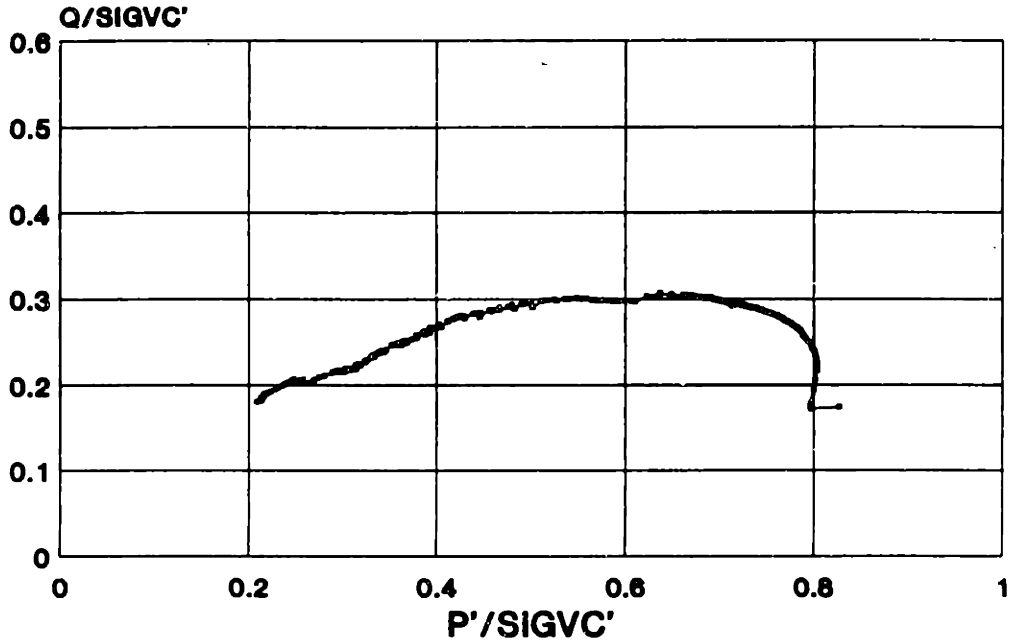

BLOCK S-2A - ELEV. 42.1'

TX095S
STRESS STRAIN
RECOMPRESSION CKoUC

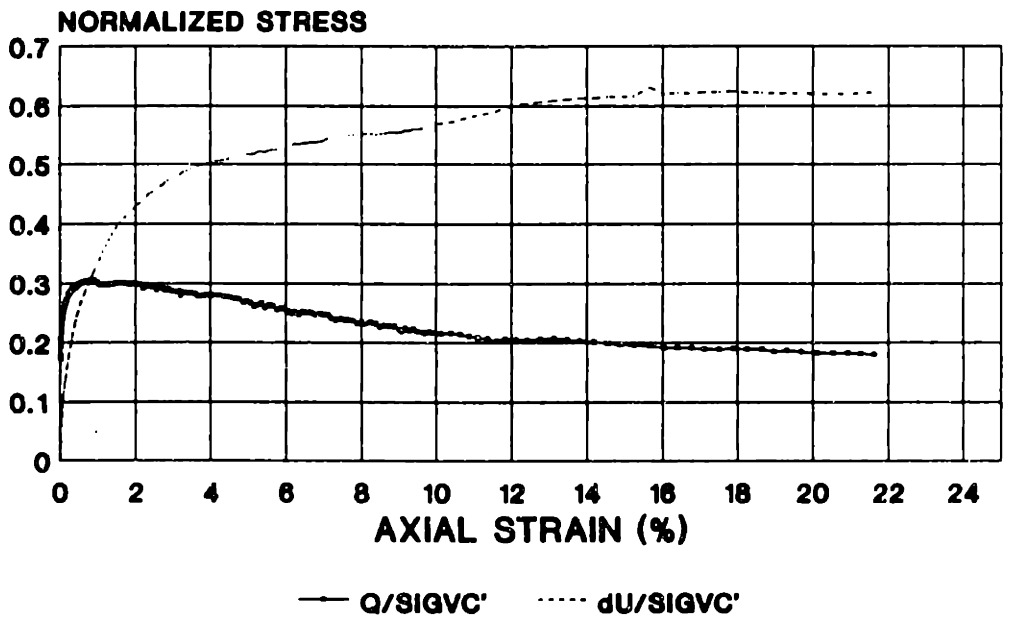

BLOCK S-2A - ELEV. 42.1'

TX095S
A PARAMETER VS. AXIAL STRAIN
RECOMPRESSION CKoUC

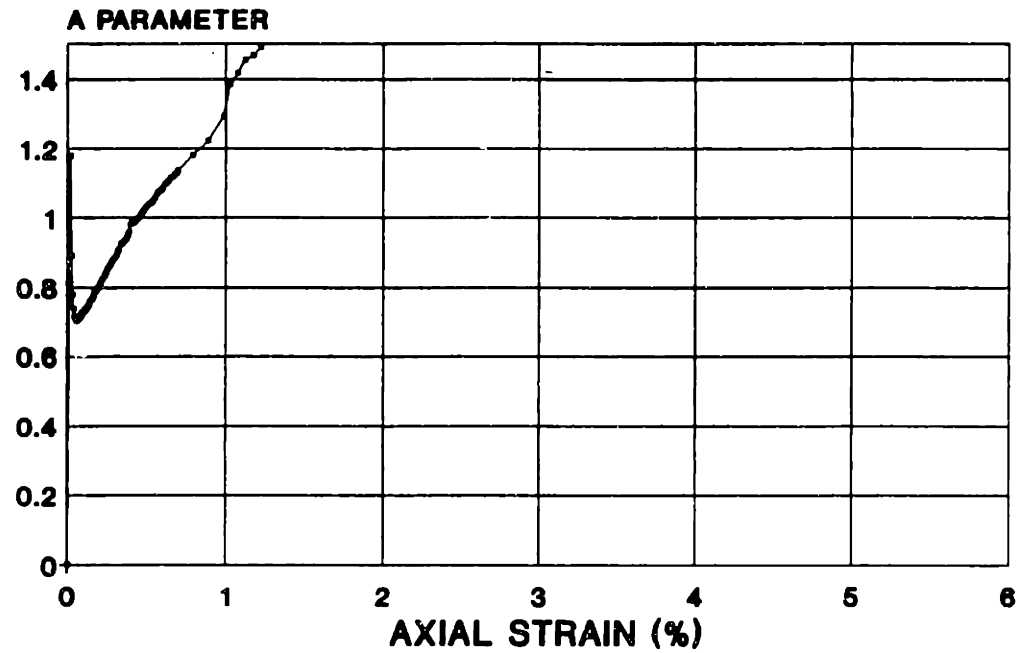

B.B.-2A - ELEV. 42.1'

TX095S
PHI VS. AXIAL STRAIN
RECOMPRESSION CKoUC

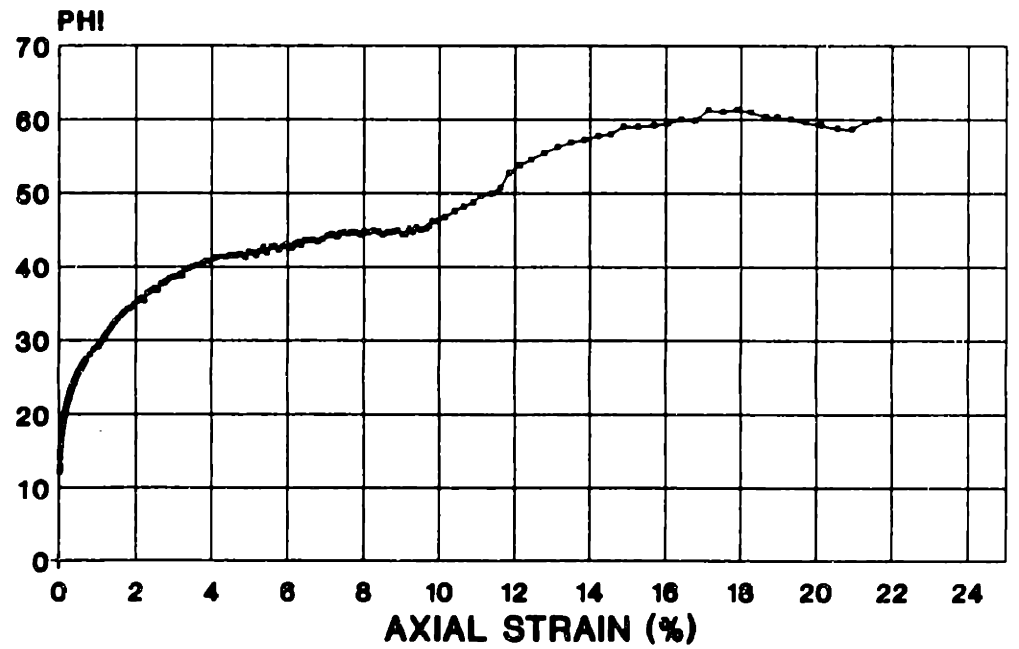

BLOCK S-2A - ELEV. 42.1'

TX096S
STRESS PATH
RECOMPRESSION CKoUE

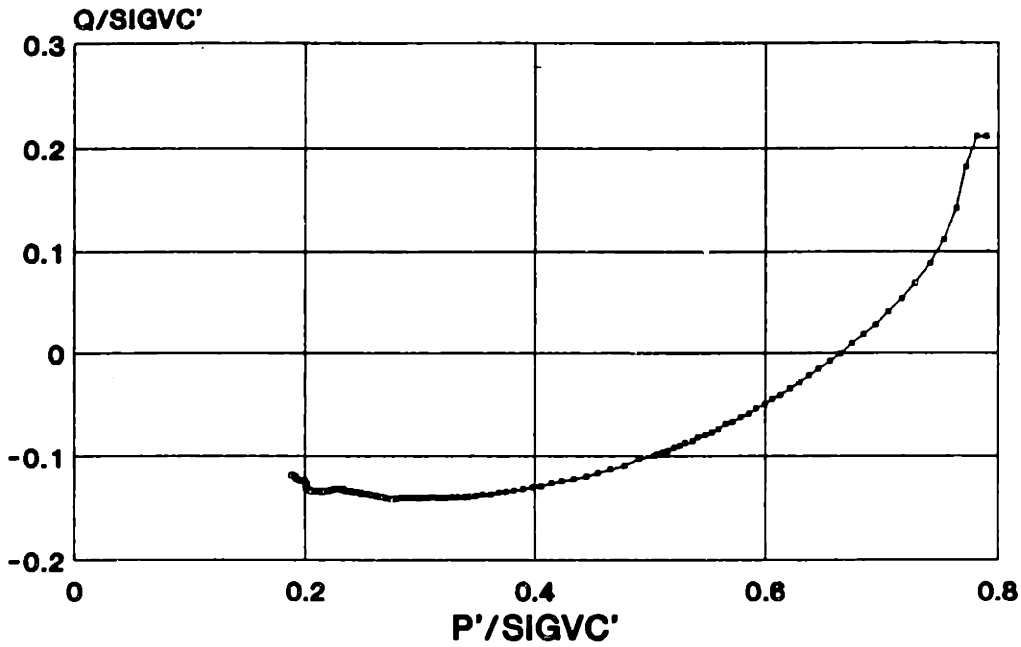

SB2-23 U22 - ELEV. -2.3'

TX096S
STRESS STRAIN
RECOMPRESSION CKoUE

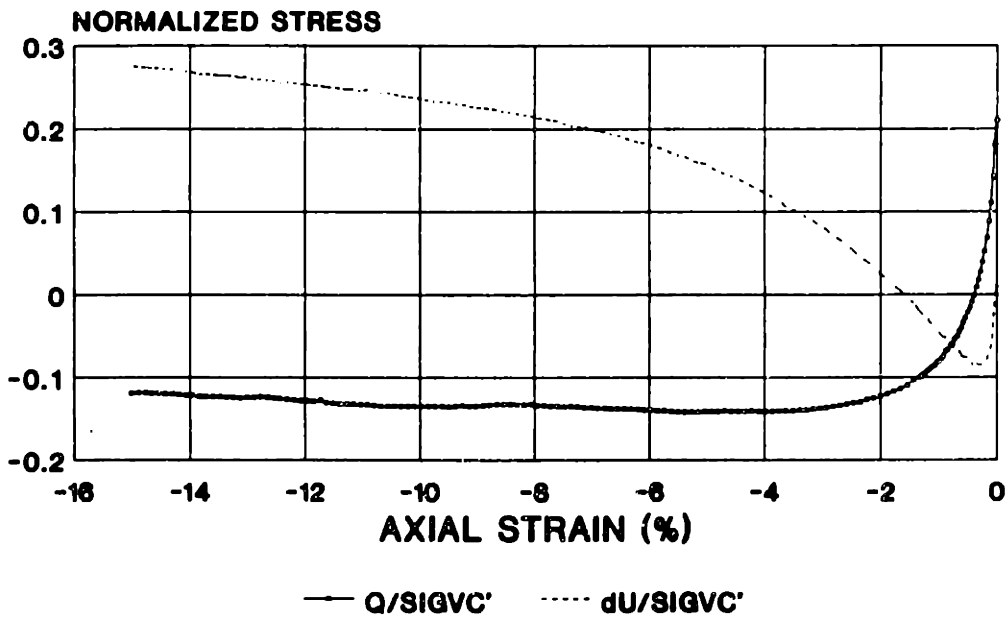

SB2-23 U22 - ELEV. -2.3'

TX096S
A PARAMETER VS. AXIAL STRAIN
RECOMPRESSION CKoUE

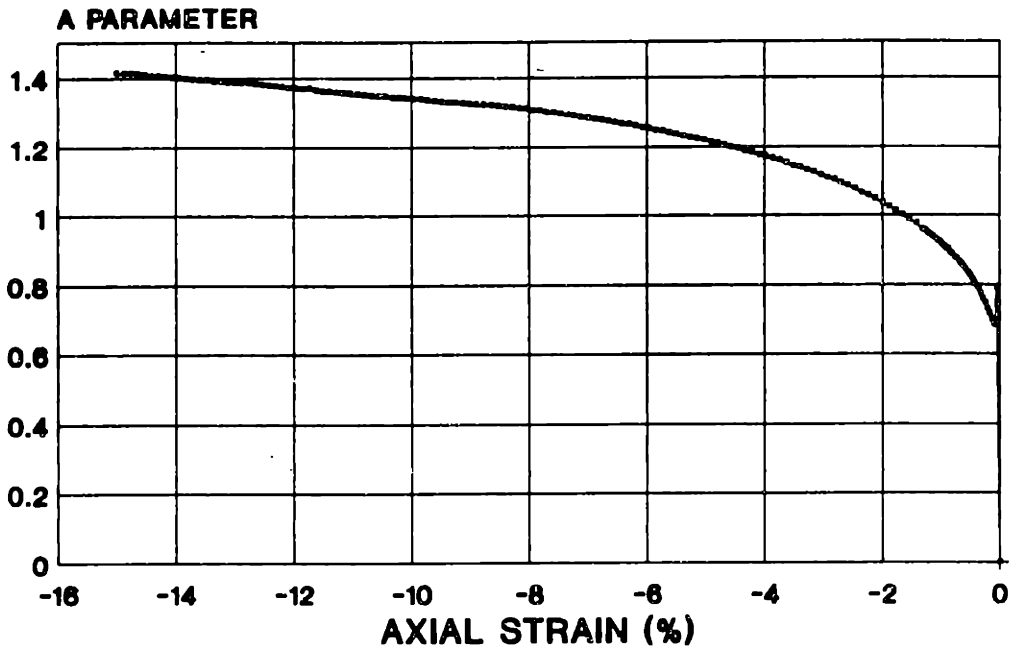

SB2-23 U22 ELEV. -2.3'

TX096S
PHI VS. AXIAL STRAIN
RECOMPRESSION CKoUE

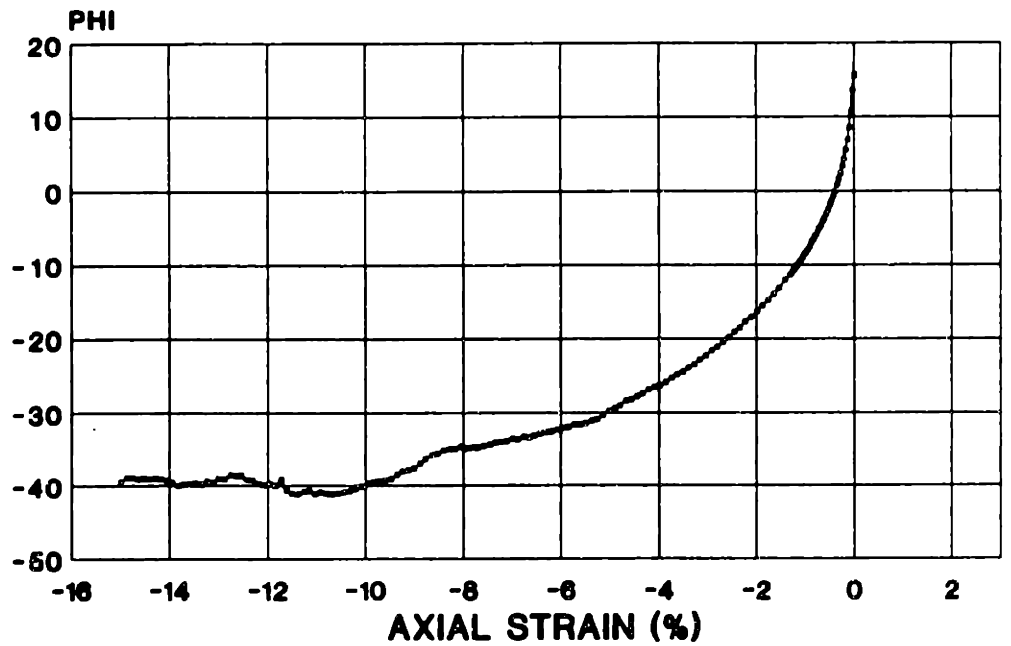

SB2-23 U22 - ELEV. -2.3'

TX098S
STRESS PATH
RECOMPRESSION CKoUC

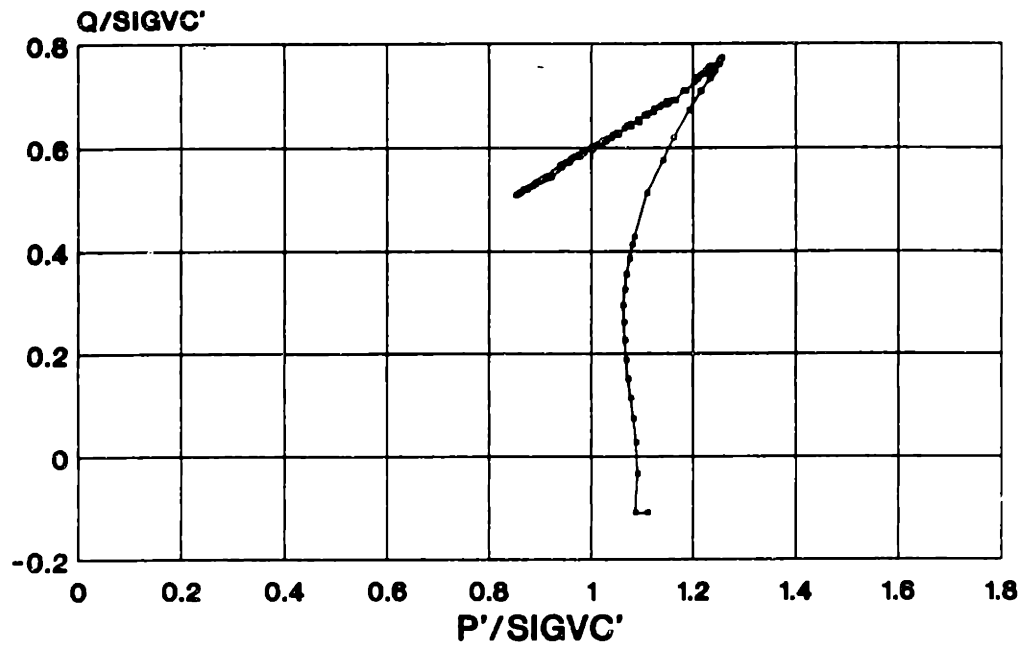

BLOCK S-2A - ELEV. 42.1'

TX098S
STRESS STRAIN
RECOMPRESSION CKoUC

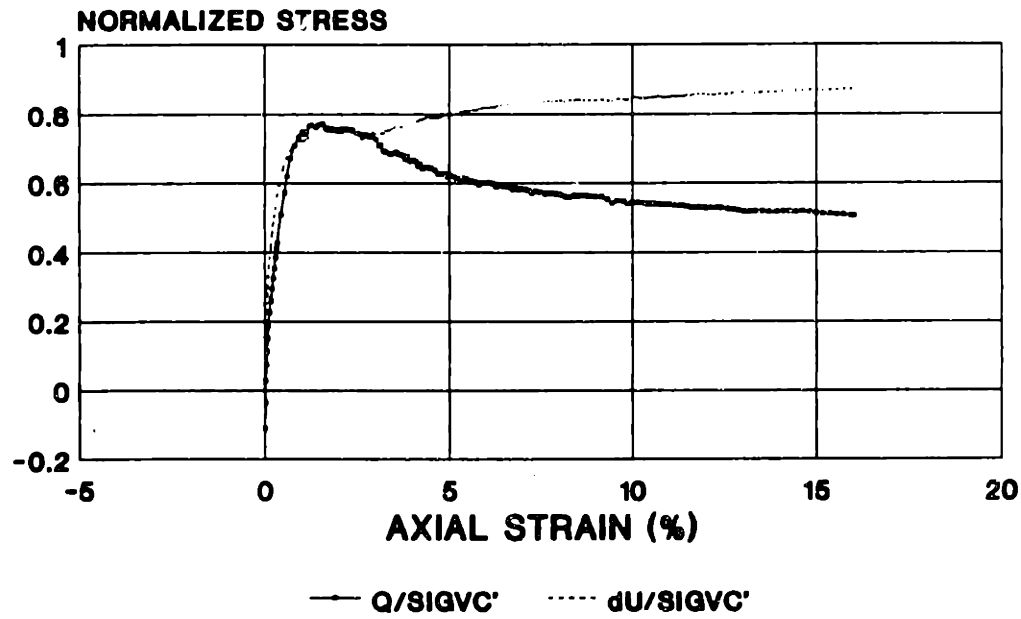

BLOCK S-2A - ELEV. 42.1'

TX098S
A PARAMETER VS. AXIAL STRAIN
RECOMPRESSION CKoUC

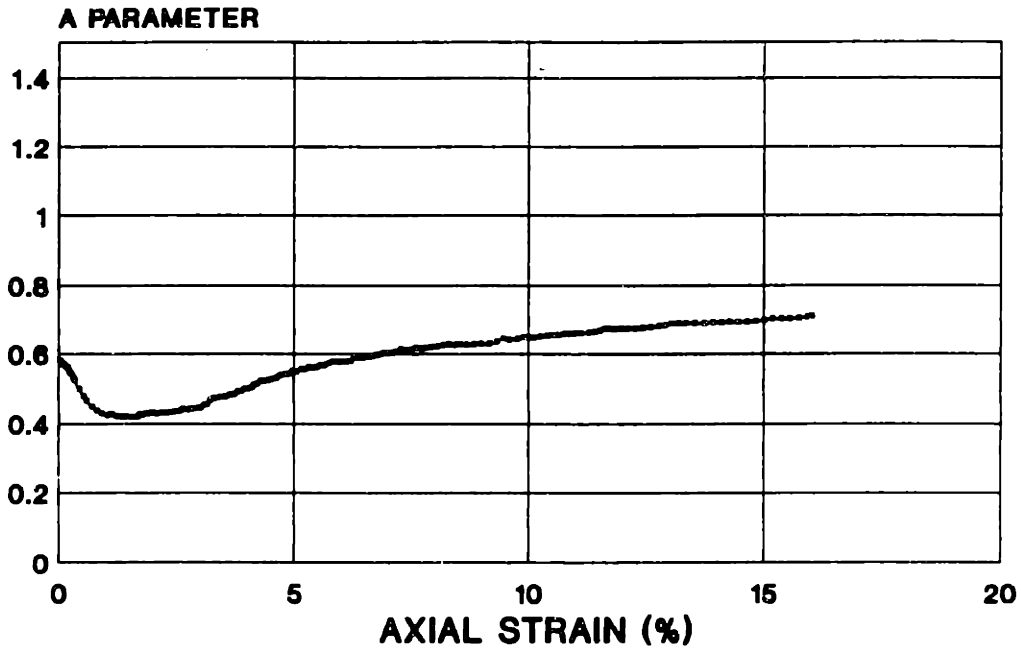

B.S.-2A - ELEV. 42.1

TX098S
PHI VS. AXIAL STRAIN
RECOMPRESSION CKoUC

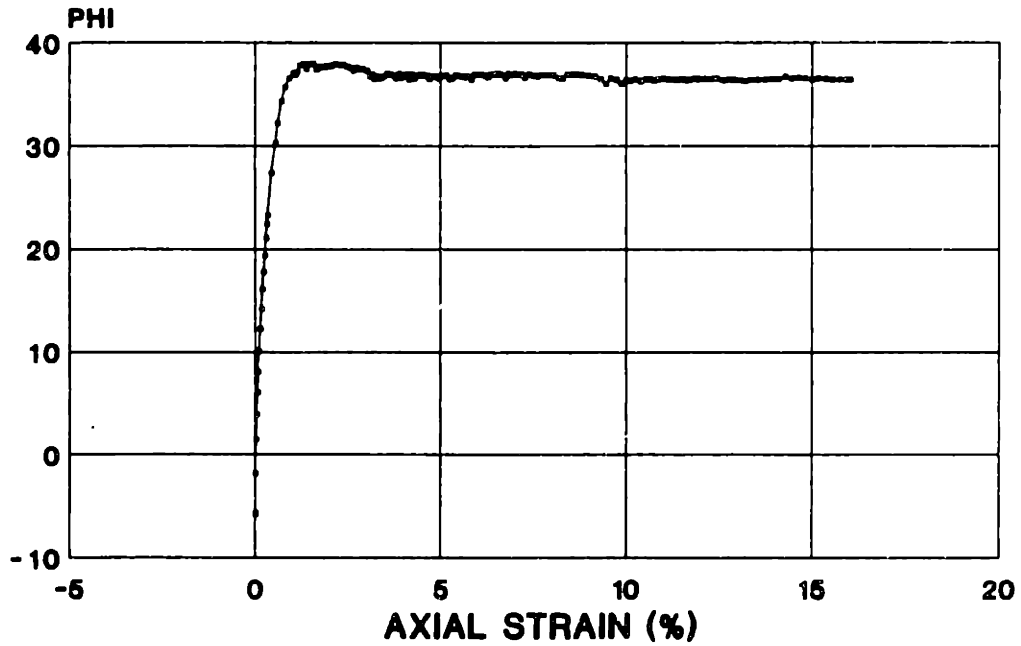

BLOCK S-2A - ELEV. 42.1'

TX099S
STRESS PATH
RECOMPRESSION CKoUE

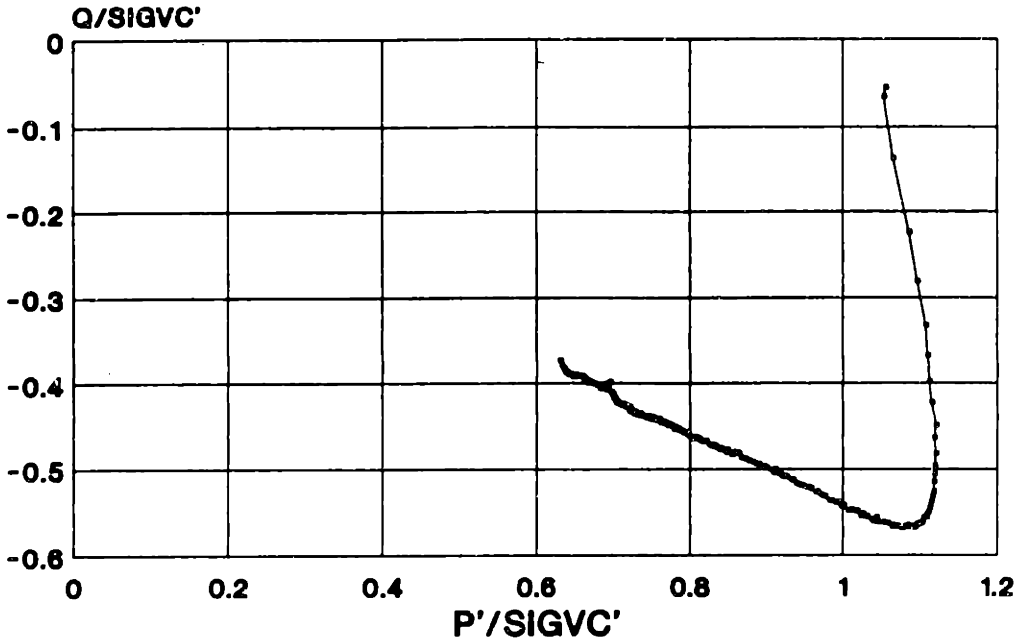

BLOCK S-7 - ELEV. 20.9'

TX099S
STRESS STRAIN
RECOMPRESSION CKoUE

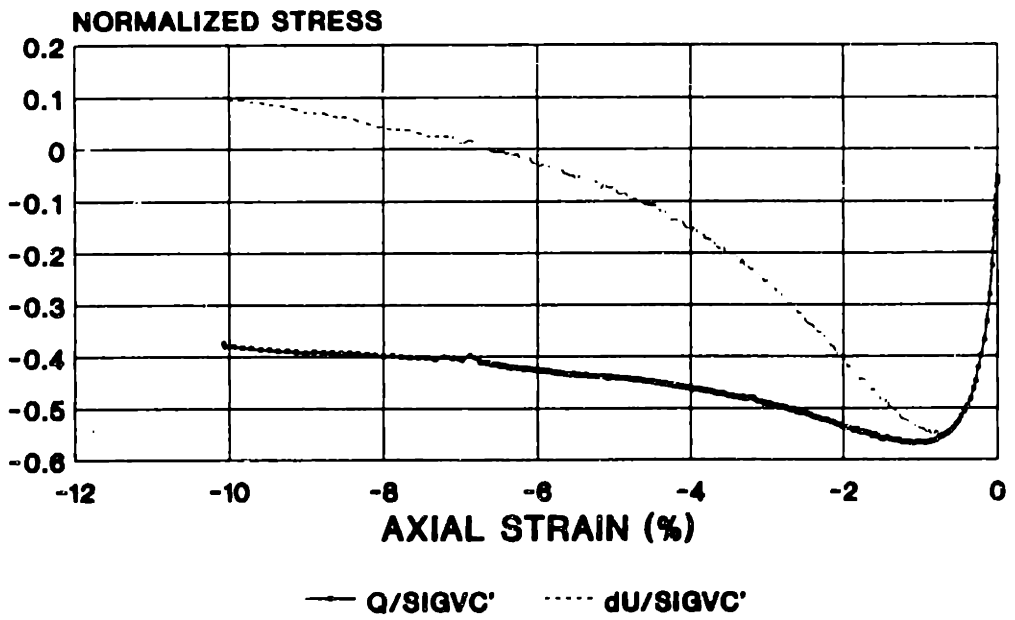

BLOCK S-7 - ELEV. 20.9'

TX099S
A PARAMETER VS. AXIAL STRAIN
RECOMPRESSION CK₀UE

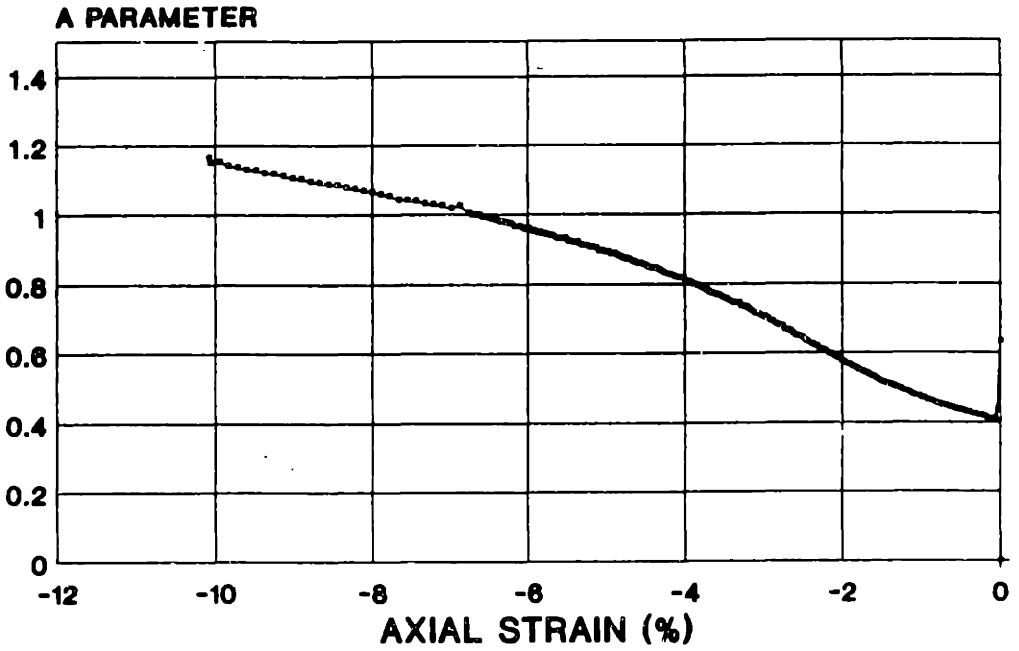

B.S.-7 - ELEV. 20.9'

TX099S
PHI VS. AXIAL STRAIN
RECOMPRESSION CK₀UE

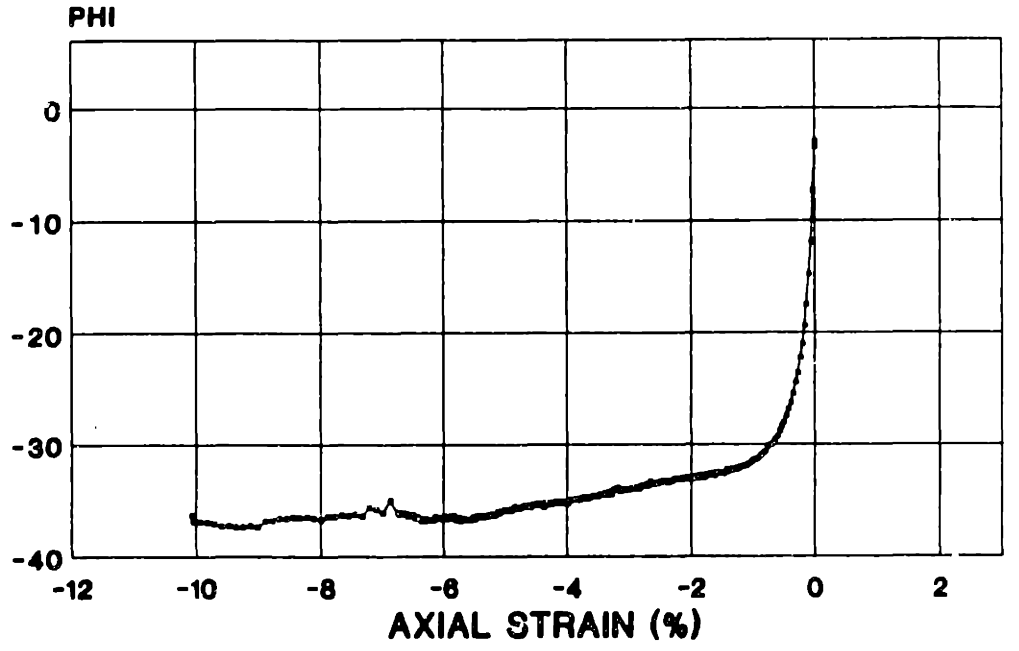

BLOCK S-7 - ELEV. 20.9'

TX101S
STRESS PATH
RECOMPRESSION CKoUC

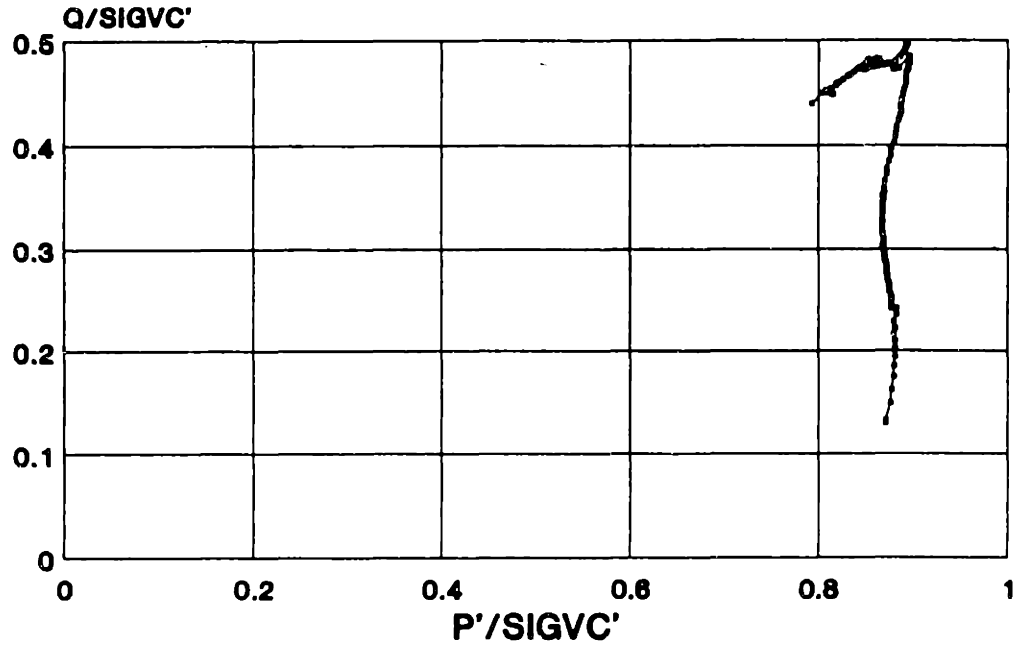

BLOCK S-2 - ELEV. 60.7'

TX101S
STRESS STRAIN
RECOMPRESSION CKoUC

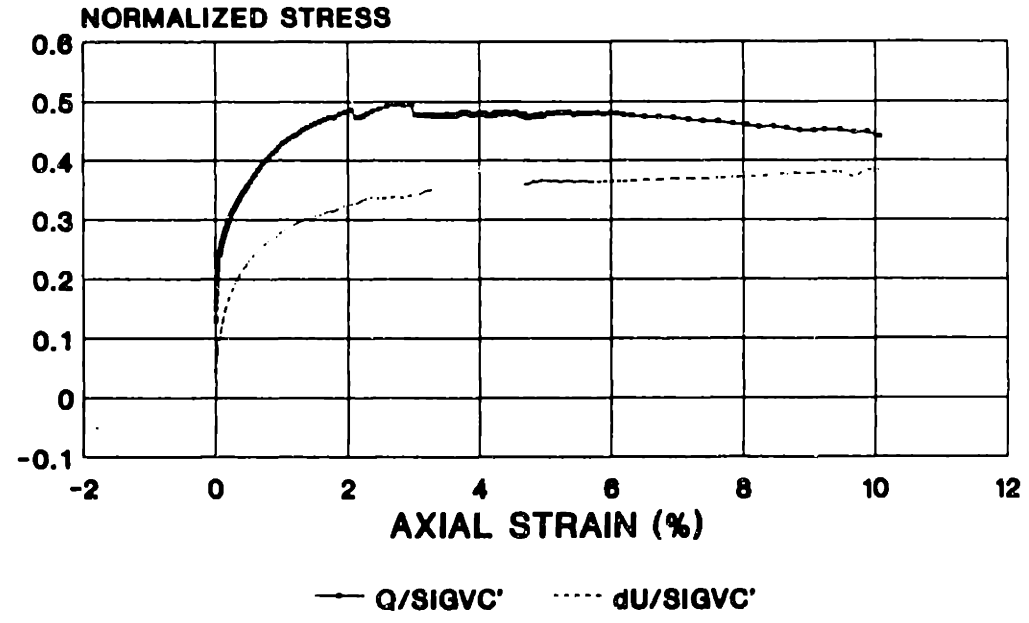

BLOCK S-2 - ELEV. 60.7'

TX101S
A PARAMETER VS. AXIAL STRAIN
RECOMPRESSION CKoUC

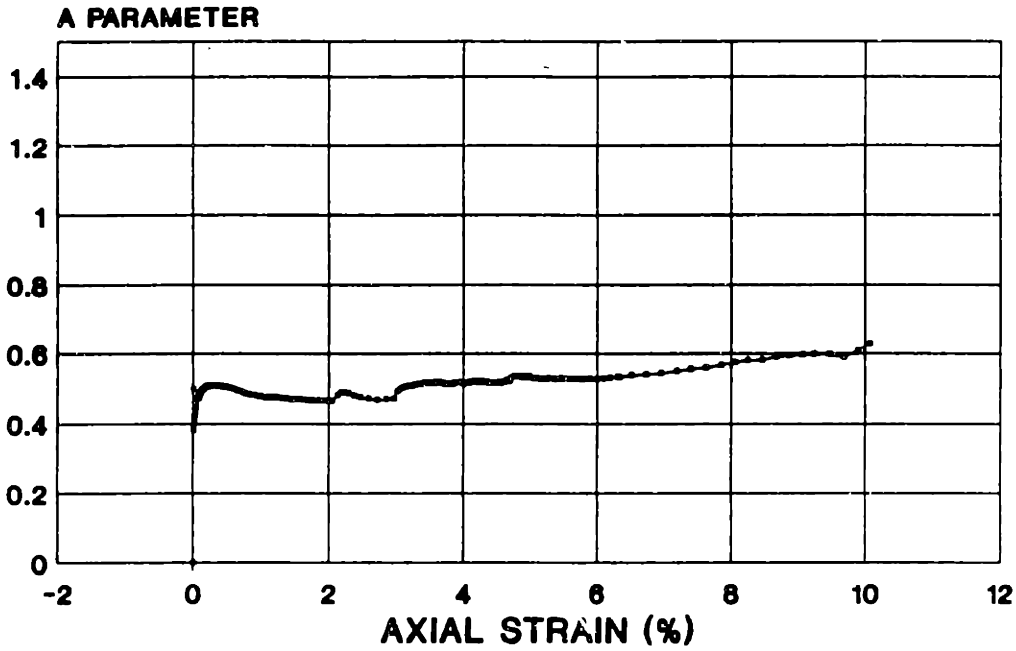

B.S.-2 - ELEV. 60.7'

TX101S
PHI VS. AXIAL STRAIN
RECOMPRESSION CKoUC

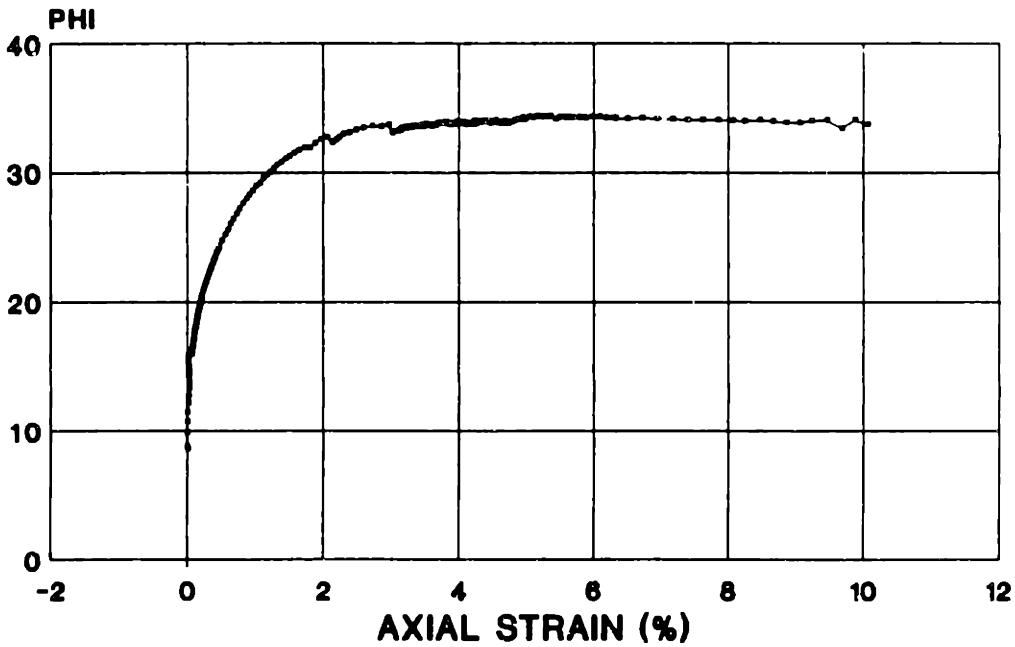

BLOCK S-2 - ELEV. 60.7'

TX103S
STRESS PATH
RECOMPRESSION CKoUC

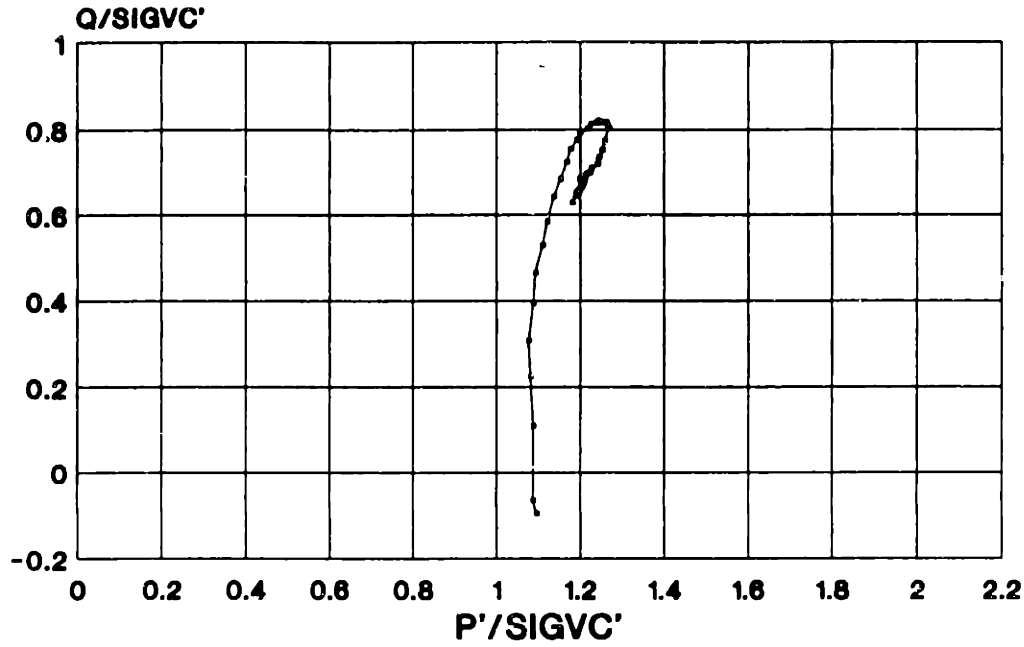

BLOCK S-2A - ELEV. 42.1'

TX103S
STRESS STRAIN
RECOMPRESSION CKoUC

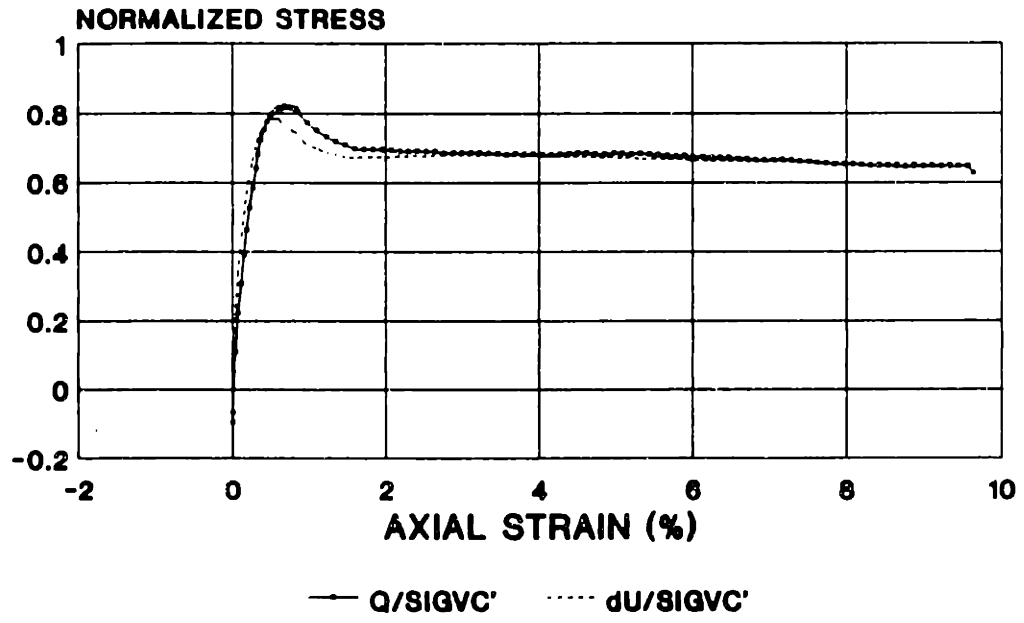

BLOCK S-2A - ELEV. 42.1'

TX103S
A PARAMETER VS. AXIAL STRAIN
RECOMPRESSION CKoUC

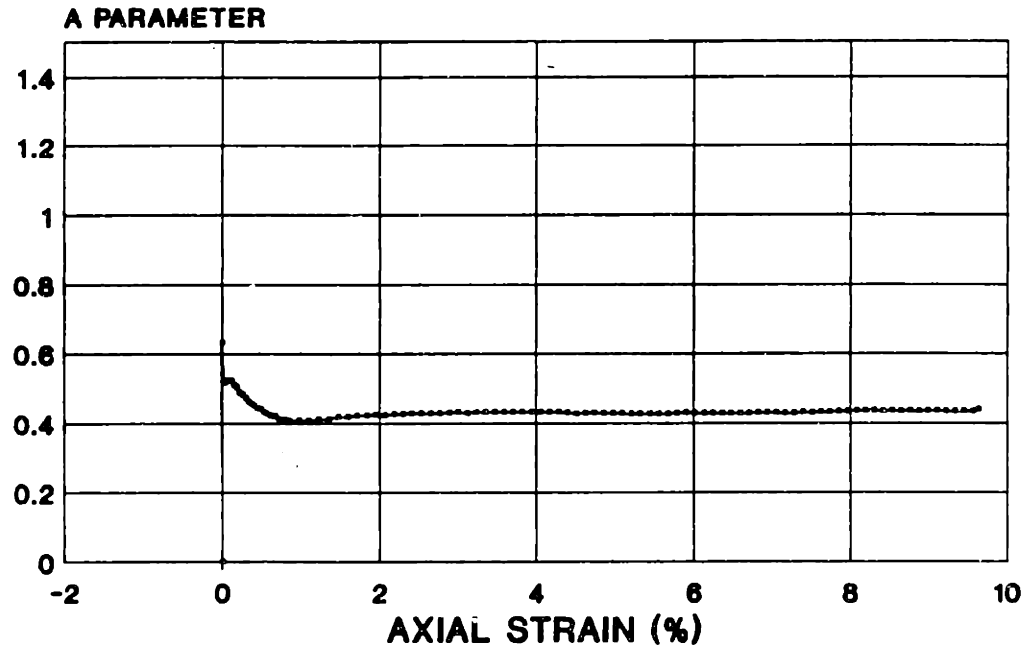

B.S.-2A - ELEV. 42.1'

TX103S
PHI VS. AXIAL STRAIN
RECOMPRESSION CKoUC

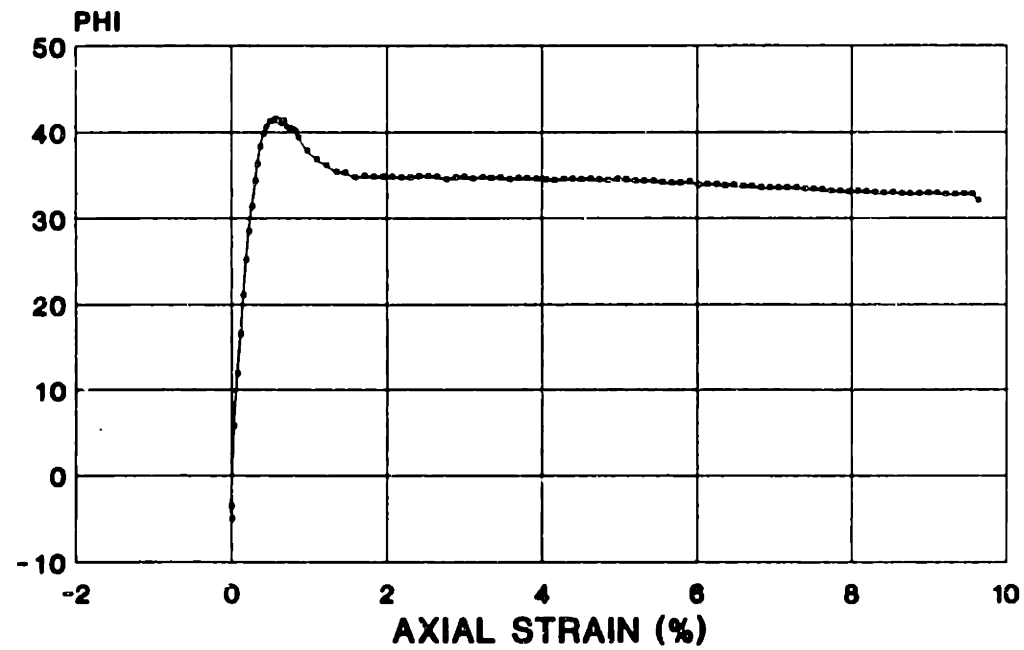

BLOCK S-2A - ELEV. 42.1'

TX104S
STRESS PATH
RECOMPRESSION CKoUC

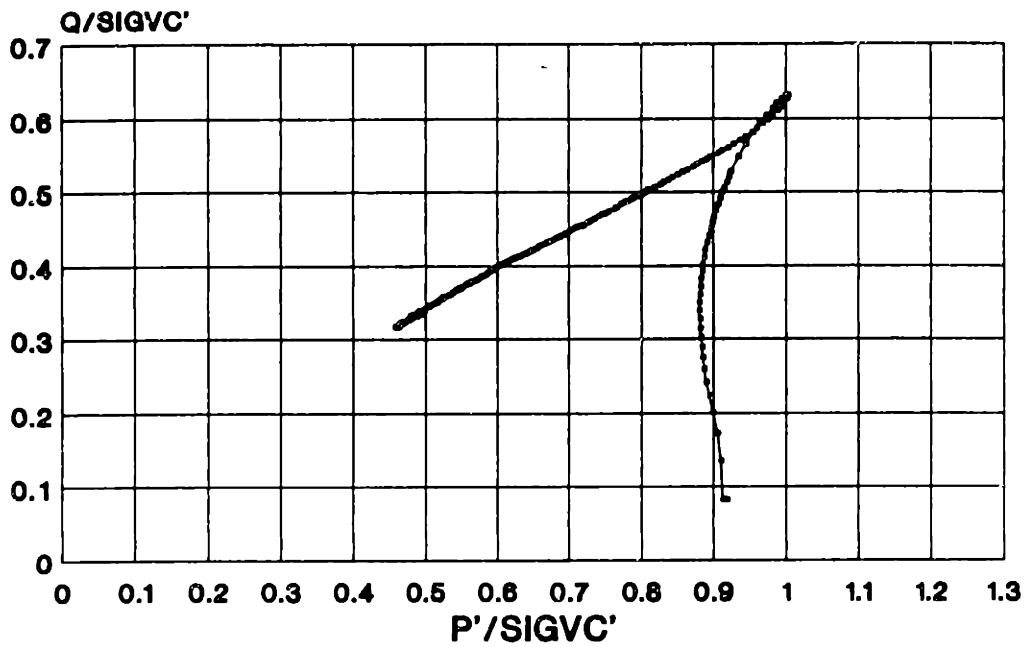

BLOCK S-7 - ELEV. 20.4'

TX104S
STRESS STRAIN
RECOMPRESSION CKoUC

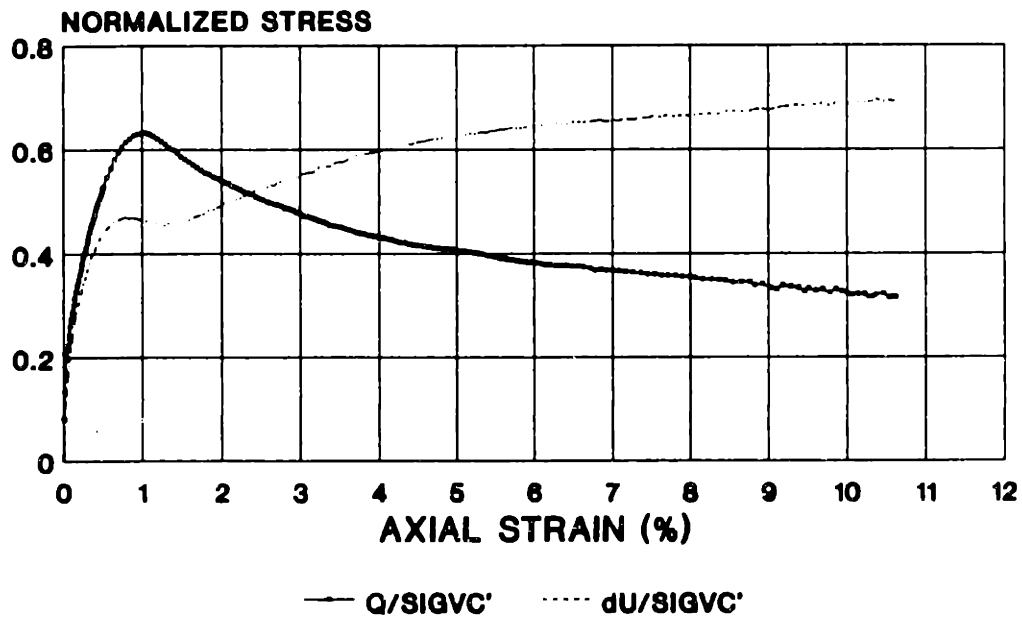

BLOCK S-7 - ELEV. 20.4'

TX104S
A PARAMETER VS. AXIAL STRAIN
RECOMPRESSION CKoUC

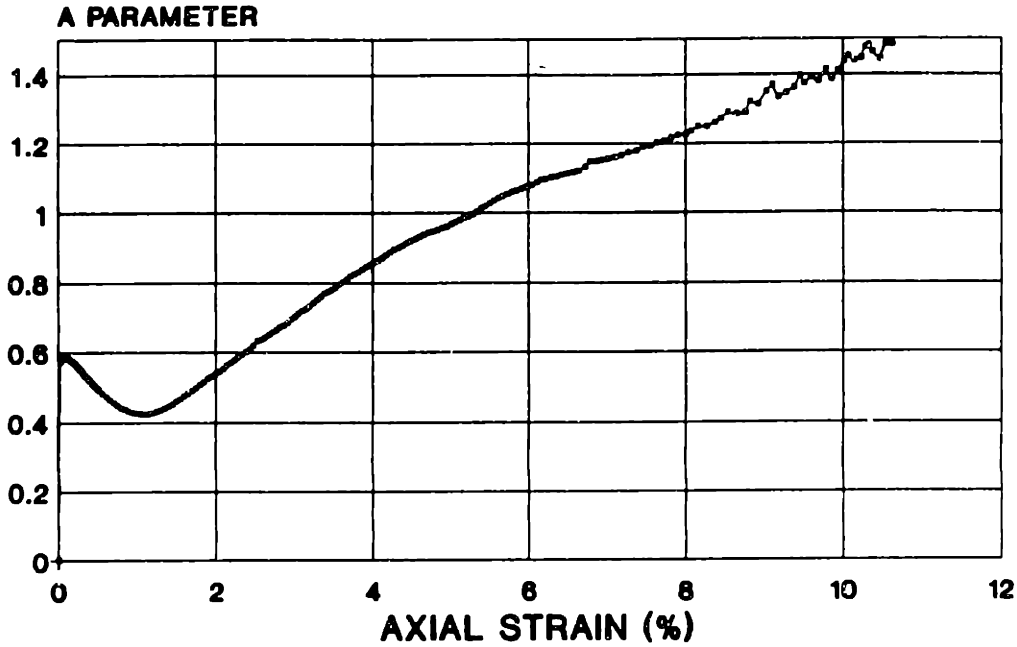

B.S.-7 - ELEV. 20.4'

TX104S
PHI 'VS. AXIAL STRAIN
RECOMPRESSION CKoUC

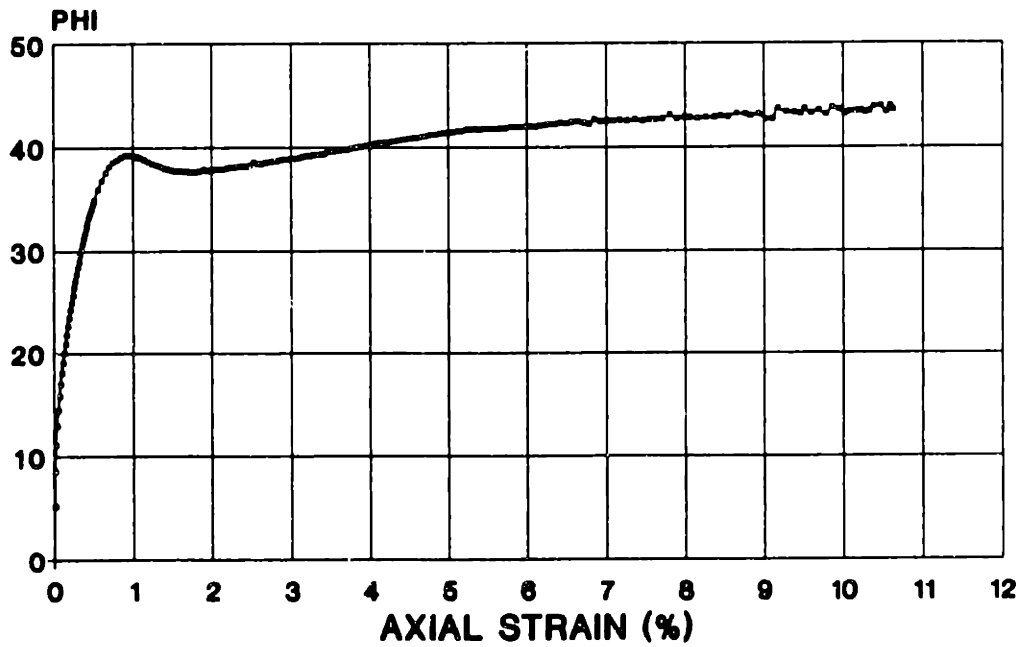

BLOCK 8-7 - ELEV. 20.4'